**stelco**
**Technology**

# DETERMINATION OF THE ABILITY OF STELCO INGOT AND STRAND CAST STRUCTURAL PLATE TO MEET THE MECHANICAL PROPERTY REQUIREMENTS FOR CANADIAN OFFSHORE STRUCTURES AND SHIPS

## - FINAL REPORT FOR DSS CONTRACT OSQ82-00211

by

D. B. McCutcheon, Stelco Inc.

Work on this project was conducted under the auspices of the Canada Centre for Mineral and Energy Technology, Energy, Mines and Resources, Canada

DSS File Number: 23SQ.23440-2-9027-1
DSS Contract Number: OSQ82-00211
CANMET Project Number:
CANMET Scientific Authority: Dr. J. D. Boyd

[illegible]
[illegible]

OCT 10 [illegible]
MICROMEDIA

[illegible]

# LIST OF REPORTS

Arctic Grade 350 Plate - Preliminary Rolling Trial

Strength and Toughness of Stelco Offshore Quality Plate

Weldability and HAZ Toughness of Stelco Offshore Quality Plate

Lamellar Tearing Resistance of Stelco Offshore Quality Plate

Controlled Rolled Grade 350 Plate for Arctic Applications

Review of Fracture Toughness Testing for Offshore Structures and Ships

# ARCTIC GRADE 350 PLATE - PRELIMINARY ROLLING TRIAL

by

D. B. McCutcheon, Stelco Inc.

Work on this project was conducted under the auspices of the Canada Centre for Mineral and Energy Technology, Energy, Mines and Resources, Canada

DSS File Number: 23SQ.23440-2-9027-1
DSS Contract Number: 0SQ82-00211
CANMET Project Number:
CANMET Scientific Authority: Dr. J. D. Boyd

# SUMMARY

Development of Canada's Arctic and East Coast oil and gas reserves will require more than 400 000 tons of Arctic grade plate during the next decade. Most of this tonnage will be 19 to 50 mm (0.75in to 20in) thick, Grade 350 plate with requirements for low temperature (-60°C, -76°F) Charpy impact toughness and adequate through-thickness ductility to prevent lamellar tearing. Traditionally, the quality level has been met with normalized steel; however, it may be possible to supply this market with more weldable, lower cost, controlled rolled plate.

Stelco is participating in a CANMET sponsored project to demonstrate the ability to provide this quality level from a Lake Erie Works strand cast, and a Hilton Works ingot cast heat. Prior to producing these trial heats, a preliminary controlled rolling trial was run using a pearlite reduced C-Mn-Cu-Ni-Cr-V-Cb grade. Fifteen slabs were controlled rolled to plate thicknesses between 19 and 60 mm (0.75in and 2.36in). The strength and toughness of plates at each thickness in the controlled rolled and normalized condition were compared with tentative Arctic grade specifications. Each plate was checked for ultrasonic cleanliness, and the Z-direction ductility determined.

In the controlled rolled condition the Grade 350 yield and tensile strength requirements were readily met in thicknesses up to 60 mm (2.36in). The tentative Charpy energy specification (40 J at -60°C, 29.5 ft-lb at -76°F) was met in thicknesses up to ≈30 mm (1.25in). The lower toughness in heavier gauge plate resulted primarily from insufficient ferrite grain refinement from controlled rolling. All plates met ASTM Level 1 ultrasonic requirements. The lamellar tearing, through-thickness tensile ductility requirement (25 percent reduction of area) was met at locations away from quarter point inclusions.

A review of the literature on the metallurgy of controlled rolled plates and recommendations to improve the toughness of heavy plate are presented.

# CONTENTS

Introduction.......................................................... 7

Strength and Toughness of Controlled Rolled and Normalized Heavy Plate....................................... 10

Plate Rolling and Testing........................................ 10
Results............................................................ 12
Discussion......................................................... 19

Ultrasonic Quality and Lamellar Tearing Resistance.................. 30

Testing............................................................ 31
Results............................................................ 31
Discussion......................................................... 39

Appendix I - Metallurgy of Controlled Rolling of Heavy Plate.. 1 AI

Appendix II - Rolling Practices.............................. 1 AII

Appendix III - Mechanical Properties.......................... 1 AIII

# INTRODUCTION

The development of Canada's East Coast and Arctic oil and gas reserves during the next decade calls for the major construction of production platforms and islands, tankers, ice breakers, barges, dredges and caissons. This equipment will require more than 400 000 tons[1] of thick steel plate (over 20 mm). The stringent service conditions for these regions coupled with the environmental hazard associated with failures of these structures result in very demanding property specifications for both structural steel plate and weldments. Although the specific property requirements have not been established for Arctic structures, it is anticipated that they will closely follow those used by other nations and classification societies for similar structures. The Canadian government is very active in this area and has commissioned two reports from Lloyds Register of Shipping[2] and Det Norske Veritas[3] that review the materials requirements for offshore structures, particularly in the North Sea. These have been used to formulate a tentative aim specification for Arctic Grade 350 structural plate (Table I).

**Table I: Aim (Minimum) Property Specifications for 20 to 100 mm (0.780in to 3.94in) Plate**

| | |
|---|---|
| Yield Strength | 350 MPa (50.8 ksi) |
| Charpy V-Notch Energy | 40 J at -60°C (29.5 ft-lb at -76°F)* |
| Through-Thickness Ductility | 25 percent reduction of area |
| Ultrasonic Cleanliness | ASTM 578 Level 1 |
| Weld HAZ Toughness | 0.25 mm CTOD at -60°C<br>(0.010in at -76°F) |

* Actual Charpy test temperatures will be dependent upon minimum service temperature as well as plate thickness and design classification.

These properties are typical of steel plate used for fabrication of North Sea structures except that the above water extreme minimum service temperatures are expected to be significantly lower [-50°C (-58°F) in Arctic and -30°C (-22°F) in Hibernia versus -10°C (-14°F) for North Sea]. Thus, most of the steels used for Canadian construction will need considerably lower impact transition temperatures than required previously for offshore applications. It is important to recognize that the base plate specification test temperatures are generally lower than the service temperature. Most international codes specify test temperatures from 20°C (35°F) to 40°C (72°F) below the service temperature depending mainly upon the thickness of the plate and the ranking of the member relative to the integrity of the structure. Furthermore allowances are made for the deterioration of plate toughness resulting from straining and aging during fabrication of cold worked tubulars. In addition, a significant tonnage will be applied for below water structures with a much higher minimum design temperature [-10°C (14°F)].

The Canadian government recognizes the benefit of having maximum Canadian participation in terms of both steel supply and fabrication of equipment for these projects. They are concerned that overspecification of steel property requirements may jeopardize the participation of Canadian steel companies. The Department of Energy, Mines and Resources has established a preliminary research program to determine the present ability of Canadian steel producers to meet Arctic grade requirements, and to pinpoint deficiencies requiring long term product development. Stelco is participating in this 50 percent funded program by the production and detailed evaluation of two trial heats - a Hilton Works CAB treated ingot cast and an LEW strand cast heat.[4] The background and detailed testing program for these steels is presented in R&D Report No. 820108. Similarly, Algoma is producing and testing a rare earth treated LT-60, low temperature normalized grade for this project.[5] Plate samples from both suppliers will be used for the development of welding procedures and consumables for this application, and testing of weld zone corrosion and fatigue crack growth rates in Arctic environments.

Stelco has not supplied heavy plate to meet the mechanical property specifications for Arctic use. Worldwide, other producers have and are continuing to develop new steel chemistries and processing practices for similar low temperature applications. Although, traditionally, heavy plate with these impact requirements have been supplied in the normalized condition, there is a strong trend to the application of controlled rolled product in gauges up to ≈50 mm (2.0in). There are several reasons for this development, including:

- the potential lower production cost of controlled rolled compared with normalized product,
- improved weldability (resistance to hydrogen induced cold cracking) and thus lower fabrication costs (no preheating or reduced preheating temperatures) because of the lower carbon equivalent of controlled rolled steels, and
- the potential for improved HAZ and weld toughness resulting from reduced carbon and microalloy contents.

At Stelco, low carbon, microalloyed (pearlite reduced) type chemistries have been used for line pipe grades (up to Grade 448) since the early seventies, however, we have little or no experience in controlled rolling this type of chemistry at gauges over ≈15 mm (0.60in). Limited trials have been run on production orders for heavy plate using high carbon equivalent, normalizing-type chemistries.[6] Although the Grade 350 strength level was consistently achieved, the impact toughness values were poor.

The key to meeting the most stringent Charpy toughness requirements is to obtain a relatively fine grained ferrite-pearlite structure throughout the plate thickness. This demands both refinement of the austenite structure by controlled reheating and rolling practices, and "optimization" of the steel chemistry in terms of carbon, alloy and particularly the microalloy contents as they interrelate with rolling practice. In this regard, there has been considerable fundamental research done on the metallurgy of microalloys and controlled rolling over the past few years. Several excellent papers have been published on the effects of steel chemistry, reheating temperatures, drafting practice, interstand hold time, etc, on austenite structure during rolling and austenite-to-ferrite phase transformation. These papers have been summarized in Appendix I along with guidelines for rolling practices to achieve the required fine-grained structures in heavy plate.

To gain some experience in controlled rolling of heavy plate, two preliminary trials were run by the Research, Metallurgical and Operating Departments during the period February to May, 1983.

This report covers the rolling and detailed testing of an LEW Stelcoloy 70 (strip grade) heat at plate gauges between 19 mm (0.75in) and ≈60 mm (2.36in). This composition, although not designed for heavy plate, is similar to the chemistries being applied by offshore suppliers for controlled rolled plate. Plate strength and toughness data are presented for both the as-rolled and normalized conditions. Normalized test results have been included to assess the potential of using normalizing as an alternative to meet the Grade 350 property requirements. In addition, the ability of the LEW strand cast steel to meet the ultrasonic and lamellar tearing resistance specifications is shown.

# STRENGTH AND TOUGHNESS OF CONTROLLED ROLLED AND NORMALIZED HEAVY PLATE

## Plate Rolling and Testing

### i) Heat Chemistry

A Stelcoloy 70 strip chemistry strand cast at LEW was used for the controlled rolling trial. The chemistry was designed for strip product, however, its carbon, manganese and microalloy levels (0.05 Cb, 0.03 V) are similar to those found in modern controlled rolled Grade 350 (50 ksi) structural plate being supplied by Japanese and European producers. Note that the sulfur level is not quite as low as believed necessary for good lamellar tearing resistance, and that the chemistry includes Cu, Ni, and Cr additions. These were originally added primarily for improved weathering resistance. They have significant but small effects on plate yield strength and UTS.

**Table II: Heat Chemistry**

| C | Mn | P | S | Si | Cu | Ni | Cr | V | Cb | ASA | N |
|---|---|---|---|---|---|---|---|---|---|---|---|
| 0.08 | 1.38 | 0.008 | 0.005 | 0.22 | 0.24 | 0.34 | 0.39 | 0.030 | 0.052 | 0.039 | 0.009 |

### ii) Plate Rolling

A total of 15 slabs were successfully controlled rolled to plate gauges ranging in thickness between 0.75in and 2.36in (Table III) in two separate rollings. The first was an R&D trial to establish the gauge/property effects on thicknesses between 0.75in and 1.50in and the second, a mill production rolling in which gauges between 1.57in and 2.36in were rolled. In both rollings, problems were experienced with excessive turnup during roughing and finishing, which resulted in four bars being rejected.

Table III: Plate Controlled Rolling Practice

| Roll Date | Charge No. | Gauge (Aim) (in) | Breakdown Bar Thickness (in) | % Reduction Below Temperature (°F) | | | | | Finish Temperature (°F) | 2-Hi-4-Hi Delay (sec) |
|---|---|---|---|---|---|---|---|---|---|---|
| | | | | | 1650 | 1600 | 1550 | 1500 | | |
| 3/09/83 | 967 | 0.750 | 2.35 | | 60 | 60 | 64 | 44 | 1389 | 25 |
| | 968 | 0.758 | 2.35 | | 60 | 60 | 64 | 59 | 1339 | 75 |
| | 969 | 0.730 | 2.35 | | 60 | 60 | 64 | 63 | 1325 | 40 |
| | 970 | 1.0 | 3.125 | | 68 | 64 | 60 | 56 | 1375 | 90 |
| | 971 | 1.0 | 3.125 | | 68 | 68 | 64 | 51 | =1400 | 30 |
| | 972 | 1.0 | 3.125 | | KO | | | | | |
| | 973 | 1.25 | 3.90 | | 65 | 62 | 60 | 38 | =1450 | 35 |
| | 974 | 1.25 | 3.90 | | 68 | 68 | 65 | 46 | =1470 | 240 |
| | 975 | 1.500 | 4.70 | | KO | | | | | |
| | 976 | 1.500 | 4.70 | | KO | | | | | |
| 5/20/83 | 158 | 1.524 | 4.70 | | 67 | 61 | 46 | 8 | 1405 | 171 |
| | 159 | 1.524 | 4.70 | | KO | | | | | |
| | 161 | 1.524 | 4.70 | | 67 | 56 | 41 | 8 | 1400 | 30 |
| | 163 | 1.524 | 4.70 | | 67 | 67 | 67 | 46 | 1368 | 68 |
| | 164 | 1.524 | 4.70 | | 67 | 64 | 61 | 26 | 1388 | 49 |
| | 165 | 1.524 | 4.70 | | 67 | 67 | 40 | 8 | 1392 | 30 |
| | 160 | 1.968 | 5.50 | | 64 | 64 | 47 | 12 | 1400 | 201 |
| | 162 | 1.968 | 5.50 | | 64 | 58 | 40 | 12 | <1473 | 40 |
| | 157 | 2.362 | 5.50 | | 63 | 48 | 6 | - | 1537 | 240 |

The main features of the controlled rolling practices were:

- 2150-2200°F maximum reheat temperature,
- 3:1 reduction below 1650°F, and
- finishing temperature as high as possible.

For the first rolling both the 2 Hi and 4 Hi drafting practice were designed by the plate mill rollers, and featured a large number of very light pass reductions during 4 Hi rolling to dissipate heat. The later rolling used a much modified 4 Hi drafting practice with an aim 10 percent reduction per pass and a fixed interpass hold time of 15 seconds. The 2 Hi drafting practice was similar on both trials. Drafting with water spray cooling during roughing was used on both trials to reduce the hold time between roughing and finishing. Specific details of the pass schedules are given in Appendix II.

### iii) Mechanical Testing and Metallography

Longitudinal and transverse tensiles were tested from each plate in the controlled rolled condition. In addition, test coupons from the first rolling were normalized at 1700°F (for 1 hr per inch of thickness) and tensile tests performed.

Full thickness bend tests were also performed on as-rolled samples representative of each plate thickness.

Full size, transverse, Charpy transitions were broken on both controlled rolled and normalized plate samples. Sample locations included:

- subsurface (0.050in below surface) from all plates,
- mid-thickness from one plate from each gauge, and
- quarter thickness position from selected plates.

Each full thickness test coupon was ultrasonically inspected prior to machining to determine the positon of quarter-point inclusions. Subsurface Charpies were taken from the "clean" side of the plate, whereas the quarter thickness Charpies came from the "dirty" side. Test coupons from the first rolling were normalized at 1700°F. This was adjusted downward to 1650°F for samples from the second rolling because of a slight coarsening of the ferrite grain structure at 1700°F. A limited number of longitudinal Charpies were also tested in both the as-rolled and normalized conditions.

Nil-Ductility Temperature (NDT) tests were done on selected plates in both the as-rolled and normalized conditions. Samples (3/4in x 2in x 5in) were tested using both surface (as per specification) and subsurface (i.e. 3/4in from rolled surface) notches. Tests were done over a series of temperatures to establish the minimum temperature for a full width fracture as per ASTM E-208-69.

The through-thickness distribution of ferrite grain size and volume fraction of pearlite and bainite were determined on all controlled rolled plates and selected normalized plates. The grain size ratings were made with the QTM 720 Image Analyzer at a minimum of seven positions through the plate thickness, depending on gauge.

The steel cleanliness was rated by manual counting of the total number and lengths of oxide and sulfide inclusions on longitudinal sections of broken Charpy coupons. Inclusion ratings were limited to selected samples covering the range of thicknesses.

## Results

### i) The Effect of Plate Gauge and Processing on Strength

In the controlled rolled condition, this chemistry easily met the minimum yield and ultimate tensile strength (UTS) requirements for

Grade 350 plate* (figure 1 and Table I, Appendix II). At lighter gauges (less than ≈1.50in), the strength was adequate for Grade 400 plate. There was only slight anisotropy in strength; the transverse yield and UTS were marginally (≈0.7 ksi, 10 MPa) higher than in the longitudinal direction. The steel showed excellent tensile ductility and readily met the minimum tensile elongation requirements over the entire gauge range. At lighter gauges (<1.0in) the yield to ultimate strength (Y/T) ratio occasionally exceeded 0.85 (figure 2). Although a Y/T upper limit is not specified by CSA (CAN3-G40.21-M81), a 0.85 maximum has often been required for heavy plate for offshore-platform-construction.

All plates passed the bend test with no sign of centerline cracking.

**Figure 1: The Effect of Plate Gauge on Controlled Rolled Plate Strength**

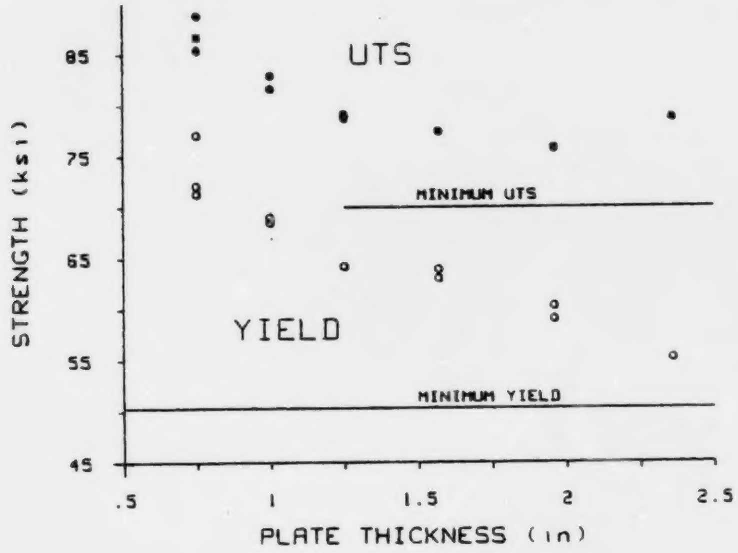

Minimum Yield - 350 MPa (50.8 ksi)
Minimum UTS - 480 MPa (70 ksi)

---

* 350 MPa = 50.8 ksi

Figure 2: The Effect of Plate Gauge on Y/T Ratio

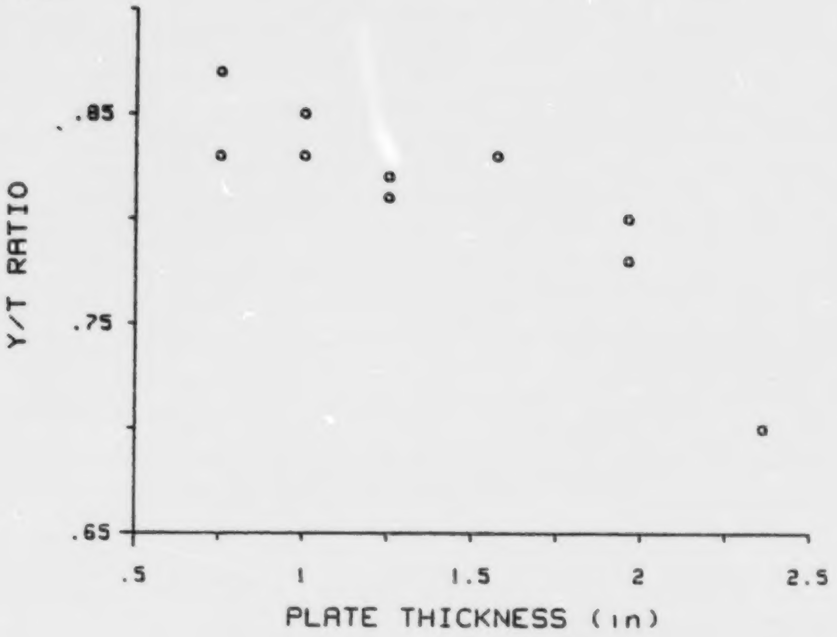

In the normalized condition, this chemistry failed to consistently achieve the minimum yield strength (Table I, Appendix III) and the UTS values just met the minimum requirements. All plates readily met the tensile ductility and Y/T specifications.

### ii) The Effect of Gauge and Processing on Toughness

Figure 3 summarizes the transverse Charpy energy data in controlled rolled plate as a function of plate gauge and sample position through the plate thickness. For Charpy tests taken from the subsurface location, the minimum Charpy energy requirement was readily met over the entire gauge range at temperatures as low as -75°F (-60°C). Charpy energy was marginal at several gauges at -100°F (-73°C). At the plate mid-thickness position, the Charpy energy requirement was met at temperatures down to -100°F (-73°C) in plate gauges up to 1.25in; however, in heavier gauges adequate Charpy toughness was achieved at temperatures down to -50°F (-45°C).

Figure 3: The Effect of Gauge and Test Temperature on Charpy Energy Absorption in Controlled Rolled Plate

(a) Plate Surface Position

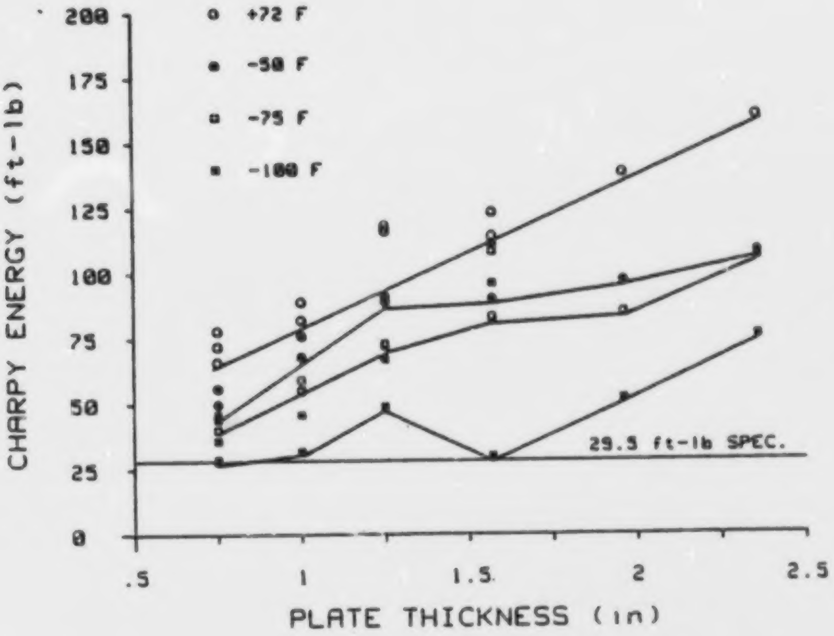

(b) Plate Mid-Thickness Position

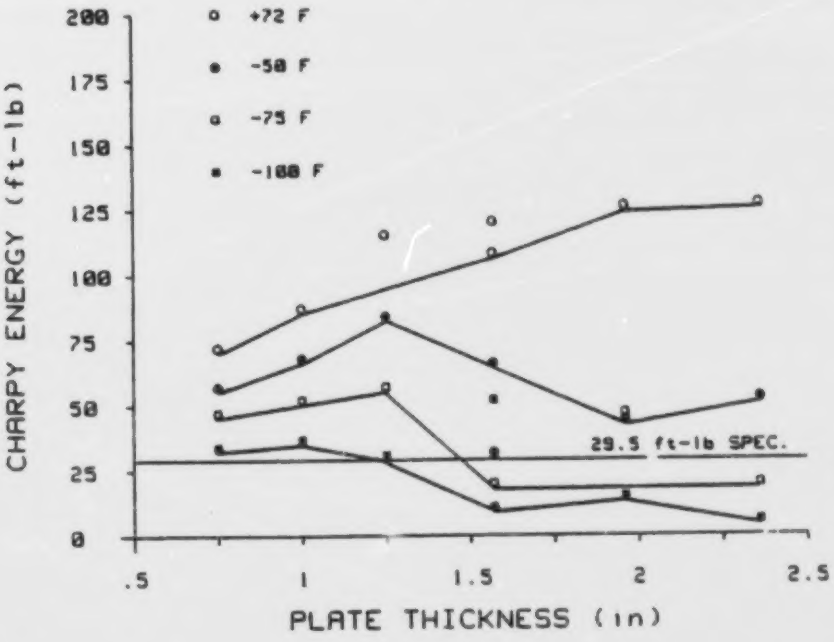

Limited tests taken from the "dirty" quarter point locations showed little difference in Charpy energy compared with the subsurface location.

The Charpy tests in the longitudinal orientation were significantly higher than the transverse tests, and the 29.5 ft-lb requirement was consistently met in all gauges at temperatures to -100°F (-73°C), Table II, Appendix III.

The Charpy energy absorption in the normalized condition was significantly higher than in the controlled rolled condition. The minimum energy requirements were easily met for both transverse and longitudinal orientations at test temperatures to -100°F (-73°C), Table II, Appendix III.

NDT temperatures for the 0.75in plates were below -100°F for both longitudinal and transverse orientations, and controlled rolled and normalized conditions. For the heavier gauges (1.0in and 1.25in) the NDT temperatures for surface notched tests were below -100°F; however, they were significantly higher (-90°F) for the subsurface tests (Table IV, Appendix III).

### iii) The Effect of Plate Thickness and Processing on Microstructure

All plates had polygonal ferrite and pearlite microstructures, with a small percentage of bainite related to the segregation band. Figure 4 shows the change in the through-thickness ferrite grain size distributions over the gauge range. Both the mean and the standard deviation in grain size of the controlled rolled plates increased significantly between plate surface and core positions and with increasing plate thickness. Whereas the mean ferrite grain size was held to less than 10 µm at the plate mid-thickness position at gauges up to 1.25in, the grain size was more than 13 µm at the same position in the heaviest plate. Representative micrographs showing the change in structure with gauge and position are shown in figure 5.

Figure 4: Through-Thickness Ferrite Grain Size Distributions for Controlled Rolled Plate

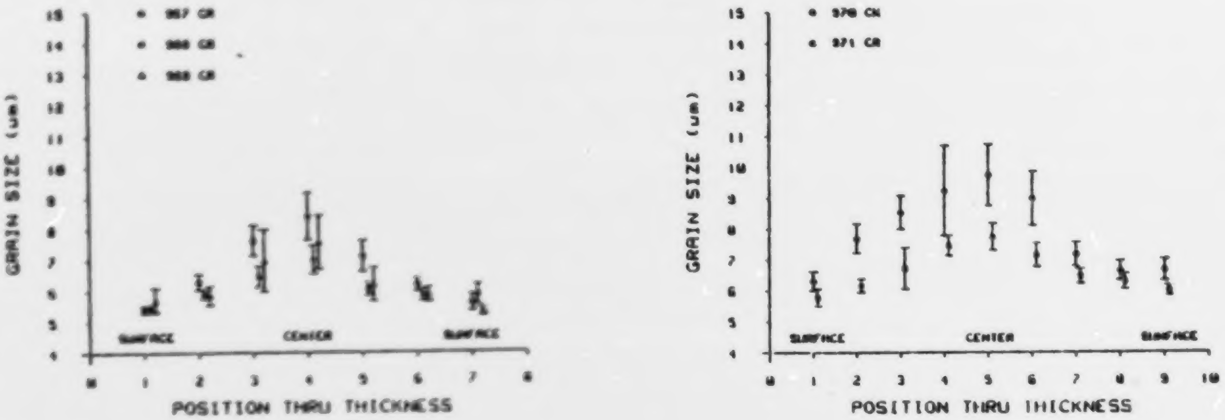

(a) 0.75in

(b) 1.0in

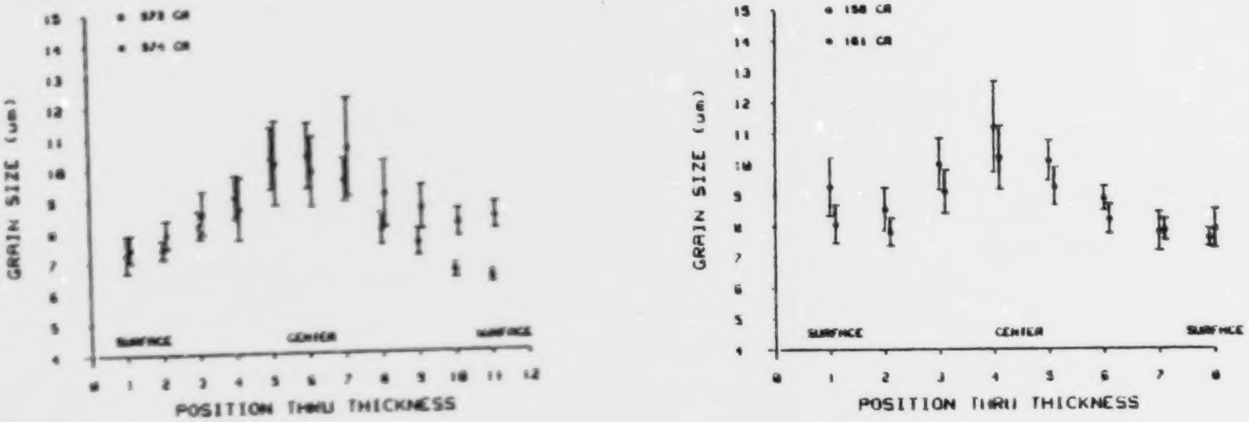

(c) 1.25in

(d) 1.57in

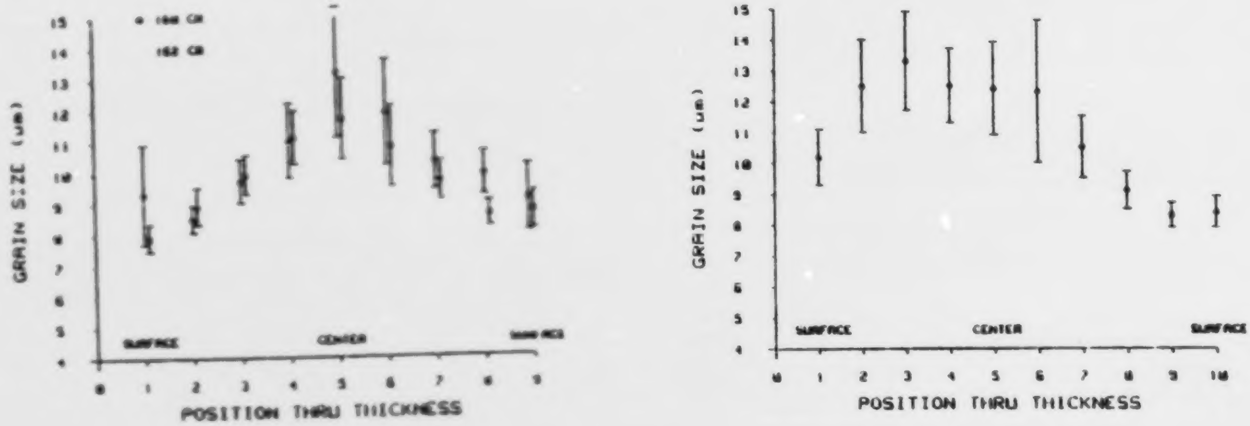

(e) 1.96in

(f) 2.36in

Figure 5: Representative Micrographs of Controlled Rolled Plate (X375)

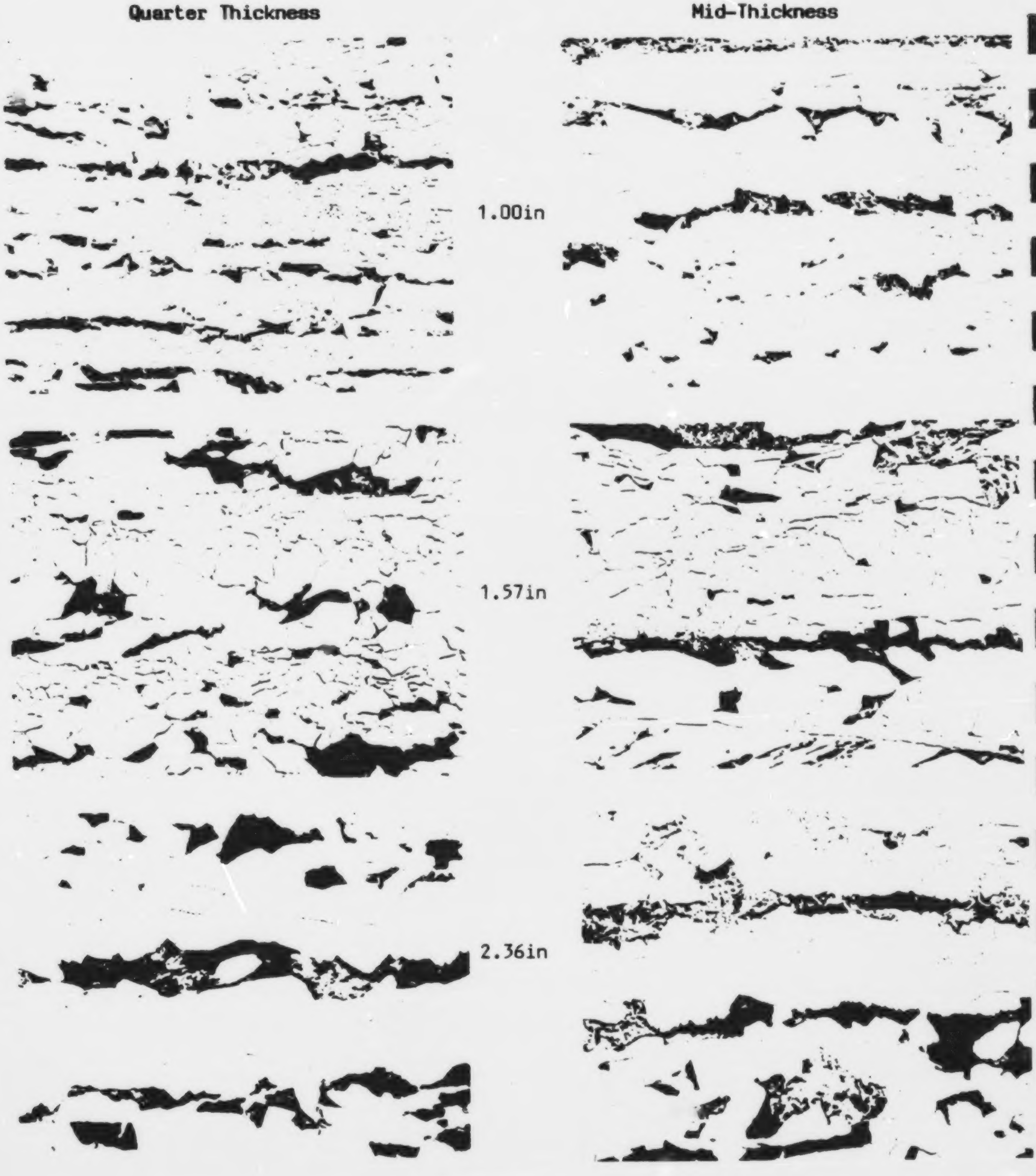
Quarter Thickness
Mid-Thickness
1.00in
1.57in
2.36in

In the normalized plate, the grain size showed little or no dependence on plate thickness (over the range 0.75in to 1.25in) but was very dependent on normalizing temperature. Reheating at 1650°F produced a very fine (≈6 μm), uniform, ferrite-pearlite microstructure throughout the plate thickness (figure 6). Increasing the normalizing temperature to 1700°F resulted in incipient abnormal grain growth (figure 7), particularly near the plate surface position, and a slight coarsening in the mean ferrite grain size. At 1800°F, there was a general coarsening in the structure to 10-12 μm.

**Figure 6: The Effect of Normalizing Temperature on Ferrite Grain Size**

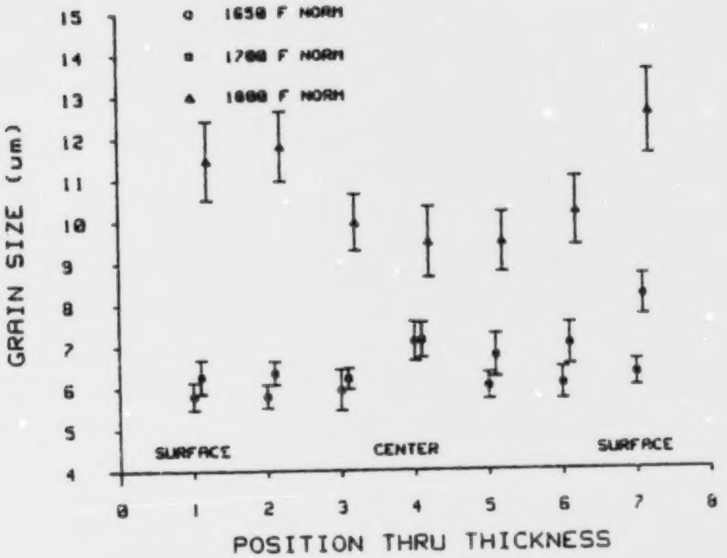

### Discussion

i) Strengthening Effects and the Design of Chemistries

These data demonstrate the ability of the Stelcoloy 70 chemistry to meet the Grade 350 strength level in the controlled rolled condition at gauges up to 2.36in. At lighter gauges, this chemistry is actually "too rich" both in microalloy (Cb, V) and alloy content (Mn, Cr, Cu, Ni), and has been modified to improve the strength-toughness combination for Arctic use.

Figure 7: Micrographs of Grain Size in Normalized Plate

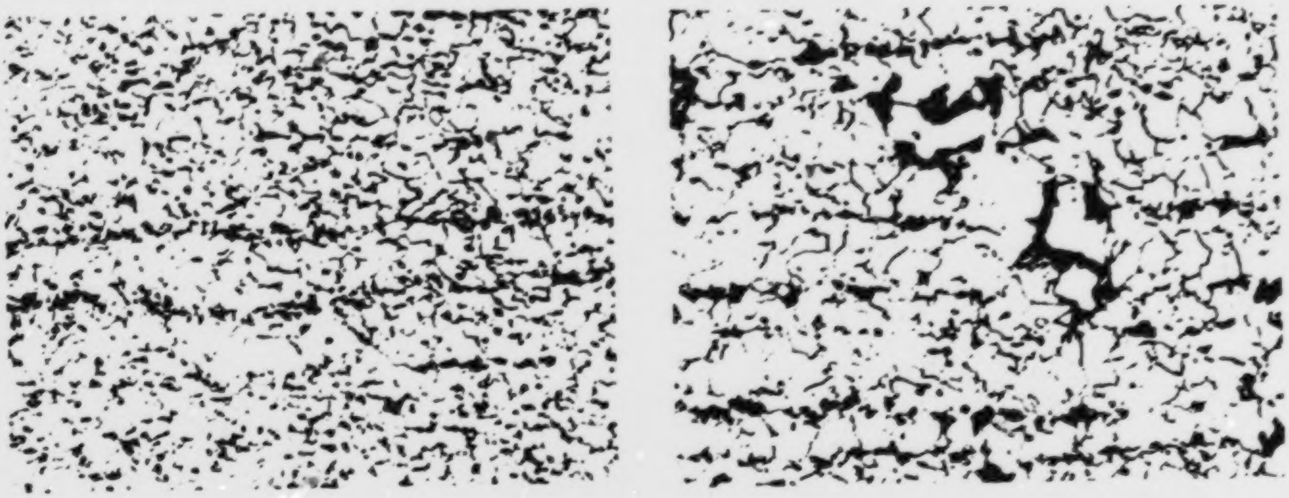

(a) 1650°F (X375)

(b) 1700°F (X375)

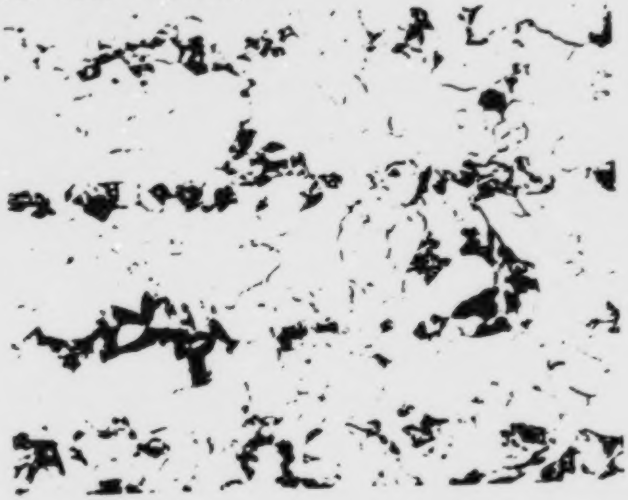

(c) 1800°F (X375)

Figure 8 shows the calculated contributions to yield strength as a function of plate gauge and demonstrates the relative effects of grain size and precipitation. It is clear that at lighter gauges (<1.50in) a significant reduction in the precipitation strengthening component is possible without jeopardizing either the yield or ultimate strength levels. Reducing precipitation strengthening is highly desirable to improve Charpy toughness (Cv FATT increases by ≈5 to 7°F per ksi increase in yield strength due to precipitation), and can be reduced by lowering the microalloy levels.

**Figure 8:** **The Effect of Gauge on Yield Strength and Contribution to Yield Strength by Different Strengthening Mechanisms**

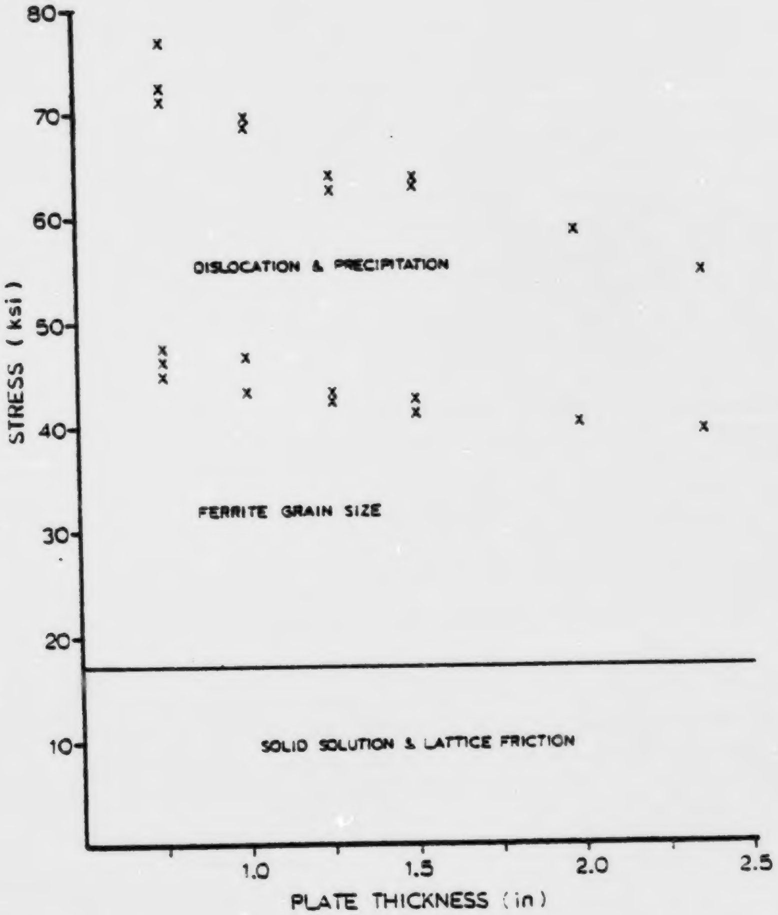

Figure 8 also demonstrates the significant loss of precipitation strengthening with increased gauge. This results from several interrelated effects including:

- increased time for precipitation of coarse microalloy carbonitrides in austenite, and
- increased time at temperature for coarsening of precipitates in ferrite.

Reduction of the microalloy content is desirable for improved HAZ toughness. Until now there has been little, if any, attention paid to the weld HAZ toughness of plate supplied to the Canadian marketplace. The specification for Arctic grade plate will require restriction on not only the total microalloy content but also the microalloys used. Although columbium is particularly effective for grain size control during controlled rolling because of its relatively low solubility in austenite (see figure 4 AI), columbium additions are being limited in modern plate grades. Several studies[7-9] have shown that columbium is particularly deleterious to HAZ crack initiation resistance in high heat input welds (> ≈2 kJ/mm). As a result, plate producers are restricting columbium levels to less than 0.02 percent for applications with HAZ toughness requirements. Some producers are making columbium-free,[10] vanadium steels to achieve this strength level in controlled rolled plates. In addition, titanium (0.01) is being used to provide HAZ grain size control and to reduce the free nitrogen content.

These concepts have been incorporated into the two experimental heats for the DSS project and recent production orders for controlled rolled Grade 350 plate (Table IV). It is important to recognize that the modification of microalloy content will have significant effects on the ferrite grain size and the degree of precipitation strengthening through their effects on reheated grain size (Ti addition), recrystallization behavior during rolling, and amount of microalloy available for precipitation in ferrite. Detailed follow-up of the rolling practices, mechanical properties and microstructures is required to fully understand the relatively complex effects of these chemistry changes on properties so that reheating and controlled rolling practices can be efficiently "optimized" for each gauge and Charpy toughness specifications.

**Table IV: Chemistries of Heats for Grade 350 Trials**

| Practice | C | Mn | S | Si | Ni | Cr | V | Cb | ASA | Ti |
|---|---|---|---|---|---|---|---|---|---|---|
| EN 142 KH5 | 0.12/0.15 | 1.30/1.45 | 0.004 Aim | 0.20/0.30 | 0.20/0.30 | - | 0.06 Aim | 0.02 Aim | 0.02/0.04 | 0.02 Max |
| DS 0608U SK | 0.06/0.08 | 1.35/1.45 | 0.005 Aim | 0.20/0.30 | 0.20/0.30 | 0.20/0.30 | 0.07 Aim | 0.02 Aim | 0.02/0.04 | 0.01 Aim |

The Stelcoloy 70 chemistry did not meet Grade 350 yield or ultimate strength levels in the normalized condition. Although a very fine-grained structure was developed by this heat treatment, there was very little precipitation strengthening. For this chemistry, the solubility product for columbium carbonitride is such that very little columbium (<0.01) is taken into solution at normalizing temperatures. Thus columbium is relatively ineffective for strengthening other than by grain refinement. Vanadium is much more soluble in austenite at normalizing temperatures, and probably was responsible for most of the observed precipitation strengthening. The UTS level in the normalized condition was particularly low because of the relatively low pearlite fraction at 0.08 percent carbon. The EN 142 chemistry has been designed with a higher carbon content to ensure meeting the strength requirements in both the as-rolled and normalized conditions.

### ii) The Effect of Orientation and Processing on Charpy Toughness

In the controlled rolled plates, there was a general deterioration in transverse Charpy toughness at low temperature with increased gauge. This loss of energy absorption is a result of complex interaction between factors which control both the absolute steel ductility (measured by Charpy shelf energy) and the ductile-to-brittle transition temperature.

The transverse Charpy shelf energy increased significantly with increased plate thickness (figure 3). This resulted largely from the significant reduction in the total inclusion length with reduced total rolling strain in the plate rolling direction (i.e. increased gauge), figure 9. The reduction in strength with increasing gauge also tended to increase ductility, whereas the slight increase in pearlite fraction with gauge tended to reduce it.

Figure 9: The Effect of Plate Gauge on Total Inclusion Length

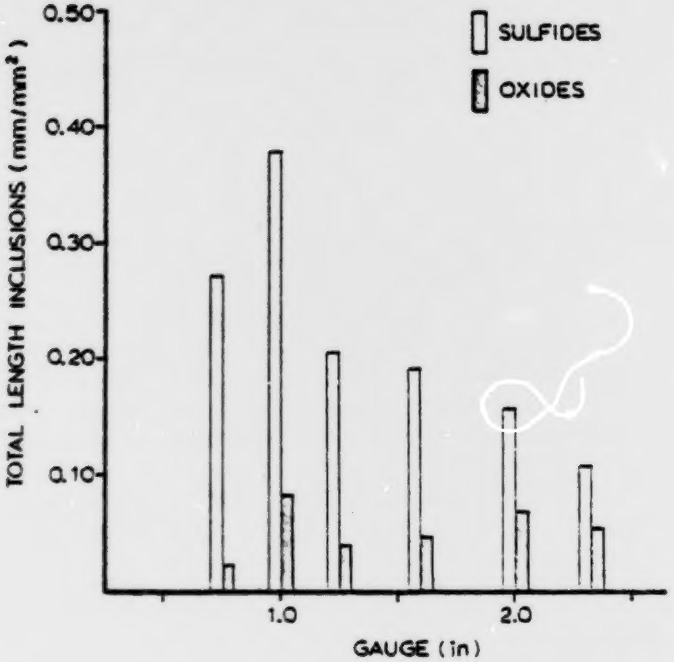

The improvement in Charpy shelf energy with increasing gauge was offset by significantly higher ductile-brittle transition temperatures, particularly at the plate mid-thickness position (figure 10). This increase in transition temperature was largely a function of increased ferrite grain size; however, other factors, including the degree of splitting, precipitation strengthening and the volume fraction of pearlite in the microstructure were also important. The reduced precipitation strengthening at heavier thicknesses tended to improve (lower) the Charpy FATT, however, the slight increase in the fraction of pearlite increased it. Estimates of the 50 percent FATT based on microstructural and strength data agree fairly well with the observed values particuarly for mid-thickness Charpy tests (Table III AIII). Subsurface Charpy tests showed much lower (≈40°F) transition temperatures than calculated. This behavior resulted from the significant degree of splitting on the subsurface Charpy tests at temperatures down to -100°F (figure 11). Little or no splitting was present in the mid-thickness Charpy tests.

Figure 10: The Effect of Gauge and Position on Ductile-Brittle Transition

(a) Mid-Thickness

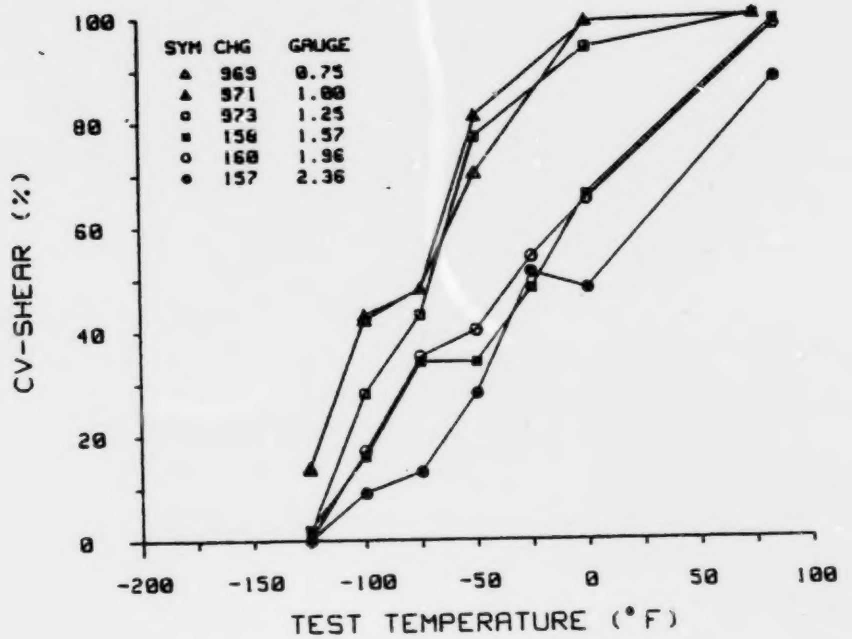

(b) Subsurface

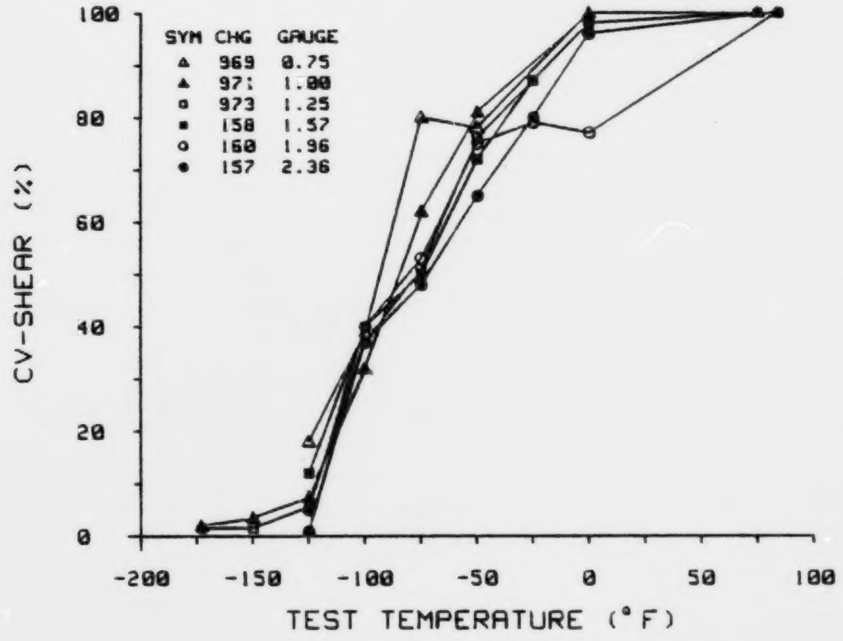

**Figure 11: Fracture Surfaces of Controlled Rolled and Normalized Charpy Tests**

(a) Controlled Rolled

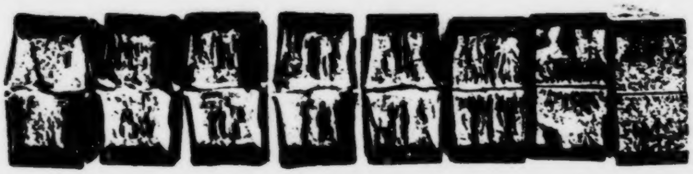

(b) Normalized

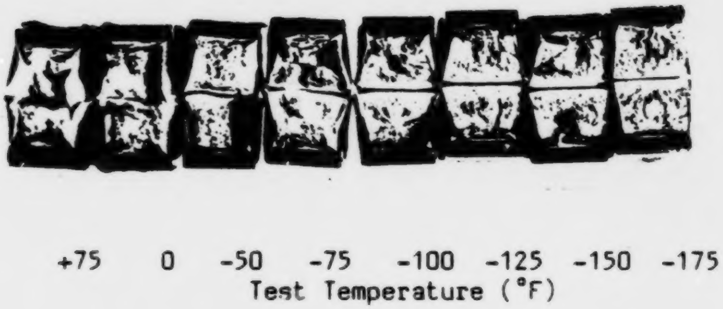

Although splitting is effective in reducing the 50 percent shear FATT and thus helps controlled rolled plate meet the nominal Charpy energy requirements at low temperatures, it is not clear that the fracture initiation resistance of controlled rolled plate is as good as normalized plate. It is notable that the fracture faces on Charpies of normalized steel, showed considerably more notch root contraction (i.e. initiation resistance) than did the controlled rolled steels with splits (figure 11). CTOD testing is required to demonstrate that controlled rolled plate has adequate fracture initiation, and this has been incorporated into the test program for the two Grade 350 heats.

The NDT tests also showed a deterioration in fracture propagation resistance in the plate core with increased thickness. This is largely attributed to increased grain size. These data suggest NDTs are adequate for the most severe applications in lighter plate (<1.0in), and that adequate toughness could be achieved in heavier plate with improved grain refinement.

The failure to meet the Charpy and NDT requirements at the mid-thickness position in heavy plate resulted primarily from a coarse ferrite grain size, plus excess precipitation strengthening. The required changes in these controlling factors can be estimated from previously defined relationships for their effects on Charpy transition temperature (see Appendix I). Figure 12 shows the effects of these variables and volume fraction pearlite on Charpy transition temperature. Based on the Charpy transition data shown in figure 10 and Table III AIII, the FATTs of the heavier plate (>1.25in) are between ≈35°F and 50°F higher than the lighter plate. To achieve this degree of improvement in FATT requires either a refinement in mean ferrite grain size from ≈12 μm to ≈8 μm, or ≈10 ksi reduction in precipitation strengthening, or a 10 percent reduction in the amount of pearlite or combinations thereof. The difference in chemistry between the Stelcoloy 70 and DSS heats should result in a reduction in precipitation strengthening, however, the pearlite fractions should be very similar (and probably higher in the HW heat). Thus, the improvement in FATT must be achieved through ferrite grain refinement, which will require a significant modification in the reheating and controlled rolling practices.

**Figure 12: The Effect of Precipitation Strengthening, Grain Size, and Percent Pearlite on FATT**

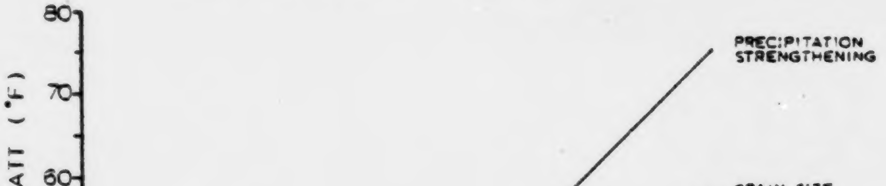

Although all plates were rolled to the same "nominal" practice in terms of percent reduction below 1650°F (Table I), there are two significant factors that resulted in coarser grain structures in the heavier plate. First, the total reduction during roughing decreased from 75 percent at 0.75in plate to only 40 percent at 1.968in and 2.36in plate. As shown in Appendix I, total reduction during high temperature rolling is a very important factor in decreasing the recrystallized grain size prior to finishing. Second, the temperature differential between surface and core increased as the slab thicknesses increases. Figure 13 gives an example of the temperature distribution through the slab/plate thicknesses of a slab rolled on the laboratory mill at CANMET. Note that the surface to core temperature differential is in excess of 180°F (100°C) in heavier gauges (>100 mm, =4in) and decreases as plate thickness is reduced. When using pyrometer measured surface temperatures for control during rolling, it is necessary to account for the surface to core temperature difference to ensure that the bulk of the bar is below the recrystallization stop temperature. As a result, the entry temperature for finishing on the trial heats has been adjusted downward with increasing gauge.

**Figure 13: Surface to Core Temperature Distribution During Plate Rolling**

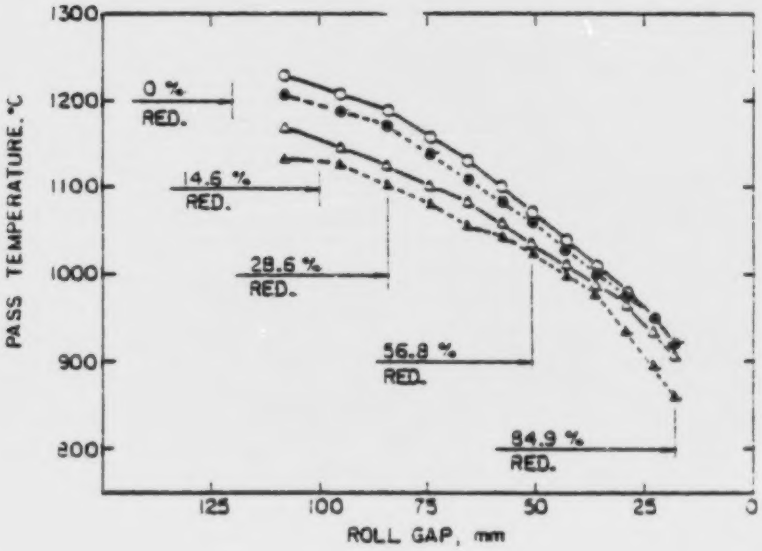

o core
Δ surface

More exact information on the temperature distribution and the effects of microalloys on the recrystallization kinetics is essential to define the surface control temperature for each gauge. We are currently working on the Lysaght strip mill computer model which incorporates a through-thickness temperature calculation. This model takes into account the effects of initial temperature profile, air and water spray cooling and rolling reduction on temperature development during rolling. We also have access to a similar, but more complete model being developed at CANMET. Calibration of these models in terms of cooling spray efficiency and temperature losses to rolls, etc, is required before they can be used with complete confidence. Initially, however, they will be used to give us a "ballpark" estimate of the corrections required to roll the two trial heats.

In addition, the LEW heat will be produced with a 0.01 percent Ti addition. This has been shown to significantly decrease the grain coarsening of strand cast slabs (see figure 5 AI). By reducing the reheated starting austenite grain size, it should be possible to achieve both a finer and more uniform ferrite grain size in heavy plate for equivalent controlled rolling practices.

Further improvement in Charpy toughness is anticipated on the trial chemistries because of improved cleanliness. This effect has been demonstrated by the improvement in transverse Charpy shelf energy with increased gauge, and also the significantly higher Charpy toughness of the longitudinal tests. The HW-CAB treated heat has been made to a lower sulfur level (0.003 percent S) and should have good sulfide shape control. Hence the anisotropy between L and T Charpy impact energy should be significantly reduced. Similarly the LEW heat has been made to a lower S level (0.003) with shrouding, which should reduce oxide inclusion content.

Overall, the strength and toughness obtained on this preliminary rolling are encouraging, however, significant improvement in the ductile-brittle transition behavior must be achieved to meet the lowest design temperature Charpy and NDT requirements in heavier plate thicknesses (i.e. over ≈1.25in). Modification of the chemistry to reduce the as-rolled strength level plus the use of a more stringent controlled rolling practice coupled with titanium addition for grain size control should significantly lower the impact transition temperatures and hopefully give adequate toughness throughout the plate thickness.

# ULTRASONIC QUALITY AND LAMELLAR TEARING RESISTANCE

Plate for Arctic use must meet ASTM A578 Level 1 ultrasonic inspection requirements. Although this level of inspection is regularly applied on pressure vessel quality steel made from ingots, we have little experience with heavy plate from LEW strand cast slabs. Ultrasonic quality has traditionally been a problem with strand cast product and the minimum reduction ratio (slab to plate thickness) required to weld up slab porosity and centerline looseness must be established for this product.

In addition to having to meet requirements for "macroscopic" soundness, a significant percentage of plate for offshore construction will need a low susceptibility to lamellar tearing in highly restrained welds. Lamellar tearing resistance is closely related to steel cleanliness, and very low total lengths of stringer sulfides and oxides can be tolerated in plate for this application. Correlations have been established between lamellar tearing and the tensile ductility measured on through-thickness tensile tests, and specifications for these applications are commonly written in terms of minimum reduction of area (RA) in a Z-direction tensile.[11] Typical requirements are between 20 and 35 percent RA depending on the level of weld joint restraint and welding procedures. Previous testing of LEW sourced plate skelp has demonstrated that this ductility will be difficult to achieve. Figure 14 shows the distribution of through-thickness values measured on several Grade 483, low sulfur (<0.006 percent) LEW heats. Low values (<10 percent reduction of area) were generally associated with quarter point stringer aluminates.

Figure 14: Through-Thickness Ductility of LEW Plate Skelp

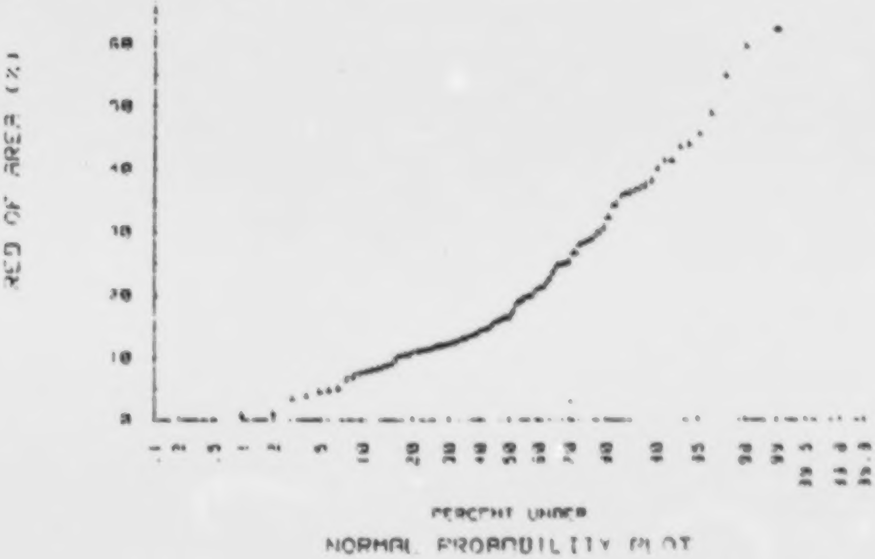

## Testing

Each slab from the first rolling was 100 percent manual ultrasonically inspected for center looseness/porosity after rolling. All plates were stack cooled from ≈700°F for hydrogen removal. The finished plates and kickover bars were ultrasonically inspected off-line using the Plate Mill Metallurgical ultrasonic procedure to detect flaking. This sensitivity is much higher than for ASTM A578 Level 1.

Coupons from each plate from both rollings were ultrasonically inspected with the R&D C-scan equipment using a sensitivity to detect a No. 3 hole (3/64in) on a calibration block. After C-scanning, through-thickness tensile tests were taken from both clean and defective areas. Through-thickness tensiles were made to both the designs recommended in ISO Draft Standard 7778 (5 mm and 6 mm diameter) and the 0.375in diameter sample that has been normally used at Stelco since 1975.

Metallographic samples were sectioned from areas showing ultrasonic indications on selected plates, and inclusions were analyzed using EDAX (Energy Dispersive Analysis of X-Rays). Similarly, the fracture surfaces of selected through-thickness samples were examined using the scanning electron microscope (SEM) to determine the cause of failure, and to analyze failure-related inclusions with the EDAX.

## Results

Four of the slabs inspected showed significant ultrasonic defects (figure 15). Two of these were finish rolled to 1.25in plate, whereas the others were only partially rolled and were kicked over at ≈4in and 3.25in.

Figure 15: Ultrasonic Indications on Slabs

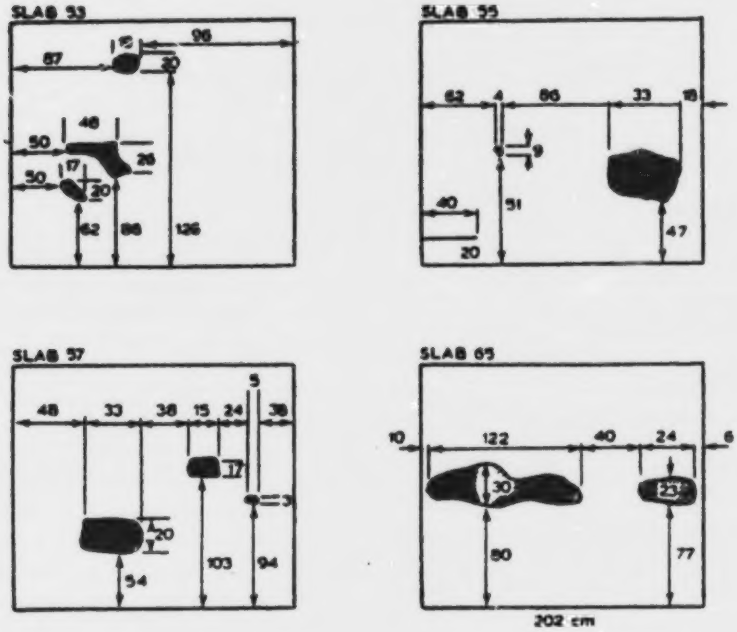
SLAB 53
15
96
87
20
48
50
26
17
50
20
62
86
126
SLAB 55
62
4
86
33
18
9
40
51
20
47
SLAB 57
5
48
33
38
15
24
38
17
3
20
103
94
54
SLAB 65
10
122
40
24
6
30
23
80
77
202 cm

None of the finished plates from either rolling (in gauges up to 2.36in) showed gross ultrasonic indications which would be cause for rejection by ASTM A578 Level 1 inspection. Several plates showed concentrations of small defects which were classified as either inclusions or flaking. One of the kickover bars showed large areas of "center looseness" which generally corresponded to the center looseness observed in the original slabs (figure 16). Metallographic observations confirmed these plate indications to be unwelded regions on the plate centerline.

Figure 16: Pattern of Ultrasonic Indications on Kickover Bar

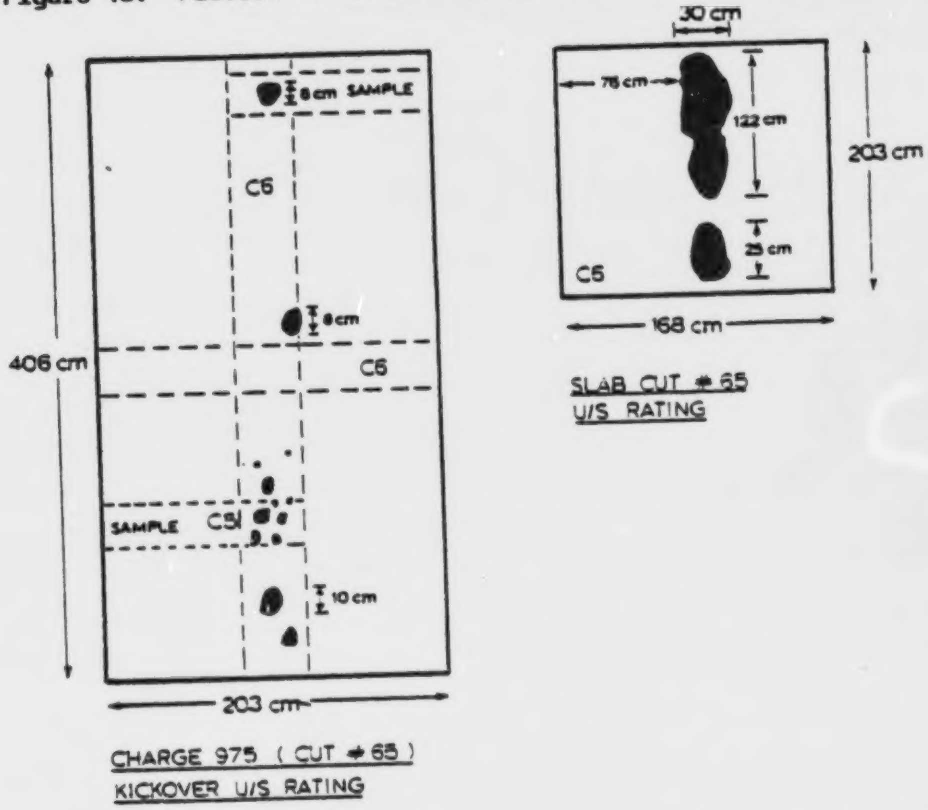

CHARGE 975 ( CUT # 65 )
KICKOVER U/S RATING

SLAB CUT # 65
U/S RATING

All plates showed a relatively high density of ultrasonic indications in laboratory C-scan tests. Figure 17 shows a typical example at 1.25in. The ultrasonic sensitivity was set to detect a No. 3 flat bottomed hole (i.e. 3/64in defect) at thicknesses between 0.75in and 1.50in; however, because of broadening of the U-sonic beam from the transducer and the irregular surface of the reflectors, there was significant magnification (≈2X) of defects particularly in the width direction. Most indications were positioned approximately quarter way through the plate thickness; a few indications were found on the plate centerline. Metallographic sections through both types of indications revealed them to be heavy oxide stringers. These were analyzed as primarily aluminum (≈70 percent) and calcium (≈20 percent) with traces of silicon, iron and sodium (figure 18). This composition suggests that they originated primarily from reoxidation of ladle and tundish slag; however, a much more detailed follow-up of inclusion formation during steelmaking, teeming and casting is required to pin down their origin. Simple calculations of stringer volumes show that they originate as ≈500-1000 μm diameter clusters in the cast slab.

Figure 17: Ultrasonic Indications on Laboratory C-Scan - Charge 974, 1.25in (Actual Size)

Figure 18: Alumina Stringers in Rolled Plate

(a) X50

(b) X200

The through-thickness tensile results showed a very strong dependence on sample position (figure 19). Tests taken from clean areas gave much higher ductilities than samples taken at defects. Test from clean areas achieved a minimum of 24.3 percent reduction in area over the gauge range tested. Tests at "dirty" areas showed considerable variability in ductility because of the inability to exactly position the defect area in the through-thickness samples. Minimum values ranged from ≈22 percent on the 0.75in plate to less than 10 percent on the 1.25in plate.

**Figure 19: The Effect of Gauge and Sample Position on Reduction of Area**

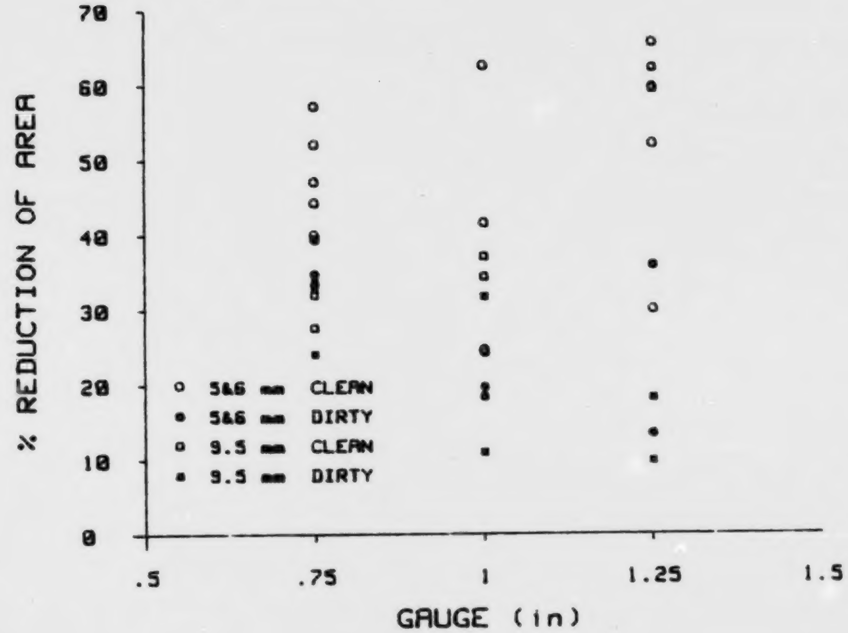

Fractography on the broken tensiles revealed that the failures in the "clean" samples were primarily related to manganese sulfide stringers. Some surfaces also showed planes of alumina and niobium oxides inclusions (figure 20). The surfaces of "dirty" tests exhibited large flat lozenge-shaped areas of broken aluminate inclusions (figure 21). No tests showed hydrogen flaking.

Figure 20: Inclusions on Through-Thickness Tensile Fracture Surfaces

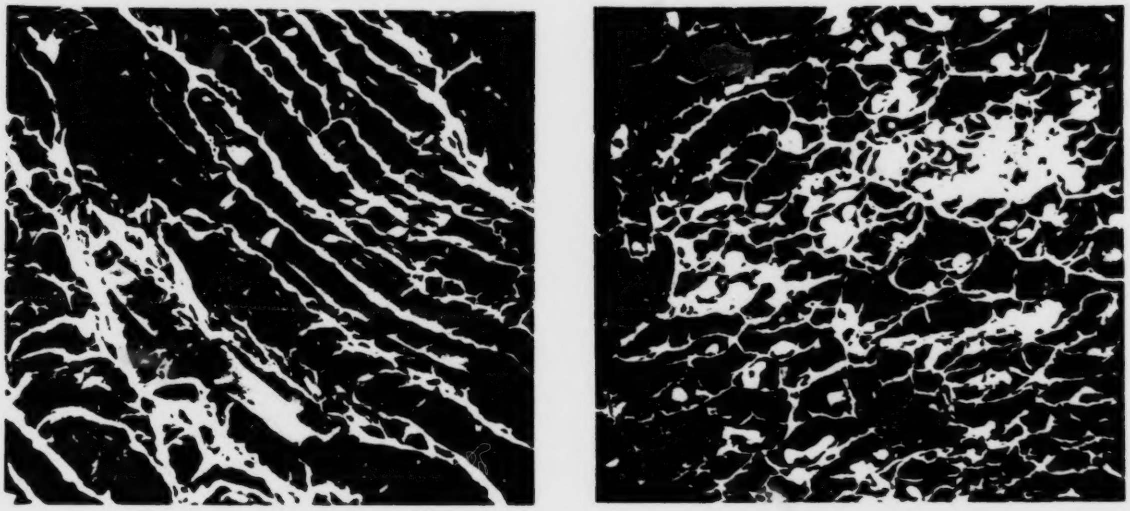

(a) Manganese Sulfide (X1000)

(b) Alumina (X1000)

(c) Niobium Oxide (X2000)

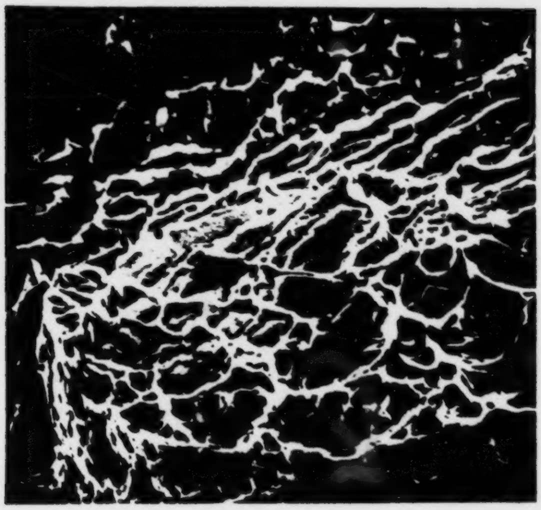

Figure 21: Gross Alumina Stringer on Through-Thickness Fracture Surface

(a) X8

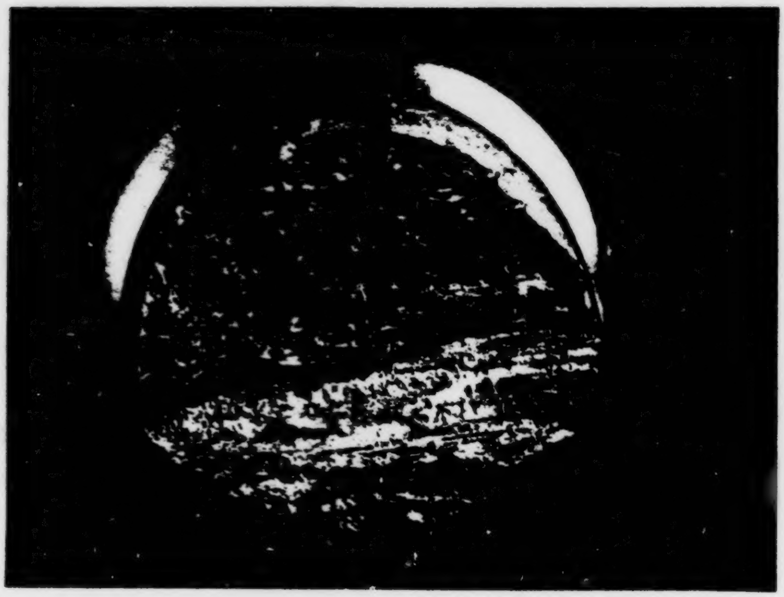

(b) X90

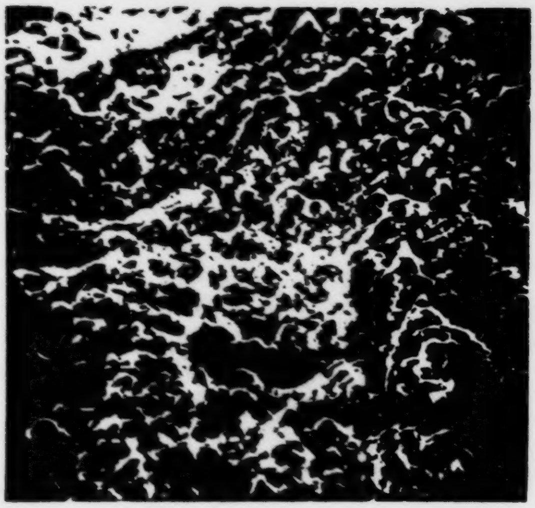

## Discussion

The plate ultrasonic tests show that the ASTM A578 Level 1 requirement can be readily met in LEW strand cast plate, and that the relatively high levels of quarter point oxide inclusions are not sufficient to cause ultrasonic rejection. Further detailed ultrasonic testing of the LEW trial heat will be done to corroborate these data.

The limited tests on slabs showing center looseness rolled to 1.25 thick plate demonstrate that a 7.5 to 1 reduction ratio can completely eliminate centerline porosity. The fact that no defects were observed in the heavier plates is encouraging; however, without information on the slab porosity prior to rolling, we cannot conclude that the minimum reduction used (4:1) is adequate for future LEW production. The unwelded zones found in the ≈4.00in thick kickover bar demonstrate that a 2.5:1 reduction is not sufficient to weld center looseness. The rolling of the LEW trial heat will provide more exact information on the critical reduction ratio required to eliminate porosity. Prior to rolling, all slabs will be ultrasonically mapped for center looseness and rolled to give a total reduction between 4:1 and 10:1.

The minimum reduction to weld up center porosity is not only dependent on the slab quality (i.e. size of porosity) but also the plate mill drafting practice. Japanese[12] work on the elimination of porosity during rolling has shown that increasing the individual pass reduction is very beneficial for welding defects. Table V gives the calculated total reduction requirements to remove different sizes of defects in 0.75in to 1.50in plate using both light and heavy reductions per pass. These calculations suggest that increasing the drafting from 5 percent up to 10 percent reduction per pass will significantly increase the plate thickness that can be applied. Unfortunately, individual pass reductions are very limited on the 148in mill 2-high rougher. Consequently, application of strand cast slabs may be limited at Stelco to lighter gauges than provided by offshore producers. Applying strand cast slabs to controlled rolled, rather than normalized product will tend to reduce the maximum thickness of plate than can be applied because of the lighter drafts used during controlled rolling. Obviously, minimization of center looseness through good casting procedures and rolling from the heaviest slabs consistent with the gauge and pattern sizes will also help increase the maximum permissible thickness.

**Table V: Effect of Light, Medium, and Heavy Drafting on Annihiliation of Porosity in Different Plate Gauges**

| Drafting Practice % Reduction per Pass | No. of Passes | | Final Plate Gauge (in) | wo = 10in, do = 0.125in | | | wo = 10in, do = 0.250in | | | wo = 10in, do = 0.500in | | |
|---|---|---|---|---|---|---|---|---|---|---|---|---|
| | 2-Hi | 4-Hi | | Shape Factor (1) | Reduction Factor (2) | Porosity Annihilated ? | Shape Factor (1) | Reduction Factor (2) | Porosity Annihilated ? | Shape Factor (1) | Reduction Factor (2) | Porosity Annihilated ? |
| 5 | 23 | 27 | 0.75 | 0.0582 | 0.0096 | yes | 0.0582 | 0.0192 | yes | 0.0582 | 0.0385 | yes |
| | 17 | 27 | 1.00 | -0.0051 | 0.0131 | no | -0.0051 | 0.0262 | no | -0.0051 | 0.0523 | no |
| | 13 | 27 | 1.25 | -0.0388 | 0.0160 | no | -0.0388 | 0.0321 | no | -0.0388 | 0.0643 | no |
| | 9 | 27 | 1.50 | -0.0663 | 0.0197 | no | -0.0663 | 0.0394 | no | -0.0663 | 0.0789 | no |
| 10 | 12 | 13 | 0.75 | 0.1565 | 0.0089 | yes | 0.1565 | 0.0179 | yes | 0.1565 | 0.0359 | yes |
| | 9 | 13 | 1.00 | 0.0990 | 0.0123 | yes | 0.0990 | 0.0246 | yes | 0.0990 | 0.0492 | yes |
| | 7 | 13 | 1.25 | 0.6770 | 0.0152 | yes | 0.0677 | 0.0304 | yes | 0.0677 | 0.0608 | yes |
| | 5 | 13 | 1.50 | 0.0413 | 0.0188 | yes | 0.0413 | 0.0375 | yes | 0.0413 | 0.0750 | no |
| 15 | 8 | 8 | 0.75 | 0.1682 | 0.0093 | yes | 0.1682 | 0.0186 | yes | 0.1682 | 0.0371 | yes |
| | 6 | 8 | 1.00 | 0.1157 | 0.0128 | yes | 0.1157 | 0.0257 | yes | 0.1157 | 0.0514 | yes |
| | 5 | 8 | 1.25 | 0.0938 | 0.0151 | yes | 0.0938 | 0.0362 | yes | 0.0938 | 0.0605 | yes |
| | 4 | 8 | 1.50 | 0.0745 | 0.0178 | yes | 0.0745 | 0.0356 | yes | 0.0745 | 0.0711 | yes |

wo = length of pore
do = thickness of pore

(1) Shape Factor $= \sum_{j=1}^{k} W_o \left(-0.051 + 0.069\, m_j + 0.013\, m_j^2\right) H_K/H_j$

where: $W_o$ = initial pore width

$H_k$ = final plate thickness

$m_j = 2\sqrt{R}\,(H_{j-1} - H_j)/(H_{j-1} + H_j)$

R = roll radius

(2) Reduction Factor $= d_o \dfrac{H_k}{H_o}$

where: do = original pore thickness

$H_o$ = initial slab thickness

The through-thickness tensile data demonstrate that relatively good lamellar tearing resistance can be achieved in desulfurized, strand cast steel provided the levels of alumina stringer inclusions are minimized. A slight reduction of both the sulfur content and the strength levels should further improve the ductility in the "clean" areas; however a significant reduction of the alumina levels is necessary to meet current through-thickness specifications. This heat was not cast with ladle to tundish shrouding and it is anticipated that the shrouded trial heat will have less oxides. Some improvement in oxide levels has been reported on shrouded LEW heats made for D&I cans.[13] In addition modification of the casting practice is being considered to reduce the alumina levels. Currently, R&D is using water modeling to study the effect of submerged nozzle design on flow patterns and inclusion removal in the mold. Also, Japanese data[14] shows that the number of gross aluminates are very dependent on the vertical length of the strand as it affects flotation time in the mold (figure 22). A reduction of casting speed at LEW by using twin strand operations could also provide a significant improvement in cleanliness.

**Figure 22: Effect of Vertical Length on Relative Number Fraction of Inclusions Entrapped in CC Slab**

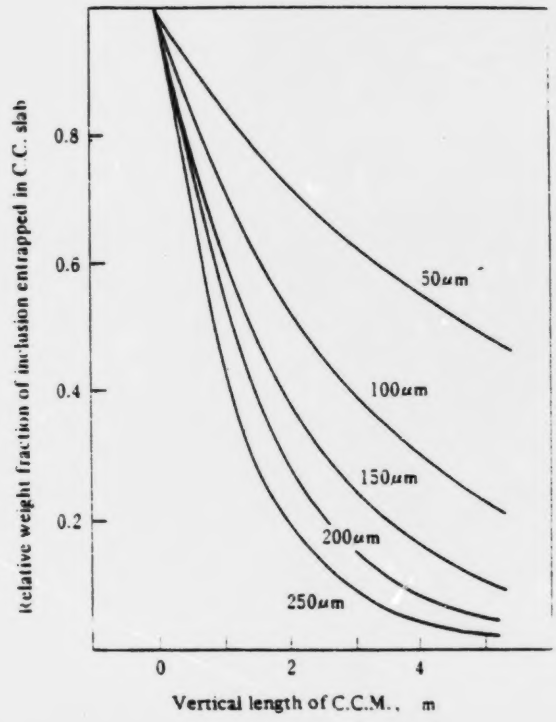

* inclusion diameter

Lamellar tearing resistant plate is most often supplied on the basis of a guaranteed minimum reduction of area; however, it has been suggested that the present standards are too conservative.[15] In steels where the through-thickness ductility is controlled by sulfide inclusions, it has been shown that improving the through-thickness ductility by reducing sulfur results in improved lamellar tearing resistance both by reducing the sites for cracking and by increasing the distance between inclusions for stepwise cracking. Isolated stringer oxide inclusions also significantly reduce the z-direction ductility; however, because of the much greater spacing between them it is not clear that they will contribute to lamellar tearing in real weldments. Full scale, high restraint welds are required on plate from the trial heats to fully assess the significance of these defects.

Finally, there is some question about the proper design of through-thickness test samples for measuring reduction of area. Recent work at ARMCO[16] and US Steel[17] has shown that, provided the specimen length-to-diameter ratio exceeds 2.0 to 2.5, there is little effect of specimen geometry on measured ductility. Lower length-to-diameter ratios tend to promote plane strain deformation with a resultant decrease in reduction of area. For the specimen designs used in this trial, only minor differences in reduction of areas were observed. These are thought to originate from sampling variability. Tests on future trial heats will be made primarily with the preferred ISO sample design.

# ACKNOWLEDGMENTS

The following people and departments are recognized as having made vital contributions to this study:

B. Armitage, W. Krestynski, J. G. Matich, R. Millsop, B. C. Branston, H. Meilach, J. H. Rennie and Machine Shop personnel, all of R&D, and the Metallurgical and Operating Departments.

## REFERENCES

1. Chinook Fuel Innovation Ltd, Survey of Requirements for Plate Steel in Offshore Structures and Arctic Vessels, May, 1982.

2. Fenco Consultants Ltd, A Review of Steel Properties at Low Temperatures, December, 1980.

3. Det Norske Veritas, Review of Steels Used in the Construction of Offshore Structures, April, 1982.

4. R&D Report No. 820018.

5. D. B. McCutcheon's Letter, Arctic Grade 350 Structural Plate - DSS Funded Research, May 3, 1983.

6. D. B. McCutcheon's Letter, Grade 350 Structural Plate - Controlled Rolling Trials, February 7, 1983.

7. W. E. Hannerz, Welding Journal Research Supplement, May, 1975, p 162.

8. R. E. Dolby, The Welding Institute Research Bulletin, September, 1977, p 250.

9. E. G. Signes and J. C. Baker, Effect of Nb and V on the Weldability of HSLA Steels, AWS 60th Annual Meeting, Detroit, April, 1979.

10. D. B. McCutcheon's "Arctic Grade 350 Structural Plate - Recent Japanese Technology", March 28, 1983.

11. J. Sommella, "Significance and Control of Lamellar Tearing of Steel Plate in the Shipbuilding Industry", Ship Structure Committee, May, 1979.

12. N. Okumura et al, "Hot Rolling Conditions for Annihilation of Porosity in Continuous Cast Slabs", Paper Presented at International Conference on Steel Rolling, Tokyo, Japan, October, 1980, p 217.

13. D. J. Harris' Letter, "Improved Slab Quality LEW - Ceramic Shrouding Trials - Inclusion Assessment", March 16, 1983.

14. NKK Technical Bulletin, "Production of Super Clean Steel by Slab Continuous Casting Process.

15. J. C. M. Farrar, J. Gisson, R. E. Dolby, The Use of Small Scale Destructive Tests to Assess Lamellar Tearing Susceptibility, The Welding of Offshore Construction, Newcastle, February, 1974.

16. R. J. Jesseman, G. J. Murphy, Proceedings of Conference, "Through Thickness Tension Testing of Steel" ASTM STP 794, p 87.

17. D. C. Ludwigson, IBID, p 40.

# APPENDIX I

## METALLURGY OF CONTROLLED ROLLING OF HEAVY PLATE

### The Effect of Grain Size on Mechanical Properties

Ferrite grain size is the principal microstructural feature that must be controlled to achieve the combination of relatively high strength and low temperature fracture toughness demanded for Arctic grade structural plate. The interrelationship between microstructural features and composition, and strength and toughness have been well defined. Figure 1 AI shows the effects of compositional and microstructural factors on strength and toughness. The equation developed by Irvine et al for silicon (2) killed steels show the dependence of both yield strength and 50 percent shear fracture appearance transition temperature (FATT) on the inverse square root of the ferrite grain size.

$$\text{Yield stress (MPa)} = 15.4\left[3.5 + 2.1\,(\%\,\text{Mn}) + 5.4\,(\%\,\text{Si}) + 23\,(\%\,\text{Nf}) + 1.13\,d^{-1/2}\right] \qquad (1)$$

$$\text{I TT } (^\circ\text{C}) = -19 + 44\,(\%\,\text{Si}) + 700\,\sqrt{\text{Nf}} + 2.2\%\ \text{Pearlite} - 11.5d^{-1/2} \qquad (2)$$

Figure 1 AI: Factors Affecting Yield Strength and Impact Transition Temperature (1) (Vectors show °C Increase in Cv FATT per 15 MPa Increase inStrength)

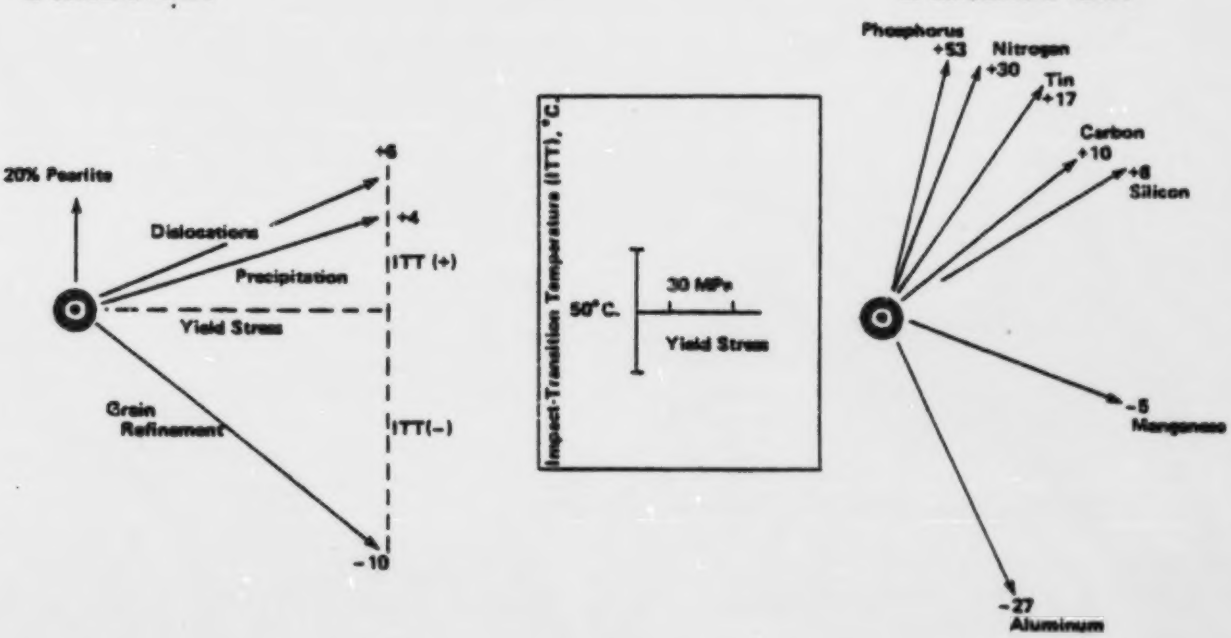
a. Structural Factors
20% Pearlite
Dislocations
Precipitation
Yield Stress
Grain Refinement
+6
+4
ITT (+)
ITT(-)
-10
Impact-Transition Temperature (ITT), °C.
50°C.
30 MPa
Yield Stress
b. Compositional Factors
Phosphorus
+53
Nitrogen
+30
Tin
+17
Carbon
+10
+8
Silicon
-5
Manganese
-27
Aluminum

Grain refinement is the only strengthening mechanism that will also improve impact toughness. Other factors that need to be considered in the design of these steels include:

- percent pearlite - increasing the pearlite fraction significantly increases FATT. Thus low carbon content steels offer significantly better toughness; however low carbon steels may give poor properties if the formation of carbides at grain boundaries is not suppressed by adding manganese.[3] Note that the ferrite grain size is slightly reduced with increasing pearlite fraction, however, its overall effect on toughness is negative.

- free nitrogen has a very detrimental effect on toughness, however in aluminum killed, microalloyed steels the amount of free nitrogen is negligible. The effect of total nitrogen on properties is complex - it may improve toughness by reducing the solubility of nitride precipitates in austenite thus promoting grain size control during reheating and retarding recrystallization during rolling. However, strengthening of ferrite by precipitates (nitrides, carbonitrides) significantly increases FATT (by ≈5 to 7°F/ksi increase in yield strength). The effect of nitrogen must be rationalized in terms of the solubility products of the microalloys in the steel.

- manganese additions can have a beneficial effect on toughness because of its effect of reducing the ferrite transformation temperature, thus promoting a finer ferrite grain size (note this effect is common to all elements which are austenite stabilizers and lower the $Ar_3$ temperature). Excessive manganese additions may, however, cause a dramatic increase in FATT related to the formation of bainitic microstructures. The level of manganese at which embrittlement occurs is very dependent upon the levels of other alloys and carbon, and the austenite processing.

- dislocation strengthening, resulting from controlled rolling at finishing temperatures below the $Ar_3$, significantly increases in yield strength but, like precipitation strengthening remarkably increases the FATT.

The other key factor that must be controlled to achieve high energy absorption at low temperatures is the steel cleanliness.

For any given percent shear value, the energy level at temperature is proportional to its shelf energy. The shelf energy is largely dependent on:

- the total length of oxide and sulfide inclusions in the fracture direction. Sulfide inclusion length can be significantly reduced simply by desulfurization, however additional improvement can be achieved with sulfide shape control elements. Oxide inclusions are generally less deleterious to toughness than sulfide inclusions in aluminum killed steels; however, oxide inclusions become increasingly important in low sulfur steels, particularly if complex stringer type oxides are formed as a result of adding desulfurization or sulfide shape control elements.

- strength level - the Charpy shelf energy generally decreases at higher strength levels. There are several factors which may contribute to the reduced ductility including:

    - a significant increase in the volume fraction of "carbide" phases (pearlite, bainite, retained austenite martensite) which act like inclusions as void initiation sites, and

    - the reduction in the plastic zone size during fracture, which relates to the reduction in strain required for void nucleation growth coalescence at higher flow stress levels.

## Development of Fine Ferrite Grain Size

The ferrite grain size (and the scale of other microstructural components) is largely controlled by the density of nucleation sites in the austenite prior to transformation. These in turn are directly related to the austenite grain boundary area and the density of other nucleation sites (e.g. deformation bands, sub-micron sized particles). The other major factor controlling the final grain size is the nucleation frequency, which varies considerably depending on the type of site.

Metallographic correlation between austenite grain size and transformed ferrite grain sizes show that the ferrite grain size is just less than one-half the austenite grain from which it is transforming (figure 2 AI). Thus, to achieve a 10 μm transformed ferrite grain size, the austenite grain size must be refined to 20 μm. This simplified correlation gives a first approximation for the austenite grain size that must be achieved in either normalized or controlled rolled steel; however, more detailed experimentation has shown that the transformation characteristics of controlled steels are significantly different than in normalized steels, and thus other factors must be included to rationalize the ferrite grain size developed in these products.

**Figure 2 AI:** **The Relationship between the Austenite and Ferrite Grain Size**[4]

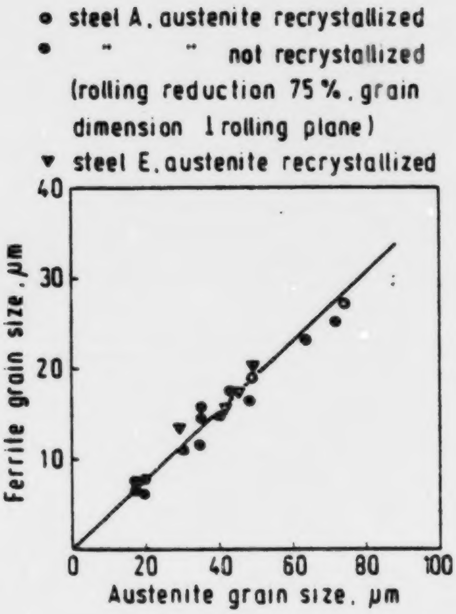

In normalized steels, transformation occurs from equiaxed, recrystallized austenite and the effective interfacial area for transformation is simply related to the equiaxed grain boundary diameter.[5]

$$S_{v,gb} = 2N_L = 2/D\gamma$$

where: $S_{v,gb}$ = interfacial area of grain boundary ($mm^2/mm^3$)
$N_L$ = intercept numbers per unit length (in any direction for equiaxed $\gamma$)
$D\gamma$ = austenitic grain diameter

In controlled rolled austenite, transformation occurs from cold-worked, unrecrystallized austenite in which the austenite grains are severely elongated and contain deformation bands. For this case:

$$S_V = S_{V.gb} + S_{V.db}$$

$$= 0.429\ (N_L)_{11} + 1.571\ (N_L)_1 + \rho/\sin\theta$$

where: $N_{L11}$, $N_{L1}$ = intercept numbers per unit length along the rolling and thickness direction
$\rho$ = density of deformation bands ($mm/mm^2$)
$\theta$ = angle between the deformation band and the thickness of the plate

The ferrite grain size achieved from deformed austenite is significantly finer than that developed from equiaxed austenite of the same size.[6] This results from the dramatic increase in the area nucleation frequency of deformed austenite. In normalized steels, the grain surfaces are not particularly favorable sites for transformation and nucleation of ferrite occurs mainly at grain edges or corners. In deformed austenite, the grain boundaries contain locally sharp curvature or bulges, formed by strain-induced grain boundary migration. These are very effective nucleation sites. Ferrite can also nucleate on subgrain boundaries close to main grain boundaries.

The initial transformation temperature ($Ar_3$) of controlled rolled Cb steels is significantly higher than in normalized steels, which results from the high ferrite nucleation rate at deformed austenite grain boundaries. However, once the favorable nucleation sites are depleted, the nucleation rate drops off drastically, because the density of intergranular sites is low. Hence, the ferrite structure from controlled rolled austenite tends to be mixed, with relatively fine ferrite grains occurring at deformed austenite boundaries and much coarser ferrite nucleated in the interior of the deformed austenite (figure 3 AI). The variation in grain size can be reduced by refining the recrystallized austenite grain size prior to finish rolling, increasing the reduction below the recrystallization stop temperature, or by increasing the cooling rate during deformation which promotes intragranular nucleation.

Figure 3 AI: Schematic Diagram of Ferrite-Transformation Types from Hot Rolled Steel[7]

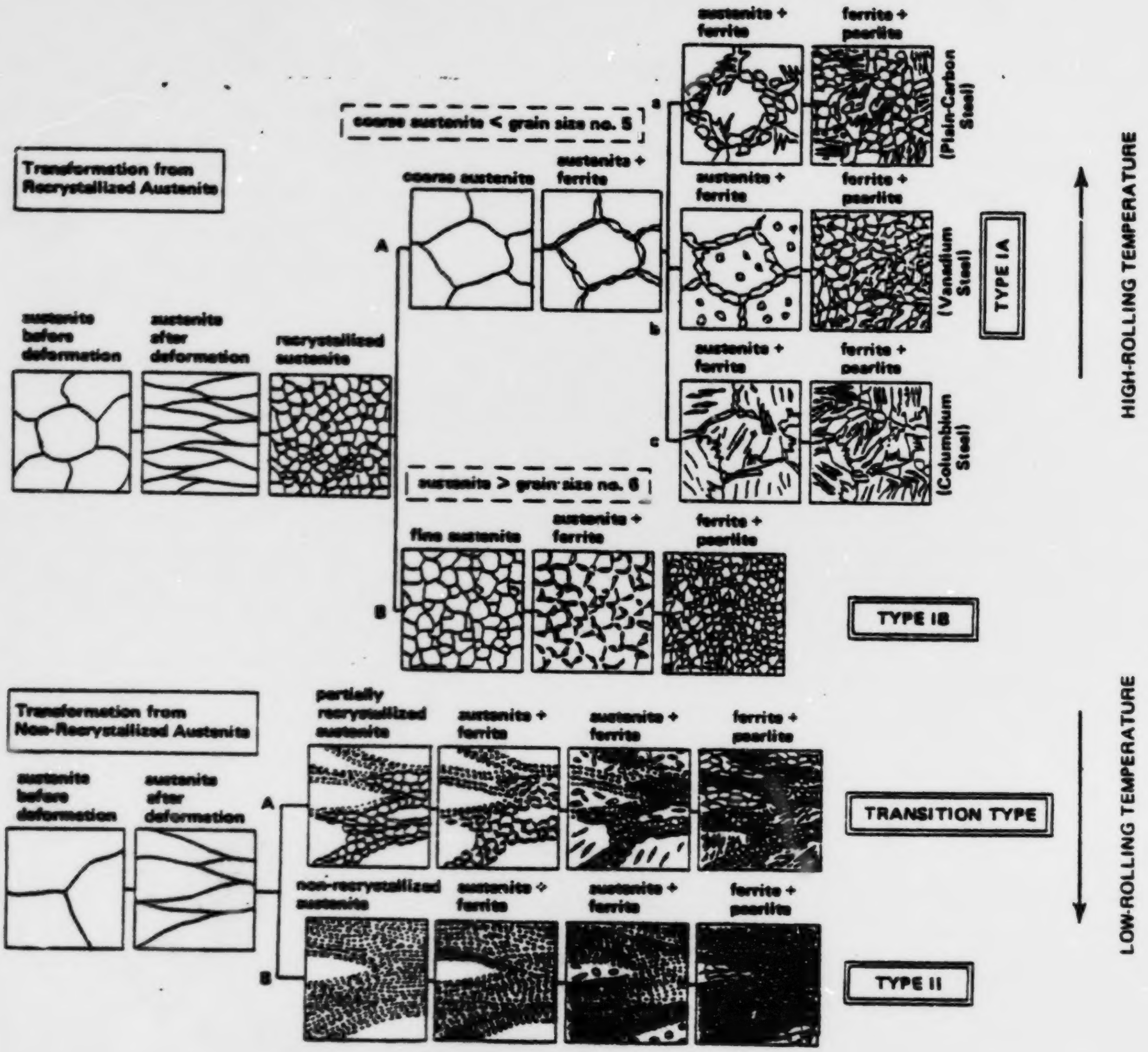

Transformation from Recrystallized Austenite
austenite before deformation
austenite after deformation
recrystallized austenite
coarse austenite < grain size no. 5
A
coarse austenite
austenite + ferrite
a
austenite + ferrite
ferrite + pearlite
(Plain-Carbon Steel)
b
austenite + ferrite
ferrite + pearlite
(Vanadium Steel)
TYPE IA
c
austenite + ferrite
ferrite + pearlite
(Columbium Steel)
austenite > grain size no. 6
B
fine austenite
austenite + ferrite
ferrite + pearlite
TYPE IB
HIGH-ROLLING TEMPERATURE
Transformation from Non-Recrystallized Austenite
austenite before deformation
austenite after deformation
A
partially recrystallized austenite
austenite + ferrite
austenite + ferrite
ferrite + pearlite
TRANSITION TYPE
B
non-recrystallized austenite
austenite + ferrite
austenite + ferrite
ferrite + pearlite
TYPE II
LOW-ROLLING TEMPERATURE

## Austenite Grain Refinement

The austenite grain size prior to the controlled rolling finishing stage is dependent upon the steel composition, the reheating condition, and the reduction sequence during roughing.

### i) Reheating Grain Size Control

The initial austenite grain size at the reheat temperature can be controlled by the addition of stable second phase particles which have the ability to restrict grain boundary movement. The key factor is a sufficient volume fraction of relatively fine particles to block coarsening. The model[7] for grain boundary motion shows that the critical particle size and volume fraction are related to the grain radius as follows:

$$r_c = \frac{6Rf}{\pi} \quad {\frac{3}{2} - \frac{2}{Z}}^{-1}$$

where: $r_c$ = critical particle radius
$f$ = volume fraction
$Z$ = grain heterogeneity factor (between 1.5 and 3.0)
$R$ = grain radius

This analysis is complicated by particle coarsening during heating and holding at temperature, resulting from Ostwald ripening.

The main practical problem to achieve grain control at conventional reheat temperatures, is that all of the commonly used microalloys (Cb, V, Al) are almost completely in solution in steels with normal levels of microalloys and interstitials (C,N). Figure 4 AI shows the solubility product data for these microalloys at typical reheat temperatures: only columbium nitride, has a low enough solubility to offer some grain size control at these temperatures. However, the columbium levels required may be prohibitive in terms of other properties (e.g. HAZ toughness). By lowering reheating temperatures, sufficient microalloy precipitates can be retained out of solution to restrict the starting austenite grain size to less than 20 µm (figure 5 AI). However, low temperature reheating may also significantly reduce reheating capacity in older designs of pusher type furnaces.

Figure 4 AI (a): CbN, VN, AlN Solublity Diagram

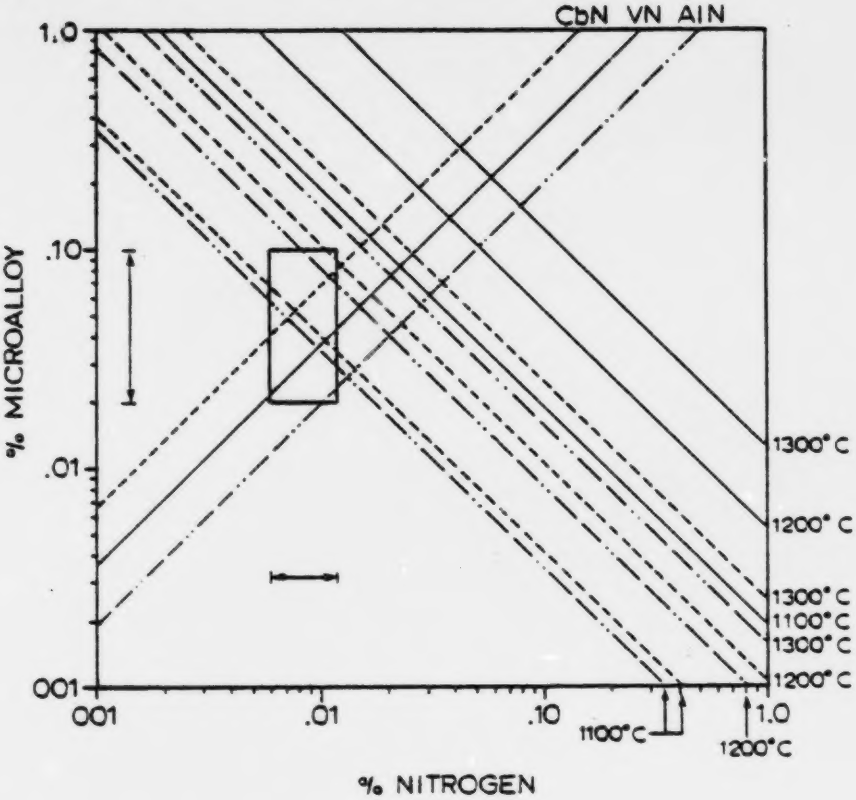

Figure 4 AI (b): CbC, VC, TiC Solubility Diagrams

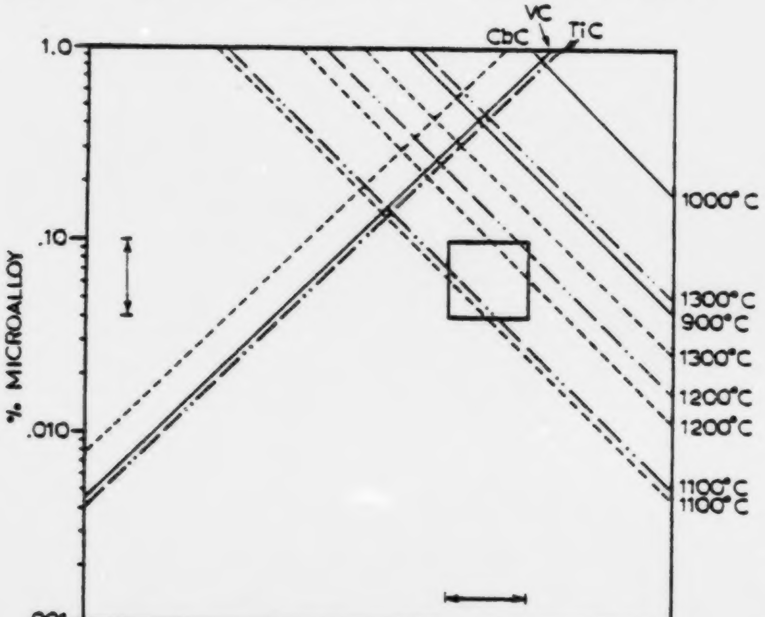

**Figure 4 AI (c): TiN Solubility Diagrams**

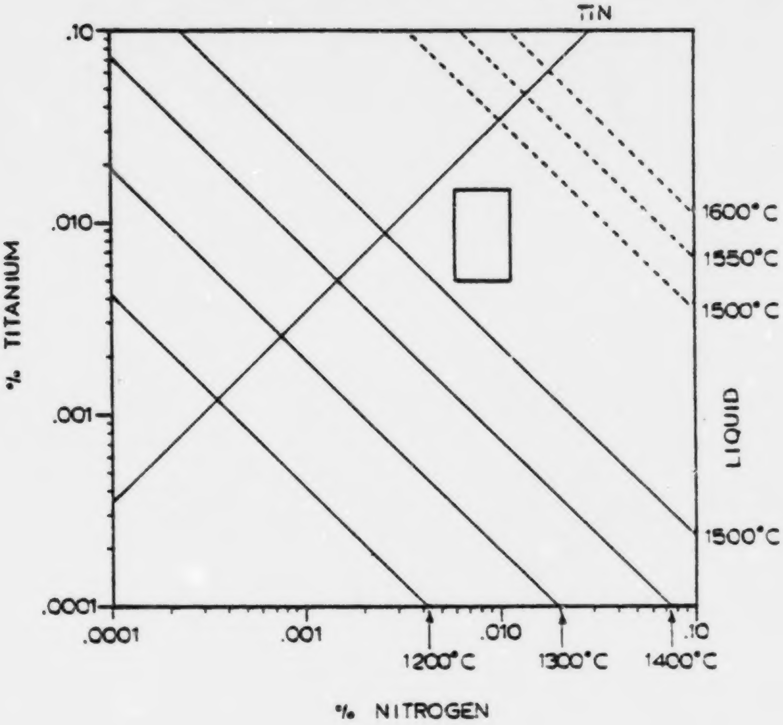

Figure 5 AI: Grain Coarsening of Austenite

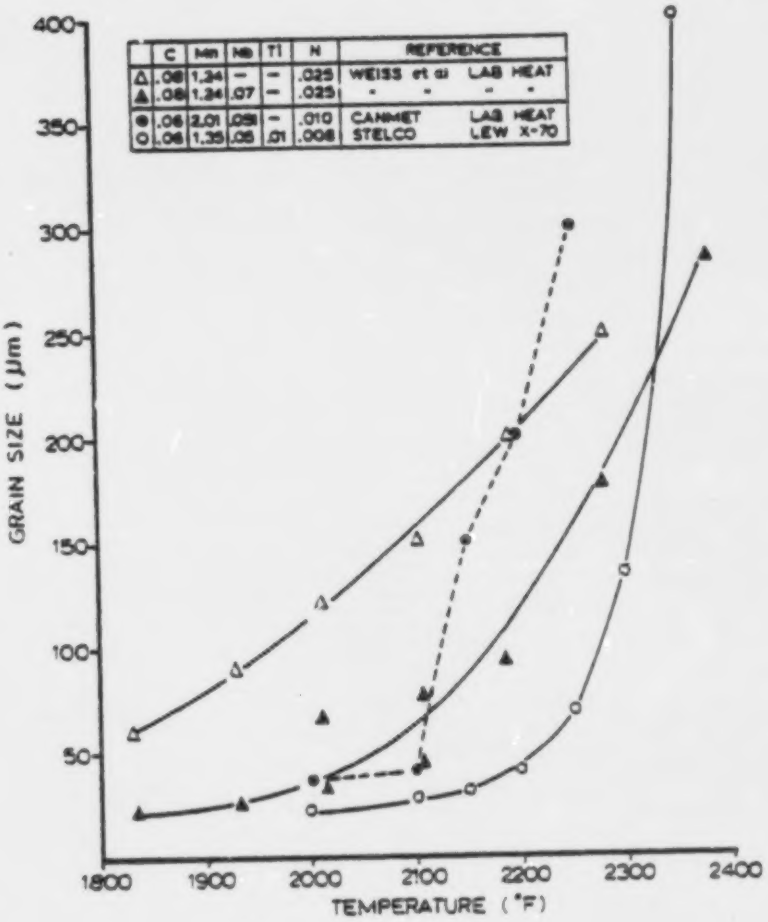

Small additions of titanium (<0.02 percent) have the potential to give grain size control up to relatively high temperatures (>2200°F). Titanium nitride has a very low solubility in both liquid steel and austenite. By adding less than the stoichrometric amount for TiN precipitation, it is possible to develop a relatively fine dispersive of submicron (≈500 A) TiN precipiates in strand cast slabs.[12,13,14] These nitrides are relatively resistant to coarsening during subsequent slab processing and plate rolling, and have been effectively used in strand cast pipe steels to reduce grain coarsening both during slab reheating and in the heat affected zone of high input welds.[14] Figure 5 AI shows the austenite grain refinement that can be achieved in a Ti-treated, LEW strand cast pipeline steel. Titanium addition offers the additional advantage of reducing the free nitrogen content which can improve both base plate and HAZ fracture toughness.

### ii) Recrystallization Rolling

The as-reheated grain size can be significantly refined during high temperature roughing by successive recrystallization of the austenite. The grain refinement occurs by static (rather than dynamic) recrystallization which takes place after the working pass. The main factors controlling the recrystallization process are:

- the initial austenite grain size,
- the pass reduction (strain),
- the temperature, and
- the steel composition.

To obtain recrystallization the steel must be given a critical minimum strain (reduction). Insufficient reduction promotes either recovery or partial recrystallization.[15] Figure 6 AI shows the effects of reduction and temperature on softening or restoration behavior in a columbium bearing steel with a ≈200 μm starting grain size. Note that:

- at least 20 percent reduction is required to achieve complete interpass recrystallization at the normal roughing temperatures (>1100°C, 2000°F), and

- decreasing the pass temperature increases the critical reduction for recrystallization.

Figure 6 AI: The Effects of Pass Reduction and Rolling Temperature on Restoration Behavior in a Cb-Bearing Steel[15] (≈200 μm d grain size)

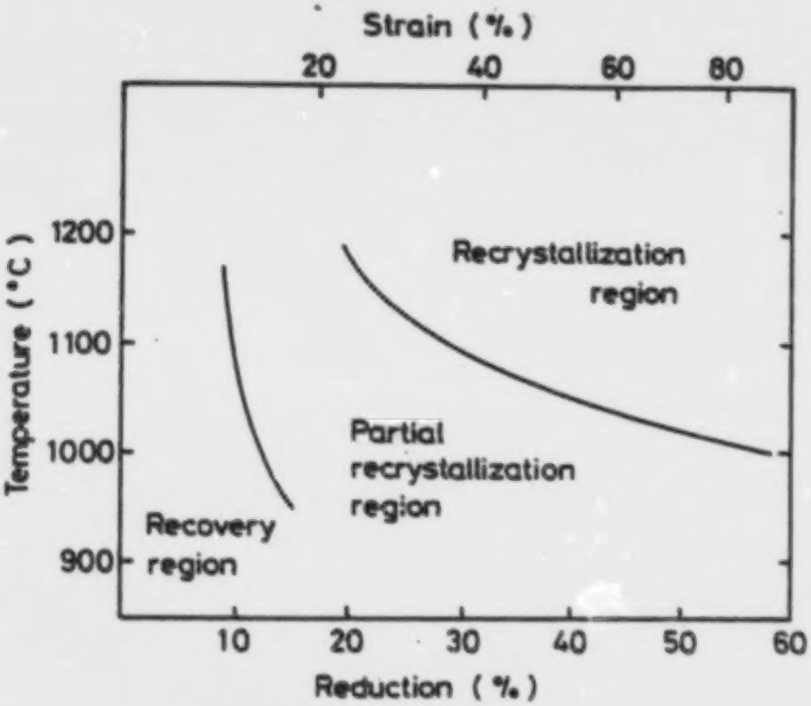

Fine grained austenite recrystallizes much more readily than coarse grained austenite (figure 7 AI) and thus there is considerable benefit to starting with a fine grained austenite in the reheated condition prior to rolling. However by rolling with successive reductions greater than the critical strain required for recrystallization, a fine austenite grain size can be developed during the roughing stage of rolling as shown in figure 8 AI.

Figure 7 AI: The Effect on Initial Austenite Grain Size and Pass Temperature on the Critical Reduction for Recrystallization[15]

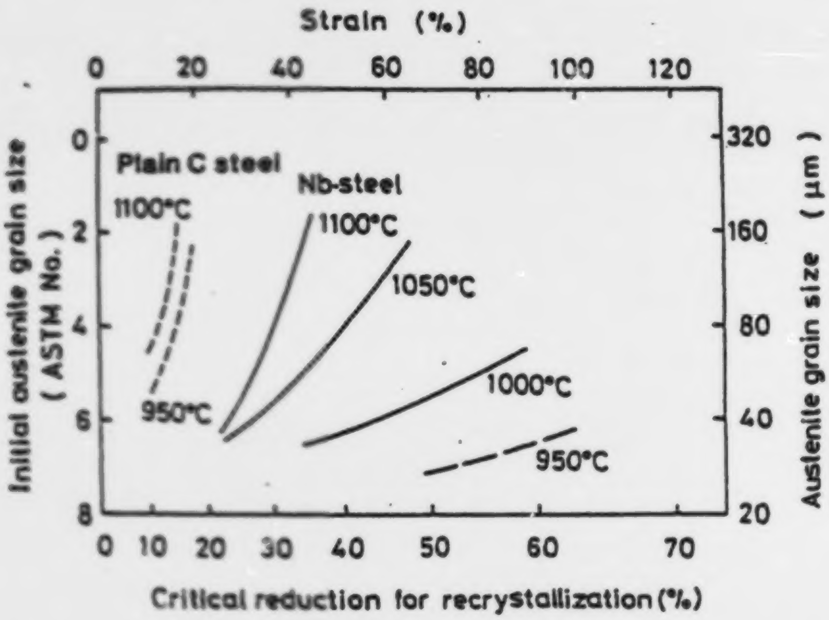

Figure 8 AI: Progressive Refinement of Austenite by Multi-Pass, Recrystallization Rolling[5]

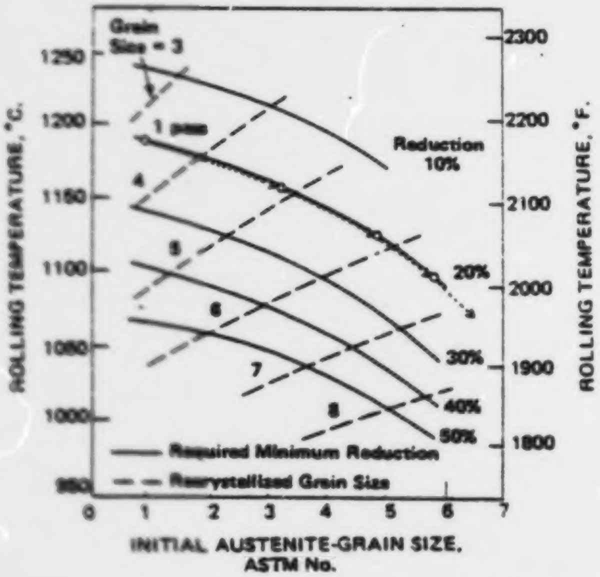

Steel composition also has a significant effect on softening behavior. Microalloys in solution at high temperature retard softening and thus higher reductions are necessary to achieve the same softening as in a plain carbon steel.

Although the rolling temperature influences the softening kinetics, it is not as important as the reduction per pass and the total reduction during roughing in determining the final recrystallized austenite grain size. Figures 9 AI and 10 AI show that effect of total reduction on final austenite grain size for multi-pass rolling in the recrystallized austenite temperature regime. Note that a coarse grained austenite requires much greater total reduction to achieve a fine grained structure. Austenite grain sizes <20 μm can be developed by choice of proper reheating temperature and high reduction sequence.

**Figure 9 AI: The Effect of Total Reduction and Increased Deformation per Pass on Austenite Grain Refinement**[16]

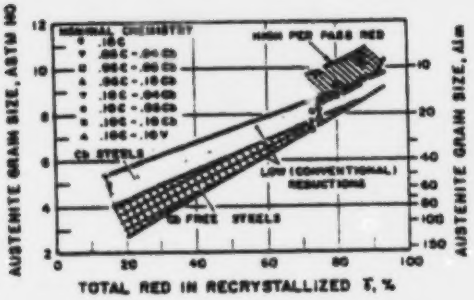

Figure 10 AI: The Effect of Total Deformation on Austenite Grain Refinement from Different Reheating Temperature[17]

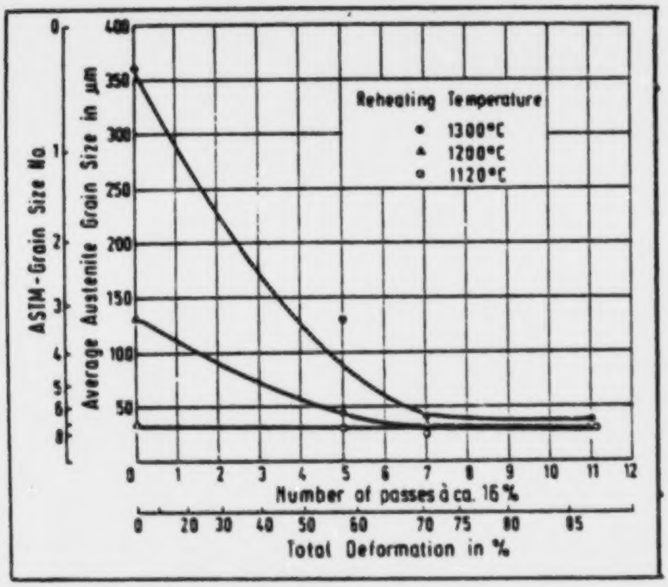

In practical mill conditions, it generally is not possible to continuously achieve recrystallization between each rolling pass. Light drafts are often used during broadside rolling on most mills, and are of necessity practised on older underpowered mills (i.e. the Stelco 148in Plate Mill 2-Hi rougher). Light drafting during rolling is potentially disastrous to austenite grain size, as shown in the next section.

## Mixed Grain Size and Grain Growth During Rolling and Hold Periods

Whereas the classical view of rolling suggests that there is a uniform austenite which recrystallizes during rolling, ultimately leading to a fine uniform transformed ferrite structure, in practice the ferrite structure is seldom uniform and often shows a duplex (mixture of coarse and fine grain) structure. Several mechanisms have been prepared to explain the formation of mixed structure, including:

- partial recrystallization during high and intermediate temperature reduction,

- grain growth between passes and during hold perio

- strain induced abnormal grain-growth due to light reduction between passes,

- insufficient refinement of austenite at high temperature, and

- inhomogeneous formation of shear bands during low temperature rolling.

i) Partial Recrystallization

Multipass rolling with strains per pass greater than required for partial recrystallization will ultimately result in a recrystallized grain structure. Austenite grains recrystallized in the previous rolling pass remain unchanged whereas the unrecrystallized grains preferentially recrystallize. It appears that a uniform fine grain structure can be developed with pass reductions in the region defined in figure 6 AI.[15]

As-reheated microallyed steels generally show a mixed austenite structure due to the effects of precipitate particles on primary austenite grain boundaries. This nonuniform starting structure will be difficult to eliminate during high temperature rolling, particularly using drafts smaller than required for recrystallization, because of the dependency of recrystallization strain energy on grain size. A few relatively large recrystallization passes appear to be required to reduce the heterogeneity in grain size. Otherwise, rolling in the partial recrystallization region will tend to aggravate the inhomogeneity in austenite.

ii) Strain Induced Abnormal Grain Growth

Light reductions (<14 percent) at high temperatures (i.e. in the recovery region) promote strain induced abnormal grain growth which results in formation of abnormally coarse grains.[15,16,17] This grain coarsening can occur in a very short time (i.e. within the interpass time normally used in high temperature rolling). Figure 11 AI shows the effect of pass reduction on percent of abnormal coarse grains for different working temperatures and initial grain sizes.

**Figure 11 AI:** Formation of Coarse Grains in the Mixed Austenite Grain Structure by Rolling with Light Reduction at High Rolling Temperatures
a) X65 Steel, Initial Grain Size Number 2.5
b) X70 Steel, Initial Grain Size Number 1.0
c) X70 Steel, Initial Grain Size No. 3.5-4.0

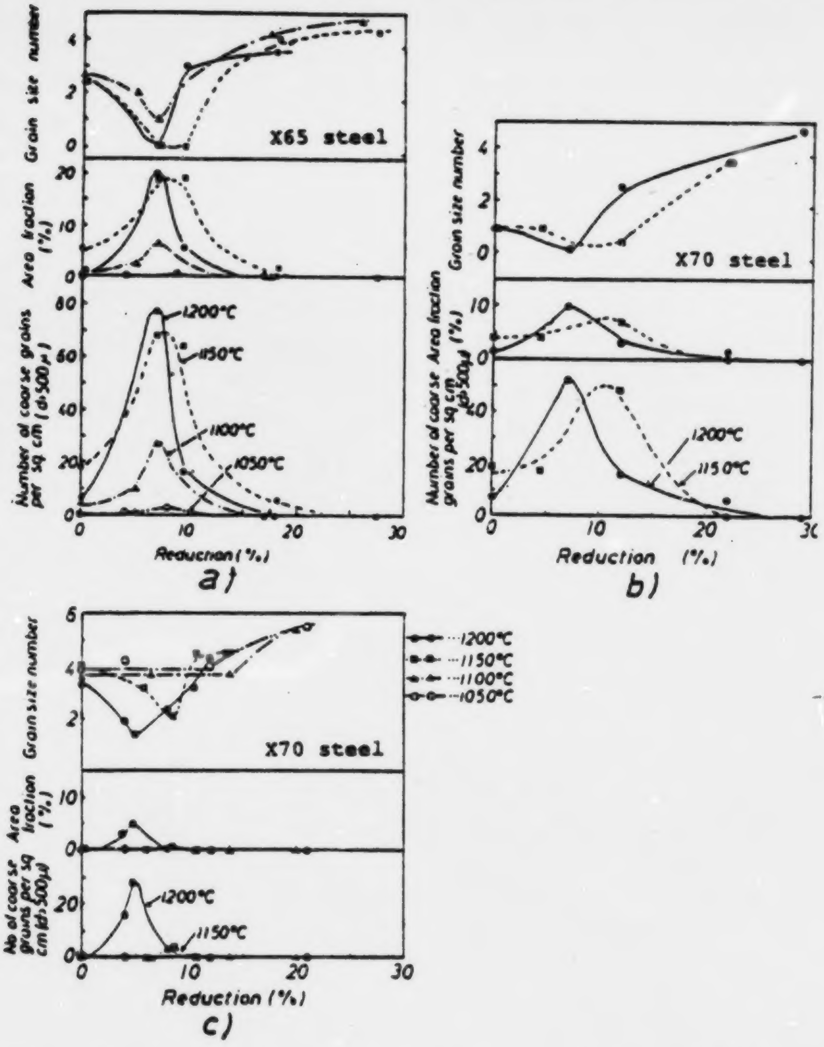

Mixed austenite grain size produced by light drafting is not completely removed by subsequent heavy drafting and thus promotes a mixed transformed ferrite structure. These structures are obtained in columbium and columbium-vanadium steels. Small titanium additions (0.01 percent) may significantly decrease the tendency for abnormal grain growth; however, it is not clear that it will completely eliminate it.[19,20]

### iii) Grain Growth During Holding

Long interpass holding times, or extended holding to remove temperature prior to low temperature rolling in the non-recrystallized region may give rise to grain growth depending upon the percent reduction prior to the delay period and the length of the delay. The most important factor is the reduction prior to holding. A light reduction (<10 percent) prior to the delay can result in more than 50 percent coarse grained structure in a matrix of relatively fine grained austenite. Increasing the delay time accentuates the degree of coarsening (figure 12 AI). Heavier reduction (>10 percent) prevents the formation of coarse grained structure. Lowering the temperature for the delay period reduces the tendency for grain coarsening, and can eliminate it entirely provided the delay temperature corresponds to the non-recrystallized temperature region in which grain boundary migration is blocked by precipitation of microalloy carbonitrides. Figure 13 AI shows the beneficial effect of reducing holding temperature and using microalloys (particularly Ti) on restricting grain coarsening.[5]

**Figure 12 AI:** The Effect of Pass Reduction Prior to Holding on Grain Coarsening During Holding[15]

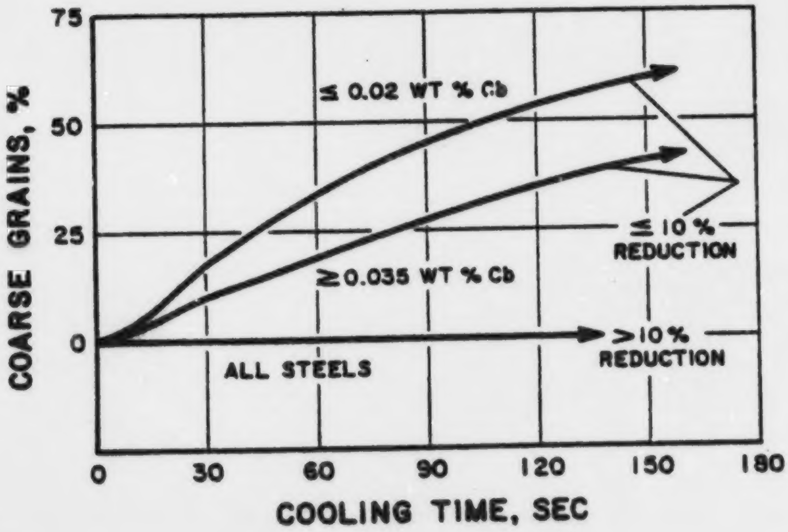

Figure 13 AI: Grain Coarsening During Holding
After Recrystallization
(C-Mn-Cb-Al Steels)[5]

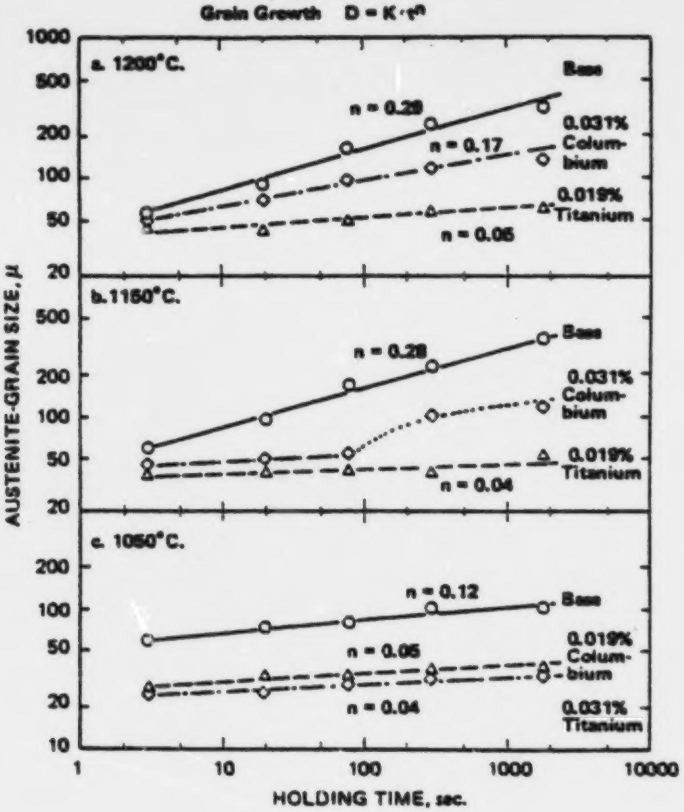

## Non-Recrystallization Rolling

Static recovery and recrystallization of austenite is significantly retarded by both lattice distortion caused by microalloys in solution and pinning of dislocations resulting from strain enhanced precipitation of microalloy carbonitrides. The former effect occurs at relatively high temperature and is relatively unimportant with respect to the softening behavior of austenite during roughing. The latter effect is very significant particularly in columbium bearing steel for which the recrystallization of austenite can be sufficiently delayed to allow strain accumulation (>80 percent) during rolling at temperatures below ≈1700°F.

The effectiveness of each microalloy on retarding softening is largely related to its tendency to precipitate in austenite, and thus is dependent on its carbide and nitride solubility product. Other elements (e.g. manganese and molybdenum) have important but complex effects on recrystallization behavior of microalloyed steels. For instance molybdenum[21] tends to lower the activity of carbon and nitrogen in solution, and thus can retard precipitation of carbonitrides in austenite. However, molybdenum in solution also retards recovery so that molybdenum bearing microalloyed steels often show greater retardation of recrystallization than non-Mo steels.

The effective recrystallization stop temperature (i.e. temperature dividing the regime of total and partial recrystallization) is dependent on the initial solute content and the microalloy. Figure 14 AI shows the increase in RS temperature with solute content for Cb, V, Ti, and Al steels.[22] Note that columbium is particularly effective in retarding recrystallization, and thus is commonly used in microalloyed steels. Similarly, high levels of titanium can be used to achieve cold-worked austenites; however at high levels of titanium the beneficial effect of Ti-N precipitation may be negated. Vanadium precipitates are also effective in preventing softening, but much higher levels of vanadium are required, and the recrystallization stop temperatures are much lower than for niobium steels. Aluminum has the potential to be used like other microalloys, however precipitation of AlN in austenite is relatively sluggish. Also aluminum levels are generally restricted because of its high affinity for oxygen.

**Figure 14 AI:** **The Increase in Recrystallization-Stop* Temperature with Increase in the Level of Microalloy[27]**

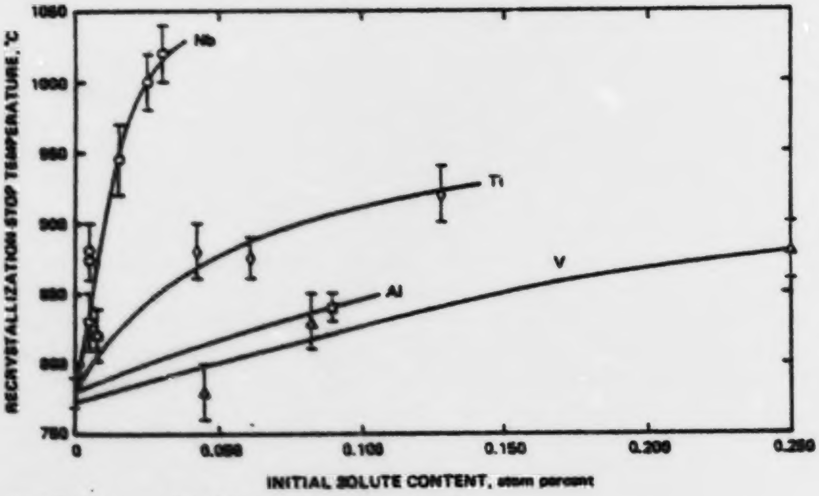

* 0.07 C, 1.40 Mn, 0.25 Si steel

Rolling below the recrystallization stop temperature produces a heavily cold worked (elongated) austenite structure. Increasing deformation increases the austenite grain boundary area and the deformation band density (figure 15 AI). Both of these contribute to the number of nucleation sites for ferrite transformation, and thus there is a significant reduction in ferrite grain size with increased low temperature (figure 16 AI). Note that the refinement achieved by this rolling is very dependent on the recrystallized austenite grain size prior to this deformation.

**Figure 15 AI:** The Effect of Total Reduction Below ≈900°C on Ferrite Nucleation Sites

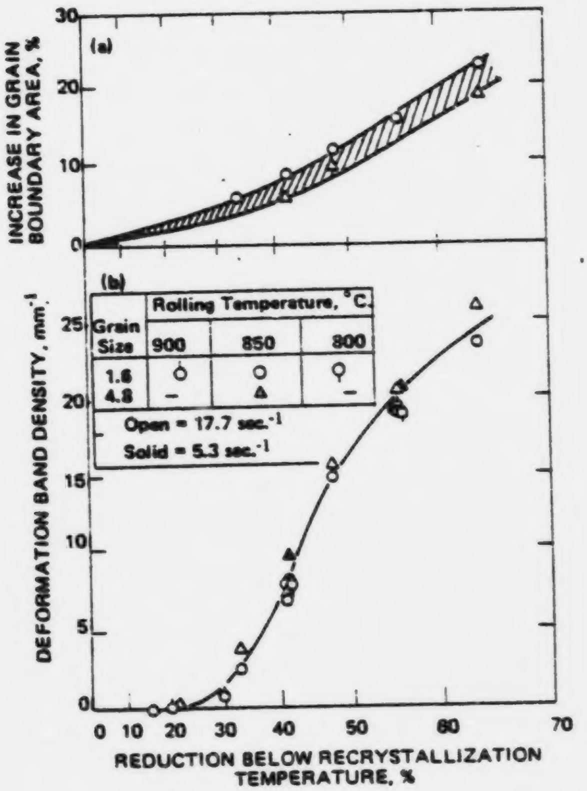

**Figure 16 AI:** The Effect of Austenite Interface Area on Ferrite Grain Size[5]

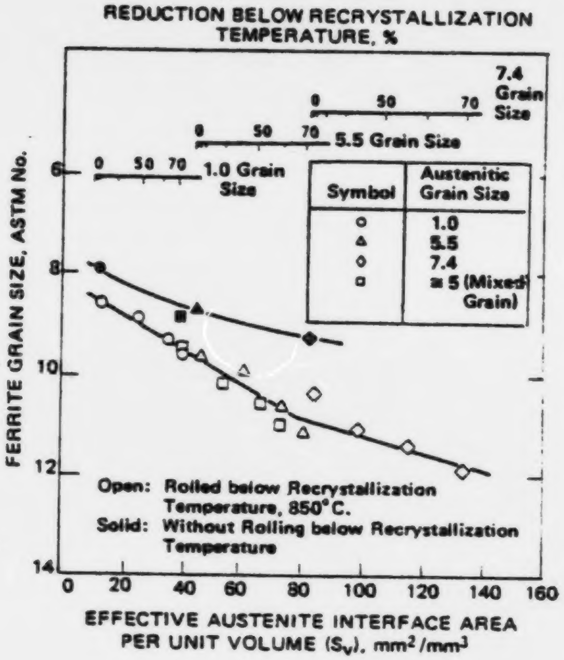

The homogeneity of the final ferrite structure is very dependent on the recrystallized austenite structure. Recrystallized grains mixed with coarse, coalesced grains develop a non-homogeneous density of deformation bands, which are more difficult to form in coarse austenite (figure 17 AI)[15]. In addition to forming coarse ferrite, coarse grain austenite structures ultimately transform into coarse bainitic patches which have a very deleterious effect on impact transition behavior (figure 18 AI).

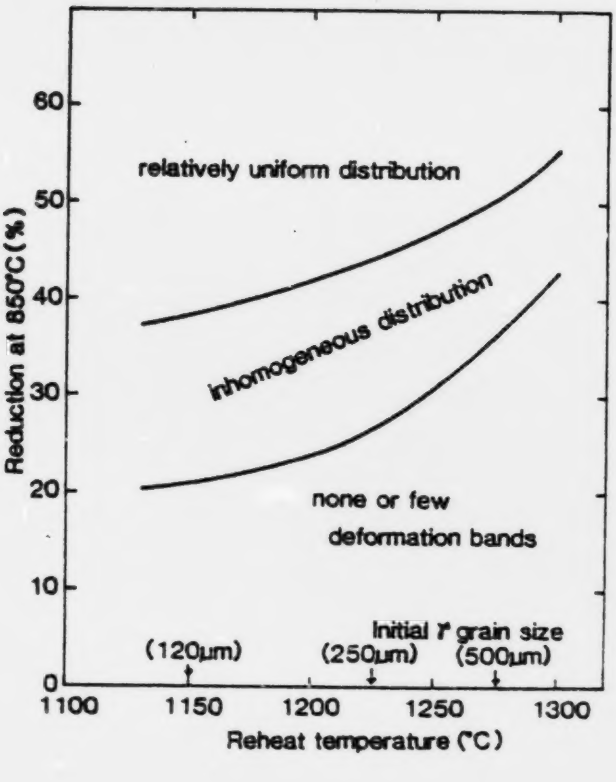

Figure 17 AI: The Effect of Total Reduction Below the Recrystallization Stop Temperature on the Ease of Forming Deformation Bands[15]

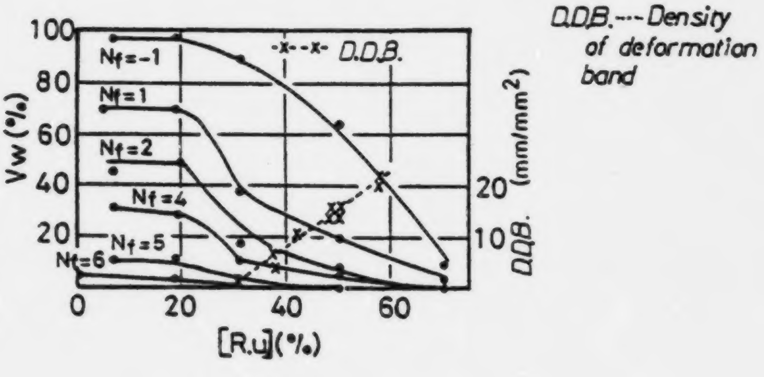

Figure 18 AI (a): The Effect of Reduction Below R-Stop Temperature and the Starting Austenite Grain Size on the Volume Fraction of of Coarse Bainite[18]

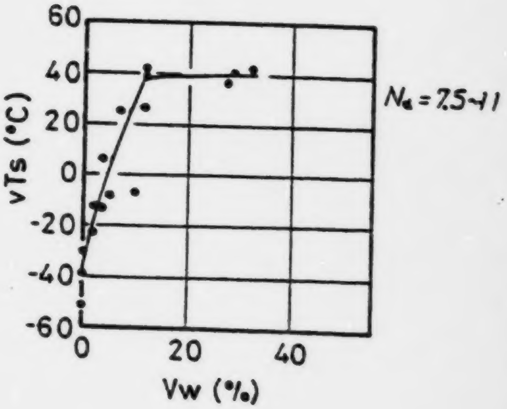

Figure 18 AI (b): The Effect of Volume Fraction of Bainite on Charpy FATT[18]

# REFERENCES - APPENDIX I

1. F. B. Pickering, Proc MicroAlloying '75, Washington, DC, 1975, pp 9-31.
2. K. J. Irvine et al: Journal of Iron and Steel Institute, 1967, Vol 205, p 161.
3. N. P. Allen et al: JISI, 1953, Vol 174, p 108.
4. B. Engl and K. Kaup, Proc Thermomechanical Processing of Microalloyed Austenite, Pittsburgh, 1981, pp 467-481.
5. I. Kozaso et al: Proc Microalloying '75, Washington, DC, 1975, pp 120-135.
6. A. Sandberg, W. Roberts, Proc Thermomechanical Processing of Microalloyed Austenite, Pittsburgh, 1981, pp 405-431.
7. M. Fukuda et al: Proc. Microalloying '75, Washington, DC, 1975, pp 136-150.
8. T. Gladman and F. B. Pickering, JISI, 205, 1967, pp 653.
9. K. Narita, Trans, ISIJ, 1975, Vol 15, p 145.
10. I. Weiss et al: Proc Thermomechanical Processing of Microalloyed Austenite, Pittsburgh, 1981, pp 33-58.
11. R. K. Amin, F. B. Pickering, IBID, pp 1-31.
12. S. Kanazawa et al: Trans ISIJ Vol 16, 1976, pp 486.
13. H. Gondoh et al: Development of Acicular Ferrite Steel for Arctic Grade Line Pipe, Nippon Steel Technical Report, No. 14, December, 1979, p 55.
14. D. B. McCutcheon et al: Proc Micon '82, STP782, Houston, Texas, 1982, p 227.
15. T. Tanaka et al: Proc Thermomechanical Processing of Microalloyed Austenite, Pittsburgh, 1981, pp 195-216.
16. D. R. MiMicco, A. I. Davenport, IBID, pp 59-81.
17. K. Hulka, C. M. Vlad, IBID, pp 121-128.

18. M. Katsumata et al, IBID, pp 101-119.

19. M. J. Godden et al, IBID, pp 253-265.

20. L. A. Leduc and C. M. Sellars, IBID, pp 641-654.

21. B. Bacroix et al, IBID, pp 293-318.

22. L. J. Cuddy, IBID, pp 129-140.

# APPENDIX II

## ROLLING PRACTICES

Table I AII summarizes the 2-High rougher and 4-High finishing practices for the two rollings.

Table I AII (a): 2-High Rougher Drafting - March 9, 1983

| Charge No. | Slab No. | Gauge (in) | | Pass No. | | | | | | | | | | | | | | | | | | | | | | No. Water Passes | 2-Hi Rolling Time (sec) | 2-Hi-Exit - 4-Hi Entry (sec) |
|---|---|---|---|---|---|---|---|---|---|---|---|---|---|---|---|---|---|---|---|---|---|---|---|---|---|---|---|---|
| | | | | 1 | 2 | 3 | 4 | 5 | 6 | 7 | 8 | 9 | 10 | 11 | 12 | 13 | 14 | 15 | 16 | 17 | 18 | 19 | 20 | 21 | 22 | | | |
| 967 | 21C | 0.75 | GAP | 8.73 | 7.99 | 7.61 | 7.16 | 7.48 | 7.10 | 6.70 | 6.30 | 5.92 | 5.52 | 5.20 | 4.81 | 4.42 | 4.02 | 3.62 | 3.27 | 2.93 | 2.63 | 2.36 | | | | 3W | 175 | 25 |
| 968 | 21D | 0.75 | GAP | 8.73 | 8.08 | 7.53 | 7.22 | 7.47 | 7.21 | 6.78 | 6.40 | 6.01 | 5.39 | 5.26 | 4.92 | 4.54 | 4.23 | 3.93 | 3.67 | 3.39 | 3.17 | 2.92 | 2.67 | 2.38 | 2.32 | 3W | 190 | 75 |
| 969 | 67 | 0.75 | GAP | 8.73 | 7.99 | 7.70 | 7.26 | 6.88 | 6.46 | 6.03 | 5.61 | 5.21 | 4.81 | 4.50 | 4.13 | 3.76 | 3.42 | 3.10 | 2.72 | 2.53 | 2.40 | 2.34 | | | | 3W | 190 | 40 |
| 970 | 51 | 1.00 | GAP | 8.74 | 8.03 | 7.73 | 7.29 | 6.93 | 6.49 | 6.10 | 5.80 | 5.41 | 5.01 | 4.62 | 4.26 | 3.92 | 3.60 | 3.33 | 3.14 | | | | | | | 5W | 165 | 90 |
| 971 | 69 | 1.00 | GAP | 8.73 | 8.07 | 7.70 | 7.26 | 6.81 | 6.41 | 6.00 | 5.60 | 5.21 | 4.83 | 4.46 | 4.13 | 3.96 | 3.53 | 3.94 | 3.29 | 3.74 | 3.14 | 3.10 | | | | 5W | 180 | 30 |
| 972 | 53 | 1.25 | GAP | 8.60 | 8.21 | 7.85 | 7.48 | 7.19 | 6.82 | 6.50 | 6.10 | 5.80 | 5.51 | 5.19 | 4.86 | 4.54 | 4.22 | 3.92 | 3.94 | 4.56 | 3.90 | | | | | 0W | 170 | 95 |
| 973 | 55 | 1.25 | GAP | 8.73 | 8.23 | 7.72 | 7.30 | 7.08 | 6.59 | 6.20 | 5.81 | 5.40 | 5.00 | 4.63 | 4.22 | 3.91 | | | | | | | | | | 7W | 140 | 35 |
| 974 | 57 | 1.25 | GAP | 8.92 | 8.46 | 8.01 | 7.61 | 7.27 | 6.76 | 6.31 | 5.91 | 5.51 | 5.12 | 4.71 | 4.42 | 4.10 | 3.90 | | | | | | | | | 5W | 172 | 240 |
| 975 | 65 | 1.50 | GAP | 8.88 | 8.44 | 8.01 | 7.58 | 7.24 | 6.78 | 6.27 | 5.78 | 5.28 | 4.87 | 4.72 | | | | | | | | | | | | 5W | 135 | 30 |
| 976 | 71 | 1.50 | GAP | 8.89 | 8.46 | 7.98 | 7.59 | 7.28 | 6.78 | 6.25 | 5.88 | 5.51 | 5.21 | 4.92 | 4.72 | | | | | | | | | | | 7W | 180 | 30 |

Table I AII (b): 4-High Finisher Drafting - March 9, 1983

| Charge No. | Slab No. | Gauge (in) |  | Pass No. |  |  |  |  |  |  |  |  |  |  |  |  |  |  |  |  |  |  | 4-Hi Pyrom (°F) | 2-Hi-4-Hi Trans Time (sec) | 4-Hi Delay (sec) | Total Time 4-Hi (sec) | Rolling Time 4-Hi (sec) |
|---|---|---|---|---|---|---|---|---|---|---|---|---|---|---|---|---|---|---|---|---|---|---|---|---|---|---|---|
|  |  |  |  | 1 | 2 | 3 | 4 | 5 | 6 | 7 | 8 | 9 | 10 | 11 | 12 | 13 | 14 | 15 | 16 | 17 | 18 | 19 |  |  |  |  |  |
| 967 | 21C | 0.75 | GAP | 2.23 | - | 2.23 | 2.12 | 2.10 | 2.01 | 2.02 | 1.93 | 1.91 | 1.81 | 1.64 | 1.49 | 1.36 | 1.13 | 0.83 | 0.76 | 0.69 | 0.61 |  |  |  |  |  |  |
|  |  |  | Temp | 1587 | - | - | 1602 | 1571 | 1575 | 1501 | 1550 | 1484 | 1529 | 1502 | 1506 | 1473 | 1469 | 1433 | 1419 | 1392 | 1390 | 1389 | 1636 | 25 | 4 | 179 | 175 |
| 968 | 210 | 0.75 | GAP | 2.12 | 2.02 | 2.01 | 1.92 | 1.92 | 1.81 | 1.71 | 1.52 | 1.42 | 1.19 | 0.93 | 0.82 | 0.73 | 0.69 | 0.68 | 0.64 |  |  |  |  |  |  |  |  |
|  |  |  | Temp | 1550 | 1555 | 1539 | 1545 | 1517 | 1521 | 1492 | 1475 | 1440 | 1461 | 1426 | 1450 | 1414 | 1395 | - | 1368 | 1339 |  |  | 1692 | 75 | 60 | 220 | 152 |
| 969 | 67 | 0.75 | GAP | 2.23 | 2.13 | 2.12 | 2.03 | 2.02 | 1.93 | 1.91 | 1.81 | 1.72 | 1.49 | 1.33 | 1.13 | 0.88 | 0.73 | 0.73 | 0.63 | 0.63 |  |  |  |  |  |  |  |
|  |  |  | Temp | 1582 | 1542 | 1516 | 1518 | 1485 | 1497 | 1436 | 1465 | 1420 | 1433 | 1397 | 1415 | 1382 | 1385 | 1327 | 1367 | 1325 | 1313 |  | 1572 | 40 | 21 | 197 | 176 |
| 970 | 51 | 1.00 | GAP | 2.92 | 2.71 | 2.61 | 2.53 | 2.43 | 2.29 | 2.01 | 1.82 | 1.64 | 1.63 | 1.28 | 1.03 | 0.93 | 0.92 | 0.88 |  |  |  |  |  |  |  |  |  |
|  |  |  | Temp | 1608 | 1633 | 1508 | 1595 | 1533 | 1529 | 1474 | 1489 | 1453 | 1477 | 1451 | 1455 | 1424 | 1415 | 1375 | 1364 |  |  |  | 1696 | 90 | 85 | 317 | 232 |
| 971 | 69 | 1.00 | GAP | 2.92 | 2.84 | 2.73 | 2.60 | 2.53 | 2.43 | 2.30 | 2.03 | 1.88 | 1.68 | 1.44 | 1.28 | 1.08 | 0.98 | 0.92 | 0.83 |  |  |  |  |  |  |  |  |
|  |  |  | Temp | 1638 | - | 1549 | 1610 | 1526 | 1577 | 1513 | - | - | 1519 | 1635 | 1506 | 1610 | - | 1617 | 1371 |  |  |  | 1667 | 30 | 23 | 263 | 220 |
| 972 | 53 | 1.25 | GAP | 3.61 | 3.53 | 3.43 | 3.32 |  |  |  |  |  |  |  |  |  |  |  |  |  |  |  |  |  |  |  |  |
|  |  |  | Temp | 1533 | 1552 | 1495 | 1516 | 1401 |  |  |  |  |  |  |  |  |  |  |  |  |  |  | 1701 | 95 | 87 | 162 |  |
| 973 | 55 | 1.25 | GAP | 3.64 | 3.59 | 3.48 | 3.33 | 3.28 | 3.19 | 3.10 | 3.10 | 2.88 | 2.72 | 2.58 | 2.34 | 2.19 | - | 1.71 | 1.53 | 1.38 | 1.33 |  |  |  |  |  |  |
|  |  |  | Temp | 1686 | 1664 | 1617 | 1629 | 1595 | 1608 | 1578 | 1576 | 1536 | 1531 | 1513 | 1524 | 1504 | 1510 | 1495 | 1506 | 1491 | 1487 | 1456 | 1661 | 35 | 28 | 306 | 278 |
| 974 | 57 | 1.25 | GAP | 3.73 | 3.62 | 3.59 | 3.43 | 3.34 | 3.28 | 3.13 | 3.10 | 3.10 | 2.83 | 2.72 | 2.58 | 2.34 | 2.18 | 1.93 | 1.73 | 1.53 | 1.34 |  |  |  |  |  |  |
|  |  |  | Temp | 1580 |  | 1535 |  | 1525 |  | 1525 |  | 1525 |  | 1510 |  | 1500 |  | 1500 |  | 1490 |  |  | 1693 | 240 | 168 | 359 | 191 |
| 975 | 65 | 1.50 | GAP | 4.48 | 4.34 | 4.28 | 4.13 | 4.08 | 3.98 |  |  |  |  |  |  |  |  |  |  |  |  |  |  |  |  |  |  |
|  |  |  | Temp | 1627 | 1647 | 1618 | 1645 | 1622 | 1635 | 1592 |  |  |  |  |  |  |  |  |  |  |  |  | 1620 | 30 | 22 | 85 |  |
| 976 | 71 | 1.50 | GAP | 4.43 | 4.39 | 4.29 | 4.13 | 4.03 | 3.99 | 3.88 | 3.73 | 3.73 |  |  |  |  |  |  |  |  |  |  |  |  |  |  |  |
|  |  |  | Temp | 1581 | 1606 | 1582 | 1602 | 1564 | 1588 | 1563 | 1554 | 1537 | 1536 |  |  |  |  |  |  |  |  |  | 1611 | 30 | 25 | 143 |  |

## Table I AII (c): 4-High Finisher Drafting - May 20, 1983

| Charge No. | Slab No. | Gauge (in) | ho | | Pass No. | | | | | | | | | | | | | | 4-HI Pyrom (°F) | 3-HI-4-HI Trans Time (sec) | 4-HI Delay (sec) | Total Time 4-HI (sec) | Rolling Time 4-HI (sec) |
|---|---|---|---|---|---|---|---|---|---|---|---|---|---|---|---|---|---|---|---|---|---|---|---|
| | | | | | 1 | 2 | 3 | 4 | 5 | 6 | 7 | 8 | 9 | 10 | 11 | 12 | 13 | 14 | | | | | |
| 157 | NA | 2.362 | 5.50 | GAP | 4.99 | 4.51 | 4.13 | 3.71 | 3.40 | 3.08 | 2.80 | 2.51 | 2.34 | | | | | | 1748 | 240 | 215 | 426 | 211 |
| | | | | Temp | 1620 | 1567 | 1582 | - | 1572 | 1550 | 1565 | 1530 | 1537 | 1489 | | | | | | | | | |
| 158 | NA | 1.574 | 4.70 | GAP | 4.39 | 3.99 | 3.58 | 3.20 | 2.93 | 2.61 | 2.39 | 2.10 | 1.90 | 1.71 | 1.59 | 1.54 | 1.49 | | 1639 | 171 | 141 | 461 | 320 |
| | | | | Temp | 1629 | 1568 | 1570 | 1541 | 1554 | 1518 | 1543 | 1500 | 1511 | 1462 | 1467 | 1400 | 1405 | 1364 | | | | | |
| 159 | NA | 1.574 | 4.70 | GAP | 4.40 | | | | | | | | | | | | | | | | | | |
| | | | | Temp | 1695 | | | | | | | | | | | | | | | | | | |
| 160 | NA | 1.968 | 5.50 | GAP | 5.01 | 4.69 | 4.29 | 3.93 | 3.60 | 3.30 | 2.99 | 2.73 | 2.49 | 2.23 | 2.00 | 1.92 | 2.04 | | 1630 | 201 | 171 | 543 | 372 |
| | | | | Temp | 1632 | 1579 | 1581 | 1551 | 1569 | 1537 | 1538 | 1491 | 1529 | 1497 | 1496 | 1444 | 1400 | 1368 | | | | | |
| 161 | NA | 1.574 | 4.70 | GAP | 4.39 | 3.99 | 3.60 | 3.20 | 2.91 | 2.64 | 2.38 | 2.14 | 1.90 | 1.70 | 1.61 | 1.59 | 1.50 | | 1605 | 30 | 15 | 357 | 342 |
| | | | | Temp | 1606 | 1606 | 1604 | 1562 | 1555 | 1540 | 1546 | 1511 | 1522 | 1455 | 1463 | 1407 | 1400 | 1367 | | | | | |
| 162 | NA | 1.968 | 5.50 | GAP | 5.01 | 4.64 | 4.30 | 3.92 | 3.60 | 3.28 | 3.00 | 2.71 | 2.49 | 2.24 | 2.03 | 1.92 | | | 1590 | 60 | 13 | 311 | 308 |
| | | | | Temp | 1591 | 1578 | 1587 | 1561 | 1575 | 1556 | 1577 | 1540 | 1553 | 1511 | 1473 | 1456 | | | | | | | |
| 163 | NA | 1.574 | 4.70 | GAP | 4.00 | 3.59 | 3.21 | 2.94 | 2.62 | 2.39 | 2.13 | 1.93 | 1.70 | 1.59 | 1.51 | | | | 1575 | 68 | 46 | 317 | 271 |
| | | | | Temp | 1531 | 1557 | 1505 | 1528 | 1492 | 1510 | 1468 | 1467 | 1407 | 1416 | 1368 | 1356 | | | | | | | |
| 164 | NA | 1.574 | 4.70 | GAP | 4.39 | 4.00 | 3.61 | 3.20 | 2.91 | 2.61 | 2.39 | 2.13 | 1.94 | 1.71 | 1.62 | 1.59 | 1.54 | | 1577 | 49 | 19 | 310 | 291 |
| | | | | Temp | 1628 | 1555 | 1538 | 1517 | 1530 | 1514 | 1520 | 1562 | 1496 | 1388 | 1446 | 1387 | 1388 | 1371 | | | | | |
| 165 | NA | 1.574 | 4.70 | GAP | 4.34 | 3.99 | 3.59 | 3.20 | 2.94 | 2.62 | 2.39 | 2.10 | 1.94 | 1.21 | 1.60 | 1.59 | 1.53 | | 1553 | 30 | 10 | 324 | 314 |
| | | | | Temp | 1574 | 1569 | 1570 | 1536 | 1558 | 1523 | 1542 | 1502 | 1506 | - | 1463 | 1397 | 1392 | 1364 | | | | | |

# APPENDIX III

## MECHANICAL PROPERTIES

Table I AIII summarizes the plate tensile and bend test data in both the as-rolled and normalized conditions.

### Table I AIII: Plate Tensile and Bend Test Data

**(a) Normalized**

| Steel | Grade | Direction | Yield | | UTS | | % RA | % Elong | | Y/T |
|---|---|---|---|---|---|---|---|---|---|---|
| | | | (ksi) | (MPa) | (ksi) | (MPa) | | 2in | 8in | |
| 967 | 0.75 | L | 46.9 | 323 | 66.3 | 457 | 70.4 | 59 | 28 | 0.71 |
| | | T | 48.7 | 336 | 66.8 | 461 | 64.0 | 57 | 30 | 0.73 |
| 968 | 0.75 | L | 46.5 | 321 | 65.9 | 454 | 71.9 | 58 | 29 | 0.71 |
| | | T | 47.4 | 327 | 66.5 | 459 | 65.5 | 58 | 30 | 0.72 |
| 969 | 0.75 | L | 50.8 | 350 | 67.4 | 464 | 73.2 | 59 | 28 | 0.75 |
| | | T | 51.5 | 355 | 67.7 | 467 | 67.3 | 58 | 29 | 0.76 |
| 970 | 1.0 | L | 53.0 | 365 | 68.9 | 475 | 74.4 | 63 | 30 | 0.77 |
| | | T | 53.0 | 366 | 69.6 | 480 | 64.2 | 60 | 30 | 0.76 |
| 971 | 1.0 | L | 46.7 | 322 | 66.1 | 456 | 73.6 | 65 | 30 | 0.71 |
| | | T | 47.9 | 330 | 66.8 | 461 | 65.4 | 54 | 27 | 0.72 |
| 973 | 1.25 | L | 54.3 | 347 | 67.6 | 466 | 77.7 | 70 | 35 | 0.74 |
| | | T | 50.1 | 346 | 68.2 | 470 | 68.0 | 68 | 33 | 0.73 |
| 974 | 1.25 | L | 51.3 | 354 | 68.7 | 474 | 73.1 | 71 | 34 | 0.75 |
| | | T | 51.7 | 357 | 68.7 | 474 | 67.6 | 68 | 32 | 0.75 |

## (b) Controlled Rolled

| Steel | Grade | Direction | Yield |  | UTS |  | % RA | % Elong |  | Y/T | Bend Test |
|---|---|---|---|---|---|---|---|---|---|---|---|
|  |  |  | (ksi) | (MPa) | (ksi) | (MPa) |  | 2in | 8in |  |  |
| 967 | 0.75 | L | 71.3 | 491 | 87.1 | 601 | 55.1 | 44 | 23 | 0.82 |  |
|  |  | T | 72.1 | 497 | 86.7 | 598 | 52.9 | 43 | 22 | 0.83 | Flat |
| 968 | 0.75 | L | 68.3 | 471 | 85.1 | 587 | 55.1 | 42 | 23 | 0.80 |  |
|  |  | T | 71.3 | 492 | 85.4 | 589 | 50.5 | 49 | 24 | 0.83 | Flat |
| 969 | 0.75 | L | 72.0 | 497 | 85.8 | 542 | 60.1 | 46 | 21 | 0.84 |  |
|  |  | T | 72.1 | 497 | 58.8 | 612 | 52.0 | 42 | 21 | 0.87 |  |
| 970 | 1.0 | L | 67.7 | 467 | 82.3 | 568 | 60.6 | 48 | 24 | 0.82 |  |
|  |  | T | 68.5 | 472 | 82.9 | 572 | 56.5 | 47 | 22 | 0.83 | Flat |
| 971 | 1.0 | L | 67.1 | 463 | 84.6 | 556 | 61.2 | 49 | 25 | 0.83 |  |
|  |  | T | 69.0 | 476 | 81.6 | 563 | 53.6 | 48 | 25 | 0.85 |  |
| 973 | 1.25 | L | 65.7 | 453 | 78.5 | 541 | 70.3 | 65 | 32 | 0.84 |  |
|  |  | T | 64.2 | 443 | 78.7 | 543 | 61.1 | 10 | 32 | 0.82 | Flat |
| 974 | 1.25 | L | 63.0 | 434 | 77.9 | 537 | 58.2 | 60 | 33 | 0.81 |  |
|  |  | T | 64.5 | 445 | 79.1 | 546 | 57.8 | 65 | 31 | 0.82 | Flat |
| 161 | 0.57 | L | 61.3 | 423 | 78.1 | 539 | NA | 50 | 30 | 0.78 | Flat |
|  |  | T | 63.9 | 441 | 77.4 | 534 | NA | 53 | 21 | 0.83 | Flat |
| 165 | 0.57 | L | 61.5 | 424 | 79.0 | 545 | NA | 63 | 27 | 0.78 | Flat |
|  |  | T | 63.1 | 435 | 77.4 | 534 | NA | 65 | 30 | 0.82 | Flat |
| 160 | 0.57 | L | 57.9 | 399 | 76.7 | 529 | NA | 75 | 31 | 0.75 | Flat |
|  |  | T | 59.0 | 407 | 75.7 | 522 | NA | 70 | 30 | 0.78 | Flat |
| 162 | 1.96 | L | 59.5 | 410 | 75.8 | 523 | NA | 50 | 30 | 0.78 | Flat |
|  |  | T | 60.3 | 416 | 75.8 | 523 | NA | 53 | 31 | 0.80 | Flat |
| 157 | 2.36 | L | 59.2 | 408 | 79.8 | 550 | NA |  | 28 | 0.74 | Flat |
|  |  | T | 55.2 | 381 | 78.7 | 543 | NA | 8 | 24 | 0.70 | Flat |
| Specification Min 350* |  |  |  |  |  | 450 |  | 22 | 19 |  |  |
| Max |  |  |  |  |  | 650 |  |  |  |  |  |

* 350 - up to 40 mm (1.571in)
330 - >40 mm ≤65 mm (2.55in)
320 - >65 mm

Table II AIII summarizes the plate full-size Charpy test data in the as-rolled and normalized conditions. These data are generally the average of two tests per temperature. Note that several of the tests in the longitudinal direction and/or the normalized condition exceeded the capacity (264 ft-lb) of the Charpy test machines.

## Table II AIII (a): Charpy Test Data - Controlled Rolled Plate, Transverse Direction

| Charge | Gauge | Condition | Position | | +75°F | | 0°F | | -25°F | | -50°F | | -75°F | | -100°F | | -125°F | | -150°F | | -175°F | |
|---|---|---|---|---|---|---|---|---|---|---|---|---|---|---|---|---|---|---|---|---|---|---|
| | | | | | ft-lb | % Shear | ft-lb | % Shear | ft-lb | % Shear | ft-lb | % Shear | ft-lb | % Shear | ft-lb | % Shear | ft-lb | % Shear | ft-lb | % Shear | ft-lb | % Shear |
| 967 | 0.75 | CR | Subsurface | | 66 | 100 | 63 | 100 | - | - | 45 | 74 | 40 | 73 | 29 | 41 | 13.5 | 12 | - | - | - | - |
| 968 | 0.75 | | | | 72 | 100 | 63 | 100 | - | - | 56 | 65 | 46 | 59 | 36 | 42 | 14.5 | 13.5 | - | - | - | - |
| 969 | 0.75 | | | | 78 | 100 | 66 | 100 | - | - | 50 | 78 | 44 | 60 | 28 | 39 | 16 | 18 | - | - | - | - |
| 970 | 1.0 | | | | 82 | 100 | 80 | 100 | - | - | 68 | 83 | 55 | 55 | 46 | 44 | 24 | 8 | 16 | 4.5 | 7.5 | 1.5 |
| 971 | 1.0 | | | | 89 | 100 | 88 | 100 | - | - | 77 | 81 | 59 | 62 | 32 | 32 | 27 | 7.5 | 12 | 3.5 | 7.5 | 2 |
| 973 | 1.25 | | | | 118 | 100 | 116 | 98 | - | - | 89 | 76 | 72 | 51 | 49 | 37 | 29.5 | 5.5 | 24 | 1.5 | 5 | 1.5 |
| 974 | 1.25 | | | | 116 | 100 | 107 | 100 | - | - | 91 | 79 | 73 | 49 | 67 | 39 | 32 | 9 | 8 | 2 | 7.5 | 1.5 |
| 158 | 1.57 | | | | 114 | 100 | 111 | 98 | 100 | 87 | 90 | 72 | 83 | 50 | 30 | 40 | 27.5 | 12 | - | - | - | - |
| 161 | 1.57 | | | +84°F | 123 | 100 | 112 | 100 | 121 | 99 | 111 | 94 | 108 | 81 | 96 | 64 | 60.5 | 72 | - | - | - | - |
| 160 | 1.96 | | | | 138 | 100 | 107 | 77 | 111 | 79 | 97 | 75 | 85 | 53 | 52 | 40 | 8 | 5 | - | - | - | - |
| 157 | 2.36 | | | | 160 | 100 | 151 | 96 | 126 | 80 | 108 | 65 | 106 | 48 | 76 | 37 | 15.5 | 1 | - | - | - | - |
| 969 | 0.75 | CR | Mid-Thickness | | 72 | 100 | 67 | 99 | - | - | 57 | 70 | 47 | 48 | 34 | 42 | 16.5 | 14 | - | - | - | - |
| 971 | 1.0 | | | | 87 | 100 | 83 | 99 | - | - | 68 | 81 | 52 | 48 | 37 | 43 | 16 | 13.5 | - | - | - | - |
| 973 | 1.25 | | | | 115 | 100 | 102 | 94 | - | - | 84 | 77 | 57 | 43 | 31 | 28 | 16 | 1.5 | - | - | - | - |
| 158 | 1.57 | | | | 108 | 99 | 90 | 66 | 61 | 48 | 32 | 34 | 20 | 34 | 11 | 16 | 13 | 2 | - | - | - | - |
| 161 | 1.57 | | | 84°F | 120 | 100 | 100 | 73 | 87 | 64 | 66 | 53 | 31 | 44 | 19 | 26 | 10 | 4 | - | - | - | - |
| 160 | 1.96 | | | | 126 | 98 | 104 | 65 | 89 | 54 | 44 | 40 | 47 | 35 | 15 | 17 | 5 | 0 | - | - | - | - |
| 157 | 2.36 | | | | 127 | 88 | 84 | 48 | 107 | 51 | 53 | 28 | 20 | 13 | 6 | 9 | 5 | 0 | - | - | - | - |
| 968 | 0.75 | CR | 1/4 PT | | 77 | 100 | 69 | 99 | - | - | 55 | 79 | 45 | 51 | 37 | 37 | 21 | 18.5 | 13 | 10.5 | 9 | 3 |
| 970 | 1.0 | | | | 83 | 100 | 82 | 99 | - | - | 69 | 83 | 45 | 55 | 33 | 41 | 14 | 7 | - | - | - | - |

## Table II AIII (b): Charpy Test Data - Controlled Rolled Plate, Longitudinal Direction

| Charge | Gauge | Condition | Position | | +75°F | | 0°F | | -25°F | | -50°F | | -75°F | | -100°F | | -125°F | | -150°F | | -175°F | |
|---|---|---|---|---|---|---|---|---|---|---|---|---|---|---|---|---|---|---|---|---|---|---|
| | | | | | ft-lb | % Shear | ft-lb | % Shear | ft-lb | % Shear | ft-lb | % Shear | ft-lb | % Shear | ft-lb | % Shear | ft-lb | % Shear | ft-lb | % Shear | ft-lb | % Shear |
| 967 | 0.75 | CR | Subsurface | | | | 136 | 99 | | | | | 75 | 74 | 72 | 85 | 40 | 75 | | | | |
| 968 | 0.75 | | | | | | 138 | 99 | | | | | 105 | 87 | 74 | 80 | 27 | 6 | | | | |
| 969 | 0.75 | | | | | | 123 | 99 | | | | | 87 | 90 | 70 | 85 | 61 | 80 | | | | |
| 970 | 1.0 | | | | | | 212 | 100 | | | | | 146 | 95 | 81 | 40 | 39 | 7 | | | | |
| 971 | 1.0 | | | | | | 258 | 100 | | | | | 169 | 95 | 93 | 35 | 96 | 63 | | | | |
| 973 | 1.25 | | | | | | X | X | | | | | 264 | 100 | 224 | 100 | 133 | 50 | | | | |
| 974 | 1.25 | | | | | | X | X | | | | | X | X | 152 | 100 | 57 | 16 | | | | |
| 158 | 1.57 | | | | | | | | | | | | | | | | | | | | | |
| 161 | 1.57 | | | | | | | | | | | | | | | | | | | | | |
| 160 | 1.96 | | | | | | | | | | | | | | | | | | | | | |
| 157 | 2.36 | | | | | | | | | | | | | | | | | | | | | |
| 969 | 0.75 | CR | Mid-Thickness | | | | 142 | 100 | | | | | 107 | 92 | 77 | 80 | 59 | 60 | | | | |
| 971 | 1.0 | | | | | | 170 | 100 | | | | | 109 | 86 | 74 | 70 | 67 | 80 | | | | |
| 973 | 1.25 | | | | | | X | X | | | | | 184 | 82 | 89 | 60 | 15 | 3 | | | | |
| 158 | 1.57 | | | | | | | | | | | | | | | | | | | | | |
| 161 | 1.57 | | | | | | | | | | | | | | | | | | | | | |
| 160 | 1.96 | | | | | | | | | | | | | | | | | | | | | |
| 157 | 2.36 | | | | | | | | | | | | | | | | | | | | | |
| 968 | 0.75 | CR | 1/4 PT | | | | 159 | 100 | | | | | 118 | 92 | 91 | 98 | 48 | 75 | | | | |
| 970 | 1.0 | | | | | | 231 | 100 | | | | | 126 | 81 | 103 | 80 | 30 | 5 | | | | |
| 158 | 1.57 | | | | | | | | | | 263 | 100 | 163 | 60 | 52 | 49 | | | | | | |
| 161 | 1.57 | | | | | | | | | | | | 264 | 100 | 263 | 100 | | | | | | |
| 160 | 1.96 | | | | | | | | | | | | 264 | 100 | 123 | 65 | | | | | | |
| 157 | 2.36 | | | | | | | | | | | | 264 | 100 | 263 | 100 | | | | | | |

X = Not tested due to energy values exceeding impact tester's limitations.

## Table II AIII (c): Charpy Test Data - Normalized Plate, Transverse Direction

| Charge | Gauge | Condition | Position | | +75°F | | 0°F | | -25°F | | -50°F | | -75°F | | -100°F | | -125°F | | -150°F | | -175°F | |
|---|---|---|---|---|---|---|---|---|---|---|---|---|---|---|---|---|---|---|---|---|---|---|
| | | | | | ft-lb | % Shear | ft-lb | % Shear | ft-lb | % Shear | ft-lb | % Shear | ft-lb | % Shear | ft-lb | % Shear | ft-lb | % Shear | ft-lb | % Shear | ft-lb | % Shear |
| 967 | 0.75 | Norm | Subsurface | | 131 | 100 | 128 | 98 | - | - | 106 | 65 | 78 | 56 | 68 | 39 | 38 | 12 | 34.5 | 5 | 21.5 | 3 |
| 968 | 0.75 | | | | 162 | 100 | 155 | 100 | - | - | 56 | 109 | 94 | 53 | 70 | 46 | 43.5 | 6 | 32.5 | 4.5 | 32.5 | 1.5 |
| 969 | 0.75 | | | | 146 | 100 | 140 | 95 | - | - | 50 | 104 | 74 | 53 | 71 | 40 | 51.5 | 14.5 | 26 | 5 | 23.5 | 2 |
| 970 | 1.0 | | | | 127 | 100 | 125 | 94 | - | - | 68 | 93 | 88 | 54 | 66 | 37 | 38.5 | 6 | 33 | 3.5 | 22 | 1 |
| 971 | 1.0 | | | | 140 | 100 | 139 | 95 | - | - | 77 | 115 | 106 | 58 | 77 | 46 | 37 | 10 | 38 | 7 | 24.5 | 3 |
| 973 | 1.25 | | | | 210 | 100 | 233 | 100 | - | - | 89 | 141 | 89 | 127 | 55 | 107 | 82 | 27 | 62 | 12 | 62 | 39.5 |
| 974 | 1.25 | | | | 262 | 100 | 215 | 100 | - | - | 91 | 137 | 85 | 124 | 54 | 101 | 79.5 | 25.5 | 79.5 | 29 | 53.5 | 11 |
| 158 | 1.57 | | | | | | | | | | | | | | | | | | | | | |
| 161 | 1.57 | | | | | | | | | | | | | | | | | | | | | |
| 160 | 1.96 | | | | | | | | | | | | | | | | | | | | | |
| 157 | 2.36 | | | | | | | | | | | | | | | | | | | | | |
| 969 | 0.75 | Norm | Mid-Thickness | | 132 | 100 | 127 | 98 | - | - | 107 | 69 | 83 | 44 | 75 | 37 | 38 | 8.5 | 20.5 | 2 | 20 | 0.5 |
| 971 | 1.0 | | | | 83 | 100 | 124 | 96 | - | - | 92 | 68 | 74 | 47 | 62 | 41 | 23.5 | 9 | 21.5 | 3 | 25.5 | 2 |
| 973 | 1.25 | | | | 231 | 100 | 233 | 100 | - | - | 127 | 77 | 119 | 63 | 93 | 43 | 86 | 23.5 | 54 | 12 | 42 | 6.5 |
| 158 | 1.57 | | | | | | | | | | | | | | | | | | | | | |
| 161 | 1.57 | | | | | | | | | | | | | | | | | | | | | |
| 160 | 1.96 | | | | | | | | | | | | | | | | | | | | | |
| 157 | 2.36 | | | | | | | | | | | | | | | | | | | | | |
| 968 | 0.75 | Norm | 1/4 PT | | 140 | 100 | 133 | 94 | - | - | 109 | 70 | 91 | 49 | 65 | 38 | 43.5 | 8 | 29.5 | 4 | 19 | 0 |
| 970 | 1.0 | | | | 142 | 100 | 137 | 100 | - | - | 106 | 75 | 85 | 56 | 59 | 41 | 41.5 | 9.5 | 30.5 | 3 | 21 | 1.5 |
| 158 | 1.57 | | | | | | | | | | | | 204 | 100 | 126 | 57 | 97 | 27 | 81 | 25 | 44 | 13 |
| 161 | 1.57 | | | | | | | | | | | | - | - | 191 | 76 | 104 | 29 | 94 | 27 | 44 | 15 |
| 160 | 1.96 | | | | | | | | | | | | 264 | 100 | 134 | 59 | 111 | 34 | 91 | 27 | 47 | 12 |
| 157 | 2.36 | | | | | | | | | | | | - | - | 178 | 75 | 64 | 22 | 83 | 25 | 54 | 17 |

## Table II AIII (d): Charpy Test Data - Normalized Plate, Longitudinal Direction

| Charge | Gauge | Condition | Position | | +75°F | | 0°F | | -25°F | | -50°F | | -75°F | | -100°F | | -125°F | | -150°F | | -175°F | |
|---|---|---|---|---|---|---|---|---|---|---|---|---|---|---|---|---|---|---|---|---|---|---|
| | | | | | ft-lb | % Shear | ft-lb | % Shear | ft-lb | % Shear | ft-lb | % Shear | ft-lb | % Shear | ft-lb | % Shear | ft-lb | % Shear | ft-lb | % Shear | ft-lb | % Shear |
| 967 | 0.75 | Norm | Subsurface | | | | 264 | 100 | | | | | 264 | 100 | | | 109 | 25 | 67 | 15 | | |
| 968 | 0.75 | | | | | | X | X | | | | | X | X | | | 254 | 100 | 105 | 27.5 | | |
| 969 | 0.75 | | | | | | X | X | | | | | X | X | | | 209 | 100 | 140 | 45 | | |
| 970 | 1.0 | | | | | | X | X | | | | | X | X | | | 187.5 | 72.5 | 92 | 22.5 | | |
| 971 | 1.0 | | | | | | X | X | | | | | X | X | | | 125 | 65 | - | - | | |
| 973 | 1.25 | | | | | | X | X | | | | | X | X | | | 264 | 100 | X | X | | |
| 974 | 1.25 | | | | | | X | X | | | | | X | X | | | 264 | 100 | X | X | | |
| 158 | 1.57 | | | | | | | | | | | | | | | | | | | | | |
| 161 | 1.57 | | | | | | | | | | | | | | | | | | | | | |
| 160 | 1.96 | | | | | | | | | | | | | | | | | | | | | |
| 157 | 2.36 | | | | | | | | | | | | | | | | | | | | | |
| 969 | 0.75 | Norm | Mid-Thickness | | | | X | X | | | | | X | X | | | 92 | 23 | 42 | 7.5 | | |
| 971 | 1.0 | | | | | | X | X | | | | | X | X | | | 65 | 15 | - | - | | |
| 973 | 1.25 | | | | | | X | X | | | | | X | X | | | 264 | 100 | X | X | | |
| 158 | 1.57 | | | | | | | | | | | | | | | | | | | | | |
| 161 | 1.57 | | | | | | | | | | | | | | | | | | | | | |
| 160 | 1.96 | | | | | | | | | | | | | | | | | | | | | |
| 157 | 2.36 | | | | | | | | | | | | | | | | | | | | | |
| 968 | 0.75 | Norm | 1/4 PT | | | | X | X | | | | | X | X | | | 62 | 15 | 46 | 100 | | |
| 970 | 1.0 | | | | | | X | X | | | | | X | X | | | 264 | 100 | 264 | 100 | | |
| 158 | 1.57 | | | | | | | | | | | | | | 264 | 100 | 264 | 100 | 200 | 73 | 96 | 27 |
| 161 | 1.57 | | | | | | | | | | | | | | X | X | X | X | 264 | 100 | 56 | 13 |
| 160 | 1.96 | | | | | | | | | | | | | | X | X | X | X | 264 | 100 | 151 | 53 |
| 157 | 2.36 | | | | | | | | | | | | | | X | X | 264 | 100 | 264 | 100 | 130 | 7 |

X = Not tested due to energy values exceeding impact tester's limitations.

Figure 1 AIII and 2 AIII show the Charpy energy and percent shear transition curves for both controlled rolled and normalized plate tested at the subsurface and plate mid-thickness positions.

For controlled rolled plate, note that:

- At the plate surface, there is little difference in the percent shear transition behavior over the entire gauge range [figure 1(a) AIII]. All plates showed similar 50 percent shear FATTs (≈75°F), which is accounted for by the similarity in grain size and degree of splitting at this position over the entire gauge range. In terms of energy absorption, however, the heavier thickness plates showed higher toughness. This results from the higher shelf energy in the thicker plate, which is in turn due to the effect of reducing the total length of inclusions with reduced strain during rolling.

- At the plate mid-thickness position, there is a significant deterioration in the Charpy percent shear transitions with increased gauge [figure 1(b) AIII]. This results primarily from the increase in grain size and percent pearlite with thickness. The Charpy 50 percent shear FATTs increased from ≈ -75°F at 0.75in to ≈ -25°F at 2.36in. The increase in transition temperature tends to offset the higher shelf energy at heavier gauges so that the energy transitions generally deteriorate with gauge.

- Longitudinal Charpy transition show both significantly higher shelf energies and lower 50 percent shear FATTs than transverse tests [figure 1(c) AIII]. It is not clear why the longitudinal percent shear transitions are improved compared with transverse transitions. It may partially relate to the finer ferrite grain dimension in the transverse to rolling direction. In addition, the longitudinal Charpies also showed a much greater degree of splitting (see figure 2 AIII) at low temperatures, which tends to artificially lower the 50 percent shear FATT.

**Figure 1 AIII: Charpy Transition Data, Controlled Rolled Plate**

**(a) Subsurface, Transverse Direction**

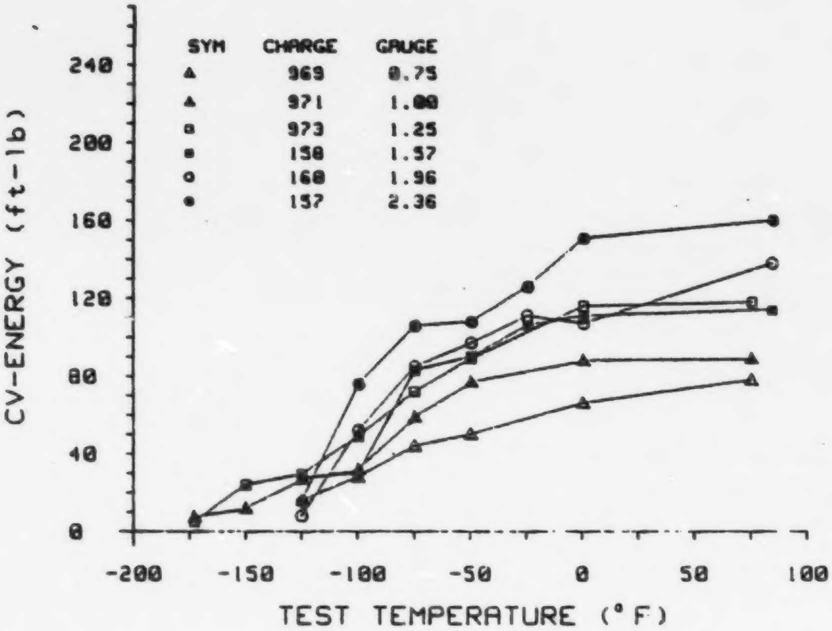

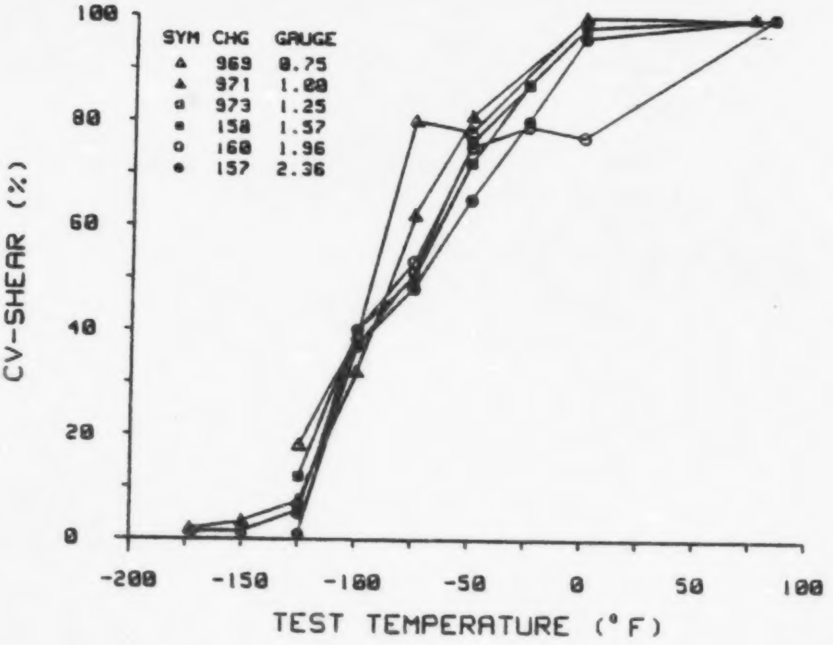

**Figure 1 AIII: Charpy Transition Data, Controlled Rolled Plate**

**(b) Mid-Thickness, Transverse Direction**

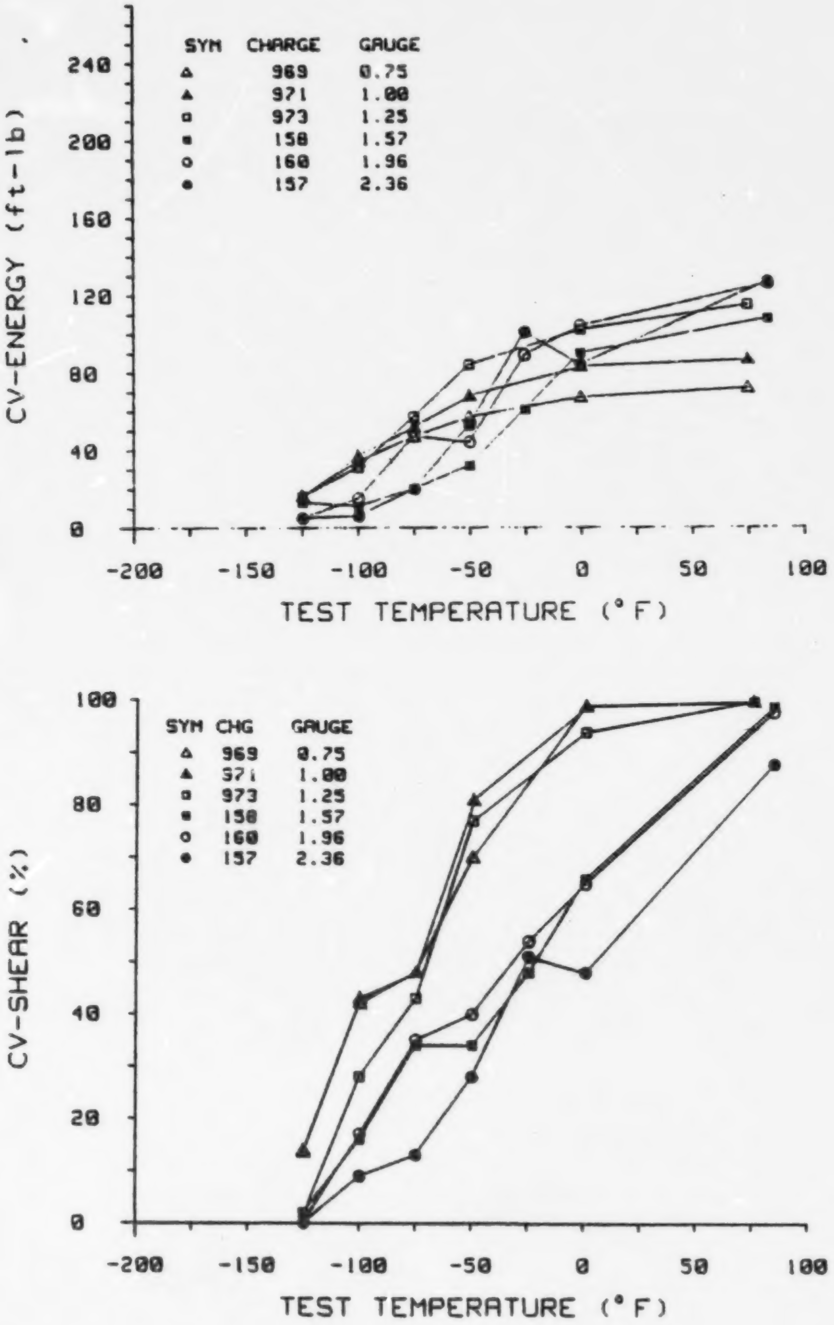

Figure 1 AIII: Charpy Transition Data, Controlled Rolled Plate

(c) Subsurface, Longitudinal Direction

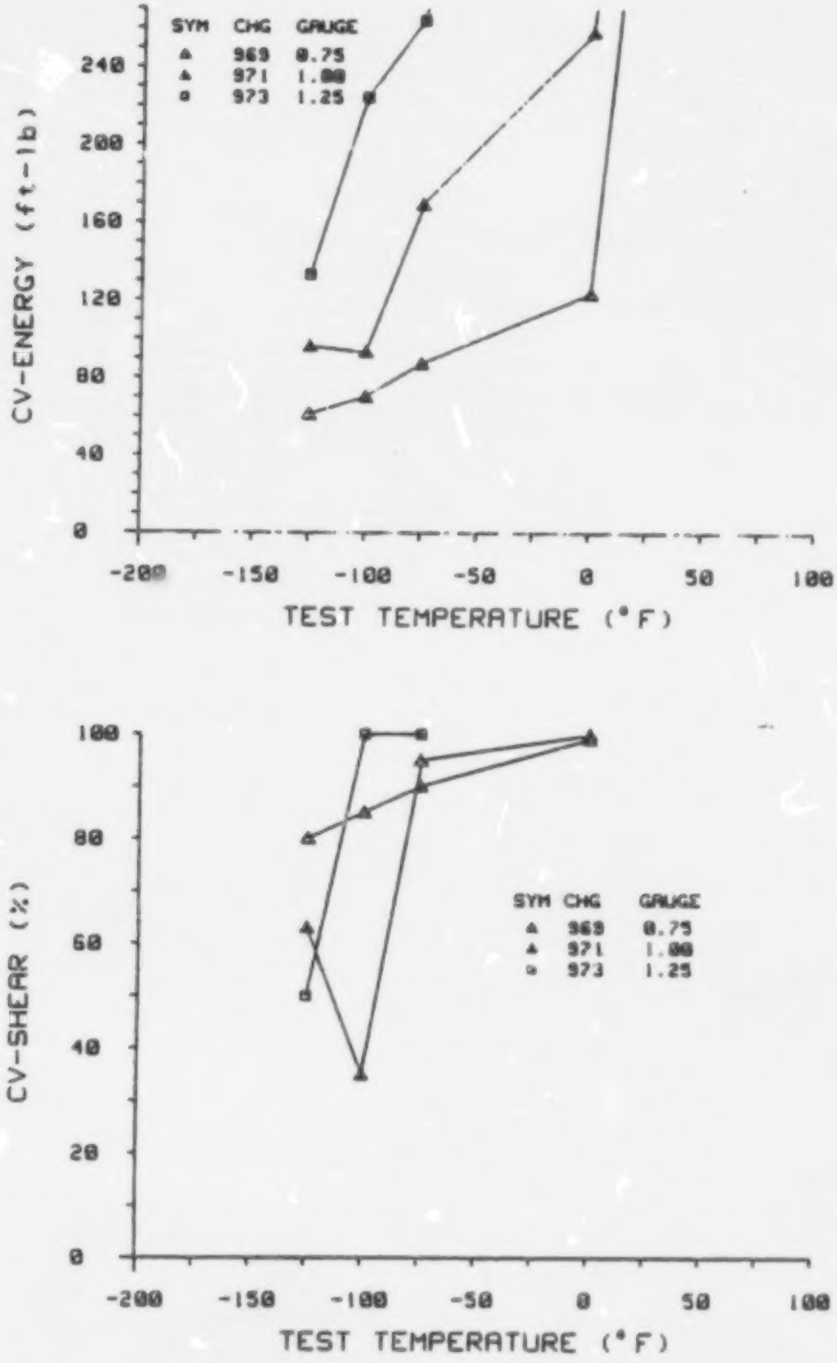

Figure 1 AIII: Charpy Transition Data, Controlled Rolled Plate

(d) Mid-Thickness, Longitudinal Direction

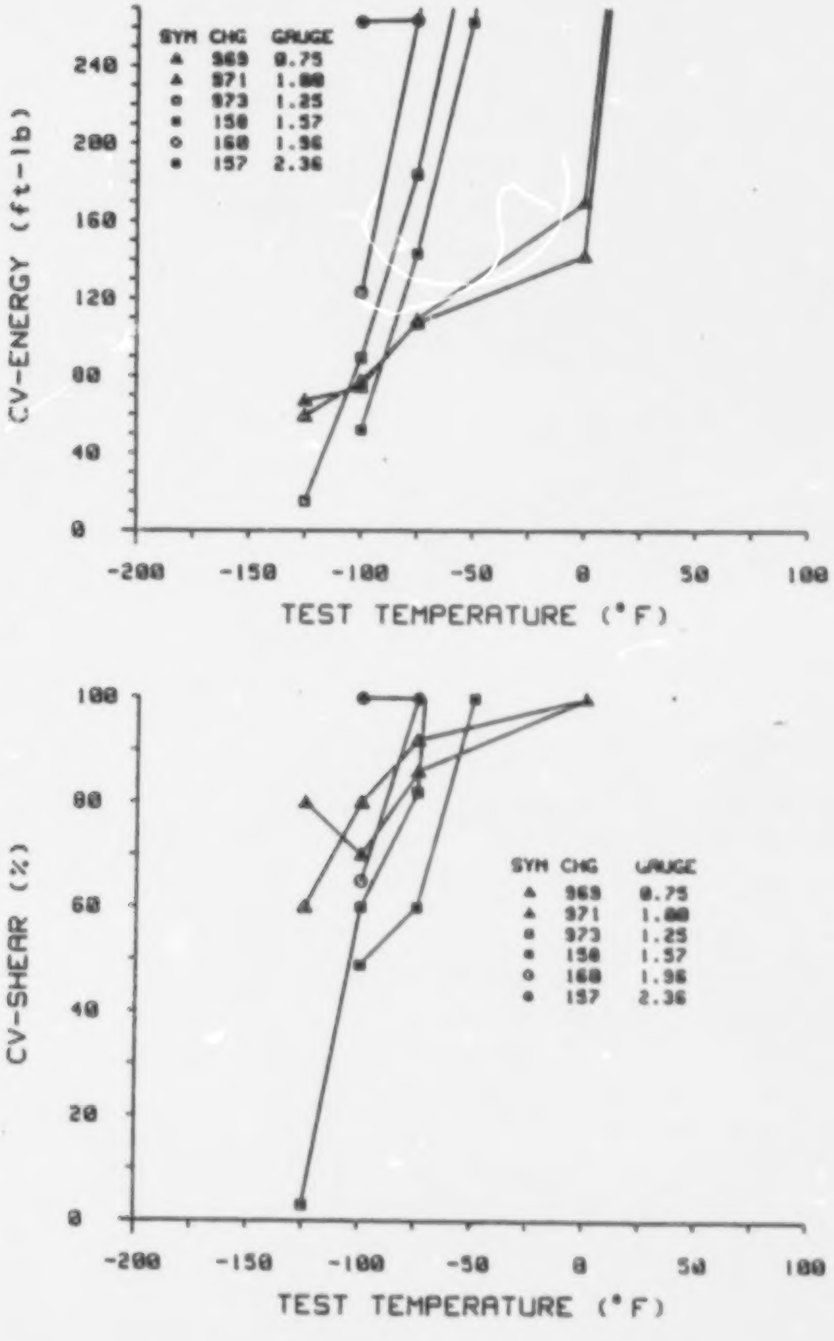

**Figure 2 AIII:**

(a) Transverse Orientation

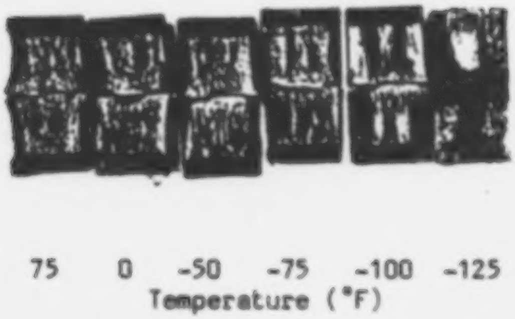

(b) Longitudinal Orientation

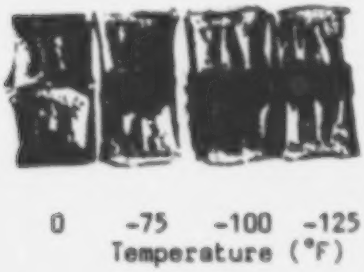

For normalized plate:

- There is no difference in the percent shear transition curves between the subsurface and mid-thickness positions [figure 3 (a) and (b) AIII]. The lighter gauge plates from the first rolling (0.75in to 1.25in) have slightly higher transitions than the heavier plates (1.57in to 2.36in) from the second rolling. This resulted from the slightly finer grain size achieved on the heavier plates normalized at 1650°F rather than 1700°F.
- The Charpy energy transition improves with increasing gauge because of the higher shelf energies of the heavier plate.

Figure 3 AIII: Charpy Transition Data, Normalized Plate

(a) Subsurface, Transverse Direction

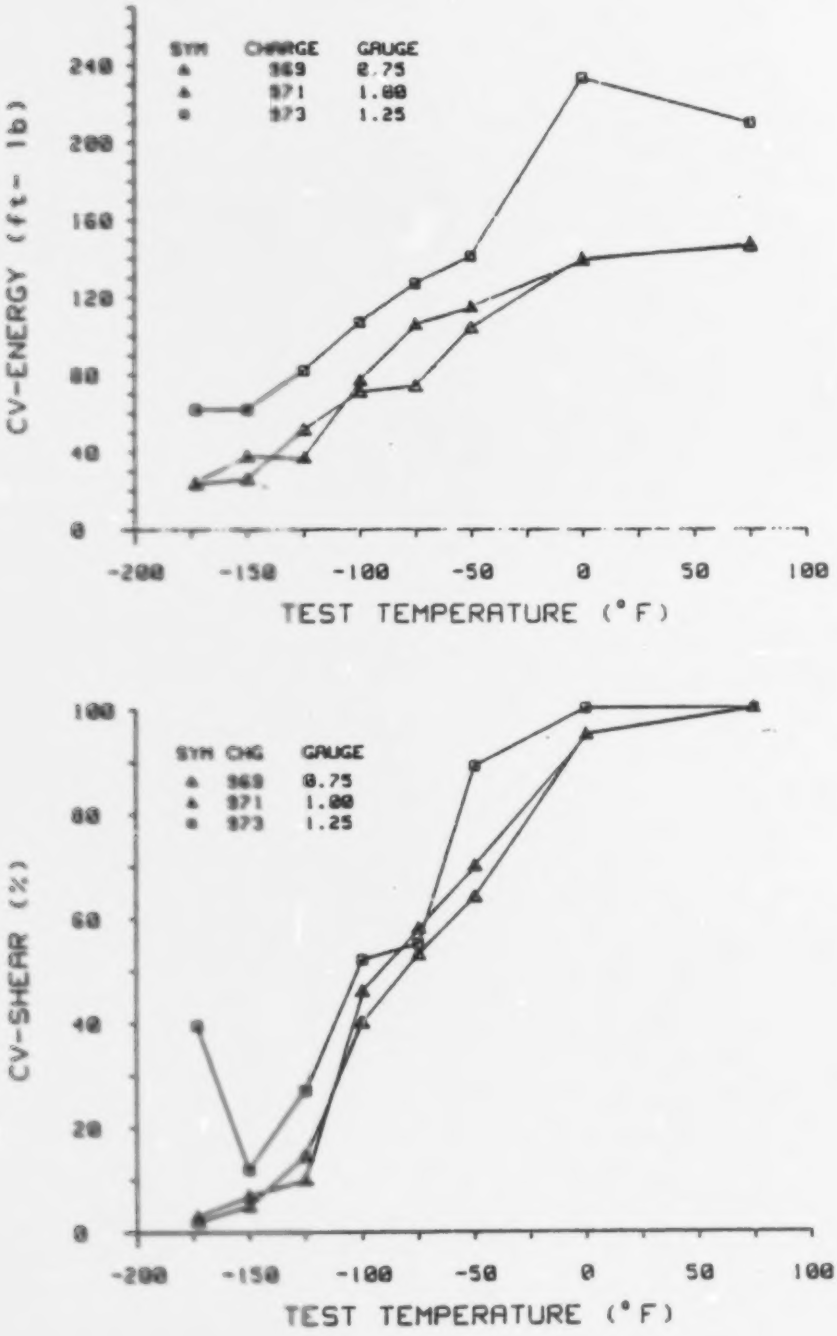

Figure 3 AIII: Charpy Transition Data, Normalized Plate

(b) Mid-Thickness, Transverse Direction

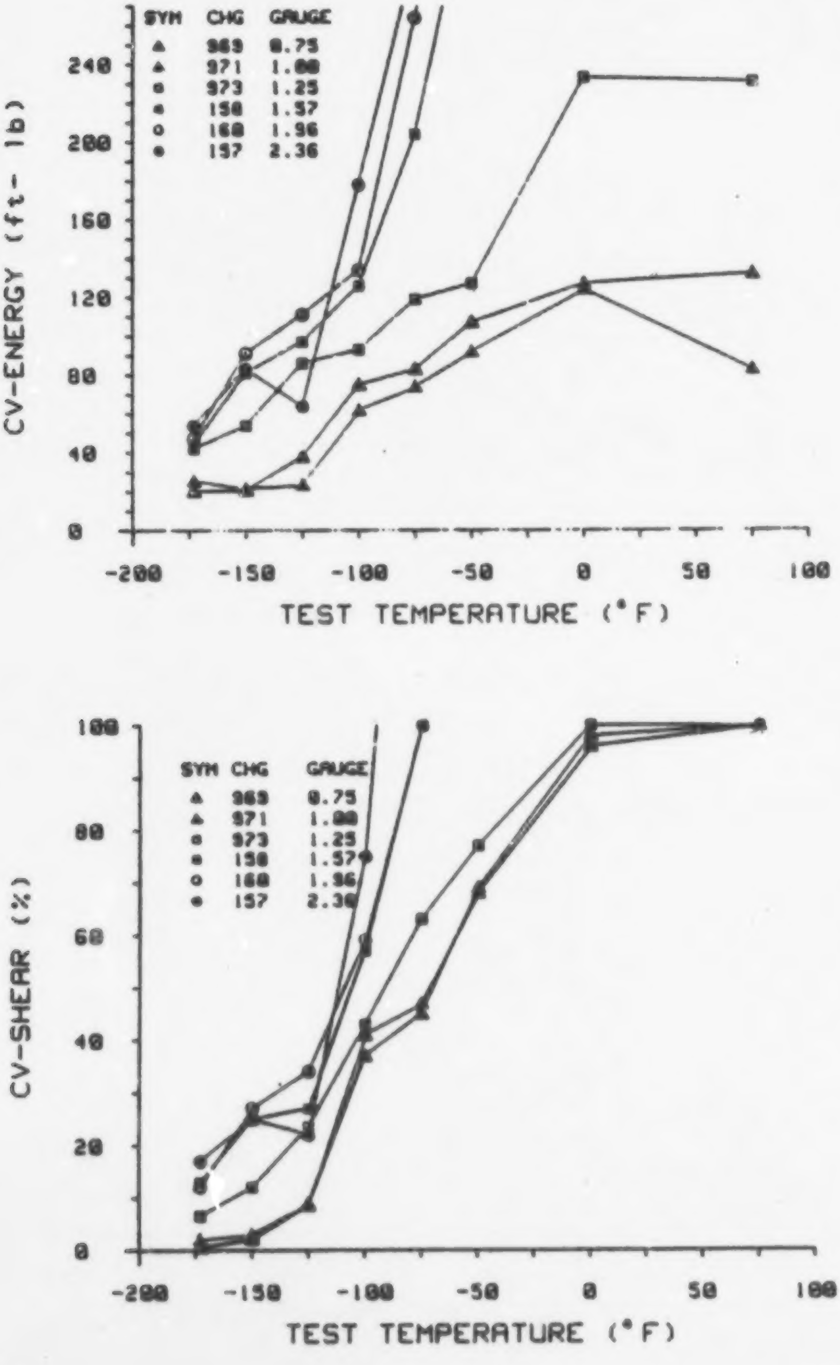

## Estimation of Impact Transition Temperature

The Charpy impact transition temperature (50 percent shear FATT) is largely dependent on the ferrite grain, the volume fraction of pearlite and the amount of dislocation/precipitation strengthening as shown in equation 1.

$$\begin{aligned} \text{ITT } (^\circ\text{C}) = -19 + 44\%\ \text{Si} + 700\ \sqrt{N_f} + 2.2\%\ \text{Pearlite} \\ - 11.5\ d^{-1/2} + \Delta\text{ppt}*2.8 \end{aligned} \qquad (1)$$

where: $N_f$ = weight percent free nitrogen

$d$ = mean ferrite grain size (mm)

$\Delta$ppt = yield strength increase due to precipitation strengthening (ksi)

The strength contribution from precipitation can be calculated using equation 2.

$$\begin{aligned} \text{Yield Strength (ksi)} = 7.8 + 4.7\%\ \text{Mn} + 12.0\%\ \text{Si} \\ + 51\%\ N_f + 2.5\ d^{-1/2} + \Delta\text{ppt} \end{aligned} \qquad (2)$$

Table III AIII summarizes the strength and metallographic data for several charges from Stelcoloy 70 trial rollings, and shows the calculated contributions to yield strength from grain size and precipitation strengthening. These were used to calculate ITTs assuming no free nitrogen. Generally there is fairly good agreement between the estimated and actual transition temperatures. Note that the actual ITTs of surface Charpies are generally lower than calculated. This is largely related to the effect of splitting on transition behavior.

## Table III AIII: Contributions to Yield Strength and FATT

| Charge No. | Gauge | Position | Strength | | Grain Size (µm) | | % Pearlite | | Calculated Yield Strength | | | Δ ITT (°C) | | | 50% FATT (°C) | |
|---|---|---|---|---|---|---|---|---|---|---|---|---|---|---|---|---|
| | | | Yield (ksi) | UTS (ksi) | $\bar{x}$ | Range | | | $\Delta d^{-1/2}$ (ksi) | $\Delta$ppt (ksi) | | $\Delta d^{-1/2}$ | $\Delta$P | $\Delta$ppt | Calc | Actual |
| 967 | 0.750 | S<br>M | 72.1 | 86.7 | 7.0<br>7.1 | 5.6 - 7.1 | 9.6 - 11.0 | | 28.4 | 26.7 | | 137<br>136 | 23 | 74 | -49<br>-48 | -65 |
| 968 | 0.750 | S<br>M | 71.3 | 85.4 | 6.2<br>6.3 | 5.3 - 6.1 | 11 - 12 | | 30.5 | 23.9 | | 146<br>145 | 25 | 66 | -64<br>-63 | -65 |
| 969 | 0.750 | S<br>M | 77.1 | 88.8 | 6.3<br>6.5 | 5.7 - 6.2 | 13 - 16.9 | | 29.7 | 30.5 | | 143<br>143 | 33 | 84 | -35<br>-35 | -65<br>-59 |
| 970 | 1.0 | S<br>M | 68.5 | 82.9 | 7.9<br>8.7 | 6.3 - 9.2 | 11.3 - 14.2 | | 26.7 | 24.9 | | 129<br>123 | 27 | 69 | -42<br>-36 | -62 |
| 971 | 1.0 | S<br>M | 69.0 | 81.6 | 6.3<br>7.2 | 6.0 - 7.4 | 11 - 14.7 | | 29.7 | 22.3 | | 143<br>136 | 28 | 62 | -62<br>-55 | -62<br>-57 |
| 973 | 1.25 | S<br>M | 64.2 | 78.7 | 8.0<br>10.1 | 7.3 - 9.1 | 11.6 - 14.8 | | 26.5 | 20.7 | | 127<br>115 | 28 | 57 | -51<br>-39 | -59<br>-49 |
| 974 | 1.25 | S<br>M | 63.0 | 77.9 | 8.2 | 7.4 - 8.7 | 8.9 - 14.6 | | 26.5 | 19.5 | | 127 | 36 | 54 | -56 | -59 |
| 158 | 1.57 | S<br>M | 63.0 | 77.4 | 8.7<br>10.7 | 7.9 - 10.1<br>10.1 - 11.2 | 17.6 - 20.7 | | 24.9 | 21.2 | | 120<br>111 | 40 | 58 | -31<br>-22 | -59<br>-32 |
| 161 | 1.57 | S<br>M | 63.9 | 77.4 | 8.4<br>9.6 | 8.1 - 9.1<br>9.1 - 10.2 | 16.9 - 22.7 | | 26.0 | 21.0 | | 125<br>117 | 45 | 58 | -31<br>-23 | <-100<br>-45 |
| 160 | 1.96 | S<br>M | 58.9 | 75.7 | 9.2<br>12.0 | 9.3 - 9.7<br>11.0 - 13.2 | 15.3 - 22.7 | | 24.4 | 17.5 | | 120<br>106 | 42 | 48 | -39<br>-23 | -62<br>-35 |
| 157 | 2.36 | S<br>M | 55.2 | 70.7 | 8.6<br>12.4 | 8.4 - 9.2<br>12 - 4 | 18.0 - 25.8 | | 22.9 | 15.4 | | 126<br>103 | 47 | 42 | -44<br>-33 | -59<br>-31 |

[1] S- Surface; M - Mid-Thickness

$$\text{Yield Strength (ksi)} = 7.8 + 4.7\%\ \text{Mn} + 12.0\%\ \text{Si} + 51\%\ \text{N}_f + 2.3\ d^{-1/2}$$

$$= 17 + 2.3\ d^{-1/2} + \Delta\text{ppt}$$

$$\text{ITT (°C)} = -19 + 44\%\ \text{Si} + 700\sqrt{\ \text{N}_f} + 2.2\%\ \text{P} - 11.5\ d^{-1/2} + \Delta\text{ppt} \cdot 2.8$$

## NDT Tests

The NDT results are shown in Table IV AIII.

**Table IV AIII: NDT Test Data**

| Charge No. | Gauge (in) | Condition | Direction | Position | NDT (°F) |
|---|---|---|---|---|---|
| 967 | 0.75 | CR | L | Rolled Surface | < -125 |
| | | | T | " | < -100 |
| | | N | L | " | < 100 |
| | | | T | " | < -100 |
| 968 | 0.75 | CR | T | " | < -100 |
| | | N | L | " | < -125 |
| 970 | 1.0 | CR | T | " | < -125 |
| | | | T | Sub-Surface | -90 |
| 973 | 1.25 | CR | T | Rolled Surface | < -100 |
| | | | T | Sub-Surface | -90 |

Most tests were made with the starter cracks on the rolled plate surface. In these cases the NDT temperatures were generally less than -100°F in both the controlled rolled and normalized conditions. For the 1.00in and 1.25in plates, NDTs were also fabricated with the starter cracks located as far as possible below the plate surface in order to evaluate the effect of coarser ferrite grain size on NDT. In these cases, the NDTs were significantly higher (-90°F as compared with <-100°F) than at the plate surface.

# STRENGTH AND TOUGHNESS OF STELCO OFFSHORE QUALITY PLATE

by

D. B. McCutcheon, Stelco Inc.

Work on this project was conducted under the auspices of the Canada Centre for Mineral and Energy Technology, Energy, Mines and Resources, Canada

| | |
|---|---|
| DSS File Number: | 23SQ.23440-2-9027-1 |
| DSS Contract Number: | 0SQ82-00211 |
| CANMET Project Number: | |
| CANMET Scientific Authority: | Dr. J. D. Boyd |

# SUMMARY

Development of Canada's East Coast and Arctic energy reserves will require a major tonnage of high toughness, Grade 350 plate. The low design temperatures of these regions (-30°C and -50°C, respectively) will demand plate steels with superior low temperature toughness. Stelco's ability to meet tentative strength and toughness requirements with either Hilton Works (HW), CAB-treated, ingot-cast or Lake Erie Works (LEW), strand-cast steels was assessed as part of the CANMET-sponsored project to evaluate the currenta ability of Canadian plate producers to supply to this market.

Two heats of Grade 350 plate were produced to optimum cleanliness steelamking practices at LEW and HW. The LEW chemistry was designed primarily for application in the controlled rolled condition, whereas the HW chemistry was designed for normalizing. Plates were rolled in thicknesses between 15 and 51 mm, and 19 and 101 mm for the LEW and HW heats, respectively. Plate strength, Charpy toughness, and nil-ductility temperature (NDT) were determined on both as-rolled and normalized plates. The Charpy impact transition data were analyzed in terms of the plate strengths and microstructures, and recommendations made for improving Charpy toughness. The Charpy impact energies for each plate thickness were compared with proposed standards for Canadian offshore construction.

The 0.07 C-Mn-Ni-Cr-V-Cb-Ti LEW chemistry met Grade 350 strength and toughness requirements for East Coast design temperatures in controlled rolled plate at thicknesses up to ≈38 mm.

The 0.13 C-Mn-Ni-V-Cb HW chemistry met Grade 350 strength and -30°C toughness requirements in the controlled rolled condition at thicknesses up to ≈32 mm. In the normalized condition, this chemistry is adequate for Grade 350 strength in thicknesses up to 100 mm, but has inadequate toughness for East Coast applications.

# CONTENTS

Background.................................................. 7

LEW Grade 350 Plate.......................................... 11

  Chemistry and Steelmaking Practice.............................. 11
  Controlled Rolling.............................................. 12
  Controlled Rolled Plate Microstructure and Mechanical Properties... 13
  Further Development of Heavy Plate Controlled Rolling.............. 22
  Normalized Plate Microstructures and Mechanical Properties......... 27
  Summary......................................................... 29

HW Grade 350 Plate........................................... 31

  Chemistry and Steelmaking Practice.............................. 31
  Controlled Rolling.............................................. 32
  Controlled Rolled Plate Microstructures and Mechanical Properties.. 33
  Further Development of Heavy Plate Controlled Rolling.............. 39
  Normalized Plate Microstructures and Mechanical Properties......... 39
  Summary......................................................... 42

References................................................... 44

Acknowledgments.............................................. 45

Appendix 1 - Austenite Grain Coarsening........................ 1 A1

Appendix 2 - Temperature Loss during Controlled Rolling........... 1 A2

Appendix 3 - Mechanical Properties and Microstructures
of Grade 350 Plate.................................. 1 A3

Appendix 4 - Cleanliness of Trial Heats........................ 1 A4

## BACKGROUND

The development of Canada's East Coast and Arctic oil and gas reserves during the next decade calls for the construction of production platforms and islands, tankers, ice-breakers, supply vessels, barges, dredges, and caissons. The exact timing of this development is uncertain, particularly considering the potential impact of the government's energy policy on exploration and the limited ability of Canadian fabricators to compete in this market; however, it is forecast that more than 30 000 tons per year of high quality heavy plate (>20 mm) will ultimately be absorbed by these projects.[1] Moreover, an order-of-magnitude greater tonnage of light gauge plate will also be required.

The Canadian government recognizes the benefit of having maximum participation by Canadian steel companies and fabricators in the supply of equipment to this market. In particular, they are concerned that the overspecification of steel property requirements (i.e. adoption of specifications based on a "best available quality" philosophy) could jeopardize the participation of Canadian steel companies. As a result, the Department of Energy, Mines and Resources established a preliminary research program to determine the ability of Canadian steelmakers to provide low temperature quality heavy plate, and to identify deficiencies in both processing and product quality requiring longer term research and development. Stelco participated in this 50 percent-funded program by characterizing the plate properties of both a CAB treated, Hilton Works (HW) ingot cast heat and a low sulfur, Lake Erie Works (LEW) strand cast heat.[2]

The specific property requirements for Canadian offshore construction have not been established; however, it is anticipated that they will closely follow those used by other nations and classification societies for similar structures. These have recently been reviewed for CANMET by Det Norske Veritas[3] and Lloyd's Register of Shipping,[4] and have been used to formulate a tentative aim specification for Arctic grade structural plate. The main requirements are shown in Table I.

**Table I: Aim Property Requirements for Arctic Grade Plate**

| | |
|---|---|
| Strength | 350 MPa Yield, 480 MPa UTS |
| Charpy Toughness | 40 J (transverse) at test temp |
| Weld HAZ Toughness | 0.25 mm CTOD at design temperature |
| Through-Thickness Ductility | 25% reduction of area |
| Ultrasonic Cleanliness | ASTM 578 Level 1 |

* test temperature dictated by application, structural category, thickness, and design temperature

Although these requirements will need to be met in plate thicknesses between ≈15 and 100 mm, the largest proportion of the plate tonnage will be in thicknesses between 20 and 50 mm.

These property requirements are typical of the steel quality supplied for North Sea construction, with one major difference - Canadian design temperatures are significantly lower. Three design temperatures have been recognized for Canadian frontier projects. For above water structures, the minimum service temperatures on the East Coast and Arctic are -30°C and -50°C, respectively. For submerged structures, the design temperature is assumed to be -5°C.

The Charpy energy requirements anticipated for low temperature service are dependent on several factors including the type of structure (mobile or fixed), the structural category, the plate thickness and the design temperature. Generally, the Charpy energy specifications for fixed structures are more stringent than for mobile units because of obvious differences in ease of inspection and repair. Specifications do not yet exist for Canadian waters. The CSA Task Group on Steel Fixed Offshore Structures and the Canadian Coast Guard are addressing this problem. Figure 1 shows the proposed interim standard for Arctic class ships, and, as an example, the DnV Rules for fixed structures. The Canadian Charpy energy requirements are expected to be higher than used in the North Sea, and it is anticipated that transverse testing will be specified. For development purposes it has been assumed that we will need to meet a minimum transverse Charpy energy of 40 J for Grade 350 plate. This energy level is slightly higher than specified by most classification societies; however, given the uncertainty in Canadian specifications plus the ability of several offshore producers (notably the Japanese) to provide very high impact toughness at low temperatures, we felt it was necessary to set a conservative aim requirement. A recent plate inquiry from the Canadian Coast Guard requested 68 J in both the longitudinal and transverse orientations.

**Figure 1 (a): Proposed Standard for Charpy Impact Requirements for Canadian Offshore Plate**

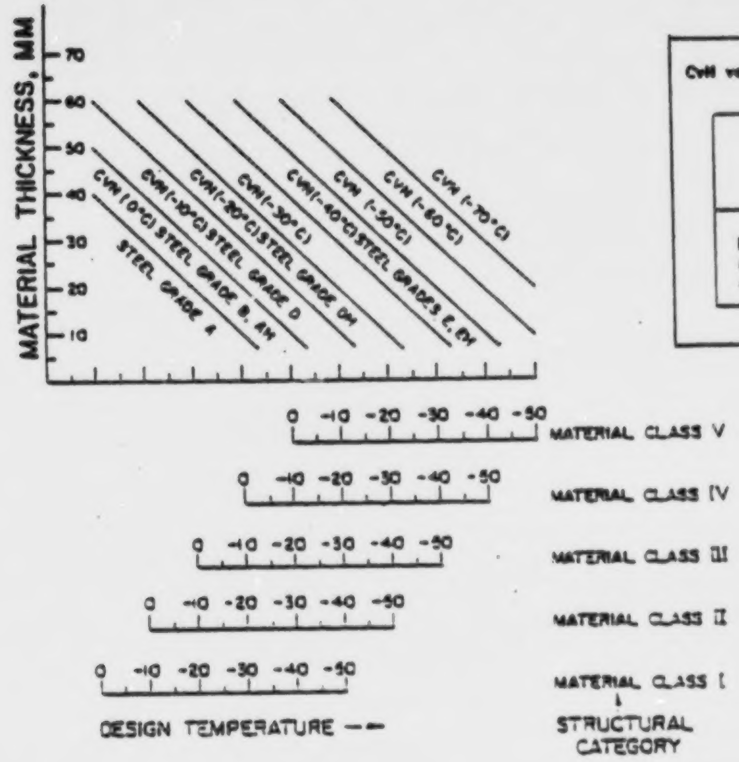

CvN values proposed for acceptance of steel grades

| Grade | Yield (MPa) | Average CvN Energy (J) | |
|---|---|---|---|
| | | Long | Trans |
| B, D, E | 235 | 27 | 20 |
| A32, D32, E32 | 315 | 31 | 22 |
| A36, D36, E36 | 355 | 34 | 24 |

**Figure 1 (b): Impact Requirements According to DnV Rules for Fixed Structures**

Impact testing temperature

| Material thickness, t mm | Special structural steel | Primary structural steel | Secondary structural steel |
|---|---|---|---|
| t≤12.5 | $T = T_D$ | $T = T_D$ | |
| 12.5<t≤25.5 | $T = T_D - 20$ | $T = T_D$ | |
| 25.5<t≤50 | $T = T_D - 40$ | $T = T_D - 20$ | $T = T_D$ |
| t>50 | $T = T_D - 40$ | $T = T_D - 40$ | $T = T_D - 20$ |

T = Impact testing temperature (°C)
$T_D$ = Design temperature (°C)

For 355 MPa yield strength:

| | |
|---|---|
| Transverse CvN Energy | 24 J |
| Longitudinal CvN Energy | 35 J |

Most steels used in offshore construction have in the past been supplied in the normalized condition. However, in the last five years there has been an increased application of controlled rolled steels for these structures. Recently, Japanese producers have also developed controlled rolled and water spray cooled plate.[5] The main advantages of replacing normalizing with these alternate approaches are:

- the lower cost of controlled rolling compared with normalizing, and
- the improved weldability (resistance to hydrogen induced cold cracking) of lower carbon equivalent controlled rolled chemistries.

Moreover, for low temperature applications, the best controlled rolled and spray cooled plate has superior toughness to normalized plate. There is a significant cost incentive (≈$120/ton) for Stelco to develop controlled rolled plate in the heaviest possible thickness as an alternative to normalizing at CHT. However, there are penalties associated with controlled rolling in terms of reduced mill productivity, poorer gauge performance, and increased mill wear and powering requirements. These aspects have been considered as part of these trials[6] and have been reported elsewhere.

Although controlled rolled steels are generally more weldable, primarily because of their reduced carbon content, there is considerable concern that they have poor weld heat-affected zone (HAZ) toughness. This is believed to result from the use of microalloys (Cb and V) to achieve the required strength levels and grain refinement in heavy plate at reduced carbon contents. Several studies are currently underway to characterize the HAZ toughness of the newly developed plate chemistries,[7,8] and Stelco is participating in the group sponsored project at The Welding Institute (UK). As part of our project we have characterized both the HAZ toughness and weldability of our trial heats, as described in R&D Report 85R009.

As well as meeting Charpy toughness requirements, a small percentage of the tonnage used for offshore platforms and ships will need to meet through-thickness ductility requirements to ensure adequate lamellar tearing resistance in highly restrained weldments. Both the LEW and HW trial heats were produced to the Stelco's "best" cleanliness steelmaking and casting practices and were extensively tested for susceptibility to lamellar tearing. These results are presented in a separate R&D report.[9]

This report details the plate strength and toughness achieved in plate from the LEW and HW trial heats in both the controlled rolled and normalized conditions. The trial heats were made, rolled and tested by the Research, Metallurgical and Operating Departments during the period May 1983 to June 1984.

# LEW GRADE 350 PLATE

## Chemistry and Steelmaking Practice

The LEW heat was produced to the chemistry shown in Table II. The main factors considered in the design of this analysis are shown in Table III. Originally, it was proposed that the heat be produced at 0.12 percent C, however, this was not supported by LEW Metallurgical because of the tendency to increase transverse slab cracking when casting in the peritectic carbon range (0.08 - 0.14 percent). In recognition of the deleterious effect of higher carbon content (>0.14 percent) on impact transition temperature the heat was produced at a low carbon content. To make up for the reduction in strength, particularly UTS, at this low carbon content, chromium and vanadium additions were made.

Table II: Heat Chemistry - 805126

| C | Mn | P | S | Si | Ni | Cr | V | Cb | Ti | ASA | N |
|---|---|---|---|---|---|---|---|---|---|---|---|
| 0.07 | 1.43 | 0.004 | 0.003 | 0.29 | 0.25 | 0.25 | 0.075 | 0.022 | 0.011 | 0.035 | 0.007 |

Table III: Design of Chemistry for LEW Grade 350 Plate

| Element | Aim | Effect | Restriction |
|---|---|---|---|
| C | 0.07 | • increased pearlite content increases UTS<br>• little effect on yield | • 0.09 - 0.014 range gives transverse slab cracking<br>• weldability<br>• increased FATT |
| Mn | 1.40 | • solid solution strengthening<br>• ferrite grain refinement through $Ar_3$ reduction | • centerline segregation<br>• bainite formation (increased FATT) |
| Cb | 0.02 | • ferrite grain refinement by controlled rolling<br>• precipitation strengthening | • promotes low toughness HAZ structures |
| V | 0.07 | • precipitation strengthening | • reduce HAZ toughness due to strain aging |
| Ti | 0.01 | • austenite grain size control during reheating; improved HAZ toughness | • reduced precipitation strengthening<br>• >3.4 Ti/N reduces HAZ toughness |
| Cr | 0.25 | • increased UTS through effect on pearlite transformation<br>• little solid solution strengthening | • bainite formation (increased FATT) |
| Ni | 0.25 | • reduced FATT<br>• little solid solution strengthening | |

A key consideration in producing the heat was high cleanliness required for both improved lamellar tearing resistance and Charpy toughness. The low sulfur content (0.004 percent) was achieved by using desulfurized hot metal and low sulfur scrap, and tapping the BOF onto 2200 lb of Canadex desulfurizing reagent. To reduce the fraction of quarter point alumina inclusions, the heat was cast with a fused silica ladle-to-tundish shroud, and an alumina-graphite tundish-to-mold shroud.

## Controlled Rolling

A total of 20 slabs were rolled to plate thicknesses between 15 and 51 mm (Table IV). The 15 and 30 mm plates were produced specifically for CANMET as test plate for corrosion fatigue and welding trials.

Table IV: Plate Controlled Rolling Practice

| Charge No. | Gauge (mm) | Width (mm) | Breakdown Bar Thickness (mm) | % Reduction Below Temperature (°C) | | | | Finish Temp (°C) | Delay Time (sec) | Total Time (sec) |
|---|---|---|---|---|---|---|---|---|---|---|
| | | | | 900 | 870 | 840 | 815 | | | |
| 24 | 19 | 2438 | 57 | 70.1 | 70.1 | 56.0 | 30.1 | 760 | 29 | 385 |
| 25 | | | | 70.6 | 70.6 | 23.4 | 23.4 | 750 | 34 | 417 |
| 26 | 25 | 2438 | 76 | 69.0 | 63.9 | 40.0 | 30.8 | 765 | 69 | 414 |
| 27 | | | | 68.8 | 57.9 | 40.4 | 21.7 | 750 | 72 | 451 |
| 28 | 32 | 2438 | 95 | 68.0 | 24.5 | 7.7 | 7.7 | 810 | 66 | 401 |
| 29 | | | | 67.8 | 22.6 | 7.7 | 7.7 | 785 | 54 | 422 |
| 30 | 38 | 2438 | 114 | 66.6 | 36.0 | 6.3 | 0 | 840 | 26 | 452 |
| 31 | | | | | | | | | | |
| 32 | 44 | 1829 | 133 | 67.6 | 8.3 | 0 | 0 | 860 | 126 | 391 |
| 33 | | | | 25.6 | 5.9 | 0 | 0 | 860 | 91 | 372 |
| 34 | 51 | 1829 | 152 | 0 | 0 | 0 | 0 | 890 | 96 | 373 |
| 35 | | | | 0 | 0 | 0 | 0 | 890 | 78 | 333 |
| 3 | 30 | 2972 | 90 | 68.1 | 57.8 | 30.9 | 30.9 | 760 | 71 | 514 |
| 36 | 15 | 2438 | 45 | 74.6 | 70.0 | 46.9 | 0 | 800 | 32 | 333 |

All plates were controlled rolled to practices designed to achieve a fine ferrite grain size. The main features of the rolling practice were:

- 1175°C (2150°F) maximum reheat temperature,
- 3:1 reduction ratio below 900°C (1650°F), and
- finishing temperature above the $Ar_3$ temperature.

A relatively low reheating temperature practice was used to limit austenite grain coarsening prior to rolling, and to reduce the holding time between roughing and finishing. Grain coarsening studies on samples taken from the as-cast slabs (Appendix 1) demonstrated that the austenite grain size could be restricted to less than 30 µm with a 1175°C maximum reheating temperature.

The trial was rolled entirely on the 4-high finishing stand of the plate mill to allow a heavy drafting practice to achieve improved grain refinement, particularly during roughing. Experimental work on the effect of pass reduction on austenite grain development during rolling has demonstrated that relatively light drafts of five to ten percent (which are typical of those used on the 2-high rougher) result in grain coarsening during high temperature rolling.[10-12] To avoid this, the 4-high-only rolling practices were designed based on previous rolling data to use maximum permissible drafts (10 to 15 percent) while staying within the mill limits of separating force, torque and horsepower. The mill powering and separating force were monitored for each pass during this trial, and these data have been analyzed to provide guidelines for production controlled rolling of these grades (R&D 840061).

The rolling practices given each bar are summarized in Table IV. Although the 3:1 reduction ratio criterion was met for plate thicknesses below ≈30 mm, as the finished plate thickness increased the percentage reduction below 870°C decreased and the finishing temperature increased. Examples of the plate surface temperature-decay measured during rolling are given in Appendix 2. For plate gauges over 30 mm, there was progressively less temperature loss during finishing as the breakdown bar thickness increased. As will be shown in the subsequent section on plate properties, the higher rolling temperatures of the heavier plate resulted in a significant deterioration in plate grain size and Charpy toughness.

## Controlled Rolled Plate Microstructure and Mechanical Properties

### 1. Microstructure

Full thickness metallographic samples were taken from the quarter width position of each plate. After polishing and etching, the ferrite grain size and volume fractions of pearlite and ferrite were measured at several positions through each plate thickness using the QTM 720 image analyzer.

All plate had polygonal ferrite-pearlite microstructures. Representative microstructures from the range of plate gauges rolled are shown in Appendix 3. The ferrite grain size was dependent on both the plate gauge and the position through the thickness. As shown in Appendix 3, at 19 mm, a ferrite grain size of ≈7 µm was achieved. It was maintained below 10 µm at gauges up to 30 mm, but increased significantly in heavier plate, and was over 15 µm at 51 mm. The volume fraction of pearlite ranged from ≈14 percent in the lighter plate down to ≈11 percent in the heavier plate.

2. Strength

The as-rolled plate yield and UTS decreased significantly with increased plate thickness (Figure 2). At 32 mm, the UTS failed to meet the aim requirement. Similarly, at 44 mm, the yield strength was less than specified for grade 350 plate.

**Figure 2: The Effect of Thickness on Yield and Ultimate Tensile Strength - Controlled Rolled**

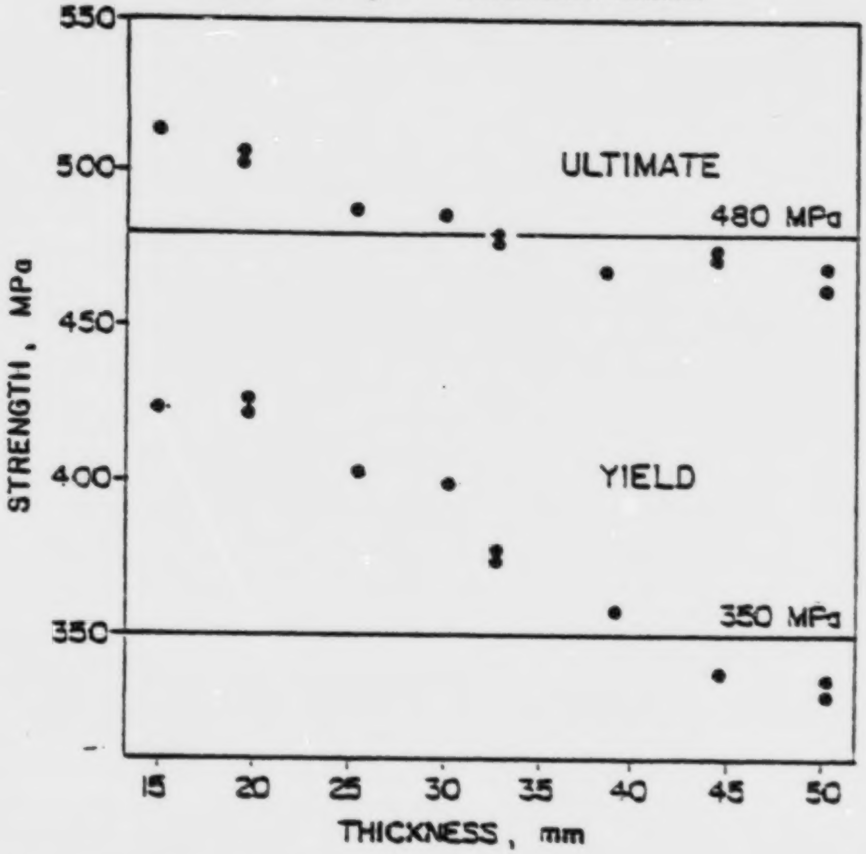

To establish what might be done to modify the chemistry or processing to meet the strength requirements, we have calculated the effective contribution to yield strength from precipitation and dislocation strengthening (Appendix 3) using previously developed relationships for the effects of grain size, solid solution strengthening, and lattice friction. These results are summarized in Figure 3. Compared with the data developed previously on the plate rolled from the LEW Stelcoloy 70 heat, the new chemistry showed significantly lower precipitation and dislocation strengthening. The earlier heat, with 0.05 Cb and 0.05 V (and with no titanium addition) gave σ (ppt) + σ (dislocation strengthening) ranging from ≈200 MPa at 19 mm to ≈125 MPa at 50 mm. The strengthening of the new chemistry was only 90 MPa at 19 mm, and 70 MPa at 50 mm.

**Figure 3: The Calculated Effect of Contributions to Yield Strength**

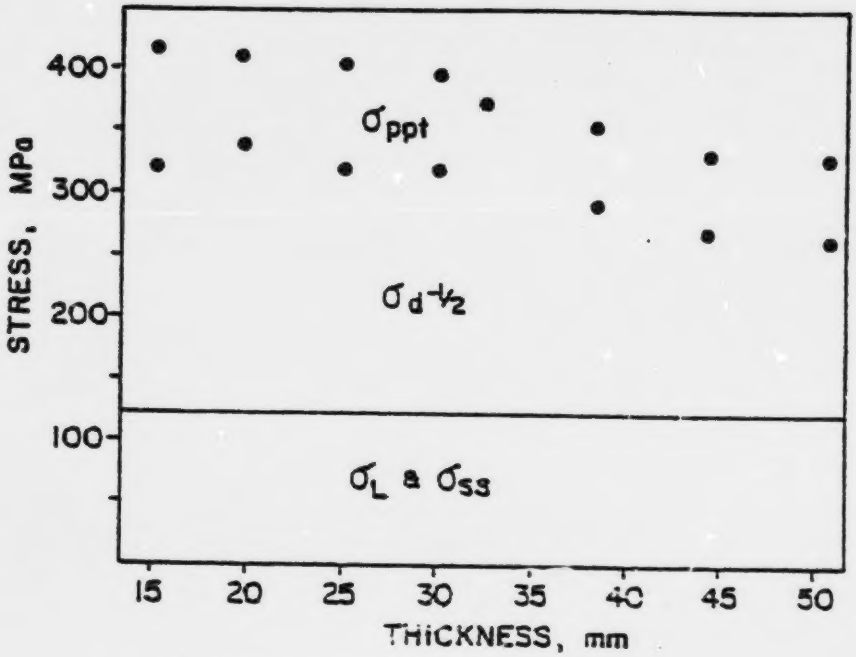

$$\sigma\ (\mathrm{MPa}) = 124.2 + 17.4\, d^{-1/2} + \sigma_{ppt}$$

where: ppt = precipitation contribution

$d^{-1/2}$ = grain size contribution
L = lattice friction
SS = solid solution contribution

The difference in strengthening on the two heats was a result of:

- the lower Cb level of the new heat. Although the vanadium level of the new heat was raised to 0.07 percent to offset the reduction in Cb, it appears that vanadium is not as effective a strengthener, particularly at low carbon contents (<0.10 percent).
- The 0.01 percent titanium addition to the new heat. A 0.010 percent Ti addition removes ≈0.003 percent N from solution as TiN. This reduces the fraction of VN available for strengthening. In addition, some of the vanadium is tied up in relatively large, complex TiVCb (C,N) primary precipitates formed in the cast slab. Moreover, a significant fraction of the precipitation in the ferrite can occur on coarse TiN type primary particles, and,
- the finishing temperature of the plates rolled from the latest heat was significantly higher than those rolled from the previous Stelcoloy 70 heat. It is possible that part of the

strengthening attributed to precipitation on the earlier heat was a result of dislocations and texture resulting from deformation at or below the $Ar_3$ temperature.

It should be possible to meet the grade 350 strength requirements in the controlled rolled condition in gauges up to 50 mm. Modification of the controlled rolling practice for improved ferrite grain refinement, particularly in heavier gauges, could increase the yield strength to meet grade 350 strength with minimal preciptation strengthening. Although this would not result in a direct improvement in UTS, the necessary reduction of the finishing temperature would result in a higher UTS through dislocation/textural strengthening. A considerable improvement in UTS could also be realized by increasing the carbon content range to 0.08 - 0.10 and would possibly allow removal of the vanadium addition, which has a deleterious effect on HAZ toughness.

## 3. Charpy Toughness

Transverse, full size Charpy V-notch transition curves were determined from the quarter width position of each plate. For plate thicknesses up to 25 mm the Charpies were taken from the plate surface position. For 30 and 32 mm plate, additional tests were taken from the plate centerline position, and in the heaviest plate, tests were done at both the quarter and mid-thickness locations.

All tests were done using the ISO, rather than ASTM striker geometry. The shelf energy of this high cleanliness, relatively low strength steel exceeded the capacity of the Stelco Charpy machines (≈350 J) when using the ASTM striker, and hence there was a risk of damaging them. Extensive testing by the JISI[13] and The Welding Institute[14] has demonstrated that the ISO striker gives significantly lower shelf energy than the ASTM striker. Preliminary testing of several plates using both geometries of striker confirmed that the ISO striker lowered the Charpy shelf energy sufficiently to allow testing on our machines, and did not significantly alter the Charpy energy absorption at energies below ≈135 J. No difference in the 50 percent shear FATT was observed between the strikers.

The Charpy energy data and representative plots of the energy and shear transition curves are summarized in Appendix 3. These results are shown in Table V in terms of the 40 J and 68 J transition temperature, as well as the 50 percent shear transition temperature, for each plate and test position. The transition temperature values were determined from lower bound curves, and thus they represent a conservative estimate of our ability. Included in this Table is an estimate of the design temperature to which the plate could be applied, assuming the criteria proposed for class V structures. It is important to recognize that cold work and subsequent strain aging resulting from tubular forming can significantly increase the Charpy FATT, and thus raise the design temperature to which the plate could be applied.

**Table V: Summary of Impact Toughness of LEW Controlled Rolled Plate**

| Gauge (mm) | Charge No. | Position | 40 J TT (°C) | 68 J TT (°C) | 50% FATT (°C) | Design* Temp (°C) |
|---|---|---|---|---|---|---|
| 15 | 36 | Sur | -70 | -65 | -55 | -50 |
| 19 | 24 | Sur | -85 | -80 | -80 | -50 |
| 19 | 25 | Sur | -95 | -90 | -80 | -50 |
| 25 | 26 | Sur | -85 | -80 | -70 | -50 |
|  | 27 | Sur | -85 | -85 | -85 | -50 |
| 30 | 3 | Sur | <-90 | <-90 | -70 | -50 |
|  |  | Mid | -85 | -80 | -55 |  |
| 32 | 28 | Sur | -85 | -80 | -55 | -50 |
|  |  | Mid | -85 | -80 | -40 |  |
|  | 29 | Mid | -70 | -65 | -55 | -50 |
| 38 | 30 | 1/4 | -85 | -80 | -50 | -30 |
|  |  | Mid | -55 | -50 | -35 |  |
| 44 | 32 | 1/4 | -55 | -50 | -25 | >-10 |
|  |  | Mid | -25 | -10 | +5 |  |
|  | 33 | 3/4 | -55 | -50 | -40 | >-10 |
|  |  | Mid | -35 | -35 | -35 |  |
| 51 | 34 | 1/4 | -65 | -65 | -65 | >-10 |
|  |  | Mid | -35 | -35 | -20 |  |
|  | 35 | 1/4 | -65 | -65 | -45 | >-10 |
|  |  | Mid | -30 | -25 | -15 |  |

* based on Coast Guard interim standard

These data indicate that the LEW chemistry has adequate strength and Charpy toughness for applications at -50°C design temperature in thicknesses up to ≈32 mm in the controlled rolled condition. At heavier thicknesses, the increase in Charpy FATTs and corresponding increase in toughness requirement (see Figure 1) makes this chemistry unsuitable for -30°C design temperature at thicknesses above ≈40 mm.

Table V also illustrates the significant increase in FATT and corresponding Charpy energy transition temperature with increased plate gauge. Whereas in plate thicknesses below ≈32 mm the FATTs are below -70°C, in heavier gauge plate the transition temperature increases to greater than -30°C, particularly at the plate mid-thickness.

Estimates of the 50 percent FATT based on grain size, volume percent pearlite, and dislocation and precipitation strengthening agree fairly well with the measured results, except at plate mid-thickness location for which the FATTs are considerably higher (worse) than expected (Figure 4). The reason for this discrepancy is not clear; however, it could be related to either bainite formation due to centreline segregation or to an increase in grain boundary carbide thickness particularly at heavier gauges. Mintz et al[15] have demonstrated the significant effect of increasing carbide thickness on the 27 J transition temperature of ferrite-pearlite and pearlite-free steels. Increases in the order of 60°C in FATT have been related to increased grain boundary carbide dimension.

**Figure 4: Comparison of Actual and Predicted 50% Shear FATT based on Grain Size and Chemistry**

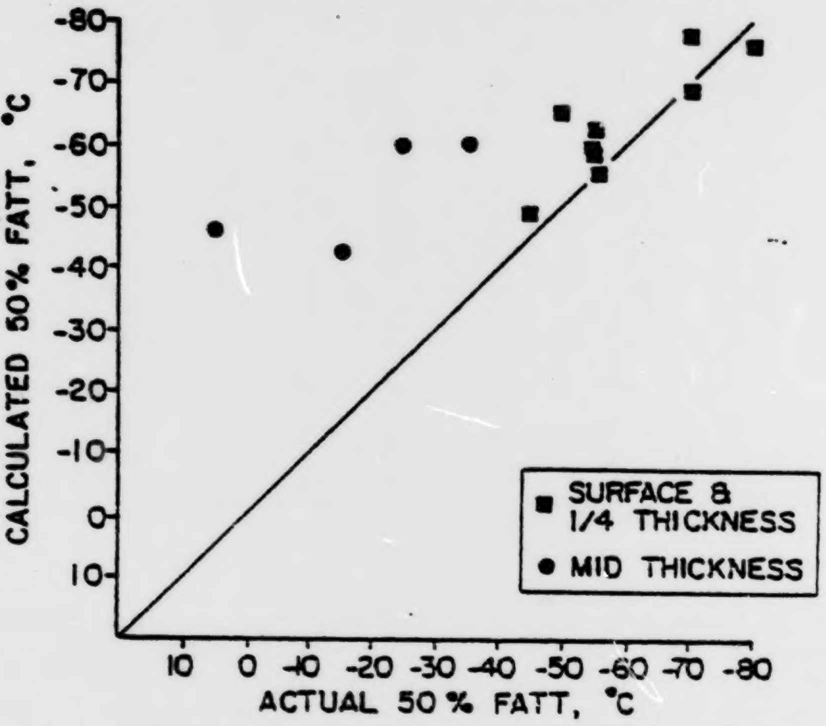

$$\mathrm{ITT}(\ \mathrm{C}) = -19 + 44\%\,\mathrm{Si} + 700\sqrt{N_f} + 2.2\,\%\,\mathrm{P} - 11.5\,d^{-1/2} + 0.41\,\sigma_{ppt}$$

Si - Silicon
$N_f$ - % free nitrogen
P - Pearlite
d - ferrite grain size (mm)
$\sigma_{ppt}$ - precipitation strengthening contribution (MPa)

It is not clear whether the low toughness at the mid-thickness position is critical to service performance. Present plate specifications do not require Charpy testing at this position. However, several offshore producers are currently evaluating the significance of this zone of low toughness. If significant, control of centerline segregation in strand cast slabs could become mandatory.

4. Nil Ductility Temperature

To further evaluate the brittle fracture initiation resistance at selected plate thicknesses, nil ductility tests (NDT) were carried out in accordance with ASTM E208 using the P-2 specimen (19 x 127 x 51 mm, t x l x w). Tests were done with starter weld beads on both the as-rolled plate surface and subsurface locations to assess the effect of differences in the through-thickness grain size on fracture resistance.

The NDT results are shown in Table VI. For comparison, the 40 J transition temperatures are also given. There is fairly good agreement between these two measures of initiation temperature. Both measures illustrate the increase in transition temperature with increasing plate thickness, particularly at the plate centerline position.

**Table VI: Nil Ductility Temperatures - LEW Controlled Rolled Plate**

| Gauge (mm) | Charge No. | Position | NDT (°C) | 40 J TT (°C) |
|---|---|---|---|---|
| 19 | 24 | Surface | -80 | -85 |
| 25 | 26 | Subsurface | -55 | -85 |
| 32 | 28 | Subsurface | -60 | -85 |
| 38 | 30 | Surface | -75 | -85 |
|  |  | Centerline | -60 | -55 |
| 44 | 32 | Centerline | -40 | -25 |
| 51 | 34 | Centerline | -45 | -35 |

The NDT temperature can be used in conjunction with the fracture analysis diagram to provide guidelines for steel usage in structures requiring fracture arrest capability (e.g. ships). Figure 5 shows the design-reference graph for fracture arrest curves, and defines the NDT relative to the nominal stress level for different plate thicknesses.[16] For welded ship hulls, in which the primary load carrying members in the main stress regions of the ship operate at up to ≈1/2 yield stress, the plate NDT temperatures must be 14°C and 22°C below the minimum operating temperature for 25 and 37 mm plate, respectively. Applying these criteria to LEW controlled rolled plate suggests that it may be applied to East Coast operating temperatures in thicknesses up to 38 mm, and to Arctic conditions up to ≈20 mm.

Figure 5: **Design Reference Graph for Fracture-Arrest Curves**

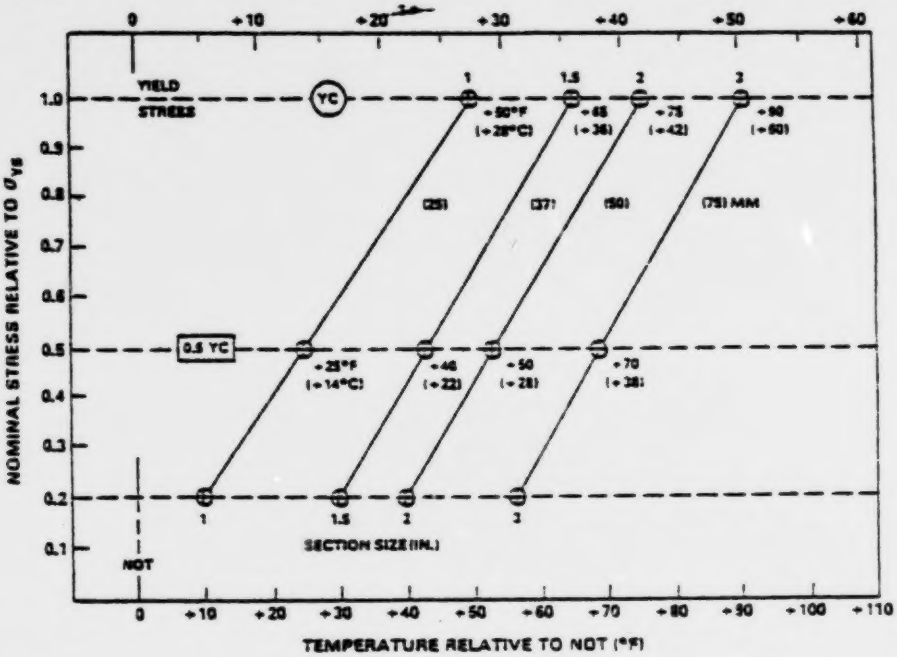

## 5. Crack Tip Opening Displacement

There has been an increasing tendency to require crack tip opening displacement (CTOD) tests to characterize the fracture initiation resistance of the weld and heat-affected zones for offshore construction. This test has several advantages over the more traditional Charpy test including:

- the test samples the full plate thickness and thus more exactly reproduces the constraint effects experienced in actual structures
- it uses a fatigue crack (sharp notch), which simulates the cracks found in service, and
- it has the ability to quantitatively relate the flaw size, geometry and operating stress to the steel fracture initiation resistance. For North Sea Construction, typical CTOD requirements for heavy plate weldments are 0.20 to 0.25 mm.

CTOD transition curves were established for both 19 mm and 38 mm plate thicknesses. All tests were done according to BS 5762-79 using the preferred BX2B (high constraint) sample with through-thickness notches.

The CTOD transition curves are shown in Figure 6. Both thicknesses exhibited 0.2 mm CTOD transition temperatures of less than -70°C.

Figure 6: CTOD Transition Curves - Controlled Rolled LEW Ht 805126

(a) Chg 24, 19 mm

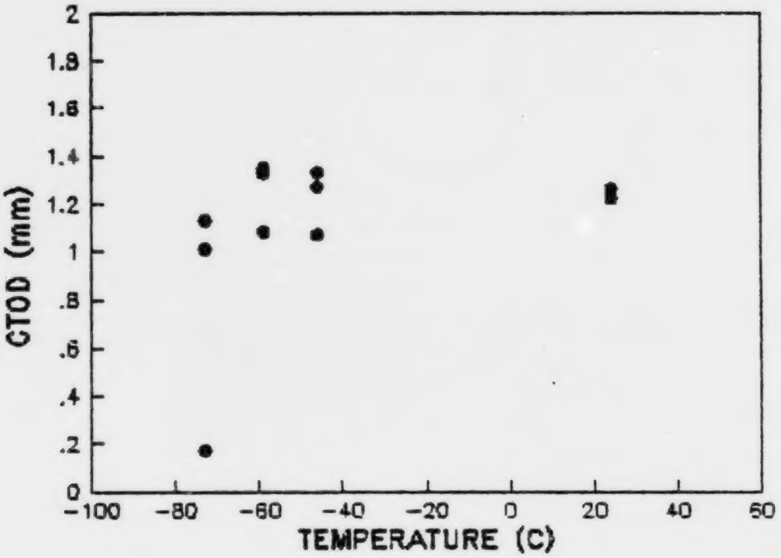

(b) Chg 30, 38 mm

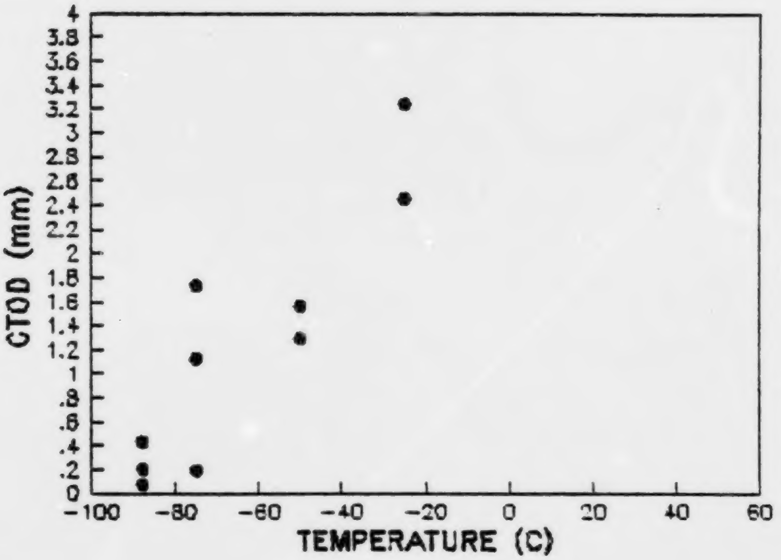

### 6. Bend Tests

Bend tests were conducted on longitudinal and transverse test samples from each gauge to evaluate the tendency for both surface cracking and centerline splitting. No cracking was observed on any bend tests.

## Further Development of Heavy Plate Controlled Rolling

This trial has demonstrated that grade 350 strength and toughness can be achieved in controlled rolled plate in thicknesses up to ≈32 mm. Further development of the controlled rolling practice and modification of mill procedures are required to both extend the range of thicknesses and to ensure property consistency on production rolling.

Key problems that must be overcome are the coarser ferrite grain sizes and the surface-to-core grain size differential that is developed in heavy plate (> ≈30 mm). These result largely from reductions in the total deformation below the austenite recrystallization-stop temperature, which in turn are related to the large surface to core temperature differentials established during rolling. To illustrate this problem, finite difference modeling was used to calculate the through-thickness temperature distribution after each pass during the rolling of 25 mm and 38 mm plates. As shown in Figure 7, a large (≈200°C) temperature differential is developed very early in the drafting sequence. This is reduced as the slab thickness decreases; however, there is still a significant surface-to-core difference at the control breakdown bar thicknesses. It is notable that for a 74 mm breakdown bar (25 mm plate) the temperature gradient is ≈50°C, whereas for a 114 mm bar (38 mm plate) it is ≈100°C. Using only surface temperature measurement to control the entry into the finishing sequence results in a large difference in the degree of deformation below the recrystallization-stop temperature. Assuming that this temperature is between 900 and 950°C for this chemistry, the core of the 74 mm transfer bar is in the unrecrystallized austenite regime after only two finishing passes; however, the core of the 114 mm transfer bar does not reach this condition until the last two or three drafts.

**Figure 7: Through-thickness Temperature Distribution During Heavy Plate Rolling**

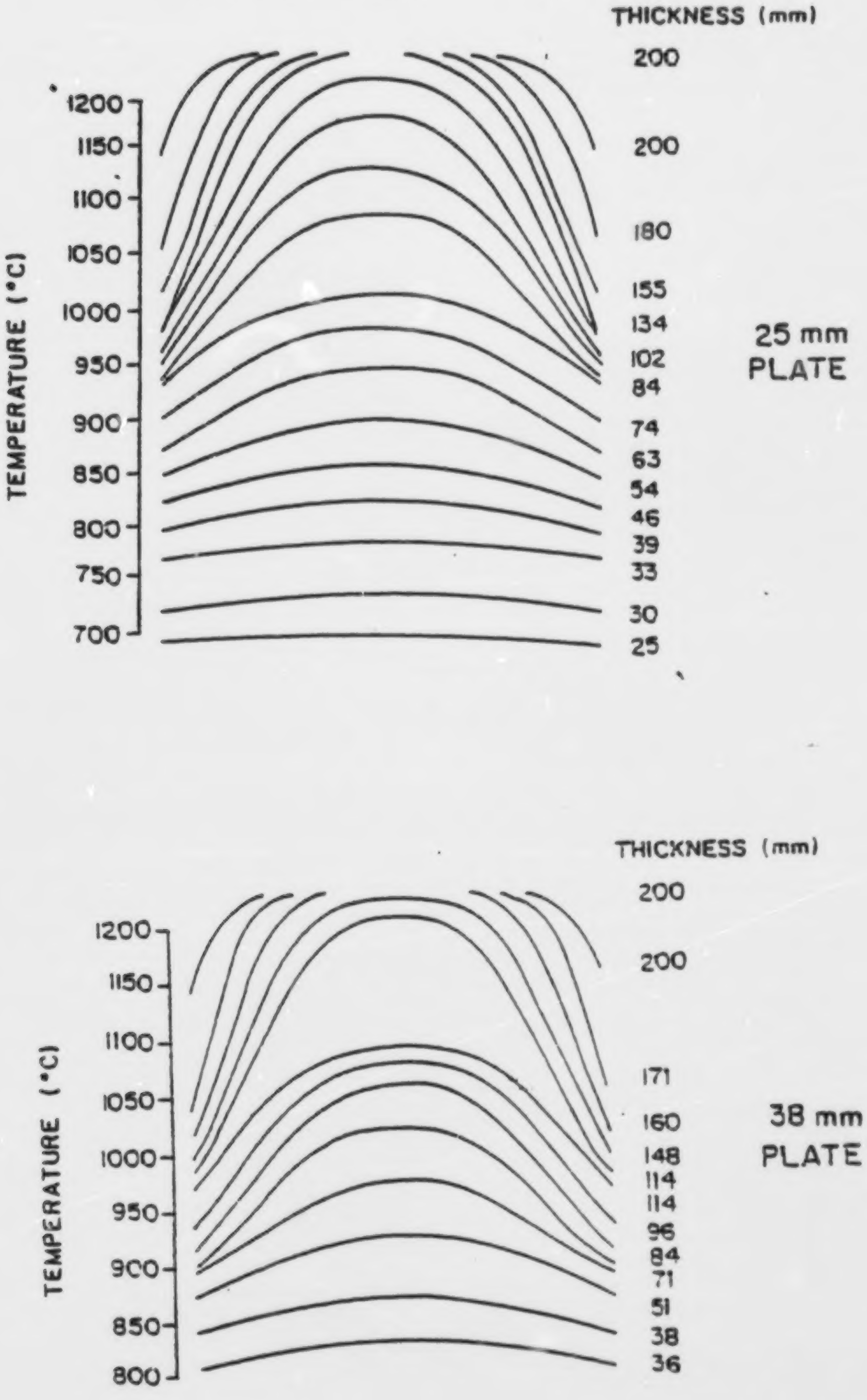

To consistently achieve the required low temperature reduction will necessitate the development of more sophisticated mill control, relying on calculated core temperatures rather than pyrometer surface measurements. As shown in Figure 1 A2, the surface temperature cooling rate is extremely slow in heavy transfer bars, and as a result, there is the potential for significant variability in actual core temperature when using only pyrometer control. Moreover, scale formation, cold spots due to uneven water spray cooling and variability in pyrometer calibration are additional sources of error when using pyrometer control. These could be eliminated by development of, in the simplest form, a "time base" rolling practice or a computer-based operator assist program. Development of either approach would require trials to confirm the temperature model and to establish "safe" mill drafting procedures.

Lowering the controlled rolling temperature to ensure rolling of unrecrystallized austenite will significantly increase the steel flow stress, and corresponding mill separating force and motor torques. Figure 8 shows the calculated flow stresses on the LEW trial as a function of surface temperature. Once below ≈900°C there is a dramatic increase in effective flow stress. We anticipate that these will be even higher if the entire plate thickness is in the unrecrystallized austenite regime. To minimize risk of overloading the mill while maintaining maximum drafting necessitates the development of a mill powering model and a computerized operator assist program to determine drafting practices. Details of the powering data taken from previous trials, together with recommendations for further development, are presented in R&D Report 840061.

**Figure 8:** **Calculated Flow Stress during Heavy Plate Rolling**

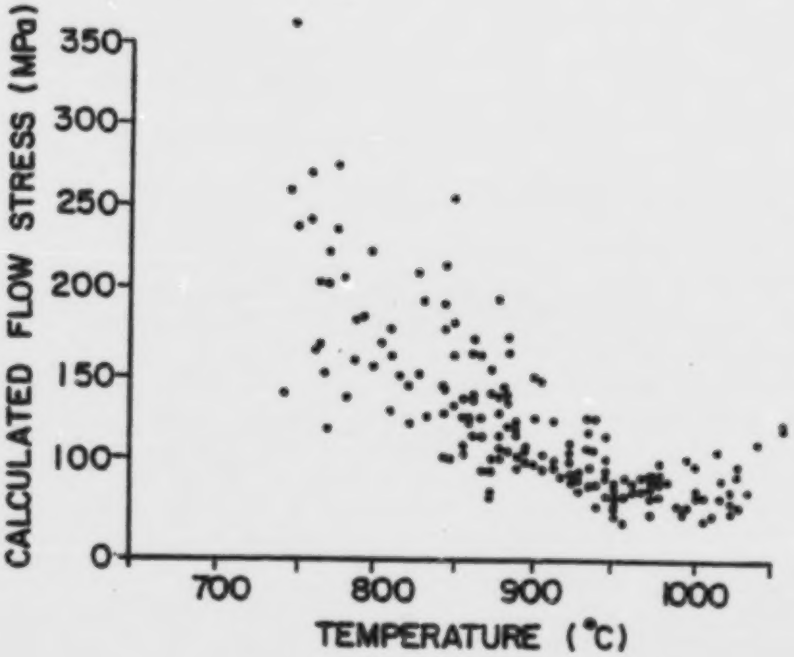

Other factors that should be evaluated to develop practices for heavy plate controlled rolling are:

- the effect of reheating temperature, and
- the effect of microalloy and interstitial content on austenite/ferrite grain refinement.

A low reheating temperature is metallurgically advantageous in that it reduces the austenite grain size prior to rolling, minimizes the hold time (during which grain growth can occur) between roughing and finishing and can minimize the surface-to-core temperature differential during rolling. Most Japanese plate producers utilize extra-low reheating temperatures (<1000°C) for controlled rolled heavy plate. The three-zone pusher furnaces of the 148in plate mill are not suited to low reheat temperature practices, and a significant increase in reheating time is required to eliminate skid marks with low reheat temperatures. To date, no information has been obtained on the actual slab temperatures achieved in the 148in plate mill reheat furnaces. It is recommended that trials be run to establish the slab reheating profiles for different reheating temperatures with particular emphasis on skid mark temperatures and their effect on plate properties/gauge during heavy plate controlled rolling.

The ability to achieve a fine ferrite grain size in controlled rolled plate is largely dependent on the refinement of the austenite grain size during roughing, and the total cumulative deformation in the austenite below its so-called recrystallization-stop temperature. In developing practices for heavy plate, it is vital to clearly establish the temperature below which recrystallization stops. This depends primarily on the microalloy and interstitial content, as they dictate the solubility product for microalloy precipitation in austenite. Little information is available on the static recrystallization behavior of our chemistries, particularly in multiple microalloyed steels with titanium additions. In addition, it is recommended that laboratory rolling trials be conducted at CANMET on both Ti-Cb and Ti-V chemistries to determine the optimum controlled rolling "control" temperature to achieve improved low temperature Charpy toughness. This would be combined with analysis of CANMET mill rolling loads to determine the ability to detect the recrystallization-stop temperatures and to develop data on the rolling loads anticipated on the 148in plate mill.

Finally it must be emphasized that considerable improvement in the low temperature Charpy impact toughness could be achieved with the application of sulfide shape control technology at LEW. Most of the testing done on this trial has been done in the transverse orientation, primarily because of the risk of damaging our Charpy impact testers with longitudinal tests. The limited number of longitudinal Charpies that were tested gave significantly higher Charpy energy absorption than the transverse tests, and significantly lower 40 J transition temperatures. The effect of using higher cleanliness sulfide shape controlled steel or low temperature Charpy toughness is clearly shown in Figure 9. Transverse Charpy transition curves are shown for three EH36 normalized steels which are identical except for their sulfur content. Although there is no effect of sulfur content on the Charpy 50 percent FATT temperature, it's clear that the high shelf energy, low sulfur steel maintains higher energy absorption than the high sulfur steels over the entire Charpy transition.

**Figure 9: The Effect of Sulfur Content on Low Temperature Charpy Toughness[17]**

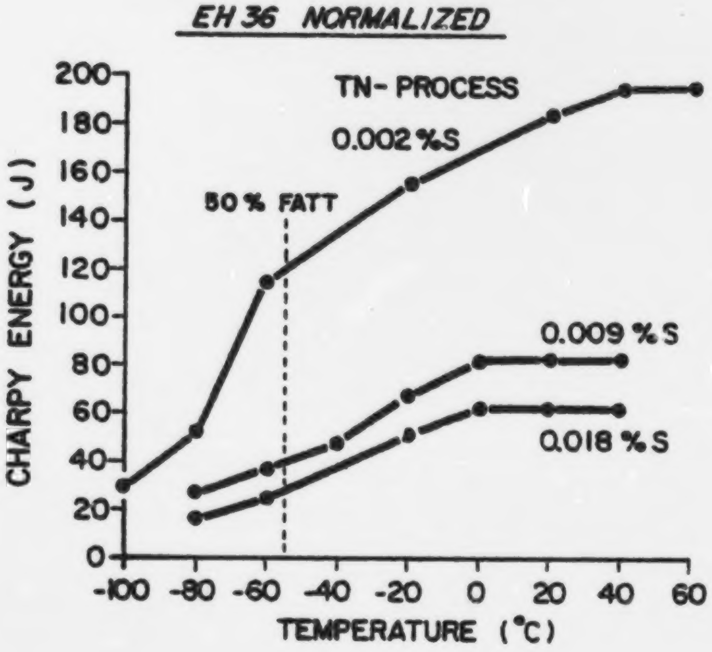

This effect of cleanliness on Charpy toughness was also demonstrated by comparison of the toughness achieved on the LEW and the HW heats. The low S LEW plate had significantly higher Charpy shelf energy than the CAB-treated HW heat (even when tested with the ISO striker!). Although this difference resulted partially from the higher strength of the HW chemistry, it was also caused by the lower inclusion levels of the strand cast steel. Limited metallography of samples from each heat demonstrated that the total inclusion lengths of the LEW plates were significantly lower than the HW plates. The total inclusion length (per unit area) of the LEW plates ranged between 0.039 and 0.096 $mm/mm^2$, whereas they ranged between 0.051 and 0.252 $mm/mm^2$ for the HW plate. Details of the inclusion measurement data are shown in Appendix 4.

## Normalized Plate Microstructures and Mechanical Properties

### 1. Normalizing

Plate coupons were normalized at 900°C for one hour per 25 mm of thickness and were cooled in air with surrounding plates to reproduce the cooling of a large plate.

### 2. Microstructure

Full thickness metallographic samples were taken from selected plate thicknesses and the volume fraction of pearlite and ferrite measured at several positions through the plate thickness using the QTM 720 image analyzer.

All plates showed polygonal ferrite and pearlite microstructures. Representative micrographs of the normalized structures are shown in Appendix 3. The ferrite grain size was dependent on the plate thickness, increasing from an average of ≈7.0 μm in the 19 mm plate to 9.5 μm in the 50 mm plate. This grain size is slightly coarser than expected for normalized plate. As seen in previous normalizing tests on the Stelcoloy 70 steel, regions of coarse grain ferrite were observed at positions near the plate surface. The cause of these "blown" grains is not clear, however it may be related to depletion of grain refining precipitates in areas containing alumina (i.e. quarter-point inclusions). The general increase in grain size at higher thicknesses results from the combined effects of longer holding times at temperature and the slower cooling rates of the heavier plates.

### 3. Strength

All gauges tested failed to meet the minimum yield and UTS requirements for grade 350 plate in the normalized condition (see Table I A3). The yield strengths decreased from just over 350 MPa to ≈330 MPa as plate thickness increased from 19 to 50 mm. Similarly the UTS dropped from ≈460 MPa to 450 MPa. The low strength of the normalized structure was due primarily to the loss of precipitation strengthening. The $\sigma_{ppt}$ calculated at between 15 and 35 MPa. Similarly the low UTS of this structure resulted primarily from a combination of the low precipitation strengthening and a relatively low fraction of pearlite.

In the normalized condition the strength just meeets the requirements for CSA Grade 300 WT, however it fails to meet the UTS specification for IACS* EH32 plate. It is clear that an improvement in both yield and UTS are necessary to apply LEW steel in the normalized condition. This could be best achieved by increasing carbon content to ≈0.12 percent (minimum).

---

* International Association of Classification Societies

## 4. Charpy Toughness

Transverse Charpy transition temperature behavior was measured on selected normalized plates. Charpy specimen positions through the plate thickness were varied as a function of gauge, as reported previously. The Charpy test results and representative energy and transition curves are presented in Appendix 3.

The Charpy energy transition data for each plate thickness are summarized in Table VII. Included in this table is an estimate of the design temperature to which the steel could be applied based on the proposed criteria for class V structures.

**Table VII: Summary of Impact Toughness of LEW Normalized Plate**

| Gauge (mm) | Charge No. | Position | 40 J TT (°C) | 68 J TT (°C) | 50% FATT (°C) | Design Temp (°C) |
|---|---|---|---|---|---|---|
| 19 | 24 | Sur | <-100 | -95 | -75 | -50 |
|  | 25 | Sur | <-100 | <-100 | -95 | -50 |
| 25 | 26 | Sur | -85 | -80 | -85 | -50 |
|  | 27 | Sur | -85 | -80 | -80 | -50 |
| 32 | 28 | Sur | <-100 | <-100 | -85 | -50 |
|  |  | Mid | -85 | -80 | -65 | -50 |
|  | 29 | Sur | -85 | -80 | -80 | -50 |
|  |  | Mid | -65 | -50 | -55 | -30 |
| 44 | 32 | 1/4 | -85 | -80 | -85 | -50 |
|  |  | Mid | -55 | -50 | -55 | -10 |
|  | 33 | 1/4 | -95 | -95 | -90 | -50 |
| 51 | 35 | 1/4 | -95 | -95 | -95 | -50 |
|  |  | Mid | -55 | -55 | -50 | -10 |

* based on Coast Guard interim standard

As with the controlled rolled plate, the Charpy transition temperatures at the plate mid-thickness position were significantly higher than at the plate surface and quarter-thickness position. Further testing is required to establish if the relatively low toughness in the mid-thickness position is in fact detrimental to the service behavior.

Based on the Charpy tests from the sub-surface and quarter-thickness positions, the normalized plate is adequate for the lowest anticipated design temperature (-50°C). The excellent toughness in this condition is in part a function of the relatively low strength and reduced pearlite fraction of this chemistry. Increasing the carbon content up to ≈0.12 percent (minimum) would significantly increase the pearlite content and Charpy FATT. It may also be necessary to increase the nickel content to ≈0.50 percent or make sulfide shape control additions to ensure meeting the 40 J transverse impact requirements in higher carbon content LEW chemistries in the normalized condition.

### 5. Nil Ductility Temperature

NDT tests were done on selected normalized plates using the procedures defined previously. The NDT temperatures are shown in Table VIII. Using the criteria of 0.5 yield operating stress (0.5 YC), shown in Figure 5, it is clear that in the normalized condition the LEW steel is adequate for East Coast (-30°C) usage up to ≈40 mm but is marginal for the Arctic. A further deterioration in NDT temperature would be anticipated for chemistries with higher strength but no significant improvement in ferrite grain size.

**Table VIII: Nil Ductility Temperature for LEW Normalized Plates**

| Gauge (mm) | Charge No. | Position | NDT (°C) |
|---|---|---|---|
| 32 | 28 | Surface | -75 |
| | | Subsurface | -60 |
| 38 | 30 | Surface | -70 |
| | | Centerline | -70 |

## Summary

Comprehensive strength and toughness evaluation of the LEW trial chemistry in both the controlled rolled and normalized condition has demonstrated the following capabilities and directions for further plate development:

### 1. Controlled Rolled

Grade 350 yield strength and ultimate tensile strength can be achieved in thickness up to 38 and 32 mm, respectively. The yield strength of the chemistry is primarily dependent on the ferrite grain size, and it should be possible to meet Grade 350 yield requirements in heavier thicknesses (up to ≈50 mm) with limited precipitation strengthening by improved controlled rolling practices. Similarly the Grade 350 tensile requirements could be met by either a slightly higher carbon content (≈0.09) and/or lower finishing temperature controlled rolling.

40 J Charpy energy transition temperatures adequate for -50°C design temperature were achieved in plate thicknesses up to 32 mm. The plate thickness limit could be extended by the development of improved controlled rolling practices which ensure adequate reduction of the entire slab thickness below the austenite recrystallization stop temperature. In addition, further improvement could be achieved by

developing sulfide shape control practices for LEW strand cast slabs. Charpy testing at the plate centerline demonstrated that this position has lower toughness than the balance of the plate thickness. This behavior is most likely caused by the formation of bainitic microstructures at centerline segregation, and may require the development of improved strand casting procedures and/or electromagnetic stirring.

## 2. Normalized

The LEW chemistry failed to meet the Grade 350 strength requirements and in fact would only be adequate for Grade 300 plate. To meet Grade 350 strength will require a significantly higher carbon content (≈0.12 percent C).

40 J Charpy energy transition temperatures adequate for -50°C designs were achieved in thicknesses up to 51 mm. However, the excellent low Charpy toughness was partially a result of low plate strength, and some deterioration in Charpy toughness would be expected at higher carbon content. Once again, the plate mid-thickness position gave significantly lower Charpy toughness than the balance of the plate thickness.

# HW GRADE 350 PLATE

## Chemistry and Steelmaking Practice

The HW heat was produced to the chemistry shown in Table IX. This chemistry was designed primarily to meet the grade 350 strength requirements in the normalized condition, and thus had a higher carbon content than the LEW chemistry. The principal factors considered in the design of this chemistry are given in Table X.

**Table IX: Heat Chemistry - 536441**

| C | Mn | P | S | Si | Ni | V | Cb | Ti | ASA |
|---|---|---|---|---|---|---|---|---|---|
| 0.13 | 1.46 | 0.013 | 0.003 | 0.24 | 0.25 | 0.064 | 0.019 | 0.005 | 0.010 |

**Table X: Design of Chemistry for HW Grade 350 Plate**

| Element | Aim | Effect | Restriction |
|---|---|---|---|
| C | 0.13 | • increased pearlite content increases UTS<br>• little effect on yield strength | • weldability<br>• increased FATT |
| Mn | 1.40 | • solid solution strengthening<br>• ferrite grain refinement through $Ar_3$ reduction | • bainite formation (increased FATT) |
| Cb | 0.02 | • ferrite grain refinement in both controlled rolled and normalized plate<br>• precipitation strengthening | • promotes low toughness HAZ structures |
| V | 0.06 | • precipitation strengthening | • reduced HAZ toughness, due to strain aging |
| Ni | 0.25 | • reduced FATT<br>• little solid solution strengthening | |
| Ti | 0.01 | • tie up free nitrogen<br>• reduced ingot panel cracking | • >3.4 Ti/N reduces base plate and HAZ toughness |

The heat was made to provide optimum steel cleanliness using current HW steelmaking, secondary steelmaking and ingot casting technology. The 0.003 percent sulfur level was achieved using desulfurized hot metal (0.005 percent S), selected low sulfur scrap, and CAB injection with CaSi in a basic lined ladle covered with a synthetic slag. Details of the heat production are provided in R&D Report 840056.

A total of six ingots were produced, and were rolled to the plate sizes shown in Table XI. The slabs were deseamed and conditioned prior to hydrogen removal at Sheet Services. All slabs were annealed for 50 or 90 hours at 650°C depending upon the slab and final plate thicknesses.

## Controlled Rolling

A total of sixteen slabs were rolled to plate thicknesses between 19 and 102 mm (Table XI).

Table XI: Plate Controlled Rolling Practice

| Chg No. | Gauge (mm) | Width (mm) | Breakdown Bar Thickness (mm) | % Reduction Below Temperature (°C) | | | | Finish Temp (°C) | Delay Time (sec) | Total Time (sec) |
|---|---|---|---|---|---|---|---|---|---|---|
| | | | | 900 | 870 | 840 | 815 | | | |
| 10 | 19 | 2438 | 53 | 77.5 | 69.0 | 55.0 | 55.0 | 740 | 37 | 481 |
| 11 | | | | 78.7 | 61.3 | 35.0 | 35.0 | 730 | 24 | 450 |
| 12 | | | | 78.8 | 61.6 | 48.4 | 35.0 | 740 | 51 | 444 |
| 13 | 25 | 2438 | 74 | 64.4 | 63.9 | 49.8 | 49.8 | 740 | 46 | 480 |
| 14 | | | | 69.0 | 58.1 | 39.9 | 30.6 | 710 | 48 | 514 |
| 15 | | | | 69.6 | 69.6 | 51.1 | 31.7 | 720 | 87 | 545 |
| 16 | 32 | 1828 | 91 | 66.9 | 61.1 | 29.4 | 14.0 | 775 | 60 | 450 |
| 17 | | | | 66.3 | 66.3 | 23.9 | 13.6 | 760 | 102 | 472 |
| 18 | | | | | | | | | | |
| 19 | 38 | 1828 | 114 | 63.1 | 63.1 | 0 | 0 | 845 | 154 | 460 |
| 20 | | | | 68.4 | 68.4 | 24.8 | - | 800 | 147 | 429 |
| 21 | | | | 68.4 | 68.4 | 24.5 | 0 | 830 | 145 | 434 |
| 22 | 64 | 1828 | 114 | 0 | 0 | 0 | 0 | 920 | - | 340 |
| 23 | | | | 0 | 0 | 0 | 0 | 905 | - | 350 |
| 2 | 102 | 1524 | NA | - - - - - - - - - Not Available - - - - - - - - - | | | | | | |
| 1 | | | | " | | | | | | |

The reheating and controlled rolling practice were the same as for the LEW portion of the trial.

The reheating temperature (1175°C) was above the austenite grain coarsening temperature for this steel (Appendix 1). It is notable that the 0.005 percent Ti addition to this ingot cast steel did not appreciably improve its grain coarsening behavior. The low cooling rate during solidification of ingots is such that the TiN precipitates formed are too large to be effective in restricting austenite grain growth.

The rolling practice given each bar is shown in Table XI. The HW plates were rolled by a different roller than the LEW steel, and there was a significant difference in the interpass delay times used by the two operators. The HW plates were rolled with about five second longer interpass times than the LEW plates, which increased their total rolling times, and thus reduced the HW plate finishing temperatures. In some cases, the last pass surface temperature was below the calculated $Ar_3$ temperature for this chemistry (≈740°C). As with the rolling of the LEW plates, the degree of controlled rolling below the austenite recrystallization stop temperature (≈900°C) decreased with increasing final plate thickness. The 64 and 102 mm plates were finish rolled entirely in the high temperature austenite regime.

### Controlled Rolled Plate Microstructure and Mechanical Properties

#### 1. Microstructure

The plate microstructures were characterized using the same procedure as for the LEW plates. All plates showed banded polygonal ferrite and pearlite microstructures. Representative micrographs of the as-rolled plates are given in Appendix 3 as well as measured grain sizes and pearlite fractions. The ferrite grain size increased from the plate surface to the core position, and also increased with plate thickness (see Figure 7 A3). In 19 mm plate, the mean ferrite grain size was 6.6 µm. In 38 mm plate, it increased to 10.6 µm. The volume fraction of pearlite ranged between ≈25 percent on the lighter gauge plate down to ≈17 percent on the heaviest (38 mm) controlled rolled plate.

The ferrite grain size achieved in the ingot controlled rolled plate was generally finer than that of the strand cast steel. It is not clear why this improvement occurred, however there are two main factors that may have effected this change:

- the increased delay time used for the HW plate rolling increased the total reduction at low temperatures and reduced the plate finishing temperature. This would tend to increase the total strain in the deformed austenite prior to ferrite transformation,

- the higher free nitrogen and carbon content of the HW chemistry increased the solubility product for Cb (C,N) and thus raised the austenite recrystallization stop temperature. Hence, the total deformation of cold worked austentite prior to transformation was higher for the HW heat.

#### 2. Strength

The as-rolled plate yield and UTS both decreased significantly with increasing plate thickness (Figure 10). The minimum plate strength requirements were readily met over the entire gauge range.

**Figure 10: Effect of Thickness on Yield and Ultimate Tensile Strength - Controlled Rolled**

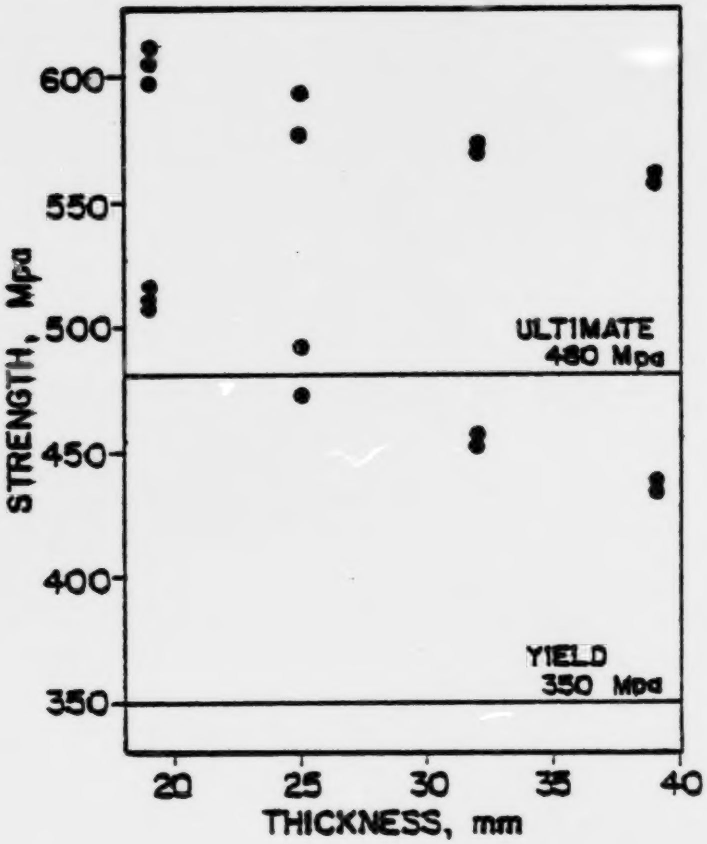

The calculated contribution to yield strength based on the previously established effects of grain size, solid solution strengthening and lattice friction are shown in Table V, Appendix 3. The precipitation strengthening ($\sigma_{ppt}$) for this chemistry is significantly higher than that for the LEW chemistry, and was relatively insensitive to gauge. The $\sigma_{ppt}$ ranged between ≈175 MPa and 140 for the 19 mm and 38 mm plate. This is about twice that observed on the LEW chemistry which had similar levels of columbium (0.02 percent) and vanadium (0.08 percent), and is similar to that on an earlier LEW heat of Stelcoloy 70 produced with 0.05 percent Cb and 0.05 percent V, but without titanium. This result suggests that either the 0.01 percent Ti addition to the LEW grade 350 heat significantly reduces the amount of precipitation strengthening, or, that low carbon steels (<0.10 percent C) give less effective precipitation.

The ability of this carbon level to meet the UTS requirement over the entire gauge range confirms the benefit of using >0.10 percent C steels to produce grade 350 plate. At this carbon level, it should be possible to achieve the grade 350 yield and UTS requirement primarily through grain refinement with little or no precipitation strengthening. Thus, it is recommended that further controlled rolled chemistry trials evaluate the potential to completely eliminate the vanadium addition, while maintaining a minimal 0.02 columbium level to provide grain refinement through control of austenite recrystallization kinetics.

### 3. Charpy Toughness

Transverse full size Charpy V-notch transition curves were measured from each plate thickness up to and including 38 mm using the same procedure as for the LEW heat. All tests were done using the ISO striker.

The Charpy energy data and representative plots of the energy and shear transition curves are given in Appendix 3. Table XII summarizes the Charpy test data for each thickness and test position in terms of the 40J, 68J and 50 percent shear transition temperatures. Included in this table is an estimate of the design temperature to which this plate could be applied based on the criteria proposed for class V structures.

**Table XII: Summary of Impact Toughness of HW Controlled Rolled Plate**

| Gauge (mm) | Charge No. | Position | 40J TT (°C) | 68J TT (°C) | 50% FATT (°C) | Design* Temp (°C) |
|---|---|---|---|---|---|---|
| 19 | 10 | Sur | -70 | -65 | -65 | -50 |
| | 11 | Sur | -70 | -65 | -65 | -50 |
| | 12 | Sur | -65 | -50 | -50 | -50 |
| 25 | 13 | Sur | -70 | -50 | -50 | -50 |
| | 14 | Sur | -70 | -55 | -50 | -50 |
| | | Sur | -70 | -65 | -65 | -50 |
| 32 | 16 | Sur | -70 | -60 | -60 | -45 |
| | | Mid | -40 | -25 | -25 | -20 |
| | 17 | Sur | -50 | -50 | -55 | -30 |
| | | Mid | -40 | -35 | -35 | -20 |
| 38 | 19 | 1/4 | -65 | -40 | -30 | -35 |
| | | Mid | -40 | -30 | -10 | -10 |
| | 20 | 1/4 | -65 | -50 | -30 | -35 |
| | | Mid | -30 | -20 | -20 | -5 |
| | 21 | 1/4 | -40 | -35 | -15 | -15 |
| | | Mid | -30 | -20 | -10 | -5 |

* based on Coast Guard Interim Standard.

The HW-CAB treated plate could be applied to -50°C design temperatures in thicknesses up to 25 mm. For heavier gauges there is a significant deterioration in the Charpy impact FATT paticularly at the mid-thickness position. At 32 mm, the plate would be marginal for East Coast application (-30°C) and at 38 mm, it would be marginal for North Sea (-10°C) and below water (-5°C) Arctic or East Coast Applications.

The deterioration in Charpy toughness with increased gauge is largely related to the increase in ferrite grain size. A comparison of the actual and predicted Charpy 50 percent FATTs based on previously established relationships with microstructure and strengthening is shown in Figure 11. For lighter gauge plate tested at the surface position, the FATTs were much lower than calculated. This discrepancy is caused by splitting (separations) on the Charpy fracture surfaces of the surface specimen. This is related to rolling the plate surface at low temperatures in the unrecrystallized austenite regime or in the austenite-ferrite phase regime.

**Figure 11:** **Comparison of Actual and Predicted 50 percent Shear FATT Based on Grain Size and Chemistry**

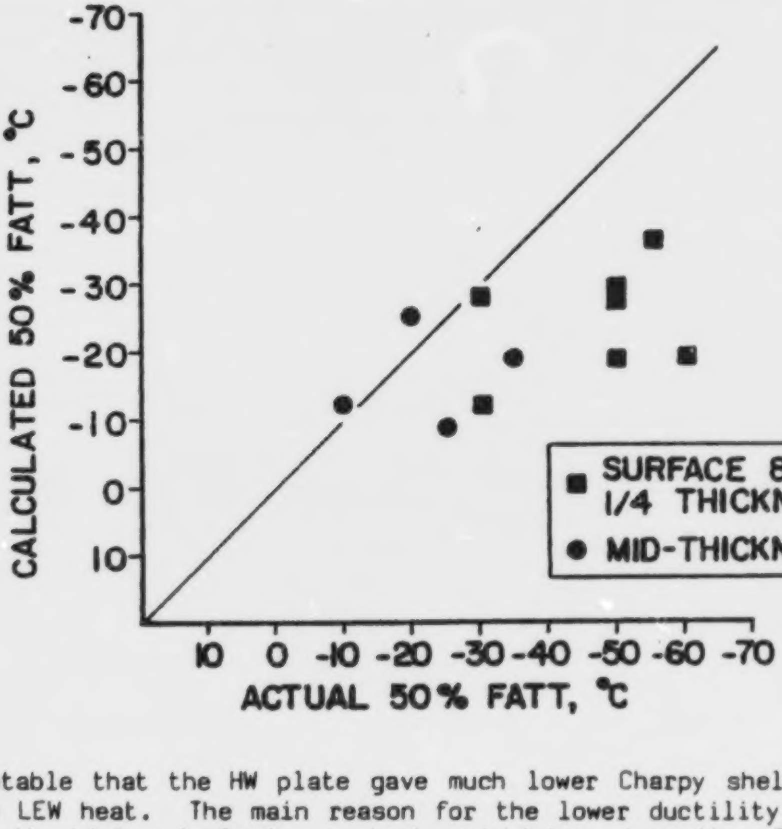

It is notable that the HW plate gave much lower Charpy shelf energies than the LEW heat. The main reason for the lower ductility of the HW plate is its higher inclusion content and higher strength. The limited inclusion analysis on the two heats indicated that there were higher total inclusion lengths in the HW heat (Appendix 4). Even at 0.003

percent sulfur, the CAB treated ingot cast steel exhibited elongated Type II manganese sulfide inclusions. Moreover, the HW steel had a significantly higher fraction of elongated oxide inclusions. It is likely that improvement in the HW steel cleanliness through the use of bottom pouring would significantly improve the low temperature Charpy toughness.

## 4. Nil Ductility Temperature

The brittle fracture arrest capability was further evaluated by NDT tests on selected plates, using the procedure described previously. The NDT results are summarized in Table XIII, together with the 40 J TT data.

**Table XIII: Nil Ductility Temperatures - HW Controlled Rolled Plate**

| Gauge (mm) | Charge No. | Position | NDT (°C) | 40J TT (°C) |
|---|---|---|---|---|
| 19 | 10 | Surface | -70 | -70 |
| 25 | 13 | Subsurface | -45 | -70 |
| 32 | 16 | Surface | -55 | -70 |
| | | Subsurface | -40 | NA |
| 38 | 19 | Mid-thickness | -40 | -40 |

Again, there was fairly good agreement between the two measures of fracture initiation temperature. Based on the criteria given in Figure 5, only the lightest gauge (19 mm) plate would have an arrest capability at -30°C.

## 5. Crack Tip Opening Displacement

CTOD transition curves were tested for both 19 mm and 38 mm plate thicknesses using the procedure outlined previously.

The CTOD transition data are shown in Figure 12. Assuming that 0.20 mm CTOD would be required at the service temperature to ensure adequate fracture initiation resistance under slow-loading conditions, the 19 mm and 38 mm plates could be applied for -60°C and ≈-10°C design temperatures, respectively.

As with the LEW plate CTOD tests, this measure of toughness tended to indicate a more favorable (lower) service temperature than either the Charpy or NDT tests.

It is notable that the absolute $\delta_{max}$ (ductile tearing) CTOD values of both the 19 and 38 mm plates from the HW-CAB heat were significantly lower than those observed for the LEW heat. This primarily reflects the superior cleanliness of the LEW steel.

Figure 12: CTOD Transition Curves - Controlled Rolled
HW Ht 536441

(a) Chg 11, 19 mm

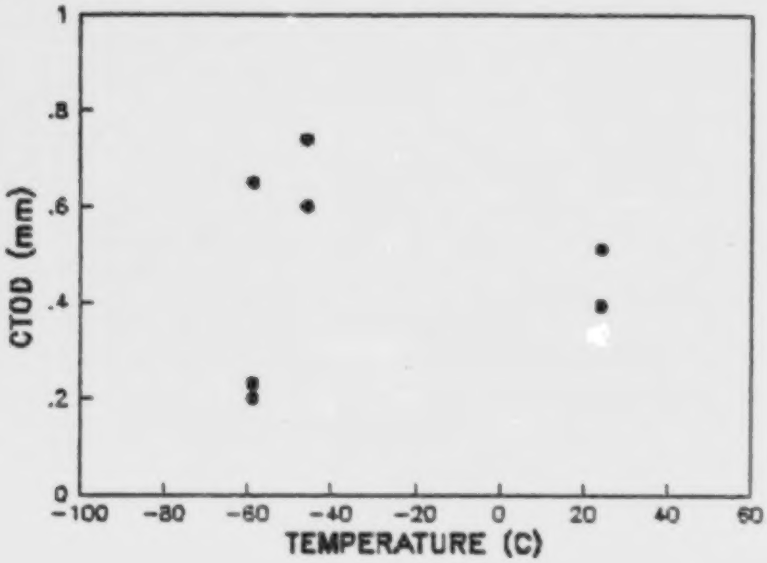

(b) Chg 20, 38 mm

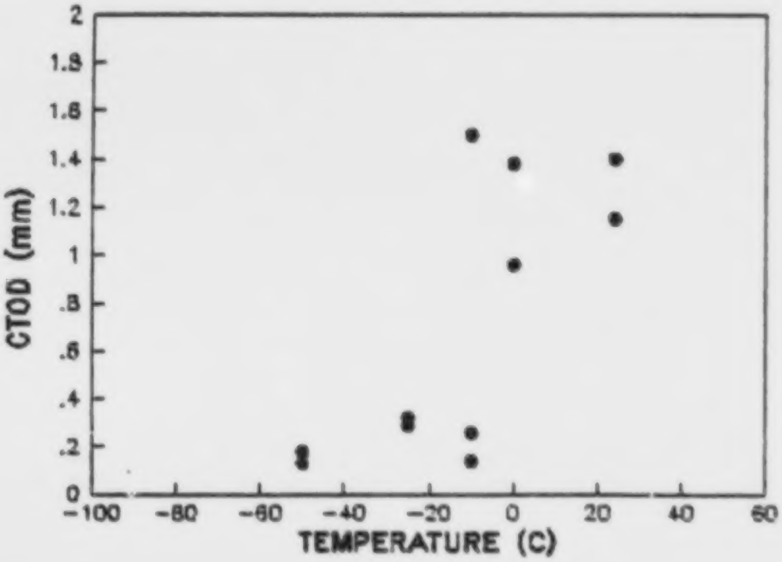

6. Bend Tests

No surface or centerline cracking was observed on either longitudinal or transverse bend tests.

## Further Development of Heavy Plate Controlled Rolling

This trial has demonstrated the rather limited ability to apply the HW-CAB EN112KHS to low temperature service in the controlled rolled condition. Based on Charpy and CTOD toughness data, this steel would be suitable for Arctic service in thicknesses to ≈25 mm and would be marginal for East Coast application at heavier gauges. However, further improvement in the base plate toughness could be achieved by increasing the degree of low temperature rolling during finishing, and reducing the plate yield strength contribution arising from precipitation strengthening. The methodology recommended to alter the controlled rolling practice has been reviewed for the LEW steel plate.

With regard to chemistry development it is clear that this practice (designed for normalized applications) can be considerably leaner and still meet the required strength levels in the controlled rolled condition. The major changes recommended are:

- reduce or eliminate the 0.06 V additions,
- reduce the carbon content to 0.10-0.12 percent.

The reduced vanadium content is anticipated to reduce the yield strength by up to 70 MPa, which would not jeopardize meeting the 350 MPa yield strength, but would improve (lower) the 50 percent shear transition temperature by as much as 30°C. Similarly, reducing the carbon content by ≈0.02 percent, would not jeopardize meeting the UTS requirement, but would reduce the pearlite content by approximately four percent, which would further reduce the 50 percent FATT by ≈10°C.

## Normalized Plate Microstructures and Mechanical Properties

1. Normalizing

Plate coupons were normalized using the same practice as for the LEW plates.

2. Microstructure

All normalized plates showed polygonal ferrite and pearlite microstructures (see Appendix 3). The ferrite grain sizes were relatively uniform through the plate thickness, however, there was a significant increase in grain size with increased plate thickness. This results primarily from the finer as-rolled plate microstructure in the lighter gauge plate, and the slower cooling rate of the heavier plate after normalizing. It is notable that the normalized ferrite grain of the ingot cast heat was significantly finer than that of the LEW heat.

### 3. Strength

As shown in Figure 13, all plate gauges met the minimum yield and tensile strength in the normalized condition. Normalizing significantly reduced the yield and ultimate strengths compared with the as-rolled condition. Calculation of the various contributions to strengthening illustrates that the precipitation hardening is reduced from ≈150 MPa down to ≈40 MPa by normalizing (Table V A3). It is clear from this analysis that the Grade 350 yield strength requirements can be met primarily through ferrite grain refinement. Similarly, the UTS requirement is readily met with the observed volume fraction of pearlite in the 0.13 percent C steel.

**Figure 13: Effect of Thickness on Yield and Ultimate Tensile Strength - Normalized**

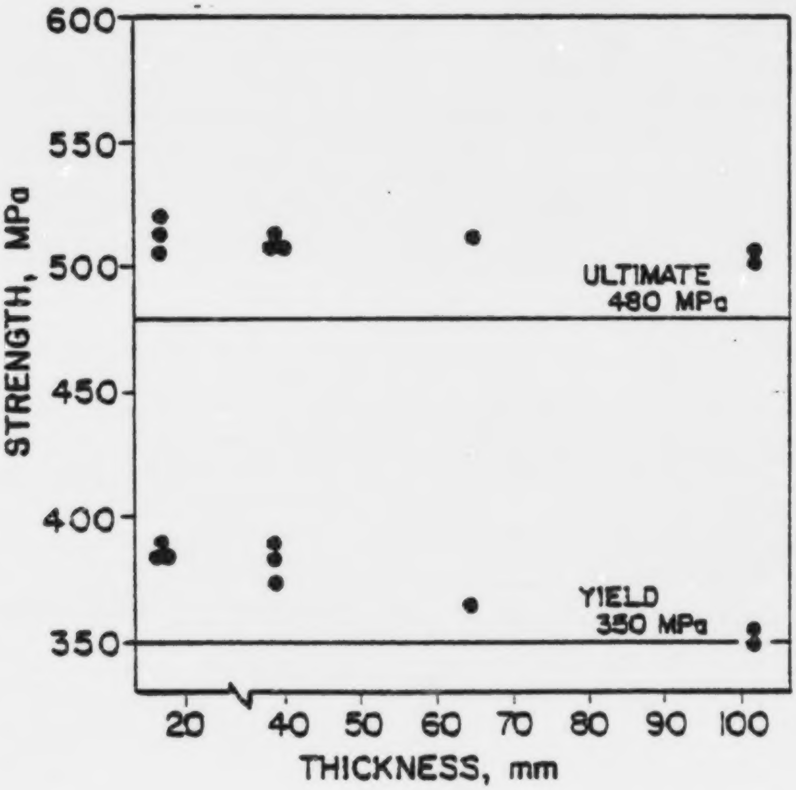

### 4. Charpy Toughness

The Charpy test data are presented in Appendix 3. The Charpy energy transition data are summarized in Table XIV.

Table XIV: Summary of Impact Toughness of HW Normalized Plate

| Gauge (mm) | Charge No. | Position | 40J TT (°C) | 68J TT (°C) | 50% FATT (°C) | Design* Temp (°C) |
|---|---|---|---|---|---|---|
| 19 | 10 | Sur | -80 | -50 | -45 | -50 |
| | 11 | Sur | -95 | -90 | -75 | -50 |
| 38 | 19 | 1/4 | -55 | -50 | -40 | -20 |
| | | Mid | -50 | -40 | -35 | -20 |
| | 20 | 1/4 | -70 | -60 | -45 | -40 |
| | | Mid | -75 | -55 | -50 | -40 |
| | 21 | 1/4 | -65 | -55 | -35 | -30 |
| | | Mid | -40 | -35 | -30 | -10 |
| 64 | 23 | 1/4 | -55 | -45 | -35 | >0 |
| | | Mid | -60 | -50 | -40 | >0 |
| 101 | 1 | 1/4 | -80 | -70 | -45 | NA |
| | | Mid | -55 | -50 | -25 | NA |
| | 2 | 1/4 | -70 | -65 | -35 | NA |
| | | Mid | -65 | -55 | -30 | NA |

* based on Coast Guard Interim Standard.

The Charpy transition temperatures of the normalized plate were similar over the entire gauge range tested. The 50 percent FATTs ranged from -25 to -50°C. This reflects the relatively consistent grain size and strength levels achieved. The 40 J transition temperatures were slightly more variable, ranging from -40 to -95°C, which is believed to result from the added dependence on steel cleanliness.

This heat generally had higher transition temperatures (≈20°C) than published Charpy transition data on similar chemistries. It is not certain why the Charpy toughness was lower than expected, however, it may be related to the low aluminum content (0.01 percent) of this heat. Such a low aluminum level would tend to increase the free nitrogen content, which would raise the FATT.

The suitability of this plate for low temperature (-30°C, -50°C) applications is very limited. Considering the significant lowering of the required Charpy test temperature with increased plate thickness, it is clear that the normalized plate would not be suitable except at the lightest thickness (19 mm) (Table XIV).

### 5. Nil Ductility Temperature

NDT tests were done on selected normalized plates using the procedure described previously. The NDT results are shown in Table XV. Again, there is fairly good agreement between the NDT and 40 J transition temperature.

**Table XV: Nil Ductility Temperatures - HW Normalized Plate**

| Gauge (mm) | Charge No. | Position | NDT (°C) | 40 J TT (°C) |
|---|---|---|---|---|
| 38 | 20 | Mid-Thickness | -60 | -60 |
| 64 | 23 | Mid-Thickness | -50 | -60 |
| 111 | 1 | Surface | -55 | NA |
| | | Mid-Thickness | -45 | -55 |

In terms of applying this steel to low temperature applications requiring fracture arrest capability, this steel is marginal for even East Coast applications (-30°C) in thicknesses above ≈40 mm.

## Summary

The detailed testing of the HW trial chemistry has demonstrated the following capabilities and directions for further development.

### 1. Controlled Rolled

Grade 350 yield and tensile strength requirements were easily met in thicknesses up to 40 mm. In fact the chemistry easily met 400 MPa strength level at 40 mm thickness, and could be considered for a higher strength class in the controlled rolled condition. Considering this result together with the LEW data, it is clear that the Grade 350 strength level can be with a relatively lean chemistry (e.g. 0.09 C, 1.40 Mn, 0.25 Ni, 0.02 Cb) provided sufficient ferrite grain refinement is achieved by controlled rolling.

40 J Charpy energy transition temperatures adequate for -50°C deseign temperature were met in thicknesses up to 25 mm. In heavier thicknesses, the Charpy energy transitions deteriorated rapidly, due primarily to the high level of precipitation strengthening and the relatively low cleanliness of the heat. A significant improvement in the heavy plate toughness levels could be achieved by modifying the heat chemistry (as above), developing improved controlled rolling practices, and increasing the ingot cast steel cleanliness by developing stream shrouding and bottom pouring practices.

### 2. Normalized

This chemistry comfortably met the Grade 350 yield and UTS requirements in gauges up to 100 mm. Slight modification of the chemistry to remove the vanadium addition is recommended to improve weld HAZ toughness. This may result in a slight reduction in yield strength, which could be compensated for by slightly higher alloy additions (Cu-Ni) or improved ferrite grain refinement. It is notable that the grain size achieved on this heat was slightly coarser than anticipated. Higher aluminum content (0.03 percent aim) and slightly higher columbium additions (0.03 percent max) are recommended.

The 40 J Charpy energy transition temperatures for the heat were generally much higher than required for either East Coast or Arctic applications, particularly in the heavy thicknesses (>40 mm) for which it is anticipated ingot cast/normalized steels will be necessary. In addition to evaluating the above mentioned methods of achieving a finer, normalized structure, the cleanliness of this must be significantly improved (through the use of bottom pouring of ingots) to give us any possibility to providing the required Charpy energy levels.

# REFERENCES

1. Chinook Fuel Innovation Ltd, Survey of Requirements for Plate Steel in Offshore Structures and Arctic Vessels, May 1982.
2. R&D Report 820018.
3. Det Norske Veritas, Review of Steels Used in the Construction of Offshore Structures, April, 1982.
4. Fenco Consultants Ltd. A Review of Steel Properties at Low Temperatures, December, 1980.
5. D. B. McCutcheon: Arctic Grade 350 Structural Plate, Recent Japanese Technology, letter of March 28, 1983.
6. R&D Report 840061.
7. The Welding Institute, Group Sponsored Proposal Normalized Steels with Improved HAZ Toughness, April, 1983.
8. Vanitec, Proposals for a Study of the Properties of Thick Plates of Normalized Vanadium Steels, and of the Properties of HAZ's in Multipass Welds, November, 1983.
9. R&D Report 840056.
10. I. Weiss et al: Proc. Thermomechanical Processing of Microalloyed Austenite, Pittsburgh, 1981, pp 35-58.
11. R. K. Amin, F. B. Pickering: IBID, pp 1-31.
12. S. Kanajawa et al: Trans ISIJ, Vol 16, 1976, p 486.
13. Investigation of the Effects on Charpy Impact Characteristics by Shape of Pendulum Striking Edge - Mechanical Tsting Subcommittee of the Joint Research Society of ISIJ, May, 1984.
14. O. L. Towers: Metal Construction, 1983, 15 (11), pp 682-686.
15. B. Mintz et al: Influence of Grain Boundary Carbide Thickness and Grain Size on the Impact Properties of Steels, Proceedings of Metals Society Conf. Advances in the Physical Metallurgy and Applications of Steels, 19782, Book 284, pp 222-228.
16. W. S. Pellini: Selection of Fracture Criteria for Steel Structures in Severe Arctic Environments, Proceedings of Fracture Toughness Evaluation of Steels for Arctic Marine Use, Oct. 1983, Ottawa, pp 4-1.
17. H. Baumgardt et al: Review of Microalloyed Structural Plate Metallurgy, Paper presented at the Int Symposium Niobium 81, San Francisco, 8-12, November, 1981.

# ACKNOWLEDGMENTS

The following people and departments are recognized as having made vital contributions to this study:

B. Armitage, W. Krestynski, J. G. Matich, B. C. Branston, R. Millsop, B. A. Buck; several people in the HW and LEW Operating and Metallurgical Departments; and the Metallurgical Test Lab at Welland Tube Works.

# APPENDIX 1

## AUSTENITE GRAIN COARSENING

To determine the austenite coarsening characteristics of both the LEW slab cast and HW ingot cast steels, samples of each steel were taken from the quarter-thickness position in the cast and rolled slabs. These were cut into 70 mm cubes, which were mounted and polished to a 1 μm finish. Cubes of each steel were reheated under vacuum in the R&D Leitz dilatometer to a series of temperatures, using a reheating time of one hour to temperature, and holding time at temperature of one hour. The samples were furnace cooled to a temperature below the temperature at which oxide would form on the polished surface. The grain size of the thermally etched samples was measured using a linear point counting method. Representative micrographs of the thermally etched surfaces are shown in Figure 1 A1. The average grain size data are summarized in Table I A1.

**Table I A1: Austenite Grain Coarsening of Slab Samples**

| Reheat Temperature (°C) | γ Grain Size (μm) | |
|---|---|---|
| | HW CAB Ht 536441 | LEW Ht 805126 |
| 1093 | 30-32 | |
| 1148 | 45-55 | 18 |
| 1176 | 52-55 | 18 |
| 1204 | 57-61 | 25-27 |
| 1226 | 62-65 | 38 |
| 1248 | 78-89 | 38-42 |
| 1300 | 98-125 | 50 |

Figure 1 A1: Micrographs of Thermally Etched Surfaces
1200°C Reheat Temperature

(a) LEW Ht 805126, d = 26 μm (200X)

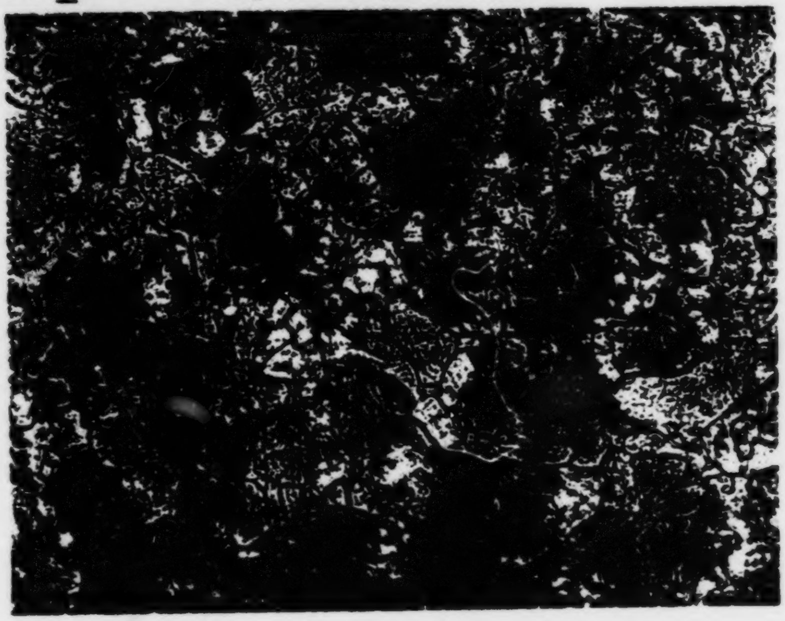

(b) HW Ht 536441, d = 61 μm (200X)

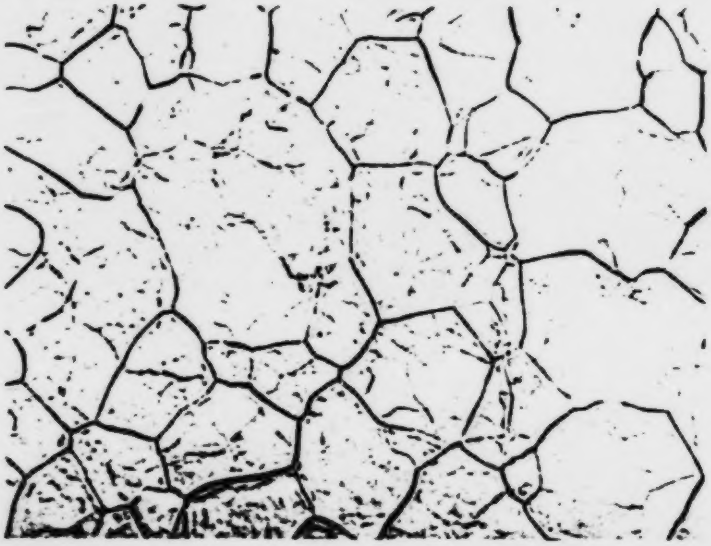

## APPENDIX 2

## TEMPERATURE LOSS DURING CONTROLLED ROLLING

Figures 1 A2 and 2 A2 give examples of the surface temperature loss during controlled rolling as a function of thickness and cumulative time, respectively.

Figure 1 A2: Surface Temperature Loss as a Function of Thickness

(a) 25 mm

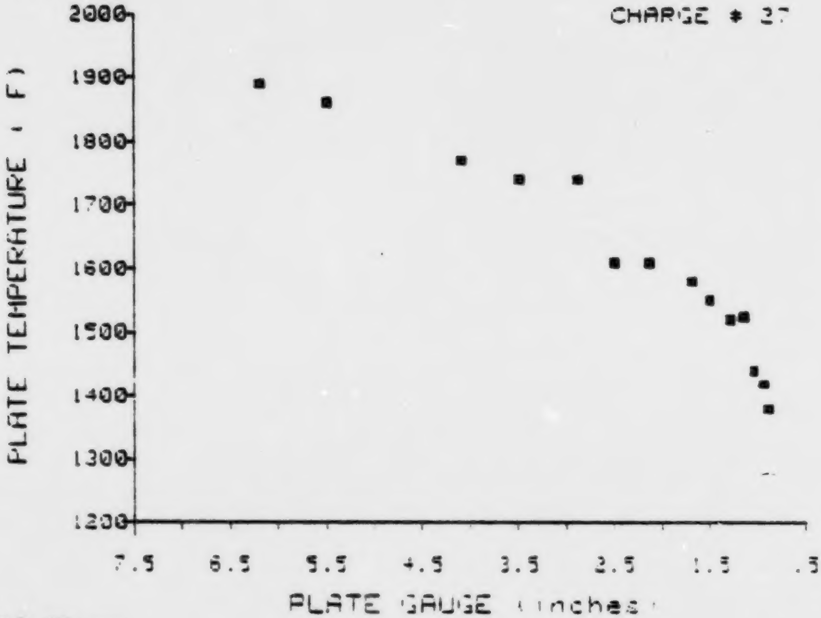

(b) 38 mm

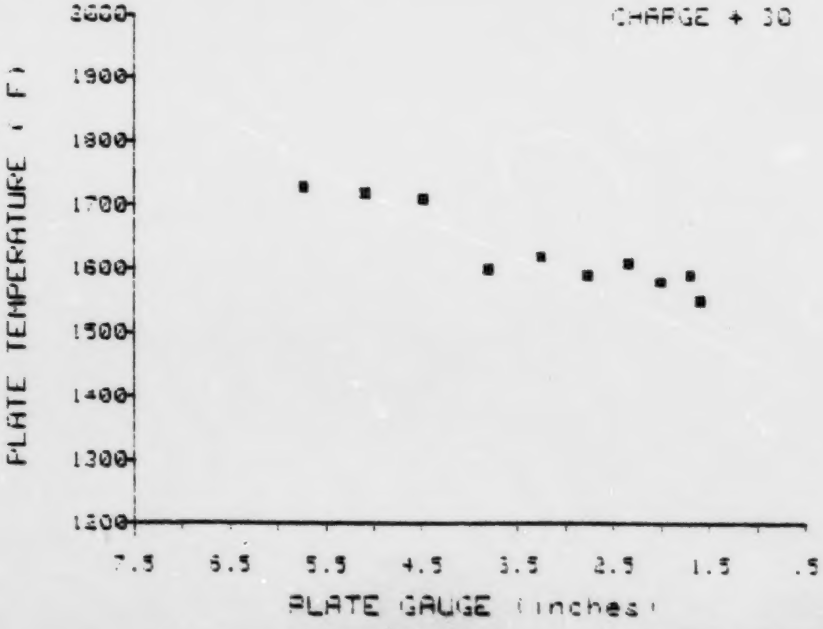

Figure 2 A2: Surface Temperature Loss as a Function of Rolling Time

(a) 25 mm

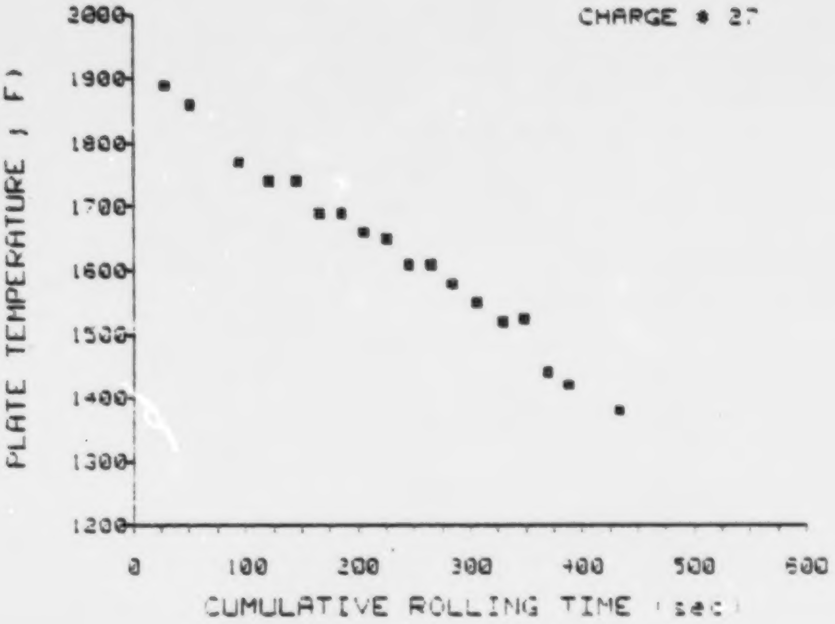

(b) 38 mm

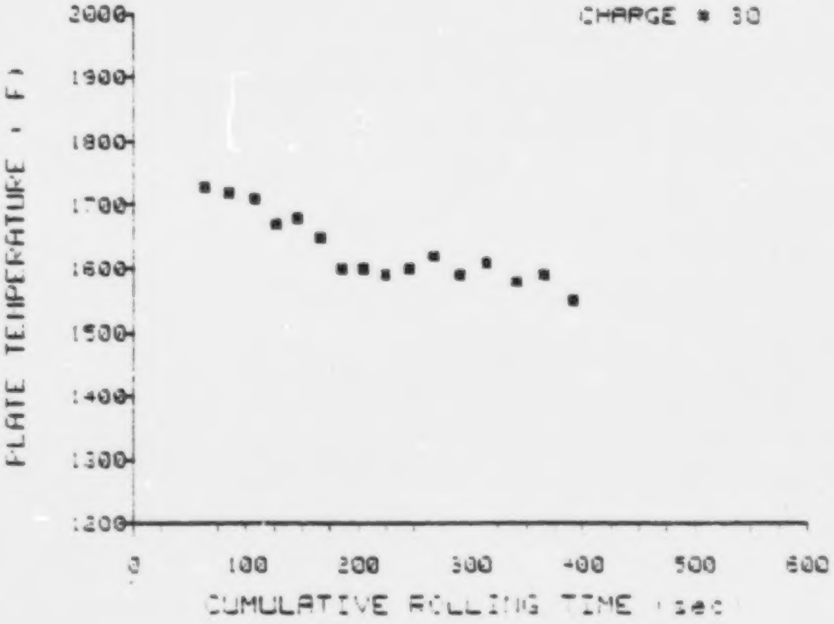

# APPENDIX 3

## MECHANICAL PROPERTIES AND MICROSTRUCTURES OF GRADE 350 PLATE

This Appendix summarizes the tensile strength and Charpy toughness data, as well as the microstructural information on the trial heats in both the controlled rolled and normalized conditions.

This includes:

Table I A3 - Tensile Data
II A3 - Charpy Data LEW Ht 805126
III A3 - Charpy Data HW Ht 536441

Figure 1 A3 - Ferrite Grain Size - LEW Ht 805126 CR
2 A3 - Microstructure - LEW Ht 805126 CR
3 A3 - Charpy Transitions - LEW Ht 805126 CR

Figure 4 A3 - Ferrite Grain Size - LEW Ht 805126 N
5 A3 - Microstructure - LEW Ht 805126 N
6 A3 - Charpy Transitions - LEW Ht 805126 N

Figure 7 A3 - Ferrite Grain Size - HW Ht 536441 CR
8 A3 - Microstructure - HW Ht 536441 CR
9 A3 - Charpy Transitions - HW Ht 536441 CR

Figure 10 A3 - Ferrite Grain Size - HW Ht 536441 N
11 A3 - Microstructure - HW Ht 536441 N
12 A3 - Charpy Transitions - HW Ht 536441 N

Tables IV A3 and V A3 give data on the calculated contributions to strength and Charpy impact transition temperature of the various strengthening mechanisms and grain size.

## Table I A3: Tensile Data

| CHG | GAUGE | WORKS | AS ROLLED LONGITUDINAL YIELD MPa | UTS MPa | %EL | %RA | AS ROLLED TRANSVERSE YIELD MPa | UTS MPa | %EL | %RA | NORMALIZED LONGITUDINAL YIELD MPa | UTS MPa | %EL | %RA | NORMALIZED TRANSVERSE YIELD MPa | UTS MPa | %EL | %RA |
|---|---|---|---|---|---|---|---|---|---|---|---|---|---|---|---|---|---|---|
| 10 | .750 | HW | 490 | 590 | 50.0 | 56.2 | 516 | 607 | 45.0 | 55.4 | 370 | 514 | 60.0 | 67.4 | 383 | 520 | 54.5 | 69.0 |
| 11 | .750 | HW | 490 | 590 | 48.0 | 66.1 | 510 | 611 | 41.0 | 53.5 | 380 | 510 | 54.5 | 63.0 | 389 | 514 | 53.0 | 60.6 |
| 12 | .750 | HW | 490 | 580 | 45.0 | 63.9 | 509 | 597 | 44.5 | 56.5 | 376 | 502 | 57.0 | 69.0 | 383 | 507 | 57.0 | 63.0 |
| 13 | 1.000 | HW | 460 | 572 | 53.0 | 63.1 | 472 | 570 | 55.0 | 56.0 | 0 | 0 | 0.0 | 0.0 | 0 | 0 | 0.0 | 0.0 |
| 14 | 1.000 | HW | 475 | 581 | 57.5 | 66.2 | 490 | 594 | 51.3 | 59.2 | 0 | 0 | 0.0 | 0.0 | 0 | 0 | 0.0 | 0.0 |
| 15 | 1.006 | HW | 469 | 575 | 56.5 | 67.6 | 0 | 0 | 0.0 | 0.0 | 0 | 0 | 0.0 | 0.0 | 0 | 0 | 0.0 | 0.0 |
| 16 | 1.250 | HW | 446 | 563 | 65.0 | 71.9 | 453 | 560 | 50.0 | 62.1 | 0 | 0 | 0.0 | 0.0 | 0 | 0 | 0.0 | 0.0 |
| 17 | 1.250 | HW | 439 | 564 | 50.0 | 65.2 | 455 | 572 | 58.0 | 63.3 | 0 | 0 | 0.0 | 0.0 | 0 | 0 | 0.0 | 0.0 |
| 19 | 1.500 | HW | 432 | 549 | 60.0 | 71.5 | 436 | 556 | 54.0 | 60.9 | 370 | 506 | 63.0 | 70.0 | 387 | 509 | 69.0 | 63.3 |
| 20 | 1.500 | HW | 429 | 552 | 60.5 | 71.4 | 436 | 557 | 43.0 | 61.6 | 372 | 509 | 70.0 | 72.2 | 383 | 512 | 66.0 | 62.6 |
| 21 | 1.500 | HW | 418 | 552 | 66.0 | 69.9 | 434 | 561 | 45.0 | 61.9 | 372 | 507 | 68.0 | 69.7 | 374 | 509 | 63.0 | 59.0 |
| 22 | 2.500 | HW | 0 | 0 | 0.0 | 0.0 | 390 | 552 | 32.0 | 70.6 | 0 | 0 | 0.0 | 0.0 | 366 | 514 | 35.0 | 72.5 |
| 23 | 2.500 | HW | 0 | 0 | 0.0 | 0.0 | 397 | 554 | 32.0 | 74.3 | 0 | 0 | 0.0 | 0.0 | 0 | 0 | 0.0 | 0.0 |
| 1 | 4.000 | HW | 0 | 0 | 0.0 | 0.0 | 392 | 580 | 31.5 | 72.3 | 351 | 500 | 30.0 | 76.3 | 356 | 503 | 38.0 | 74.3 |
| 2 | 4.000 | HW | 0 | 0 | 0.0 | 0.0 | 382 | 564 | 32.5 | 73.1 | 0 | 0 | 0.0 | 0.0 | 350 | 502 | 38.0 | 74.9 |
| | | | | | | | | | | | | | | | | | | |
| 36 | .390 | LEW | 421 | 509 | 53.0 | 60.3 | 423 | 514 | 40.0 | 64.3 | 0 | 0 | 0.0 | 0.0 | 0 | 0 | 0.0 | 0.0 |
| 24 | .750 | LEW | 410 | 496 | 50.0 | 69.4 | 424 | 505 | 56.0 | 67.0 | 340 | 463 | 64.0 | 74.7 | 347 | 461 | 56.5 | 68.7 |
| 25 | .750 | LEW | 415 | 502 | 50.5 | 71.4 | 423 | 502 | 56.5 | 66.6 | 347 | 466 | 65.0 | 76.7 | 351 | 460 | 61.5 | 70.1 |
| 26 | 1.000 | LEW | 396 | 486 | 63.5 | 72.6 | 401 | 489 | 64.5 | 70.3 | 327 | 447 | 71.0 | 70.2 | 330 | 449 | 69.5 | 72.1 |
| 27 | 1.000 | LEW | 390 | 486 | 66.0 | 74.0 | 0 | 0 | 0.0 | 0.0 | 332 | 450 | 70.0 | 76.5 | 337 | 461 | 60.0 | 72.1 |
| 3 | 1.100 | LEW | 387 | 470 | 72.0 | 76.6 | 390 | 487 | 70.0 | 70.0 | 0 | 0 | 0.0 | 0.0 | 0 | 0 | 0.0 | 0.0 |
| 28 | 1.250 | LEW | 371 | 474 | 73.0 | 70.1 | 374 | 479 | 62.5 | 70.9 | 327 | 450 | 74.0 | 76.3 | 332 | 451 | 60.0 | 72.1 |
| 29 | 1.250 | LEW | 370 | 470 | 40.0 | 75.9 | 374 | 470 | 46.0 | 71.7 | 330 | 449 | 74.0 | 77.4 | 329 | 447 | 60.0 | 73.0 |
| 30 | 1.500 | LEW | 355 | 463 | 77.0 | 76.2 | 357 | 467 | 60.0 | 73.0 | 325 | 461 | 55.0 | 76.0 | 332 | 464 | 57.0 | 73.2 |
| 32 | 1.750 | LEW | 0 | 0 | 0.0 | 0.0 | 369 | 473 | 38.0 | 80.5 | 0 | 0 | 0.0 | 0.0 | 336 | 462 | 40.0 | 81.4 |
| 33 | 1.750 | LEW | 0 | 0 | 0.0 | 0.0 | 336 | 473 | 38.0 | 78.5 | 0 | 0 | 0.0 | 0.0 | 335 | 461 | 40.0 | 80.7 |
| 34 | 2.000 | LEW | 336 | 460 | 39.0 | 80.7 | 335 | 466 | 39.5 | 80.3 | 0 | 0 | 0.0 | 0.0 | 330 | 450 | 41.0 | 81.0 |
| 35 | 2.000 | LEW | 0 | 0 | 0.0 | 0.0 | 330 | 469 | 37.5 | 80.3 | 0 | 0 | 0.0 | 0.0 | 0 | 0 | 0.0 | 0.0 |

## Table II A3: Charpy Data - Ht 805126

### (a) Average

| CHG | GAUGE | TEST POS. | WORKS | COND | ENERGY(Joules)/%SHEAR | | | | | | | | |
|---|---|---|---|---|---|---|---|---|---|---|---|---|---|
| | | | | | +20 | 0 | -15 | -30 | -45 | -60 | -75 | -90 | -100 |
| 24 | .750 | sur | LEW | H | NA /NA | NA /NA | NA /NA | 282/100 | 188/68 | 229/85 | 161/56 | 114/30 | 87 /23 |
| 25 | .750 | sur | LEW | H | NA /NA | NA /NA | NA /NA | 274/100 | 262/83 | 236/83 | 201/67 | 180/53 | 140/40 |
| 26 | 1.000 | sur | LEW | H | NA /NA | NA /NA | NA /NA | 297/100 | 264/88 | 198/67 | 206/73 | 103/31 | 38 /9 |
| 27 | 1.000 | sur | LEW | H | NA /NA | NA /NA | NA /NA | NA /NA | 283/100 | 191/63 | 163/63 | 95 /41 | 14 /8 |
| 28 | 1.250 | sur | LEW | H | NA /NA | NA /NA | 274/100 | 229/100 | 217/84 | 210/77 | 178/60 | 146/40 | 125/33 |
| 28 | 1.250 | mid | LEW | H | NA /NA | NA /NA | NA /NA | 331/100 | 243/75 | 194/60 | 193/53 | 61 /22 | 98 /30 |
| 29 | 1.250 | sur | LEW | H | NA /NA | NA /NA | NA /NA | NA /NA | 279/100 | 247/79 | 240/84 | 87 /25 | 89 /25 |
| 29 | 1.250 | mid | LEW | H | NA /NA | NA /NA | NA /NA | 316/93 | 187/72 | 144/59 | 153/46 | 38 /13 | 14 /5 |
| 30 | 1.500 | 1/4 | LEW | H | NA /NA | NA /NA | NA /NA | NA /NA | NA /NA | NA /NA | NA /NA | NA /NA | NA /NA |
| 30 | 1.500 | mid | LEW | H | NA /NA | NA /NA | NA /NA | NA /NA | NA /NA | NA /NA | NA /NA | NA /NA | NA /NA |
| 32 | 1.750 | 1/4 | LEW | H | NA /NA | NA /NA | NA /NA | NA /NA | 290/100 | 290/88 | 236/83 | 94 /27 | 19 /6 |
| 32 | 1.750 | mid | LEW | H | NA /NA | NA /NA | NA /NA | NA /NA | 323/90 | 194/60 | 127/50 | 60 /15 | 19 /4 |
| 33 | 1.750 | 1/4 | LEW | H | NA /NA | NA /NA | NA /NA | NA /NA | NA /NA | 266/100 | 228/80 | 203/56 | 47 /11 |
| 33 | 1.750 | mid | LEW | H | NA /NA | NA /NA | NA /NA | NA /NA | NA /NA | NA /NA | NA /NA | NA /NA | NA /NA |
| 34 | 2.000 | 1/4 | LEW | H | NA /NA | NA /NA | NA /NA | 358/100 | 273/95 | 263/92 | 250/92 | 191/52 | 103/27 |
| 34 | 2.000 | mid | LEW | H | NA /NA | NA /NA | NA /NA | NA /NA | NA /NA | 321/100 | NA /NA | NA /NA | NA /NA |
| 35 | 2.000 | 1/4 | LEW | H | NA /NA | NA /NA | NA /NA | NA /NA | 305/100 | 233/75 | 256/93 | 201/66 | 9 /3 |
| 35 | 2.000 | mid | LEW | H | NA /NA | NA /NA | NA /NA | 357/100 | 317/91 | 184/57 | 111/35 | 28 /11 | 46 /11 |
| 36 | .590 | sur | LEW | CR | 240/100 | 255/91 | 190/75 | 140/64 | 188/65 | 98 /41 | 28 /25 | 15 /6 | NA /NA |
| 24 | .750 | sur | LEW | CR | NA /NA | NA /NA | NA /NA | 226/95 | 186/80 | 195/82 | 174/73 | 64 /32 | 23 /20 |
| 25 | .750 | sur | LEW | CR | NA /NA | NA /NA | 206/99 | 194/94 | 179/83 | 156/75 | 130/57 | 100/37 | 20 /20 |
| 26 | 1.000 | sur | LEW | CR | NA /NA | NA /NA | 240/99 | 237/93 | 198/82 | 190/77 | 129/51 | 80 /34 | 11 /7 |
| 27 | 1.000 | sur | LEW | CR | NA /NA | NA /NA | NA /NA | 256/98 | 240/87 | 202/79 | 210/82 | 133/51 | 79 /30 |
| 3 | 1.180 | sur | LEW | CR | NA /NA | NA /NA | NA /NA | 300/100 | 308/99 | 271/93 | 197/55 | 174/48 | NA /27 |
| 3 | 1.180 | mid | LEW | CR | NA /NA | NA /NA | NA /NA | 339/96 | 292/85 | 138/62 | 197/57 | 22 /10 | NA /NA |
| 28 | 1.250 | sur | LEW | CR | NA /NA | 297/100 | 252/91 | 141/59 | 179/53 | 180/51 | 142/36 | 34 /9 | 7 /2 |
| 28 | 1.250 | mid | LEW | CR | NA /NA | 350/100 | 259/67 | 229/66 | 182/45 | 176/49 | 111/27 | 14 /3 | NA /NA |
| 29 | 1.250 | mid | LEW | CR | NA /NA | 298/100 | 241/69 | 226/78 | 228/72 | 138/54 | 80 /22 | 5 /3 | NA /NA |
| 30 | 1.500 | 1/4 | LEW | CR | NA /NA | 305/100 | 258/71 | 254/84 | 221/64 | 174/49 | 153/37 | 11 /4 | NA /NA |
| 30 | 1.500 | mid | LEW | CR | NA /NA | 325/100 | 236/74 | 229/64 | 146/40 | 20 /18 | 37 /13 | 9 /2 | NA /NA |
| 32 | 1.750 | 1/4 | LEW | CR | NA /NA | 354/100 | 282/86 | 199/57 | 193/51 | 42 /15 | 20 /5 | NA /NA | NA /NA |
| 32 | 1.750 | mid | LEW | CR | 171/44 | 126/51 | 167/58 | 117/38 | 39 /14 | 20 /11 | 7 /2 | NA /NA | NA /NA |
| 33 | 1.750 | 1/4 | LEW | CR | NA /NA | 281/93 | 243/78 | 205/66 | 172/48 | 104/31 | 7 /4 | NA /NA | NA /NA |
| 33 | 1.750 | mid | LEW | CR | NA /NA | 302/95 | 354/100 | 245/77 | 37 /13 | 96 /23 | 8 /4 | NA /NA | NA /NA |
| 35 | 2.000 | 1/4 | LEW | CR | NA /NA | 334/100 | 353/100 | 301/95 | 231/67 | 197/61 | 9 /4 | NA /NA | NA /NA |
| 35 | 2.000 | 1/4 | LEW | CR | 311/100 | 279/90 | 240/71 | 224/60 | 210/54 | 136/34 | 30 /6 | NA /NA | NA /NA |
| 35 | 2.000 | mid | LEW | CR | NA /NA | 353/100 | 245/63 | 182/40 | 22 /9 | 34 /9 | 9 /3 | NA /NA | NA /NA |
| 35 | 2.000 | mid | LEW | CR | NA /NA | 268/78 | 357/100 | 110/32 | 11 /7 | 9 /6 | NA /NA | NA /NA | NA /NA |

**(b) Minimum**

| CHG | GAUGE | TEST POS. | WORKS | COND | ENERGY(Joules)/%SHEAR +20 | 0 | -15 | -30 | -45 | -60 | -75 | -90 | -100 |
|---|---|---|---|---|---|---|---|---|---|---|---|---|---|
| 24 | .750 | sur | LEN | N | NA /NA | NA /NA | NA /NA | 201/100 | 104/65 | 197/69 | 152/52 | 76 /22 | 45 /14 |
| 25 | .750 | sur | LEN | N | NA /NA | NA /NA | NA /NA | 270/100 | 239/90 | 195/65 | 190/61 | 136/55 | 130/36 |
| 26 | 1.000 | sur | LEN | N | NA /NA | NA /NA | NA /NA | 285/100 | 225/81 | 186/66 | 183/70 | 7 /10 | 16 /7 |
| 27 | 1.000 | sur | LEN | N | NA /NA | NA /NA | NA /NA | NA /NA | 268/100 | 190/68 | 136/57 | 5 /8 | 5 /6 |
| 28 | 1.250 | sur | LEN | N | NA /NA | NA /NA | 267/100 | 209/100 | 174/67 | 157/53 | 175/59 | 133/33 | 119/32 |
| 28 | 1.250 | mid | LEN | N | NA /NA | NA /NA | NA /NA | 325/100 | 210/66 | 190/59 | 171/20 | 20 /7 | 19 /12 |
| 29 | 1.250 | sur | LEN | N | NA /NA | NA /NA | NA /NA | NA /NA | 262/100 | 239/76 | 186/67 | 23 /12 | 23 /11 |
| 29 | 1.250 | mid | LEN | N | NA /NA | NA /NA | NA /NA | 277/85 | 113/56 | 50 /41 | 132/37 | 20 /11 | 9 /4 |
| 30 | 1.500 | 1/4 | LEN | N | NA /NA | NA /NA | NA /NA | NA /NA | NA /NA | NA /NA | NA /NA | NA /NA | NA /NA |
| 30 | 1.500 | mid | LEN | N | NA /NA | NA /NA | NA /NA | NA /NA | NA /NA | NA /NA | NA /NA | NA /NA | NA /NA |
| 32 | 1.750 | 1/4 | LEN | N | NA /NA | NA /NA | NA /NA | NA /NA | 285/100 | 231/75 | 210/71 | 8 /7 | 10 /5 |
| 32 | 1.750 | mid | LEN | N | NA /NA | NA /NA | NA /NA | NA /NA | 300/95 | 31 /36 | 35 /20 | 12 /7 | 11 /2 |
| 33 | 1.750 | 1/4 | LEN | N | NA /NA | NA /NA | NA /NA | NA /NA | NA /NA | 260/100 | 207/75 | 186/51 | 4 /3 |
| 33 | 1.750 | mid | LEN | N | NA /NA | NA /NA | NA /NA | NA /NA | NA /NA | NA /NA | NA /NA | NA /NA | NA /NA |
| 34 | 2.000 | 1/4 | LEN | N | NA /NA | NA /NA | NA /NA | 350/100 | 260/90 | 236/83 | 240/85 | 184/51 | 33 /10 |
| 34 | 2.000 | mid | LEN | N | NA /NA | NA /NA | NA /NA | NA /NA | NA /NA | 300/100 | NA /NA | NA /NA | NA /NA |
| 35 | 2.000 | 1/4 | LEN | N | NA /NA | NA /NA | NA /NA | NA /NA | 287/100 | 176/57 | 236/85 | 178/56 | 7 /3 |
| 35 | 2.000 | mid | LEN | N | NA /NA | NA /NA | NA /NA | 354/100 | 270/82 | 60 /25 | 12 /10 | 15 /7 | 11 /5 |
| 36 | .590 | sur | LEN | CR | 235/100 | 243/86 | 179/72 | 100/57 | 182/64 | 80 /30 | 16 /23 | 11 /5 | NA /NA |
| 24 | .750 | sur | LEN | CR | NA /NA | NA /NA | NA /NA | 210/90 | 179/75 | 161/74 | 174/72 | 37 /29 | 18 /19 |
| 25 | .750 | sur | LEN | CR | NA /NA | NA /NA | 201/90 | 187/90 | 175/70 | 144/71 | 134/57 | 71 /35 | 20 /14 |
| 26 | 1.000 | sur | LEN | CR | NA /NA | NA /NA | 243/90 | 220/85 | 179/91 | 168/69 | 117/47 | 20 /27 | 11 /7 |
| 27 | 1.000 | sur | LEN | CR | NA /NA | NA /NA | NA /NA | 255/96 | 229/83 | 190/79 | 195/80 | 102/44 | 30 /19 |
| 3 | 1.100 | sur | LEN | CR | NA /NA | NA /NA | NA /NA | 289/100 | 304/90 | 244/86 | 178/30 | 167/46 | NA /10 |
| 3 | 1.100 | mid | LEN | CR | NA /NA | NA /NA | NA /NA | 320/92 | 258/91 | 80 /40 | 167/50 | 20 /8 | NA /NA |
| 28 | 1.250 | sur | LEN | CR | NA /NA | 240/100 | 218/81 | 114/51 | 171/52 | 167/47 | 125/32 | 9 /3 | 4 /2 |
| 28 | 1.250 | mid | LEN | CR | NA /NA | 350/100 | 255/64 | 212/64 | 164/42 | 176/45 | 79 /21 | 7 /2 | NA /NA |
| 29 | 1.250 | mid | LEN | CR | NA /NA | 290/100 | 226/62 | 206/67 | 217/69 | 171/48 | 18 /11 | 5 /3 | NA /NA |
| 30 | 1.500 | 1/4 | LEN | CR | NA /NA | 277/100 | 240/65 | 220/60 | 220/61 | 156/41 | 146/35 | 7 /3 | NA /NA |
| 30 | 1.500 | mid | LEN | CR | NA /NA | 293/100 | 201/71 | 226/62 | 85 /30 | 18 /17 | 33 /12 | 8 /2 | NA /NA |
| 32 | 1.750 | 1/4 | LEN | CR | NA /NA | 350/100 | 247/74 | 140/45 | 138/48 | 15 /10 | 5 /3 | NA /NA | NA /NA |
| 32 | 1.750 | mid | LEN | CR | 136/65 | 85 /43 | 64 /35 | 23 /23 | 28 /13 | 11 /8 | 5 /2 | NA /NA | NA /NA |
| 33 | 1.750 | 1/4 | LEN | CR | NA /NA | 251/85 | 176/55 | 201/66 | 146/42 | 12 /8 | 4 /4 | NA /NA | NA /NA |
| 33 | 1.750 | mid | LEN | CR | NA /NA | 240/70 | 350/100 | 231/73 | 12 /10 | 43 /13 | 5 /3 | NA /NA | NA /NA |
| 34 | 2.000 | 1/4 | LEN | CR | NA /NA | 334/100 | 346/100 | 250/90 | 210/57 | 176/56 | 9 /3 | NA /NA | NA /NA |
| 35 | 2.000 | 1/4 | LEN | CR | 309/100 | 212/60 | 163/42 | 217/59 | 203/52 | 87 /21 | 9 /2 | NA /NA | NA /NA |
| 34 | 2.000 | mid | LEN | CR | NA /NA | 347/100 | 222/50 | 170/37 | 7 /3 | 4 /3 | 8 /2 | NA /NA | NA /NA |
| 35 | 2.000 | mid | LEN | CR | NA /NA | 180/56 | 357/100 | 41 /13 | 7 /6 | 7 /5 | NA /NA | NA /NA | NA /NA |

## Table III A3: Charpy Data - HW Heat 536441

### (a) Average

| CHG | GAUGE | TEST POS. | WORKS | COND | ENERGY(Joules)/%SHEAR | | | | | | | | |
|---|---|---|---|---|---|---|---|---|---|---|---|---|---|
| | | | | | +20 | 0 | -15 | -30 | -45 | -60 | -75 | -90 | -100 |
| 10 | .750 | sur | HW | N | 171/100 | 155/84 | 130/76 | 122/54 | 80 /51 | 46 /32 | 57 /24 | 20 /11 | 8 /3 |
| 11 | .750 | sur | HW | N | NA /NA | NA /NA | NA /NA | 160/100 | 151/78 | 115/50 | 85 /52 | 69 /36 | 30 /23 |
| 12 | .750 | sur | HW | N | NA /NA | NA /NA | NA /NA | NA /NA | NA /NA | NA /NA | NA /NA | NA /NA | NA /NA |
| 19 | 1.500 | 1/4 | HW | N | 179/100 | 161/84 | 155/75 | 140/55 | 104/46 | 20 /27 | 16 /11 | 12 /8 | NA /NA |
| 19 | 1.500 | mid | HW | N | 144/100 | 132/78 | 130/62 | 91 /56 | 43 /41 | 27 /25 | 8 /10 | NA /NA | NA /NA |
| 20 | 1.500 | 1/4 | HW | N | NA /NA | 202/100 | 157/75 | 122/62 | 87 /50 | 65 /41 | 33 /25 | 22 /14 | 9 /10 |
| 20 | 1.500 | mid | HW | N | NA /NA | 170/95 | 125/56 | 122/50 | 80 /53 | 60 /36 | 42 /26 | 15 /14 | 12 /5 |
| 21 | 1.500 | 1/4 | HW | N | 187/100 | 167/80 | 136/70 | 107/51 | 76 /44 | 62 /29 | 30 /13 | 16 /9 | NA /NA |
| 21 | 1.500 | mid | HW | N | 149/100 | 133/84 | 119/72 | 76 /50 | 33 /39 | 31 /25 | 15 /12 | NA /NA | NA /NA |
| 22 | 2.500 | 1/4 | HW | N | NA /NA | NA /NA | NA /NA | NA /NA | NA /NA | NA /NA | NA /NA | NA /NA | NA /NA |
| 22 | 2.500 | mid | HW | N | NA /NA | NA /NA | NA /NA | NA /NA | NA /NA | NA /NA | NA /NA | NA /NA | NA /NA |
| 23 | 2.500 | 1/4 | HW | N | NA /NA | 165/100 | 137/95 | 107/54 | 65 /41 | 30 /29 | 23 /17 | 9 /9 | NA /NA |
| 23 | 2.500 | mid | HW | N | NA /NA | 172/100 | 152/60 | 149/57 | 100/47 | 41 /20 | 12 /14 | 12 /6 | NA /NA |
| 1 | 4.000 | 1/4 | HW | N | NA /NA | 212/100 | 152/63 | 136/49 | 130/51 | 123/41 | 54 /23 | 7 /8 | NA /NA |
| 1 | 4.000 | mid | HW | N | NA /NA | 175/100 | 142/62 | 100/40 | 103/38 | 12 /21 | 24 /14 | 4 /9 | NA /NA |
| 2 | 4.000 | 1/4 | HW | N | 201/100 | 226/82 | 159/64 | 146/55 | 114/43 | 75 /34 | 30 /13 | 12 /4 | NA /NA |
| 2 | 4.000 | mid | HW | N | 201/100 | 190/77 | 156/63 | 133/50 | 117/39 | 53 /23 | 12 /7 | NA /NA | NA /NA |
| 10 | .750 | sur | HW | CR | NA /NA | 127/100 | 126/99 | 107/95 | 104/100 | 75 /90 | 16 /35 | NA /NA | NA /NA |
| 11 | .750 | sur | HW | CR | NA /NA | 130/90 | 110/95 | 113/90 | 77 /60 | 73 /44 | 12 /20 | NA /NA | NA /NA |
| 12 | .750 | sur | HW | CR | NA /NA | 136/100 | 132/100 | 119/100 | 85 /95 | 52 /69 | 22 /32 | 7 /10 | NA /NA |
| 13 | 1.000 | sur | HW | CR | NA /NA | 171/100 | 156/90 | 157/90 | 110/63 | 53 /42 | 34 /39 | 14 /13 | NA /NA |
| 14 | 1.000 | sur | HW | CR | NA /NA | 155/99 | 132/90 | 126/87 | 90 /75 | 60 /32 | 11 /11 | NA /NA | NA /NA |
| 15 | 1.000 | sur | HW | CR | NA /NA | 141/100 | 110/95 | 114/90 | 80 /90 | 73 /73 | 11 /20 | NA /NA | NA /NA |
| 16 | 1.250 | sur | HW | CR | 160/100 | 164/100 | 134/85 | 130/85 | 60 /43 | 60 /39 | 10 /17 | NA /NA | NA /NA |
| 16 | 1.250 | mid | HW | CR | 130/95 | 125/60 | 121/73 | 49 /45 | 61 /32 | 20 /15 | NA /NA | NA /NA | NA /NA |
| 17 | 1.250 | sur | HW | CR | NA /NA | 146/99 | 145/92 | 107/92 | 76 /70 | 23 /30 | 27 /25 | 7 /5 | NA /NA |
| 17 | 1.250 | mid | HW | CR | 136/96 | 141/90 | 125/71 | 89 /59 | 22 /23 | 14 /12 | NA /NA | NA /NA | NA /NA |
| 19 | 1.500 | 1/4 | HW | CR | 175/100 | 176/85 | 146/74 | 99 /50 | 53 /39 | 62 /17 | 11 /8 | NA /NA | NA /NA |
| 19 | 1.500 | mid | HW | CR | 149/85 | 111/64 | 80 /47 | 71 /44 | 20 /20 | 9 /6 | NA /NA | NA /NA | NA /NA |
| 20 | 1.500 | 1/4 | HW | CR | NA /NA | 149/94 | 141/35 | 83 /52 | 102/50 | 50 /31 | 14 /10 | NA /NA | NA /NA |
| 20 | 1.500 | mid | HW | CR | 119/90 | 90 /60 | 87 /50 | 79 /36 | 22 /26 | 8 /9 | NA /NA | NA /NA | NA /NA |
| 21 | 1.500 | 1/4 | HW | CR | 140/95 | 107/55 | 92 /50 | 87 /47 | 34 /27 | 9 /7 | NA /NA | NA /NA | NA /NA |
| 21 | 1.500 | mid | HW | CR | 119/72 | 96 /56 | 87 /45 | 39 /25 | 20 /12 | 5 /7 | NA /NA | NA /NA | NA /NA |

## (b) Minimum

| CHG | GAUGE | TEST POS. | WORKS | COND | ENERGY(Joules)/%SHEAR | | | | | | | | |
|---|---|---|---|---|---|---|---|---|---|---|---|---|---|
| | | | | | +20 | 0 | -15 | -30 | -45 | -60 | -75 | -90 | -100 |
| 10 | .750 | sur | HW | N | 172/100 | 165/92 | 140/76 | 123/57 | 91/53 | 62/35 | 77/20 | 33/11 | 11/4 |
| 11 | .750 | sur | HW | N | NA/NA | NA/NA | NA/NA | 171/100 | 170/89 | 123/59 | 80/55 | 71/36 | 39/26 |
| 12 | .750 | sur | HW | N | NA/NA | NA/NA | NA/NA | NA/NA | NA/NA | NA/NA | NA/NA | NA/NA | NA/NA |
| 19 | 1.500 | 1/4 | HW | N | 190/100 | 164/87 | 159/79 | 146/62 | 115/52 | 60/22 | 34/15 | 24/10 | NA/NA |
| 19 | 1.500 | mid | HW | N | 145/100 | 144/83 | 136/64 | 90/60 | 49/43 | 39/26 | 11/11 | NA/NA | NA/NA |
| 20 | 1.500 | 1/4 | HW | N | NA/NA | 209/100 | 164/98 | 126/69 | 95/52 | 83/43 | 38/26 | 26/15 | 16/11 |
| 20 | 1.500 | mid | HW | N | NA/NA | 180/90 | 133/77 | 123/60 | 100/55 | 80/40 | 56/20 | 30/17 | 14/6 |
| 21 | 1.500 | 1/4 | HW | N | 188/100 | 180/90 | 130/72 | 118/54 | 96/46 | 65/30 | 50/18 | 20/9 | NA/NA |
| 21 | 1.500 | mid | HW | N | 149/100 | 142/89 | 126/74 | 85/55 | 39/41 | 45/27 | 22/13 | NA/NA | NA/NA |
| 22 | 2.500 | 1/4 | HW | N | NA/NA | NA/NA | NA/NA | NA/NA | NA/NA | NA/NA | NA/NA | NA/NA | NA/NA |
| 22 | 2.500 | mid | HW | N | NA/NA | NA/NA | NA/NA | NA/NA | NA/NA | NA/NA | NA/NA | NA/NA | NA/NA |
| 23 | 2.500 | 1/4 | HW | N | NA/NA | 174/100 | 146/90 | 115/62 | 81/47 | 35/33 | 23/10 | 12/10 | NA/NA |
| 23 | 2.500 | mid | HW | N | NA/NA | 190/100 | 156/69 | 153/63 | 110/48 | 66/34 | 46/22 | 19/10 | NA/NA |
| 1 | 4.000 | 1/4 | HW | N | NA/NA | 216/100 | 156/63 | 140/50 | 145/53 | 134/43 | 65/24 | 12/9 | NA/NA |
| 1 | 4.000 | mid | HW | N | NA/NA | 207/87 | 152/66 | 100/47 | 114/40 | 66/32 | 26/14 | 7/9 | NA/NA |
| 2 | 4.000 | 1/4 | HW | N | 210/100 | 205/91 | 171/65 | 140/57 | 114/44 | 99/36 | 57/17 | 15/4 | NA/NA |
| 2 | 4.000 | mid | HW | N | 209/100 | 205/82 | 156/66 | 144/55 | 122/41 | 61/24 | 14/10 | NA/NA | NA/NA |
| 10 | .750 | sur | HW | CR | NA/NA | 137/100 | 127/99 | 117/90 | 106/100 | 81/90 | 20/40 | NA/NA | NA/NA |
| 11 | .750 | sur | HW | CR | NA/NA | 133/90 | 121/96 | 121/93 | 80/73 | 76/45 | 15/20 | NA/NA | NA/NA |
| 12 | .750 | sur | HW | CR | NA/NA | 144/100 | 137/100 | 127/100 | 91/80 | 61/71 | 30/39 | 9/12 | NA/NA |
| 13 | 1.000 | sur | HW | CR | NA/NA | 175/100 | 163/98 | 157/99 | 123/77 | 79/55 | 47/43 | 16/14 | NA/NA |
| 14 | 1.000 | sur | HW | CR | NA/NA | 159/99 | 144/90 | 132/92 | 107/80 | 61/36 | 12/12 | NA/NA | NA/NA |
| 15 | 1.000 | sur | HW | CR | NA/NA | 145/100 | 123/90 | 115/99 | 100/93 | 76/77 | 15/20 | NA/NA | NA/NA |
| 16 | 1.250 | sur | HW | CR | 160/100 | 167/100 | 144/80 | 137/89 | 81/56 | 39/50 | 19/22 | NA/NA | NA/NA |
| 16 | 1.250 | mid | HW | CR | 142/95 | 141/73 | 132/77 | 69/51 | 60/35 | 23/16 | NA/NA | NA/NA | NA/NA |
| 17 | 1.250 | sur | HW | CR | NA/NA | 140/99 | 149/93 | 110/83 | 102/79 | 31/34 | 34/27 | 8/6 | NA/NA |
| 17 | 1.250 | mid | HW | CR | 145/97 | 140/82 | 125/72 | 90/60 | 45/31 | 16/14 | NA/NA | NA/NA | NA/NA |
| 19 | 1.500 | 1/4 | HW | CR | 186/100 | 179/88 | 152/75 | 123/64 | 83/46 | 65/22 | 20/20 | NA/NA | NA/NA |
| 19 | 1.500 | mid | HW | CR | 135/90 | 117/65 | 84/49 | 75/47 | 27/21 | 11/6 | NA/NA | NA/NA | NA/NA |
| 20 | 1.500 | 1/4 | HW | CR | NA/NA | 164/91 | 149/90 | 110/61 | 117/58 | 65/34 | 15/10 | NA/NA | NA/NA |
| 20 | 1.500 | mid | HW | CR | 126/93 | 102/72 | 89/60 | 46/40 | 23/27 | 15/11 | NA/NA | NA/NA | NA/NA |
| 21 | 1.500 | 1/4 | HW | CR | 152/95 | 113/60 | 114/57 | 100/49 | 56/29 | 19/10 | NA/NA | NA/NA | NA/NA |
| 21 | 1.500 | mid | HW | CR | 133/78 | 90/57 | 94/46 | 57/30 | 23 17 | 7 7 | NA/NA | NA/NA | NA/NA |

Figure 1 A3: Ferrite Grain Size* Distributions Controlled Rolled LEW Ht 805126

(a) Chg 24, 19 mm

(b) Chg 3, 30 mm

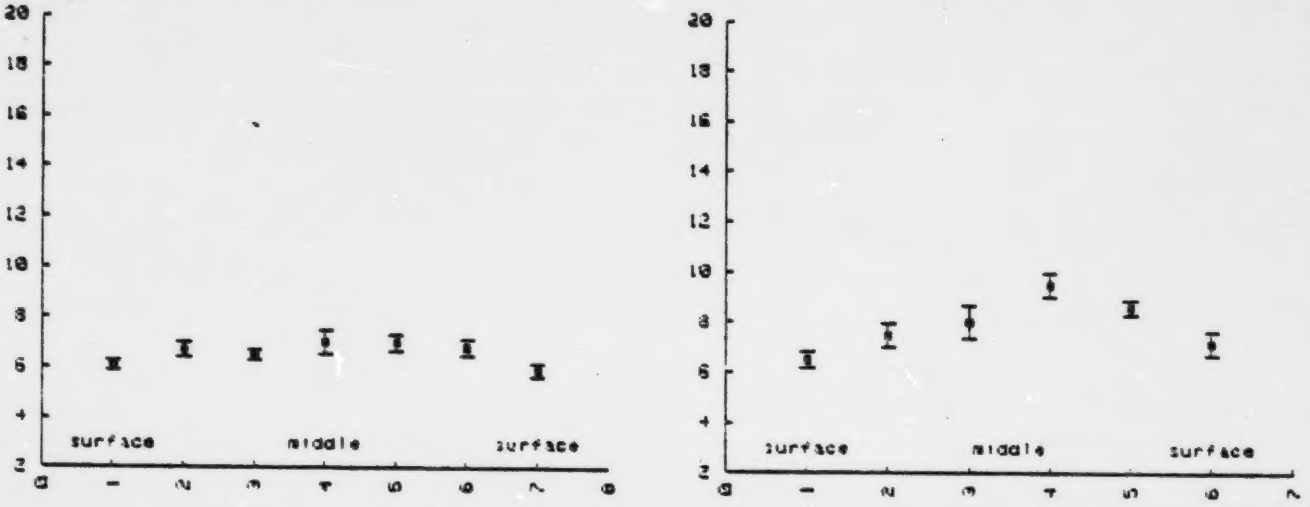

(c) Chg 30, 38 mm

(d) Chg 35, 51 mm

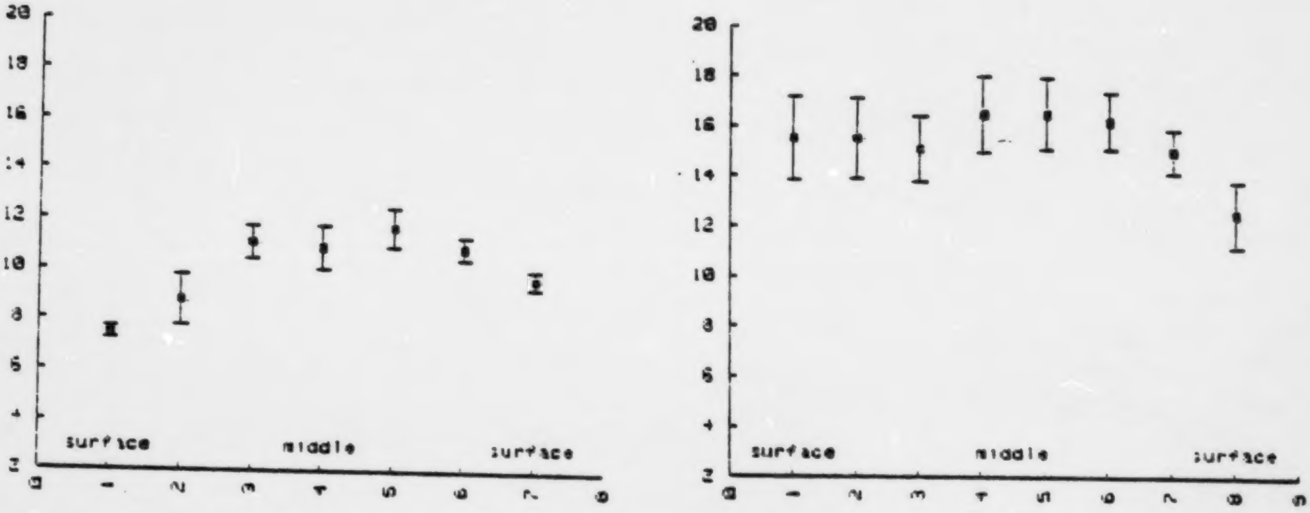

* ferrite grain size in microns.

Figure 2 A3: Microstructures LEW Ht 750126 Controlled Rolled (200X)

(a) Chg 24, 19 mm, 1/4 T

(b) Chg 3, 30 mm, 1/4 T

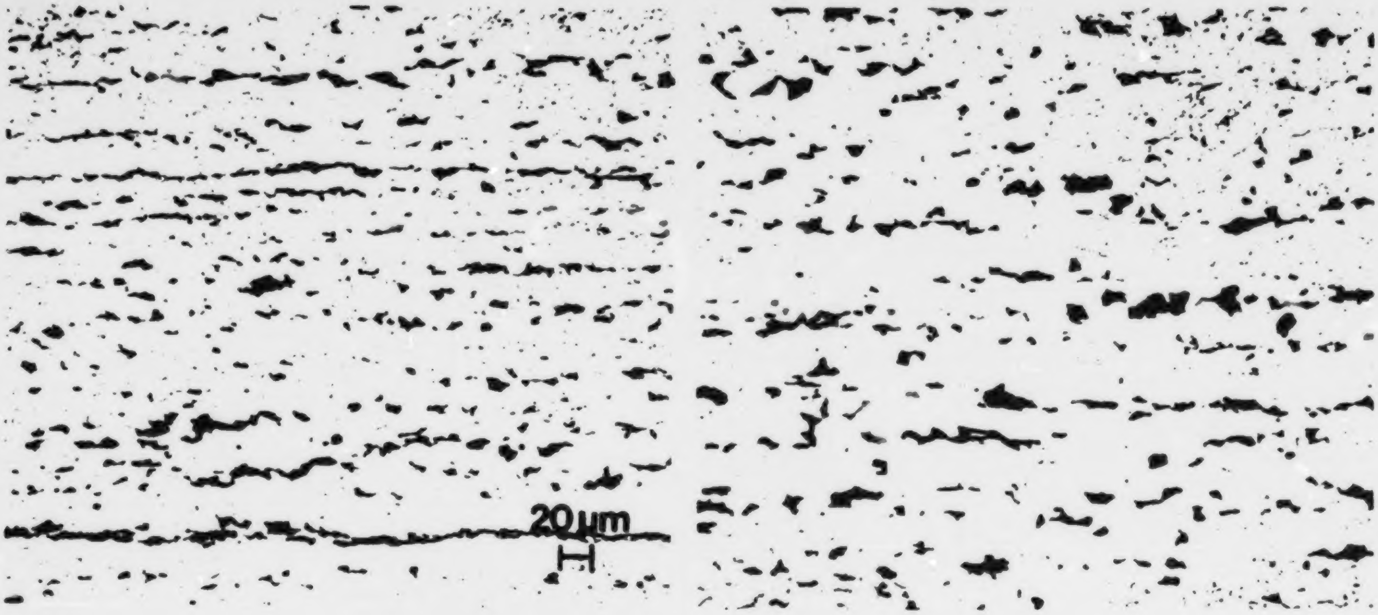

(c) Chg 30, 38 mm, 1/2 T

(d) Chg 35, 51 mm, 1/2 T

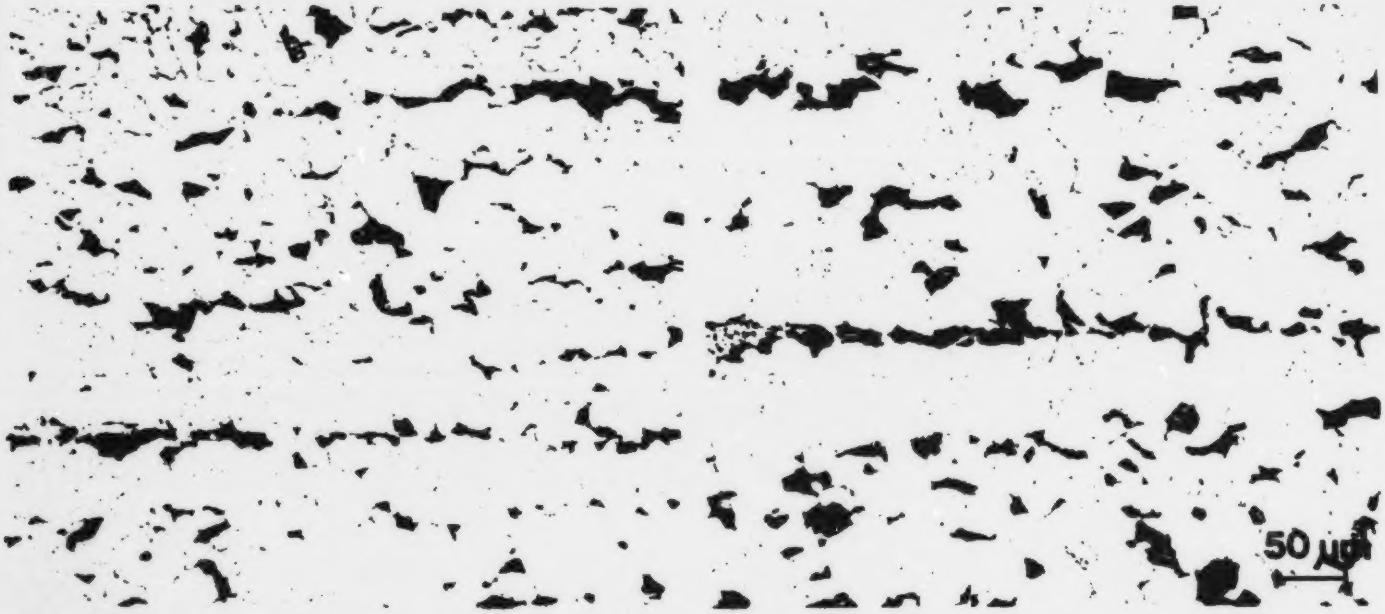

Figure 3 A3: Charpy Transition Curves Controlled Rolled LEW 805126

(a) Chg 3, 30 mm, Surface

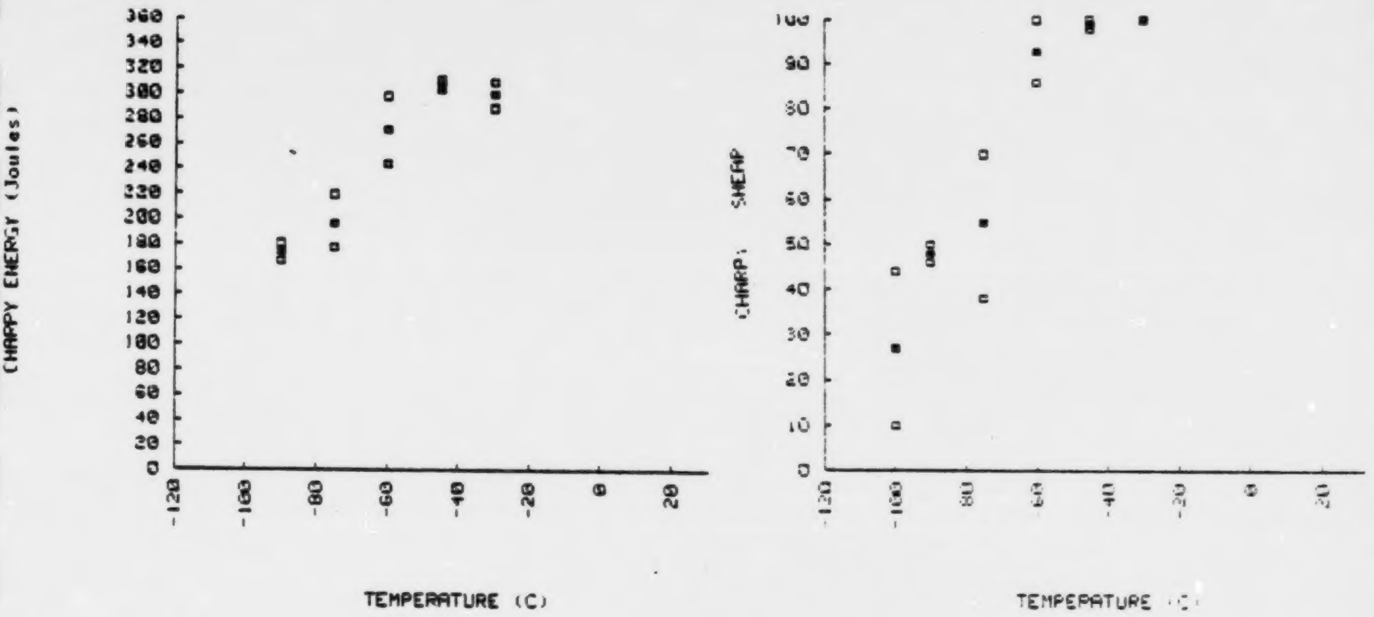

(b) Chg 3, 30 mm, Mid Thickness

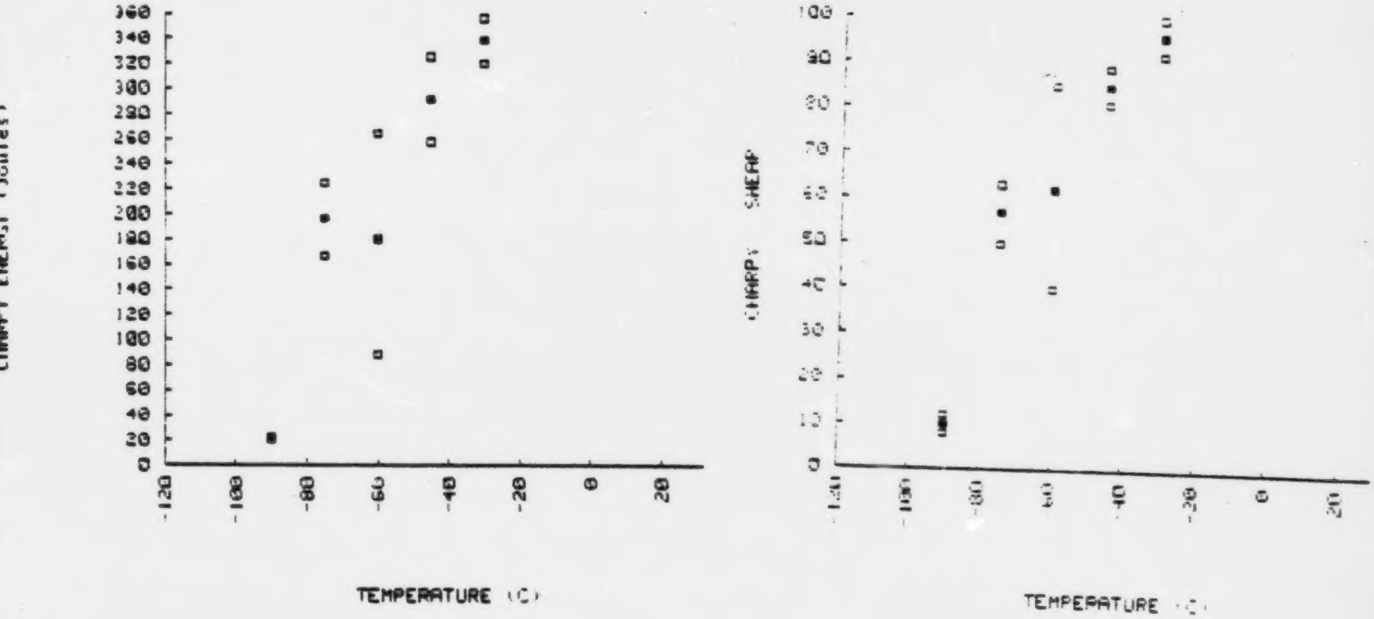

**igure 3 A3 (contd)**

**:) Chg 30, 38 mm, 1/4 Thickness**

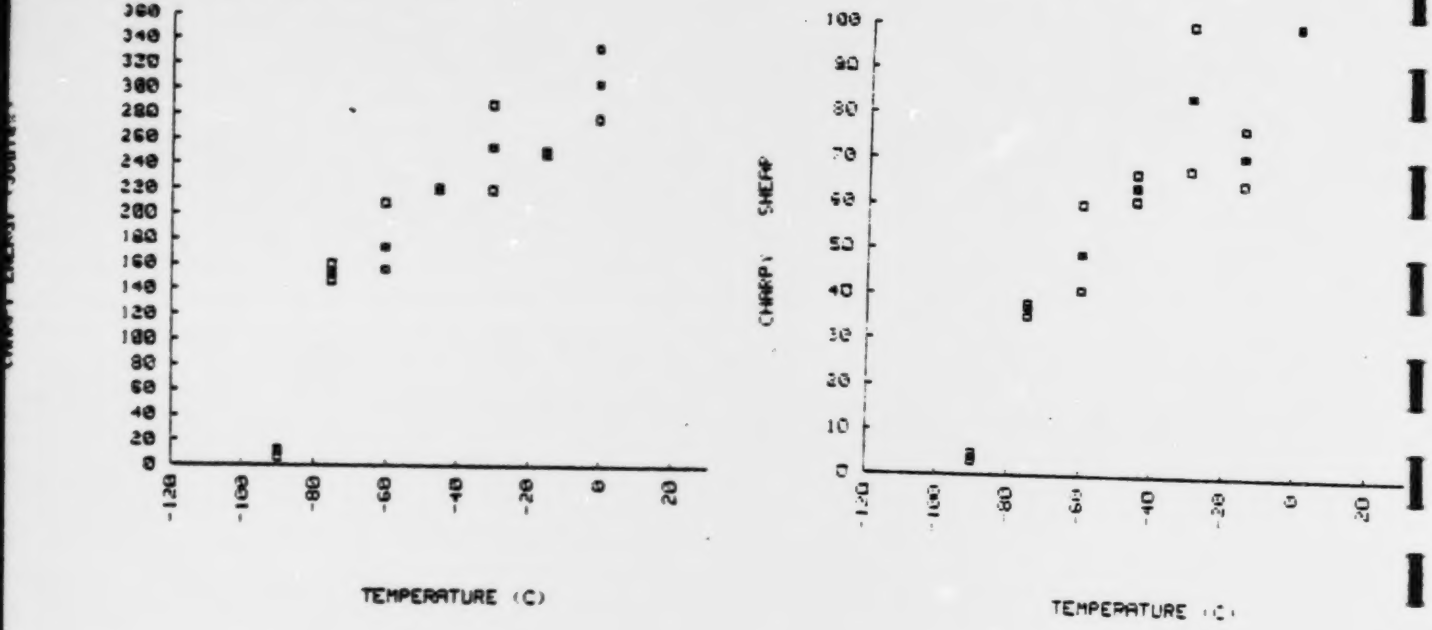

**d) Chg 30, 38 mm, Mid Thickness**

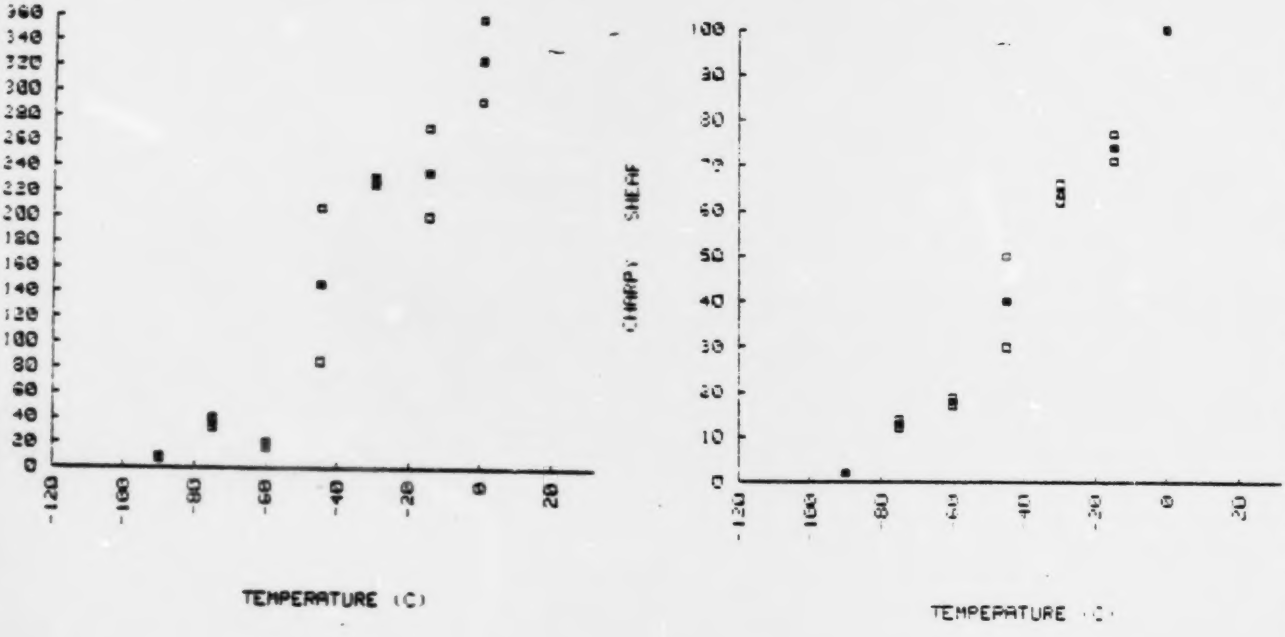

Figure 3 A3 (contd)

(e) Chg 35, 51 mm, 1/4 Thickness

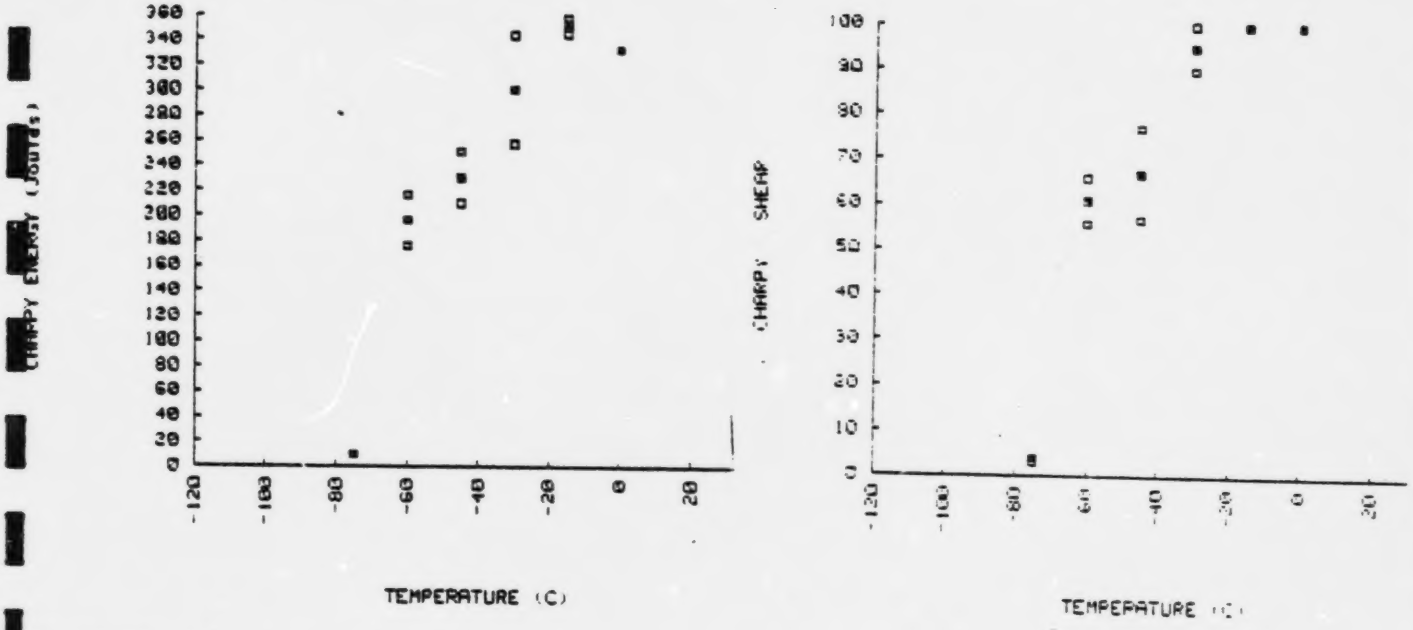

(f) Chg 35, 51 mm, Mid Thickness

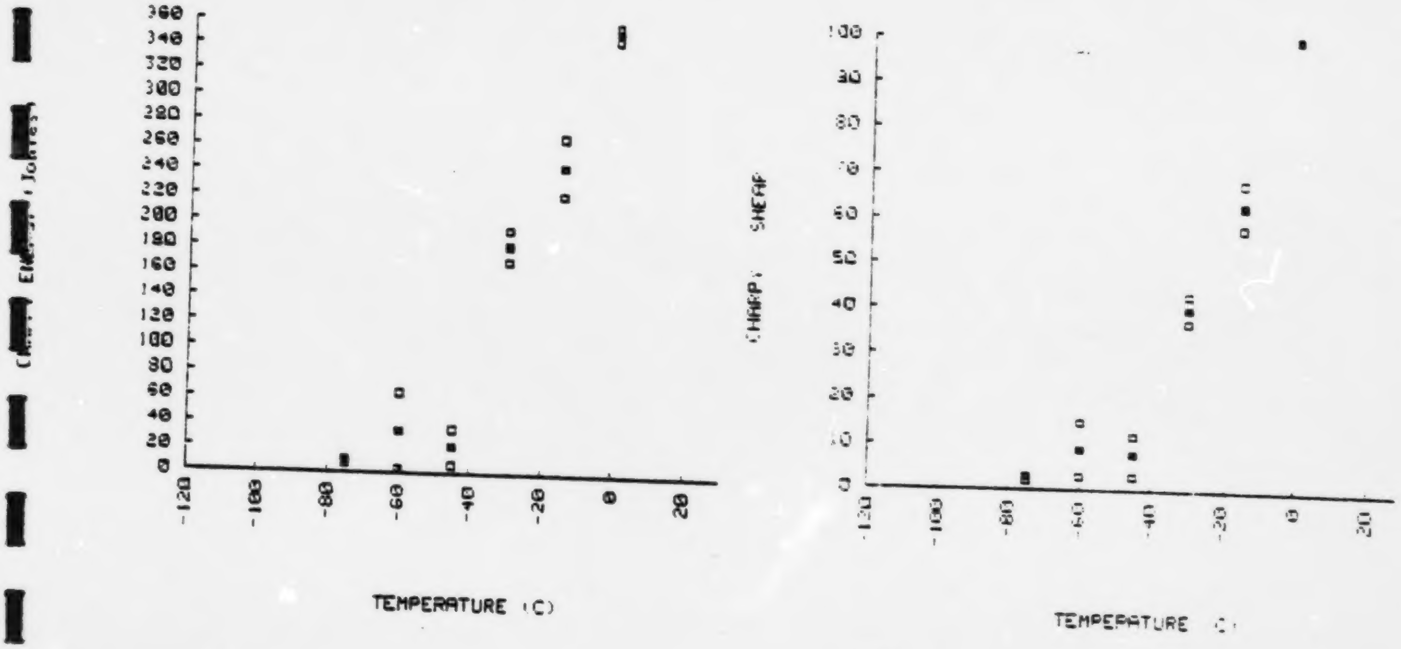

**Figure 4 A3: Ferrite Grain Size* Distributions Normalized LEW Ht 805126**

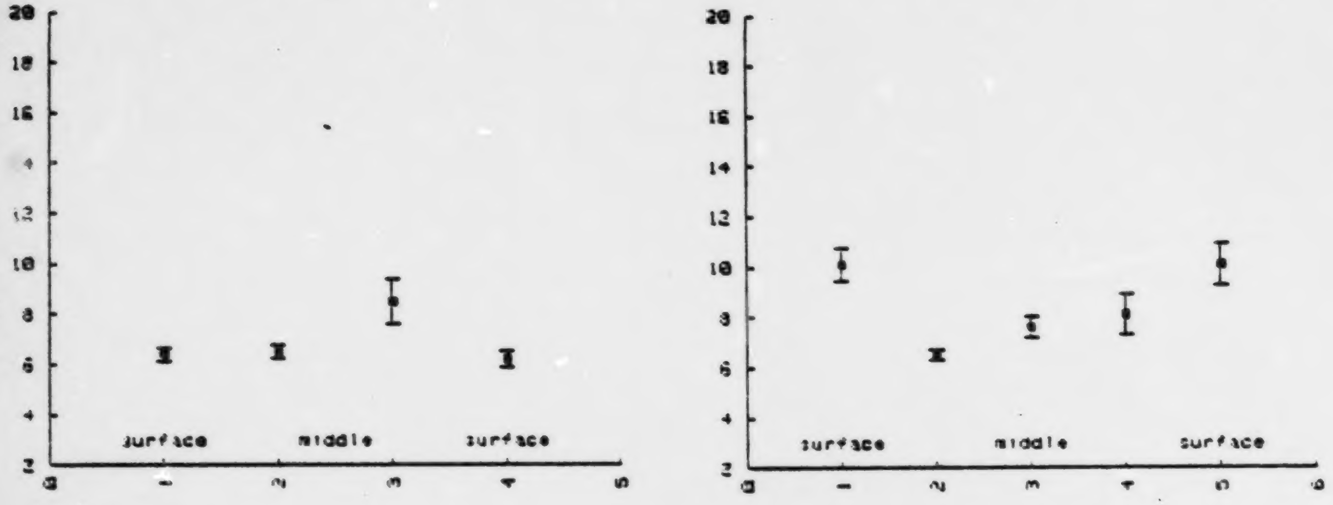

**(a) Chg 24, 19 mm**

**(b) Chg 27, 25 mm**

**(c) Chg 30, 38 mm**

**(d) Chg 35, 51 mm**

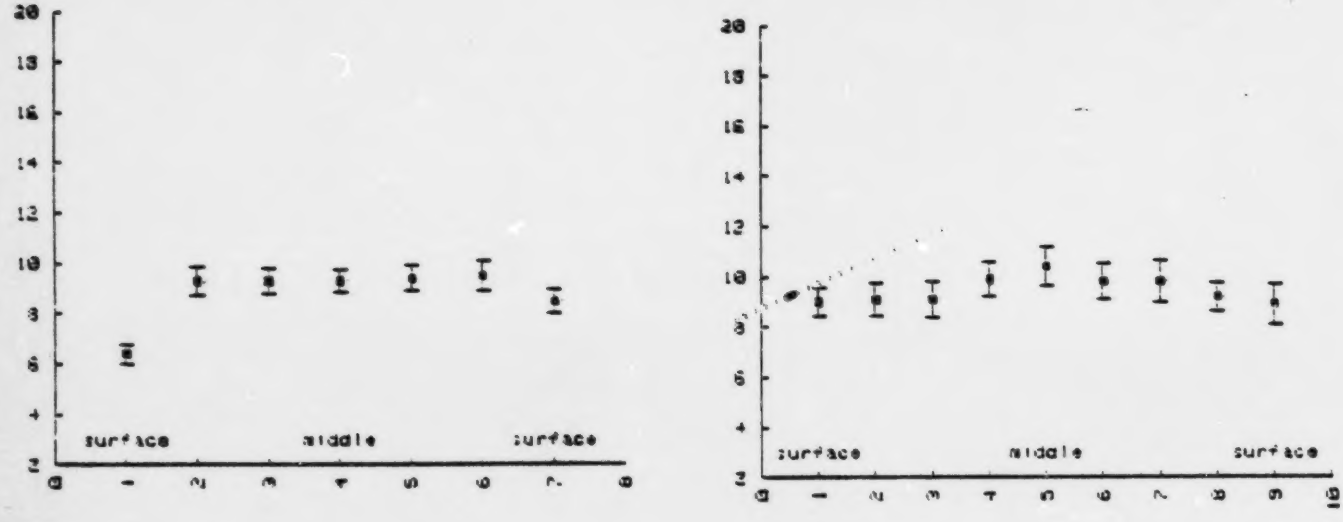

* Ferrite Grain Size in Microns

Figure 5 A3: Microstructures LEW Ht 805126 Normalized

(a) Chg 27, 25 mm, 1/4 Thickness (200X)

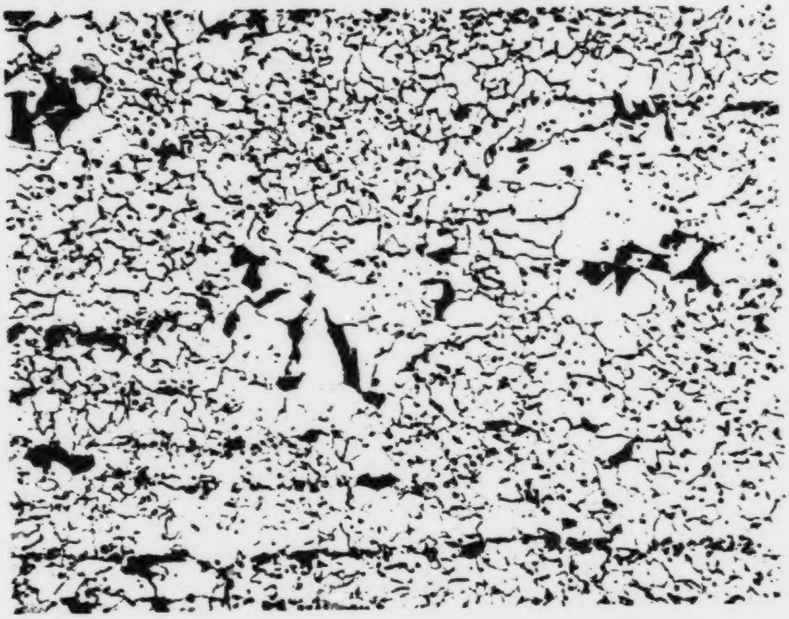

(b) Chg 35, 51 mm, 1/4 Thickness (200X)

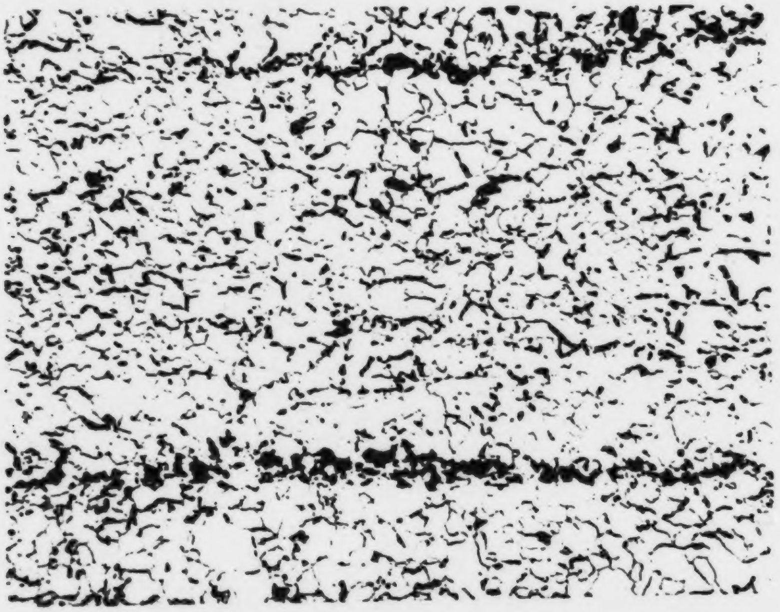

igure 6 A3: Charpy Transition Curves Normalized LEW 805126

a) Chg 24, 19 mm, Surface

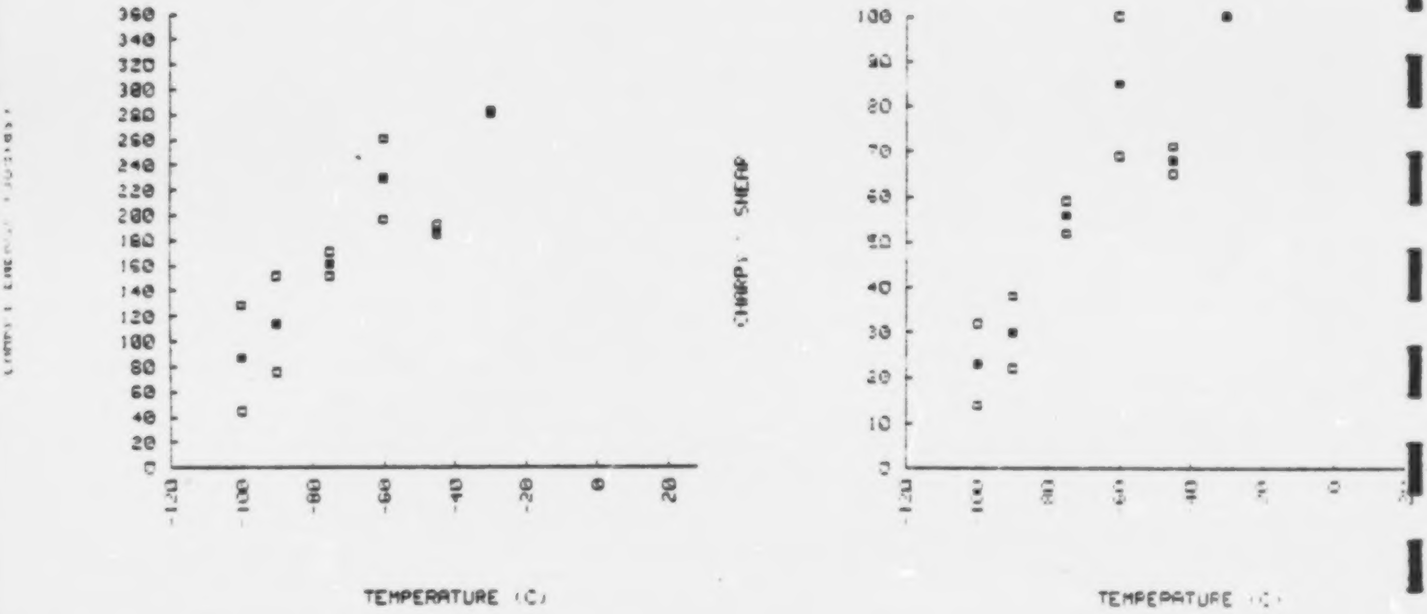

b) Chg 35, 51 mm, 1/4 Thickness

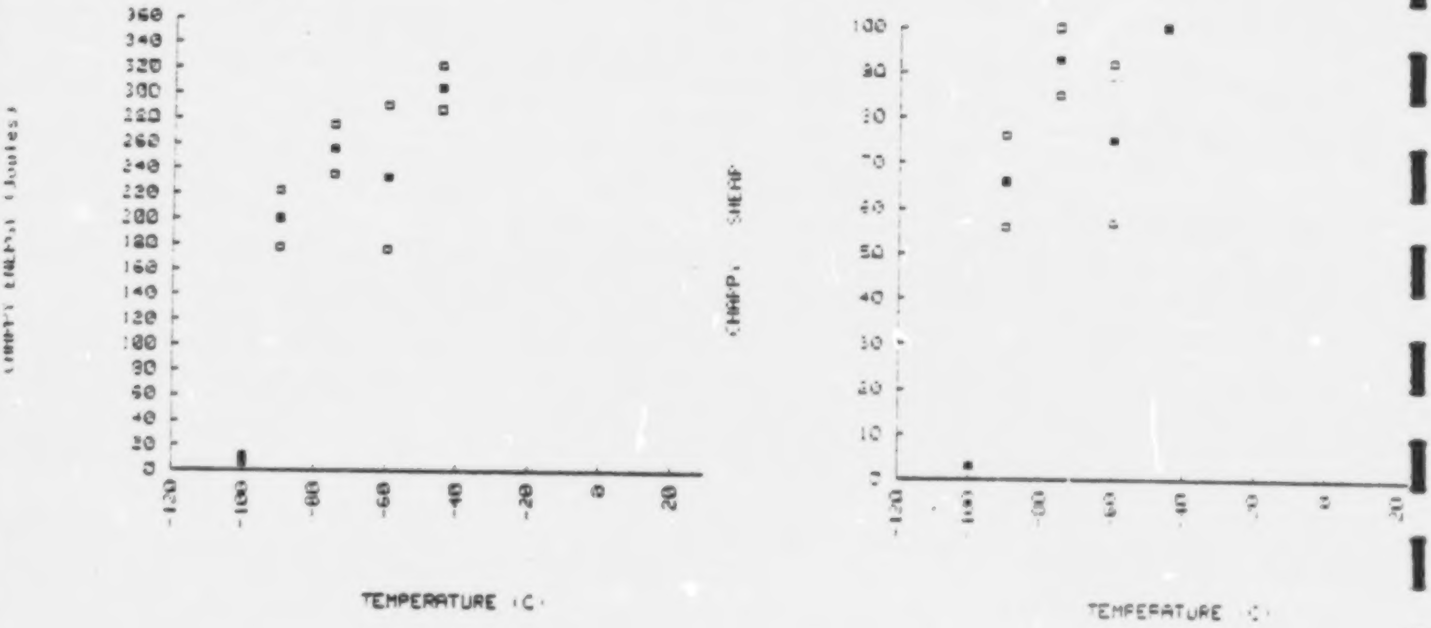

Figure 6 A3 (contd)

(c) Chg 35, 51 mm, Mid-Thickness

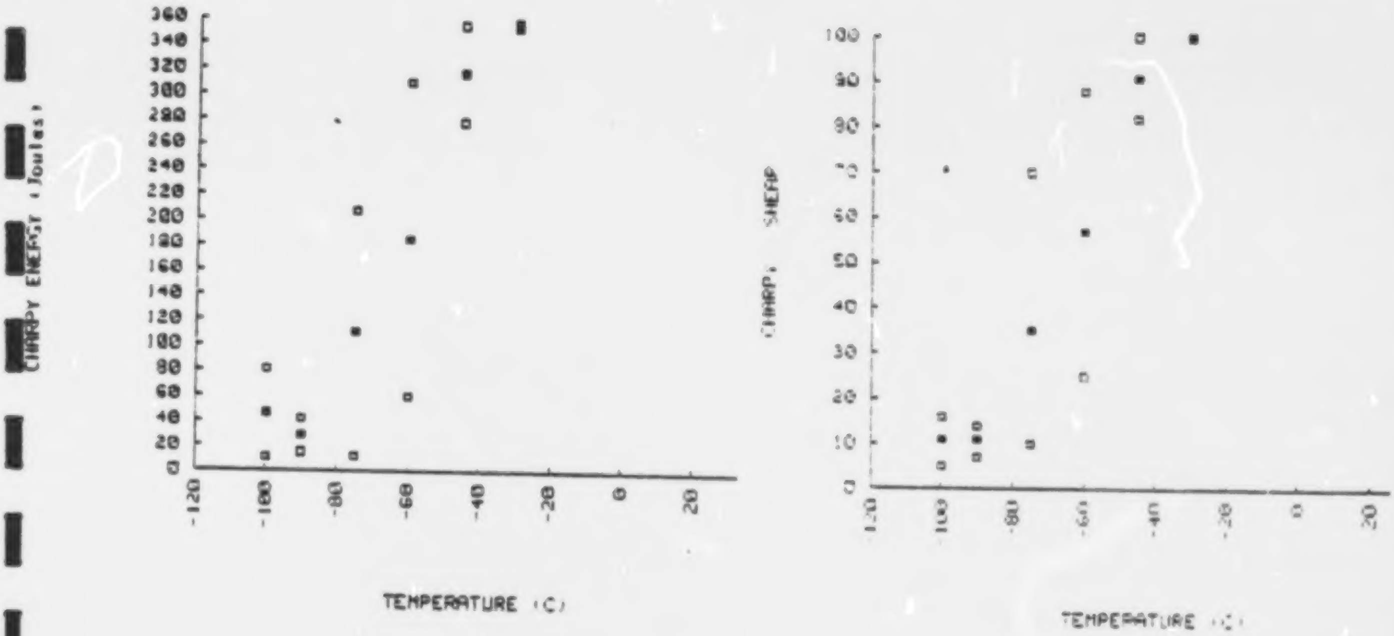

**Figure 7 A3: Ferrite Grain Size Distributions Controlled Rolled HW Ht 536441**

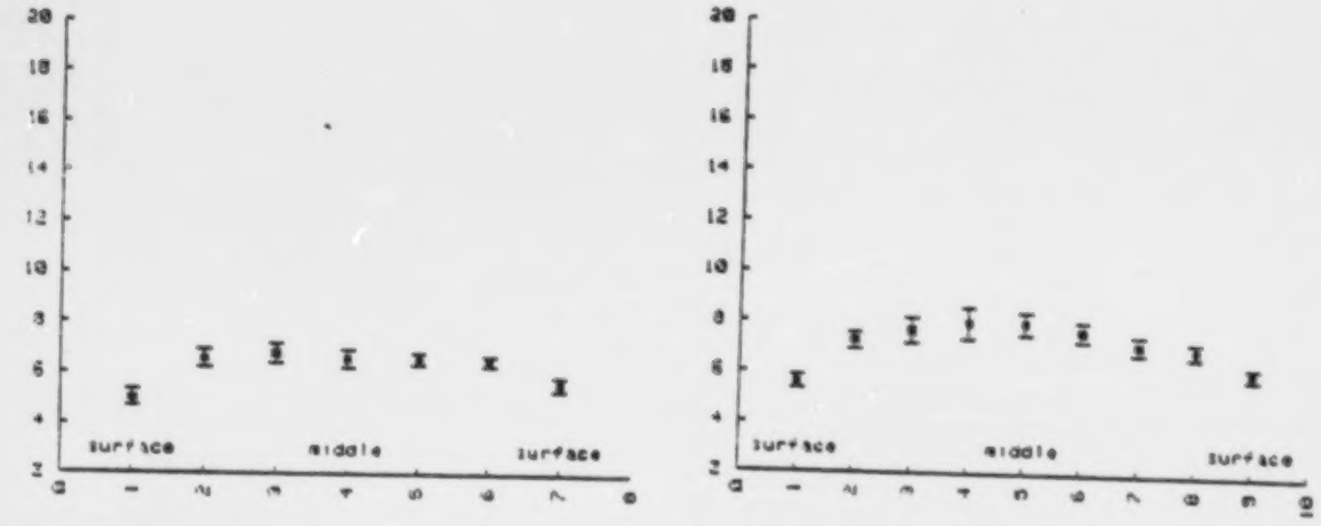

(a) Chg 11, 19 mm

(b) Chg 14, 25 mm

(c) Chg 17, 32 mm

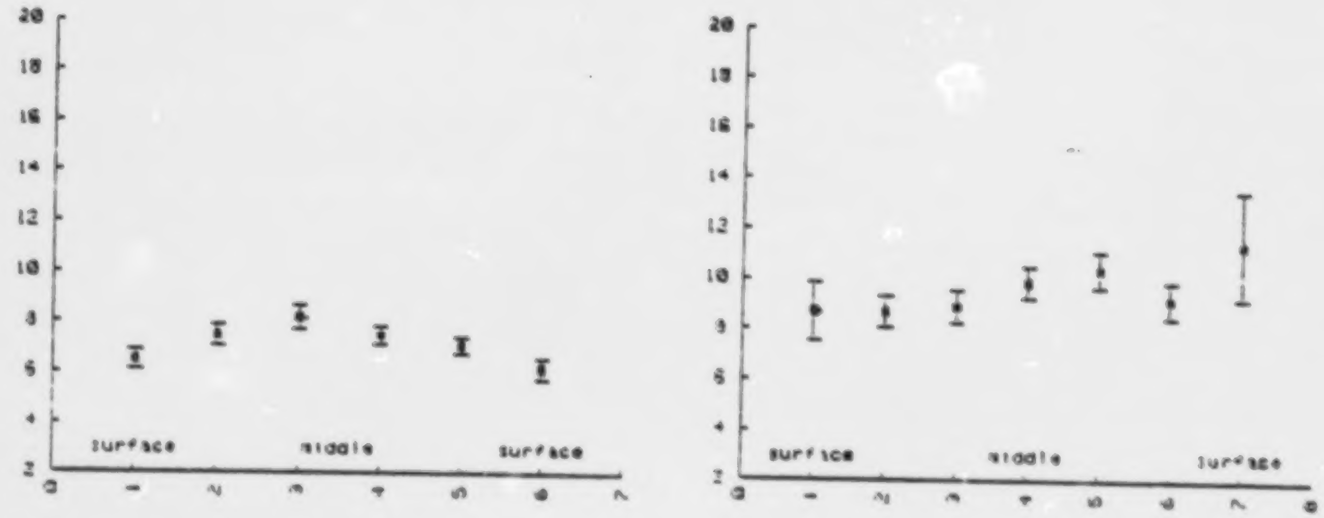

(d) Chg 20, 38 mm

ure 8 A3: Microstructures HW Ht 536441 Controlled Rolled (200X)

Chg 11, 19 mm

(b) Chg 17, 32 mm

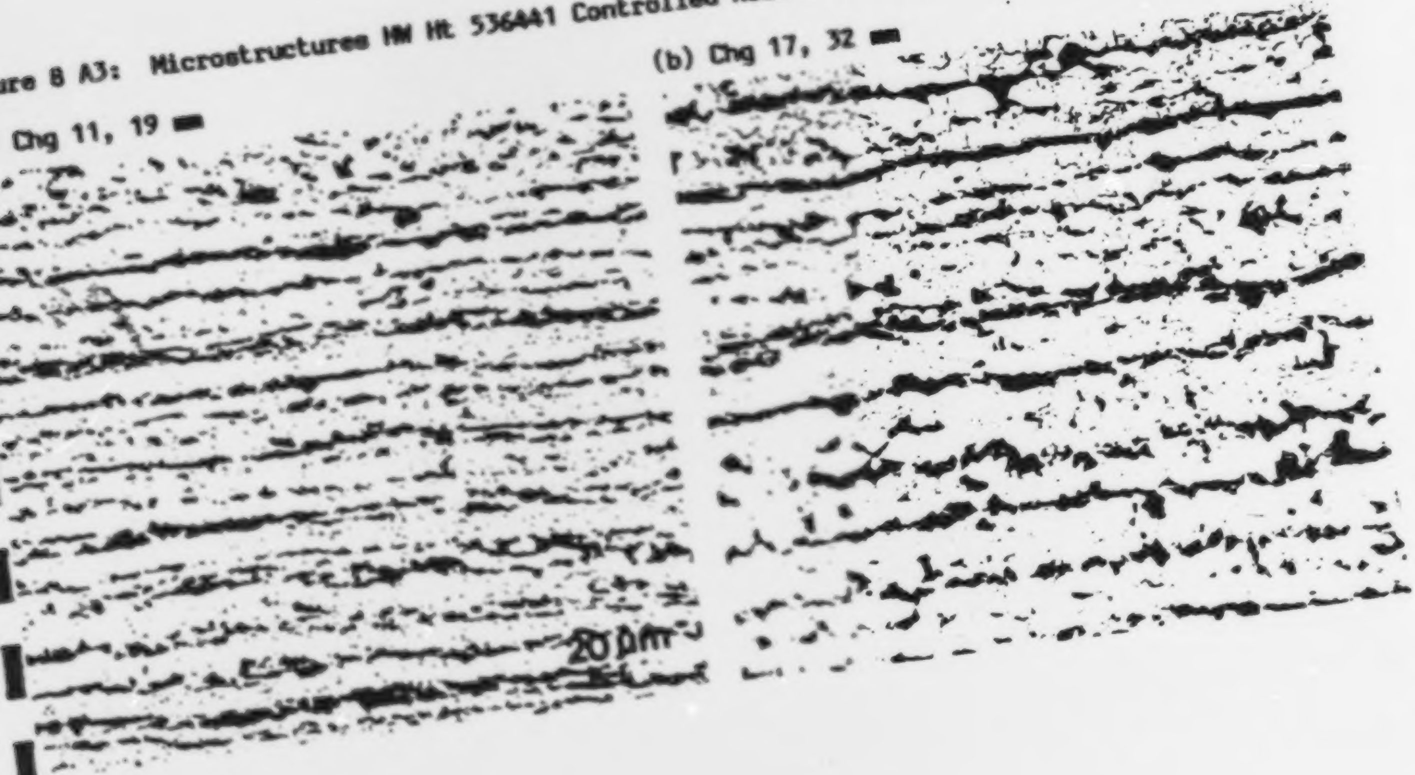

(c) Chg 20, 38 mm

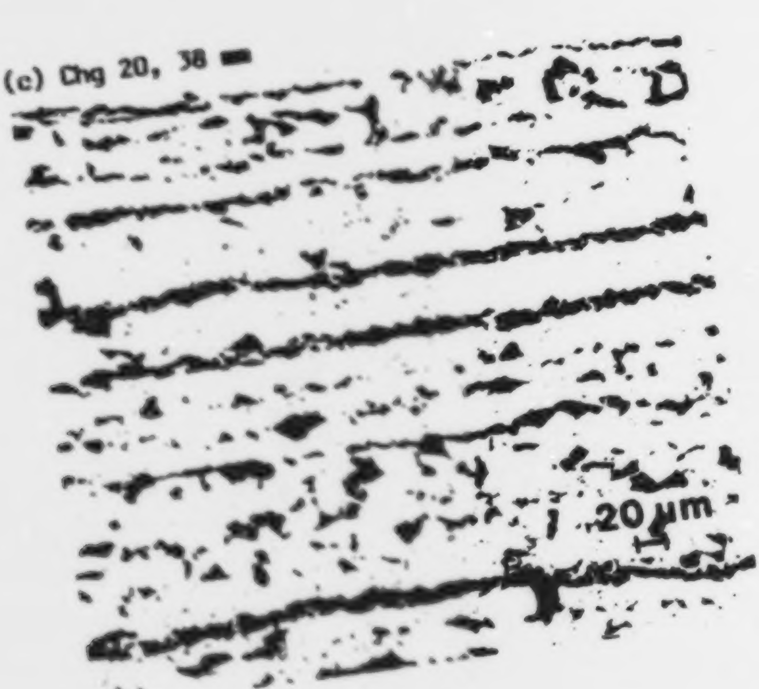

**Figure 7 A3: Ferrite Grain Size Distributions Controlled Rolled HW Ht 536441**

(a) Chg 11, 19 mm

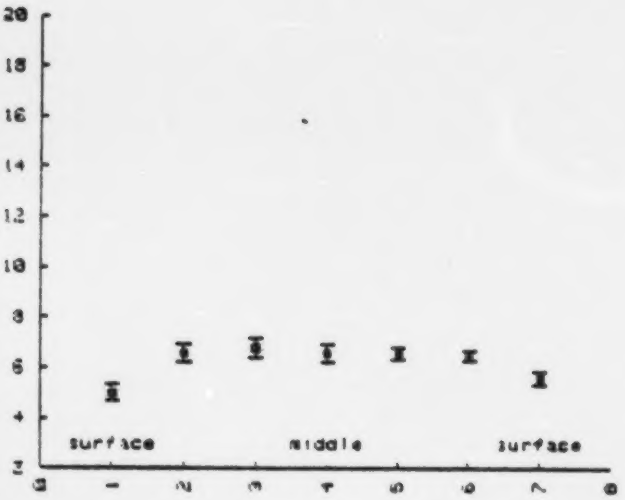

(b) Chg 14, 25 mm

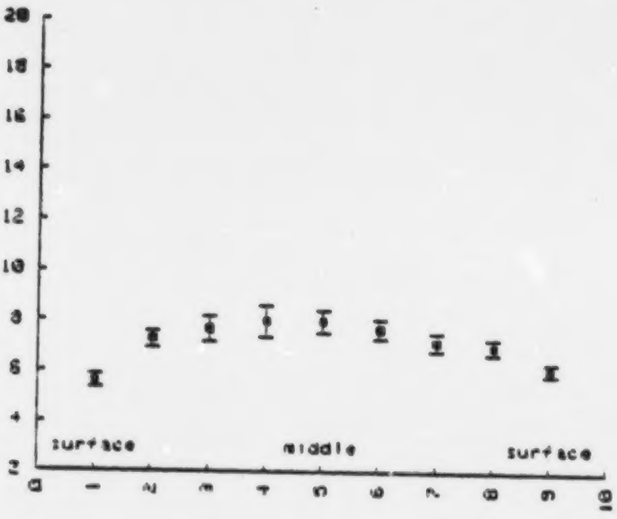

(c) Chg 17, 32 mm

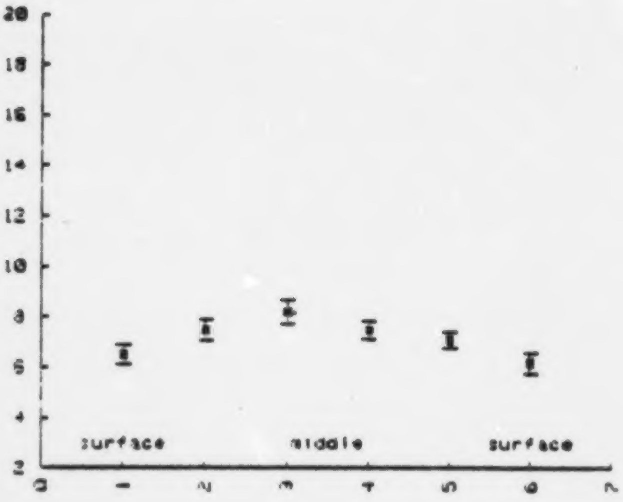

(d) Chg 20, 38 mm

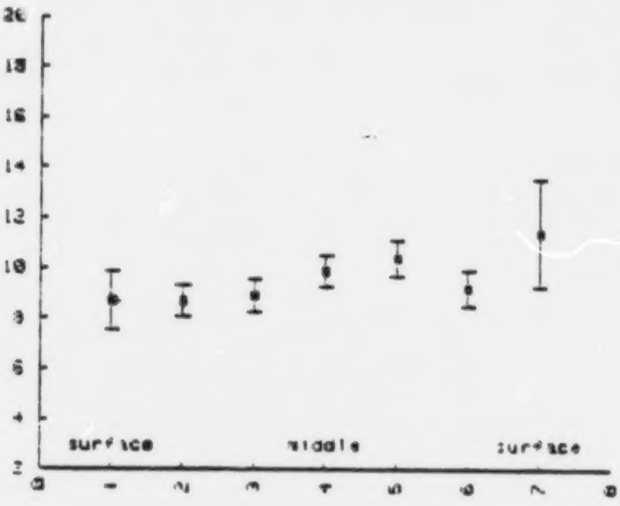

Figure 8 A3: Microstructures HW Ht 536441 Controlled Rolled (200X)

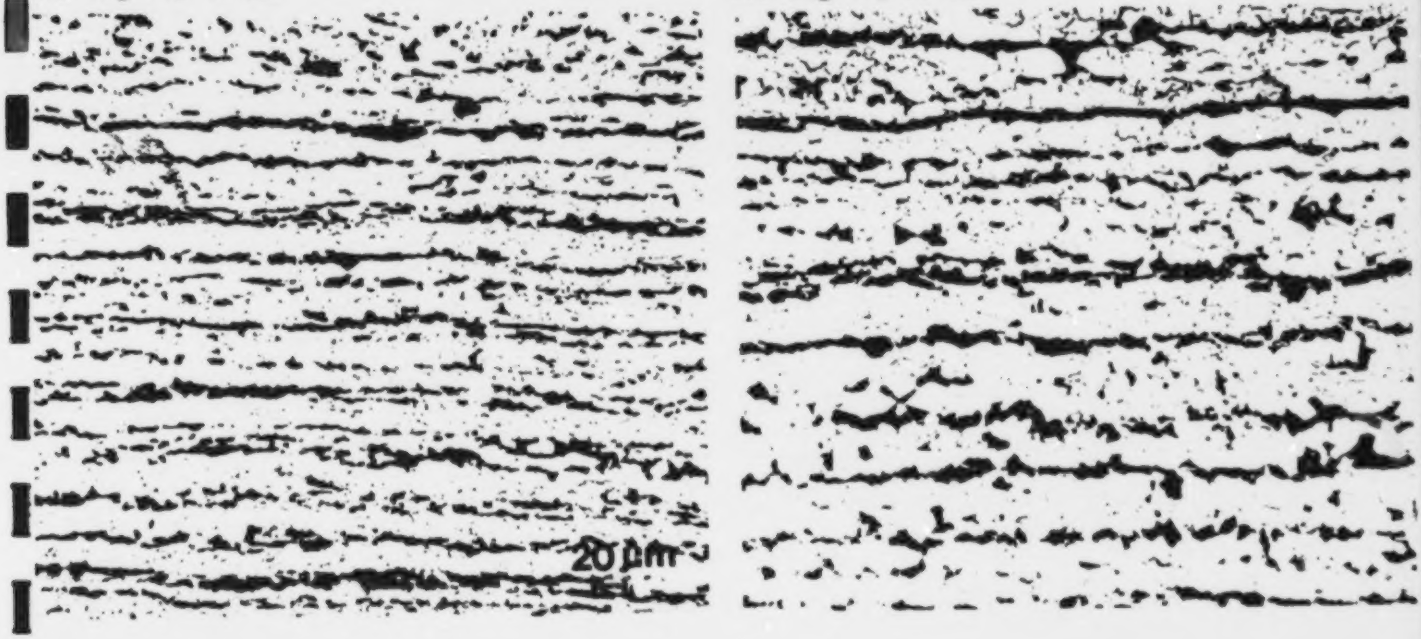
(a) Chg 11, 19 mm

(b) Chg 17, 32 mm

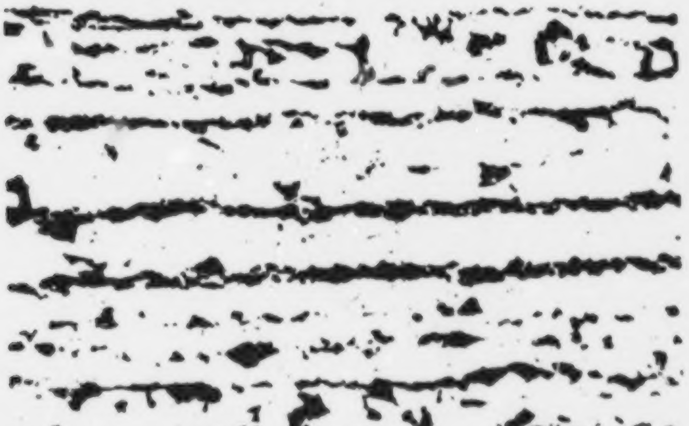
(c) Chg 20, 38 mm

**Figure 9 A3: Charpy Transition Curves Controlled Rolled HW 536441**

**(a) Chg 11, 19 mm, Surface**

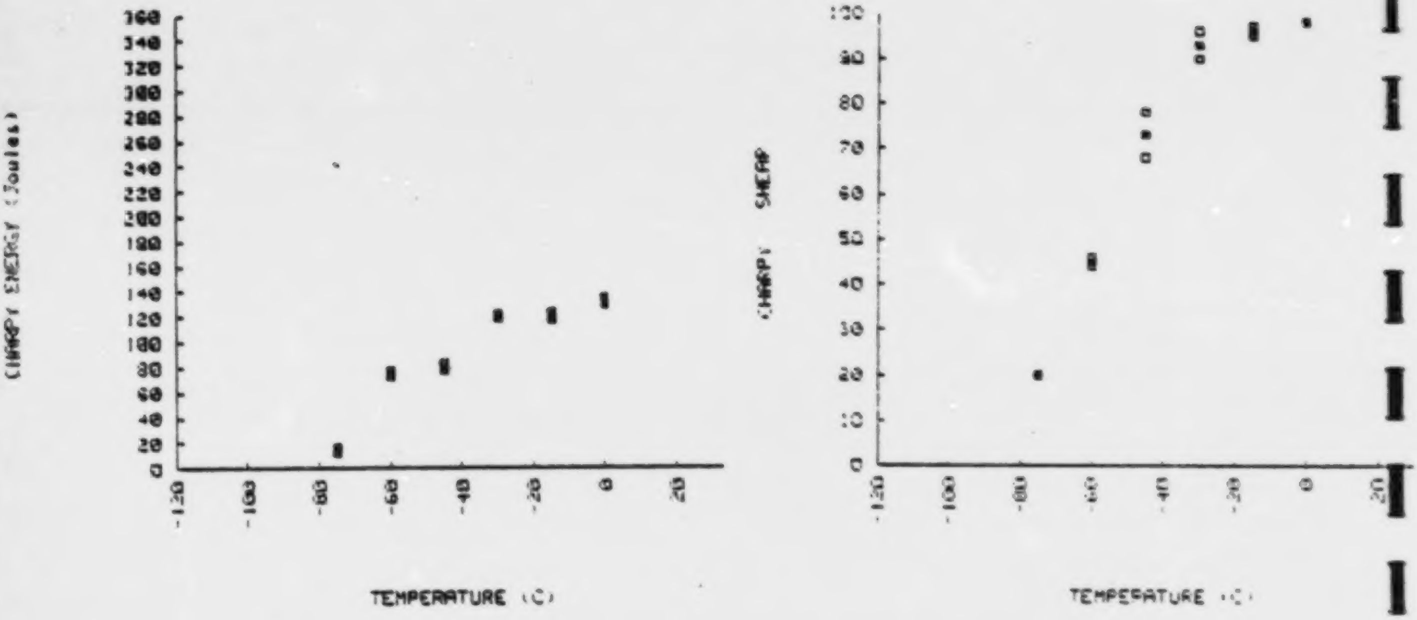

**(b) Chg 14, 25 mm, Surface**

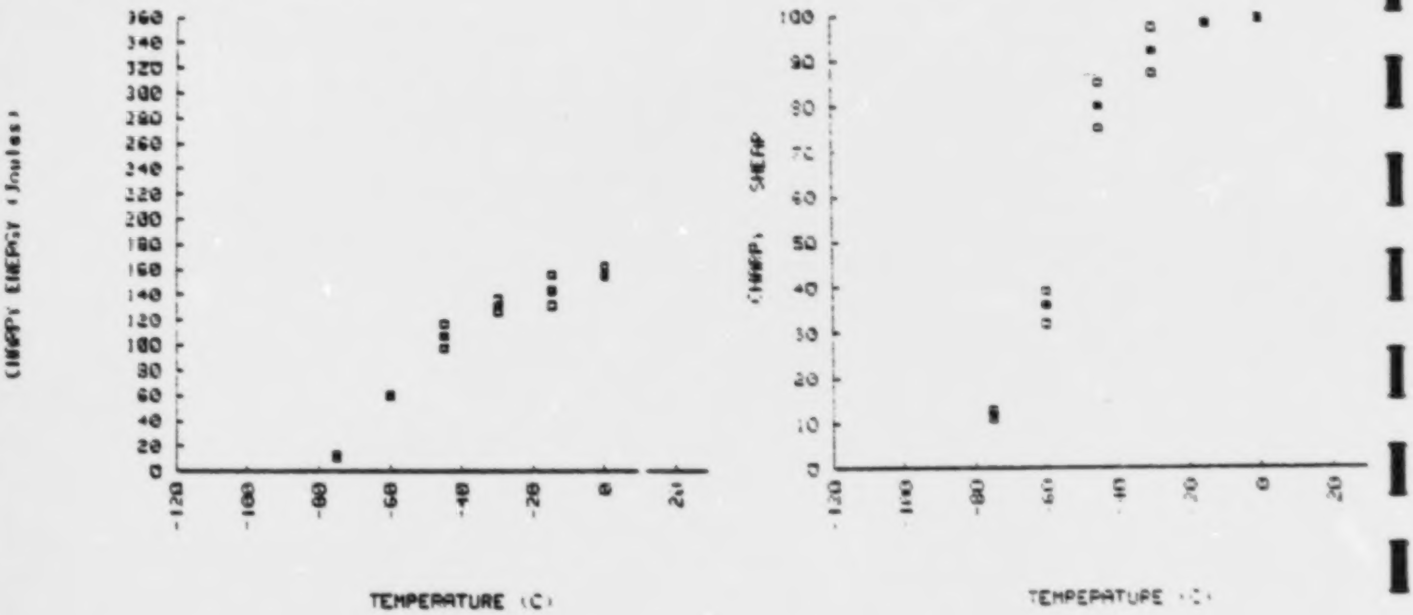

Figure 9 A3 (contd)

(c) Chg 17, 32 mm, Surface

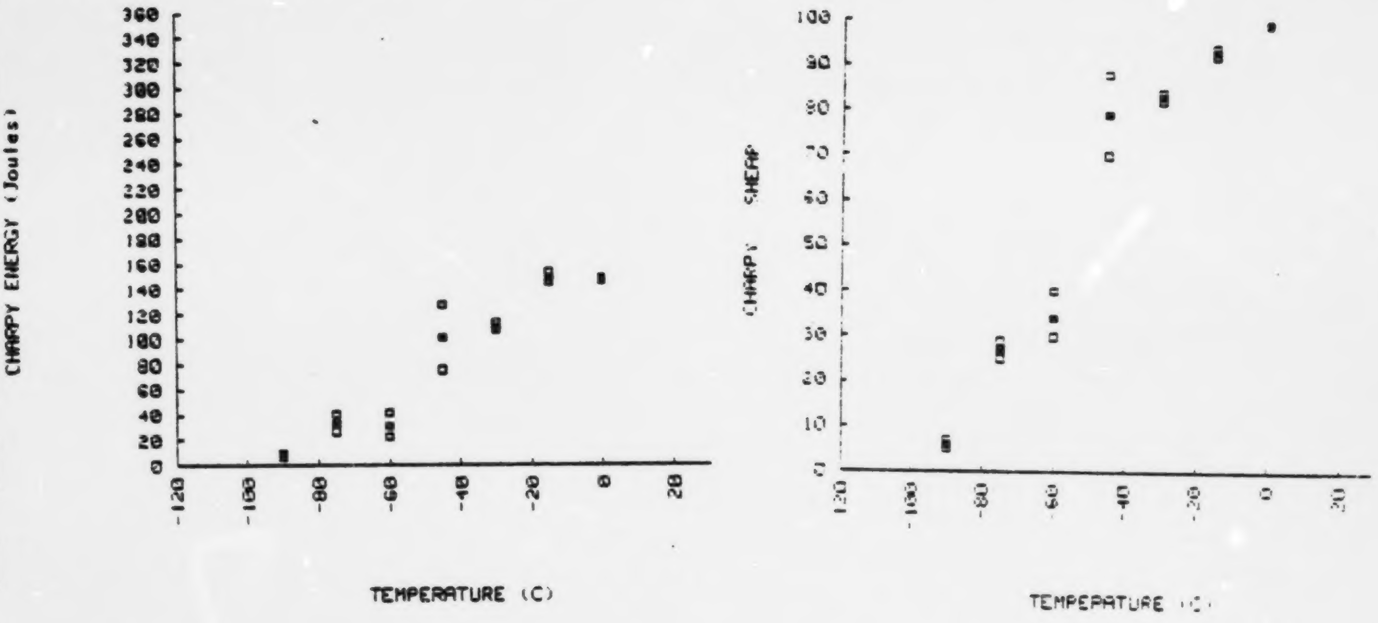

(d) Chg 17, 32 mm, Mid-Thickness

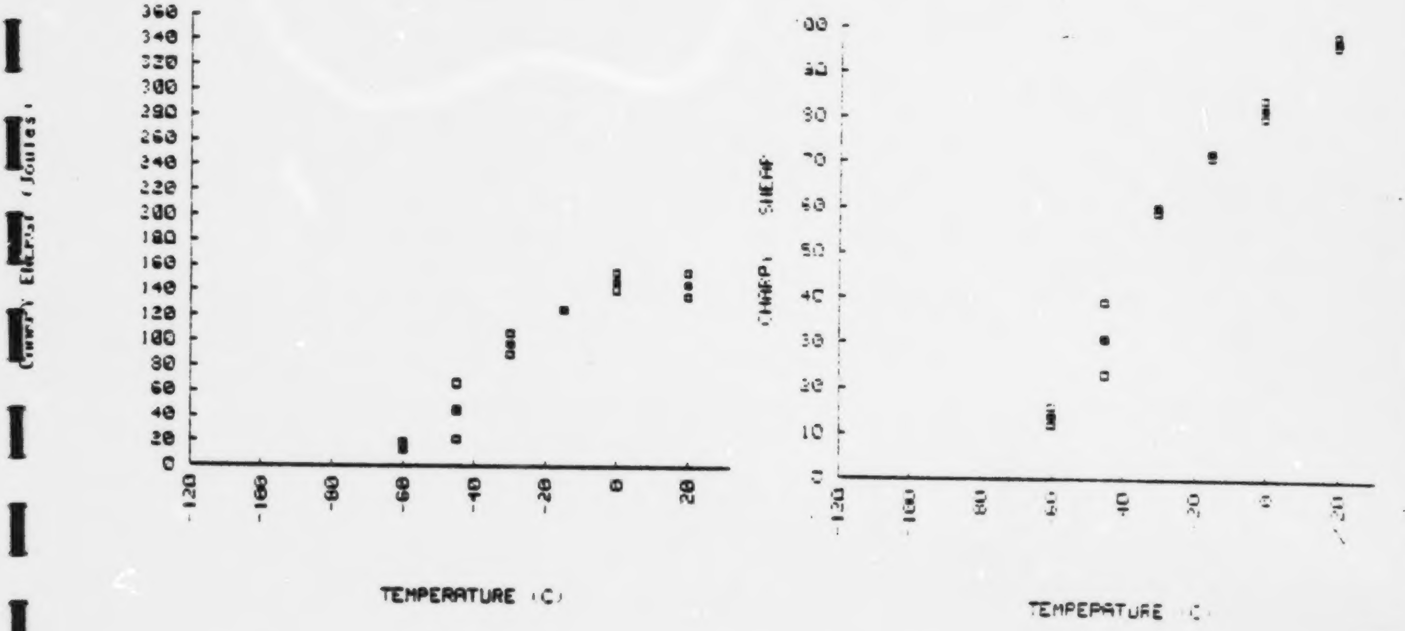

Figure 9 A3 (contd)

(e) Chg 21, 38 mm, 1/4 Thickness

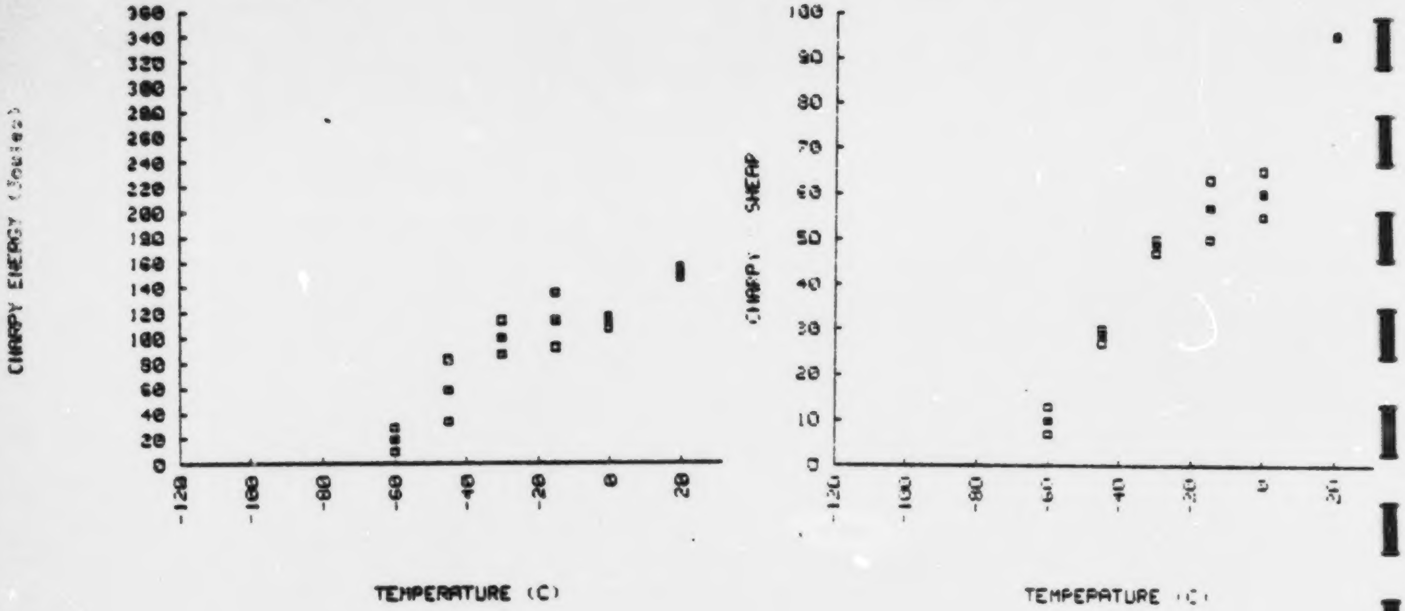

(f) Chg 21, 38 mm, Mid-Thickness

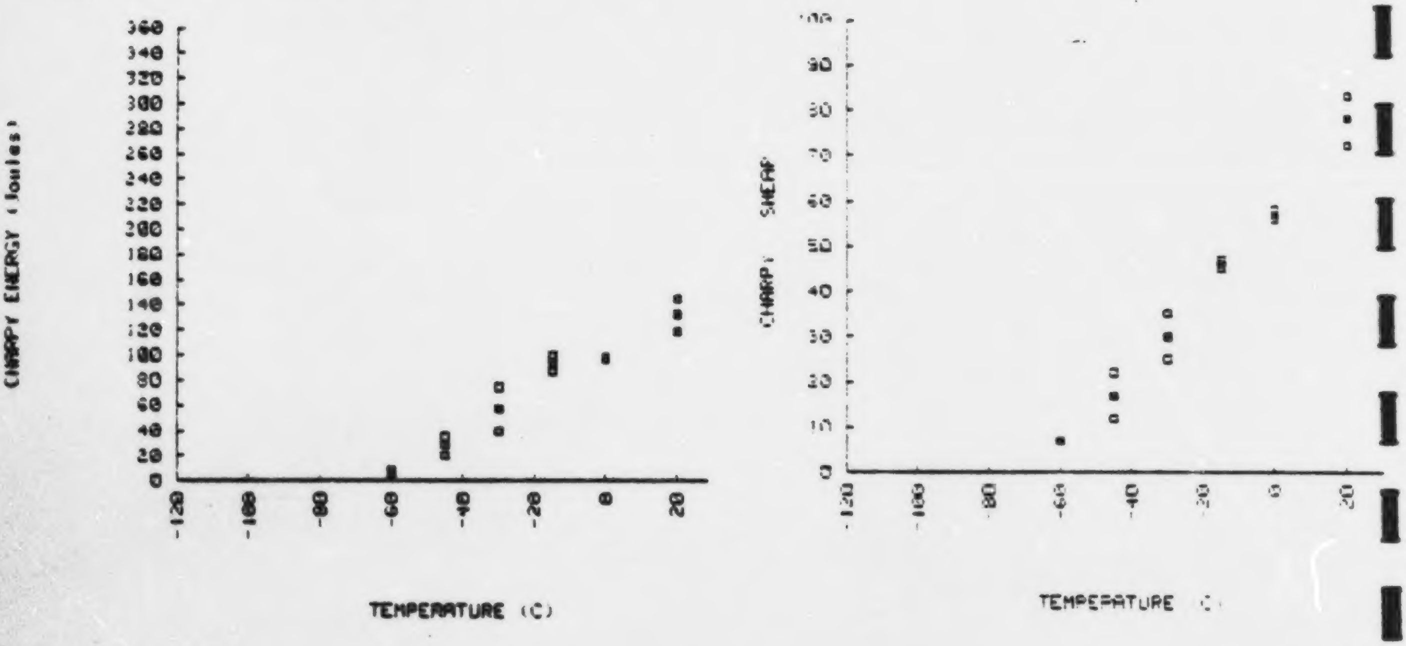

**Figure 10 A3: Ferrite Grain Size* Distributions Normalized HW Ht 536441**

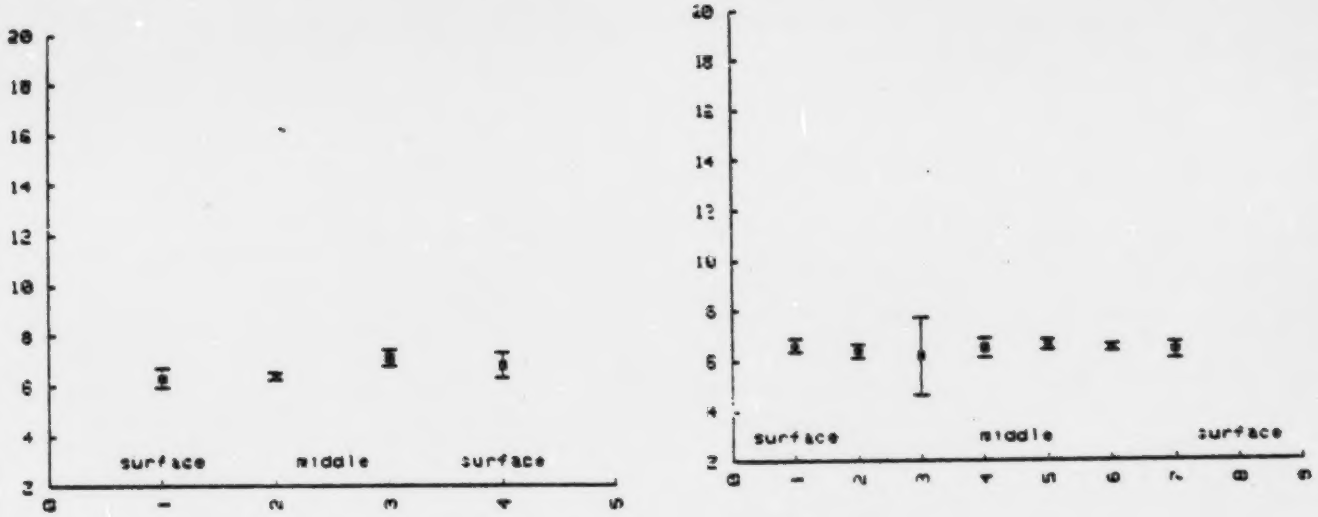
(a) Chg 11, 19 mm

(b) Chg 20, 38 mm

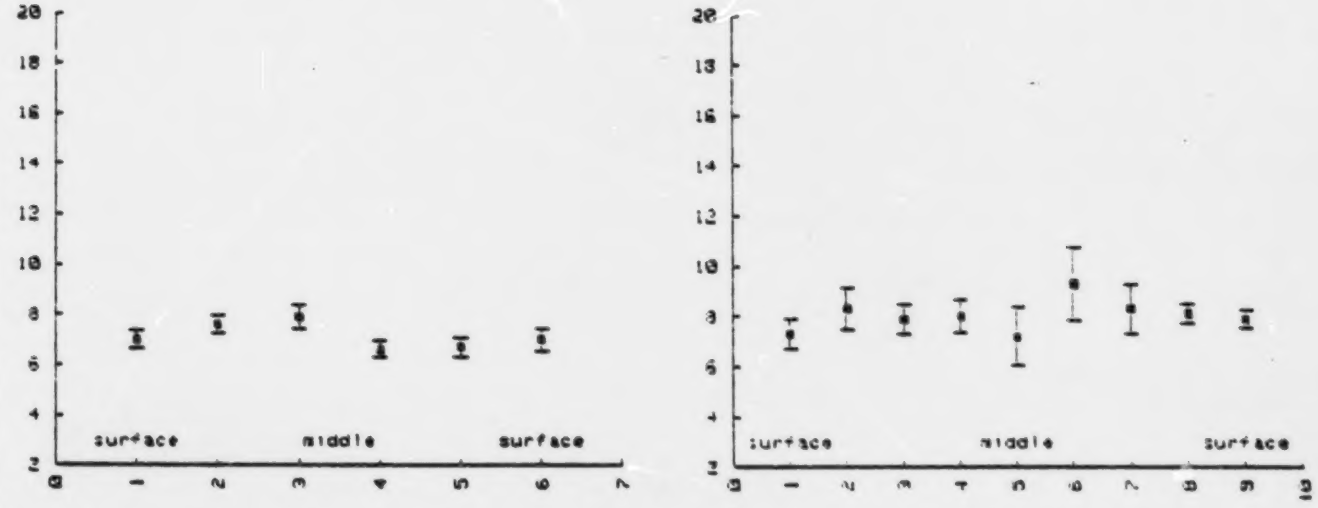
(c) Chg 23, 64 mm

(d) Chg 2, 101 mm

* ferrite grain size in microns.

Figure 11 A3: Microstructures HW Ht 536441 Normalized (200X)

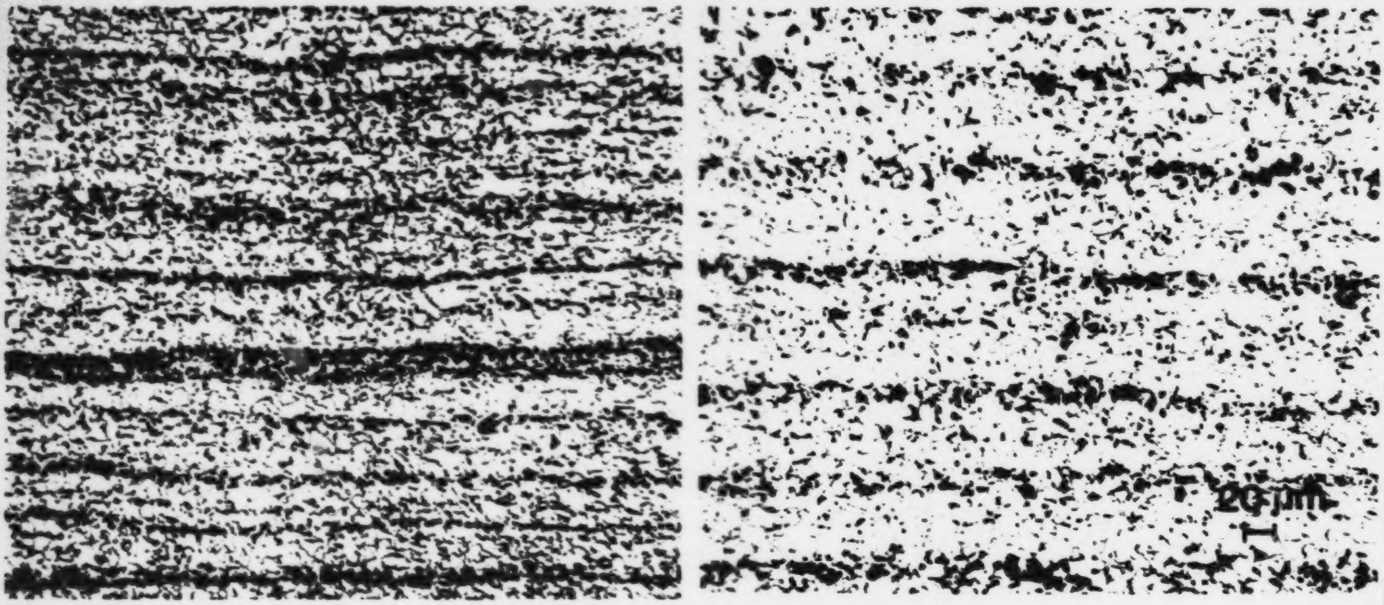

(a) Chg 11, 19 mm

(b) Chg 20, 38 mm

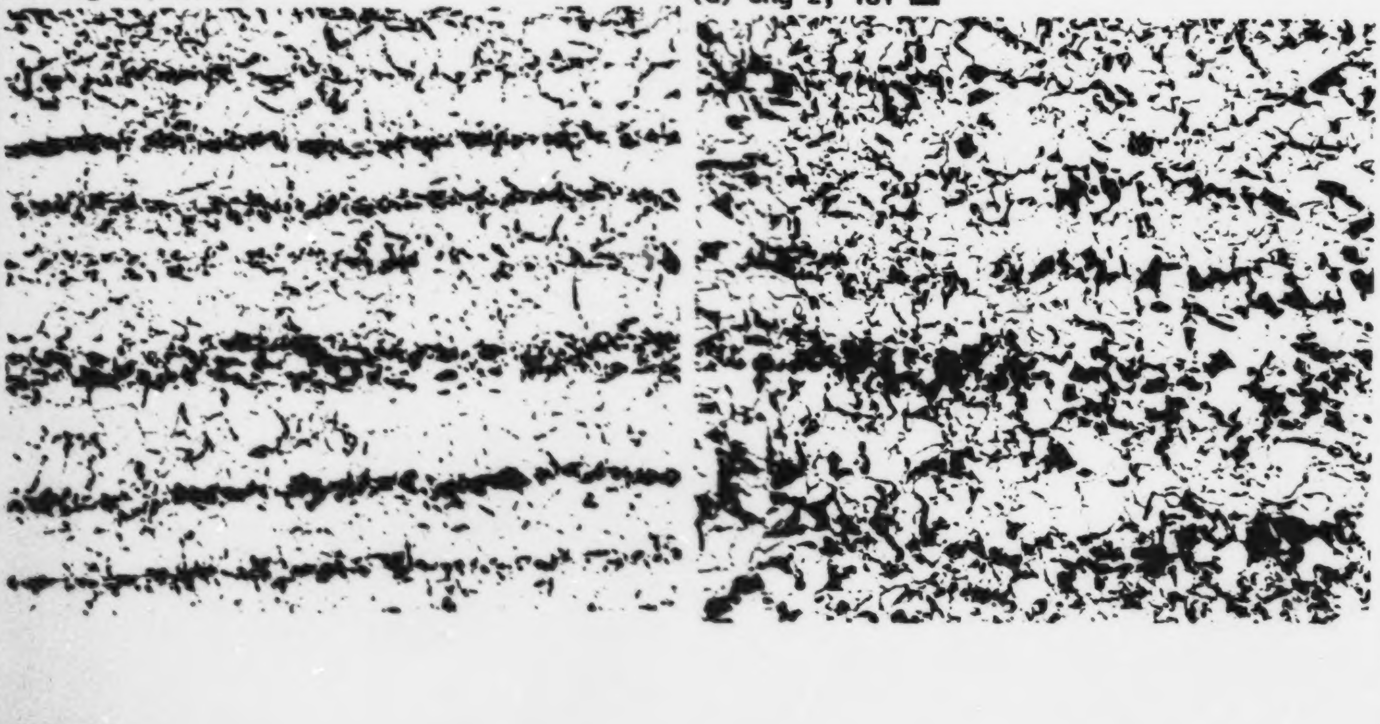

(c) Chg 23, 64 mm

(d) Chg 2, 101 mm

Figure 12 A3: Charpy Transition Curves Normalized, HW Ht 536441

(a) Chg 1, 101 mm, 1/4 Thickness

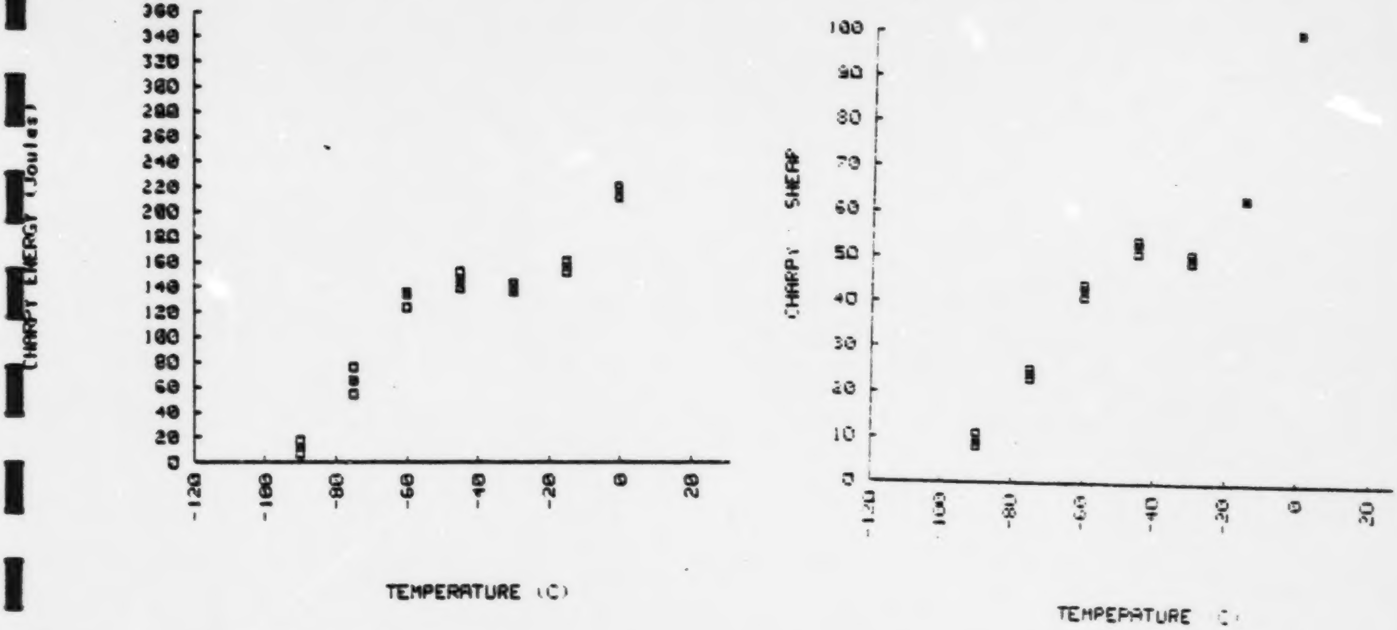

(b) Chg 1, 101 mm, Mid-Thickness

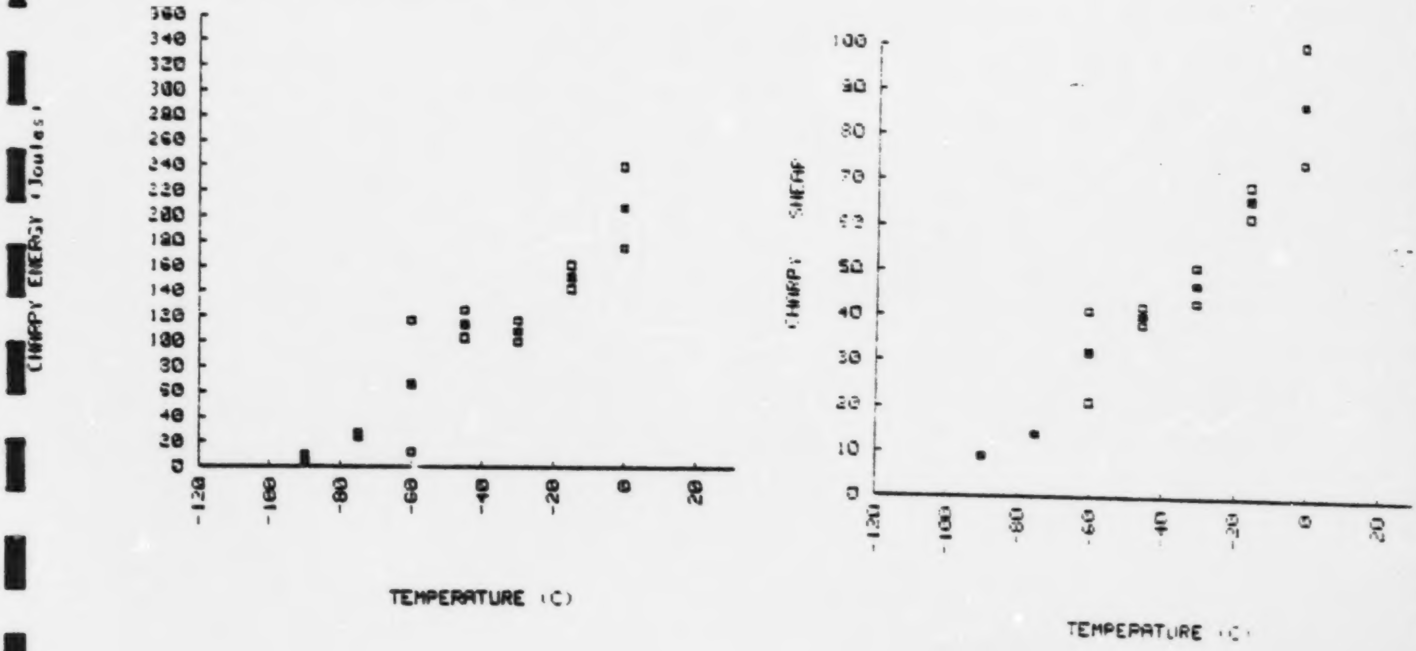

## Table IV A3: LEW Controlled Rolled and Normalized

| Chg | Gauge (mm) | Pos | Yield (MPa) | UTS (MPa) | Grain Size | | % P | | Δ Yield (MPa) | | ΔITT(°C) | | | 50% FATT (°C) | |
|---|---|---|---|---|---|---|---|---|---|---|---|---|---|---|---|
| | | | | | $\bar{x}$ | Range | $\bar{x}$ | Range | $d^{-1/2}$ | Δppt | $\Delta d^{-1/2}$ | Δp | Δppt | Act | Calc |
| 36 | 15 | Sur | 423 | 514 | 8.6 | 7.7 - 9.6 | 12.1 | 10.2 - 14.7 | 186 | 113 | -124 | 26.6 | 46 | -55 | -58 |
| 24 | 19 | Sur | 424 | 505 | 6.6 | 5.9 - 7.0 | 16.5 | 15.0 - 18.4 | 212 | 88 | -142 | 36.3 | 36 | -80 | -75.9 |
| 26 | 25 | Sur | 401 | 489 | 8.0 | 6.7 - 9.4 | 14.6 | 12.5 - 17.0 | 193 | 84 | -129 | 32.2 | 34 | -70 | -69 |
| 27 | 25 | Sur | - | - | 7.7 | 6.5 - 8.8 | 13.2 | 11.7 - 16.3 | 197 | | -131 | 29.0 | | -85 | |
| 3 | 30 | Sur | 398 | 487 | 7.5 | 6.5 - 8.6 | 14.4 | 10.8 - 18.4 | 199 | 74 | -133 | 31.7 | 30 | -70 | -77.5 |
| 17 | 32 | Mid | | | 8.8 | 8.0 - 9.5 | 13.7 | 11.9 - 15.4 | 184 | 90 | -123 | 30.1 | 36 | -55 | -63.1 |
| 28 | 32 | Sur | 374 | 478 | 10.9 | 9.7 - 11.6 | 9.9 | 9.2 - 10.9 | 165 | 86 | -110 | 21.8 | 35 | -55 | -59.4 |
| 19 | 38 | Mid | | | 12.0 | 11.5 - 12.5 | 9.9 | 8.8 - 10.9 | 157 | 93 | -105 | 21.8 | 38 | -40 | -51.4 |
| 29 | 32 | Sur | 374 | 479 | 9.3 | 8.2 - 10.7 | 12.3 | 10.1 - 17.4 | 179 | 72 | -119 | 27.1 | 29 | | |
| 20 | 38 | Mid | | | 11.1 | 11.1 - 11.2 | 11.1 | 10.8 - 11.3 | 163 | 87 | -109 | 24.4 | 35 | -55 | -55.8 |
| 30 | 38 | 1/4 | 357 | 467 | 10.6 | 8.8 - 11.7 | 11.5 | 10.0 - 13.2 | 168 | 66 | -112 | 25.3 | 27 | -50 | -65.9 |
| | | Mid | | | 11.2 | 10.9 - 11.7 | 11.8 | 10.8 - 12.9 | 163 | 70 | -109 | 26.0 | 29 | -35 | -60.2 |
| 32 | 44 | 1/4 | 336 | 473 | 13.6 | 12.3 - 14.7 | 8.7 | 7.5 - 10.1 | 148 | 64 | -99 | 19.1 | 26 | -25 | -60.1 |
| | | Mid | | | 15.0 | 13.7 - 16.2 | 10.9 | 10.2 - 11.5 | 140 | 71 | -94 | 24.0 | 29 | +5 | -47.2 |
| 35 | 51 | 1/4 | 330 | 470 | 15.5 | 15.0 - 16.2 | 10.2 | 9.6 - 10.7 | 139 | 68 | -92 | 22.4 | 27 | -45 | -48.8 |
| | | Mid | | | 16.5 | 16.5 | 10.7 | 10.3 - 11.0 | 134 | 72 | -90 | 23.5 | 29 | -15 | -43.7 |
| 24 | 19 | Sur | 347 | 461 | 6.9 | 6.2 - 8.5 | 18.0 | 16.3 - 19.9 | 208 | 16 | -138 | 39.6 | 6.4 | -75 | -98 |
| 27 | 25 | Sur | 337 | 461 | 8.7 | 6.5 - 10.1 | 16.4 | 12.6 - 20.1 | 184 | 28 | -123 | 36.1 | 11.4 | -80 | -82 |
| 30 | 38 | 1/4 | 331 | 448 | 9.4 | 9.3 - 9.5 | 9.8 | 8.6 - 11.0 | 178 | 29 | -119 | 21.6 | 11.8 | | -92 |
| | | Mid | | | 9.3 | | 10.4 | | | | | 22.9 | | | |
| 35 | 51 | 1/4 | 331 | 448 | 9.1 | 8.9 - 9.2 | 14.4 | 14.1 - 14.7 | 181 | 26 | -121 | 31.7 | 10.6 | -95 | -85 |
| | | Mid | | | 10.0 | 9.8 - 10.4 | 14.0 | 13.6 - 14.4 | 172 | 35 | -115 | 30.8 | 14.0 | -50 | -64 |

## Table V A3: HW Controlled Rolled and Normalized

| Chg | Gauge (mm) | Pos | Yield (MPa) | UTS (MPa) | Grain Size | | % P | | Δ Yield (MPa) | | ΔITT(°C) | | | 50% FATT (°C) | |
|---|---|---|---|---|---|---|---|---|---|---|---|---|---|---|---|
| | | | | | $\bar{x}$ | Range | $\bar{x}$ | Range | $d^{-1/2}$ | Δppt | $\Delta d^{-1/2}$ | Δp | Δppt | Act | Calc |
| 11 | 19 | Sur | 510 | 611 | 6.6 | 6.5 - 6.8 | 22.2 | 21.0 - 24.0 | 212 | 176 | -142 | 55.5 | 73.1 | -50 | -22 |
| 13 | 25 | Sur | 471 | 597 | 7.7 | 6.5 - 8.4 | 18.9 | 12.2 - 26.7 | 197 | 157 | -131 | 47.3 | 63.8 | -50 | -29 |
| 14 | 25 | Sur | 490 | 579 | 7.3 | 7.8 - 7.7 | 19.3 | 17.9 - 20.6 | 202 | 170 | -135 | 48.3 | 69.2 | -50 | -27 |
| 16 | 32 | Sur | 453 | 568 | 7.8 | 7.3 - 9.3 | 24.1 | 23.3 - 24.8 | 195 | 140 | -130 | 60.1 | 56.8 | -60 | -22 |
| | | Mid | | | 8.8 | 8.3 - 9.2 | 25.1 | 24.0 - 26.1 | 184 | 151 | -123 | 62.8 | 61.3 | -25 | -8 |
| 17 | 32 | Sur | 455 | 572 | 7.3 | 7.1 - 7.5 | 21.1 | 21.1 - 21.2 | 202 | 135 | -135 | 52.8 | 54.9 | -55 | -36 |
| | | Mid | | | 7.9 | 7.5 - 8.2 | 24.6 | 23.7 - 24.5 | 194 | 143 | -129 | 61.5 | 58.2 | -35 | -18 |
| 19 | 38 | 1/4 | 436 | 555 | 10.5 | 10.4 - 10.7 | 19.0 | 17.7 - 20.0 | 168 | 150 | -112 | 47.5 | 60.8 | -30 | -13 |
| | | Mid | | | 10.6 | 10.4 - 11.0 | 19.3 | 18.6 - 20.0 | 168 | 150 | -112 | 48.3 | 61.0 | -10 | -12 |
| 20 | 38 | 1/4 | 436 | 557 | 9.3 | 9.2 - 10.4 | 17.1 | 14.6 - 19.2 | 179 | 139 | -119 | 42.8 | 56.6 | -30 | -28 |
| | | Mid | | | 9.7 | 8.9 - 10.4 | 17.1 | 14.6 - 19.2 | 175 | 143 | -117 | 42.8 | 58.0 | -20 | -25 |
| 11 | 19 | Sur | 399 | 514 | 6.7 | 6.3 - 7.1 | 15.4 | 13.4 - 17.2 | 210 | 61 | -140 | 38.5 | 24.6 | -75 | -86 |
| 20 | 32 | 1/4 | 372 | 510 | 6.4 | 6.2 - 6.6 | 24.3 | 21.6 - 23.8 | 216 | 39 | -144 | 60.8 | 15.7 | -45 | -77 |
| | | Mid | | | 6.3 | 6.2 - 6.5 | 26.5 | 24.6 - 28.4 | 217 | 37 | -145 | 66.3 | 15.1 | -50 | -73 |
| 23 | 64 | 1/4 | 366 | 514 | 7.2 | 6.6 - 7.9 | 19.8 | 17.3 - 24.2 | 203 | 45 | -136 | 49.5 | 18.2 | -35 | -113 |
| | | Mid | | | 7.2 | 6.6 - 7.9 | 19.8 | 17.3 - 24.2 | 203 | 45 | -136 | 49.5 | 18.2 | -40 | -77 |
| 2 | 102 | 1/4 | 350 | 502 | 8.1 | 7.9 - 8.3 | 20.6 | 18.4 - 22.9 | 192 | 41 | -128 | 51.5 | 16.5 | -35 | -69 |
| | | Mid | | | 8.2 | 7.2 - 9.3 | 23.2 | 20.5 - 26.6 | 190 | 42 | -127 | 58.0 | 17.0 | -30 | -61 |

## APPENDIX 4

## CLEANLINESS OF TRIAL HEATS

The cleanliness of the trial heats was assessed by doing detailed metallographic inclusion counting and length measurements on representative plate samples from each of the trial heats. For the HW heat, full thickness plate samples were rated from the 19, 32, 64 and 101 mm plate thicknesses, whereas for the LEW heat the plate thicknesses were 15, 25, 38, and 51 mm. For each sample, the inclusions were counted and measured manually on Leitz metallographic. Inclusion counts were made on each field of three, full thickness traverses for each specimen. For each rating the inclusions were classified according to whether they were isolated or stringers, and whether they were the following types, based on aspect ratio and optical appearance:

- oxides with aspect ratios less than two,
- complex chape controlling sulfides with aspect ratios between two and five, and
- long thin sulfides (primarily Type II MnS) with aspect ratios greater than five.

Representative micrographs showing the different types of inclusions rated are shown in Figure 1 A4.

The summary of the inclusion ratings in terms of length are given in Table I A4. Comparing the LEW and HW heats, it's clear that the strand cast low S LEW steel shows both higher cleanliness and less variability in cleanliness than the CAB-treated ingot cast HW heat. Comparing the two heats on the basis of total length of sulfides, the LEW plates show total lengths ranging between 0.012 and 0.025 $mm/mm^2$ whereas the HW plates show lengths between 0.006 and 0.146 $mm/mm^2$ (an order of magnitude higher than the LEW steel in the worst positions). Similarly the oxide content of the shrouded strand cast heat was significantly less than the ingot cast steel. The total oxide lengths ranged between 0.0273 and 0.0763 $mm/mm^2$ for the LEW plate and between 0.0395 and 0.121 $mm/mm^2$ for the HW plate.

Figure 1 A4: Characteristic Inclusions in LEW and HW Trial Plates

HW Plate

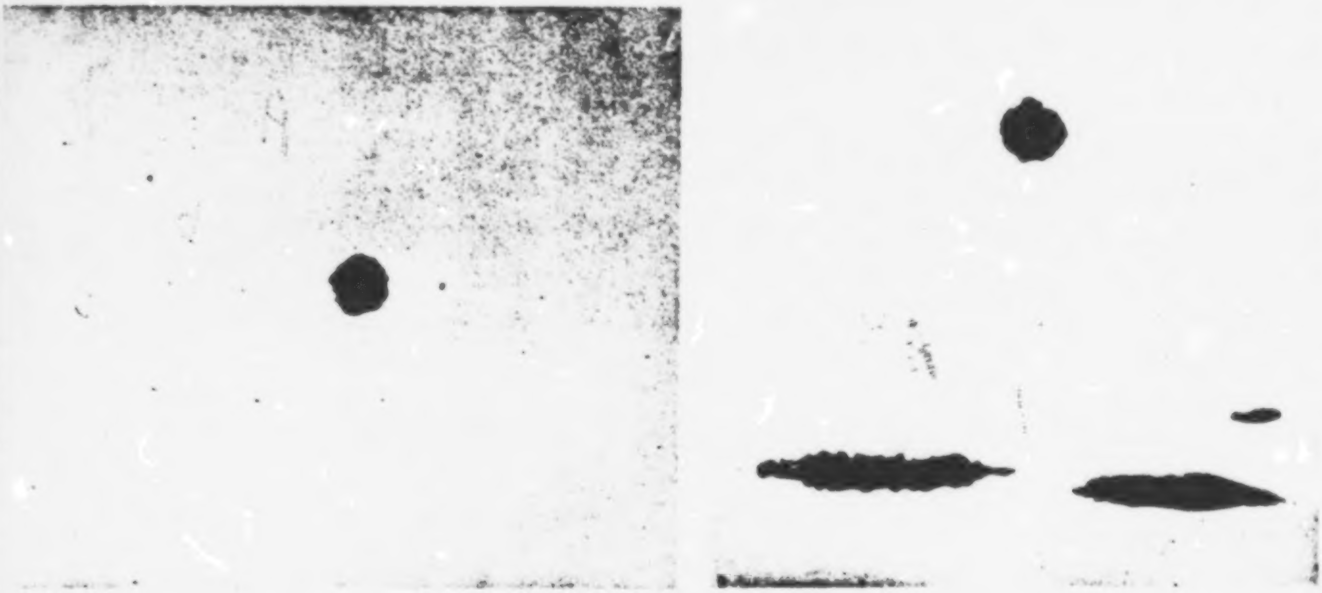

(a) Isolated Duplex Calcium Aluminate (L/T <2) (500X)

(b) Isolated Duplex Aluminate and Elongated Complex Alumina-sulfide (2 < L/T <5) (500X)

(c) Type II MnS (L/T >5) (500X)

Figure 1 A4: Characteristic Inclusions in LEW and HW Trial Plates

LEW Plate

(d) Isolated Aluminate (L/T <2) (500X)

(e) Stringer Aluminate (500X)

(f) Type II MnS (L/T >5) (500X)

Table I A4: Total Inclusion Lengths in LEW and HW Trial Plates ($mm/mm^2$)

| Code No. | Thickness (mm) | Oxide (L/T < 2) | | | Sulfides (L/T > 2 < 5) | | | Sulfides (L/T > 5) | | | Total Sulfides (L/T > 2) | All Inclusions |
|---|---|---|---|---|---|---|---|---|---|---|---|---|
| | | I | S | T | I | S | T | I | S | T | I | T |
| 11 CR 536441 | 19 | 0.0593 | 0.0104 | 0.0697 | 0.0146 | 0.0014 | 0.0160 | - | 0.0047 | 0.0047 | 0.0207 | 0.0904 |
| 17 CR 536441 | 32 | 0.0598 | 0.0609 | 0.1207 | 0.0082 | 0.0510 | 0.0592 | 0.0091 | 0.0076 | 0.0167 | 0.0759 | 0.1966 |
| 23 N SS 536441 | 64 | 0.0547 | 0.0509 | 0.1056 | 0.0055 | 0.1384 | 0.1439 | 0.0009 | 0.0012 | 0.0021 | 0.1460 | 0.2516 |
| 23 N OC 536441 | 64 | 0.0485 | 0.0017 | 0.0502 | 0.0041 | 0.0557 | 0.0598 | 0.0035 | - | 0.0035 | 0.0633 | 0.1135 |
| 2 N SS 536441 | 101 | 0.0790 | 0.0028 | 0.0818 | 0.0031 | 0.0029 | 0.0060 | - | - | - | 0.0060 | 0.0878 |
| 2 N OC 536441 | 101 | 0.0313 | 0.0082 | 0.0395 | 0.0029 | 0.0061 | 0.0090 | 0.0015 | - | 0.0015 | 0.0106 | 0.0511 |
| 36 CR 805126 | 15 | 0.0202 | 0.0107 | 0.0309 | 0.0037 | 0.0099 | 0.0136 | 0.0030 | - | 0.0030 | 0.0166 | 0.0475 |
| 27 N 805126 | 25 | 0.0212 | 0.0061 | 0.0273 | 0.0061 | 0.0059 | 0.0120 | - | - | - | 0.0120 | 0.0393 |
| 30 SS 805126 | 38 | 0.0414 | 0.0150 | 0.0564 | 0.0068 | 0.0026 | 0.0094 | 0.0035 | 0.0072 | 0.0107 | 0.0201 | 0.0765 |
| 30 OC 805126 | 38 | 0.0268 | 0.0005 | 0.0273 | 0.0071 | 0.0064 | 0.0135 | 0.0010 | - | 0.0010 | 0.0145 | 0.0418 |
| 35 N SS 805126 | 51 | 0.0685 | 0.0078 | 0.0763 | 0.0063 | 0.0015 | 0.0078 | 0.0059 | 0.0055 | 0.0114 | 0.0192 | 0.0955 |
| 35N OC 805126 | 51 | 0.0431 | 0.0037 | 0.0468 | 0.0052 | 0.0059 | 0.0111 | 0.0100 | 0.0037 | 0.0137 | 0.0248 | 0.0716 |

I - Isolated; S - Stringer; T - Total (I + S)

# WELDABILITY AND HAZ TOUGHNESS OF STELCO OFFSHORE QUALITY PLATE

by

D. B. McCutcheon, Stelco Inc.

Work on this project was conducted under the auspices of the Canada Centre for Mineral and Energy Technology, Energy, Mines and Resources, Canada

| | |
|---|---|
| DSS File Number: | 23SQ.23440-2-9027-1 |
| DSS Contract Number: | OSQ82-00211 |
| CANMET Project Number: | |
| CANMET Scientific Authority: | Dr. J. D. Boyd |

# SUMMARY

Development of Canada's offshore oil and gas reserves will create a demand for significant tonnages of Grade 350 plate. In addition to meeting base plate strength and toughness requirements, this grade must exhibit excellent weldability (resistance to hydrogen induced cold cracking) and weld HAZ toughness. Stelco's ability to produce weldable Grade 350 plate which meets tentative HAZ CTOD toughness requirements was assessed as part of a CANMET-sponsored project to determine the current capability of Canadian plate producers to supply to this market.

Two trial heats of Grade 350 plate were produced at Lake Erie and Hilton Works to low carbon equivalent chemistries designed to minimize weld preheating requirements and to exhibit good low temperature HAZ toughness. The weldability of each steel was evaluated using Y-groove cracking, controlled thermal severity and implant tests. The HAZ toughness was determined using CTOD and Charpy tests on actual weldments, as well as CTOD tests on Gleeble simulated HAZ samples.

Both the LEW (0.38 CE, 0.17 $P_{CM}$) and HW (0.40 CE, 0.22 $P_{CM}$) chemistries exhibited excellent resistance to cold cracking with low hydrogen (E7018) electrodes and would require no preheat at 25 mm thickness. With cellulosic, high hydrogen (E7010) electrodes, the LEW chemistry has superior cold cracking resistance, and requires correspondingly lower preheat to prevent cracking.

The titanium treated, LEW chemistry has better low temperature HAZ toughness than the HW chemistry. By restricting the weld heat input to 3 kJ/mm, the LEW chemistry could be considered for East Coast design temperatures. The HW chemistry has very poor HAZ toughness, and could not be applied even to North Sea (-10°C) design temperatures.

# WELDABILITY AND HAZ TOUGHNESS OF STELCO OFFSHORE QUALITY PLATE

by

D. B. McCutcheon, Stelco Inc.

Work on this project was conducted under the auspices of the Canada Centre for Mineral and Energy Technology, Energy, Mines and Resources, Canada

| | |
|---|---|
| DSS File Number: | 23SQ.23440-2-9027-1 |
| DSS Contract Number: | 0SQ82-00211 |
| CANMET Project Number: | |
| CANMET Scientific Authority: | Dr. J. D. Boyd |

# SUMMARY

Development of Canada's offshore oil and gas reserves will create a demand for significant tonnages of Grade 350 plate. In addition to meeting base plate strength and toughness requirements, this grade must exhibit excellent weldability (resistance to hydrogen induced cold cracking) and weld HAZ toughness. Stelco's ability to produce weldable Grade 350 plate which meets tentative HAZ CTOD toughness requirements was assessed as part of a CANMET-sponsored project to determine the current capability of Canadian plate producers to supply to this market.

Two trial heats of Grade 350 plate were produced at Lake Erie and Hilton Works to low carbon equivalent chemistries designed to minimize weld preheating requirements and to exhibit good low temperature HAZ toughness. The weldability of each steel was evaluated using Y-groove cracking, controlled thermal severity and implant tests. The HAZ toughness was determined using CTOD and Charpy tests on actual weldments, as well as CTOD tests on Gleeble simulated HAZ samples.

Both the LEW (0.38 CE, 0.17 $P_{CM}$) and HW (0.40 CE, 0.22 $P_{CM}$) chemistries exhibited excellent resistance to cold cracking with low hydrogen (E7018) electrodes and would require no preheat at 25 mm thickness. With cellulosic, high hydrogen (E7010) electrodes, the LEW chemistry has superior cold cracking resistance, and requires correspondingly lower preheat to prevent cracking.

The titanium treated, LEW chemistry has better low temperature HAZ toughness than the HW chemistry. By restricting the weld heat input to 3 kJ/mm, the LEW chemistry could be considered for East Coast design temperatures. The HW chemistry has very poor HAZ toughness, and could not be applied even to North Sea (-10°C) design temperatures.

# CONTENTS

Introduction.................................................. 7

Resistance to Hydrogen-induced Cold Cracking........................ 9

- Carbon Equivalent........................................ 9
- Weldability Tests........................................ 10
- Summary.................................................. 19

HAZ Toughness.................................................. 20

- Welding.................................................. 20
- Metallography............................................ 21
- CTOD and Charpy Testing.................................. 26
- Simulated HAZ Testing.................................... 35
- Discussion............................................... 41

References..................................................... 44

Acknowledgments................................................ 46

# INTRODUCTION

The forecast Canadian shortages of oil and gas early in the next century will create a demand for thick, low temperature plate for frontier oil and gas projects. As an initial step in the development plate for this market, Stelco participated in a CANMET funded project to assess our current ability to produce Grade 350 structural plate that meets East Coast and Arctic specifications.[1] In addition to evaluating the base plate strength and toughness[2] and lamellar tearing resistance[3] of two trial heats, extensive testing has been done to determine weldability in terms of both weld heat-affected zone (HAZ) toughness, and resistance to hydrogen-induced cold cracking.

For steels applied to welded construction it is essential (for the plate producer) to recognize the risk of fracture initiation in the HAZ and to ensure adequate toughness through chemistry control. The fracture initiation resistance of welded structures is primarily controlled by the weld metal and HAZ toughness, which are often significantly lower than that of the base plate. Although the HAZ is a relatively narrow region (usually less than a few millimetres wide), it is relatively brittle and is a likely site for defects in the form of either fusion line discontinuities or HAZ cracks. Several catastrophic failures have initiated from HAZs.[4] Although the base plate and weld metal structures surrounding the HAZ may have excellent initiation toughness under static loading conditions, they frequently cannot arrest fast running cracks.

HAZ toughness is currently a major concern in the selection of steels for offshore structures. Most of the data on HAZ properties has come from North Sea fabrication. Extensive HAZ toughness testing of BS4360 type steels as part of the UK Offshore Steels Research Program in the mid-1970s[5] concluded that the toughness of these steels was adequate at -10°C. Testing covered a range of thicknesses from 50 to 134 mm welded at heat inputs between 1.5 and 4.0 kJ/mm. More recently, however, concern has been expressed by several companies about exceptionally low HAZ toughness in newer, low carbon, microalloyed chemistries. The low toughness appears to be related to local segregation (potentially centerline segregation in strand cast slabs) and the high levels of microalloy additions used to achieve the required strength in low carbon chemistries. Unconfirmed comments from several independent sources have indicated that this problem has resulted in the abandonment of at least one partially completed platform. The Welding institute UK has initiated a group sponsored program[6] (including several major oil companies, steel producers and fabricators) to determine the HAZ toughness of a cross section of both conventional normalized and modern controlled rolled 50 mm Grade 350 steels. Similarly, Det norske Veritas is attempting to initiate an extensive program to assess the significance of local brittle zones on platform structural integrity.[7]

Canadian and North American plate producers have done little or no work to either assess or improve the HAZ fracture toughness of structural plate grades. However, most Japanese and several European steelmakers have developed new steels designed to provide HAZ fracture initiation resistance, particularly in high heat input welds. In the early 70s Japanese plate producers pioneered the use of small titanium additions (<0.02 percent) for HAZ grain size control,[8] as well as the use of low nitrogen steels (<0.005 percent), to improve HAZ toughness.[9] More recently, they have developed low nitrogen, high aluminum (≈0.06 percent) steels designed to reduce the HAZ free nitrogen content[10] as well as calcium treatment to restrict HAZ grain coarsening.[11] Moreover, their development of heavy plate controlled rolling and most recently, water spray cooling of heavy plate[12] has allowed the production of Grade 350-type plate with little or no microalloy content and exceptional HAZ fracture resistance. It is anticipated that for Canadian offshore construction (with its significantly lower design temperatures), the HAZ properties of currently available Canadian Grade 350 plate will not be acceptable, and hence significant development of plate chemistry and processing will be necessary to meet HAZ toughness requirements.

The other major property to be considered in the development of new Grade 350 steels is their inherent susceptibility to HAZ, hydrogen-induced cold cracking. Welding procedures to eliminate cold cracking have been developed through the use of low hydrogen consumables and preheating. However, there is a significant cost advantage to the fabricator in reducing or eliminating preheating, and thus there has been a strong trend to develop more weldable structural steels for offshore applications. Cracking susceptibility is primarily dependent on carbon and alloy content, which controls the microstructure produced in the HAZ, and the resistance to cracking has been related to the chemical analysis through carbon equivalent formulae. The other factors controlling cold cracking are the weld hydrogen content and the weld restraint stresses.

Prediction methods are available for determining suitable welding conditions to avoid HAZ cold cracking. The most commonly used are The Welding Institute (TWI) approach, covered in BS5135, and the $P_W$ approach developed in Japan by Ito and Bessyo. These approaches are significantly different in origin, in terms of their carbon equivalent formulae and the degree to which they account for the effects of other factors controlling cracking.[13] It is important to recognize that there are deficiencies in the predictive methods. Recent studies by TWI have shown that the BS5135 and TWI approaches do not, in all cases, adequately safeguard against hydrogen cracking during the fabrication of low carbon equivalent steels.[14] Thus it is necessary for the steel producer, particularly when developing new chemistries of plate, to provide data on a steels' susceptibility to cracking during actual fabrication.

This report describes both the HAZ toughness and weldability testing done on the LEW and HW Grade 350 trial heats during the period January 1984 to August 1984.

## RESISTANCE TO HYDROGEN-INDUCED COLD CRACKING

### Carbon Equivalent

Carbon equivalents are used as the preliminary measure of a steel's sensitivity to HAZ cold cracking. They are essentially measures of a steel's hardenability during fairly rapid cooling from austenite. The two most used carbon equivalent formulae are:

- $\mathrm{CE} = \mathrm{C} + \frac{\mathrm{Mn}}{6} + \frac{\mathrm{Cr} + \mathrm{Mo} + \mathrm{V}}{5} + \frac{\mathrm{Ni} + \mathrm{Cu}}{15}$ (%), and

- $P_{CM} = \mathrm{C} + \frac{\mathrm{Si}}{70} + \frac{\mathrm{Mn}}{20} + \frac{\mathrm{Cu}}{20} + \frac{\mathrm{Ni}}{60} + \frac{\mathrm{Cr}}{20} + \frac{\mathrm{Mo}}{15} + \frac{\mathrm{V}}{10} + 5\mathrm{B}$ (%)

The CE formulae has been developed for relatively high carbon steels (>0.18 percent C) and is used in the TWI approach for predicting safe welding procedures based primarily on a critical HAZ hardness criterion. The $P_{CM}$ formula used in the Japanese approach was developed more for lower carbon (<0.17 percent) steels, and thus is more applicable to modern low C normalized and controlled rolled plate steels, particularly for butt-welds.

For offshore structures, steels are commonly purchased with maximum CE (and sometimes carbon) restrictions. These vary considerably with both end user and classification society. Examples of recent requirements are available in the DnV Review of Steels used in Construction of Offshore Structures. A typical maximum allowable CE is 0.43.

It has generally been suggested that modern low carbon steels (less than ≈0.15) have better weldability than predicted by the CE formula. However, there are indications that other factors, in addition to the potential deficiencies of the TWI prediction procedures, may need to be considered in fully describing a steels resistance to cold cracking. These are primarily factors which have secondary effects on the chemistry's hardenability, including cleanliness, nitrogen content and austenite grain coarsening behavior. In particular, modern low sulfur steels (required for lamellar tearing resistance and improved notch toughness) have been reported to have an increased susceptibility to cracking.[15] This has been attributed to both the increased hardenability of steels with low inclusion content, and the reduction in sites for hydrogen trapping. Similarly, the recent trend to reduce microalloy content to improve HAZ toughness may adversely affect cracking resistance by increasing HAZ hardenability and allowing more grain coarsening in the HAZ.

The chemistries and calculated carbon equivalents for the trial heats are given in Table I.

**Table I: Heat Chemistries**

| | C | Mn | S | Si | Ni | Cr | V | Cb | Ti | ASA | N | CE | $P_{CM}$ |
|---|---|---|---|---|---|---|---|---|---|---|---|---|---|
| LEW | 0.07 | 1.43 | 0.004 | 0.29 | 0.25 | 0.25 | 0.075 | 0.02 | 0.011 | 0.038 | 0.007 | 0.38 | 0.17 |
| HW | 0.13 | 1.40 | 0.003 | 0.23 | 0.24 | - | 0.06 | 0.02 | 0.005 | 0.010 | 0.011 | 0.40 | 0.22 |

Both heats were designed with lower carbon equivalent (CE) and lower carbon contents than previous Stelco Grade 350 chemistries, and meet current, known restrictions for CE. It is notable that in terms of CE value, both steels would be expected to have similar cold cracking resistance, whereas their $P_{CM}$ values would suggest superior performance by the LEW chemistry.

**Weldability Tests**

1. Y-Groove Cracking Tests

Y-groove cracking tests were performed on 25 mm plate from each chemistry to determine the minimium preheat temperature required to prevent cracking. All tests were done in accordance with JIS Z3158, with the exception that the percentage of cracking was rated by a heat tinting method rather than metallographic examination.

A unique method was developed to fabricate the test specimen. As shown in Figure 1, the coupons are self-restrained, and contain a Y-groove test section. It is critical that the joint gap be reproducibly fabricated to 2 ±0.2 mm to ensure the same conditions for all tests. Normally, the gap is produced by placing shims along the test portion during restraint welding. This procedure was abandoned after preliminary testing in favor of a modified edge preparation in which the double-bevel test length was offset 2 mm.

Figure 1: Y-Groove Cracking Test

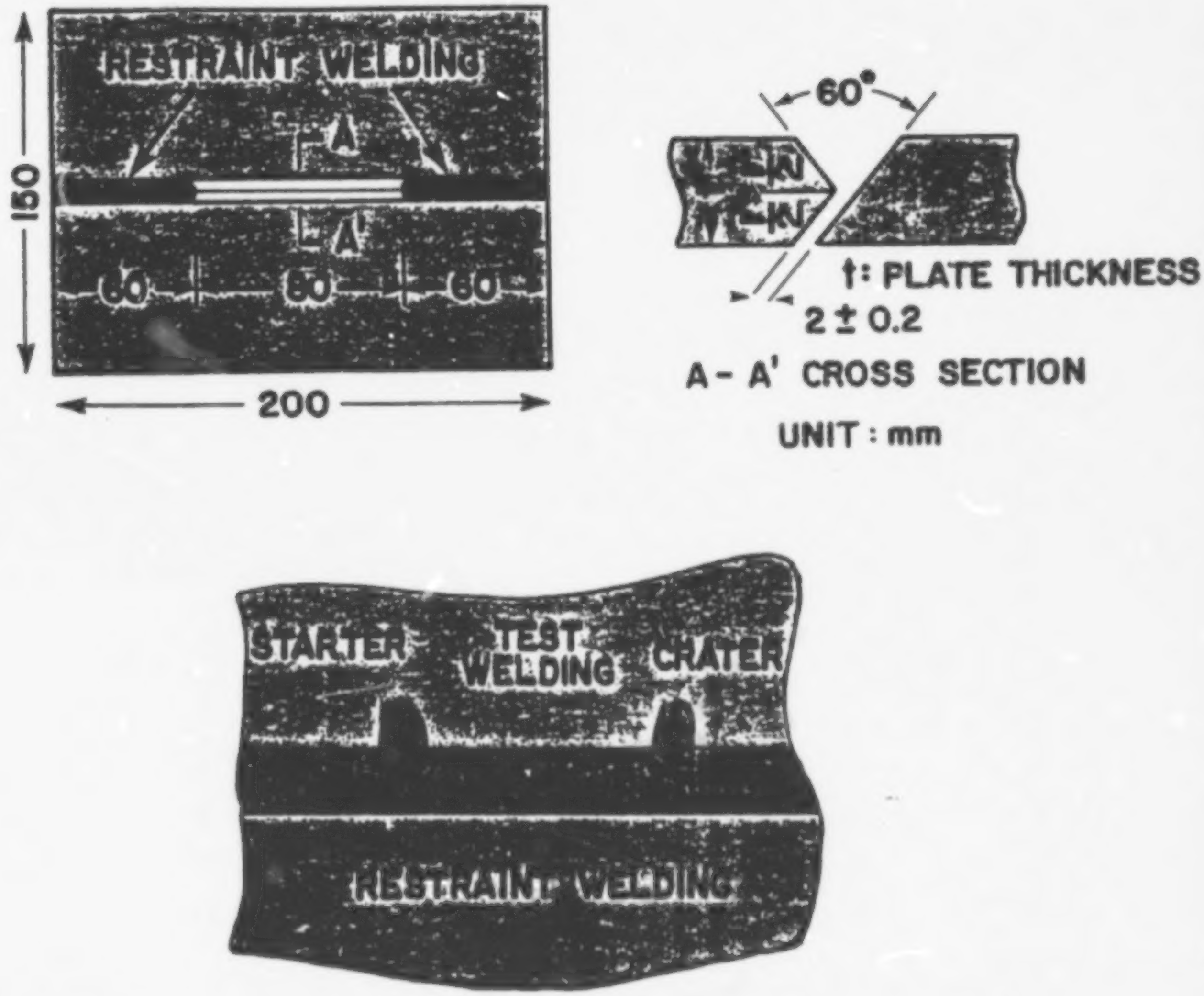
RESTRAINT WELDING
A
A'
60
60
60
150
200
60°
t: PLATE THICKNESS
2 ± 0.2
A - A' CROSS SECTION
UNIT : mm
STARTER
TEST WELDING
CHATER
RESTRAINT WELDING

The Y-groove tests were welded manually using both E7010 and E7018 SMAW 4 mm Ø electrodes to attain two levels of weld hydrogen. The E7010 electrodes were taken from a new canister and were protected from moisture by wrapping in plastic during the period of test welding. Similarly, the E7018 electrodes were new and were baked at 250°C for one hour (according to the manufacturer's recommendation) immediately prior to welding to achieve a consistently low hydrogen content. The hydrogen content of each electrode type was measured in accordance with ISO 3690-1976 (Welding-Determination of Hydrogen in Deposited Weld Metal Arising from the use of Covered Electrodes for Welding Mild and Low Alloy Steels). This technique uses mercury as a eudiometric fluid and gives a significantly higher hydrogen content than that determined by the JIS glycerin method. The hydrogen levels for the electrodes are given in Table II.

Table II: Test Electrode Hydrogen Contents

| Electrode | Hydrogen Content (mL/100 g) | | | |
|---|---|---|---|---|
| | Deposited Metal | | Fused Metal | |
| | IIW | JIS* | IIW | JIS* |
| E7010 | 74.3 | 49.0 | 30.3 | 19.5 |
| E7018 | 7.6 | 4.3 | 4.6 | 2.3 |

* $H_{JIS} = 0.67\ H_{IIW} - 0.8$

The Y-groove tests were done on nominal 25 mm plates from both the LEW and HW heats. Because of the potential effects of the centerline segregation zone on cold cracking resistance, the LEW coupons were machined from 32 mm plate down to 25 mm so that the segregation region was offset from the weld zone. Additional tests were also done with an as-rolled thickness of 25 mm, so that the segregation zone would be located near the weld line.

All tests were welded in the flat position with a nominal heat input of 1.7 kJ/mm. Weld amperage, current and travel speed were measured for each weld. The calculated heat input ranged from 1.5 to 1.9 kJ/mm. Test temperatures ranged from 0 to 200°C. Sub-ambient temperatures were achieved by precooling the test samples in dry ice, and allowing the samples to heat to test temperature. Moisture on the low temperature samples was removed by flame drying immediately prior to welding. All tests were held at ambient temperature for 48 hours prior to heat tinting at 350°C. After tinting the samples were cooled in a dry ice-alcohol mixture and were bent to failure to reveal the degree of cracking. This technique has the advantage, compared with the recommended metallographic procedure, of being able to more reliably detect isolated low percentages of cracking. Representative fracture faces showing different degrees of cracking are shown in Figure 2.

**Figure 2: Fracture Surface of Heat Tinted Y-Groove Tests**

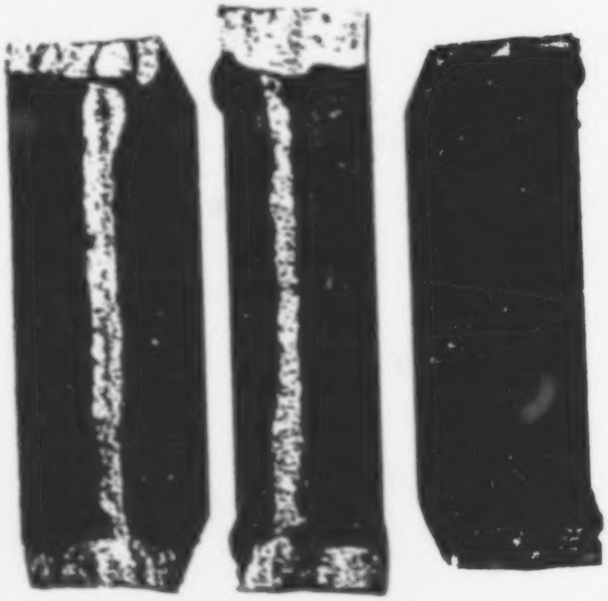

The Y-groove cracking test results are shown in Table III. For low hydrogen, E7018 electrodes, both steels exhibited similar weldability with To (preheat temperature for no cracking) temperatures of 23°C. The LEW centerline weld tests showed no deterioration in weldability, however, a more complete evaluation of centerline segregation effects is recommended. For high hydrogen E7010 electrodes the HW steel had a slightly higher To temperature than the LEW steel (150°C versus 100°C).

**Table III: Y-Groove Cracking Results**

| Heat | Electrode | % Cracking | | | | | |
|---|---|---|---|---|---|---|---|
| | | 0°C | 23°C | 50°C | 100°C | 150°C | 200°C |
| HW | E7018 | 10 | 0 | 0 | - | - | - |
| | E7010 | - | 100 | 100 | <2 | 0 | 0 |
| LEW | E7018 | <2 | 0 | 0 | - | - | - |
| | E7010 | | 100 | 95 | 0 | | |
| LEW $C_L$ | E7018 | 0 | 0 | - | - | - | - |
| | E7010 | - | 100 | - | 0 | 0 | - |

The preheat requirement for the LEW steel welded with low hydrogen electrodes was in good agreement with that predicted by the Ito-Bessyo formula:

$$T = 1440 \left( P_{CM} + \frac{t}{600} + \frac{H}{60} \right) -392^{\circ}C$$

where: t = plate thickness (mm)
H = diffusible hydrogen in deposited weld metal (mL/100 g)

The term H/60 applies to relatively low hydrogen welds (<5 mL/100 g). For high hydrogen welds its effect is accounted for by the factor 0.093 log H.

For the low hydrogen E7018 electrode the predicted To was 21°C and 89°C for the LEW and HW chemistries, respectively. For the cellulosic E7010 electrodes To was 138°C and 210°C for the LEW and HW steels. The Y-groove results for the LEW steel welded with E7018 electrode was in good agreement with the predicted performance. However, the measured actual To temperatures on the other tests were significantly lower than predicted, which suggests the $P_{CM}$ approach is conservative for these steels.

It is important to recognize that the Ito-Bessyo approach includes a factor for the effect of plate thickness on preheat requirement. This approach predicts an increase in preheat requirement of 60 and 180°C for increases in plate thickness from 25 to 50 mm and 25 to 100 mm, respectively. Also, because of the higher than normal restraint intensity in the Y-groove test design, the Y-groove tests tend to give a higher (more conservative) preheat requirement than necessary in practical applications.

Additional weldability testing has been done by Kawasaki Heavy Industries Limited (KHI) on Stelco LEW chemistries similar to that of the LEW heat.[17] Y-groove, maximum hardness and fillet weld cracking tests were done on a composition without the 0.25 Ni and 0.25 Cr additions in 20, 35 and 45 mm thicknesses, and a composition similar to the Grade 350 trial heat at 20 mm thickness. These results are in good agreement with our results, and clearly demonstrate the significant effect of plate thickness (weld restraint) on preheat requirements.

## 2. Controlled Thermal Severity (CTS) Tests

CTS tests were done on 25 mm plates from each trial heat. The tests were performed using the procedure recommended by Pedder and Hart of TWI.[18] Figure 3 shows the specimen dimensions. Note that the test contains a 1.6 mm root gap, which simulates the gap found in normal fabrication and increases the risk of cracking. The anchor welds were made with dried E7018 electrodes using a preheat temperature of 150°C to ensure freedom from cracking. The test welds were deposited in a flat position using E7010 and pre-dried E7018 electrodes at a nominal heat input of 1.7 kJ/mm. To reproduce the cooling conditions experienced in the welding of large structures, the end of the CTS specimen was immersed in cold water to a depth of 50 mm immediately after welding. To ensure sufficient time for possible cracking, a time of at least 72 hours elapsed between welding the first and second test weld, and also between completing the second weld and sectioning.

**Figure 3: CTS Test Specimen**

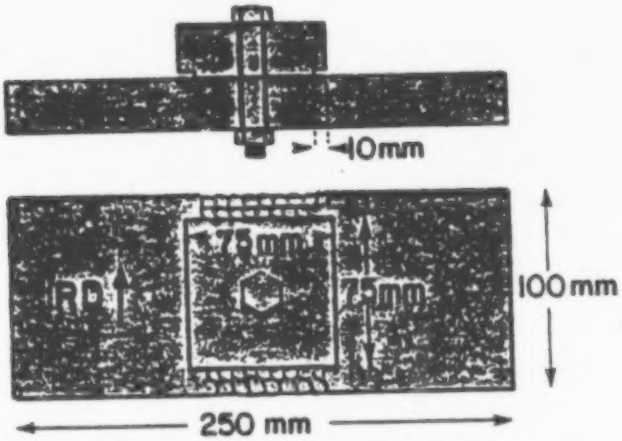

Cracking was measured by sectioning each test weld at six equidistant positions along the weld length. The sections were mounted, polished, etched and metallographically examined for cracking at magnifications up to 500X. The weld and HAZ hardness were measured using the test pattern shown in Figure 4. These HAZ hardness tests were made along both the vertical and horizontal legs.

Figure 4: CTS Test Section with Hardness Impressions (8X)

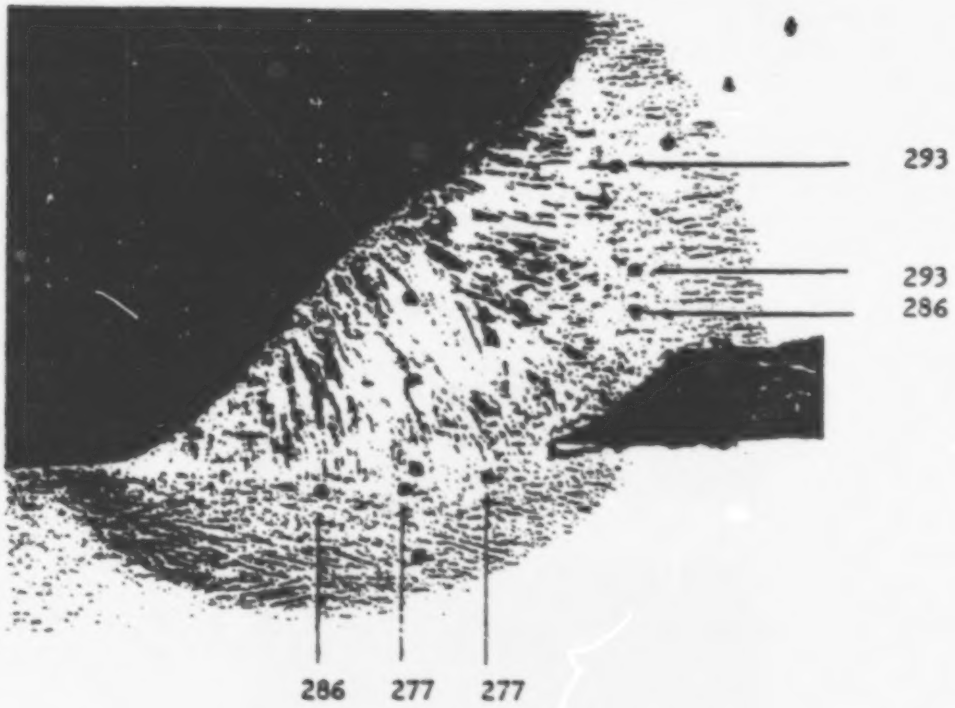

The CTS results are summarized in Table IV. Neither the LEW or the HW chemistries exhibited cracking in room temperature tests when welded with the low hydrogen electrodes. With the cellulosic electrodes, the LEW steel showed significantly better cold cracking resistance than the HW steel. The LEW steel had a critical preheat of 50°C to avoid cracking, compared with a preheat of more than 75°C for the HW steels. Although both steels had similar IIW CE values, the maximum HAZ hardness measured on the LEW chemistry was significantly lower than that of the HW chemistry (293 HV5 versus 358 HV5).

Table IV: CTS Results

| Steel | Electrode | Temperature | Cracking |  | Max HAZ Hardness HV5 |
|---|---|---|---|---|---|
|  |  |  | HAZ | WM |  |
| LEW | E7010 | 23 | 1/6* | 1/6* | 293 |
|  |  | 23 | 3/12 | 10/12 | 288 |
|  |  | 50 | 0/12 | 0/12 | 298 |
|  | E7018 | 23 | 0/12 | 0/12 | 293 |
| HW | E7010 | 23 | 4/6* | 5/6* | 358 |
|  |  | 50 | 8/12 | 0/12 | 347 |
|  |  | 75 | 4/12 | 0/12 | 349 |
|  | E7018 | 23 | 0/12 | 0/12 | 381 |

* welds on one side of CTS test were made with smaller diameter (1/8in) electrodes. These results were not included in the evaluation and thus the results are based on six rather than twelve sections.

The cellulosic CTS test data as well as the maximum HAZ hardness results suggest that the low carbon LEW steel has improved weldability compared with the HW chemistry. Both steels should require little or no preheat when welded with low hydrogen electrodes and heat inputs greater than ≈1.7 kJ/mm. It should be emphasized that although the exact preheat requirements of the HW chemistry should be safely predicted by the TWI procedure, low carbon steels (like the LEW chemistry) do not fall within the range of chemistries or hardness levels originally used to develop it. Hence, welding procedural tests are advised for demonstration of the preheat requirements for all new low carbon chemistries.

KHI fillet weld cracking tests on similar chemistries confirmed the excellent cracking resistance of the LEW steel. Tests done with low hydrogen electrodes at 1.9 kJ/mm heat input exhibited no cracking at 0°C.

### 3. Implant Tests

Implant tests were done on both steels using a test procedure similar to that used by Ito et al.[16] The test specimens were 7 mm diameter with a 0.5 mm deep helical notch with 0.05 mm notch radius (Figure 5). The test samples were taken parallel to the rolling direction and were welded into 25 mm backing plates made from the HW chemistry. All tests were made with E7010 cellulosic electrodes using a nominal 1.7 kJ/mm heat input. The tests were loaded to predetermined stress levels after cooling to 150°C. Up to 10 tests were made over a range of stress levels to determine the maximum stress (critical stress) that could be sustained without failure after loading for 1000 minutes.

**Figure 5: Implant Test Specimen**

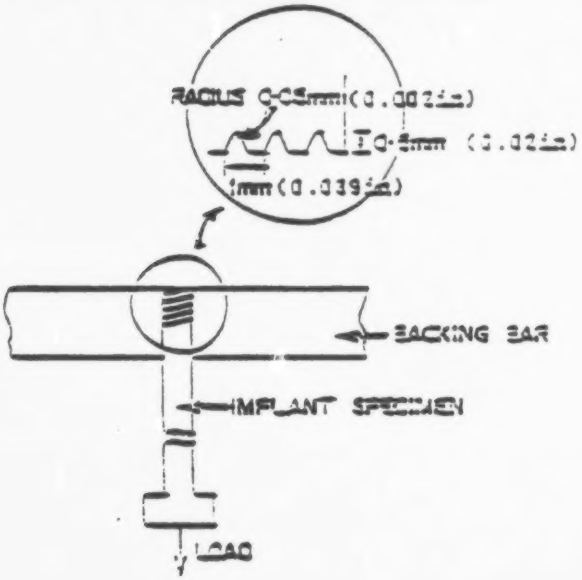

The stress versus rupture time results for each steel are summarized in Figure 6. The LEW chemistry had a significantly higher critical stress ($\sigma_{CR}$) than the HW chemistry (480 MPa versus 365 MPa).

**Figure 6: Implant Test Results**

**(a) LEW**

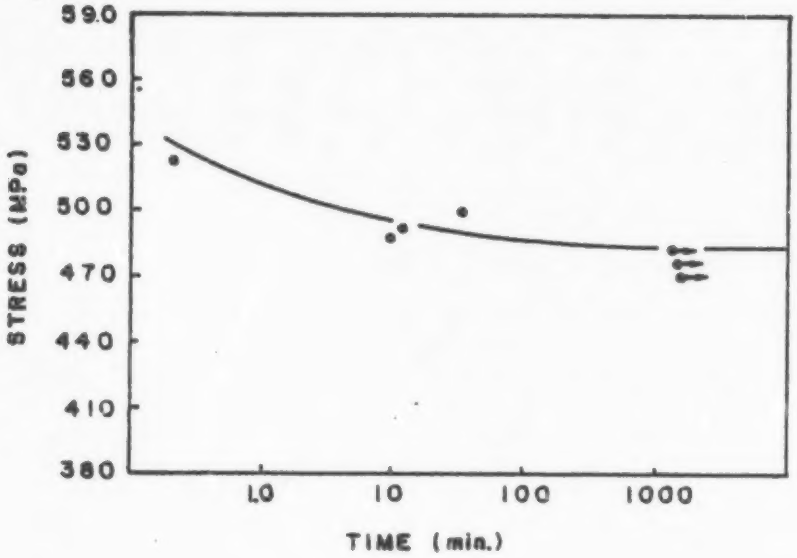

**(b) HW**

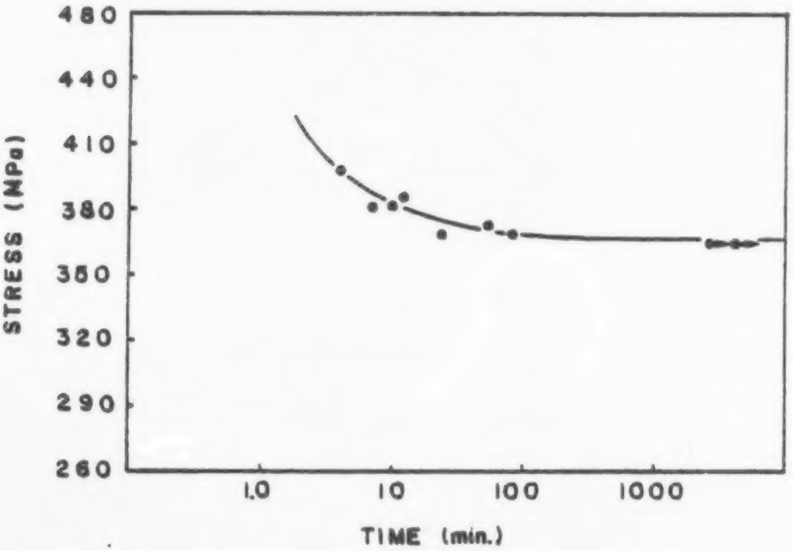

Ito et al have shown a relationship between $\sigma_{CR}$ derived from the implant test and the values of $P_{CM}$, the diffusible weld hydrogen content and the cooling time from the peak temperature to 100°C. They showed that the change in critical stress could be related to the change in $P_{CM}$ by the equation:

$$\Delta\sigma_{CR} = -240\ \Delta P_{CM}$$

where: $\Delta\sigma_{CR}$ is in $kg/mm^2$

This approach predicts a $\Delta\sigma_{CR}$ of ≈120 MPa between the two chemistries, which is in good agreement with the observed difference.

## Summary

The results of several weldability tests have demonstrated the excellent resistance to cold cracking of both the LEW and HW trial chemistries. Both butt and fillet weld tests suggest that these steels can be readily welded without preheat using low hydrogen electrodes. With cellulosic type electrodes, preheat is required, however, under this condition of hydrogen, the low $P_{CM}$ LEW chemistry exhibits superior performance to the HW chemistry. This result was substantiated by the difference in critical stress derived from implant tests made with cellulosic electrodes.

Although our tests suggest excellent weldability for both chemistries it is important to note the recent findings of the TWI who report that their current procedures may give rise to cracking particularly with the newer low carbon plate grades. It is strongly recommended that the weldability of current Stelco plate grades and those under development be characterized using laboratory tests and that these be correlated with fabricator's experience during weld procedure approval testing. In addition, weldability results at sub-ambient temperatures under weld repair conditions are required to characterize the applicability of these steels to Arctic conditions and to provide potential end users with guidelines on cold temperature repair procedures. Clearly, the low carbon equivalent type LEW steels offer some potential in this regard. Japanese development of ultra-low carbon equivalent, water spray cooled plate will undoubtedly promote this aspect, which may be considered as a significant quality advantage for future low temperature construction.

Finally, it should be recognized that despite excellent resistance to HAZ cold cracking, preheat may be required to prevent weld metal chevron cracking. It is very important that we work closely with fabricators and end users in the development of welding procedures for low temperature steels so that we develop technical expertise in this area, both to update our in-house test program and to offer technical guidance to potential end users.

## HAZ TOUGHNESS

The HAZ toughness of the two trial heats was evaluated using both actual and simulated HAZ tests. Actual welds were made in both 19 and 38 mm plates from each heat, and the toughness measured using fatigue precracked CTOD tests and Charpy V-notch tests. Because of the well-known scatter in HAZ CTOD test results, additional CTOD tests were done using Gleeble simulated HAZ samples to provide a comparative measure of the two chemistries' performance over a range of heat inputs. For all HAZ tests, detailed metallography and HAZ hardness testing was performed.

### Welding

It was necessary to develop a welding procedure that would produce relatively straight HAZs in heavy plate for fracture testing. Originally, we considered using a K-type preparation, however, we later adopted the inclined plate procedure recommended by TWI (Figure 7). Following preliminary trials to refine the edge-preparation and bead-sequencing, test welds (400 mm x 1000 mm) were made in 19 mm and 38 mm plate samples from each heat using both 2 and 4 kJ/mm heat input. All plate coupons were cut from parent plates so that the welds ran in the plate rolling direction. The welds were made with a Lincoln SA-800 Amp DC submerged arc welder with a Lincoln LAF-3 controller. The consumables used were Stelco 80 wire and ESAB-1071 flux. The root pass was made in the flat position, and the filler and capping passes were made with the plate inclined at 22° to the flat.

**Figure 7: Schematic of the Inclined Plate Welding Test Procedures**

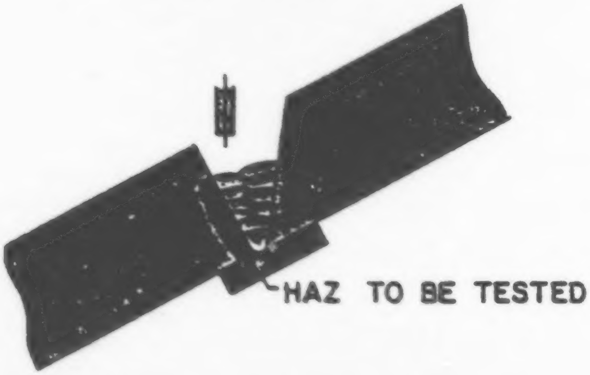

HEAT INPUT 2KJ/mm & 4KJ/mm

SAW CONSUMABLES ESAB 10.71 FLUX
STELCO 80 WIRE
( 0.08 C , 1.59 Mn, .23 Si, .53 Mo, .26 Ni )

PREHEAT & INTERPASS TEMP. 150 °C

To confirm that the test welds were suitable for CTOD testing, full thickness etch tests were taken from the quarter, mid and three-quarter length positions of each weld. Generally, the low heat input welds gave much straighter through-thickness HAZs than the high heat input welds. In addition, significant butterflying of the plates was encountered on several of the 38 mm test coupons. To overcome the effects of this distortion and the slight rotation of the HAZ plane relative to the original plate surface, the plates/welds were machined to 32 mm.

### Metallography

Detailed metallographic examination of the weld HAZ cross sections was done to determine with the extent of the grain coarsened regions through the plate/weld thickness and to determine the types and hardnesses of the different microstructural regions produced by the multi-pass welds. For 2 kJ/mm heat input in the 38 mm plates, the weld bead overlap was such that it produced primarily a normalized type structure along the weld fusion line (Figure 8). At the higher heat input, the bead size was sufficient to produce clear zones of coarse grained structure which made up ≈20 percent of the total fusion line length.

As anticipated from previous results on line pipe steels, the strand cast, 0.01 percent Ti LEW steel exhibited a significantly narrower coarse grained HAZ as well as a finer coarse grained structure than the HW steel. Figure 9 shows the near-fusion line coarse grained HAZs for the two steels in 19 mm plate welded at 2 kJ/mm. Grain coarsening was restricted to a distance of ≈250 μm in the LEW heat, but extended over ≈600 μm in HW heat. In addition, the fusion line prior austenite grain size was ≈60 μm in the LEW plate and over 150 μm in the HW plate. These effects are important in that the cleavage resistance of the HAZ bainitic structures deteriorate with increased grain size. Moreover, the probability of a fatigue crack remaining in this low toughness region is lessened by restricting its width.

For multi-pass welds several different microstructures are produced in the HAZ due to the thermal cycles caused by subsequent weld passes. The main discrete HAZ structures are (see Figure 10):

- coarse-grained - reheated above the austenite grain coarsening temperature,
- normalized - reheated between the $Ar_3$ and the grain coarsening temperatures,
- intercritical - reheated between the $Ar_1$ and $Ar_3$ temperatures, and
- sub-critical - reheated below the $Ar_1$.

Figure 8: Overlap in 2 kJ/mm and 4 kJ/mm Welds in 38 mm Plate (3X)

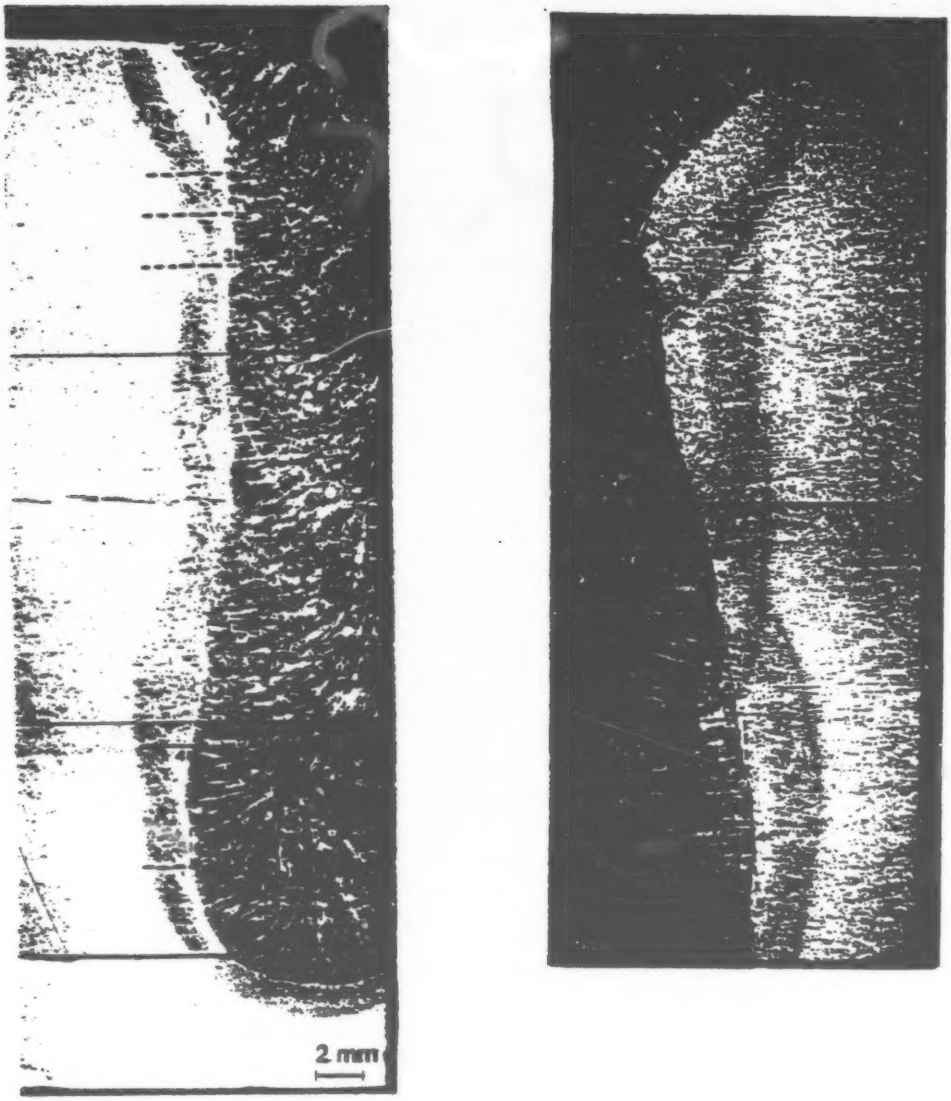

2 kJ/mm

4 kJ/mm

Figure 9: Comparison of HAZ Grain Coarsening in Ti and non-Ti Treated Plate (200X)

(a) LEW (2 kJ/mm, 19 mm Plate)

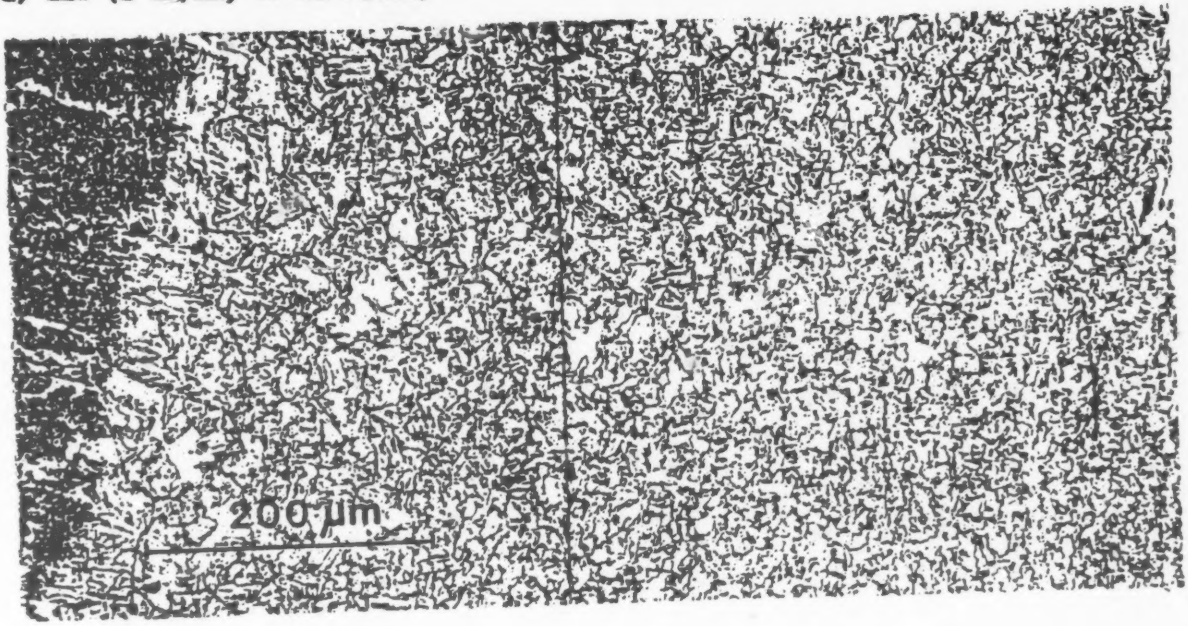

(b) HW (2 kJ/mm, 19 mm Plate)

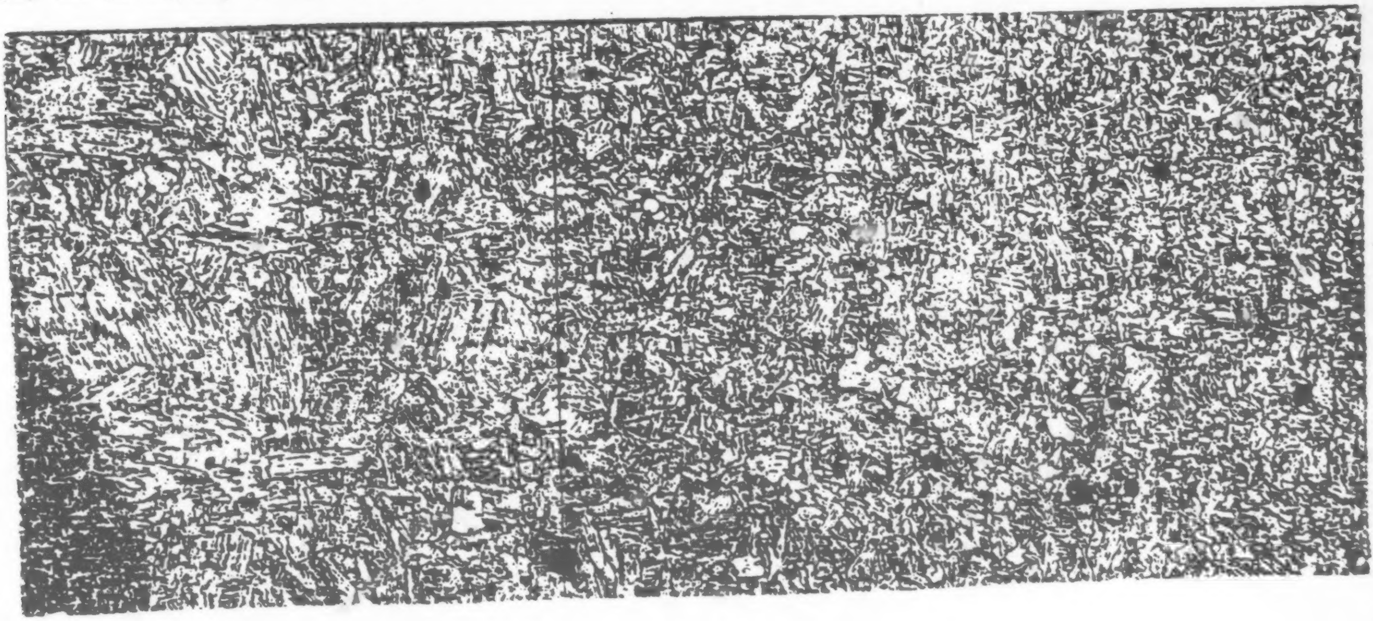

Figure 10: HAZ Regions in Multi-pass Welds (500X)

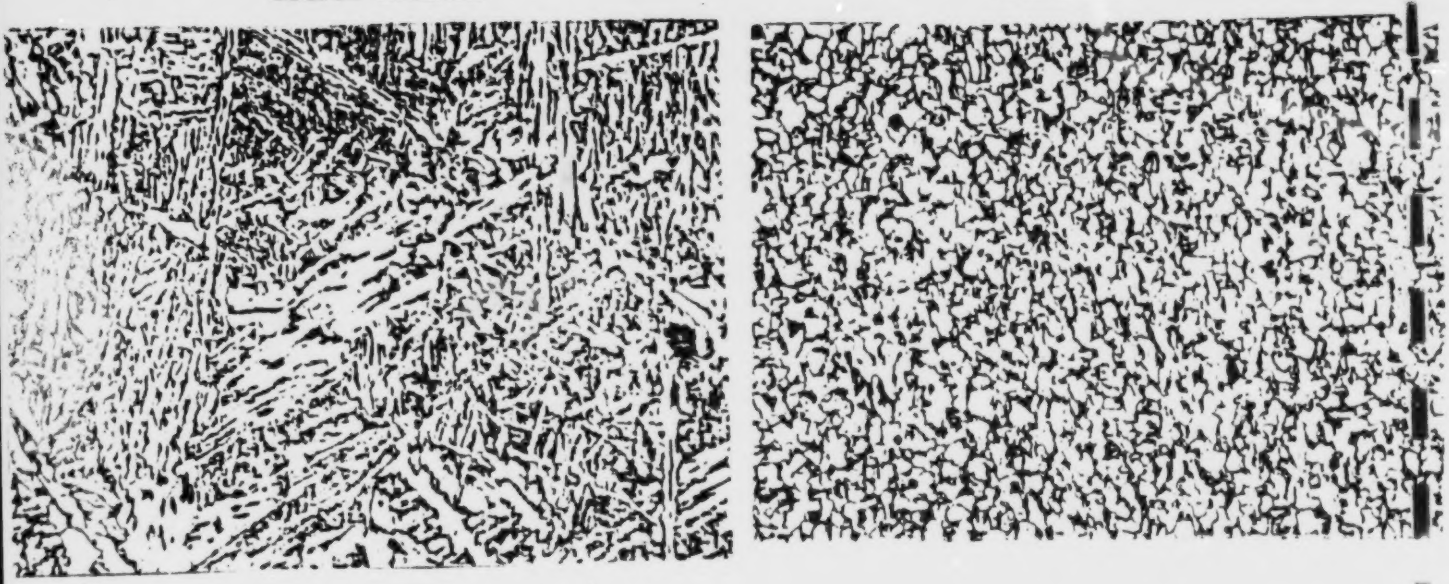
Coarse Grained

Normalized

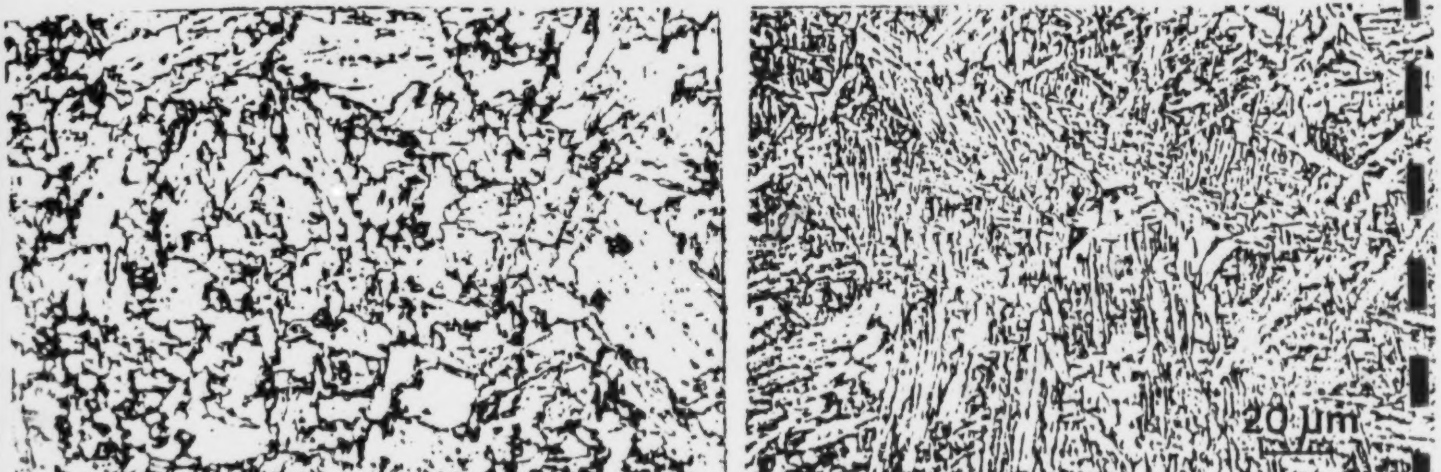

Intercritical

Sub-critical

The main difference in the microstructures between the two heats was evident in the coarse grained and sub-critical regions. Besides the previously mentioned difference in grain coarsening behavior, the HW chemistry tended to have a upper bainitic structure with predominantly cementite inter-lath carbides, whereas the higher alloy content LEW chemistry had a significant percentage of retained austenite-martensite inter-lath constituent. Moreover, the higher carbon HW heat tended to have a higher fraction of inter-lath particles.

Hardness tests were done in each discrete region using a 0.10 kg load. This small load allowed the hardness impressions to be located entirely within a region and resulted in slightly higher (≈20 HV) hardnesses than measured with the more commonly used 5 and 10 kg loads. The hardness results are summarized in Table V. The two heats exhibited similar maximum hardnesses in each region. The highest hardnesses were generally observed in the intercritical region, whereas the lowest hardnesses were found in the normalized structures.

**Table V: Maximum HAZ Hardness**

(a) LEW

| Weld | | Region | | | |
|---|---|---|---|---|---|
| Thickness (mm) | Heat Input (kJ/mm) | Coarse Grain | Normalized | Inter-Critical | Sub-Critical |
| 19 | 2 | 256 | 222 | 263 | 249 |
| | 4 | 264 | 233 | 278 | 245 |

(b) HW

| Weld | | Region | | | |
|---|---|---|---|---|---|
| Thickness (mm) | Heat Input (kJ/mm) | Coarse Grain | Normalized | Inter-Critical | Sub-Critical |
| 19 | 2 | 258 | 224 | 268 | 263 |
| | 4 | 248 | 216 | 264 | 247 |
| 38 | 2 | 251 | 219 | 270 | 258 |
| | 4 | 246 | 222 | 268 | 242 |

Hardness is important not only with respect to hydrogen-induced cold cracking during fabrication but also in the context of stress-corrosion cracking (SCC) during service in severe marine environments. Often a maximum hardness of 325 HV5 is specified in as-welded procedure qualification tests in order to prevent cold cracking. Lower hardness (down to 280 HV) has been specified to protect against SCC. Although neither of the chemistries tested would fail to meet these limits under the welding conditions used here (150°C preheat), lower preheat temperatures and/or lower heat input could significantly increase peak hardness results, particularly for the HW chemistry. Further evaluation of welding effects on hardness will be required if SCC susceptibility becomes part of the Canadian requirements.

## CTOD and Charpy Testing

Up to 15 CTOD specimens were prepared to the preferred BX2B geometry from each weld(s). To ensure that each test coupon was suitable for CTOD testing, each test weld was completely sectioned into oversize coupons. The through-thickness weld and HAZ of both sides of each coupon were ground and nital etched to reveal the HAZ microstructure. If suitable for testing, each sample was subsequently laid out and machined with reference to the "best fit" line, positioned to give the maximum length of HAZ coarse-grained structure. The precrack notches were milled to give a starting a/W of 0.45 with a final notch radius of 0.1 mm. Prior to fatigue precracking the notch root of each sample was precompressed to a strain of 1.0 percent in order to produce a planar fatigue crack front. Fatigue precracking and testing were done in accordance with BS5762:1979.

The CTOD test results are summarized in Figures 11 and 12 for the LEW and HW steels, respectively.

**Figure 11: LEW HAZ CTOD Results**

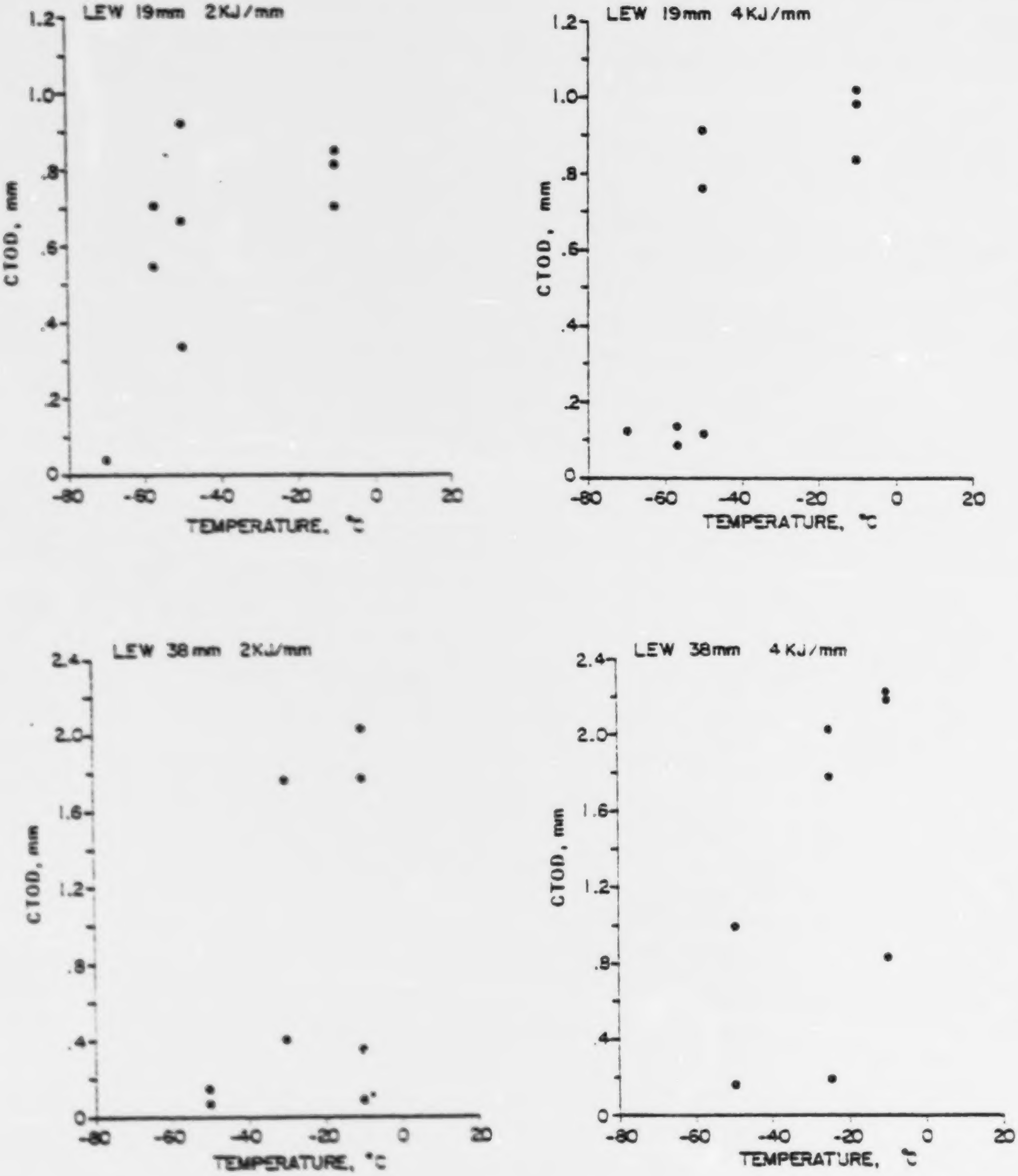

Figure 12: HW HAZ CTOD Results

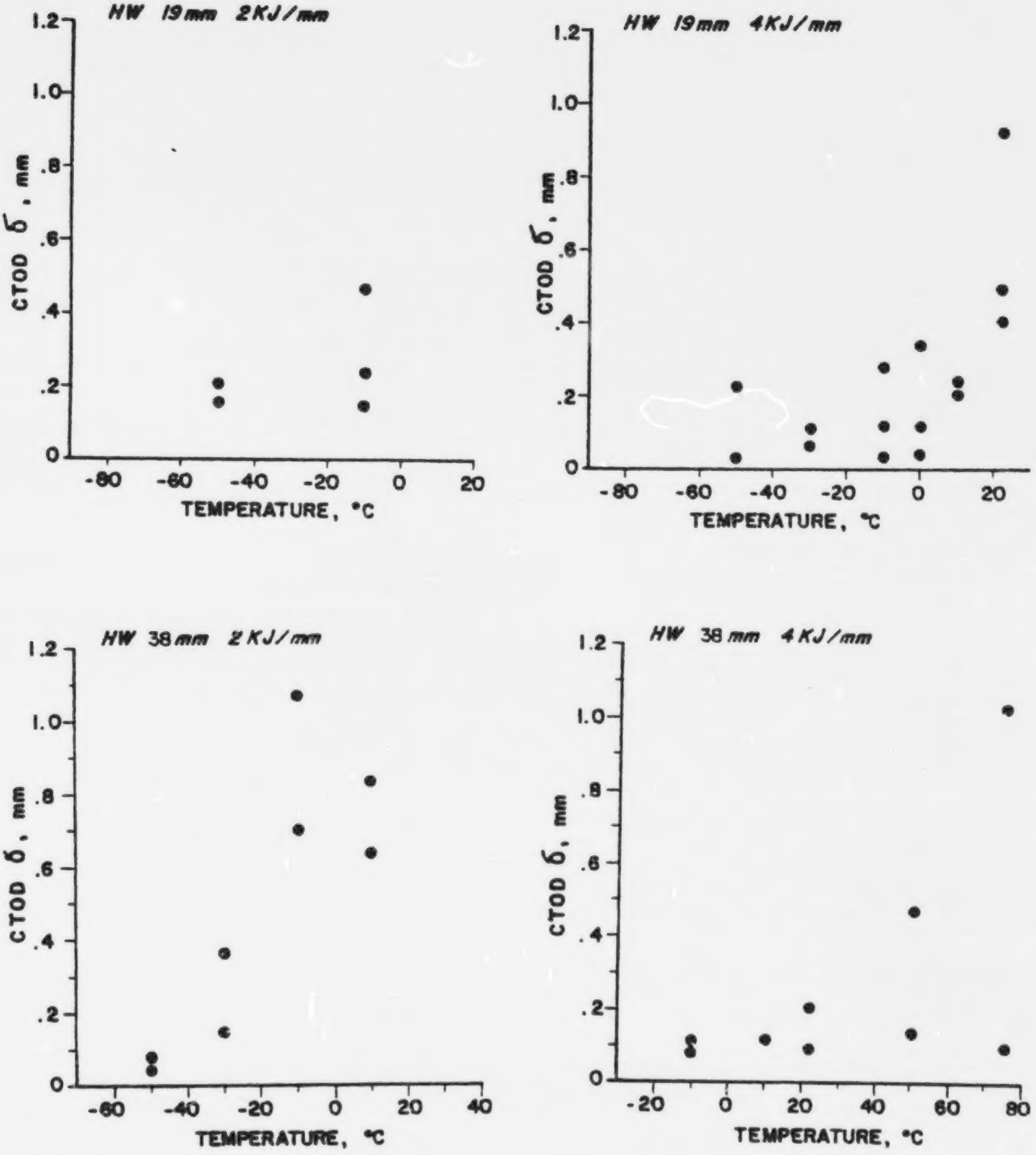

CTOD toughness requirements have not yet been established for Canadian offshore structures. However, CTOD specifications are common in the North Sea, and to a lesser extent, in the Gulf of Mexico. The acceptance requirements are quite variable and like base plate Charpy requirements depend on several factors including the zone of the structure, the structural importance of the weld, combined weld thickness, and weld conditions, a reduction in CTOD requirements being given for PWHT. Typical North Sea requirements are 0.20 to 0.25 mm CTOD at -10°C or 0°C depending on whether the weld is exposed or submerged. Translating this to Canadian conditions, we anticipate the same CTOD levels will need to be met at -50°C (Arctic), -30°C (East Coast) or -5°C (submerged).

Comparing the results obtained from our test program to these criteria, it is clear that only the LEW chemistry has any potential for low temperature applications. In 19 mm plate, at 2 kJ/mm heat input, the LEW heat had adequate toughness down to -50°C; however, at 4 kJ/mm heat input the CTOD values were inadequate at -50°C; additional testing is required to substantiate applications at -30°C. In 38 mm plate (30 mm test thickness), the CTOD toughness is marginal at -30°C at 4 kJ/mm. Results at 2 kJ/mm included one low "pop-in" value at -10°C. At best, these results suggest that the LEW type chemistry is applicable to East Coast design temperatures, however, weld procedural HAZ testing is definitely required to ensure adequate performance with this chemistry in different weld conditions and thicknesses.

The CTOD performance of the HW chemistry was very poor, and it is questionable if this steel could be applied even at North Sea design temperatures. The HAZ toughness at the lowest heat input failed to meet the 0.2 mm criteria at -30°C, at 2 kJ/mm heat input, and at temperatures as high as +75°C at 4 kJ/mm heat input!

Selected CTOD tests were sectioned to determine the position of the fatigue pre-crack relative to the weld fusion line and to identify the microstructure where crack initiations occurred. The sampling positions and typical metallographic sections are shown in Figure 13. As shown, it was confirmed that the fatigue cracks could be located within a few grains of the weld fusion line at different locations along the crack front. With the multi-pass welds, a planar HAZ was not achieved; however, by ensuring that the fatigue crack sampled one or two coarse grain fusion line regions near the center of the plate thickness, we feel that representative minimum CTOD values were measured. Low test values (<0.1 mm) corresponded generally to cleavage initiation at the coarse grain region. This often appeared as a large cleavage "pop-in" on the fracture face. Figure 14 illustrates this behavior on a HW, 38 mm plate sample tested at +75°C. Cleavage fracture in the central "pop-in" was contained in a coarse-grained region related to a single weld bead. Either side of this bead, ductile fracture was observed.

Figure 13: CTOD HAZ Mtallographic Sections

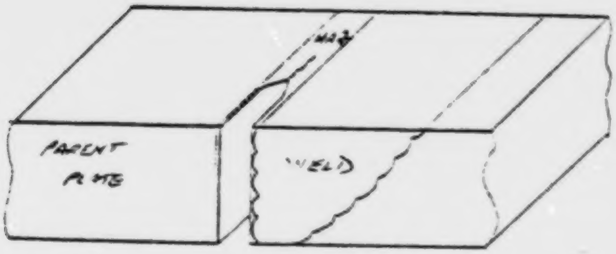
HAZ
PARENT PLATE
WELD

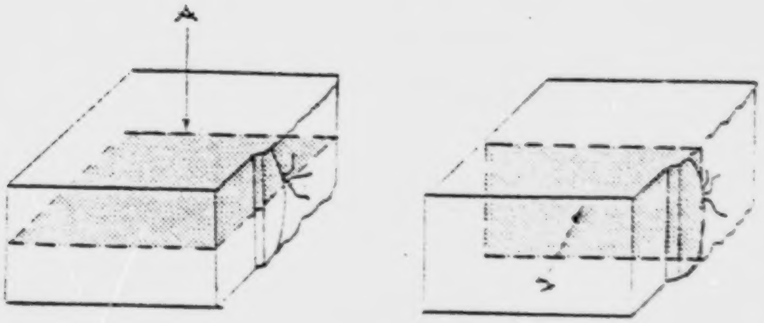

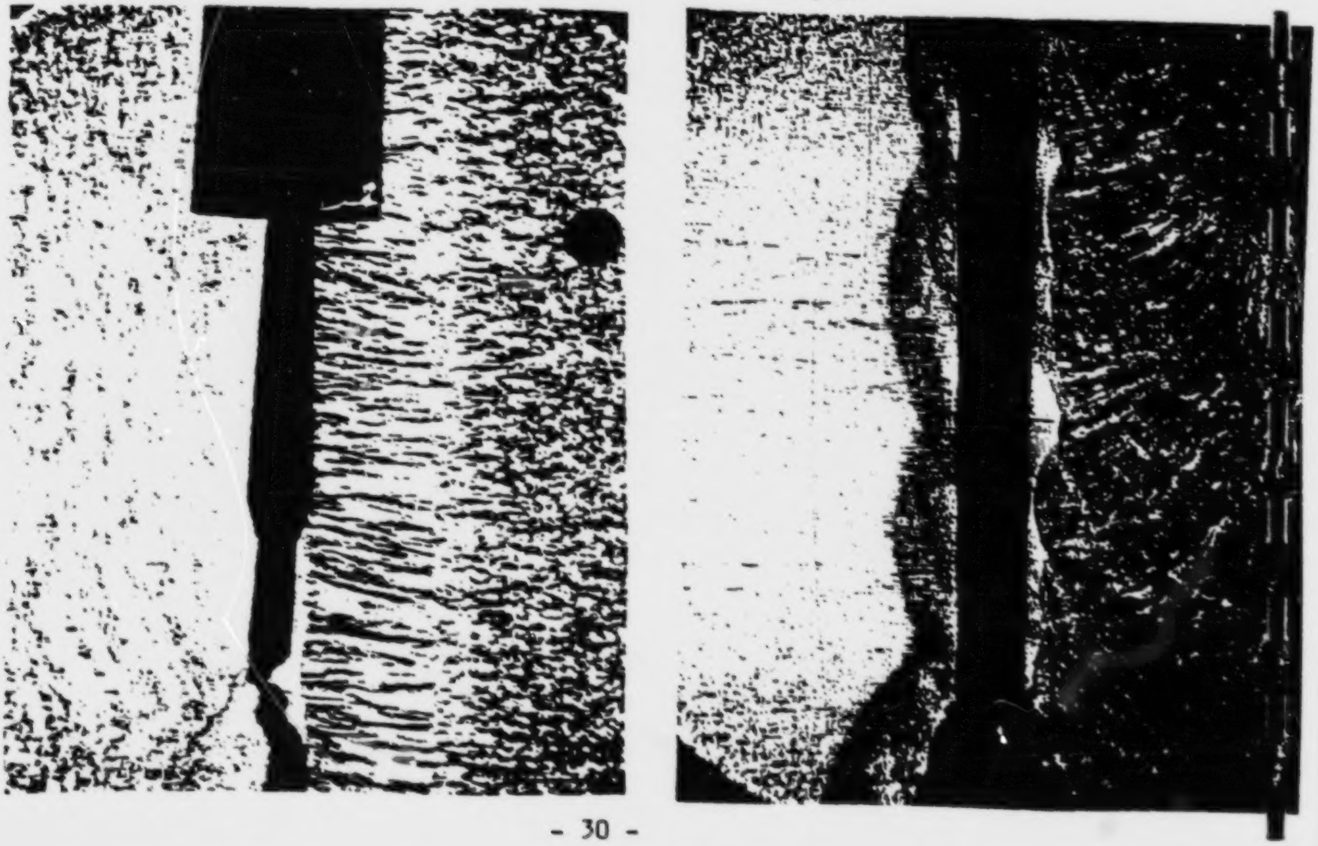

(b) HW 19 mm Plate (15X)
2 kJ/mm

(c) HW 19 mm Plate (5X)
2 kJ/mm

Figure 14: Cleavage Initiation in the Coarse-grained HAZ

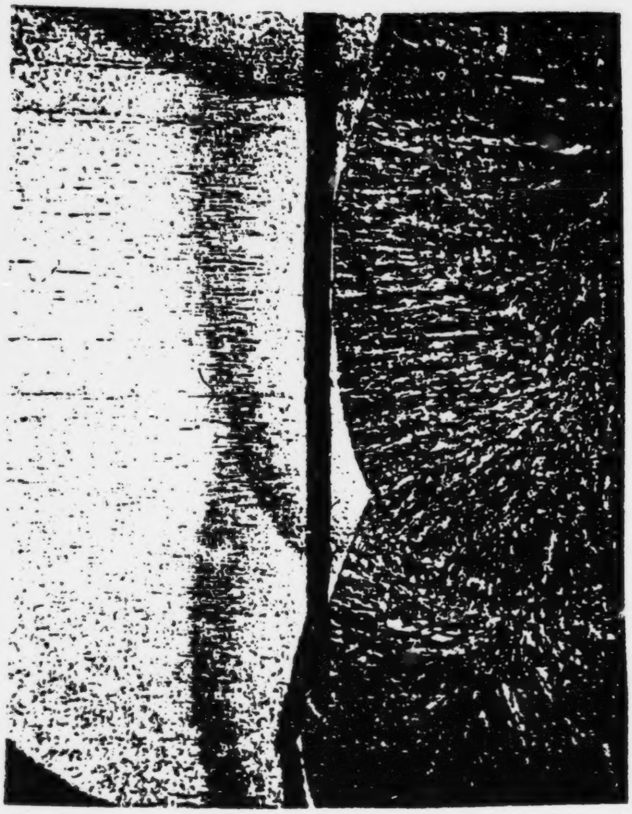

Weld bead overlap
in HW 38 mm Plate
4 kJ/mm Heat Input
(5X)

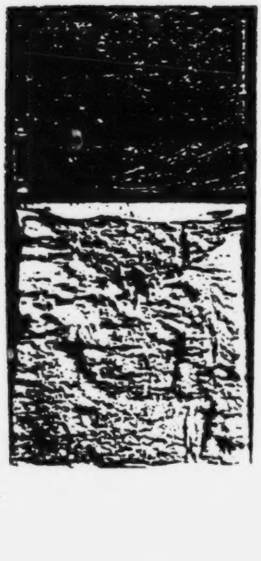

CTOD fracture face
showing cleavage
cracking in CG HAZ
(Actual Size)

Full size Charpy V-notch transitions were also measured on each plate weld. All Charpies were taken from test positions near the weld root and were oriented so that a maximum length of coarse-grained structures would be sampled. This was considered to be more valid than simply specifying a test position at a fixed distance from the plate surface for which the HAZ structures (and toughness) could vary significantly with weld heat input and plate thickness. All Charpies were rough machined and etched prior to notching to position the notch root on the weld fusion line. Because of both weld bead curvature and bead overlap it was not always possible to locate the notch so as to contain only weld fusion line. In these cases the notch was positioned so as to sample the fusion line and HAZ, rather than weld metal.

The Charpy transition curves are shown in Figures 15 and 16 for the LEW and HW heats, respectively. As with the base plate Charpy results, the LEW heat gave significantly higher Charpy shelf energies than the HW heat (>360 J versus ≈180 J). Table VI summarizes the lower bound 40 J transition temperatures for each steel and test condition. Generally, the LEW steel showed significantly better Charpy toughness than the HW chemistry except in the 38 mm plate welded at 4 kJ/mm heat input. If base plate Charpy requirements are used a guideline for applications (with respect to the HAZ) in terms of minimum design temperature, the LEW chemistry could be used in Arctic conditions at 19 mm, and in East Coast conditions at 38 mm (with restricted weld heat input). However, the Charpy approach also suggests that the HW chemistry is applicable to East Coast design temperatures. This result clearly demonstrates the problem inherent with using HAZ Charpy V-notch tests for design applications. It is not sufficiently sensitive to the toughness of the narrow HAZ region to discriminate between acceptable and unacceptable fracture initiation resistance, and thus its use in future development trials or weld procedure testing should be treated with caution and must be supplemented by CTOD testing.

Figure 15: LEW HAZ Charpy Results

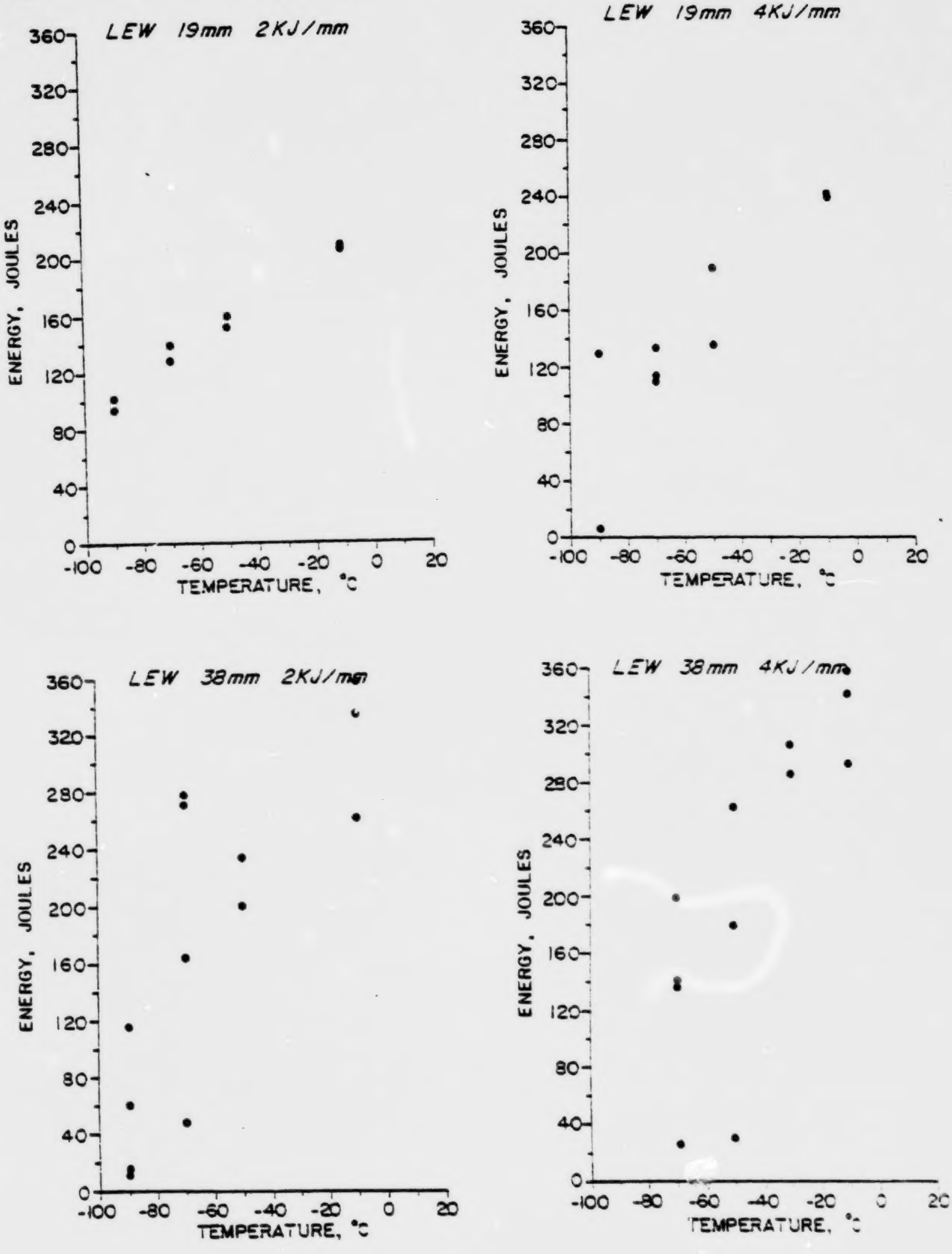

Figure 16: HW HAZ Charpy Results

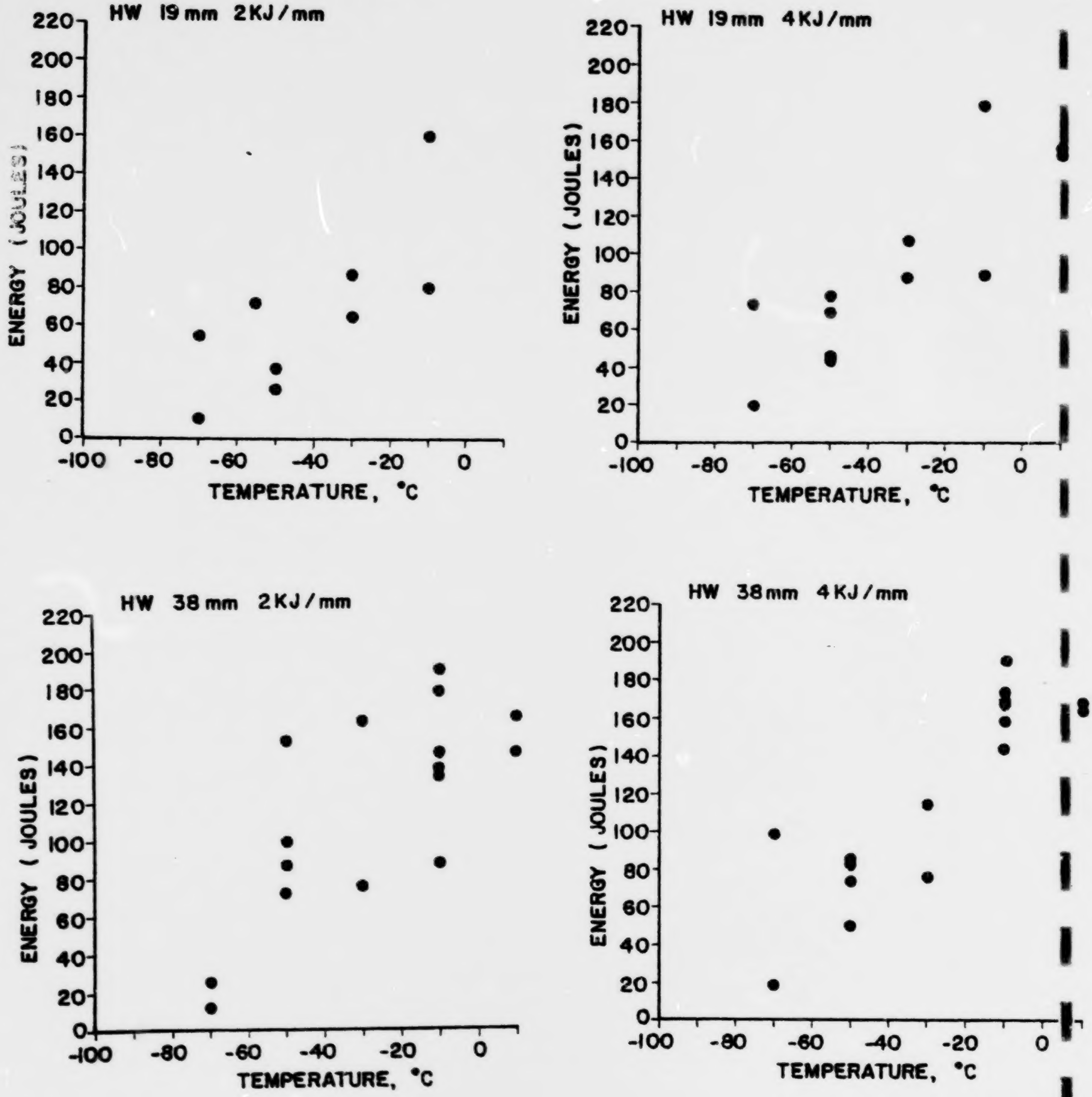

**Table VI: HAZ Charpy Toughness Results**

| Steel | Weld Thickness (mm) | Heat Input (kJ/mm) | 40 J TT (40°C) |
|---|---|---|---|
| LEW | 19 | 2 | < -90 |
| | | 4 | < -80 |
| | 38 | 2 | -70 |
| | | 4 | -40 |
| HW | 19 | 2 | -40 |
| | | 4 | -50 |
| | 38 | 2 | -50 |
| | | 4 | -50 |

## Simulated HAZ Testing

As an alternative to large scale, real weld CTOD testing, the testing of Gleeble simulated HAZ microstructures has been used to develop comparative fracture data on different steel chemistries and weld HAZ regions. Although there are some concerns about the ability of the simulation to exactly reproduce the grain coarsening behavior and microstructures of real HAZs, previous testing at Stelco, and our current work indicate that Gleeble thermal simulations are adequate for HAZ toughness comparisons. One drawback of the Gleeble approach, however, is that because of the relatively small cross section (10 mm x 10 mm) of the Gleeble specimen, the fracture data is not suitable for fracture resistance calculations in more highly constrained structures.

Gleeble simulated HAZ samples were produced in 10 mm x 10 mm x 85 mm coupons taken from the quarter-thickness position of 38 mm plate from each chemistry. All tests were oriented transverse to the plate rolling direction. The thermal cycles reproduced are shown in Table VII. Three of these cycles were chosen to reproduce the single pass coarse grained HAZ for a range of heat inputs between ≈2 and 5 kJ/mm in 30 mm plate preheated to 100°C, based on data developed by Inagaki.[19] The main factors controlled in these were the peak temperature (1350°C), the time above 1000°C, and the cooling rate between 800 and 500°C ($\Delta T_{800-500}$). The fourth cycle was designed to simulate the normalized structure produced in a coarse grained HAZ by a subsequent weld bead. The peak temperature of this cycle was restricted to 1000°C.

Table VII: Gleeble Thermal Cycles

| Cycle | Peak Temperature (°C) | Time Above 1000°C (sec) | $\Delta T_{800-500}$ (sec) |
|---|---|---|---|
| 1 | 1350 | 8 | 19 |
| 2 | 1350 | 11 | 36 |
| 3 | 1350 | 18 | 75 |
| 4 (i) | 1350 | 11 | 36 |
| (ii) | 1000 | - | 36 |

The microstructures and hardnesses of the simulated structures agreed well with those in the actual weldments. Figures 17 and 18 show actual and Gleeble HAZ structures for both steels. The effect of increased cooling time (heat input) was to coarsen the structures and to promote more grain boundary ferrite, and a coarser upper bainitic structure in both steels. The LEW chemistry at a $\Delta T$ of 20 seconds contained little or no proeutectoid ferrite, and was similar to a low carbon upper bainite structure with lath ferrite and primarily M/A particles along lath boundaries. Increasing the cooling time to 35 and 75 seconds caused some proeutectoid ferrite to form at prior austenite grain boundaries, and a coarsening of the lath ferrite together with formation of an increased fraction of larger cementite (rather than M/A) inter-lath particles. The microstructural changes in the HW chemistry were similar, except that in all cases the HW chemistry showed a larger fraction of inter-lath particles, which were predominantly cementite.

Figure 17: Simulated and Actual HAZ Structures - LEW Heat

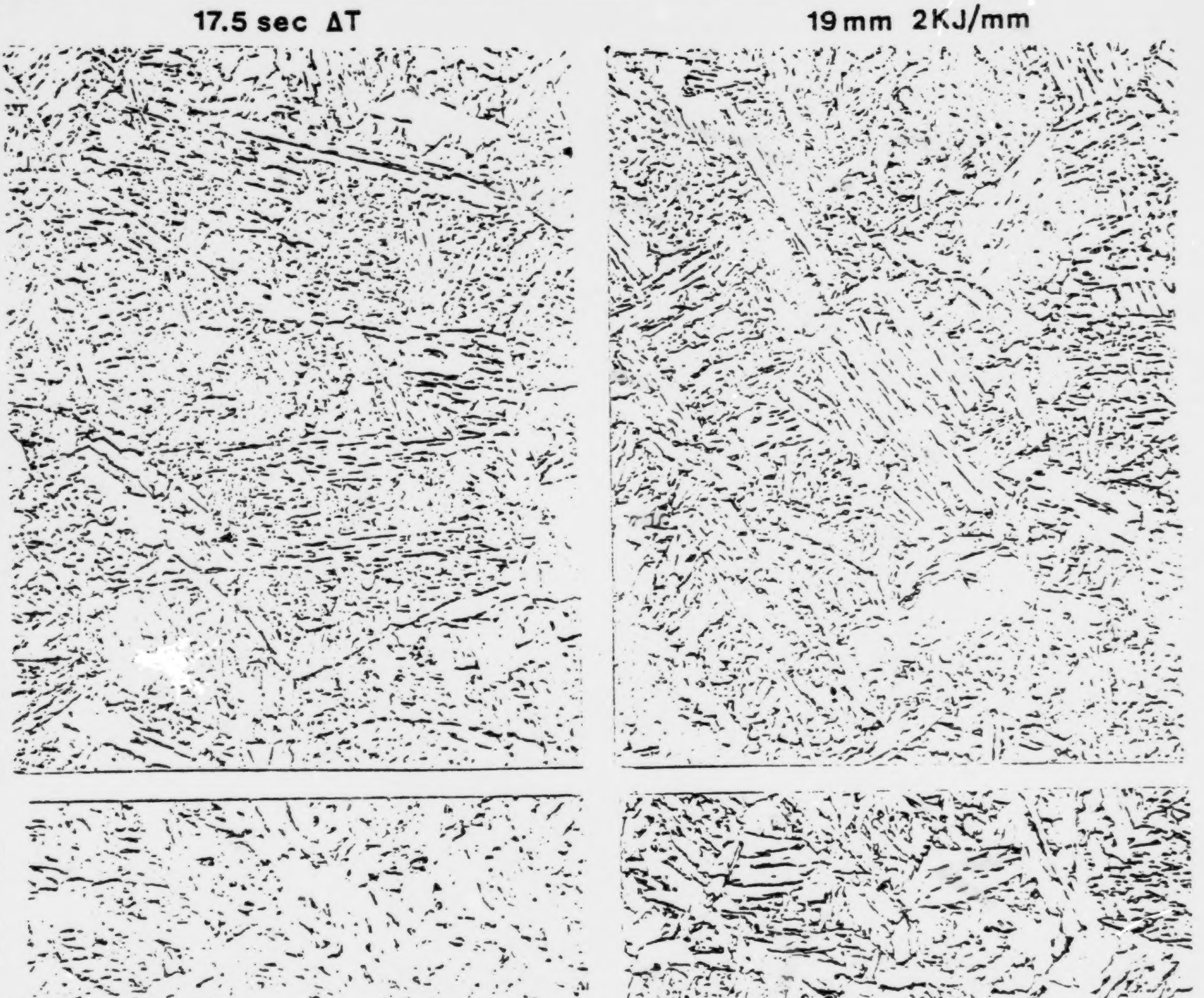

17.5 sec ΔT

19mm 2KJ/mm

75 sec ΔT

19mm 4KJ/mm

Figure 18: Simulated and Actual HAZ Structures - HW Heat

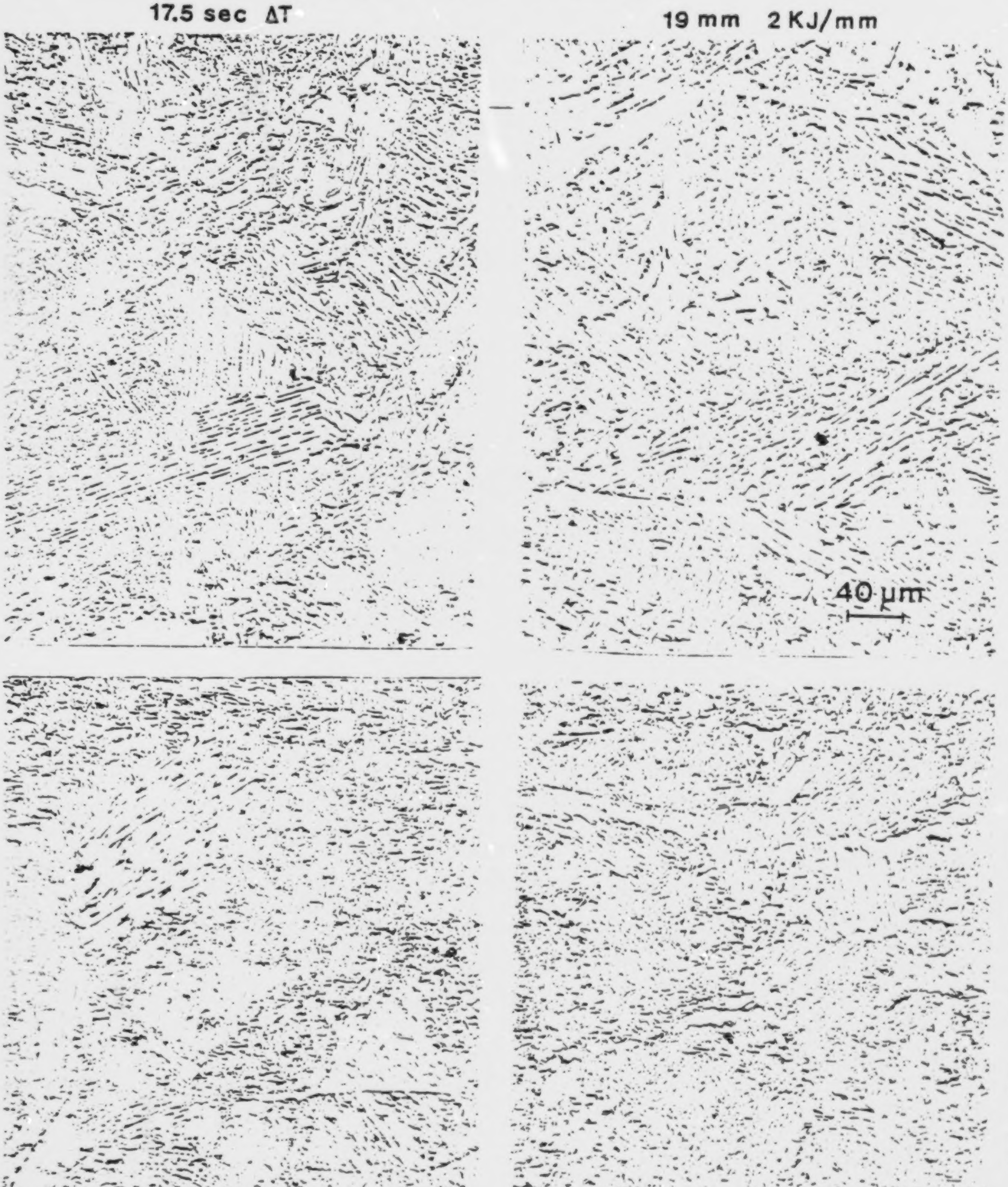
17.5 sec ΔT
19 mm 2 KJ/mm
40 µm
75 sec ΔT
19mm 4KJ/mm
20 µm

The major difference between the actual and simulated structures was the prior austenite grain size. The grain size of the Gleeble simulations was finer than that at the weld fusion line of actual weldments. The smaller grain size of the Gleeble samples reflects their lower peak temperature, and hence the microstructures developed are probably more representative of a position in the bulk of the coarse grained regions. The exact position simulated would depend on thermal gradient developed in the actual weld, which in turn would depend on the weld heat input, preheat, and plate thickness. The mean grain sizes in the LEW and HW simulations were 53, 60 and 53 microns, and 20, 85, 120 microns for the 20, 35 and 75 second $\Delta T_{800-500}$ simulations respectively. It is notable that the LEW (Ti-treated) steel gave much finer grain sizes and was less sensitive to heat input than the HW steel.

Tensile tests were taken from Gleeble samples with the reduced gauge length containing the HAZ structure. The tensile results (Table VIII) illustrate the general softening of the HAZ structures with reduced cooling rate. All single pass simulations exhibited continuous stress-strain behavior which is believed to result from the significant proportion of M/A constitutent in these structures. Thus 0.2 percent offset yield stress values are listed. Comparing the two steels, the LEW chemistry was slightly stronger than the HW chemistry in each condition.

**Table VIII: Gleeble Simulated HAZ Tensile Strength**

**(a) LEW**

| Cycle | Yield Strength (MPa) | UTS (MPa) |
|---|---|---|
| 1 | 575 | 729 |
| 2 | 542 | 680 |
| 3 | 502 | 647 |
| 4 | 476 | 659 |

**(b) HW**

| Cycle | Yield Strength (MPa) | UTS (MPa) |
|---|---|---|
| 1 | 509 | 683 |
| 2 | 512 | 646 |
| 3 | 435 | 616 |
| 4 | 401 | 618 |

Fifteen CTOD (10 mm x 10 mm) tests were prepared from each thermal condition. All tests were through-thickness notched and were fatigue precracked to give a nominal a/W of 0.35. Fatigue precracking and testing were done in accordance with BS5762 1979. Triplicate CTODs were done at each temperature over the range -70 to +50°C. The lowest CTOD results at each temperature were used to define the CTOD transition curves shown in Figure 19. As with our full weld tests, the LEW heat had superior fracture initiation resistance in all conditions. For the LEW chemistry, the 20 and 35 second $\Delta T_{800-500}$ cycles gave 0.2 mm transition temperature of -40°C. At 75 seconds the 0.2 mm transition increased to ≈0°C.

Figure 19: Simulated HAZ CTOD Results

(a) LEW

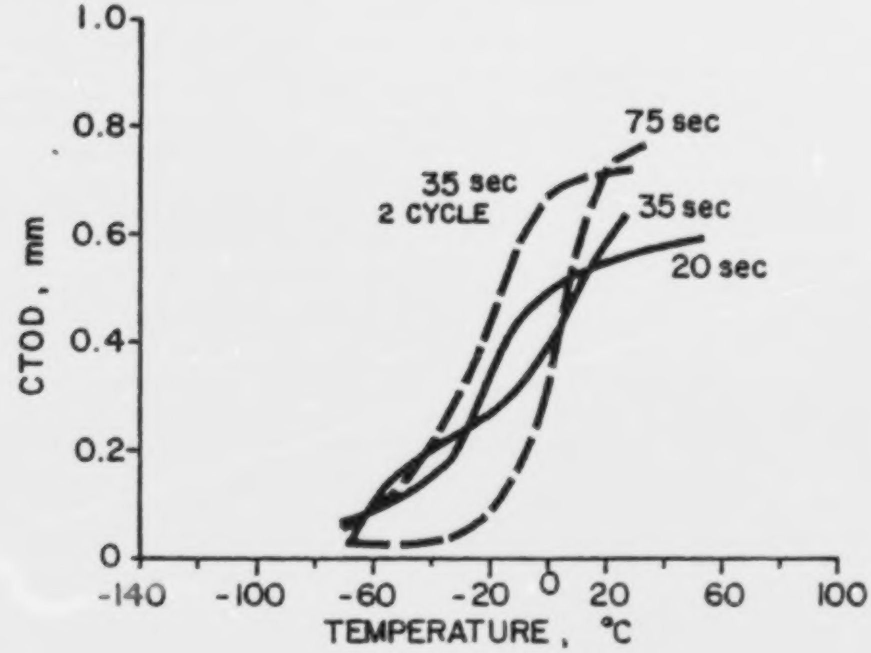

(b) HW

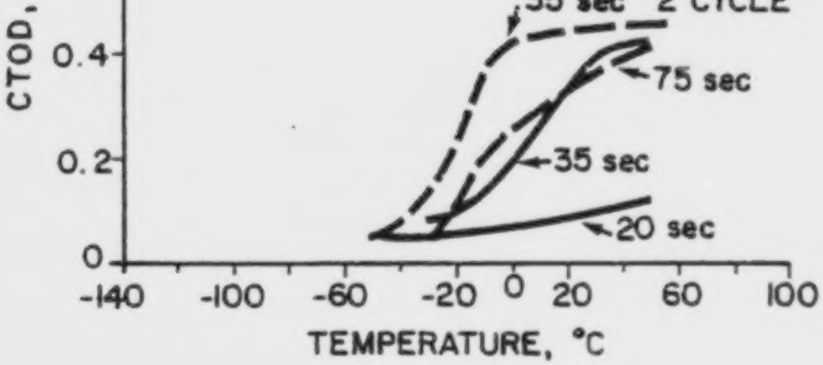

For the HW chemistry, the 20 second $\Delta T_{800-500}$ condition gave extremely poor toughness, and a 0.2 mm CTOD value was not reached even at +50°C. For the 35 and 75 second cycles, the fracture initiation resistance improved, 0.2 mm values being maintained at ≈0°C and -10°C, respectively.

For both steels the normalized (two cycle) condition gave the best CTOD performance. The 0.2 mm temperatures were ≈-40°C and -30°C for the LEW and HW steels, respectively.

These results confirm that only the LEW steel should be considered for low temperature application. They suggest that this chemistry has adequate toughness for North Sea application and is marginal for East Coast design temperatures (-30°C). Moreover, welding heat input should be restricted to achieve the toughest heat-affected zone structures, corresponding to a $\Delta T_{800-500}$ cooling time of between 20 and 35 seconds. Additional testing has been done at the Welding Institute of Canada on this chemistry using bead on plate welds with nominal heat inputs between 3 and 6 kJ/mm.[20] Tests were done using 10 mm x 10 mm cross section CTODs with the fatigue precrack grown in the through-thickness direction and the notch tip located in the coarse grained HAZ. An a/W of 0.5 was used, which gave lower upper shelf CTOD values than we observed because of the reduced ligament size. Consequently, a 0.1 mm CTOD was used as a relative measure of fracture initiation resistance. The 0.1 mm CTOD values were achieved at -61, -18, +5, and -45°C for the 3, 4, 5 and 6 kJ/mm heat inputs, respectively. The 3 and 4 kJ/mm CTOD values agree very well with the Gleeble results on the 20 and 35, and 75 second $\Delta T_{800-500}$ simulations. These results confirm the relatively good HAZ toughness of the LEW chemistry at low heat inputs, but also suggest a significant deterioration in performance at slightly higher heat inputs. The reason for the improvement at the high heat input (6 kJ/mm) is under study.

The results from the HW heat also confirm the poor HAZ toughness of this chemistry. At the lowest simulated heat input the toughness was very low at temperatures up to +50°C. This low toughness probably reflects a combination of factors, including a coarse prior austenite grain size, a low toughness microstructure, and a high base nitrogen content. The apparent improvement in HAZ toughness with increased heat input demonstrates one of the major problems associated with designing steels for improved HAZ fracture initiation resistance. It is not clear, without doing more fundamental studies, what structure gives the best performance.

## Discussion

The results of the HAZ toughness evaluation have demonstrated the superior performance of LEW strand cast steel over HW ingot cast steel. Modification in both steel chemistries is, however, recommended to achieve improved HAZ toughness.

The LEW chemistry is considered marginal for applications down to -30°C, and the following approaches should be studied to develop improved toughness.

### 1. Lower Nitrogen Content

Recent results by NKK have correlated the HAZ fracture toughness with the free nitrogen content.[10] NKK claim that titanium's grain refining effect is only partially responsible for the improved toughness of titanium-bearing steels. The other key factor is its ability to reduce the free nitrogen content. At the weld fusion line peak temperatures are such that even TiN can be taken into solution, and its grain refining effect is only partially effective. Similarly, dissolution of TiN will result in free nitrogen. This can be overcome by reducing the starting nitrogen content and by using high aluminum contents to form stable nitride precipitates during the HAZ cooling. Japanese producers are now regularly achieving 0.003 nitrogen for these grades, and NKK is using 0.08 ASA.

The adoption of low nitrogen contents is problematic - both from the practical aspect of achieving these levels in steelmaking, and from the aspect that nitrogen content is important in terms of its role in forming stable nitride precipitates during controlled rolling and for subsequent precipitation strengthening. Development of low nitrogen steels will require extensive trials in steelmaking and controlled rolling to ensure reproducibility in nitrogen content and base plate properties. Moreover, optimization of the Ti content will be required.

### 2. Single Microalloy Addition

Both trial heats were produced with Cb and V additions for grain refinement and strengthening. This "belt and braces" approach must be refined to a straight Cb or straight V approach, depending on the base plate toughness requirements, and whether the plate is produced by controlled rolling or normalizing. Cb additions will give the best base plate strength/toughness combination in the controlled rolled and the normalized conditions, however, Cb is known to have a deleterious effect on HAZ toughness in that it promotes the formation of a brittle bainitic HAZ microstructure. V is not as effective in retarding austenite recrystallization during controlled rolling, as thus cannot achieve the fine grain size developed with Cb steels. Similarly, it does not give as fine a grain size in the normalized condition. Thus, V-only steels will be limited in application in terms of both design temperature and thickness. However, V does not have the same deleterious effect as Cb on HAZ structure, and thus may offer a significant advantage in terms of HAZ toughness.

Trials are required to develop both base plate and HAZ property data on both steel types. Preliminary studies by both Vanitec and the Welding Institute of Canada are underway to evaluate these approaches. When completed, the results of these programs will be incorporated into full heat trials.

Other factors that could be varied to improve toughness are the alloy content, particularly the manganese, chromium, and nickel levels. Nickel additions (0.50 percent) are being used in North Sea steels for improved low temperature performance. Similarly, Rautaruukki is using a low manganese (<1.0 percent), low alloy content chemistry for its Polar class steels. Although the latter approach was primarily developed for improved HAZ corrosion resistance, it's also reported to have good HAZ toughness.

The low toughness of the HW ingot cast steel will be difficult to improve. The ingot cast approach, which will be required for the heaviest plate thicknesses (which will also demand the best HAZ toughness), cannot take advantage of the titanium addition technology used in strand casting. The slow cooling rates and double reheating required for ingot cast slabs cause relatively coarse TiN particles to form, which are ineffective in preventing austenite grain growth during either slab or HAZ reheating. The other approaches mentioned above should be evaluated to improve the ingot cast HAZ toughness. Again the most important of these would be development of steelmaking/ingot casting procedures for low nitrogen contents. Given the long-term phasing out of ingot casting at Hilton Works, there would be limited payback on these developments.

# REFERENCES

1. R&D Report No. 820108.

2. R&D Report No. 85R027.

3. R&D Report No. 840056.

4. J. D. Harrison, Why does Low Toughness in the HAZ Matter?, The Welding Institute Seminar, Coventry, England, 1983.

5. H. G. Pisarski, J. D. Harrison: Fracture Resistance of Steels used in Offshore Structures, European Offshore Steels Research, November, 1978, Cambridge, Paper 2.

6. TWI GSP 5543, HAZ Toughness of Thick Section Steels.

7. DnV Proposal for a Sponsored Research Project 1984-1986 Local Brittle Zones - Strength and Risk of Failure.

8. S. Kanazawa et al: Development of New Steels for High Heat Input Welding, IIW Doc IX-952-76.

9. Y. Kasamatsu et al: Tetsu-to-Hagane, Vol 65, No. 8, 1979, pp 1232-1241.

10. M. Suzuki et al: Newly Developed Arctic Grade High Al/Low N/micro Ti Offshore Structural Steel, Second International Conference on Offshore Welded Structures, November, 1982, London, Paper 16.

11. I. Watanabe: Development of NK-HIWEL Steels Suitable for High Heat Input Welding, Nippon Kokan Technical Report, Overseas No. 38, 1983, pp 33-41.

12. K. Yasuda: A Synopsis of High Tensile Hull Structural Steels through the Thermo Mechanical Control Process (TMCP) in Japan, NK Technical Bulletin, 1983, pp 62-74.

13. P. H. M. Hart and A. R. Jones: The Prediction of Safe Welding Conditions for C:Mn Steels, Proceedings of ASM Conference Solutions to Hydrogen Problems in Steel.

14. P. J. Booth and P. Rodgerson: Offshore Structrual Steels; Weldabilitly and Hardenability, Proceedings of TWI Conference, Towards Rational and Economic Fabrication of Offshore Structures - Overcoming the Obstacles, London, November 22-23, 1984.

15. P. H. M. Hart: The Influence of Steel Cleanliness on HAZ Hydrogen Cracking: The Present Position, IIW Doc IX-1308-04.

16. Y. Ito et al: Sumitomo Search No. 17, May, 1977, pp 56-65.

17. Performance Testing for the Plate Samples Supplied by Stelco Inc, Kawasaki Heavy Industries Limited, May, 1984.

18. C. Pedder and P. H. M. Hart: CTS Testing Procedures, The Present Position, TWI Research Bulletin, 1975, 16, (9), p 264.

19. Inagaki, reported by F. Matuda: Welding Metallurgy, Nikkan Kogyo Papers, 1975, pp 192-193.

20. T. W. Lau and R. B. Lazor: HAZ Toughness of Ti-Bearing Steel, Welding Institute of Canada Report, RC 200/1/84.

# ACKNOWLEDGMENTS

The following people and departments are recognized as having made vital contributions to this study:

W. Krestynski, B. Gris, J. G. Matich, B. C. Branston, E. F. Paterson, R. Millsop, H. Meilach, B. A. Buck, the R&D Machine Shop, and the Metallurgical Test Lab at Welland Tube Works.

# LAMELLAR TEARING RESISTANCE OF
# STELCO OFFSHORE QUALITY PLATE

by

D. B. McCutcheon, Stelco Inc.

Work on this project was conducted under the auspices of the Canada Centre for Mineral and Energy Technology, Energy, Mines and Resources, Canada

| | |
|---|---|
| DSS File Number: | 23SQ.23440-2-9027-1 |
| DSS Contract Number: | 0SQ82-00211 |
| CANMET Project Number: | |
| CANMET Scientific Authority: | Dr. J. D. Boyd |

# SUMMARY

Development of Canada's East Coast and Arctic oil and gas reserves is forecast to require more than 400 000 tons of Grade 350 structural plate for the construction of offshore platforms and ships. A significant percentage of the tonnage for platforms will require resistance to lamellar tearing. The tearing resistance of a Hilton Works, CAB-treated and a Lake Erie Works strand-cast heat was assessed as part of a CANMET-sponsored project to evaluate the current capability of Canadian plate producers to meet offshore and Arctic requirements.

Two heats of Grade 350 plate were made to optimum cleanliness steelmaking practices at LEW and HW. The low sulfur (0.004 percent S) LEW heat was strand cast using full ladle to tundish and tundish to mold shrouding, and was rolled to plate thicknesses between 0.75in and 2.00in. The CAB-treated, HW heat was made with 0.003 percent S, and rolled to plate between 0.75 and 4.0in. All plates were ultrasonically inspected to the quality levels required for offshore production. The lamellar tearing resistance was assessed by through-thickness tensile and window tests.

The low sulfur, strand-cast LEW steel is shown to have adequate lamellar tearing resistance to meet the most stringent offshore quality requirements in gauges between 0.75 and 2.0in.

CAB-treated, ingot cast HW steel does not have consistent enough cleanliness and lamellar tearing resistance to be classified as Z-plate.

## CONTENTS

Background.................................................. 7

LEW Continuously Cast Plate................................. 13

  Method.................................................... 13
  Results................................................... 17
  Discussion................................................ 24

HW CAB-treated Ingot-cast Plate............................. 28

  Method.................................................... 28
  Results................................................... 29
  Discussion................................................ 36

Acknowledgments............................................. 37

References.................................................. 38

Appendix 1 - Slab Inspection................................ 1 A1

Appendix 2 - Lab Ultrasonic Inspection...................... 1 A2

Appendix 3 - Through-thickness Tensile Data................. 1 A3

## BACKGROUND

The development of Canada's East Coast and Arctic oil and gas reserves will require the fabrication of a significant number of marine structures (offshore platforms, ships, supply vessels, caissons, etc) which in turn will create a demand for high quality structural plate. The mechanical properties of plate for these applications must take account not only of structural design requirements but also of the forming and welding processes used in fabrication. One of the most onerous specifications is for the plate used for multi-column connections or node joints of offshore platforms (Figure 1). These weld joints require a great amount of weld deposition and develop a high degree of restraint in the plate through-thickness direction, and thus they are very susceptible to a defect known as lamellar tearing. In addition, several of the corner, T, and cruciform joints of ships are susceptible to tearing, although documented cases of this defect are much more infrequent in ships than in offshore platforms.

**Figure 1: Jacket Structure showing Multi-column Connections**

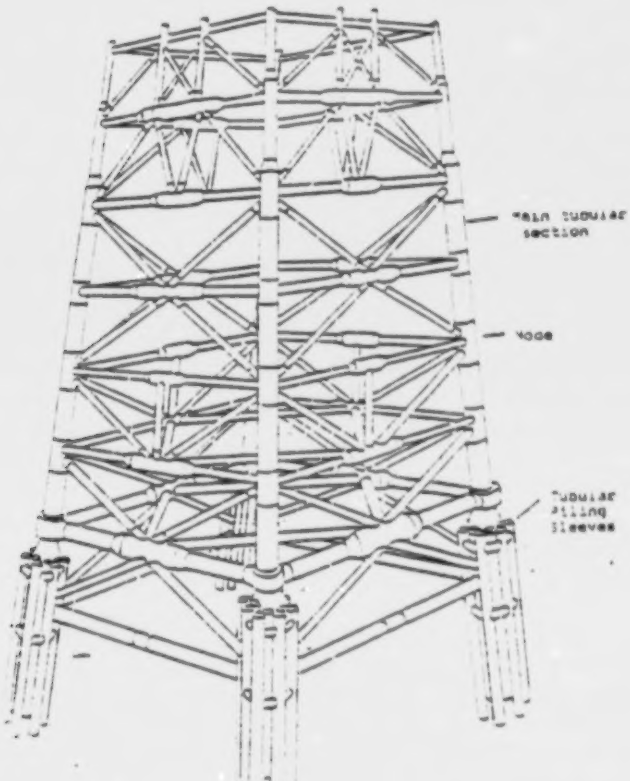

Lamellar tearing (Figure 2) is the separation of the base metal along planes parallel to the plate rolling plane, and is caused primarily by the through-thickness strains developed by weld metal shrinkage.[1] Tearing occurs usually in the parent metal, just outside the visible heat affected zone (HAZ), however, its location may vary from just below the HAZ to well within the base plate. It may also initiate at hydrogen induced cracks in the weld toe or root. Tearing is principally caused by decohesion and shear linkage of individual or clusters of inclusions. A steel's susceptibility to tearing is primarily governed by the steels inclusion content, however, other properties such as the susceptibility to hydrogen induced cold cracking during welding, yield strength level and sensitivity to strain aging and hydrogen embrittlement may be important in governing the extent of cracking. In addition, ferrite-pearlite banding has been reported to cause both initiation and propagation of tears.

**Figure 2 (a): Lamellar Tearing Below a Multi-pass Weld**

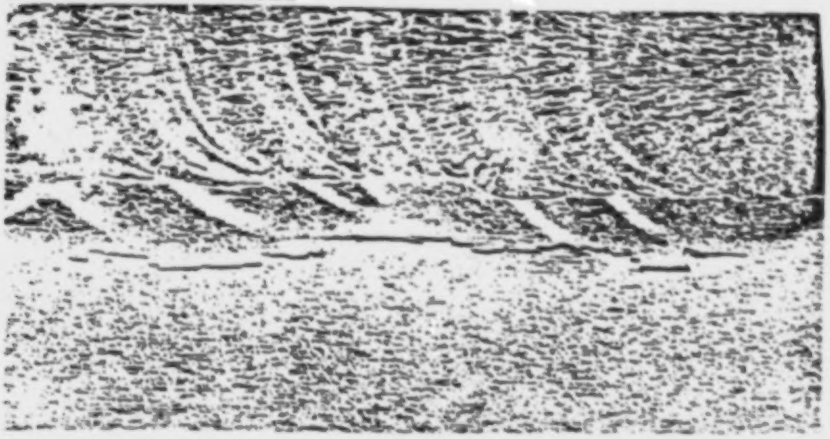

**Figure 2 (b): Typical Joints Susceptible to Lamellar Tearing**

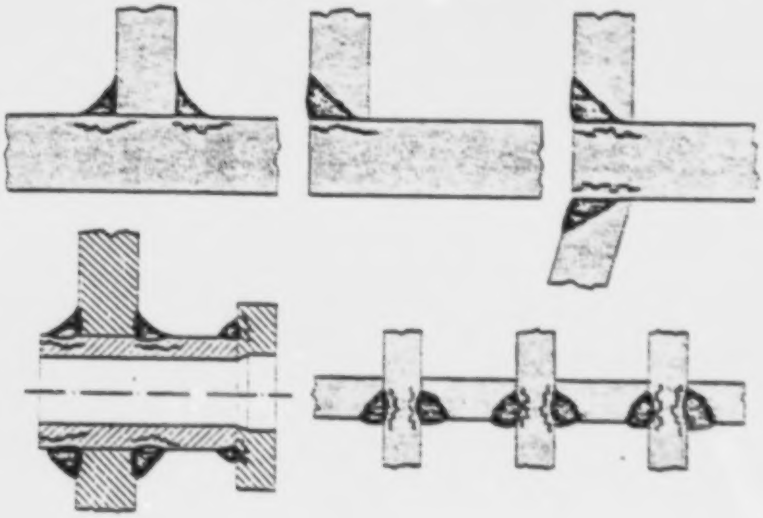

Lamellar tearing can be partially controlled by proper design and fabrication techniques. Key design factors that should be considered to help avoid tearing include:[2]

- design of joints to minimize the creation of weld shrinkage strains in the through-thickness direction,
- reduction of joint restraint, and
- modification of the structural configuration to reduce the component restraint.

Similarly, considerations in welding fabrication to minimize tearing include:[2]

- the use of low hydrogen electrodes, preheating and maintenance of interpass temperatures to prevent root cracking and to reduce residual stress,
- proper sequencing of the weld beads to reduce the level and concentration of weld shrinkage strains,
- buttering, i.e. depositing layer(s) of low yield strength weld metal directly on the plate surface, and
- utilization of the highest heat input welding process, consistent with other weldment requirements (e.g. toughness).

Although design and fabrication guidelines have been established to suppress this form of cracking, the high cost of repairing these defects together with the cost penalties associated with fabrication delays have created a demand for lamellar tearing resistant or node quality steel for highly restrained joints. This grade of steel was developed by several offshore plate producers in the early to mid-70s, largely for application in offshore structures. No Canadian supply of this quality level is yet available, and it is one of the purposes of the CANMET-sponsored Grade 350 program to establish the ability of both LEW strand-cast and HW CAB-treated ingot-cast plate to meet the cleanliness standards for Z-plate.

Several laboratory tests have been used to quantify the susceptibility of plate to tearing. The most informative tests are actual restrained weld tests, such as the Welding Institute Window test, the Cranfield test and Lehigh restraint test. These offer the advantage of not only simulating the restraint conditions but also producing the weld HAZ microstructure and hydrogen levels, however, they are expensive and not always practical for production or quality control.

The most widely accepted quality control test to measure a steel's resistance to tearing is the through-thickness tensile test. Good correlations have been established between the Z-direction reduction of area and observed incidences of tearing. The reduction of area in the through-thickness direction (RAz) is being increasingly used by classification societies to define and approve Z-grade steels for both ships and offshore structures. The RAz requirements are defined in up to three categories of Z-plate which are classified in terms of the minimum, mean and minimum individual values of RAz. The guidelines for these categories have become more standardized in the past few years. Both the ISO[3] and ASTM[4] have similar test standards, as shown in Table I. The selection of Z-grade steel is dependent on the importance of the component to the overall integrity of the structure and the level of restraint at the weld connection. Figure 3[5] shows a typical guide for selection of minimum RAz values.

**Table I: Classification of Z-Plate**

| Class | Minimum RAz Average Value* | Minimum RAz Individual Value |
|---|---|---|
| Z15 | 15% | 10% |
| Z25 | 25% | 15% |
| Z35 | 35% | 25% |

* Average of three tests.

**Figure 3: Through-thickness Ductility Requirements for Different Joint Restraints**

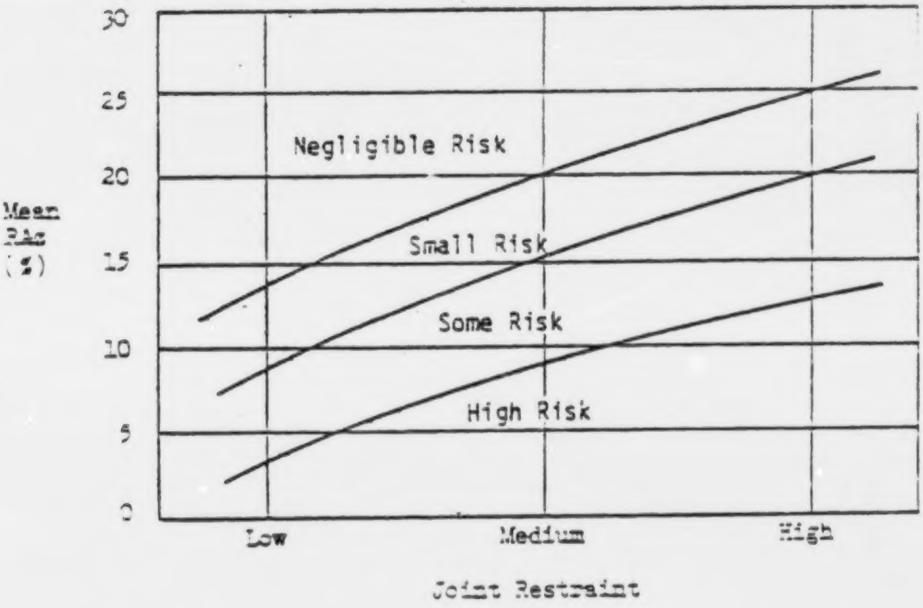

Ultrasonic inspection of plates prior to fabrication has also been partially successful in measuring susceptibility to tearing. The Welding Institute[6] has extensively studied the use of a high gain ultrasonic pulse echo technique to correlate the "integrated echo" per unit thickness with the steel's short-transverse or through-thickness tensile ductility. Their system was capable of accurately predicting the through-thickness reduction of area in steels containing primarily Type II MnS inclusions with a relatively high risk of lamellar tearing (i.e. less than 20 percent reduction of area).

The main feature of node quality steels is high cleanliness. Several workers[7-9] have demonstrated the strong correlation between RAz and the projected total length of inclusions. In particular, long inclusions, which individually or in a cluster are greater than ≈50 μm in length, appear to have the dominant effect on Z-direction ductility. In fully killed steels, these are primarily Type II manganese sulfides and, possibly, large reoxidation oxides. Thus, node quality steels are desulfurized to less than approximately 0.005 percent S (Figure 4), and/or treated with sulfide shape control elements.[10] Removal of oxide inclusions by argon stirring or vacuum degassing, flotation of inclusions in the tundish and mold during strand casting and complete shrouding of the pouring stream to prevent reoxidation during ingot and strand casting are also practiced for these grades.

**Figure 4: The Effect of Sulfur Content on Through-thickness Ductility**

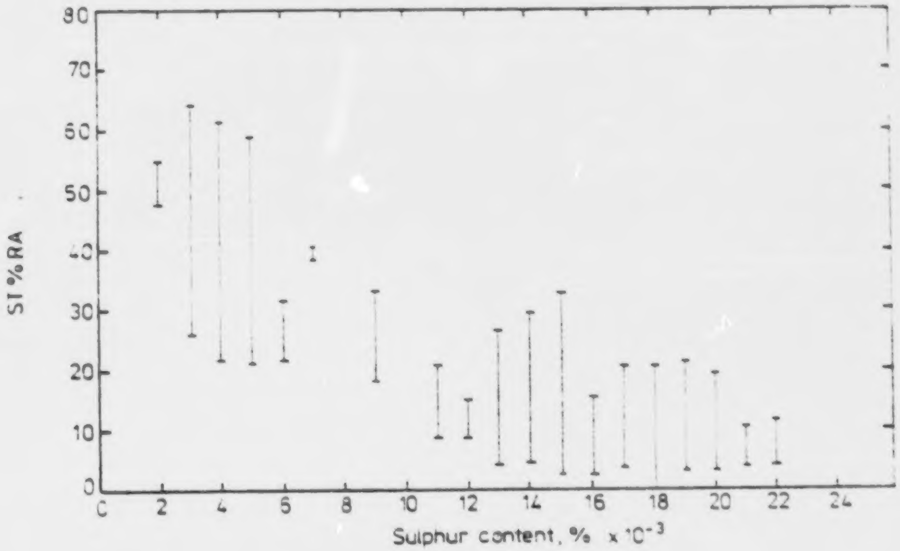

Low Z-direction ductility has also been related to hydrogen embrittlement[11] and the formation of "fish-eyes" on the fracture faces. Thus, low hydrogen steelmaking practices and slab/plate diffusion treatments (beyond those required to prevent flaking) are used in the production of node quality steel.[12] In plate produced from strand-cast slabs, poor ductility may also be caused by lack of welding of centerline looseness in the cast slab. Thus RAz in strand-cast plate tends to go through a maximum in relation to plate thickness or total reduction ratio. In heavy plate, RAz may be low due to there being insufficient reduction to weld the centre looseness, whereas in light plate it is low because of significant elongation of deformable inclusions in the rolling plane.

This report documents the production and detailed assessment of the lamellar tearing resistance of two heats produced as part of the CANMET-supported Arctic Grade 350 Plate Project. These trials took place between May 1983 and May 1984.

## LEW CONTINUOUSLY CAST PLATE

### Method

1. Steelmaking, Casting and Hydrogen Removal

A 250 ton BOF heat was produced using desulfurized hot metal (0.002 percent S) and selected low sulfur scrap, to the heat analysis shown in Table II. The heat was cast singly (i.e. non-sequence) using a fused silica ladle to tundish shroud and an alumina-graphite tundish to mold shroud. The main features of the casting procedure are shown in Table II.

**Table II: Production of Heat 805126**

| | C | Mn | P | S | Si | Ni | Cr | V | Cb | Ti | ASA | N | H |
|---|---|---|---|---|---|---|---|---|---|---|---|---|---|
| Plate Check | 0.070 | 1.43 | 0.003 | 0.004 | 0.29 | 0.25 | 0.25 | 0.075 | 0.02 | 0.011 | 0.037 | 0.007 | - |

- Hot metal S - 0.002% (CaSi desulfurized)
- Vessel tap S - 0.006
- Tap onto 2200 lb Canadex
- Argon Stir - 8 min
- Silica ladle to tundish shroud
- Chrome - magnesite tundish boards with dam/weir configuration
- Alumina graphite tundish to mold shroud -15° bifurcated up
- Teem temperature -2850°F
- Casting speed - 1.0 - 1.2 m/min
- Water practice 0.65 L/kg (No. 36)

Mold hydrogen samples were taken at the front, middle and back of the heat and the hydrogen content (5.2 ppm) was determined using a LECO RH2 hot extraction hydrogen analyzer. All parent slabs were stacked into a single pile, which was completely covered with vermiculite. The temperature of the stack was monitored by two thermocouples inserted in the middle and one slab below the top of the stack. The slab stack was held for 116 hours prior to breakup, giving a total time of 100 hours between 1400 and 900°F for removal of hydrogen by diffusion in ferrite.

Parent slabs were cut while warm into the ordered plate slab sizes and conditioned to remove all injurious surface defects. All slabs were ultrasonically mapped to determine the position and degree of center looseness (Appendix 1). Sulfur prints were taken from each parent slab to further assess the size of center looseness, and to qualitatively measure the steel cleanliness in terms of quarter point inclusions.

To further evaluate the effectiveness of the slab cooling procedure in precluding hydrogen flaking and minimizing hydrogen effects on through-thickness ductility, one slab for each finished plate thickness was annealed at 1200°F for periods of 50 and 80 hours (depending on plate gauge).

## 2. Plate Rolling and Ultrasonic Testing

Plates were rolled to the finished sizes shown in Table III. Immediately after rolling and leveling all plates were stacked in the Plate Mill torch cut area and held for 48 hours prior to inspection and cutting. All plates were ultrasonically tested to ASTM-578 Level I. The central area of each plate was also tested to a Stelco U-sonic specification to detect flaking.

**Table III: Production of Heat 805126**

| Slab No. | Slab Size (in) | Slab Anneal (hr) | Charge No. | Plate Size (in) |
|---|---|---|---|---|
| 2 | 7.87 x 72 x 280.5 | —— held as parent —— | | |
| 4 C | 7.87 x 72 x 93.5 | 50 | 24 | 0.75 x 96 x L |
| D | " | none | 25 | " |
| 4 E | 7.87 x 72 x 93.5 | 50 | 26 | 1.00 x 96 x L |
| 6 C | " | none | 27 | " |
| 6 D | 7.87 x 72 x 93.5 | 80 | 28 | 1.25 x 96 x L |
| 6 E | | none | 29 | |
| 8 C | 7.87 x 72 x 93.5 | 80 | 30 | 1.50 x 96 x L |
| 8 D | | none | 31 | |
| 8 E | 7.87 x 72 x 93.5 | 80 | 32 | 1.75 x 72 x L |
| 10 C | | none | 33 | |
| 10 D | 7.87 x 72 x 93.5 | 80 | 34 | 2.0 x 72 x L |
| 10 E | | none | 35 | |
| 12 C | 7.87 x 72 x 93.5 | 50 | 3 | 1.18 x 117 x L |
| D | | 50 | 4 | " |
| E | | 50 | 5 | " |
| 14 C | | 50 | 6 | " |
| D | | 50 | 7 | " |
| E | | 50 | 8 | " |
| 16 C | | 50 | 9 | " |
| 16 D | 7.87 x 72 x 110 | 50 | 36 | 0.59 x 96 x L |
| 16 E | 7.87 x 72 x 82.5 | —— cut for slab samples —— | | |
| 18 | 7.87 x 72 x 280.5 | —— held as parent —— | | |
| 20 | " | | " | |
| 22 | " | | " | |

A 6in long, full width strip from each plate was sectioned and ultrasonically C-scanned at R&D to detect gross oxide inclusions and flaking. The ultrasonic system was calibrated to detect a known size of flat bottomed hole, as described in Appendix 2.

## 3. Testing for Lamellar Tearing Resistance

### 3.1 Through-thickness Tensile

Six through-thickness tensiles were tested at selected positions from each full width strip sample. All samples were prepared by trepanning 0.5in diameter, full thickness cylinders from the base plate and friction welding 0.5in diameter prolongations onto the test pieces. The tensile tests were then machined to 0.394in (10 mm) diameter, with the radius reduction initiating at the plate surface. This procedure agrees with the ISO/TC17/SC 3N 415 and ASTM A770M-84 draft proposals, except that these proposals recommend using 6 mm diameter specimens for plates less than 25 mm thick. Additionally, they recommend that all tests be taken from a coupon centered on the longitudinal axis of the plate. To establish the variability in RAz across the cast slab width, duplicate tests were taken at the edge, quarter-width and center width positions. All tests were taken with reference to the indications found by C-scanning, and at least two tests per plate were centered on defects.

### 3.2 Window Tests

Window tests[13] were done on test sections taken from 1.25in and 1.75in rolled plates. Figure 5 shows the specimen dimensions and an example of a prepared test. The 1.18in (30 mm) rigid restraining plate was prepared from a controlled rolled plate of the same heat, which had 56.0 ksi and 70.0 ksi yield and ultimate tensile strength, respectively. To maintain standardized restraint levels for all tests, all test plates were milled to 20 mm thickness, leaving a rolled surface intact. All test coupons were C-scanned prior to machining to ensure that representative gross oxide inclusions were located below the test welds.

The test welds were made using fresh 1/8in diameter E7018 electrodes which had been dried at 250°F for one hour. The welding heat input was 43 kJ/in (1.7 kJ/mm). The preheating and interpass temperatures were controlled to 300°F and 167°F, respectively, using a contact thermocouple. The welds were made in the sequence shown in Figure 5 and held for at least 48 hours prior to sectioning to examine for tearing.

Figure 5: Window Test Samples*

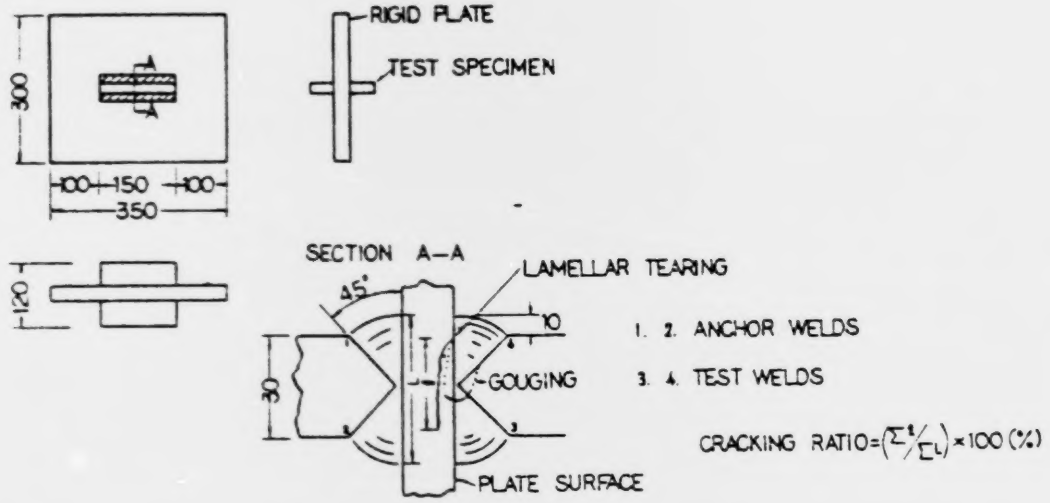
RIGID PLATE
TEST SPECIMEN
300
100
150
100
350
120
SECTION A—A
45°
LAMELLAR TEARING
10
30
GOUGING
PLATE SURFACE
1. 2. ANCHOR WELDS
3. 4. TEST WELDS
CRACKING RATIO=(Σl/ΣL)×100(%)

* dimensions in mm

## Results

### 1. Ultrasonic Testing

None of the plates (except the ≈4.0in thick kickover bar) showed any ultrasonic indications as inspected to the ASTM Level I and the Stelco hydrogen flaking standard. The kickover bar exhibited gross centerline defects and a sample was torch cut out for lab ultrasonic and metallographic examination.

The C-scan data are summarized in Table II A2. The lab C-scan inspection revealed isolated quarter-point inclusions located 0.15in to 0.20in and 0.30in to 0.70in below the plate surface in the 0.75in and 2.0in thick plate, respectively. Most of the plate full-width samples showed few or no defects. However, a concentration of quarter-point type indications was observed on one side of several of the lighter gauge plates. Examples of the different densities of inclusions are shown in Figure 6.

**Figure 6: Indications Detected by Laboratory Ultrasonic C-Scans (0.5X)**

**(a) Light Rating (Chg 27, 1.0in, Pos 4-5)**

**(b) Medium Rating (Chg 28, 1.25in, Pos 2-3)**

No flaking was observed in any of the plates finished up to 2in thick. The kickover bar showed gross centerline discontinuities which were identified metallographically as flaking (Figure 7).

**Figure 7 (a): Mid-wall Ultrasonic Indications in 4.0in Kickover Bar (Charge 31) - 0.5X**

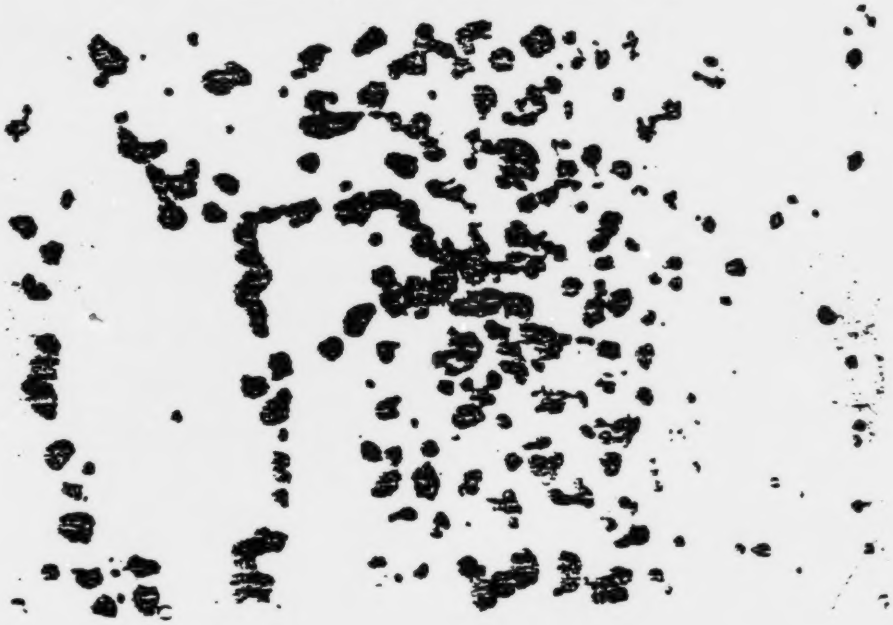

**Figure 7 (b): Flaking on Centerline Segregation Band (4X)**

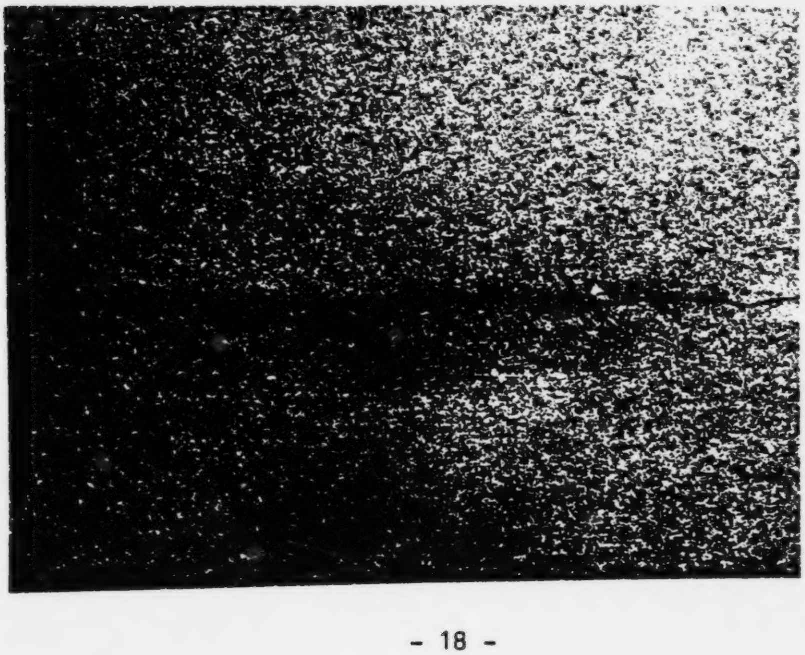

## 2. Through-thickness Ductility

The LEW strand-cast plate showed excellent through-thickness ductility at all of the plate gauges tested. The RAz values are summarized in Figure 8 and Table I A3. Except for one test which gave 21.6 percent RAz, the LEW plate would be classified as Z35, with greater than 35 percent mean RAz on the six tests and greater than 25 percent RAz minimum individual test value.

The through-thickness ductility tended to increase with increased plate thickness. This is believed to result from the greater elongation of inclusions and higher strength levels in the lighter plate. Moreover at the lightest thickness, the lower ductility may be caused by increased constraint resulting from the reduced test gauge length.

Figure 8: Summary of Through-thickness Ductility in LEW Sourced Plate

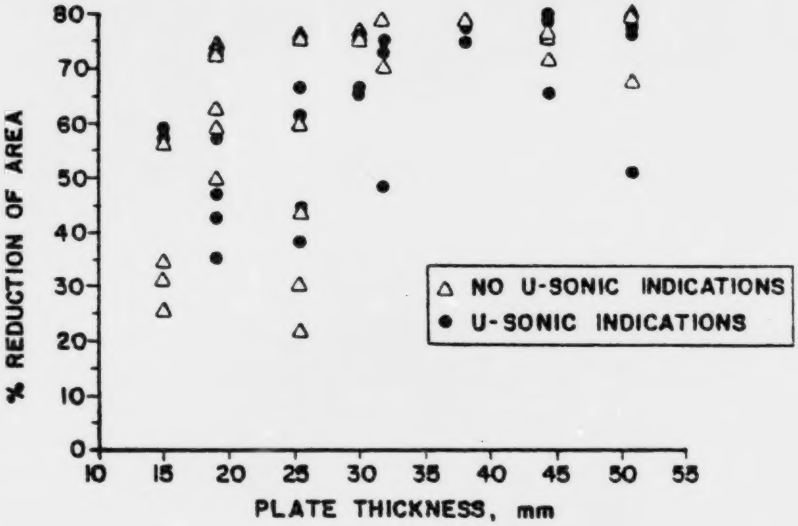

Most tests exhibited cup-cone fracture which is indicative of high ductility (Figure 9b). Fracture generally occurred at the quarter thickness location for the heavier gauge plates and the half thickness position for the lighter gauge plates (Figure 9a). Some tests taken from areas showing ultrasonic discontinuities showed reduced through-thickness ductility related to gross alumina stringers (Figure 10). Other samples, located away from U-sonic indications, showed low ductility related to Type II manganese sulfide inclusions and columbium oxides (Figure 11).

Figure 9 (a): Broken Through-Thickness Tensiles from Plates of Varying Thickness (0.5X)

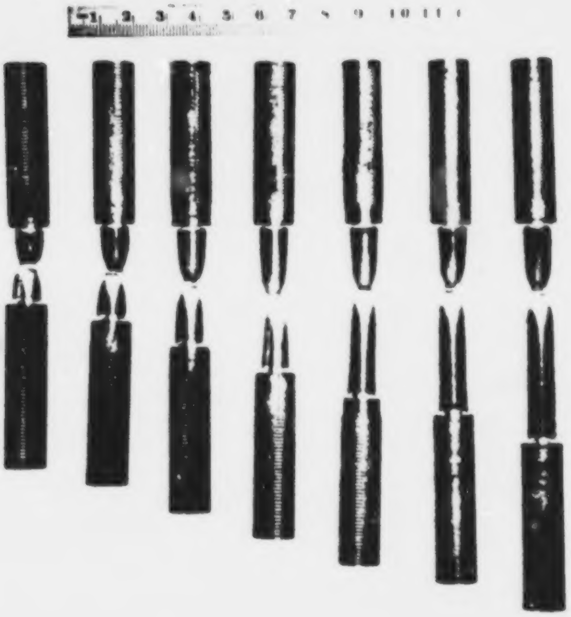

Figure 9 (b): Cup-Cone Fracture on Through-Thickness Tensile (Chg 32, 1.75in) - 8X

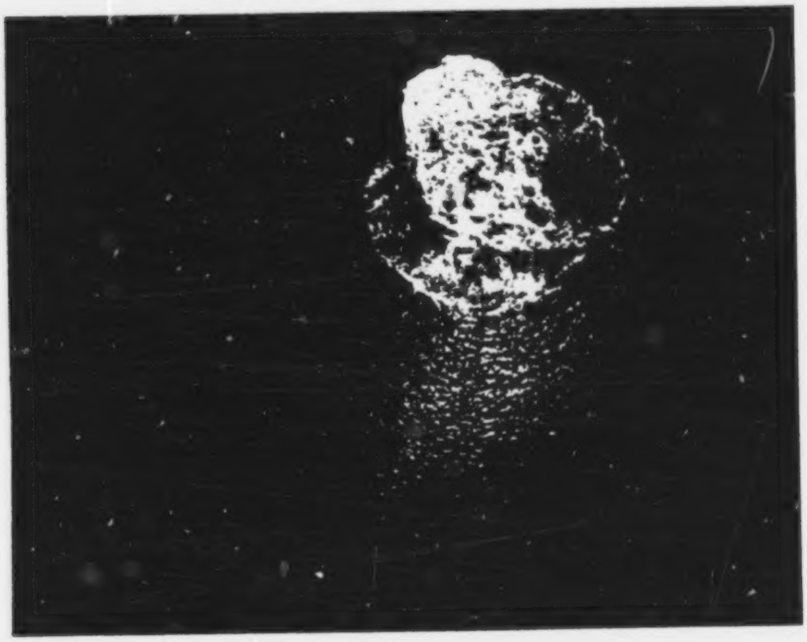

Figure 10 (a): Alumina Stringer on Through-Thickness Tensile Fracture Surface (Chg 29, 1.25in) - 8X

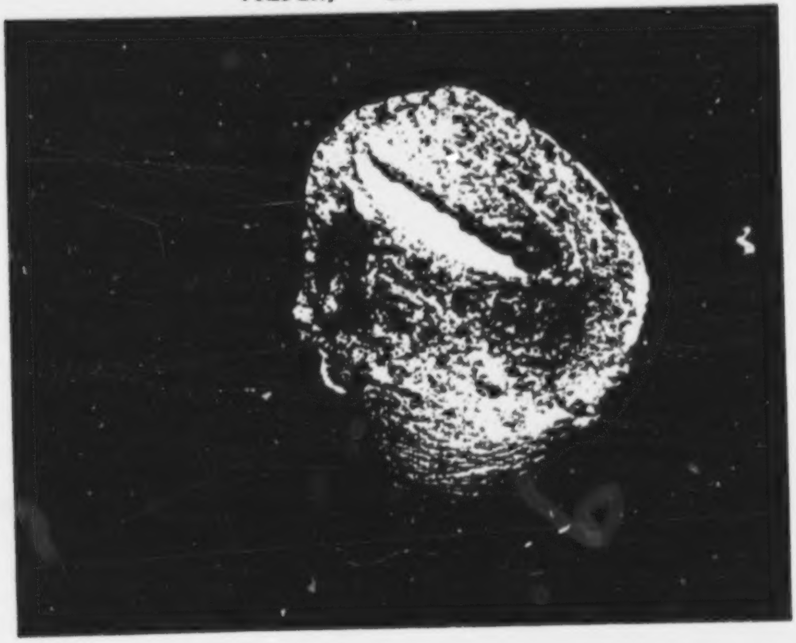

Figure 10 (b): 500X

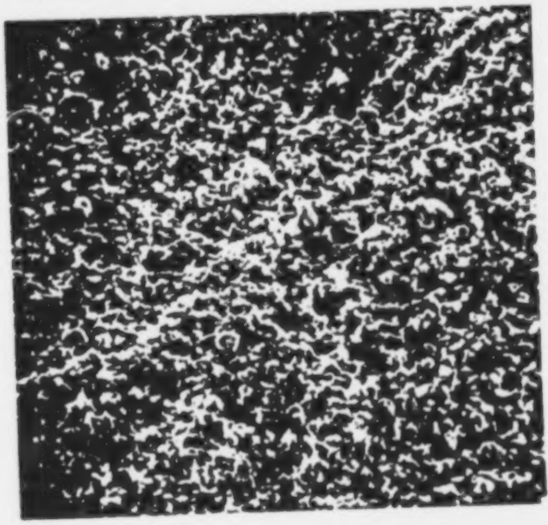

Figure 11 (a): Manganese Sulfide-Columbium Oxide Inclusions on Through-Thickness Tensile Fracture Surface (Chg 26, 1.0in) - 8X

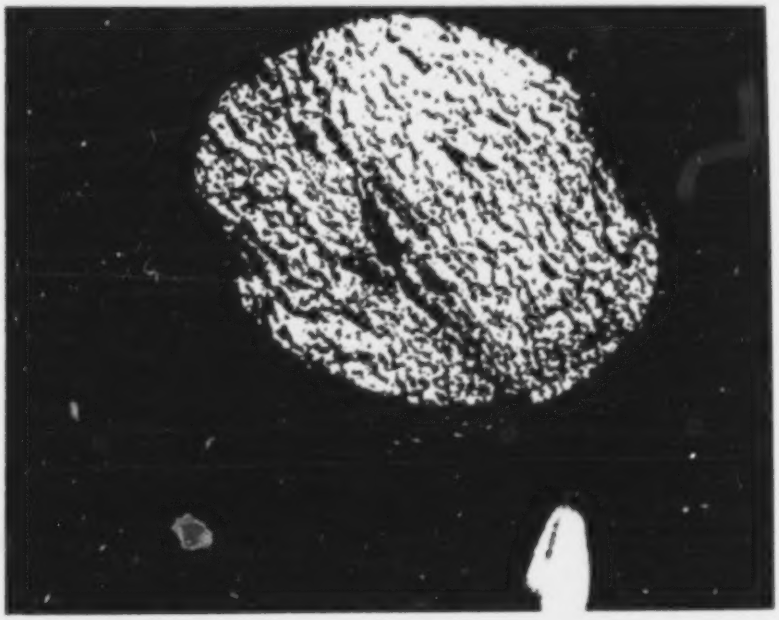

Figure 11 (b): 2000X

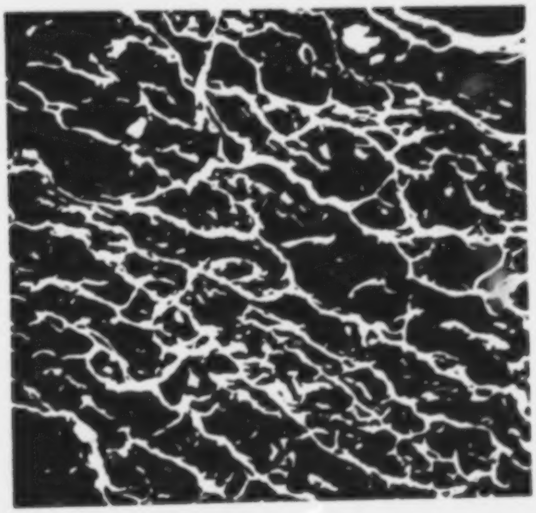

### 3. Window Tests

No lamellar tearing was observed on the window test taken from either plate charge. Figure 12 shows a typical cross section from the window test, taken specifically through a plane containing quarter-point inclusions. There was no evidence of cracking at inclusions.

**Figure 12: Window Test Through Quarter-Point Inclusion (Charge 28, 1.25in Plate)**

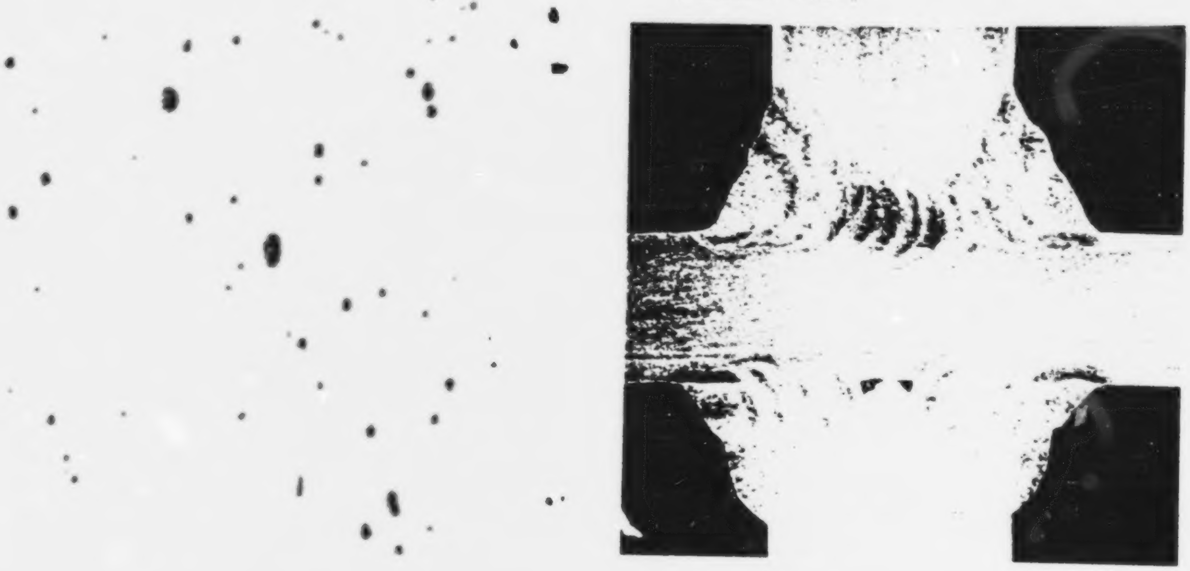

**(a) C-Scan of Test Plate (0.65X)**

**(b) Etched Section through Window Test (Actual Size)**

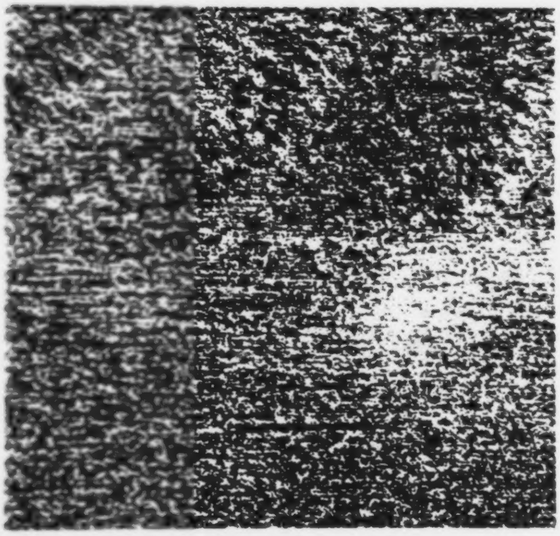

**(c) Quarter-Point Inclusion below Weld HAZ (8X)**

## Discussion

The extensive through-thickness tensile testing on this heat has demonstrated that low sulfur, shrouded LEW strand-cast steel can meet Z-plate standards. Further trials and production testing, however, are required to fully develop our knowledge of the steelmaking, casting and plate rolling factors that must be controlled to consistently provide this quality level. Factors that need to be addressed include:

### 1. Start-up, Sequence, and Cap Off Slab Cleanliness

The application of these slabs to Z-plate applications is questionable because of the potentially high levels of oxide inclusions generated during these operations. We need to establish what length of parent slab must be downgraded at each of these stages based on cleanliness/through-thickness ductility testing.

### 2. Improved Shrouding, Twin Strand Casting

The through-thickness ductility measured on this shrouded heat is significantly better than tests on a 0.005 percent S, unshrouded Stelcoloy 70, LEW heat tested previously. Since the trial heat was made, further improvements have been reported in steel cleanliness, particularly for D&I can applications, related to modifications in ladle to tundish shrouding. Similarly, improvements in oxide removal can be expected as a result of reduced casting speed by twin strand operations. These changes should significantly reduce gross quarter-point inclusion contents, and thus increase the consistency in meeting the reduction of area criteria.

### 3. Slab to Plate Reduction Ratio

The slab-to-plate reduction ratio is important for node quality plate as it affects both welding up of centerline looseness and through-thickness ductility. Moreover the reduction ratio also strongly controls austenite grain refinement during roughing and subsequent controlled rolling. The fact that no U-sonic defects were found in the 2in thick plate demonstrates that a 4:1 reduction ratio is adequate to weld up porosity. It should be noted, however, that this trial was rolled entirely in the 4-high finishing stand using maximum allowable drafts. Utilization of a 2-Hi rougher - 4-Hi finisher drafting practice (to improve mill productivity) would reduce the individual pass reduction, and thus possibly limit the finished plate thickness that can be applied to this quality. Application of the heavier slab thickness (9.45in) hopefully will offset this. Detailed U-sonic inspection of heavy plate produced from this slab size is required to define the thickness limitation.

Increasing the total reduction ratio will also increase the elongation of inclusions during rolling. This effect is most significant in relatively light gauge (<0.750in) plate. Thus, provided the sulfur level is maintained at less than 0.005 percent, RAz values should still meet Z-plate requirements.

Other factors that will also significantly affect RAz are the rolling temperature and the degree of cross rolling. To meet the Charpy impact requirements in heavier plate (>1.25in) will require a significant increase in the degree of low temperature (<1650°F) deformation, which will tend to increase the elongation of Type II manganese sulfides. Similarly, increasing the amount of cross rolling, while advantageous for transverse Charpy shelf energy, will also tend to reduce Z-direction ductility. The reduction in RAz resulting from changes in these variables needs to be established by monitoring future LEW sourced plate production. Reduction of the steel sulfur content and/or sulfide shape control may be required to offset negative effects.

### 4. Hydrogen

Commercial production of this grade will require development of slab and plate hydrogen removal treatments to avoid both reduced ductility through hydrogen embrittlement and hydrogen flaking. The fact that no significant difference in RAz was observed between the annealed and non-annealed tests confirm that slab and plate diffusion treatments can reduce the finished plate hydrogen contents to sufficiently low levels to avoid embrittlement. Similarly, the freedom from flaking in all plates confirms that adequate hydrogen removal can be achieved by slab and plate slow cooling.

Calculations of hydrogen removal based on our experience with light gauge (<0.600in) plate skelp demonstrate that flaking can be prevented in plate gauges up to ≈2.0in by using a combination of slab and plate stack cooling (Table V). Note that plate stack cooling by itself is not adequate for plate gauges over ≈1.0in and hydrogen levels over ≈4 ppm (this hydrogen level is regularly exceeded in low sulfur LEW production). Plate thickness has a dominant effect on hydrogen removal rate, and specific slab stack cooling procedures must be developed by R&D, Operating and Metallurgical for the entire range of gauges to be produced from LEW.

**Table IV: Calculated Hydrogen Removal Procedure to Prevent Flaking***

| Plate Gauge (in) | Plate Stacking Time (hr) | Slab Stacking Time (hr) | |
|---|---|---|---|
| | | 4 ppm* | 6 ppm* |
| 0.75 | 8 | not required | not required |
| 1.00 | 8 | not required | not required |
| 1.25 | 8 | not required | 24 |
| 1.50 | 8 | 24 | 60 |
| 1.75 | 8 | 40 | 80 |
| 2.0 | 8 | 70 | 140 |

* Assumptions:

1. 9.45in thick slabs.
2. Plate stacking from 550°F to 200°F.
3. Slab stacking start at 1450°F, 8 heat pile, vermiculite on ends.
4. Initial slab hydrogen content 6 ppm and 4 ppm; final plate centerline hydrogen to preclude flaking 1.5 ppm.

It must be recognized that in addition to the high cleanliness of LEW steel, its relatively low carbon equivalent also contributed to its resistance to lamellar tearing. Extensive laboratory testing by Sumitomo[14-16] has shown that tearing can be a hydrogen related form of cracking, and is dependent on the cold cracking susceptibility of the steel and the diffusible hydrogen content of the weld deposit. Ito[16] proposed the relationship shown in Figure 13 between cracking and steel chemistry and hydrogen content.

**Figure 13: Relation between Tearing Susceptibility and Cracking**

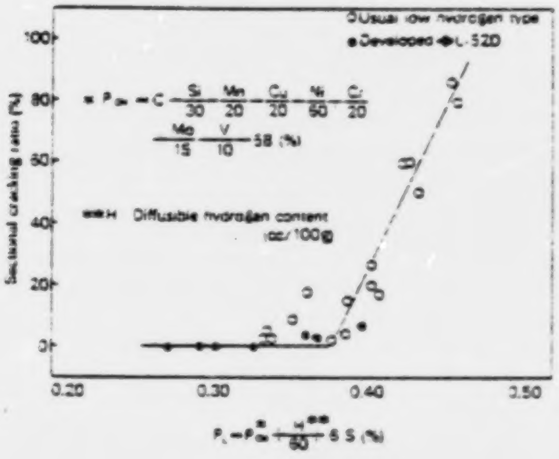

Based on this relationship, the LEW chemistry has a $P_L$ factor of ≈0.25 when welded with low hydrogen (≈3 cc/100 g) electrodes. No cracking would be expected in the window test samples, particularly those for which preheat was used. Any modifications to the chemistry to achieve higher UTS levels, such as higher carbon content, or increased sulfur content would tend to reduce the tearing resistance. It is recommended that in addition to doing through-thickness tensile tests, window type restraint tests should be done simulating actual fabrication welding prior to supplying this steel for Z-plate applications.

## HW CAB-TREATED INGOT-CAST PLATE

### Method

1. Steelmaking and Casting

A 130 ton HW BOF heat was produced to the chemical analysis shown in Table V. The heat was processed through the HW CAB station to practice No. EN112 KHS which was designed to provide optimum, reproducible steel cleanliness using current HW steelmaking, secondary steelmaking and ingot casting technology. The key features of the steelmaking practice used are summarized in Table V. The hot metal was desulfurized to 0.005 percent S using mag-coke injection and the hot metal slag was skimmed prior to charging. The BOF vessel was charged with selected low sulfur scrap, and the heat made with a single turndown practice with LBE argon treatment to minimize nitrogen pickup during steelmaking. Slag carry-over in tapping was restricted to 2.5in by blocking the tap hole prior to tap and using a floating slag cutoff device and a hot heel practice.

**Table V: Production of Heat 536441**

| | C | Mn | P | S | Si | Ni | V | Cb | Ti | ASA | N | H* |
|---|---|---|---|---|---|---|---|---|---|---|---|---|
| Ingot | 0.13 | 1.44 | - | 0.003 | 0.24 | 0.24 | 0.062 | 0.020 | 0.006 | 0.015 | 0.010 | 5.1 - 7.4 |
| Plate Check | 0.13 | 1.46 | 0.013 | 0.003 | 0.24 | 0.25 | 0.064 | 0.019 | 0.005 | 0.013 | 0.010 | - |

* ppm

- Hot metal S - 0.005% (Mag coke desulfurized)
- Vessel tap S - 0.007
- Slag carry-over - 2.5in
- Synthetic Slag - 1100 lb lime
  1000 lb $CaO \cdot Al_2O_3$ prefused
  1000 lb Fluorspar
- CaSi injection - 610 lb
- Teem temperature -2825°F

The heat was CAB injected with 610 lb CaSi in a basic lined ladle covered with a synthetic slag (1100 lb lime, 1000 lb fluorspar, 1000 lb CaO $Al_2O_3$ prefused slag). The aluminum drop during injection was limited to 0.006 percent and the nitrogen increase was only 20 ppm. The final sulfur level was 0.003 percent.

The heat was tapped at 2825°F into prime Nalcote treated molds.

Standard hot topping practice was followed for each ingot, and hydrogen tests were taken through the hot top. To minimize bottom cone segregation the ingot string was held in the shop until fully solidified.

The ingots were rolled to the slab sizes shown in Table VI and deseamed and conditioned prior to hydrogen removal at Sheet Services. The slabs were annealed for 50 or 90 hours at 1200°F depending on slab thickness and reinspected prior to shipment to the 148in plate mill for rolling.

Table VI: Production from HW Heat 536441

| Ingot No./Cut | | Ingot Size | Slab Size (in) | Slab Anneal (hr) | Charge No. | Plate Size (in) |
|---|---|---|---|---|---|---|
| 1 | T | 72in BED | 7.5 x 62 x 95 | 50 | 10 | 0.750 x 96 x L |
| | M | | | | 11 | |
| | B | | | | 12 | |
| 2 | T | 72in BED | 7.5 x 62 x 95 | 50 | 13 | 1.00 x 96 x L |
| | M | | | | 14 | |
| | B | | | | 15 | |
| 3 | T | 72in BED | 7.5 x 62 x 95 | 50 | 16 | 1.25 x 72 x L |
| | M | | | | 17 | |
| | B | | | | 18 | |
| 4 | T | 72in BED | 7.5 x 65 x 98 | 90 | 19 | 1.50 x 72 x L |
| | M | | | | 20 | |
| | B | | | | 21 | |
| 5 | T | 72in BED | 8 x 66 x 120 | 90 | 22 | 2.50 x 72 x L |
| | B | | | | 23 | |
| 6 | T | 54in BED | 8 x 50 x 85 | 90 | 2 | 4.0 x 60 x L |
| | B | | 8 x 50 x 120 | | 1 | |

### 2. Plate Rolling and Ultrasonic Testing

The plates were rolled to the finished sizes shown in Table VI. After rolling and leveling, all plates were taken off-line and stacked for hydrogen removal in the Plate Mill torch cut area in two piles and held for 48 hours prior to removal. All plates were visually and ultrasonically inspected and test samples cut according to the procedures described previously for LEW plate.

### 3. Testing for Lamellar Tearing Resistance

Through-thickness tensiles were tested from each plate following the same procedures as for the LEW plate.

Window tests were taken from the 1.00in and 1.50in thick plate at positions showing medium density of oxide inclusion stringers. The same test procedure was used as for the LEW plates.

## Results

### 1. Ultrasonic Testing

All plates showed no ultrasonic indications as tested by the ASTM 578 Level I and Stelco hydrogen flaking standards.

The laboratory C-scan data are summarized in Table III A2. All of the full-width strips showed heavy multi-layer inclusions at the plate edge extending up to 3.5in into the plate body. Figure 14 shows examples of the heavy concentration of inclusions located throughout the plate thickness. The density of these reflectors appeared to be greater in the lighter gauge plates, presumably because of increased elongation and concentration of the inclusions at higher reduction ratios. The width of the edge indications also appeared to be greater in lighter plate, which had increased cross rolling to ≈100in width.

**Figure 14: Ultrasonic C-Scans of Edge Inclusions (0.45X)**

**(a) Charge 10, 0.75in, 1 Top**

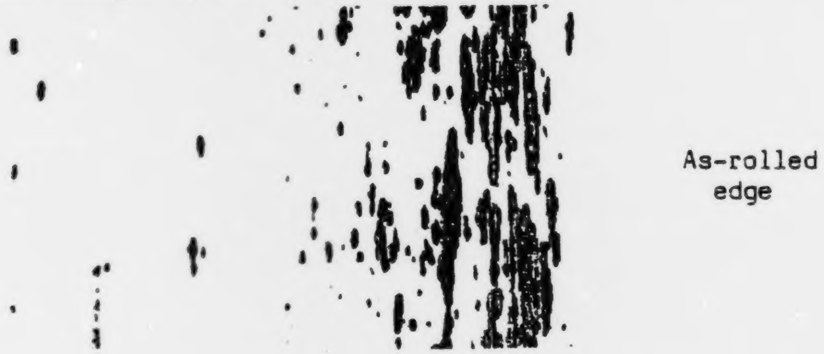

**(b) Charge 20, 1.50in, 4 Mid**

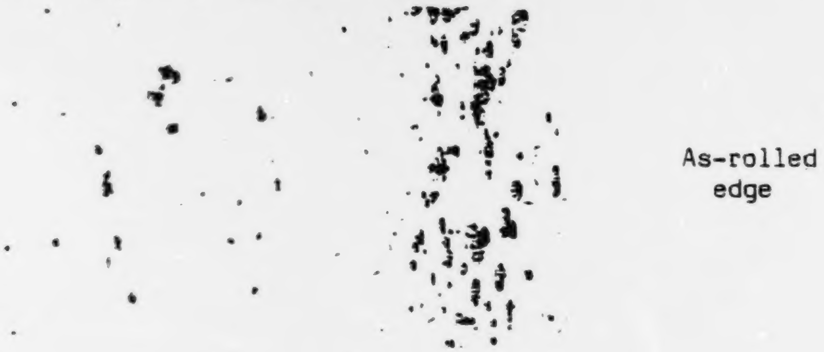

**(c) Charge 22, 2.50in, 5 Top**

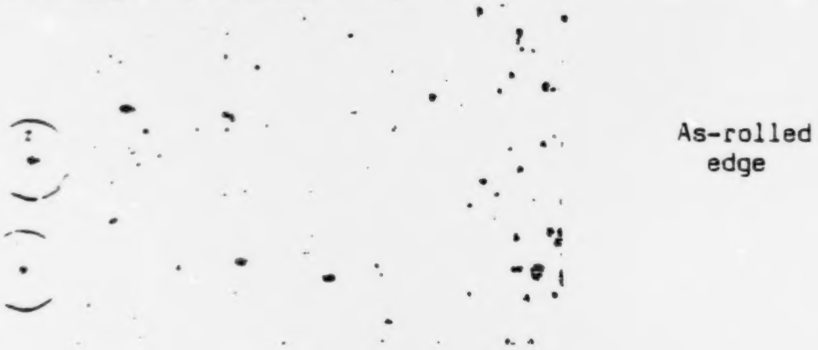

Away from the plate edges the rolled plates exhibited variable densities of U-sonic reflectors. Generally, the strip taken from the position corresponding to the ingot bottom showed nil to light indications. In terms of through-thickness position, the indications were generally much closer to the plate surface than in strand-cast steel and increased in depth below surface with increased thicknesses, ranging from 0.050in below in 0.75in plate to 0.25in below in 4.0in plate.

## 2. Through-thickness Ductility

None of the ingots and corresponding plate gauges tested had the consistently high through-thickness reduction of area required to be classified as Z-plate. Although the average values met Z-25 standards, low minimum values (often less than 10 percent) were experienced in most ingots (Table II A3, Figure 15).

**Figure 15: Summary of Through-Thickness Ductility in HW Sourced Plate**

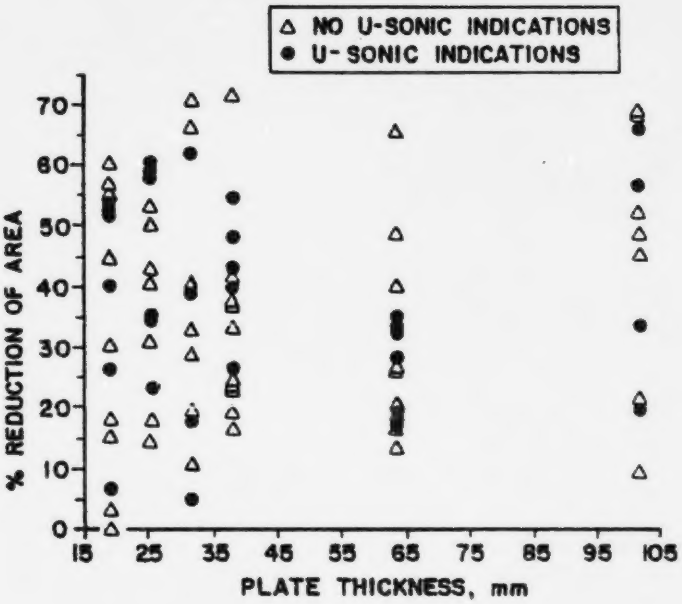

Samples taken from areas showing subsurface reflectors often showed low ductility associated with heavy sheets of broken calcium aluminate inclusions (Figure 16). There was considerable variability in the RAz values taken from defect areas, ranging from 5.0 percent to more than 60 percent. This variability resulted from problems in exactly locating the through-thickness samples on defect areas and the multi-planar nature of some reflectors which resulted in stepwise failure. In some cases, tests fractured at subsurface inclusions located in the friction weld heat-affected zone.

**Figure 16:** Sheets of Broken $CaO \cdot Al_2O_3$ Inclusions on Through-Thickness Tensile Fracture Surface (500X)

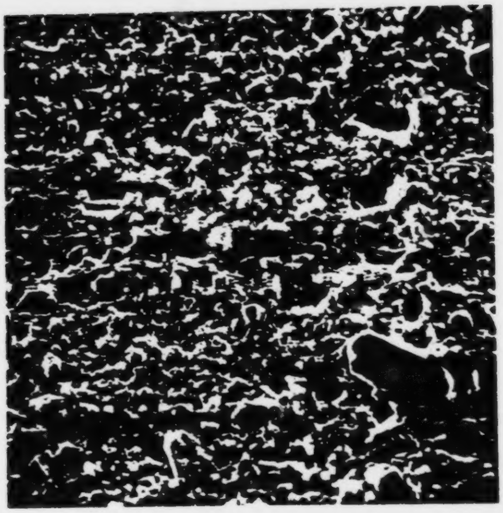

Low ductility was also encountered at non-defect locations. Examination of the fracture surfaces of several of these samples showed planar or step fracture caused by either Type II MnS (Figure 17) or sheets of broken calcium aluminate inclusions (Figure 18).

Figure 17: Low Z-direction Ductility resulting from MnS Inclusions

(a) Charge 11, 0.75in, 8X

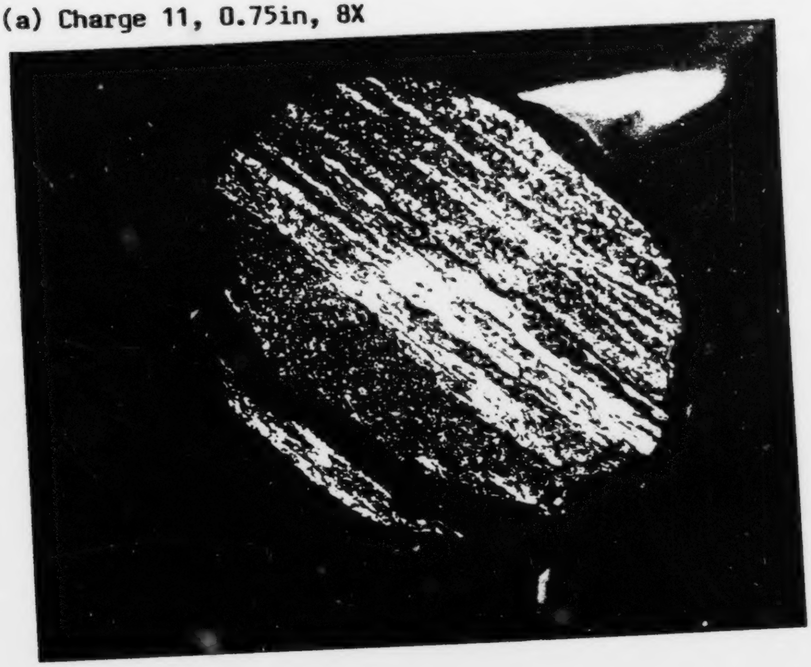

(b) 500X

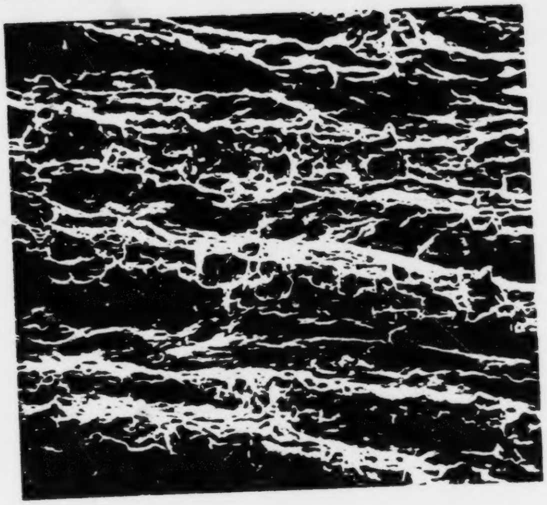

Figure 18: Low Z-direction Ductility related to $CaO-Al_2O_3$ Inclusions

(a) Charge 17, 1.25in, 8X

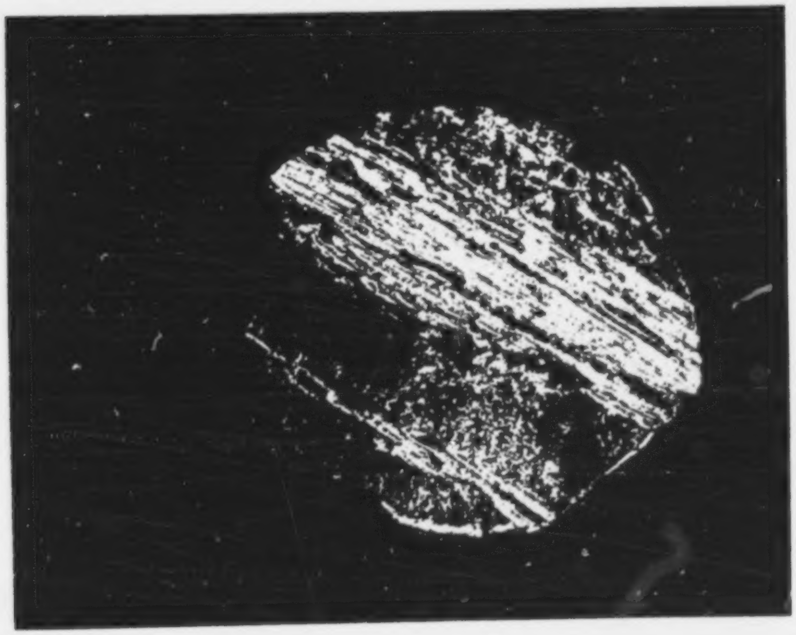

(b) 1000X

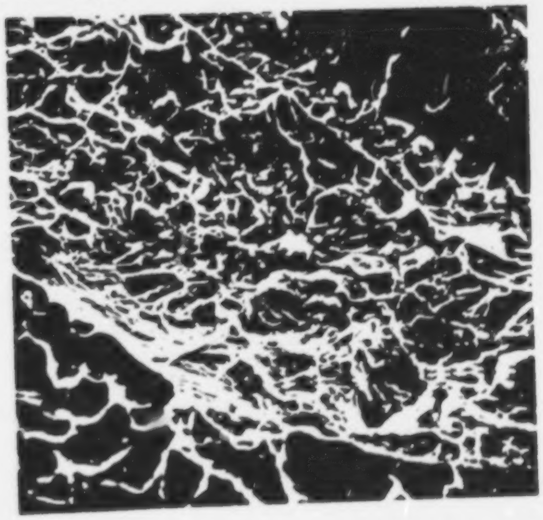

### Window Test

No lamellar tearing was observed in the window tests taken from either plate charge. Figure 19 shows a cross section from a test section taken through a plane containing subsurface calcium aluminate stringers.

Figure 19: Window Test* Through Subsurface Inclusions

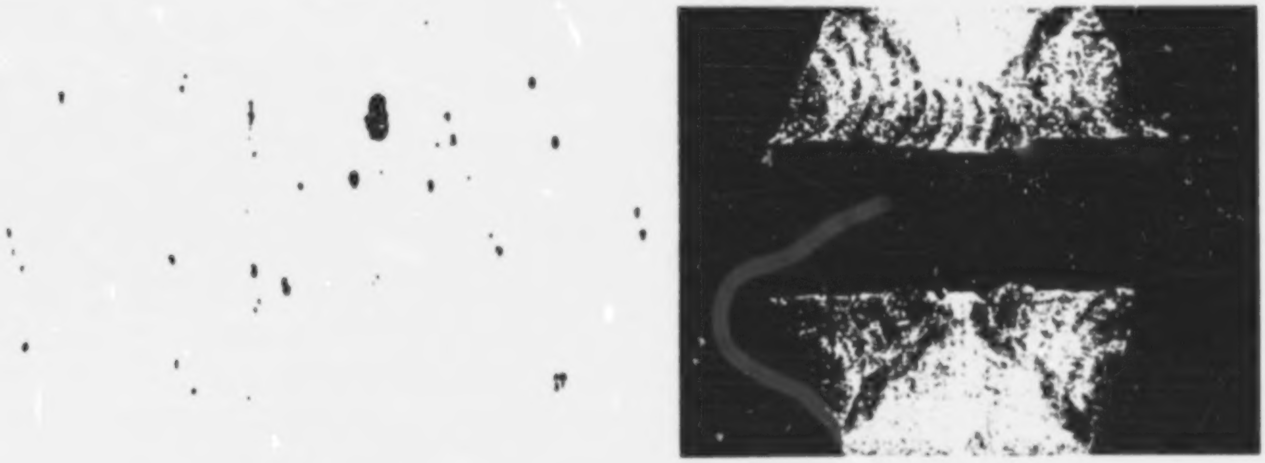

(a) C-Scan of Test Plate (0.65X)

(b) Etch Section through Window Test (Actual Size)

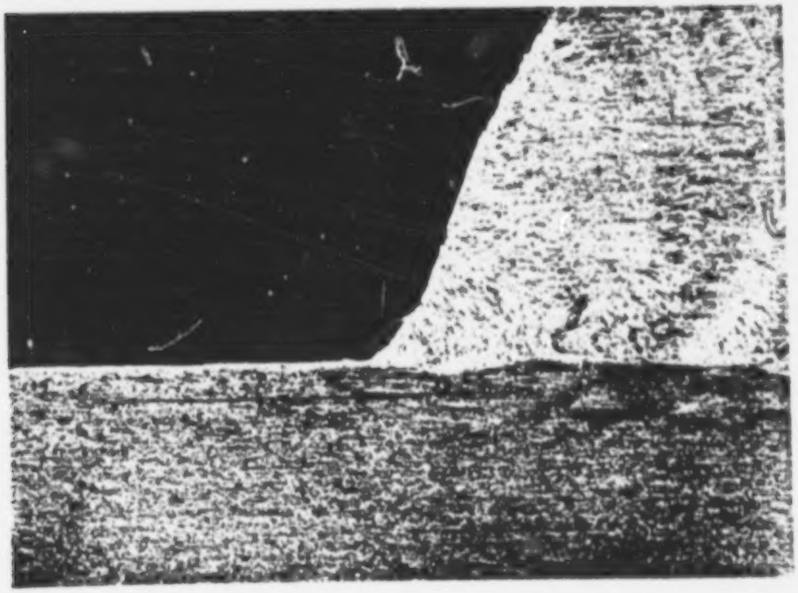

(c) Subsurface Oxide Stringer below Weld HAZ (3X)

## Discussion

The through-thickness tensile testing of the HW CAB-treated heat has demonstrated the tremendous variability in cleanliness of top poured ingot-cast steel. Despite the low S content (0.003 percent), poor through-thickness ductility was measured at several positions throughout this heat. The low ductility was a result of both gross calcium aluminate (reoxidation) inclusions and Type II MnS formed by segregation during solidification. Moreover, near-surface oxides trapped during solidification are also potential sites for tearing. Although no cracking was observed in window test samples, it is clear from the variability in tensile ductility that this plate would not pass current mill test requirements for Z-plate.

The results of these tests confirm our previous testing of top-poured, CAB-treated steel for both large diameter and ERW sour-service pipe. The key problem with our processing appears to be the reoxidation that occurs during teeming, which results in agglomerated calcium aluminates and subsurface oxides. A potential solution to this problem is the use of bottom pouring with gas shrouding between the ladle and the down sprue. R&D is investigating the equipment and associated cost to run a trial on bottom pouring a CAB-treated Grade 350 heat.

The window test results confirm the Sumitomo experience that cracking can be avoided by control of steel carbon equivalent and by the use of low hydrogen electrodes (to prevent hydrogen induced root cracking). If the levels of subsurface oxide inclusions can be reduced, then further restraint type weld testing is recommended to confirm the resistance of these plates to tearing under actual fabrication conditions.

As with LEW sourced heavy plate, hydrogen control procedures must be established to ensure freedom from hydrogen flaking. R&D, Metallurgical and Operating will review the steelmaking and slab and plate stack cooling practices required and assess the need to run further trials to develop these practices.

# ACKNOWLEDGMENTS

The following people and departments are recognized as having made vital contributions to this study:

B. Armitage, W. Krestynski, J. G. Matich, B. C. Branston, H. Meilach, J. H. Rennie, R&D Machine Shop and Photographic Lab, personnel, B. A. Buck, and several people in the HW Steelmaking, Plate Mill and LEW Steelmaking, Metallurgical and Operating Departments.

# REFERENCES

1. J. C. M. Farrar and P. E. Dolby: "Lamellar Tearing in Welded Steel Fabrication, the Role of Sulfide Inclusions", ASM Conference, Sulfide Inclusions in Steels, Port Chester, New York, November, 1974, pp 252-268.

2. J. Somella: "Significance and Control of Lamellar Tearing of Steel Plate in the Shipbuilding Industry", Ship Structure Committee, 1979.

3. 4th Draft Proposal on Plate with Specified Through-thickness Characteristics", ISO 17/SC, 3N415, August, 1981.

4. Through-thickness Tension Testing of Steel Plate for Special Applications, A770M-84, 822-6, January, 1984.

5. Australian Welding Research Association, "Control of Lamellar Tearing", AWRA Technical Note 6, April, 1976.

6. R. E. Dolby et al: "Susceptibility to Lamellar Tearing - Development of General Techniques".

7. I. D. Simpson et al: "Effect of Size and Shape of Inclusions and Through-thickness Properties", BHP Technical Bulletin, Vol 20, April, 1976, No. 1, pp 30-36.

8. A. J. DeArdo and E. G. Hamburg: "Influence of Elongated Inclusions on the Mechanical Properties of High Strength Steel Plate", ASM Conference Sulfide Inclusions in Steel, Port Chester, New York, November, 1974, pp 252-268.

9. G. Bernard et al: "Inclusions in Steel Plates and Mechanical Anisotropy", Metals Technology, November, 1975, pp 512-521.

10. S. Kanazawa et al: "Lamellar Tearing Resisting Steels and the Directions for Use of Them", Nippon Steel Corporation, Japan, 1974 (IIW Doc IX-873-74).

11. R. Blondeau et al: "Investigations of Factors Influencing the Reduction of Area through the Thickness of Heavy-Gauge HSLA Plates", ASM Conference, Welding of HSLA (Microalloyed) Structural Steels, Rome, Italy, November, 1976, pp 530-552.

12. Y. Tomita et al: "Prevention of Hydrogen Cracking in Thick Steel Plates Produced from Continuous Casting Slabs", ASM Conference, Hydrogen Problems in Steels, Washington, DC, November, 1982, pp 63-69.

13. S. Kanazawa et al: "On the Assessment of the Lamellar Tearing Susceptibility of Steel Plate", IIW Doc IX-040-73.

14. S. Hasebe et al: "Lamellar Tearing and Through-thickness Properties of Steel Plate", Sumitomo Search, No. 11, May, 1974, pp 25-30.

15. S. Hasebe et al: "Factors for Lamellar Tearing of Steel Plate", Sumitomo Search, No. 13, May, 1975, pp 19-27.

16. Y. Ito et al: "Lamellar Tearing in Welded HT 50 Steel Plate", Sumitomo Search No. 13, May, 1975, pp 8-18.

# APPENDIX 1

# SLAB INSPECTION

## Ultrasonic Testing

All slabs produced from heat 805126 were manual ultrasonically inspected at LEW to map out the areas of gross center looseness. Intermittent areas of centerline indications were found throughout the length of the cast (Figure 1 A1). Its notable that only minor areas of center looseness were present in the first two and last two parent slabs cast. The areas of porosity were generally confined to the center portion of the slab width, and ranged from ≈20 cm (8in) to ≈80 cm (30in) in width. In the front half of the heat the looseness was semi-continuous, whereas in the last half the looseness was confined to discrete, almost regularly spaced islands.

## Sulfur Prints

Sulfur prints taken from the end of each parent slab were examined for quarter point inclusions. Table I A1 summarizes the quarter point inclusion densities throughout the heat. The information from the sulfur prints agrees well with the C-scan data, and confirms the buildup of quarter point inclusions on first one side and then the other of the strand. Figure 2 A1 shows a typical sulfur print section containing inclusions.

Figure 1 AI: Center Looseness in HT 805126

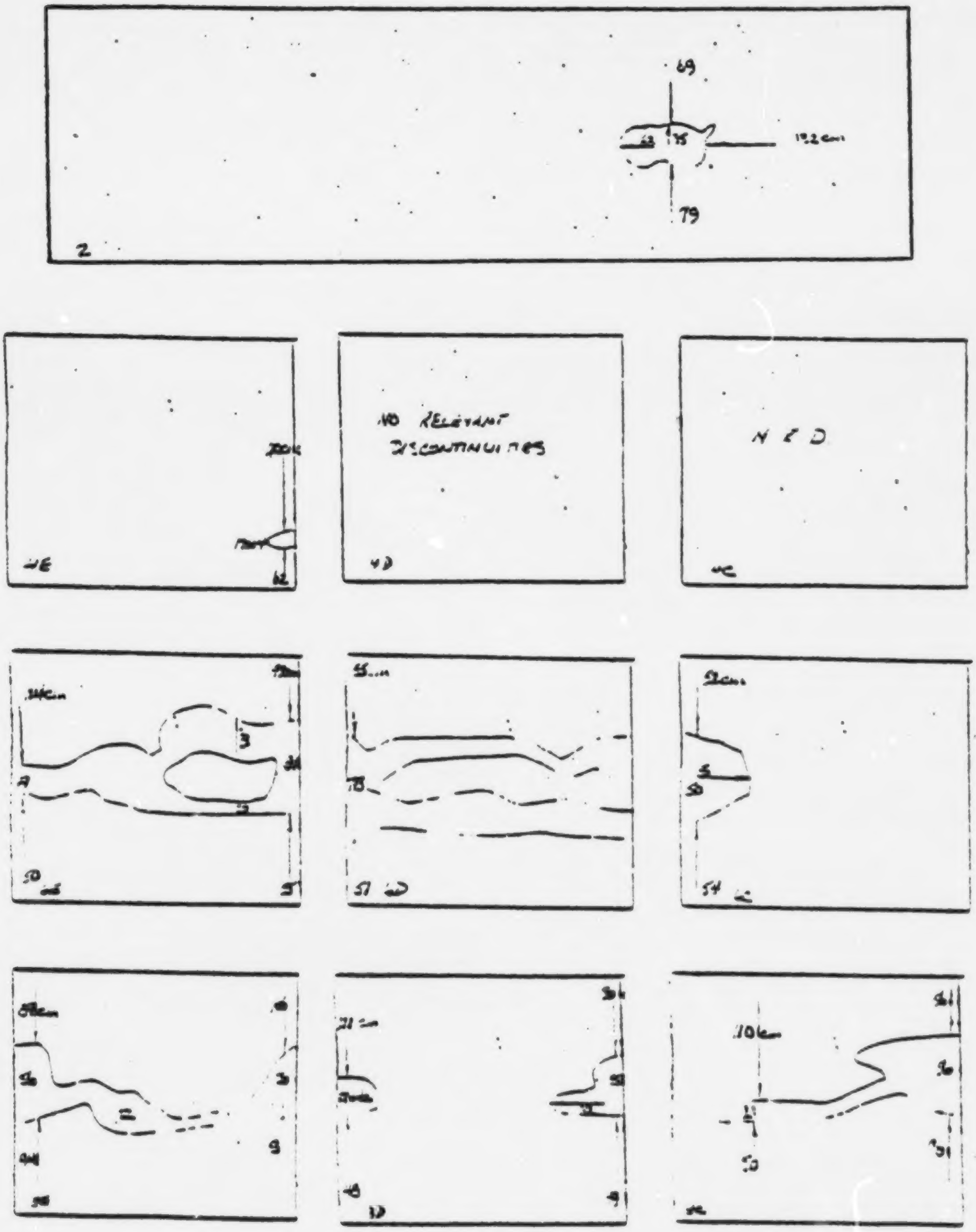
69
75
79
19.2 cm
2
4E
NO RELEVANT DISCONTINUITIES
4D
N E D
4C
50
51
57
54
21 cm
10 cm
56

Figure 1 AI (contd)

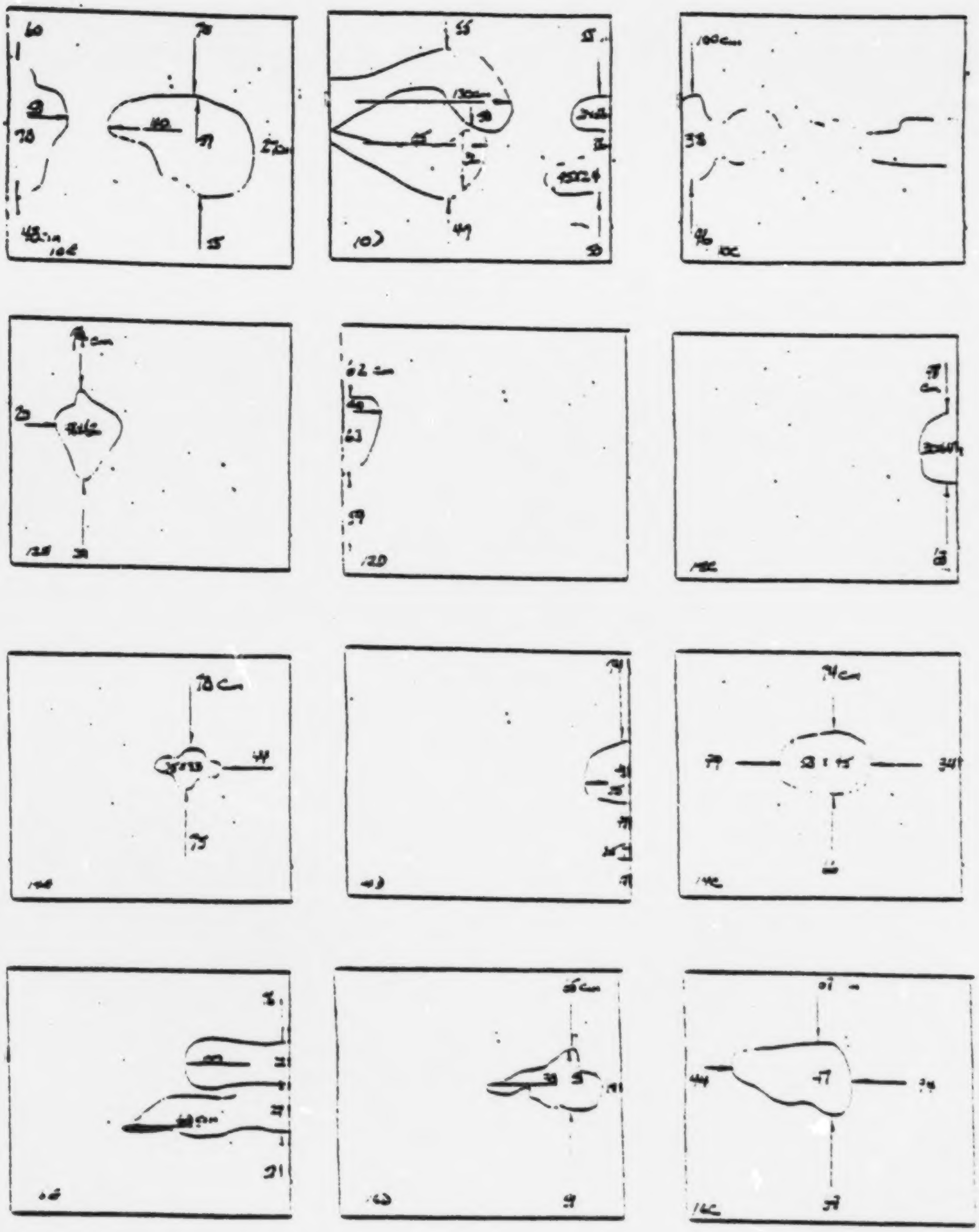

60
70
100cm
38
62 cm
73 cm
74 cm
25cm

Figure 1 AI (contd)

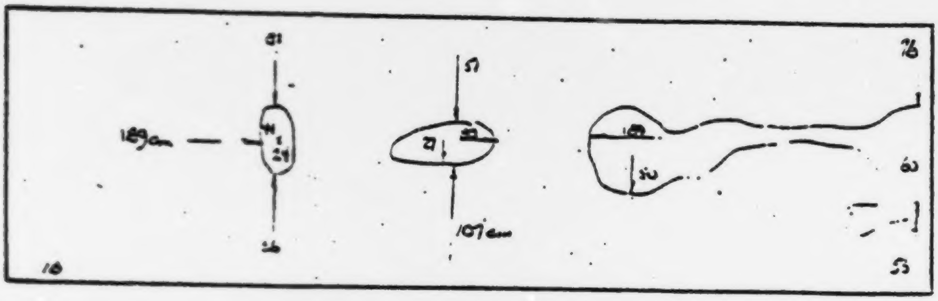
81
57
76
189cm
44
29
21
52
180
50
60
107cm
26
18
53

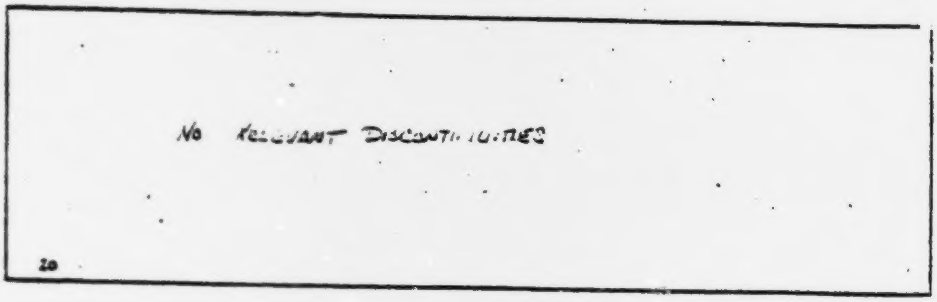
NO RELEVANT DISCONTINUITIES
20

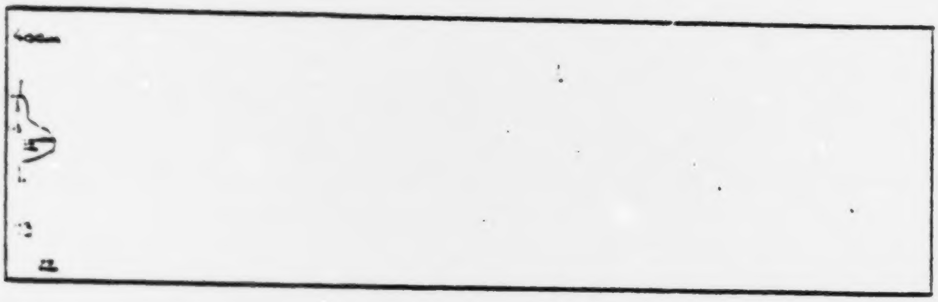

**Table I A1: Quarter Point Inclusion Densities in Ht 805126**

| Parent Slab | Slab Section* | | | |
|---|---|---|---|---|
| | 1 | 2 | 5 | 6 |
| 2 | √ | 0 | 0 | √ |
| 4 | 0 | 0 | √ | √ |
| 6 | 0 | 0 | √ | √ |
| 8 | 0 | 0 | √ | √ |
| 10 | 0 | 0 | √ | 0 |
| 12 | 0 | 0 | √ | √ |
| 14 | 0 | 0 | 0 | √ |
| 16 | √ | √ | √ | 0 |
| 18 | √ | √ | √ | √ |
| 20 | √ | 0 | 0 | 0 |
| 22 | √ | √ | 0 | 0 |

√ - significant quarter-point inclusions
0 - no quarter-point inclusions
* position across the width of the cast slab

Figure 2 A1: Sulfur Print from Ht 805126 showing Quarter-Point Inclusions and Centerline Porosity

# APPENDIX 2

## LAB ULTRASONIC INSPECTION

### U-sonic Test Procedure

Full-width strips from the ends of each plate rolled were sectioned into approximately 12in wide coupons for laboratory ultrasonic inspection. All coupons were inspected using the American NDT Model AX8000 Integrity Tester combined with the Automation U-S-450 lab scanner. The C-scan of each coupon was done with 0.010in step increments.

To cover the wide range of plate thicknesses tested, the system was calibrated using a resolution block to a known size of flat bottomed hole (Table I A2). For plate thicknesses up to 1.5in, the calibration hole size was 3/64in, and it was increased to 5/64in on plate gauges up to 2.5in, and to 8/64in on the 4.0in plate. To ensure adequate detection of discontinuities at both the near and far surfaces, the dB gain was increased with plate thickness. With the focused probes used, this increase in gain produced enlargement (up to 2.5X) particularly of near-surface discontinuities. Figure 1 A2 shows examples of the C-scan outputs for different plate thicknesses.

### U-sonic Results

Tables II A2 and III A2 summarize the C-scan indications for the LEW and HW heats respectively. As noted in the body of the report, the LEW heat exhibited quarter point inclusions. These were distributed inhomogeneously across the plate width and tended to be concentrated initially at one edge of the strand, and later at the other edge. The position of the inclusions below the plate rolled surface varied between 0.08 to 0.15in for the 0.59in plate to 0.30 to 0.70in for the 2.0in plate.

The HW heat showed variable indications throughout the height and width of the ingot, as shown in Table II A2. Very heavy concentrations of inclusions were found at the as-rolled edge. These penetrated up to 3.5in into the plate body. Generally, the ingot cast inclusions were much closer to the plate surface than those in strand cast plate. At 0.750in thickness, the inclusions were 0.050in below surface. This increased up to 0.25in below in the 4.0in plate.

Figure 1 AII: Calibration of Lab C-Scan using Resolution Block (0.75X)

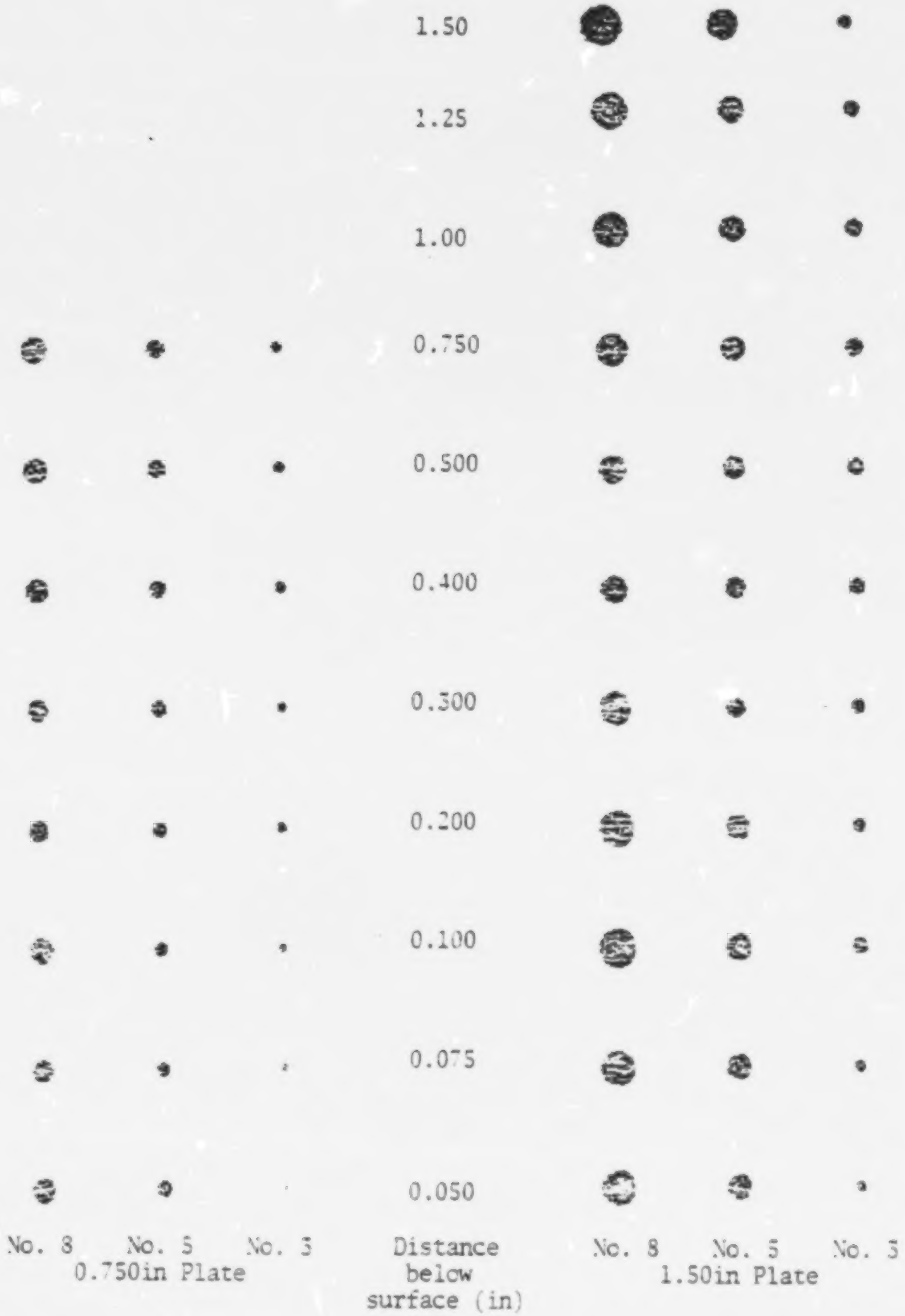
1.50
1.25
1.00
0.750
0.500
0.400
0.300
0.200
0.100
0.075
0.050
No. 8
No. 5
No. 3
0.750in Plate
Distance below surface (in)
No. 8
No. 5
No. 3
1.50in Plate

Table I A2: Calibration of American NDT AX-8000

| Plate Gauge | Dynamic Range in % db Gain | Display Mode | Reject Baseline Noise | Alarm Level % SH | Pulse Rep Rate | Transducer | Screen Height Response to Flat Bottom Hole | |
|---|---|---|---|---|---|---|---|---|
| 0.590 | 73 | positive | <25% | 35 | 1000 | 10 MHz | 80% @ 0.600in | No. 3 |
| 0.750 | 75 | positive | <25% | 35 | 1000 | 0.375 dia | 80% @ 0.750in | |
| 1.0 | 78 | positive | <25% | 35 | 1000 | 3in focus | 80% @ 1.0in | |
| 1.18 | 81 | positive | <25% | 35 | 1000 | " | 80% @ 1.18in | |
| 1.25 | 82 | positive | <25% | 35 | 1000 | " | 80% @ 1.25in | |
| 1.5 | 76 | positive | <25% | 35 | 1000 | 10 MHz | 20% @ 1.5in | |
| 1.75 | 77 | positive | <25% | 35 | 1000 | 0.500 dia | 100% @ 1.75in | No. 5 |
| 2.0 | 78 | positive | <25% | 35 | 1000 | 4in focus | 100% @ 2.0in | |
| 2.5 | 80 | positive | <25% | 35 | 1000 | " | 755 @ 2.5in | |
| 4.0 | 85 | positive | <25% | 35 | 1000 | " | 60% @ 4.0in | No. 8 |

## Table II AII: Summary of C-Scans Ht 805126

| Charge No. | Gauge (in) | Slab | Width (in) | Width (in) |  |  |  |  |  |  |  | Location of U-Sonic Indication |
|---|---|---|---|---|---|---|---|---|---|---|---|---|
|  |  |  |  | 0 – 10 – 20 – 30 – 40 – 50 – 60 – 70 – 80 – 90 – 100 – 110 – 120 |  |  |  |  |  |  |  |  |
| 24 | 0.75 | 4C | 105 | NIL** | VL | VL | *VL* | L | L-M | L | L | 0.15 - 0.20in |
| 25 |  | 4D | 105 | NIL** | VL | VL | **L* | L | L-M | M | M | 0.15 - 0 20in |
| 26 | 1.0 | 4E | 104 | NIL** | NIL* | VL | VL* | L | M | M | M | 0.15 - 0.20in |
| 27 |  | 6C | 104 | *L* | L | M** | M** | M | M | M | M | 0.15 - 0.20in |
| 28 | 1.75 | 6D | 81 | **M | M | *M* | M* | M | L | L | VL | 0.10 - 0.30in |
| 29 |  | 6E | 81 | L** | M | **M | M** | M | L | L | NIL | 0.20 - 0.30in |
| 30 | 1.50 | 8C | 81 | VL** | VL | **VL | VL** | NIL | NIL | NIL | NIL |  |
| 31 | 8D | 8D | 0X |  |  |  | FLAKING |  |  |  |  |  |
| 32 | 1.75 | 8E | 81 | NIL** | NIL | *NIL | NIL* | NIL | VL | NIL | VL | 0.25 - 0.30in |
| 33 |  | 10C | 81 | VL* | *L* | **VL | VL** | NIL | NIL | NIL | NIL | 0.25 - 0.30in |
| 34 | 2.0 | 10D | 81 | VL** | VL | *L | VL** | NIL | NIL | NIL | NIL | 0.30 - 0.70in |
| 35 |  | 10E | 81 | VL** | NIL | *NIL | VL** | NIL | NIL | NIL | NIL | 0.30in |
| 3 | 1.18 | 12C | 121 | **L | L** | L | L** | L | L | L | L | 0.20 - 0.30in |
| 36 | 0.590 | 16D | 114 | NIL** | NIL | **NIL | NIL** | NIL | VL | VL | VL | 0.08 - 0.15in |

Table III AII:  Summary of C-Scans Ht 536441

| Charge No. | Gauge (in) | Cut | Width (in) | Width (in) 0 10 20 30 40 50 60 70 80 90 100 | | | | | | | | | | | Location of U-Sonic Indications |
|---|---|---|---|---|---|---|---|---|---|---|---|---|---|---|---|
| 10 | 0.75 | 1 Top | 102 | 2.5 | L** | *L* | L | L** | L | M | M | M | | 3.0 | 0.050 - 0.100in below |
| 11 | | 1 Mid | 102 | 3.0 | L** | M** | L | L** | L | L | L | L | | 3.5 | 0.050 - 0.100in below |
| 12 | | 1 Bot | 102 | 1.0 | NIL** | NIL | **NIL | NIL** | NIL | NIL | NIL | NIL | | | No Indications |
| 13 | 1.0 | 2 Top | 102 | 3.0 | M** | M | **M | M** | M | M | M (Window) | M-H | | 3.0 | - 0.100in below |
| 14 | | 2 Mid | 101 | 3.0 | M** | M** | L | L* | L | L | L | L | | 3.0 | - 0.100in below |
| 15 | | 2 Bot | 101 | 2.0 | L** | L** | V-L | NIL** | NIL | NIL | NIL | L | | | 0.100in below |
| 16 | 1.25 | 3 Top | 78 | 1.75 | *L* | L** | L | LM** | NIL | L | L | L | | 1.75 | 0.100in below |
| 17 | | 3 Mid | 78 | 2.0 | *L* | **L | L | L** | L | VL | NIL | L | | 2.0 | 0.100 - 0.200in below |
| 18 | | 3 Bot | 78 | | | | | | | | | | | | |
| 19 | 1.50 | 4 Top | 78 | 2.25 | *L* | L*-M* | L-M | L** | L | L | L | L | | 2.25 | 0.120 - 0.200in below |
| 20 | | 4 Mid | 78 | 2.0 | **NIL | **L | L | NIL** | L | L | *L (Window) | L-M | | 2.0 | 0.150 - 0.200in below |
| 21 | | 4 Bot | 78 | 2.25 | *L* | *L* | L | L** | L | L | L | L | | 2.5 | 0.120 - 0.180in below |
| 22 | 2.50 | 5 Top | 80 | 2.0 | L** | VL** | VL | VL** | VL | VL | VL | VL | | 2.0 | 0.150 - 0.250in below |
| 23S | | 5 Mid | 80 | 2.0 | L** | VL | VL** | VL** | L | L | L | L | | 2.0 | 0.150 - 0.300in below |
| 23N | | 5 Bot | 80 | 1.25 | **L | VL | *VL* | NIL** | NIL | NIL | NIL | L | | 1.5 | 0.100 - 0.300in below |
| 1 | 4.0 | 6 Mid | 66 | 2.5 | M** | M-H | *M* | M | M** | M | M | M-H | | | 0.250 - 0.750in below |
| 2 | | 6 Top | 66 | 2.5 | M** | M | NIL ** M | M-H | **L-M | M-L | L | | | 3.0 | 0.250 - 0.750in below |

# APPENDIX 3

## THROUGH-THICKNESS TENSILE DATA

The through-thickness tensile test results for the LEW and HW heats are summarized in Tables I A3 and II A3, respectively. Included are the reduction of area, the position of the fracture in the plate through-thickness (TT) and the appearance of the fracture surface.

# Table I A3: Summary of Through-Thickness Tensile Data - LEW Ht 805126

| Chg No. | Gauge (in) | Slab Cut | Edge | | | | | | | 1/4 Width | | | | | | | 1/2 Width | | | | | | | RAz Avg | RAz Min |
|---|---|---|---|---|---|---|---|---|---|---|---|---|---|---|---|---|---|---|---|---|---|---|---|---|---|
| | | | | Test 1 | | | Test 2 | | | | Test 3 | | | Test 4 | | | | Test 5 | | | Test 6 | | | | |
| | | | C-Scan | % RA 1 | TT 2 | FR 3 | % RA | TT | FR | C-Scan | % RA | TT | FR | % RA | TT | FR | C-Scan | % RA | TT | FR | % RA | TT | FR | | |
| 24 | 0.75 | 4C | Nil | 75.2 | 1/2 | CC | 71.9 | 1/2 | CC | VL | 42.3 | 1/2 | Woody | 47.0 | 1/2 | Woody | VL | 61.9 | 1/2 | CC | 62.3 | 1/2 | CC | 60.1 | 42.3 |
| 25 | | 4D | Nil | 76.2 | 1/2 | CC | 72.7 | 1/2 | CC | L | 57.1 | 1/2 | CC | 34.9 | 1/4 | Flat | L | 58.0 | 1/2 | CC | 49.5 | 1/2 | CC | 57.9 | 34.9 |
| 26 | 1.0 | 4E | Nil | 76.5 | 1/2 | CC | 75.4 | 1/2 | CC | Nil | 61.6 | 1/2 | CC | 66.3 | 1/2 | CC | VL | 21.6 | 1/2 | Flat | 29.9 | 1/2 | Flat | 55.2 | 21.6 |
| 27 | | 6C | L | 76.2 | 1/2 | CC | 75.0 | 1/2 | CC | M | 44.5 | 1/2 | Woody | 38.1 | 1/4 | Woody | M | 43.4 | 1/2 | Woody | 59.3 | 1/2 | CC | 56.0 | 38.1 |
| 28 | 1.25 | 6D | M | 75.2 | 1/2 | CC | 74.2 | 1/2 | CC | MM | 75.0 | 1/3 | CC | 72.7 | 1/3 | CC | M | 74.5 | 1/2 | CC | 78.2 | 1/2 | CC | 75.0 | 72.7 |
| 29 | | 6E | L | 78.5 | 1/2 | CC | 70.1 | 1/2 | CC | M | 48.4 | 1/4 | Alumina | 48.6 | 1/4 | Flat | M | 75.0 | 1/2 | CC | 74.5 | 1/3 | CC | 65.9 | 48.4 |
| 30 | 1.50 | 8C | VL | 78.5 | 1/3 | CC | 72.9 | 1/3 | CC | VL | 77.5 | 1/3 | CC | 75.1 | 1/3 | CC | VL | 78.4 | 1/3 | CC | 75.0 | 1/3 | CC | 77.1 | 75.0 |
| 31 | | 8D | | | | CC | | | CC | | | | CC | | | | | | | CC | | | CC | | |
| 32 | 1.35 | 8E | Nil | 79.6 | 1/4 | CC | 79.8 | 1/4 | CC | Nil | 78.6 | 1/4 | CC | 77.2 | 1/4 | CC | Nil | 76.7 | 1/4 | CC | 79.1 | 1/4 | CC | 78.5 | 76.7 |
| 33 | | 10C | VL | 77.8 | 1/3 | CC | 80.0 | 1/3 | CC | L | 65.4 | 1/2 | CC | 77.7 | 1/2 | CC | VL | 71.6 | 1/2 | CC | 75.0 | 1/2 | CC | 74.9 | 65.4 |
| 34 | 2.0 | 10D | VL | 78.3 | 1/3 | CC | 78.0 | 1/3 | CC | L | 78.2 | 1/4 | CC | 51.4 | 1/5 | Alumina | VL | 67.4 | 1/2 | CC | 80.8 | 1/3 | CC | 72.3 | 51.1 |
| 35 | | 10E | VL | 78.3 | 1/4 | CC | 79.1 | 1/4 | CC | Nil | 76.4 | 1/4 | CC | 76.7 | 1/4 | CC | VL | 77.7 | 1/4 | CC | 78.6 | 1/4 | CC | 77.8 | 76.4 |
| 3 | 1.18 | 12C | L | 74.9 | 1/3 | CC | 77.8 | 1/3 | CC | L | 66.4 | 1/2 | CC | 65.5 | 1/2 | CC | L | 76.3 | 1/3 | CC | 77.1 | 1/3 | CC | 73.0 | 65.5 |
| 36 | 0.590 | 12D | Nil | 56.1 | 1/2 | CC | 34.0 | 1/2 | Woody | Nil | 58.8 | 1/2 | CC | 57.1 | 1/2 | CC | Nil | 25.1 | 1/2 | Woody | 30.7 | 1/2 | Woody | 43.6 | 25.1 |

Notes:

①

$$\% RA = \frac{Ao - A}{Ao}$$

where: Ao = original area (6 mm)
A = final area

② TT denotes position of fracture through the plate thickness.

③ FR describes the type of fracture surface.

CC = Cup and Cone

## Table II A3: Summary of Through-Thickness Tensile Data - HW Ht 536441

| Chg No. | Gauge (in) | Slab Cut | Edge | | | | | | | 1/4 Width | | | | | | | 1/2 Width | | | | | | | RAz Avg | RAz Min |
|---|---|---|---|---|---|---|---|---|---|---|---|---|---|---|---|---|---|---|---|---|---|---|---|---|---|
| | | | | Test 1 | | | Test 2 | | | | Test 3 | | | Test 4 | | | | Test 5 | | | Test 6 | | | | |
| | | | C-Scan | % RA | TT | FR | % RA | TT | FR | C-Scan | % RA | TT | FR | % RA | TT | FR | C-Scan | % RA | TT | FR | % RA | TT | FR | | |
| 10 | 0.75 | 1T | L | 54.4 | 1/2 | CC | 0 | Surf | - | VL | 7.0 | Surf | - | 52.3 | 1/2 | CC | VL | 30.2 | 1/2 | Step | 18.0 | 1/2 | Woody | 32.4 | 7.0 |
| 11 | | 1M | L | 44.7 | 1/2 | Woody | 56.4 | 1/2 | CC | L | 26.4 | 1/3-1/2 | Step | 40.1 | 1/2 | Woody | L | 15.2 | 1/2 | Flat | 3.0 | 1/2 | Flat | 40.0 | 3.0 |
| 12 | | 1B | Nil | 56.1 | 1/2 | CC | 59.7 | 1/2 | CC | Nil | 52.3 | 1/2 | CC | 53.7 | 1/2 | CC | VL | 52.2 | 1/2 | CC | 52.0 | 1/2 | CC | 54.3 | 52.0 |
| 13 | 1.0 | 2T | M | 39.9 | 1/3 | Flat | 42.7 | 1/2 | Woody | M | 23.3 | 1/2 | Woody | 34.0 | 1/3 | Woody | M | 14.3 | 1/2 | Step | 17.6 | 1/2 | Woody | 28.6 | 14.3 |
| 14 | | 2M | M | 58.8 | 1/2 | CC | 52.7 | 1/2 | CC | MH | 34.9 | 1/2 | Step | 52.3 | 1/2 | CC | M | 30.7 | 1/2 | Step | 23.4 | 1/2-1/3 | Flat | 42.1 | 23.4 |
| 15 | | 2B | L | 57.0 | 1/2 | CC | 57.3 | 1/2 | CC | M | 57.6 | 1/2 | CC | 60.0 | 1/2 | CC | M | 50.0 | 1/2 | CC | 58.4 | 1/2 | CC | 56.7 | 50.0 |
| 16 | 1.25 | 3T | L | 19.2 | 1/2 | Step | 10.3 | 1/2 | Flat | VL | 61.6 | 1/3 | CC | 5.0 | Surf | | VL | 65.7 | 1/3 | CC | 70.4 | 1/3 | CC | 38.7 | 5.0 |
| 17 | | 3M | L | 28.7 | 1/2T | Flat | 32.7 | 1/2 | Step | | 39.0 | 1/4 | CC | 17.4 | Surf | Woody | | 40.2 | 1/2 | Woody | 40.6 | 1/2 | Woody | 33.1 | 17.4 |
| 19 | 1.50 | 4T | L | 23.3 | 1/4 | Step | 32.8 | 1/4 | CC | Nil | 39.6 | 1/4 | Flat | 54.4 | 1/4 | CC | Nil | 41.3 | 1/4 | CC | 19.3 | 1/4 | Woody | 35.1 | 19.3 |
| 20 | | 4M | Nil | 24.2 | 1/3 | Flat | 37.1 | 1/2 | Step | L | 26.4 | Surf | Step | 26.5 | Surf | Step | VL | 41.5 | 1/2 | Step | 36.2 | 1/2 | Woody | 32.0 | 24.2 |
| 21 | | 4B | L | 17.2 | Surf | Woody | 23.5 | 1/4 | Woody | L | 43.4 | 1/4 | CC | 48.2 | 1/4 | CC | VL | 41.1 | 1/2 | Woody | 16.3 | Surf | Woody | 31.6 | 16.3 |
| 22 | 2.50 | 5T | L | 13.2 | 1/4 | Flat | 20.0 | 1/5 | Flat | Nil | 28.7 | 1/5 | Woody | 17.5 | 1/8 | Flat | VL | 65.3 | 1/4 | CC | 17.5 | 1/4 | Flat | 27.0 | 13.2 |
| 235 | | 5M | L | 48.4 | 1/5 | Ductile | 16.1 | 1/6 | Woody | L | 33.2 | 1/4 | Ductile | 34.9 | 1/6 | Slant | L | 39.7 | 1/6 | Ductile | 26.6 | 1/6 | Ductile | 33.2 | 16.1 |
| 23N | | 5B | L | 28.4 | 1/4 | Step | 25.7 | 1/3 | Flat | Nil | 19.5 | 1/3 | Step | 32.3 | 1/2 | Step | Nil | 33.4 | 1/4 | Step | 18.7 | 1/4 | Flat | 26.3 | 18.7 |
| 1 | 4.0 | 6 | M | 21.4 | 1/4 | Ductile | 45.0 | 1/6 | Slant | L | 33.8 | Surf | Flat | 19.7 | 1/4 | Ductile | L | 51.8 | 1/5 | CC | 68.4 | 1/5 | CC | 40.0 | 19.7 |
| 2 | | 6T | M | 9.3 | 1/2 | Flat | 48.4 | 1/5 | Ductile | Nil | 65.8 | 1/5 | Ductile | 56.7 | 1/5 | Ductile | Nil | 67.4 | 1/5 | Ductile | 67.6 | 1/5 | CC | 52.5 | 9.3 |

TT - Position of fracture through the plate thickness
FR - Fracture surface appearance

# ABSTRACT

Development of Canada's East Coast and Arctic energy resources will create a demand for significant tonnages of Grade 350 structural plate with low temperature impact requirements. This market has traditionally been supplied with normalized plate. This paper presents data on the development of controlled rolled, low carbon - Mn-Cr-Ni-Cb-V-Ti strand cast steel for this application. In addition to plate strength and Charpy toughness data, results on the steel's lamellar tearing and HAZ cold cracking resistance, and SAW weld HAZ fracture toughness are presented.

# INTRODUCTION

The development of Canadian oil and gas reserves in the Arctic and along our East Coast during the next decade will require the construction of major capital equipment including production platforms and islands, tankers, ice-breakers, supply vessels, and caissons. Although the exact timing of the major activities in these areas is somewhat uncertain, it is forecast that up to 30 000 tons per year of relatively high quality structural plate will be absorbed by this market.[1] In an effort to maximize Canadian participation of both steelmakers and fabricators in this market the Department of Energy, Mines and Resources[2] has sponsored a preliminary research program to define the present Canadian capabilities of plate supply and welding technology. Stelco has participated in this program by producing and testing trial heats of Grade 350 steel.[3]

The specific property requirements for Canadian offshore construction have not yet been established, however, it is anticipated that they will closely follow those used by other nations and classification societies for similar structures. These have recently been reviewed by both Det Norske Veritas[4] and Lloyds Register of Shipping,[5] and have been used to formulate a tentative aim specification for base plate strength and toughness, lamellar tearing resistance, and heat affected zone fracture initiation resistance, as shown in Table I. Most of the plate tonnage will be Grade 350 (350 MPa yield strength) in thicknesses between approximately 15 and 100 mm, with the largest tonnage in the range 20 to 50 mm. These requirements are typical of the steel quality provided for North Sea construction with the major difference that both East Coast and Arctic design temperatures (-30 and -50°C) are significantly lower than that of the North Sea (-10°C). The lower design temperature will necessitate steels with significantly improved impact toughness (lower transition temperatures) in both the base plate and the weld zone.

Although steels for offshore fabrication have generally been supplied in the normalized condition, since the mid-70s there has been considerable development of new, low carbon controlled rolled and, more recently, water spray cooled plate for similar applications. These steels offer the advantage of lower production cost by replacing a relatively expensive heat treatment, together with potentially improved weldability compared with the more traditional normalized chemistries. There is some concern that the new steels have relatively poor resistance to HAZ fracture initiation; however, there is a potential to minimize deterioration in the HAZ region through the use of grain refining additions and reduced nitrogen content. In particular, small titanium additions (≈0.01 percent) have been shown to restrict grain coarsening during the weld thermal cycle by the formation of a relatively fine (<500Å) stable dispersion of TiN particles.[6,7] This technology has been successfully applied at

Stelco for strand cast large diameter pipe,[8] and was incorporated into the design of the Grade 350 trial heat.

This report gives a detailed description of the processing and mechanical properties of a new low carbon, microalloyed chemistry developed to meet Canadian design requirements for offshore service.

## Heat Chemistry

The heat chemistry was essentially designed to meet the Grade 350 strength requirements in the controlled rolled condition, while achieving improved low temperature toughness, compared with conventional normalizing chemistries, through reduced pearlite content. The main factors considered in developing the analysis are shown in Table II. Note that at the 0.07 carbon level, the reduced pearlite content results in significantly lower ultimate strength (UTS). To make up this loss of UTS, high manganese (1.40 percent) as well as 0.25 percent chromium and 0.25 percent nickel were added. It is important to note that it may not be necessary to meet the aim UTS levels in that current design philosophy is based on yield strength. The 0.02 percent columbium addition was made to provide grain refinement (through its well established effect on austenite recrystallization kinetics) and precipitation hardening. The 0.01 percent titanium addition was made primarily to restrict austenite grain growth, during both slab reheating and the HAZ thermal cycle, and to improve brittle fracture resistance by reducing the free nitrogen content.

## Heat Production

A 250 tonne BOF heat was produced at Stelco Lake Erie Works to the chemistry shown in Table III. The heat was made to a low sulfur practice using desulfurized hot metal, selected low sulfur scrap, and tapping onto a desulfurizing reagent to achieve a 0.004 percent sulfur product analysis. To reduce the level of oxides, particularly aluminates, the heat was fully shrouded between ladle and tundish and tundish and mold, and inclusion removal was promoted in the tundish by using a dam/weir system and an oxide absorbing tundish slag. The heat was cast singly (non-sequenced) to a 200 mm x 1830 mm slab cross section. All parent slabs were stack-cooled under vermiculite to achieve hydrogen removal to prevent flaking.

A total of 20 slabs were rolled to plate thicknesses between 15 and 51 mm (Table IV). All plates were controlled rolled using a low reheating (1175°C) temperature practice to restrict grain coarsening during reheating and to reduce the time available for austenite grain growth between roughing and finishing. Grain coarsening studies on samples taken from the as-cast slabs demonstrated that the grain coarsening temperature of the titanium treated steel was significantly above 1200°C. All plates were rolled using a breakdown bar thickness of three times the finished plate thickness. After roughing, the breakdown bars were held to achieve a surface control temperature below 950°C, and were finished using mill-limited drafts of 10 to 15 percent reduction per pass. The plates were rolled to finish above this chemistry's estimated $Ar_3$ temperature (755°C) to avoid rolling in the austenite-ferrite phase regime. Immediately following rolling all plates were stack cooled below 400°C to promote hydrogen removal to prevent flaking.

## Plate Microstructure, Strength and Toughness

### i) Microstructure

Full thickness, longitudinal metallographic samples were taken from the quarter-width position of each plate. After polishing and etching, the ferrite grain size and volume fraction of ferrite were measured at several positions through the plate thickness using a QTM 720 image analyzer.

The plate microstructure at all thicknesses was polygonal ferrite and pearlite. Representative microstructures from several plate thicknesses are shown in figure 1. The ferrite grain size was dependent on both the plate gauge and the position through the plate thickness. As shown in figure 2, a 7 μm ferrite grain size was achieved in the 19 mm plate and it was maintained below 10 μm in gauges up to 30 mm, however it increased significantly in heavier plate up to 16 μm in the 51 mm plate. The volume fraction of pearlite ranged from ≈14 percent in the lighter thicknesses down to ≈11 percent in the heaviest plate.

ii) Strength

Full-thickness plate tensile tests were taken from the mid-width plate position for thicknesses up to and including 40 mm. For heavier gauges, 12 mm diameter round tensiles were machined from the plate quarter-thickness position.

Both the plate yield strength and UTS decreased significantly with increased plate gauge (figure 3). The minimum yield strength requirement was achieved in plate thicknesses up to 38 mm, whereas the minimum UTS requirement was met in gauges up to 32 mm.

To rationalize the loss of strengthening with increased thickness, the effects of the different strengthening mechanisms on yield strength were calculated using previously developed relationships for ferrite-pearlite steels. Figure 4 illustrates the significant loss in strength due to grain refinement with increased gauge. For 19 mm plate, approximately 210 MPa in strength is related to grain size; this is reduced to only 140 MPa in 51 mm plate. Similarly, the estimated contribution from precipitation strengthening is reduced by ≈20 MPa with increased thicknesses. This analysis demonstrates that a ferrite grain size of less than ≈11 μm is required to consistently meet the Grade 350 strength level with this chemistry. As will be shown in a subsequent section, it should be possible to achieve this with modified controlled rolling procedures. Alternatively, additional precipitation strengthening would be beneficial for meeting both the yield and UTS levels. However, this latter approach is not attractive because of the detrimental effect of particle strengthening on plate Charpy transition temperature and the potential embrittling effect of certain microalloys on HAZ toughness.

### iii) Bend Tests

Bend tests were conducted on full thickness plate samples from each thickness to establish the potential for either surface or centerline cracking during forming. No cracking was observed on any sample (figure 5).

### iv) Charpy Toughness

Transverse, full size Charpy V-notch transitions were determined from the quarter-width position of each plate. For thicknesses up to 25 mm, the tests were taken 2 mm below the plate surface. For 30 and 32 mm plate additional tests were taken from the plate mid-thickness positions, whereas for heavier plate, tests were taken from the quarter and mid-thickness positions.

All tests were done using the ISO rather than the ASTM Charpy striker geometry. The very high ductility of this high cleanliness, relatively low strength steel was such that the Charpy shelf energy of all tests exceeded the capacity of our Charpy impact machines (≈350 J) even for transverse orientation tests. Extensive testing by the JISI[9] and The Welding Institute,[10] has demonstrated that the ISO striker gives significantly lower shelf energy than the ASTM striker. Preliminary testing of several trial plates using both geometries of striker confirmed this effect for Charpy energies above ≈135 J (ASTM), as shown in figure 6. No difference in fracture appearance transition temperature was observed using the two striker geometries.

Representative plots of the Charpy energy and shear transition curves are given in figure 7. The Charpy test data are summarized in Table V in terms of the 40 J, 68 J and 50 percent shear transition temperatures for each plate thickness and test position. It was notable that in the region of the shear transition temperature, there was considerable scatter in the impact energy absorption. To give a conservative estimate of the toughness of this steel, all transition data reported in Table V have been taken from lower bound energy results. Moreover, as anticipated from the increase in ferrite grain size, there was a significant increase in the impact transition temperatures between the surface and core positions and with increased thickness.

The transition data can be used to give estimates of the minimum design temperature to which the steel could be applied. As mentioned previously, there is yet no consensus on the Charpy energy requirements for Canadian offshore structures. This is being addressed by the CSA Task Force on Steel for Fixed Offshore Structures. Several approaches[4] are used by the different Classification Societies to account for the effects of yield stress, plate thickness, test direction and the structural importance and loading of the member. For the range of thickness with which we are concerned in the present study (20 to 50 mm), these approaches would suggest that the actual Charpy impact test temperature should be as much as 20°C and 40°C below the design temperature for primary and special applications, respectively. Accordingly, the controlled rolled strand cast plate could be applied to -30°C design temperature at thicknesses up to ≈38 mm and 32 mm for primary and special applications, respectively. At -50°C design temperature it could be used for primary structures in thicknesses up to 32 mm.

### iv) Nil Ductility Tests

To further evaluate the brittle fracture resistance of the controlled rolled plate, nil-ductility temperature (NDT) tests were conducted on selected plate thicknesses in accordance with ASTM E208. All tests were done with the P-2 specimen (19 x 127 x 51 mm), using crack starter welds located on both the as-rolled plate surface and sub-surface locations, to assess the effect of through-thickness ferrite grain size differences on fracture resistance.

The NDT results were consistent with the Charpy tests and illustrated the reduction in fracture resistance with increased plate thicknesses and between plate surface and core. Table VI shows the NDTs determined together with the Charpy 40 J transition temperatures. Note that there is fairly good agreement between the two measures of fracture initiation temperature.

NDT can be used together with Pellini's fracture analysis diagram[11] (FAD) to provide guidelines for low temperature steel usage. Limiting the service temperature to slightly above the NDT provides fracture initiation resistance for most types of structures subject to dynamic loading conditions. For welded steel ship hulls it is recommended that all steels used for primary load carrying plate members in the main stress regions of ships have a maximum NDT 18°C below the minimum service temperature.[12] Using this criterion, this steel is adequate for East Coast (-30°C) applications at thicknesses up to 38 mm, and for Arctic (-50°C) up to 25 mm.

## Further Development of Controlled Rolling

This preliminary trial has demonstrated that controlled rolled plate can meet tentative strength and impact toughness requirements for design temperatures down to -30°C in plate thicknesses up to ≈32 mm. Above this gauge, the trial plate failed to meet both strength and mid-thickness Charpy impact requirements. Although modification of the chemistry could be used to ensure improved strength, improved ferrite grain refinement is the only factor which can be used to meet both the strength and impact requirements in the heavier thicknesses. Figure 8 shows the significant positive effect of grain refinement, and the deleterious effects of precipitation strengthening and pearlite fraction on FATT. It is noteworthy that estimates of the 50 percent FATT based on the microstuctural and strengthening factors[13] agree fairly well with the measured results, except at the mid-thickness position of heavier gauges (figure 9). The reason for this discrepancy is not known, however, it could be related to bainite formation in the core due to center segregation or perhaps increases in the grain boundary carbide content.[14] Further detailed metallography and testing are required to rationalize this behavior.

For controlled rolled plate the main factor that controls the transformed ferrite grain size is the total reduction below the so-called austenite recrystallization stop temperature. Increased deformation of non-recrystallized austenite increases the nucleation sites for ferrite transformation at both the austenite grain boundaries and at deformation bands in the interior of the austenite grain.[15,16] Although very high total deformations can be achieved in relatively light plate (<20 mm), in heavier plate it becomes increasingly difficult to achieve equivalent reductions at low rolling temperatures. This is further complicated by the extreme surface to core temperature difference which develops in the heavy slabs during roughing and holding prior to finishing.

To appreciate the effect of this temperature gradient on grain refinement during controlled rolling, finite difference temperature modeling was done for several plate thicknesses and holding times between roughing and finishing. Figure 10 shows the calculated through-thickness temperature distributions during the rolling of 25 and 38 mm plate. Very early in the rolling sequence, a large surface to core differential (≈250°C) is developed. As the slab thickness is reduced this differential decreases, but is still more than 150°C for a 115 mm transfer bar and at least 85°C for a 75 mm transfer bar. When starting to finish roll at ≈950°C using surface temperature measurements for control, it takes several passes before the core temperature is below the estimated austenite recrystallization stop temperature (≈900°C). This situation is considerably worse with heavier transfer bars, and is further complicated by the uncertainty in the actual recrystallization stop temperature for this chemistry. Thus there is a significant gradient in the total amount cold worked austenite developed between the surface and core, which results in the observed gradient in ferrite grain size, particularly in heavier plate.

Further rolling trials are planned using this base chemistry to evaluate the effect of improved controlled rolling practice on the ferrite grain refinement that can be achieved in thicknesses up to 50 mm. Additional factors that will be studied to improve grain refinement are the starting slab thickness and the reheat temperature. Laboratory studies[17,18] have demonstrated the effect of total reduction during roughing on austenite grain refinement at high temperatures. As the plate and corresponding breakdown bar thickness increase, the total strain during roughing decreases. This can be partially offset by using the heaviest possible slab thickness consistent with the finished plate size. For LEW strand cast slabs, the thickness can be increased to 240 mm. A low reheating temperature is beneficial because it reduces the hold time between roughing and finishing in which austenite grain coarsening can occur.[19] Morever, reheating below the austenite grain coarsening temperature can restrict the starting austenite grain size to ≈20 μm in Ti microalloyed steels.

## Lamellar Tearing Resistance

It is anticipated that a small proportion of the plate tonnage required for both platforms and ships will require lamellar tearing resistance. This defect occurs most commonly in highly restrained joints such as T-butt or fillet welds in which there is significant through-thickness strains developed by weld metal shrinkage. Tearing appears as the separation of the base metal along planes parallel to the rolling plane and is principally caused by decohesion and shear linkage of individual inclusions or clusters of inclusions (figure 11). A steel's susceptibility to tearing is primarily governed by its inclusion content, however, other properties including its susceptibility to hydrogen induced cold cracking, its yield strength level, and sensitivity to strain aging and hydrogen embrittlement may be important in governing the extent of cracking.

Although tearing can be partially controlled by proper design and fabrication techniques, the relatively high cost of repairing these defects together with the cost penalties associated with fabrication delays have created a demand for lamellar tearing resistant plate. The main feature of these steels is high cleanliness. Several workers[21,22] have demonstrated the strong correlation between through-thickness ductility and the projected total length of inclusions. In particular, inclusions which are greater than ≈50 μm in length appear to have a dominant effect on Z direction ductility. In fully killed steels these are primarily Type II manganese sulfides and large reoxidation oxides.

The tearing resistance of the trial heat was evaluated using both through-thickness tensile tests and a high restraint welding test.

### i) Through-Thickness Tensile Tests

Through-thickness tensile tests were taken from each plate at selected positions across the plate width. To locate the test positions, a full width strip from each plate was ultrasonically C-scanned to detect any gross oxide-type inclusions or discontinuities. The ultrasonic system was calibrated for each plate thickness to detect a 1.2 mm diameter flat bottomed hole. In most instances no reflectors were found, however, indications were recorded from quarter-point inclusions in some plates. A typical C-scan recording from an area with these inclusions is shown in figure 12. A total of six tensiles were tested from each plate, two from clean areas near the plate mid-width, two from clean areas near the plate edge and, where possible, two from an area showing quarter-point inclusions.

All samples were prepared by trepanning 12 mm diameter full thickness cylinders from the base plate and friction welding 12 mm diameter prolongations onto the test pieces. The tensile tests were then machined to 10 mm diameter with the radius reduction initiating at the original plate rolled surface. This procedure is in agreement with that recommended by the ISO/TC17/SC 3N 415 and the ASTM A770 M-84 draft proposals except that they recommend using 6 mm diameter specimens for plates less than 25 mm thick to avoid the effect of sample constraint on through-thickness ductility.

The strand cast plate showed excellent through-thickness ductility at all test positions over the entire gauge range (figure 13). Except for one test in 25 mm plate that gave 21.6 percent reduction of area ($RA_Z$) all tests had minimum individual $RA_Z$s of over 25 percent and mean $RA_Z$s of over 55.2 percent. Most tests showed cup-and-cone type fracture which generally occurred near the plate quarter-thickness (figure 14). Tests taken at ultrasonic indications were not consistently the lowest results. Some tests showed reduced ductility related to gross alumina stringers on the fracture surface (figure 15). Other low $RA_Z$ values corresponded to Type II MnS inclusions and columbium oxides (figure 16).

$RA_Z$ values are being increasingly used by classification societies to define and approve Z-grade steels for both ships and offshore structures. The $RA_Z$ requirements are defined in up to three categories of Z-plate which are classified in terms of the mean and minimum individual values of $RA_Z$, as shown in Table VII. The selection of Z-grade is dependent on the importance of the component to the overall integrity of the structure and the level of restraint at the weld connection. Based on these criteria, the low sulfur LEW steel could be approved for the most stringent application, Z35.

### ii) Window Tests

To further evaluate the susceptibility of the trial heat to tearing, window tests were conducted on test coupons from both 32 and 44 mm plate. The tests were done according to the procedure described by Kanazawa.[23] Figure 17 shows the weld preparation and an example of the welded test. To maintain constant restraint, the test plates were milled to 20 mm thickness, leaving one rolled surface intact. The rigid restraining plate was prepared from a controlled rolled 30 mm trial plate. To evaluate the effect of quarter-point inclusions on tearing susceptibility, the test plates were machined from locations showing quarter-point inclusion during C-scanning. The test plates were machined to ensure that the representative inclusions were located immediately below the welds.

The tests were made using fresh 3.2 mm E7018 electrodes which had been dried at 250°C for one hour. The weld heat input was maintained at 1.7 kJ/mm for all passes, and the preheating and interpass temperatures were controlled to 150°C and 75°C, respectively using a contact thermocouple. The welds were made in the sequence shown in figure 17 and were held for at least 48 hours prior to sectioning. Each weld was sectioned at three locations in the test plate. The test positions were located to ensure that the test planes contained quarter point inclusions below the welds. Each section was ground and polished and metallographically examined for cracking at magnifications up to

500 power in both the etched and unetched condtion. No cracking was observed in any test section (figure 18).

**Weldabilty**

A major consideration in the development of steels for welded fabrication is their susceptibility to HAZ hydrogen induced cold cracking. Although welding guidelines have been developed to prevent cold cracking, there is a significant cost advantage to be obtained by reducing or eliminating preheat requirements or perhaps allowing high hydrogen content consumables. The resistance to cold cracking has been correlated with the steel chemistry through various carbon equivalent formulae, which in effect give a measure of the steel's hardenability during fairly rapid cooling from austenite. The two most commonly used formulae are:

$$CE = C + \frac{Mn}{6} + \frac{Cr + Mo + V}{5} + \frac{Ni + Cu}{15} \quad (\%)$$

$$P_{CM} = C + \frac{Si}{30} + \frac{Mn}{20} + \frac{Cu}{20} + \frac{Ni}{60} + \frac{Cr}{20} + \frac{Mo}{15} + \frac{V}{10} + 5B \quad (\%)$$

The CE (or IIW) formula was developed for relatively high carbon steels (>0.18 percent) and is used in the Welding Institute approach to predict safe welding procedures based primarily on a maximum HAZ hardness criteria.[24] The $P_{CM}$ formula developed by Ito and Bessyo[25] is used extensively in Japan, and is more applicable to modern low carbon (<0.17 percent C) chemistries particulary for butt-welds. The CE for the trial heat was 0.38 which is slightly lower than that of more conventional normalized type steels of the same strength level. Moreover, it is generally recognized that for low carbon steels, a higher value of CE should be permitted. The $P_{CM}$ value, 0.17, is significantly lower than that of conventional Grade 350 plate.

Two laboratory tests were used to evaluate the steel's resistance to cold cracking:

- y-groove test, and
- controlled thermal severity (CTS) test.

### i) Y-groove Test

Y-groove cracking tests (figure 19) were performed on 25 mm plate in accordance with the procedure outlined in JIS Z 3158, with the exception that the percentage of cracking was determined by heat tinting and back-bending rather than metallographic sectioning. The tests were welded using both E7010 and E7018 SMAW 4 mm diameter electrodes to achieve two levels of hydrogen. The E7010 electrodes were used from a fresh canister and were protected from moisture over the period of test welding. Similarly, the E7018 electrodes were fresh and were baked at 250°C for one hour immediately prior to usage. The hydrogen content of each electrode type was measured in accordance with ISO 3690-1976. The hydrogen content of the deposited melt were 74.3 mL/100 g and 7.6 mL/100 g for the E7010 and E7018 electrodes, respectively. All tests were welded in the flat position with a nominal heat input of 1.7 kJ/mm. The preheat temperature was varied btween 0 and 100°C to define the no-crack condition. The test results are summarized in Table VIII. For the low hydrogen electrode, no cracking was observed at 23°C, whereas for the high hydrogen electrode a preheat of 100°C was required.

### ii) CTS Test

CTS tests were done on 25 mm plate using the test procedure recommended by The Welding Institute.[26] The test specimens (figure 20) contained a 1.6 mm root gap to simulate the fit-up found in normal fabrication, which increases the risk of cracking. The test welds were deposited in the flat position using 4 mm diameter E7010 and pre-dried E7018 electrodes with a nominal heat input of 1.7 kJ/mm. To reproduce the cooling conditions normally experienced in large welded structures, the end of the CTS test was immersed in cold water to a depth of 30 mm immediately after welding. To ensure sufficient time for cracking, at least 72 hours was allowed to elapse between the welding of the first and second test welds, and also between completion of the second weld and sectioning.

Cracking was measured on six test sections along each weld. Each section was mounted, polished and etched in nital prior to metallographic examination at magnifications up to 500X. The weld and HAZ hardness were measured in both the vertical and horizontal legs using HV5 load.

No cracking was observed in either the weld metal or HAZ using E7018 electrodes at +23°C (Table IX). However, a preheat temperature of +50°C was required to eliminate cracking with the cellulosic E7010 electrodes. The maximum HAZ hardness was 293 HV5.

Both the Y-groove cracking and CTS tests demonstrate that this chemistry is weldable at +23°C without preheat using low hydrogen electrodes. It is important to recognize that the actual preheat requirement predicted by both WI and Japanese approaches is dependent on the plate thickness. The Ito-Bessyo approach use the following equation to predict preheat temperature (T) in Y-groove type joints.

$$T\ (^\circ C) = 1440\ (P_{CM} + t/600 + H/60) - 382$$

where: t = plate thickness (mm)

H* = diffusible hydrogen in deposited weld metal (cc/100 g)

* determined by JIS method, $H_{JIS} = 0.67\ H_{IIW} - 0.8$

This predicts a preheat of 20°C for the conditions used in our tests. For 40 mm plate, the preheat requirement would be increased by 36°C up to ≈50°C.

It is of interest to note that low sulfur steels have been shown to have increased susceptibility to cold cracking.[27] This has been related to both increased hardenability and reduced sites for hydrogen trapping at low inclusion levels. The good agreement between predicted and actual cracking behavior for this steel would suggest that its low sulfur content has not adversely affected its weldability.

In actual construction, preheat requirements may be somewhat different than found in the laboratory tests. In particular the Y-groove test tends to give a higher restraint intensity, and thus tends to give a more conservative (higher) preheat requirement than necessary in actual fabrication. However, this assumes other factors, such as weld electrode hydrogen level and heat input, which have significant effects on cracking resistance will not vary in field fabrication. Moreover, preheating requirements may be dictated by the need to prevent transverse weld metal or chevron cracking.

### HAZ Toughness

The fracture resistance of welded structures is controlled primarily, not by the base plate, but rather the weld zone toughness. In the development of new steels for critical applications, attention must be given to the deterioration of toughness on the weld HAZ. Although this is typically a very narrow region (often less than a few hundred microns) it is a relatively low toughness region and a likely site for crack initiation from either fusion line defects or HAZ cracks. Even though the HAZ can be surrounded by metal and base plate with excellent fracture initiation resistance, they may not be capable of arresting fast running cracks. Several catastrophic failures have been initiated in weld HAZs,[28] and the toughness of this region is a major concern for selection of offshore structural steels.

The steels used for North Sea offshore construction have generally been considered to have adequate HAZ toughness for North Sea design temperatures. Extensive CTOD testing of BS4360 type steels as part of the UK Offshore Steels Research Program[29] in the mid-70s concluded that there was no HAZ fracture problem in the as-welded condition with heat inputs between 1.5 and 4.0 kJ/mm in thickness of 50 to 82 mm. This finding was supported by additional work by Eide.[30] More recently, however, concern has been expressed about the low HAZ toughness of new low carbon, microalloy chemistries. This is potentially related to modification of the HAZ microstructure or excess precipitation strengthening by the microalloy additions. Unfortunately, detailed data on what steels have given problems are not available. The extent of this problem will hopefully be defined by the current group-sponsored Welding Institute program.[31]

To evaluate the HAZ toughness of the trial heat, HAZ CTOD and Charpy tests on SAW welds, as well as CTOD tests on Gleeble simulated HAZ microstructures were performed.

### i) Submerged Arc Weld HAZ Toughness

Test welds were prepared in 19 mm and 38 mm plates using both 2 kJ/mm and 4 kJ/mm heat input. To obtain a relatively planar HAZ for fracture testing, all welds were produced using an inclined plate weld procedure (figure 21). The test welds (t x 400 x 1000 mm) were made from plate coupons oriented parallel to the plate rolling direction. The weld consumables used were a proprietary Stelco 80 wire and ESAB 10.71 flux, which had previously been shown to give good low temperature toughness in similar heat input large diameter pipe seam welds. The root pass was made in the flat position, and the filler and capping passes were made with the test inclined at 22°. All welds were made with a nominal preheat temperature and interpass temperature of 150°C.

Representative macrographs of the weld cross section produced in each plate thickness are shown in figure 22. Generally, the 38 mm welds gave more planar HAZs than the 19 mm welds. Significant butterflying was encountered on several of the 38 mm plate welds. To overcome the effects of distortion and the slight rotation of the HAZ front relative to the rolling plane it was necessary to reduce the thickness of the CTOD tests taken from these welds to 32 mm.

Detailed metallographic examination of the weld HAZ cross sections was done to determine the extent of the HAZ grain coarsened region. For the 2 kJ/mm heat input in the 38 mm plate, the overlap of the weld beads was such that most of HAZ structure region primarily contained "normalized" structure (figure 23a). At 4 kJ/mm, the bead size was sufficient to produce ≈20 percent coarse grained structure (figure 23b). For the 19 mm tests, significant grain coarsened HAZs were produced at both heat inputs.

For multipass welds several different microstructures are produced in the HAZ because of the thermal cycles of subsequent passes. The main discrete HAZ structures are (figure 24):

- coarse grained - reheated above the grain coarsening temperature,
- normalized - reheated between the $Ar_3$ and the grain coarsening temperatures,
- intercritical - reheated between the $Ar_1$ and $Ar_3$ temperature, and
- sub-critical - reheated below the $Ar_1$.

These microstructural regions were identified in each weld and hardness tests done. Because of the relatively small size of several of these zones, a HV 0.1 microhardness test was used. This allowed the hardness impressions to be located entirely within each region and resulted in slightly higher hardnesses (≈20 HV) than measured using the more commonly used 5 or 10 kg loads. Table X summarizes the hardness results. The maximum hardness was generally found in the intercritical HAZ structure. In the coarse grain region developed by the capping pass, the maximum hardness ranged from 256 to 264 HV 0.1, whereas it was between 255 and 278 HV 0.1 in the intercritical region. The normalized structure was significantly softer at between 222 and 233 HV 0.1.

Up to 15 CTOD tests were prepared from each weld to the preferred B x 2B specimen geometry. Prior to final machining, all rough sample coupons were etched to locate the notch position so that it sampled the coarse grain HAZ/fusion line near the mid-thickness. The precrack notches were milled to give a starting a/w of 0.45. Prior to fatigue precracking, the notch root of each test was precompressed by 1.0 percent strain in order to produce a planar fatigue crack front. Fatigue cracking and testing were done in accordance with BS 5762 1979.

The CTOD test results are summarized in figure 25. For the 19 mm plate welds, the 0.25 mm requirement was met at test temperatures down to -60°C and -40°C for the low and high heat input conditions, respectively. For the 38 mm welds, this value was met at temperatures down to -20°C for both heat inputs. It is important to note that these results have ignored one minor "pop-in" that occurred in testing the 38 mm, 2 kJ/mm heat input weld. The CTOD value at the "pop-in" was equivalent to 0.1 mm at -10°C. Subsequent sectioning of the sample test indicated that the cleavage fracture initiated in a coarse grained structure but subsequently arrested. It is not clear from current CTOD procedures whether this result should be considered as the critical event for design purposes. Further CTOD testing is required to resolve whether this result is significant for this steel chemistry.

Several of the broken CTOD specimens were subsequently sectioned, as shown in figure 26, to determine the position of both the fatigue crack notch relative to the weld fusion line and the microstructure at the crack initiation zone. Figure 27 shows a typical macrograph taken at the fracture initiation position in a 19 mm weld oriented parallel to the plate rolling plane. Similarly, figure 28 shows sections at the fracture initiation point in 38 mm welds, oriented through the weld thickness. At 2 kJ/mm heat input, the structure was essentially normalized (figure 28); whereas at 4 kJ/mm fracture initiated in both the intercritical and coarse grained structures.

Full size Charpy-V-notch transitions were also tested on each plate weld. All Charpies were taken from test positions near the weld root and were oriented so that the maximum length coarse-grained structure would be sampled. It was felt that this was more valid than simply specifying a test position at a fixed distance from the plate surface for which the HAZ structure could vary significantly with weld heat input and plate thickness. All Charpies were rough machined and etched prior to notching to position the notch root on the weld fusion line. Because of both fusion line curvature and bead overlap it was not possible to sample only the weld fusion line in most tests. In these cases the notch position was adjusted so as to sample both fusion line and HAZ structures rather than weld metal.

The Charpy transition curves are shown in figure 29. Note that these tests were done using the ASTM rather than the ISO striker used for the base plate tests. Both the 2 and 4 kJ/mm heat input welds in the 19 mm plate showed Charpy transitions similar to that of the base plate. The 40 J transition temperature was less than -90°C for the low heat input and at -80°C for the high heat input. The low heat input weld in the 38 mm plate gave a 40 J transition temperature of ≈-70°C; however, in the high heat input weld it was ≈-50°C.

### ii) Simulated HAZ Toughness

As already mentioned, there is considerable difficulty in developing good CTOD toughness data on HAZ structures in heavy weldments because of first, the difficulty in producing a near planar HAZ that provides the HAZ structures found in actual fabrication and secondly, the problem of locating the CTOD fatigue crack notch exactly in the most brittle region. As an alternative to the large scale real weld test, the testing of Gleeble simulated HAZ microstructures has been used to develop comparative fracture data on different steel chemistries and different microstructural regions within the multipass HAZ. It is recognized that there is some question about the ability of the simulation to exactly reproduce the HAZ structure; however, previous testing[8] and the work done in this project suggest that very similar HAZ microstructures and microhardness can be produced provided the Gleeble thermal cycle reproduces that of the actual weldment. The relatively small size of the Gleeble test specimen develops significantly reduced constraint compared with actual structures, and thus the fracture data is not suitable for fracture resistance calculations in more highly constrained structures.

Gleeble simulated HAZ samples were produced in 10 x 10 x 85 mm test coupons taken from the quarter-thickness position of 38 mm plate and oriented transverse to the plate rolling direction. Three of the cycles used (Table XI) were chosen to simulate the single pass, coarse grained HAZ structure for a range of heat inputs between 2 and 5 kJ/mm in ≈30 mm plate preheated to 100°C. The main factors controlled in the thermal cycle were the maximum temperature (1350°C), the time above 1000°C, and the cooling rate between 800 and 500°C ($\Delta T_{800-500}$). The three $\Delta T_{800-500}$ were nominally 20, 35 and 75 seconds. The fourth cycle was designed to simulate the normalized structure produced in a coarse grained HAZ by a subsequent weld bead. The peak temperature of the second cycle was restricted to 1000°C, and the $\Delta T_{800-500}$ was 35 seconds.

The microstructures and hardness of the simulated HAZ were very similar to those of the actual weldments. Figure 30 shows the microstructures produced in both the Gleeble simulations and weldments. The HV 0.1 hardnesses of the simulated structures were 259, 252 and 241 for the 20, 30, and 75 second $\Delta T_{800-500}$, and 231 for the simulated normalized structure. These agree well with the hardnesses shown in Table X except for the hardness of the 75 second $\Delta T_{800-500}$ which is significantly lower than that of the actual weldment.

At a $\Delta T_{800-500}$ of 20 seconds the structure contained little or no proeutectoid ferrite, and was similar to a low carbon upper bainite structure with lath ferrite and martensite retained austenite (M/A) particles on the lath boundaries. At a $\Delta T_{800-500}$ of 35 seconds the structure was similar, except that there was a small amount of ferrite nucleated at the prior austenite boundaries, and a greater percentage of the lath boundary particles were cementite. At the $\Delta T_{800-500}$ of 75 seconds, the structure changed significantly, containing more ferrite at the prior austenite boundaries a coarser lath ferrite structure and an increased percentage of large cementite particles. It is notable that the prior austenite grain size of this titanium treated steel was significantly finer than that of another non-titanium trial steel tested concurrently, and that the grain size did not coarsen significantly with increased cycle time above 1000°C. The mean grain sizes were 53, 60 and 53 microns for the 20, 35 and 75 second $\Delta T_{800-500}$, respectively. Note that the grain size developed in the Gleeble simulations is smaller than that developed at the fusion line of the actual weldments. Detailed HAZ grain size measurements done on this chemistry at the Welding Institute of Canada[32] have shown that the fusion line austenite grain size increases from $\approx 65$ μm to $\approx 110$ μm as the heat input increases from 3 to 6 kJ/mm. The smaller grain size of the simulated HAZ structures reflects the lower peak temperature used in the Gleeble thermal cycle compared with that at the fusion line. It is important to recognize that in the titanium treated steels, the grain coarsening is restricted to a narrow zone within $\approx 200$ μm of the weld fusion line. Hence the toughness results on the Gleeble tests are representative of the bulk of the transformed HAZ, but probably not the worst test position (at the weld fusion line), particularly for higher heat input welds (>3 kJ/mm).

Tensile tests taken from the Gleeble samples confirmed the general softening of the structure with decreased cooling rate (Table XII). Note that all the single pass simulations showed continuous-stress strain behavior which is believed to result from the significant percentage of M/A in the structure.

Fifteen CTOD (13 x 13) tests were prepared from each thermal cycle. The tests were through-thickness notched, and were fatigue precracked to give a nominal a/w of 0.35. Fatigue precracking and testing were done in accordance with BS 5762 1979. Triplicate CTODs were done at each temperature over a range of temperature between -70°C and +50°C. The lowest CTOD results at each temperature were used to define the CTOD transition curves shown in figure 31. Both the 20 and 35 second thermal cycles gave 0.20 mm CTOD transition temperatures of ≈-40°C, which is consistent with their similar prior austenite grain sizes, structures and strength levels. The 75 second $\Delta T_{800-500}$ condition gave a significantly higher 0.20 mm CTOD, ≈0°C, even though it had a significantly lower strength. This suggests that the lower strength structure containing an increased fraction of proeutectoid ferrite and coarser bainite ferrite laths and cementite particles has a lower cleavage fracture stress than the structure developed at higher cooling rates. The normalized cycle gave a 0.2 mm transition temperature of ≈-40°C similar to that measured for the 20 and 35 second coarse grained austenite thermal cycles.

The simulated HAZ CTOD results indicate that this steel has marginal resistance to cleavage fracture initiation for East Coast design temperature (-30°C), and that welding heat input should be limited to achieve the toughest HAZ structure, corresponding to a $\Delta T_{800-500}$ between 20 and 35 seconds.

The Gleeble simulated HAZ results are in fairly good agreement with the toughness data derived from the actual weldments. The deterioration in 0.25 mm transition temperature in the 19 mm plate with increased heat input was ≈20°C, which is similar to that found on the Gleeble tests ongoing between 20 or 35 seconds and 75 sec $\Delta T_{800-500}$. The comparison of absolute CTOD transition temperatures is complicated by the different levels of constraint, the finer prior austenite grain size of the Gleeble microstructure, and the differences in the uniformity of structure sampled by the notch root. The higher CTOD transition temperature measured in the 38 mm plate may be related primarily to the increased sample constraint, however, more testing is required to fully rationalize the difference in the CTOD toughness measured on the actual and Gleeble simulated HAZ structures.

Additional HAZ CTOD testing has been done at The Welding Institute of Canada using bead-on-plate welds with nominal heat inputs between 3 and 6 kJ/mm.[32] Tests were done using 10 x 10 x 50 mm CTODs with the fatigue crack grown in the through-thickness direction and the notch tip located in the coarse grained HAZ.

The a/w was 0.5 which, because of the reduced ligament, gave lower upper shelf CTOD values than measured in this study; consequently, a 0.1 mm CTOD was used to compare the effect of heat input. The 0.1 mm CTOD values were achieved at -61, -18, +5, and -45°C for the 3, 4, 5, and 6 kJ/mm heat inputs, respectively. The 3 and 4 kJ/mm values agree very well with the 0.1 mm CTOD temperatures obtained from the 20 or 35 second and the 75 second $\Delta T_{800-500}$ thermal cycles, respectively. These results confirm that relatively good HAZ toughness can be achieved with this chemistry by limiting the heat input below ≈3 kJ/mm, and that adequate HAZ toughness can be achieved for design temperatures down to ≈-30°C. However, the HAZ toughness tends to deteriorate rapidly at higher heat inputs.

## Conclusions

1. The C-Mn-Ni-Cr-V-Cb-Ti chemistry can meet Grade 350 strength and toughness requirements for -30°C design temperature in thicknesses up to ≈32 mm with a moderate controlled rolling practice. The controlled rolled thickness to which this chemistry can be applied could be extended by ensuring that the core of the slab is below the austenite recrystallization stop temperature during the entire controlled rolling finishing practice.

2. The low sulfur strand cast steel has excellent resistance to the lamellar tearing and meets the most stringent through-thickness ductility Z-plate requirement.

3. The low carbon equivalent chemistry has excellent resistance to HAZ hydrogen induced cold cracking, and does not require preheat with low hydrogen E7018 electrodes at 25 mm thickness.

4. The HAZ toughness of this chemistry is dependent on the weld thickness and heat input. The weld heat input should be limited to $\leq 3$ kJ/mm to achieve adequate CTOD and Charpy toughness for design temperatures down to -30°C.

# ACKNOWLEDGMENTS

Stelco Inc. wishes to acknowledge the funding of the Department of Supply and Services and the support of CANMET for the research. In particular the author would like to thank Dr. J. Bowker of CANMET for providing the Gleeble test samples and the personnel in the Stelco Operating and Metallurgical, and particularly the R&D Department who have made vital contributions to this work.

## REFERENCES

1. Chinook Fuel Innovation Limited, Survey of Plate Steel in Offshore Structures and Arctic Vessels, May, 1982.

2. Department of Energy, Mines and Resources, Request for Proposal, Research into the Development and Fabrication of Steels for Use in the Construction of Offshore Structures and Arctic Vessels, July, 1982.

3. Stelco R&D Report 820108, Development of Grade 350 Structural Steel for Offshore Structures and Arctic Vessel.

4. Det Norske Veritas, Review of Steels used in the Construction of Offshore Structures, April, 1982.

5. Fenco Consultants, A Review of Steel Properties at Low Temperatures, December, 1980.

6. S. Kanazawa et al, Development of New Steels for High Heat Input Welding, IIW Doc IX-952-76.

7. Y. Kasamatsu et al, Tetsu-to-Hagane, Vol 65, No. 8, (1979), pp 1232-1241.

8. D. B. McCutcheon et al, Proc Micon '82, Optimization of Processing, Properties and Service Performance Through Microstructural Control, Houston, 1982, pp 227-255.

9. Investigation of the Effects on Charpy Impact Characteristics by Shape of Pendulum Striking Edge, Mechanical Testing Subcommittee of the Joint Research Society of ISIJ, May, 1984.

10. O. L. Towers, Metal Construction, 1983, 15 (11), pp 682-686.

11. W. S. Pellini, 1971 AWS Adams Lecture, Principles of Fracture Safe Design, Part I and Part II, Welding Journal Research Supplement, March and April, 1971.

12. S. T. Rolfe, J. M. Barsom, Fracture and Fatigue Control in Structures, Prentice Hall, New Jersey, 1977, p 477.

13. F. B. Pickering, Proc Microalloying '75, Washington, DC, 1975, pp 9-31.

14. B. Mintz et al, Proc, Metals Society Conference, Advances in the Physical Metallurgy and Applications of Steels, 1978, Book 284, pp 222-228.

15. I. Kozasu et al, Proc Microalloying '75, Washington, DC, 1975, pp 120-135.

16. A. Sandberg, W. Roberts, Proc Thermomechanical Processing of Microalloyed Austenite, Pittsburgh, 1981, pp 405-431.

17. D. R. DiMicco, A. T. Davenport, IBID, pp 59-81.

18. K. Hulka, C. M. Vlad, IBID, pp 121-128.

19. T. Tanaka et al, IBID, pp 195-216.

20. J. Sommella, Significance and Control of Lamellar Tearing of Steel Plate in the Shipbuilding Industry, Ship Structure Committee, May, 1979.

21. I. D. Simpson et al, BHP Technical Bulletin, Vol 20, April, 1976, No. 1, pp 30-36.

22. G. Bernard et al, Metals Technology, November, 1975, pp 512-521.

23. S. Kanazawa et al, On the Assessment of the Lamellar Tearing Susceptibility of Steel Plate, IIW Doc IX-040-73.

24. N. Bailey, Welding Journal, April, 1972, pp 169B-177B.

25. Y. Ito and K. Bessyo, IIW Doc IX-631-69.

26. C. Pedder and P. H. M. Hart, 'CTS Testing Procedures, The Present Position, TWI Research Bulletin, 1975, 16 (9), p 264.

27. P. H. M. Hart, The Influence of Steel Cleanliness on HAZ Hydrogen Cracking: The Present Position, IIW Doc IX-1308-84.

28. J. D. Harrison, WHy Does Low Toughness in the HAZ Matter? The Welding Institute Seminar, Coventry, England, 1983.

29. H. G. Pisarski, J. D. Harrison, Fracture Resistance of Steels used in Offshore Structures, European Offshore Steels Research, Nov, 1978, Cambridge, Paper 2.

30. G. H. Eide, Fracture Mechanics for Assessing the Safety Against Brittle Fractures in Offshore Installations, Welding Institute Seminar - COD Fact or Fiction, Sheffield, 1980.

31. Welding Institute Group Sponsored Proposal, Normalized Steels with Improved HAZ Toughness, April, 1983.

32. T. W. Lau, R. B. Lazor, HAZ Toughness of Ti-Bearing Steel, Welding Institute of Canada Report RC 200/1/84.

**Table I: Aim Specifications for Grade 350 Plate**

| | |
|---|---|
| Yield Strength<br>Ultimate Tensile Strength | 350 MPa<br>480 MPa |
| Charpy Energy | 40 J Transverse at<br>ΔT* below design temperature |
| Through-Thickness Ductility | 25% min reduction of area |
| HAZ Toughness | 0.25 mm CTOD at design temperature |

* ΔT dependent on thickness and structural category.

**Table II: Design of Chemistry for LEW Grade 350 Plate**

| Element | Aim | Effect | Restriction |
|---|---|---|---|
| C | 0.07 | • increased pearlite content increases UTS<br>• little effect on yield strength | • 0.09 - 0.014 range gives transverse slab cracking<br>• weldability<br>• increased FATT |
| Mn | 1.40 | • solid solution strengthening<br>• ferrite grain refinement through $Ar_3$ reduction | • centerline segregation<br>• bainite formation (increased FATT) |
| Cb | 0.02 | • ferrite grain refinement by controlled rolling<br>• precipitation strengthening | • promotes low toughness HAZ structures |
| V | 0.07 | • precipitation strengthening | • potential to reduce HAZ toughness |
| Ti | 0.01 | • austenite grain size control during reheating; improved HAZ toughness | • reduced precipitation strengthening<br>• >3.4 Ti/N reduces HAZ toughness |
| Cr | 0.25 | • increased UTS through effect on pearlite transformation<br>• little solid solution strengthening | • bainite formation (increased FATT) |
| Ni | 0.25 | • reduced FATT<br>• little solid solution strengthening | |

Table III: Product Analyses

| C | Mn | P | S | Si | Ni | Cr | V | Cb | Ti | ASA | N |
|---|---|---|---|---|---|---|---|---|---|---|---|
| 0.070 | 1.43 | 0.003 | 0.004 | 0.29 | 0.25 | 0.25 | 0.075 | 0.020 | 0.011 | 0.037 | 0.007 |

Table IV: Plate Production - Controlled Rolling Practice

| Gauge (mm) | Width (mm) | Breakdown Bar Thickness (mm) | % Reduction below Temperature (°C) |  |  |  | Finish Temp (°C) |
|---|---|---|---|---|---|---|---|
|  |  |  | 900 | 870 | 840 | 815 |  |
| 15 | 2438 | 45 | 74.6 | 70.0 | 46.9 | 0 | 800 |
| 19 | 2438 | 57 | 70.1 | 70.1 | 56.0 | 30.1 | 760 |
|  |  |  | 70.6 | 70.6 | 23.4 | 23.4 | 750 |
| 25 | 2438 | 76 | 69.0 | 63.9 | 40.0 | 30.8 | 765 |
| 30 | 2972 | 90 | 68.1 | 57.8 | 30.9 | 30.9 | 760 |
|  |  |  | 68.8 | 57.9 | 40.4 | 21.7 | 750 |
| 32 | 2438 | 95 | 68.0 | 24.5 | 7.7 | 7.7 | 810 |
|  |  |  | 67.8 | 22.6 | 7.7 | 7.7 | 785 |
| 38 | 2438 | 114 | 66.6 | 36.0 | 6.3 | 0 | 840 |
| 44 | 1829 | 133 | 67.6 | 8.3 | 0 | 0 | 860 |
|  |  |  | 25.6 | 5.9 | 0 | 0 | 860 |
| 51 | 1829 | 152 | 0 | 0 | 0 | 0 | 890 |
|  |  |  | 0 | 0 | 0 | 0 | 890 |

Table V: Summary of Transverse Charpy Transition Data

| Gauge (mm) | Position | 40 J TT (°C) | 68 J TT (°C) | 50% FATT (°C) |
|---|---|---|---|---|
| 15 | Sur | -70 | -65 | -55 |
| 19 | Sur | -85 | -80 | -80 |
| 19 | Sur | -95 | -90 | -80 |
| 25 | Sur | -85 | -80 | -70 |
|  | Sur | -85 | -85 | -85 |
| 30 | Sur | <-90 | <-90 | -70 |
|  | Mid | -85 | -80 | -55 |
| 32 | Sur | -85 | -80 | -55 |
|  | Mid | -85 | -80 | -40 |
|  | Mid | -70 | -65 | -55 |
| 38 | 1/4 | -85 | -80 | -50 |
|  | Mid | -55 | -50 | -35 |
| 44 | 1/4 | -55 | -50 | -25 |
|  | Mid | -25 | -10 | - 5 |
|  | 3/4 | -55 | -50 | -40 |
|  | Mid | -35 | -35 | -35 |
| 51 | 1/4 | -65 | -65 | -65 |
|  | Mid | -35 | -35 | -20 |
|  | 1/4 | -65 | -65 | -45 |
|  | Mid | -30 | -25 | -15 |

Table VI: Summary of NDT Data

| Gauge (mm) | Position | NDT (°C) | 40 J TT (°C) |
|---|---|---|---|
| 19 | Surface | -80 | -85 |
| 25 | Subsurface | -55 | -85 |
| 32 | Subsurface | -60 | -85 |
| 38 | Surface | -75 | -85 |
|  | Centerline | -60 | -55 |
| 44 | Centerline | -40 | -25 |
| 51 | Centerline | -45 | -35 |

Table VII: Classification of Z-plate

| Class | Min $RA_Z$ Avg Value* | Min $RA_Z$ Ind Value |
|---|---|---|
| Z-15 | 15% | 10% |
| Z-25 | 25% | 15% |
| Z-35 | 35% | 25% |

* Avg of three tests.

Table VIII: Y-groove Cracking (%)

| Electrode | Deposited Metal Hydrogen (mL/100g) | Preheat (°C) | | | |
|---|---|---|---|---|---|
| | | 0 | 23 | 50 | 100 |
| E7010 | 74.3 | - | 100 | 95 | 0 |
| E7018 | 7.6 | <2 | 0 | 0 | - |

Table IX: CTS Cracking

| Electrode | Deposited Metal Hydrogen (mL/100 g) | Preheat (°C) | | Max HAZ Hardness (HV 5) |
|---|---|---|---|---|
| | | 23 | 50 | |
| E7010 | 74.3 | 3/12 | 0/12 | 293 |
| E7018 | 7.6 | 0/12 | - | 293 |

Table X: Maximum HAZ Hardness (HV 0.1)

| Weld | | Region | | | |
|---|---|---|---|---|---|
| Thickness (mm) | Heat Input (kJ/mm) | Coarse Grain | Normalized | Intercritical | Subcritical |
| 19 | 2 | 256 | 222 | 263 | 249 |
| | 4 | 264 | 233 | 278 | 245 |
| 38 | 2 | 261 | 225 | 257 | NA |
| | 4 | 257 | 225 | 255 | 252 |

Table XI: Gleeble Simulated HAZ Thermal Cycles

| Cycle | Peak Temperature (°C) | Time Above 1000°C (sec) | $\Delta T_{800-500}$ |
|---|---|---|---|
| 1 | 1350 | 8 | 19 |
| 2 | 1350 | 11 | 36 |
| 3 | 1350 | 18 | 75 |
| 4 (i) | 1350 | 11 | 36 |
| (ii) | 1000 | - | 36 |

Table XII: Gleeble Simulated HAZ Tensile Strength

| Cycle | Yield Strength (MPa) | UTS (MPa) |
|---|---|---|
| 1 | 575 | 729 |
| 2 | 542 | 680 |
| 3 | 502 | 647 |
| 4 | 476 | 659 |

Figure 1: Microstructure of Controlled Rolled Plate - 2% Nital Etch (200X)

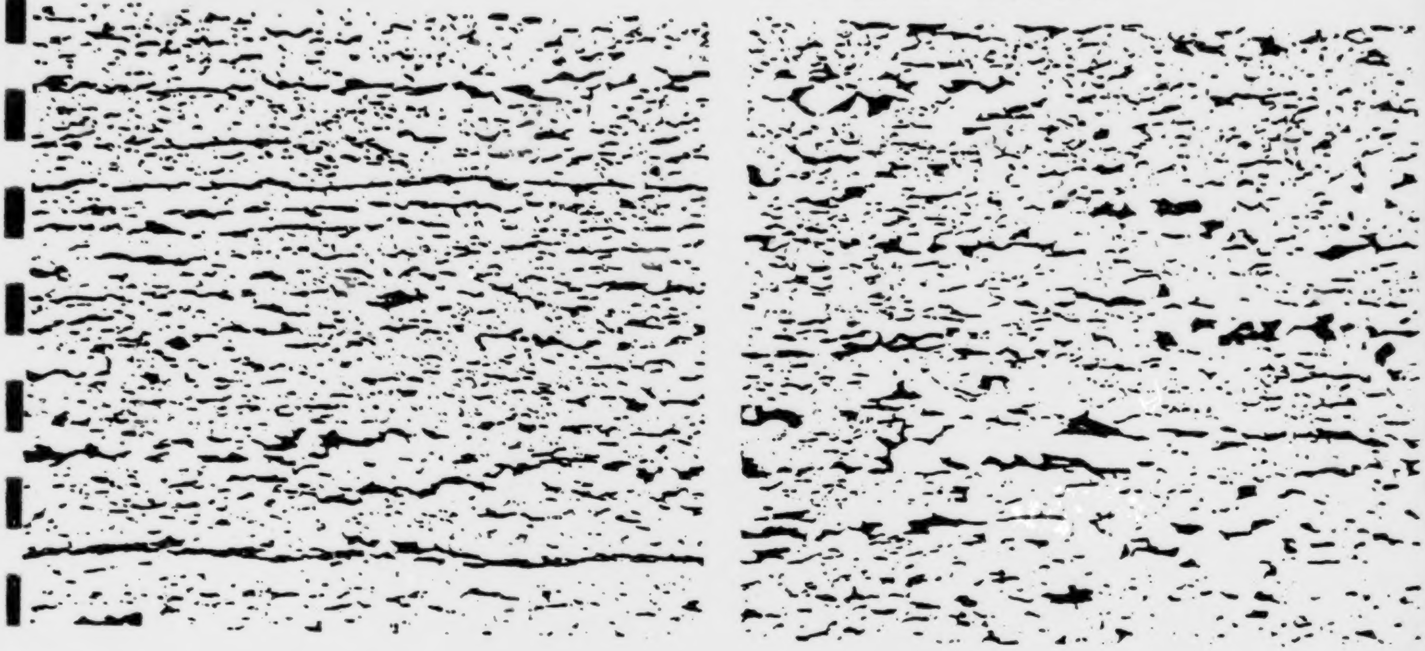

(a) 19 mm, 1/4 Thickness

(b) 30 mm, 1/4 Thickness

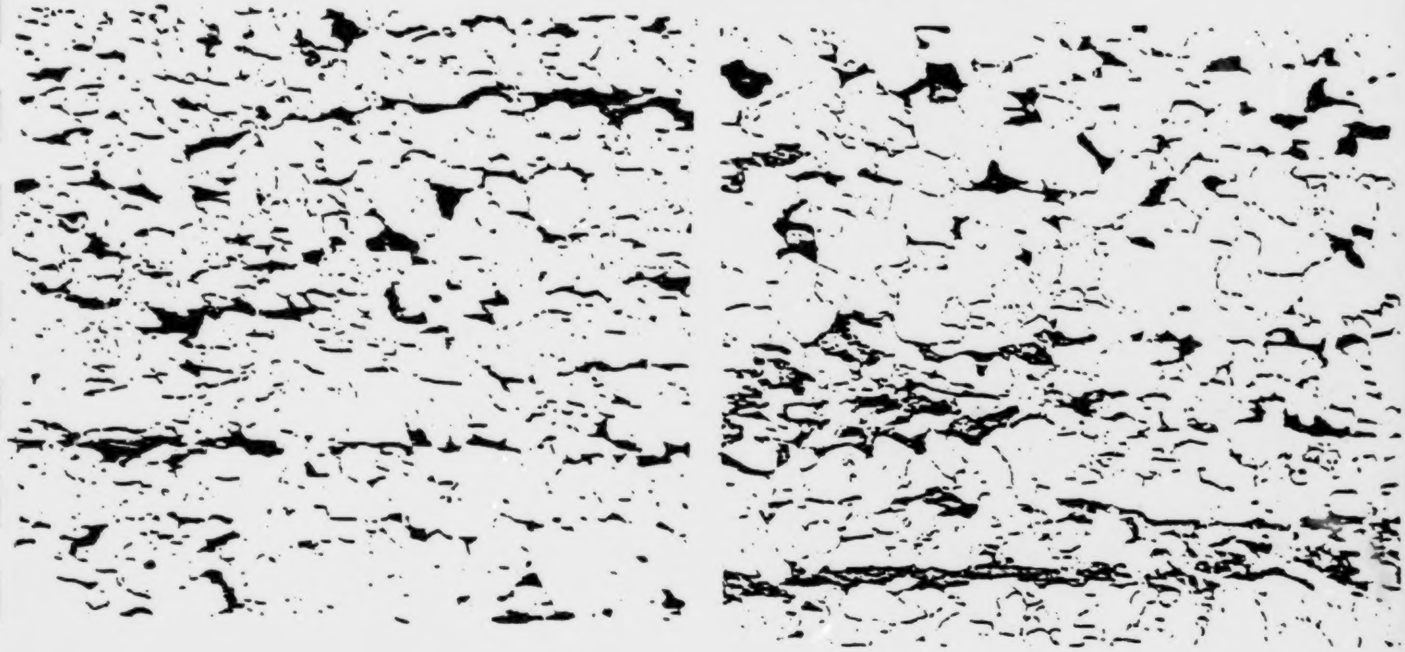

(c) 38 mm, Mid-thickness

(d) 51 mm, Mid-thickness

Figure 2: Through-thickness Ferrite Grain Size Distribution

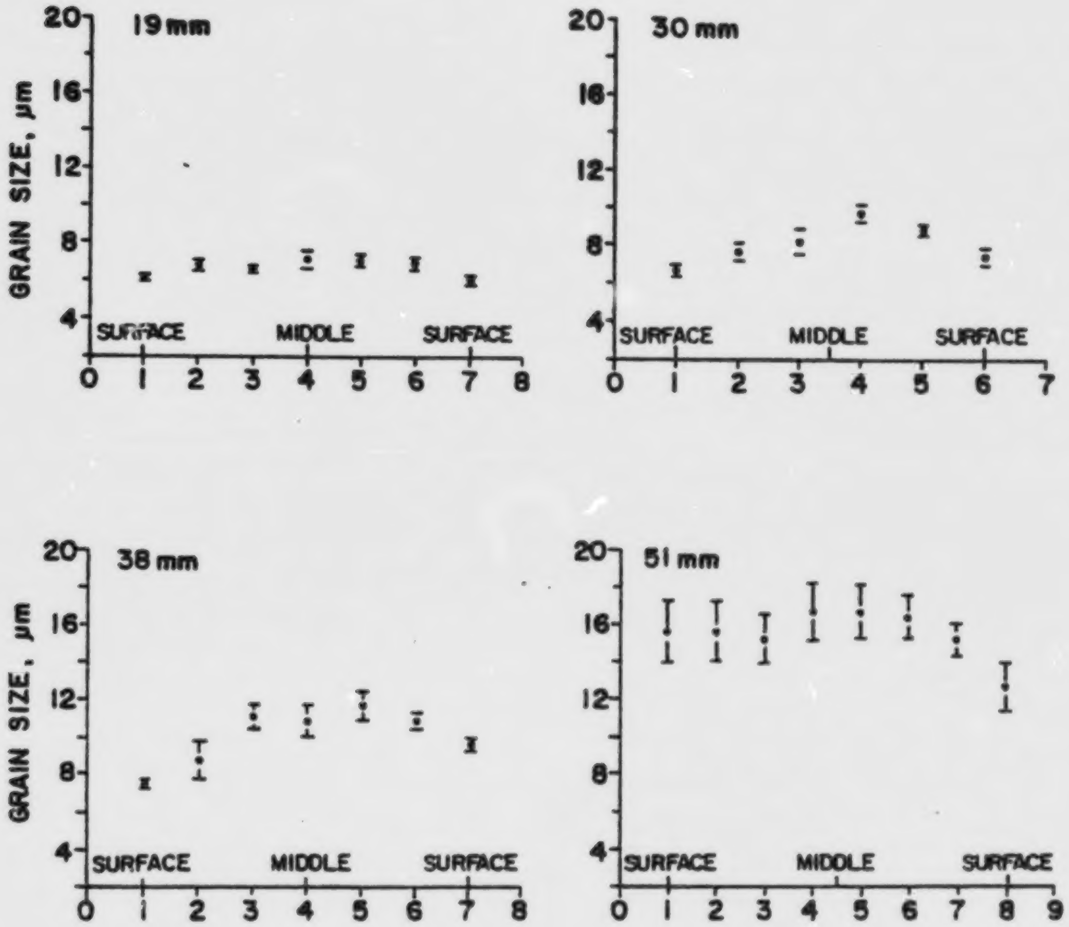

Figure 3: The Effect of Thickness on Yield and Ultimate Tensile Strength

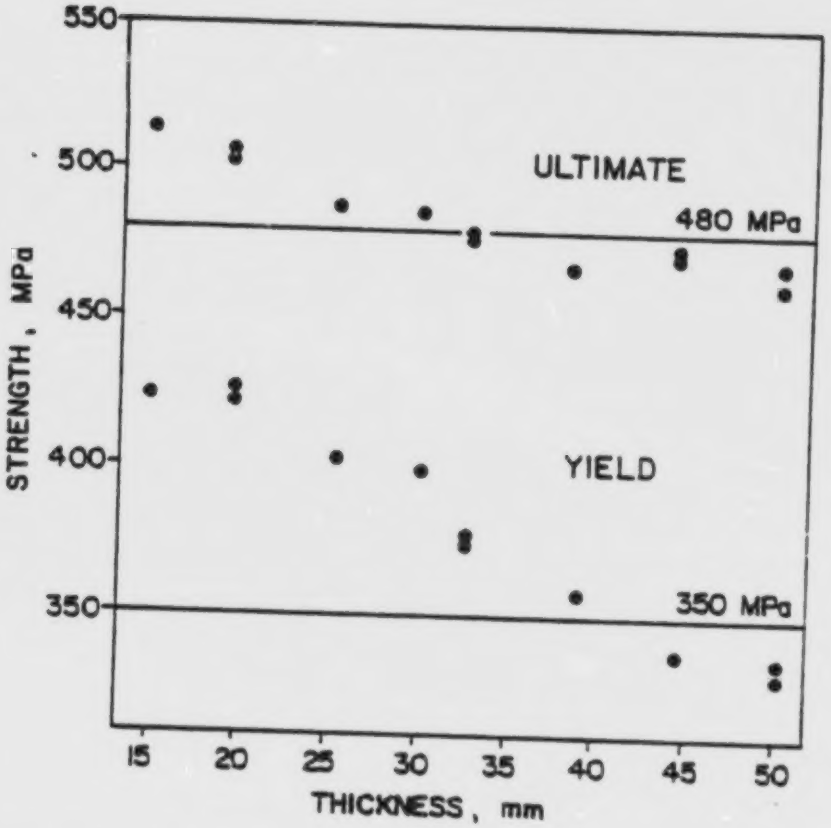

Figure 4: The Calculated Effect of Contributions to Yield Strength

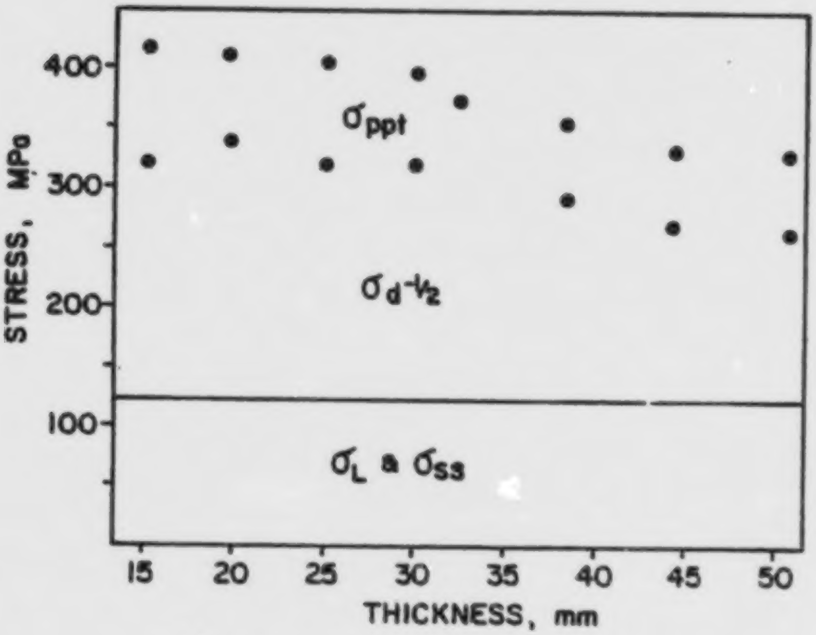

$$\sigma \text{ (MPa)} = 124.2 + 17.4\, d^{-1/2} + \sigma_{ppt}$$

where: ppt = precipitation contribution

$d^{-1/2}$ = grain size contribution

L = lattice friction

SS = solid solution contribution

Figure 5: Full-Thickness Bend Tests

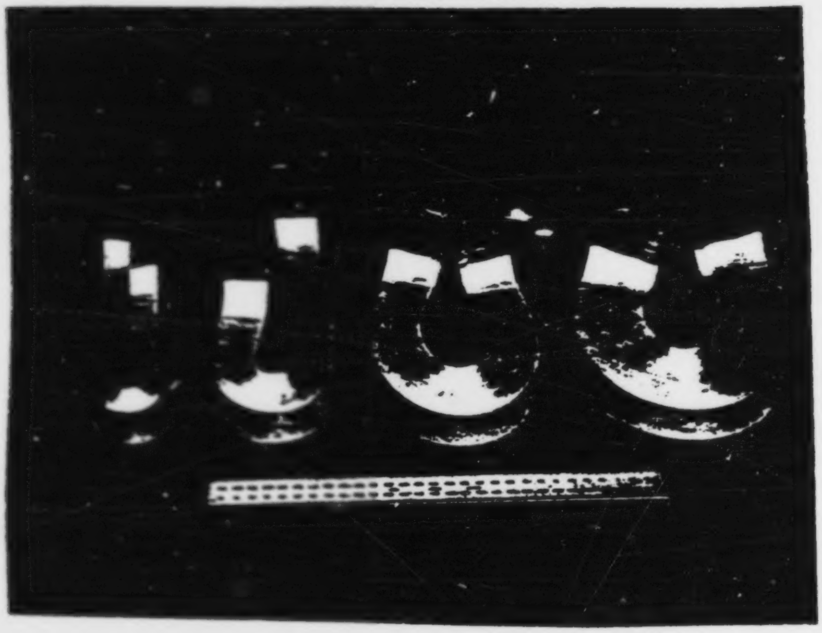

19 30 44 51

Figure 6: The Effect of Charpy Striker Geometry on Energy Absorption

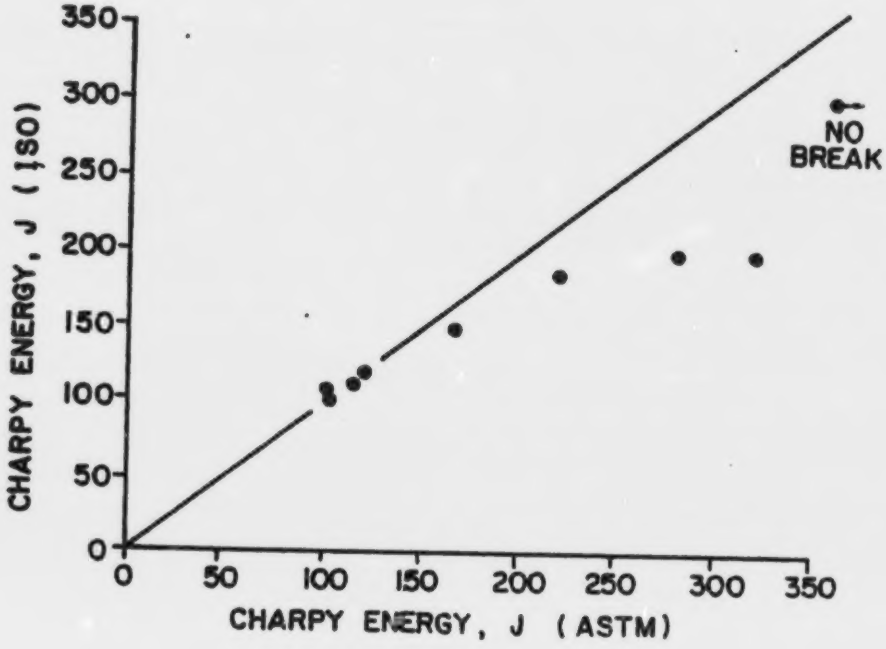

Figure 7: Charpy Energy (Joules) Transition Curves

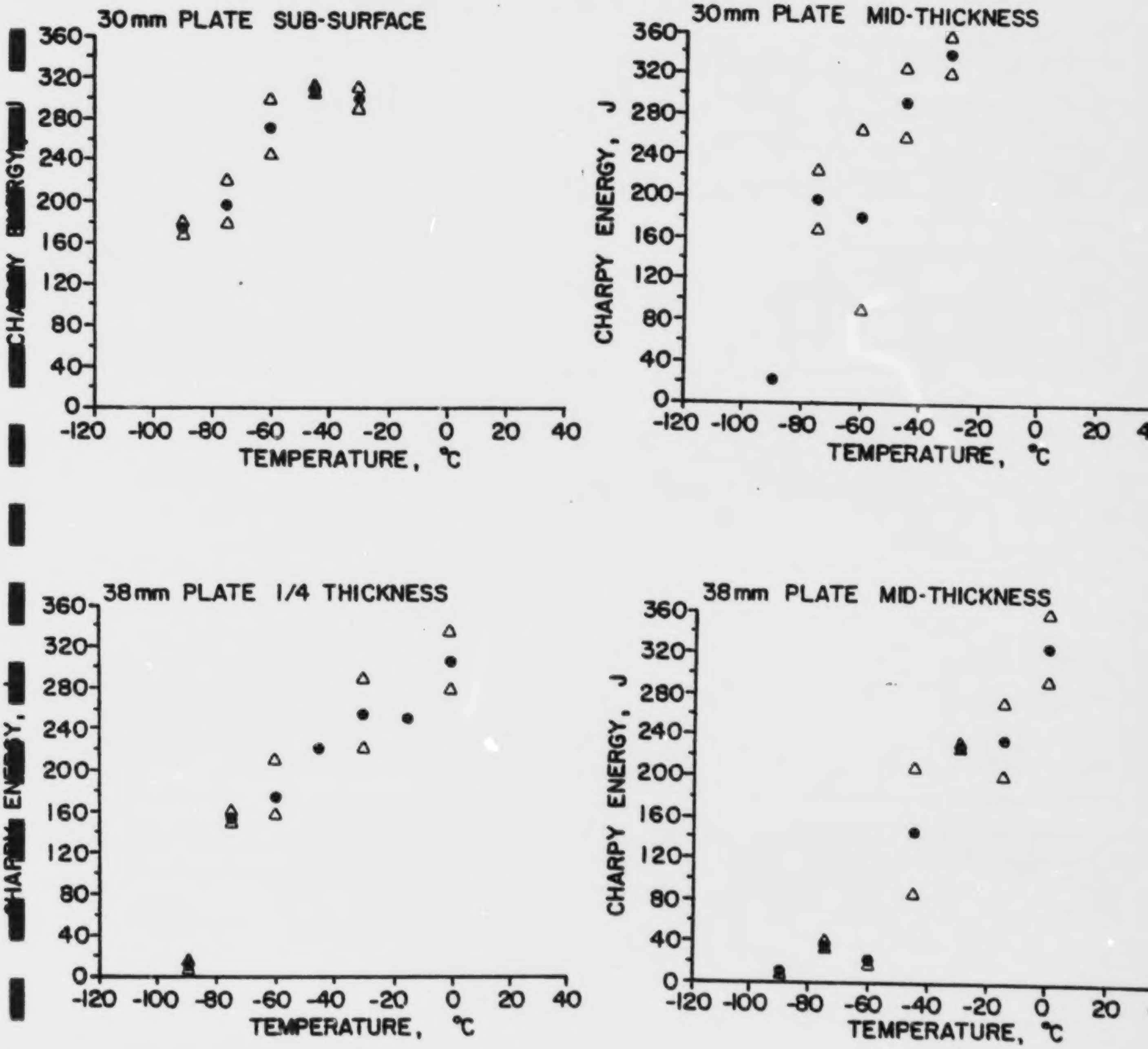

Figure 8: The Effect of Precipitation Strengthening, Grain Refinement and % Pearlite on 50% FATT

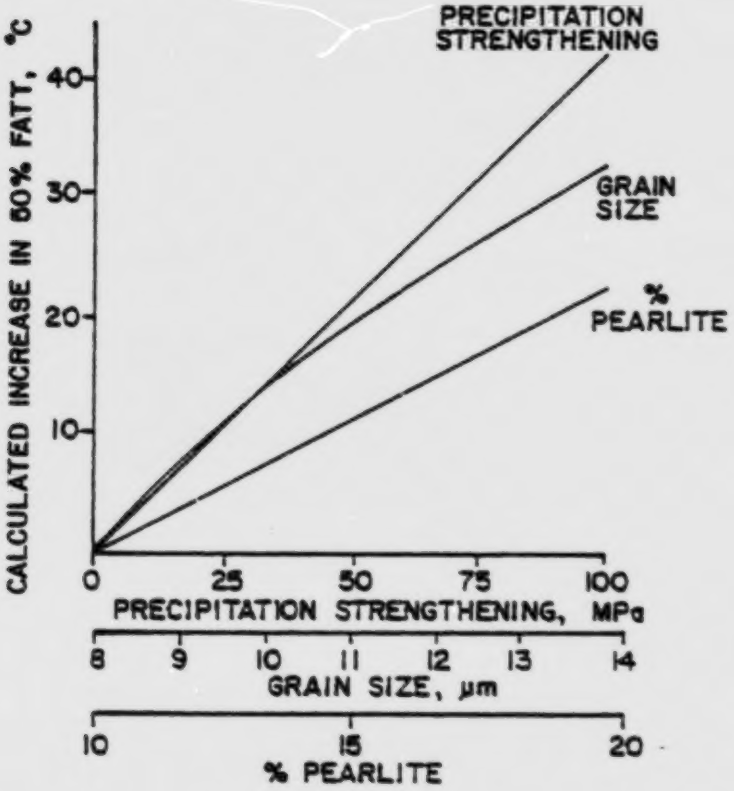

Figure 9: Comparison of Actual and Predicted 50% Shear FATT based on Grain Size and Chemistry

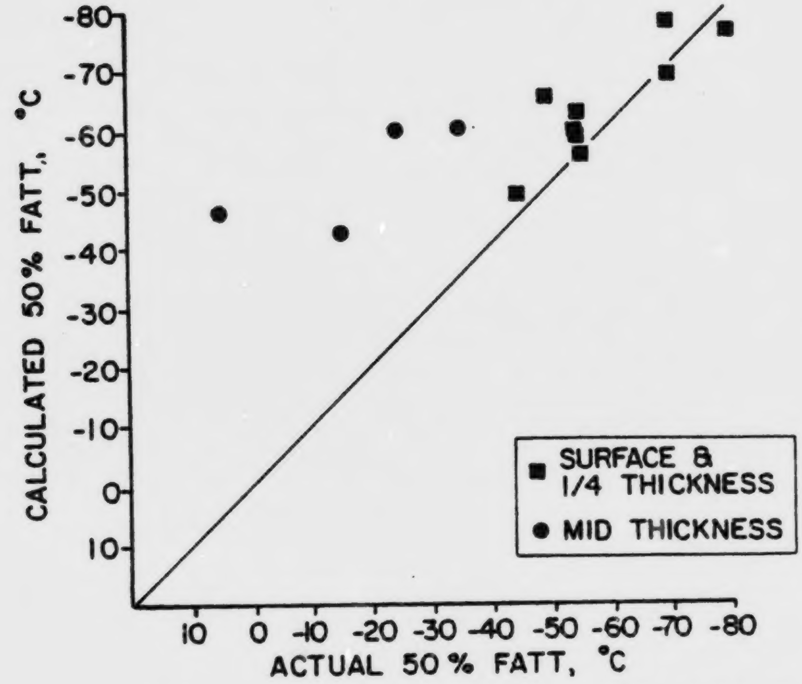

$$ITT(\ C) = -19 + 44\%S_i + 700\sqrt{N_f} + 2.2\%P$$
$$-11.5d^{-1/2} + 0.41\,\sigma_{ppt}$$

Si - Silicon
$N_f$ - % free nitrogen
P - Pearlite
d - ferrite grain size (mm)
$\sigma_{ppt}$ - precipitation strengthening contribution (MPa)

Figure 10: Through-thickness Temperature Distribution during Heavy Plate Rolling

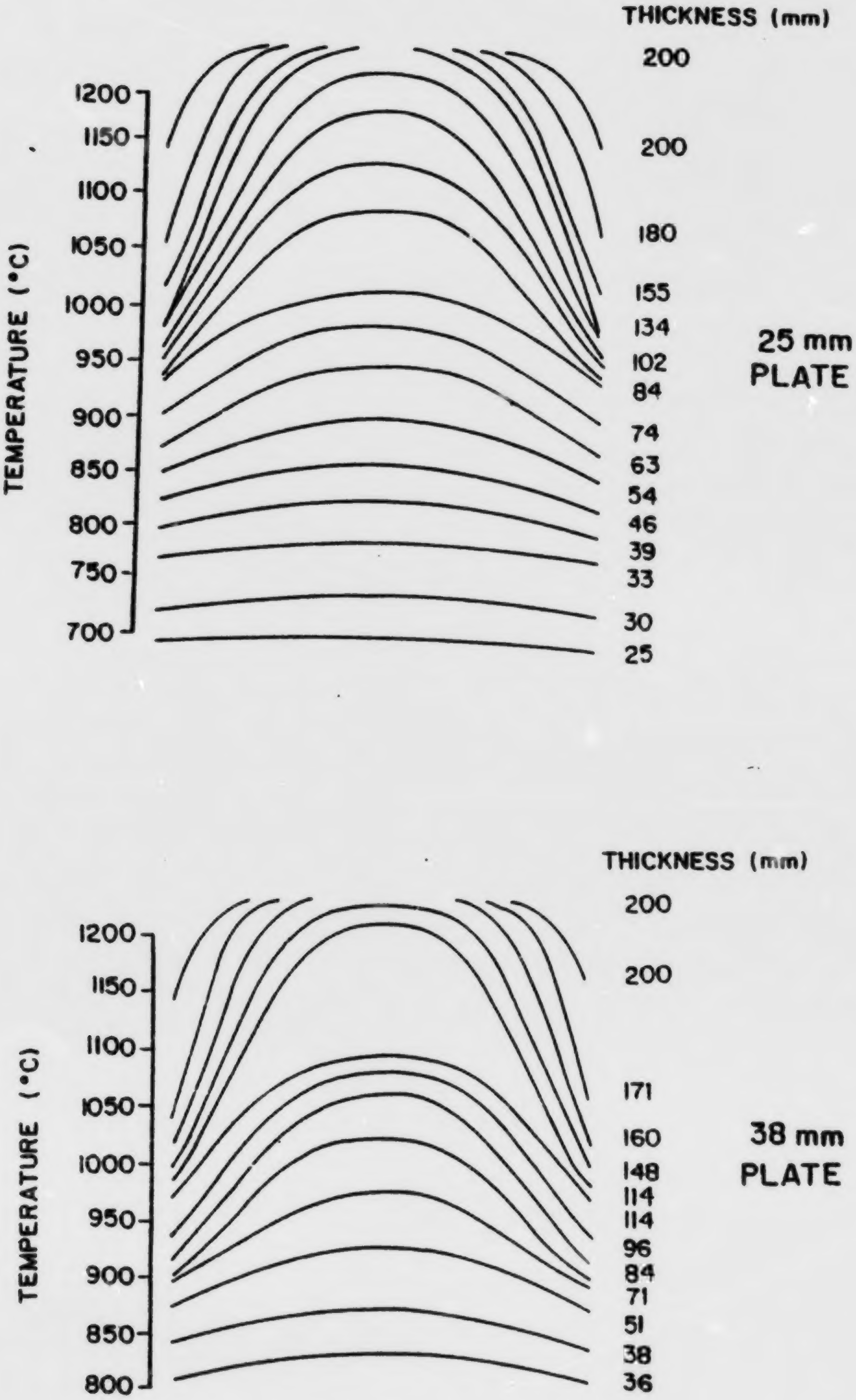

Figure 11: Lamellar Tearing

(a) Lamellar Tearing below a Multi-pass Weld

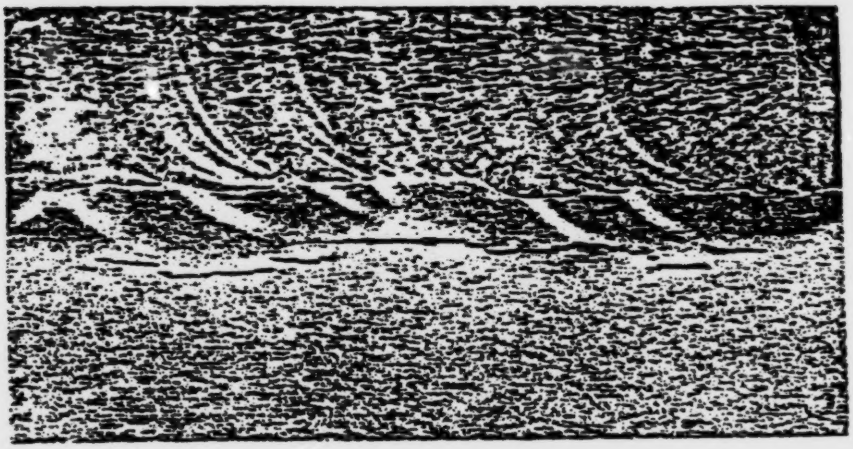

(b) Typical Joints Susceptible to Tearing

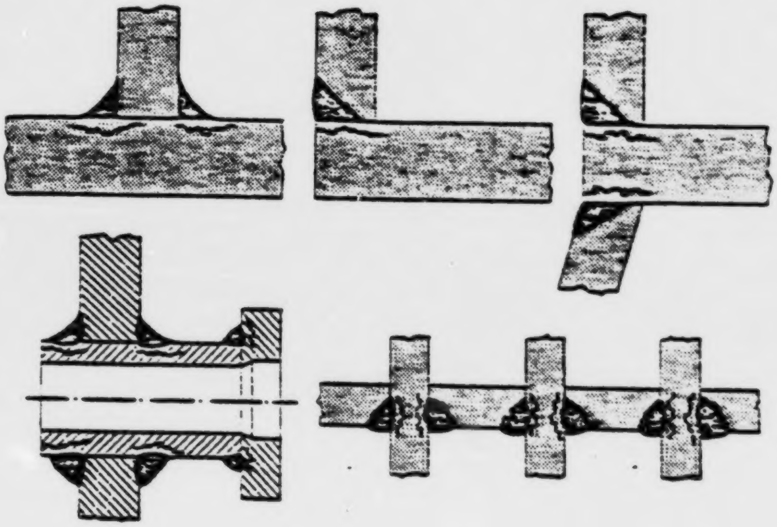

Figure 12: Quarter-Point Inclusions in Rolled Plate

(a) Ultrasonic C-Scan (0.5X)

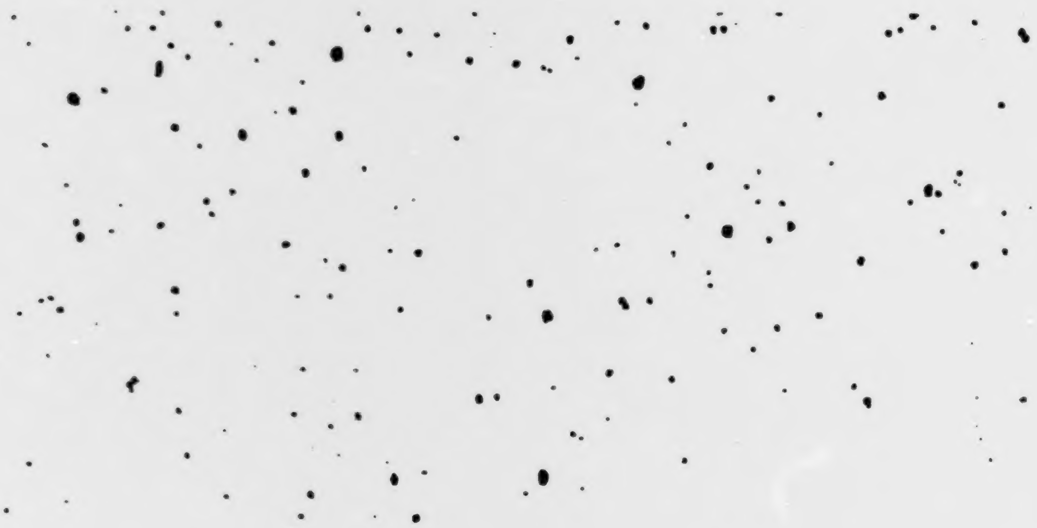

(b) Metallographic Cross Section (16X)

Figure 13: Through-thickness Ductility

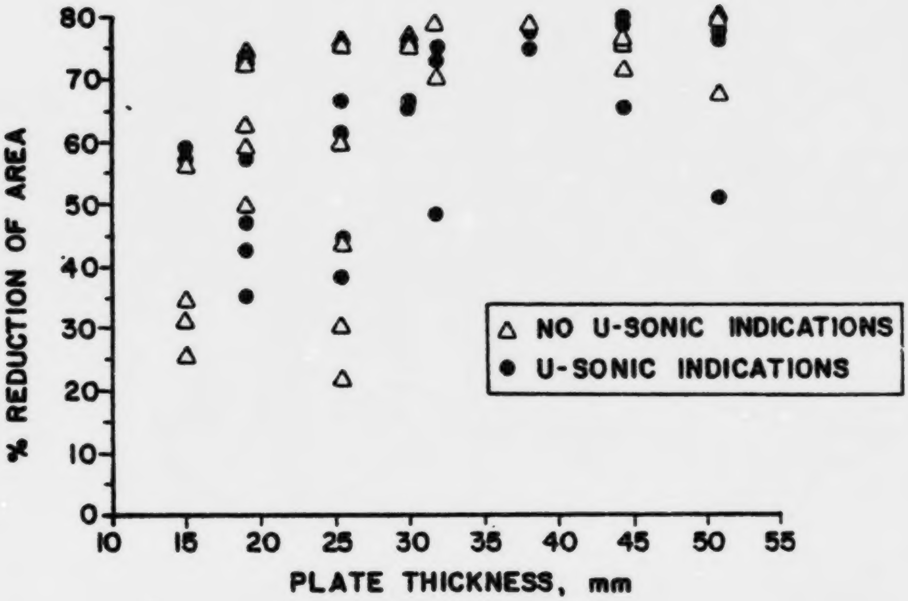

Figure 14: Broken Through-thickness Tensiles

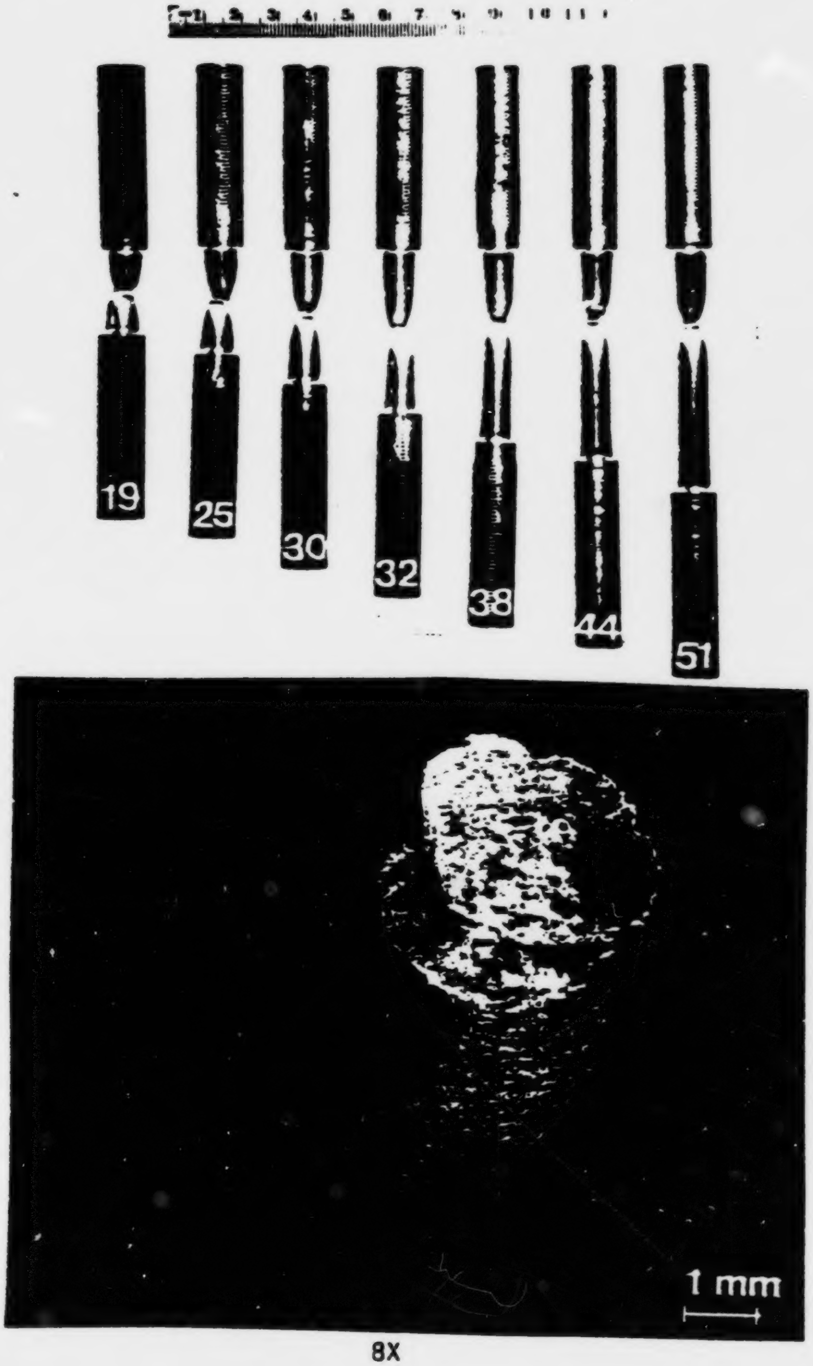
19
25
30
32
38
44
51
1 mm

8X

Figure 15: Alumina Cluster on Through-thickness Tensile Fracture Surface

(a) 8X

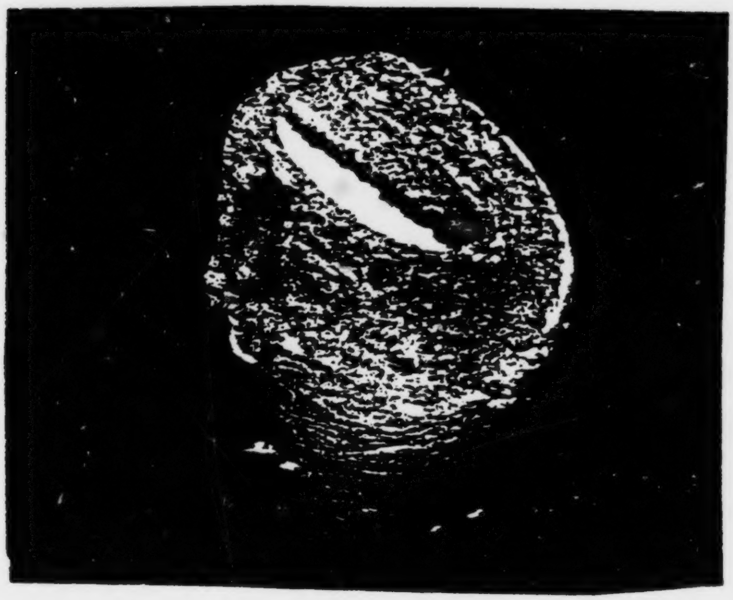

(b) 500X

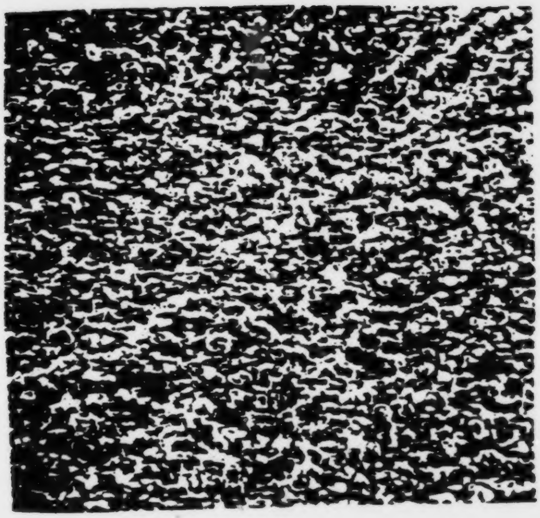

Figure 16: Type II Manganese Sulfide Inclusions on Through-thickness Tensile Fracture Surface

(a) 8X

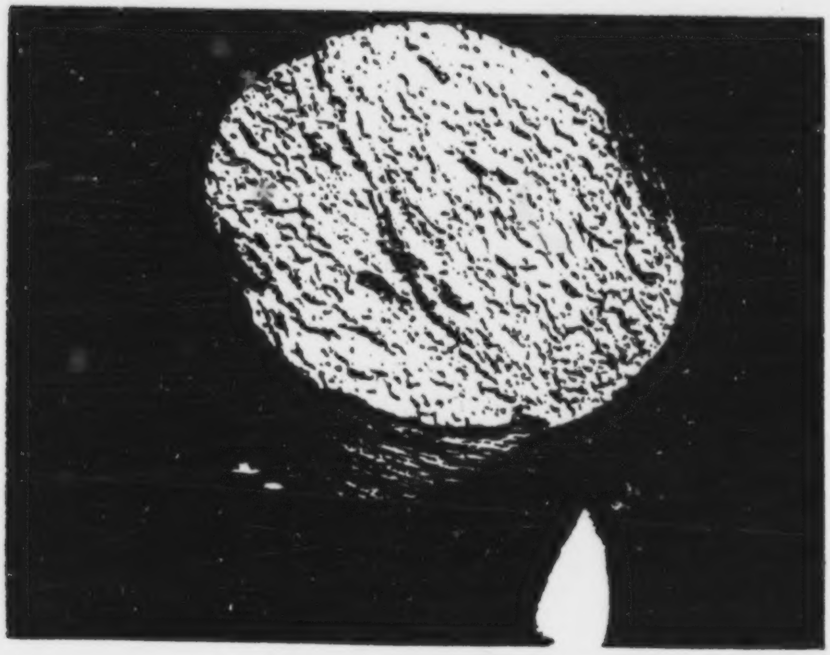

(b) 2000X

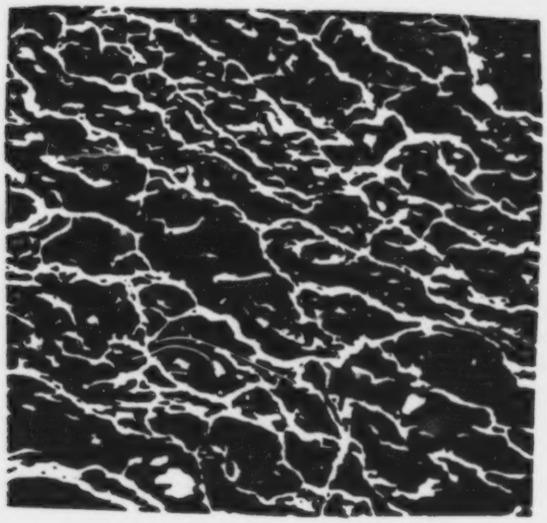

Figure 17: Window Test for Susceptibility to Lamellar Tearing

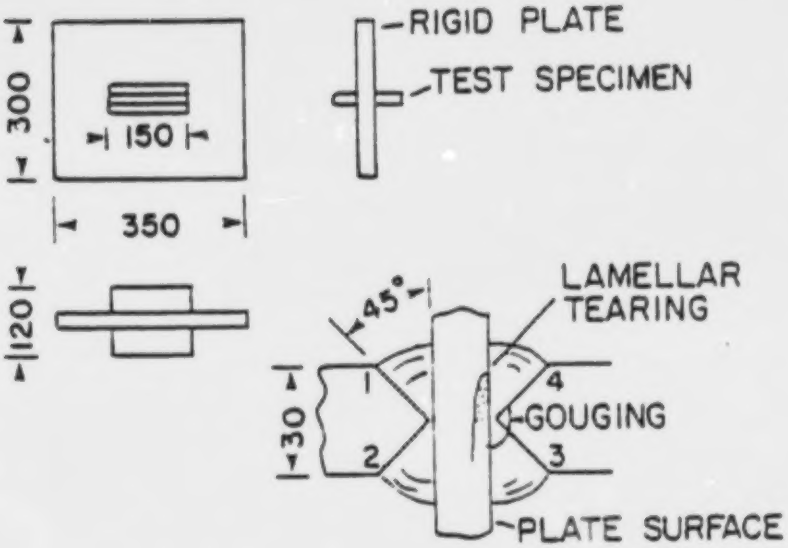
300
150
350
120
RIGID PLATE
TEST SPECIMEN
45°
LAMELLAR TEARING
30
1
2
3
4
GOUGING
PLATE SURFACE

* dimensions in mm

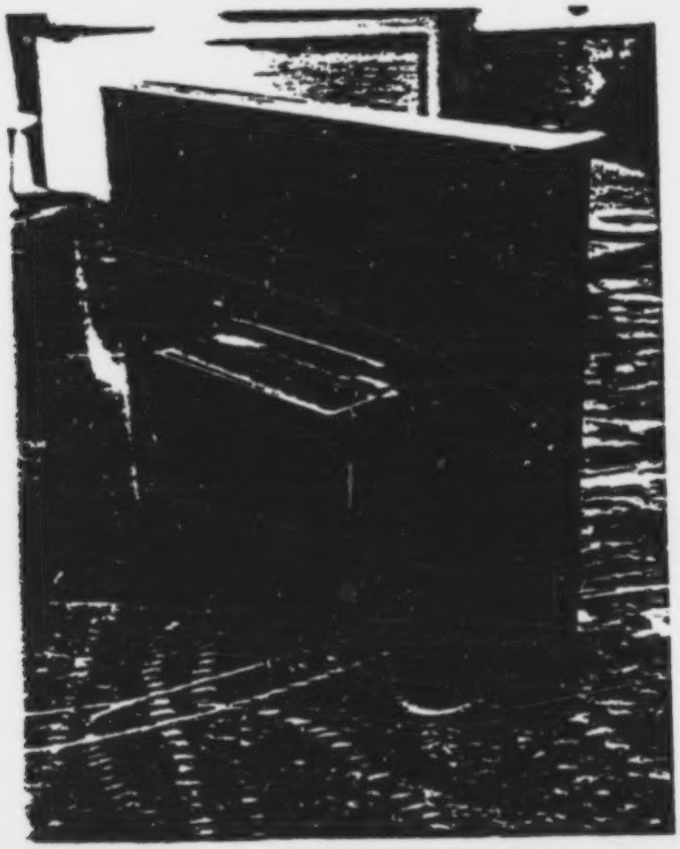

Figure 18: Window Test Cross Section through Quarter Point Oxides

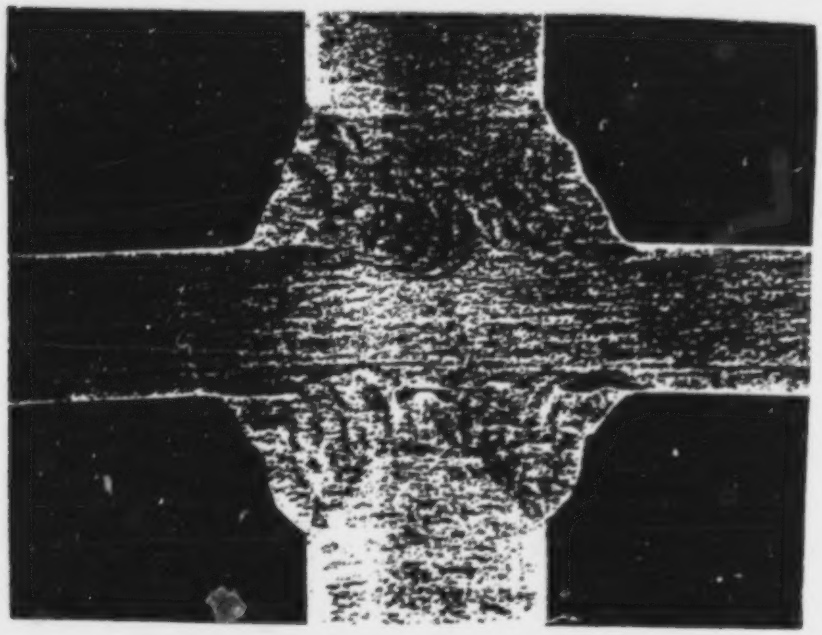

Actual Size

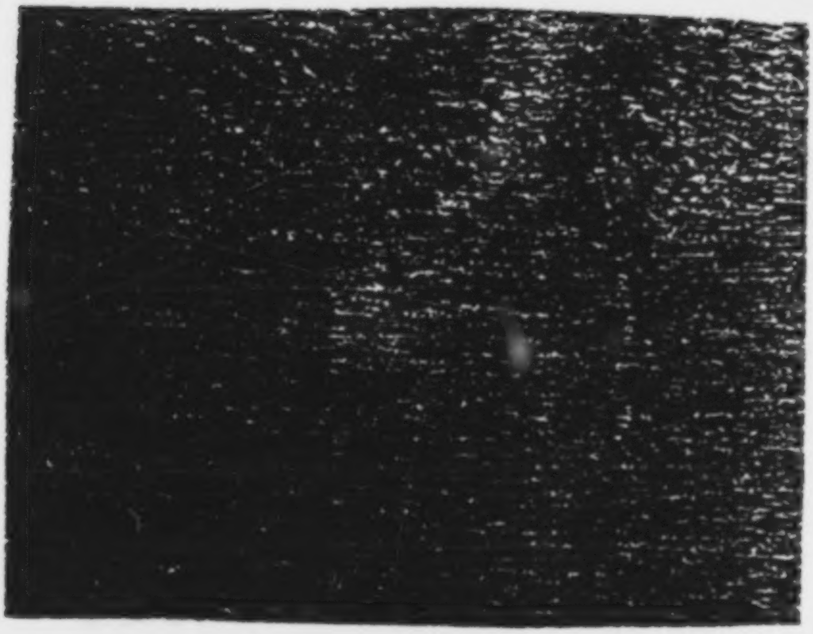

5X

Figure 19: Y-groove Cracking Test

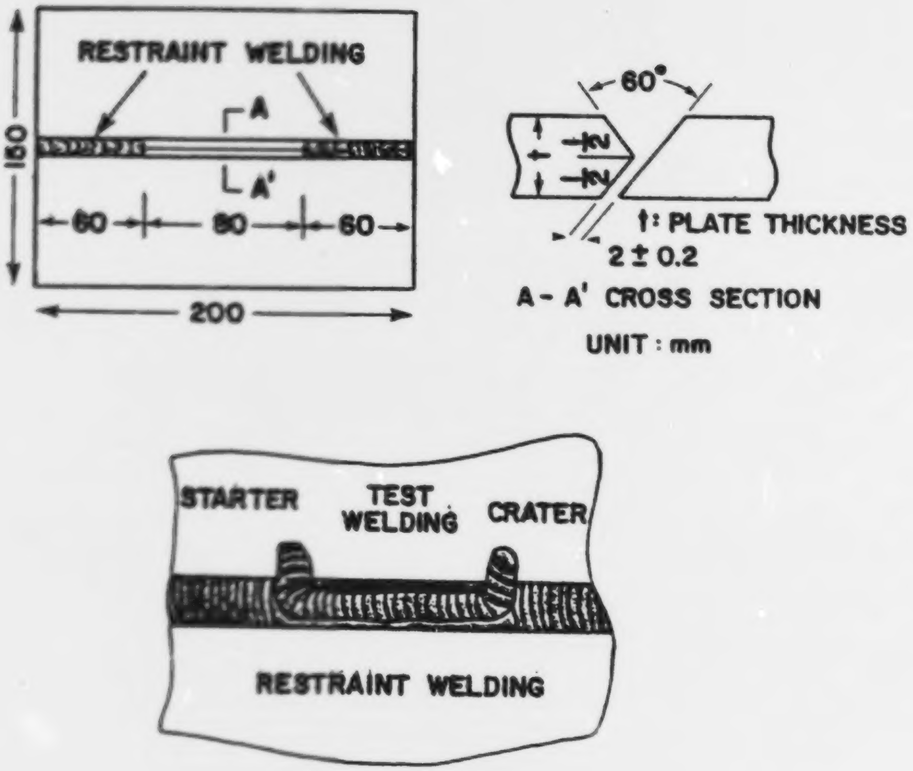
RESTRAINT WELDING
A
A'
150
60
80
60
200
60°
t: PLATE THICKNESS
2 ± 0.2
A - A' CROSS SECTION
UNIT : mm
STARTER
TEST WELDING
CRATER
RESTRAINT WELDING

*WELDING CONDITIONS*

| | |
|---|---|
| WELDING METHOD | SMAW |
| WELDING POSITION | FLAT |
| CORE DIAMETER | 4 mm ϕ |
| WELDING CURRENT | 170 ± 10A |
| WELDING VOLTAGE | 24 ± 3V |
| WELDING SPEED | 10~15 cm/min |

Figure 20: Controlled Thermal Severity Test

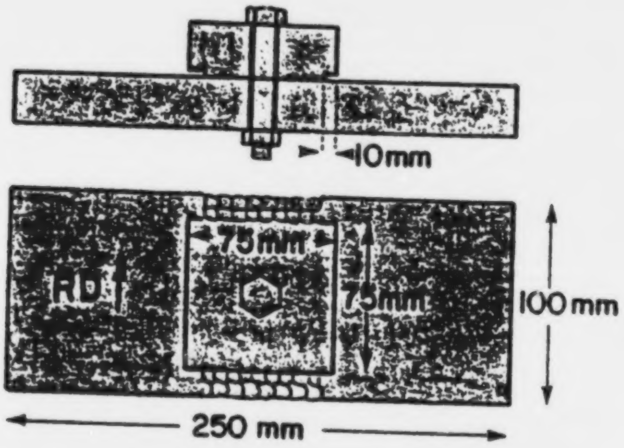
10mm
75mm
RD
75mm
100mm
250 mm

*WELDING CONDITIONS*

| | |
|---|---|
| WELDING METHOD | SMAW |
| WELDING POSITION | FLAT |
| CORE DIAMETER | 4 mm ϕ |
| WELDING CURRENT | 170 ± 10A |
| WELDING VOLTAGE | 24 ± 3V |
| WELDING SPEED | 10 – 15 cm/min |

Figure 21: Inclined Plate Welding Test

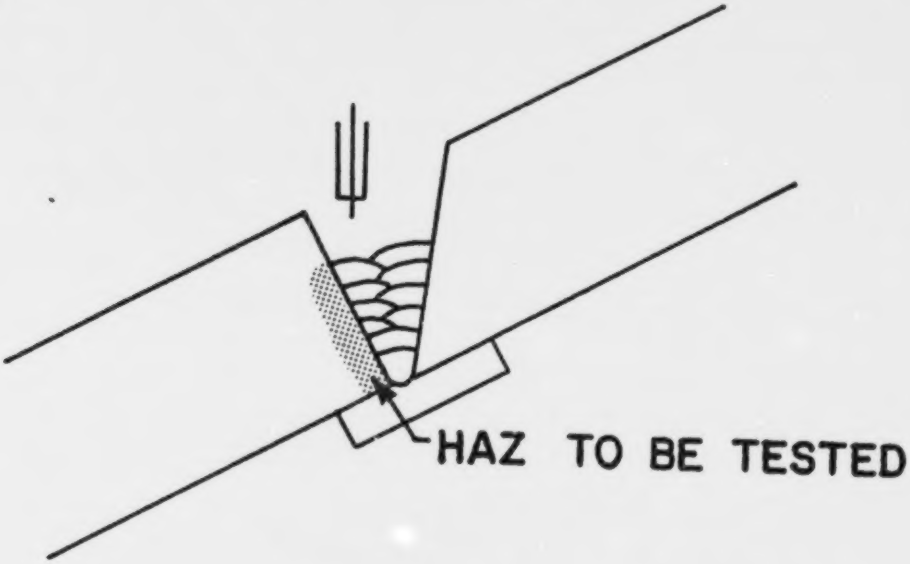

| | |
|---|---|
| Heat Input | 2 kJ/mm and 4 kJ/mm |
| SAW Consumables | ESAB 10.71 Flux<br>Stelco 80 Wire<br>(0.08 C, 1.59 Mn, 0.23 Si, 0.53 Mo, 0.26 Ni) |
| Preheat and Interpass Temperature | 150°C |

Figure 22: Macrostructure of Test Welds

19 mm

(a) 2 kJ/mm

(b) 4 kJ/mm

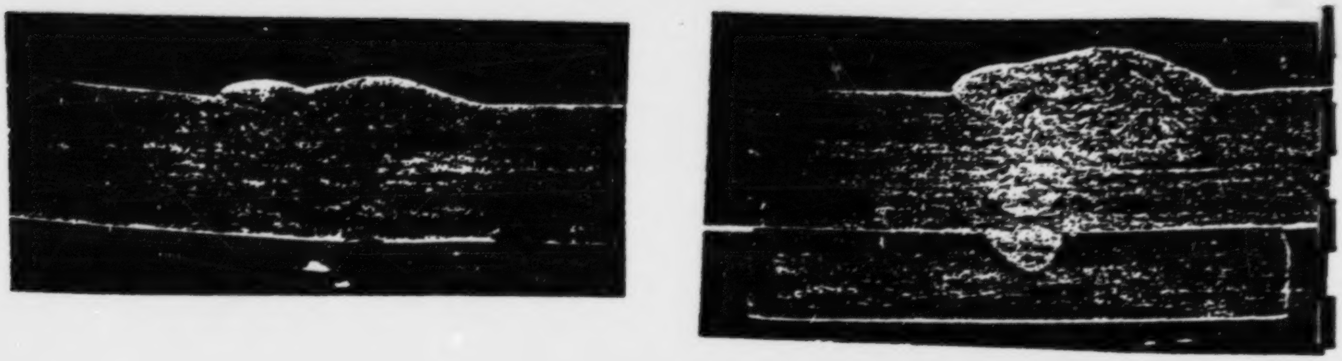

38 mm

(c) 2 kJ/mm

(d) 4 kJ/mm

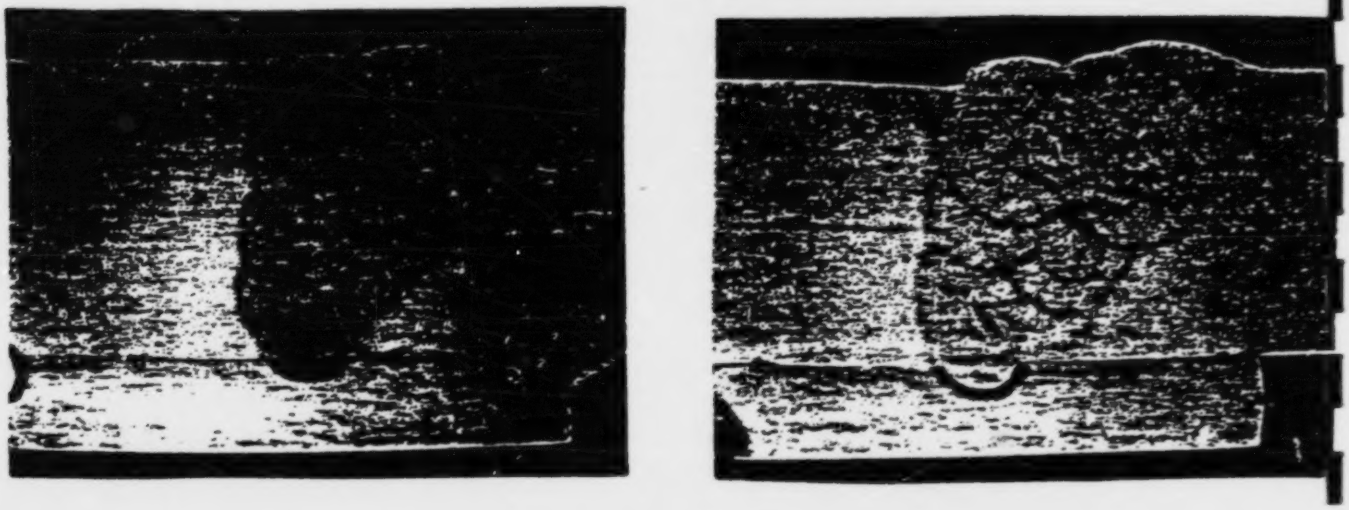

Figure 23: Comparison of Weld Bead Overlap at 2 kJ/mm and 4 kJ/mm Heat Input

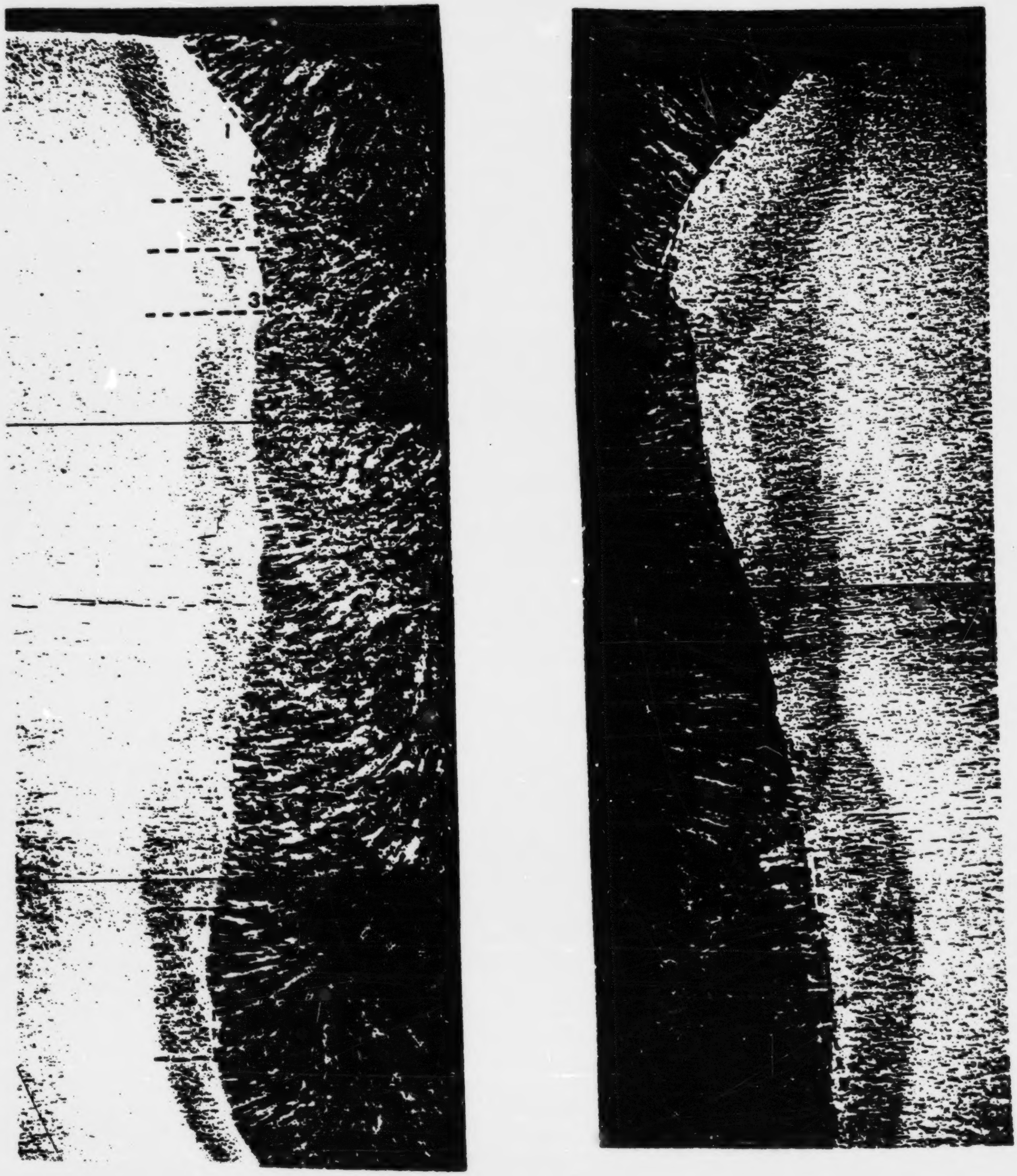

(a) 2 kJ/mm

(b) 4 kJ/mm

Figure 24: Specific Heat Affected Zone Microstructures in Multi-pass Welds (500X)

(a) Coarse Grain (b) Normalized

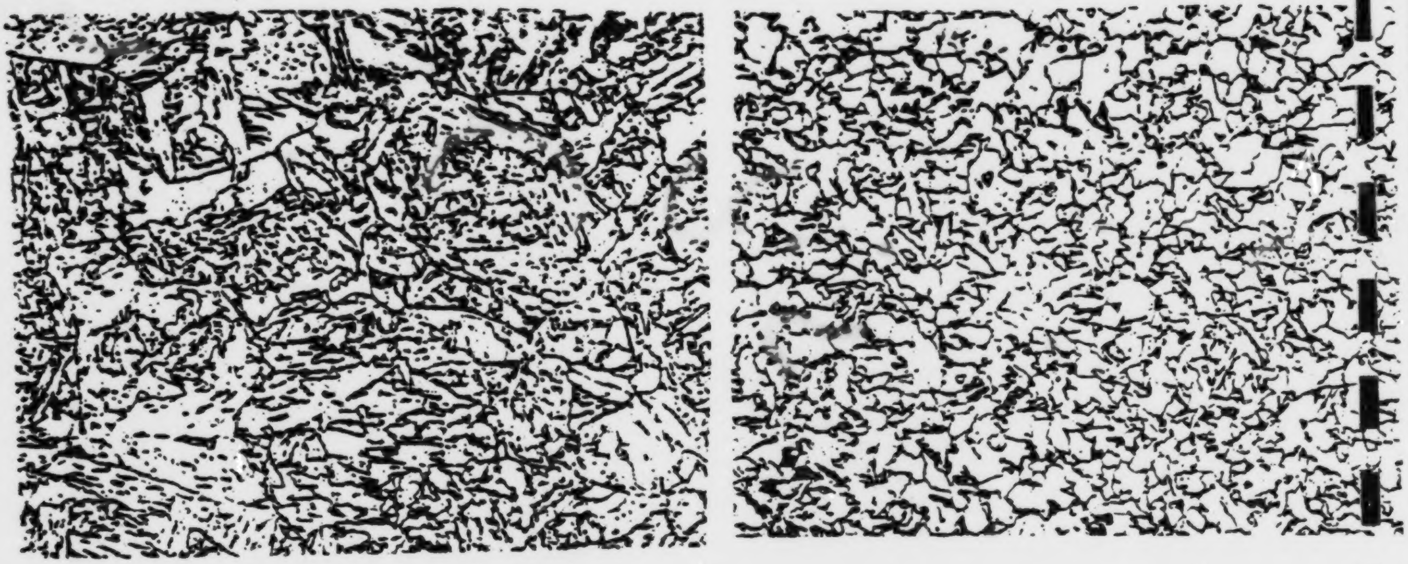

(c) Intercritical (d) Sub-critical

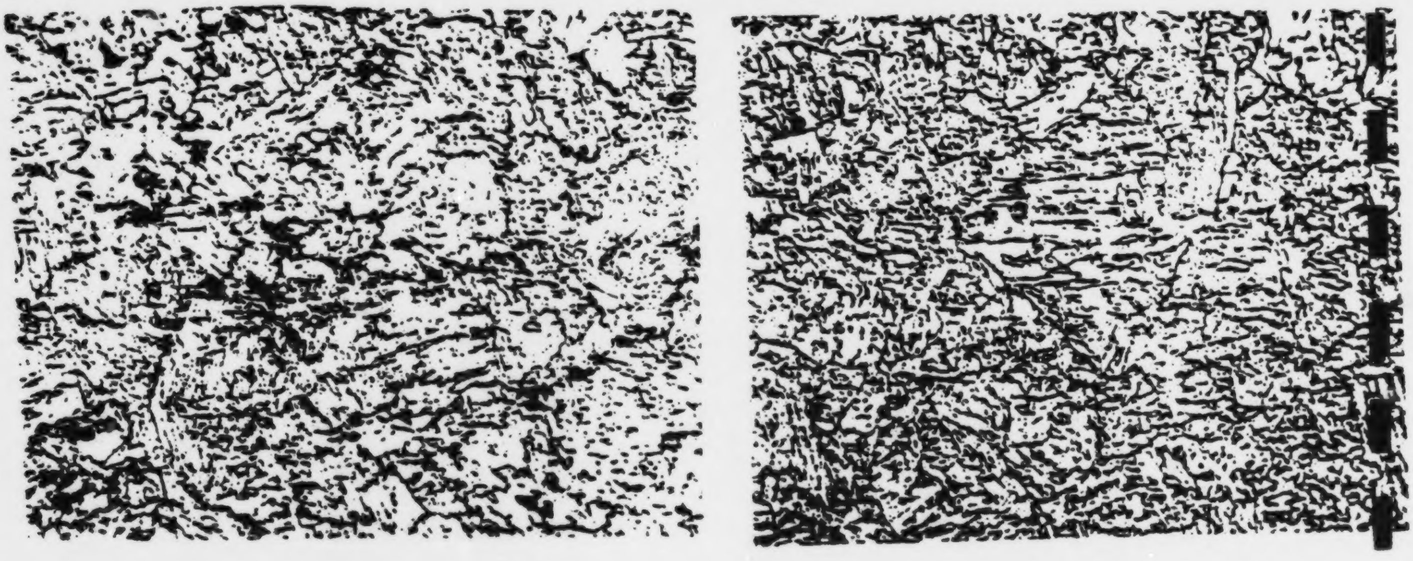

Figure 25: HAZ CTOD Transition Curves

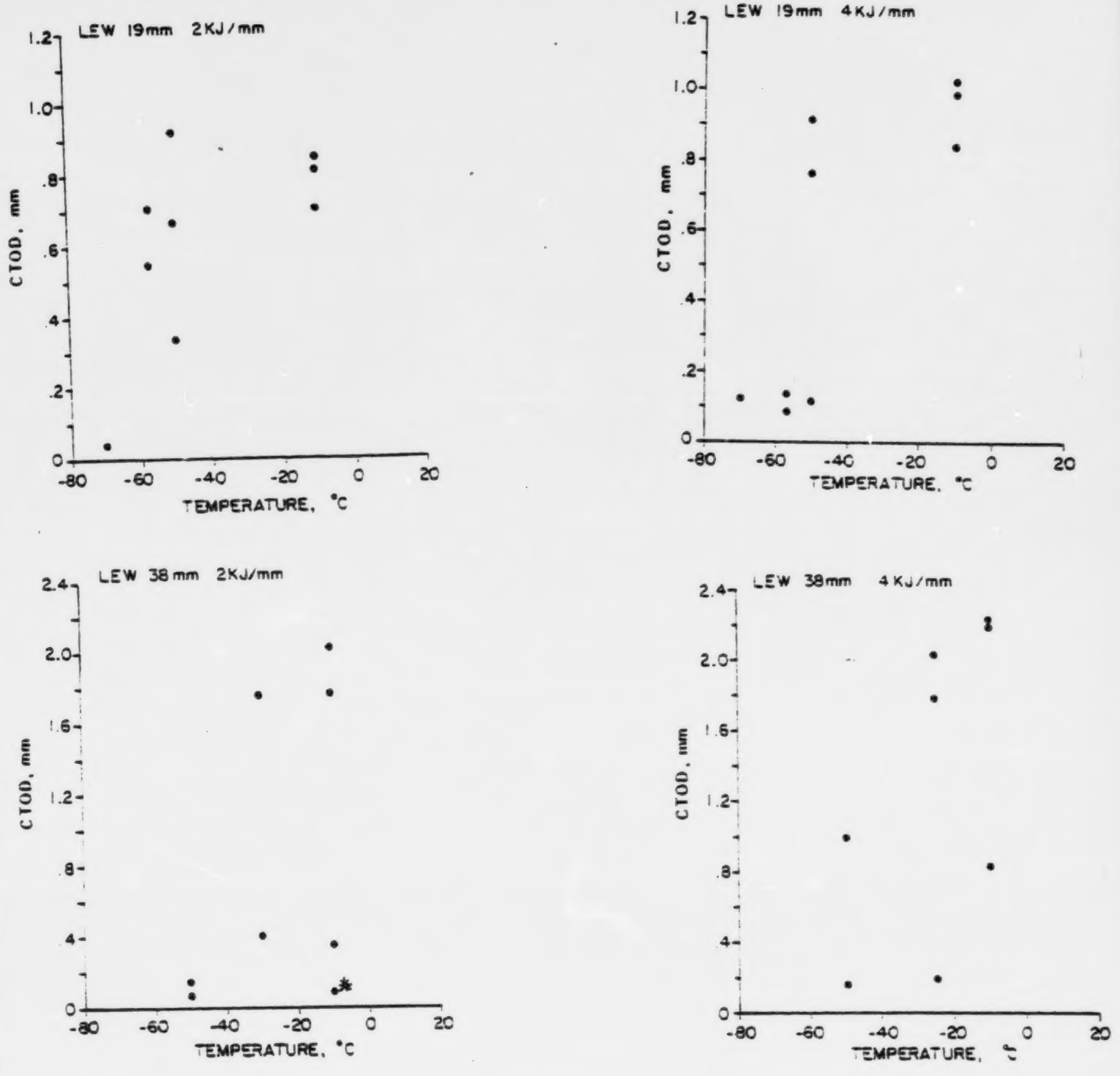

* "pop in"

Figure 26: Sectioning of CTOD Tests to determine Fatigue Precrack and Fracture Initiation Position

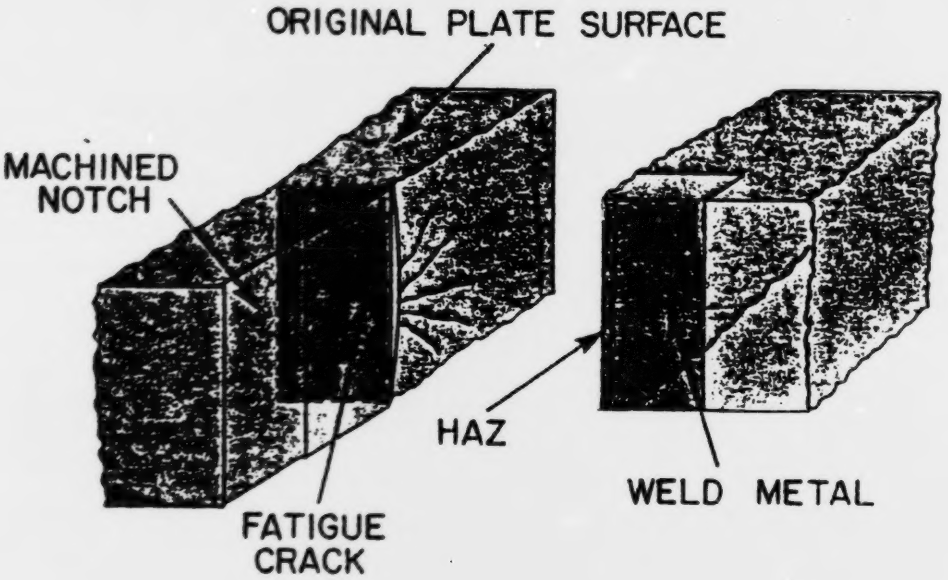
ORIGINAL PLATE SURFACE
MACHINED NOTCH
HAZ
WELD METAL
FATIGUE CRACK

Figure 27: Fracture Initiation Position in 19 mm Plate - 4 kJ/mm Heat Input

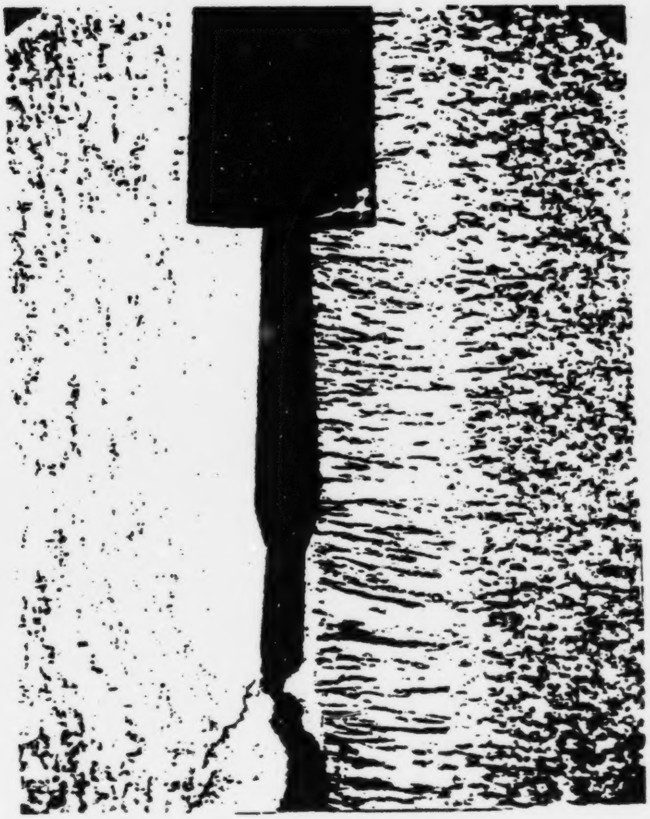

Figure 28: Fracture Initiation Position in 38 mm Weld - 2 kJ/mm Heat Input

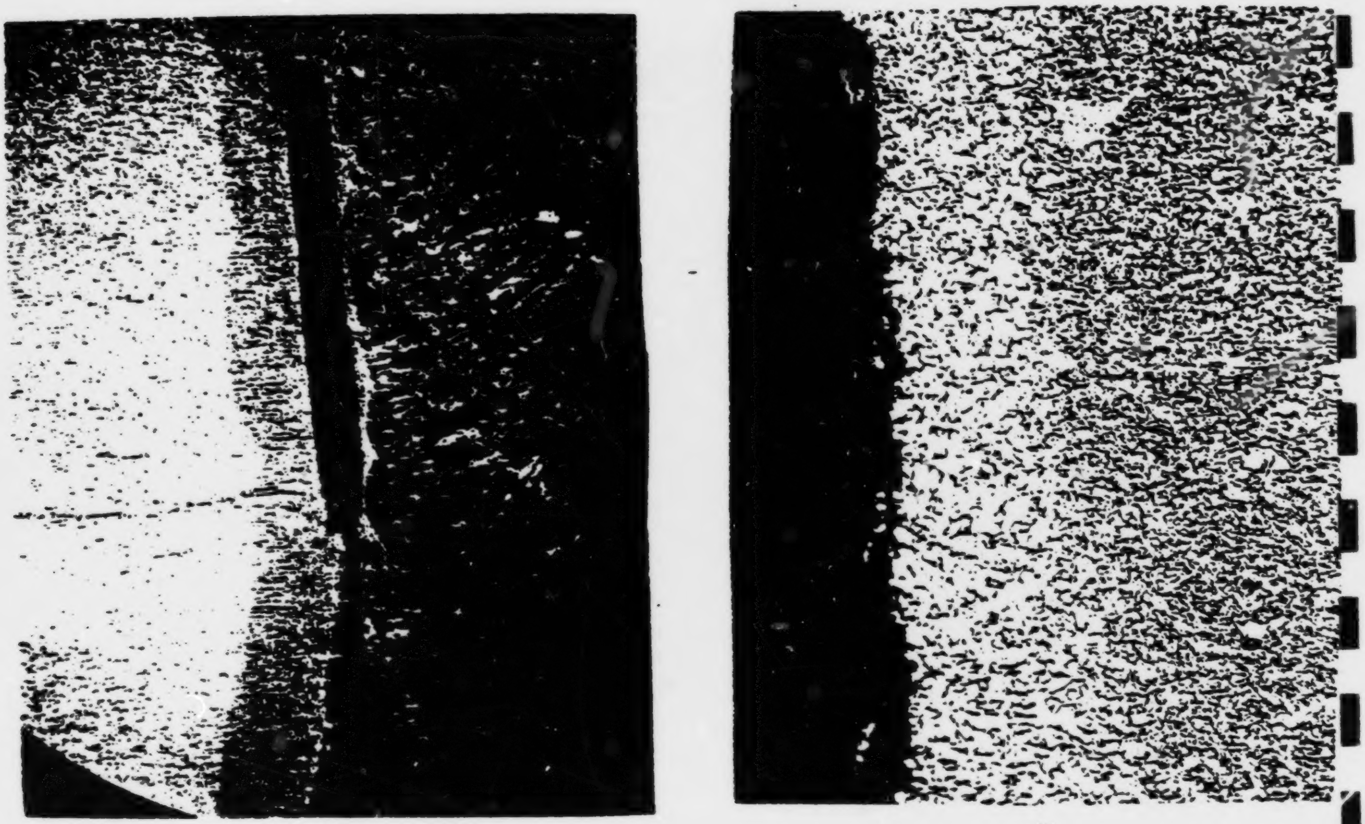

Figure 29: Energy Transitions of SAW Weld Heat Affected Zones

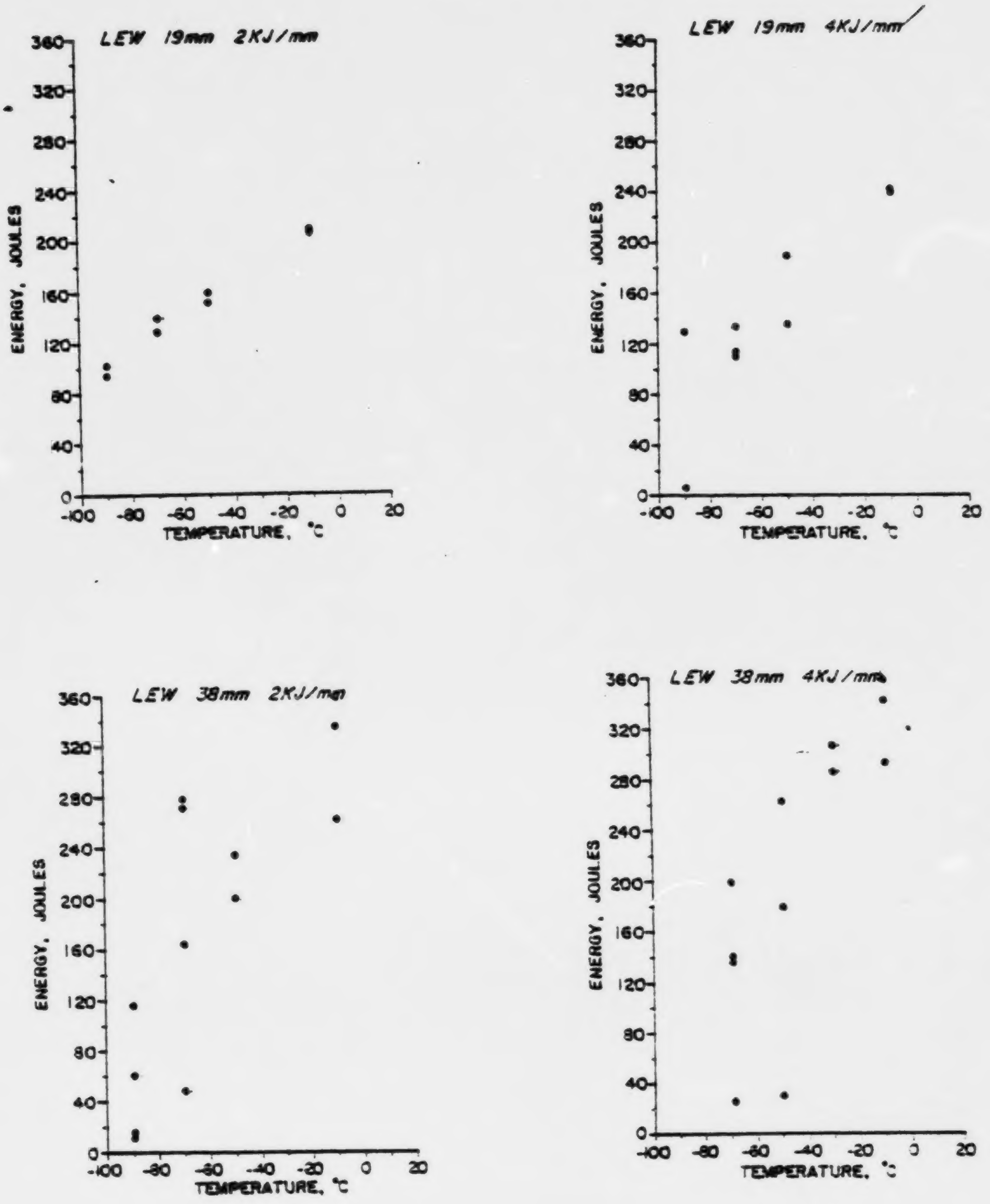

Figure 30: Comparison of Actual and Gleeble Simulated HAZ Structures

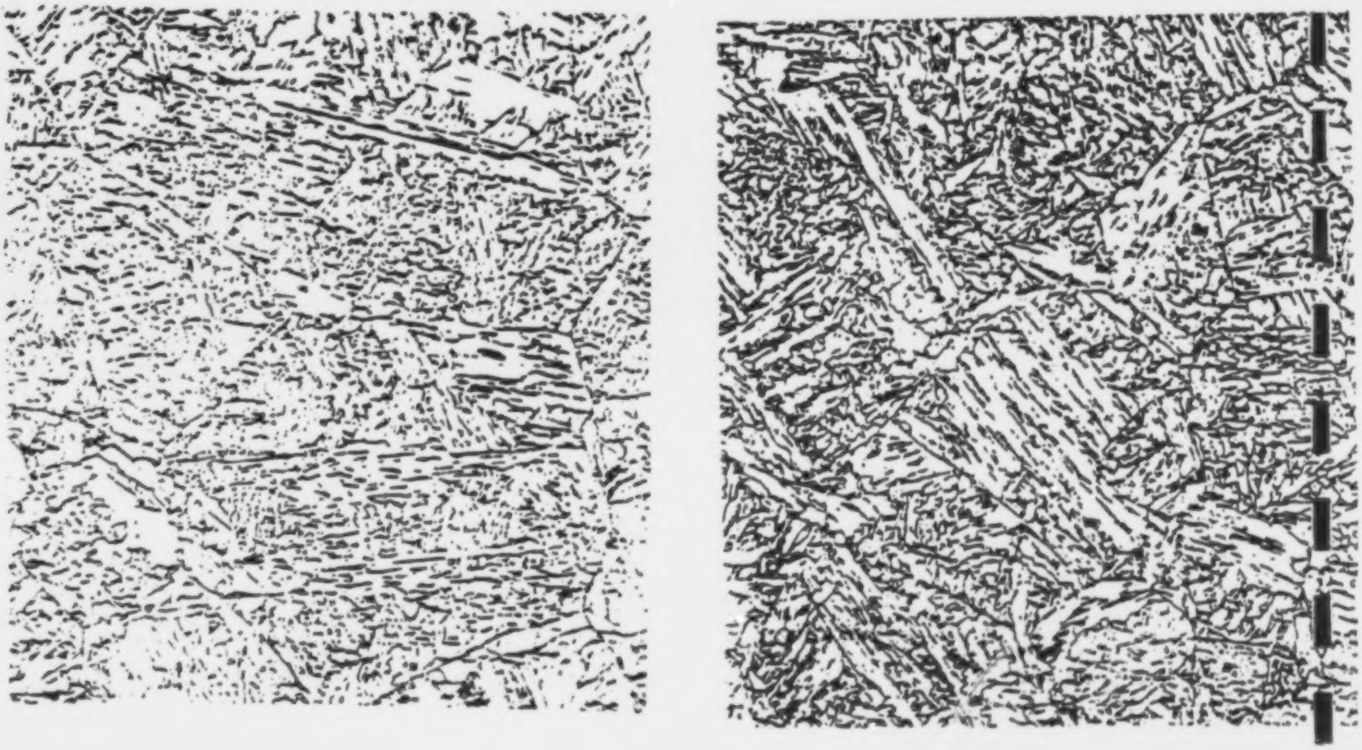

(a) Gleeble Simulated HAZ 20 sec $\Delta T_{800-500}$

(b) 19 mm Plate - 2 kJ/mm Heat Input

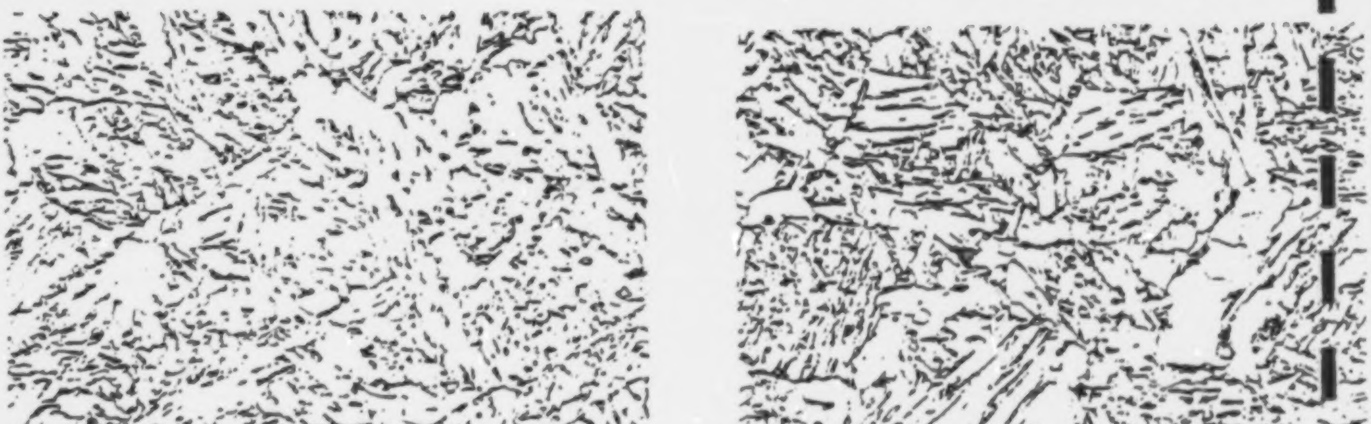

(c) Gleeble Simulated HAZ 75 sec $\Delta T_{800-500}$

(d) 19 mm Plate - 4 kJ/mm Heat Input

Figure 31: Simulated HAZ CTOD Results

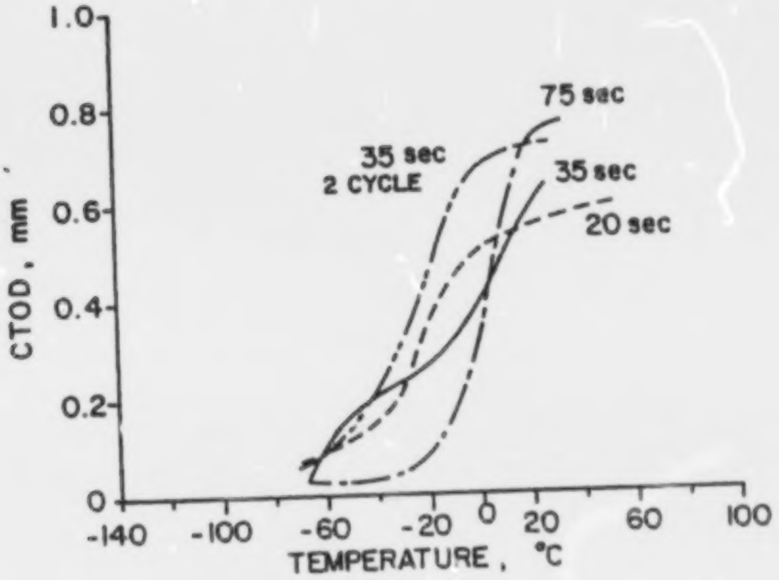

# REVIEW OF FRACTURE TOUGHNESS TESTING
# FOR OFFSHORE STRUCTURES AND SHIPS

J. D. Embury and Ligeng Luo
Department of Metallurgy and Materials Science
McMaster University

D. B. McCutcheon
Research and Development Department
Stelco Inc.

April 1985
R&D 85R046 TM

## TABLE OF CONTENTS

1. Introduction........................................................ 1-1

2. Fracture Mechanisms................................................. 2-1

2.1 Definition......................................................... 2-1

2.2 Fracture Mechanisms and Toughness.................................. 2-2
  (1) Fracture Toughness............................................... 2-2
  (2) Cleavage Initiation Mechanism.................................... 2-4
  (3) Fibrous Initiation Mechanism..................................... 2-5
  (4) Stable Crack Extension Mechanism................................. 2-7

2.3 Transition of Crack Initiation Mechanisms.......................... 2-8
  (1) Crack Initiation Mechanisms - Transition Temperature.. 2-8
  (2) Effect of Thickness.............................................. 2-11
  (3) Transition Temperature Range..................................... 2-13

References............................................................. 2-16

3. Fracture Criteria................................................... 3-1

3.1 General............................................................ 3-1

3.2 Validity of $K_1$ Criteria......................................... 3-1
  (1) General Aspects of $K_{IC}$...................................... 3-1
  (2) Tensile Stresses................................................. 3-3
  (3) Bending Stresses................................................. 3-4
  (4) Stress Concentration Effects..................................... 3-8
  (5) Influence of Residual Stresses................................... 3-9

3.3 CTOD Criterion..................................................... 3-10
  (1) CTOD Calibration Curve........................................... 3-10
  (2) Superposition of Stresses and Strains............................ 3-11
  (3) Effect of Constraint............................................. 3-11

3.4 Other Criteria..................................................... 3-12

References............................................................. 3-13

**4. Fracture Toughness and Fracture Toughness Testing** ............... 4-1

4.1 Fracture Toughness of Medium Strength Steels................ 4-1

4.1.1 General Aspects.......................................... 4-1
  (1) Literature Survey.................................... 4-1
  (2) Transition Temperature and Fracture Toughness....... 4-3
  (3) Effect of Constraint................................. 4-6

4.1.2 Fracture Toughness Data.................................. 4-10
  (1) Scatter Toughness Data............................... 4-10
  (2) Fracture Toughness Data.............................. 4-11

4.2 Fracture Toughness Testing Methods.......................... 4-16

4.2.1 Testing Methods.......................................... 4-16
  (1) Test for $K_i$ and $K_c$................................. 4-16
  (2) Test for $CTOD_c$..................................... 4-19
  (3) Test for $J_{ic}$ (or $J_i$)................................ 4-23

4.2.2 Some Additional Aspects for Investigation................. 4-26
  (1) "Pop-in" Processes................................... 4-26
  (2) Statistical Analysis of Data......................... 4-27
  (3) Fracture Toughness Tests for Weldments.............. 4-29

References..................................................... 4-32

**5. Assessment of Fracture Toughness** ................................ 5-1

5.1 Principles.................................................. 5-1
  (1) Preparation of Data.................................. 5-1
  (2) Determination of Fracture Criterion.................. 5-4
  (3) Assessment of Fracture Toughness..................... 5-5

5.2 Empirical Assessment of Toughness........................... 5-6
  (1) Based on Failure..................................... 5-6
  (2) Based on Safety Factors.............................. 5-7

5.3 Assessment of Some Current Structural Steels................ 5-10
  (1) Assessment of BS4360 Grade 50D....................... 5-10
  (2) Asssessment of KST 248 and KST 33.................... 5-11

References..................................................... 5-13

# OVERVIEW

In considering the ability of steel producers to supply structural steels with yield strength levels up to 350 MPa and in section sizes suitable for Arctic service there are major philosophical differences to be reconciled. The standard approach to a product may be in terms of control of composition or cleanliness or in attempting to specify the relationship between engineering properties such as yield strength or ductility and the detailed microstructure of the material. However, from a design viewpoint the materials may have to be in section sizes up to 100 mm in thickness, fabricated for economic reasons by high heat input welding, and have a design temperature down to -50°C.

Hence from a design viewpoint the tendency is to assume a constant set of mechanical properties and microstructures in order to focus on the macroscopic problems of load bearing capacity and fracture resistance. Clearly in considering the fracture we must encompass both the designers need and the steel producers need to relate the behavior and fitness for service of the product to the structure and processing route. In the present work emphasis is given to the problems of specifying fracture resistance and the precautions needed in applying concepts of fracture mechanisms which were developed for high strength materials to structural steels.

Consideration is given to the variation of fracture mode, to the problems of the influence of stress state, to the extent of residual stresses and to the influence of section size on a variety of fracture resistance parameters.

It is clear that for large scale welded structures it is important to develop a fracture resistance philosophy which takes cognizance not only of minimum specified values of fracture resistance but the significance of the observed scatter in fracture resistance values and the methods of correlating test results and service behavior.

The various sections of the report are provided with a bibliography and a brief summary and some general conclusions and recommendations are given at the end of the report.

It is important to emphasize that a review of the type presented here does not seek to propose a unique and definite specification for the fracture resistance of grade 350 structural steels, but attempts to outline a variety of possible criteria and to consider the factors relating to the utilization and applicability to design.

## Summary of Section 2

For structural steels the fracture toughness can be defined in terms of the attainment of critical values of parameters such as $K_I$, $\delta$, and J. It is important to realize that there are in essence three critical conditions, viz initiation specified by $\delta_i$, $J_i$ and $K_i$, unstable crack growth specified by $\delta_u$, $J_u$, $K_{Ic}$ and crack growth due to the onset of plastic instability at $\delta_m$, $J_m$ and $K_{Im}$.

Clearly comparison between values of fracture toughness parameters demands that cognizance be taken of which of the three stages indicated above is operative.

Further the fracture toughness depends on the microstructural mechanism which is operative. For example initiation at a given temperature may occur by cleavage or fibrous initiation depending on the level of yield stress and the cleanliness of the steel. The importance of considering both the microstructural and macroscopic aspects of fracture resistance arises because for low alloy structural steels the fracture initiation mechanisms vary with operating temperature, loading rate and the degree of constraint as well as with microstructural variables such as grain size the degree of precipitation hardening and the character of the transformation products.

In devising test procedures it is important to specify the minimum design temperature, the expected maximum loading rate and to attempt to obtain data under conditions of full constraint.

If the initiation mechanism under conditions of full constraint is ductile fibrous initiation the toughness becomes independent of sample size. However attention should be given to the concept of the initiation transition temperature and its variation with specimen size so that the initiation process is well characterized both for the base plate and the weldment.

## Summary of Section 3

The fracture behavior of large scale welded structures such as pressure vessels, ships and offshore structures can be considered using either a $K_I$ or CTOD criterion. However the factors of safety which should be applied in conjunction with these two criteria are not universally accepted and should be defined in relation to Arctic exposure. The reasons for adopting a $K_I$ criterion are:

- large-scale structures hold large amounts of elastic energy and have high elastic constraint factors, thus final failure under design loads involves only small-scale yielding
- the use of a $K_I$ criterion has the advantage that from the experience with high strength materials there is a large available design literature related to various geometrical structures, crack configurations and combinations of loading systems
- for offshore structures used in Arctic conditions it is of value to use a $K_I$ criterion because it it necessary both to determine the behavior under conditions of full constraint and to consider the application of the $K_I$ criterion through the temperature range where there is a transition in fracture mechanism.

In considering the application of a CTOD criterion it is important to note the following points:

- much depends on the accuracy of the CTOD calibration curves and at low values of CTOD there are considerable errors in calibration
- there is some difficulty in establishing equivalent crack length based on CTOD data
- the assumption of linear stress-strain field may not be justifiable with the CTOD method

The main advantage of the CTOD method is that data can be obtained readily from standard full thickness samples for various elastic-plastic conditions.

**Summary of Section 4**

In considering the measurement of fracture toughness in structural steels the design temperature and loading rate can be specified, but it is important to consider the role of constraint when considering the behavior of large-scale structures.

When crack initiation occurs in either the elastic or small scale yielding condition, the influence of constraint can be determined by increasing the uncracked ligament length in three point bend samples. This will enable a determination of the fracture initiation mechanism at full constraint to be made.

For the determination of the parameters of initiation toughness, say $K_i$ or $\delta_i$, it is recommended that multispecimen tests and interrupted tests be used.

In considering the determination of fracture toughness data there remain a number of problems which need further consideration, viz:

- the minimum specimen size needed to represent the full constraint conditions of a large-scale structure
- the number of specimens needed to provide adequate confidence limits for the data, and the role of metallurgical variability on the definition of these limits
- the importance of "pop-in" processes and their significance in relation to the behavior of structures
- the need to consider the influence of specimen location for cases where samples are extracted from the weldment or heat-affected-zone

The existing data in the literature indicates that the values of $\delta_c$ for weld metals may range from 0.01 to 0.40 mm, indicating that attention must be given both to the confidence limits and extreme values of the test data.

## Summary of Section 5

In considering the application of fracture mechanics parameters to both design and material selection, it is useful to consider current experience in relation to failure probabilities.

There are a variety of CTOD initiation specifications in use. In many cases the specified value of $\delta_c$, $\delta_u$ is 0.25 mm. However for welded material the measured values are of the order of 0.03 to 0.10 mm, and yet the materials are satisfactory in service. Thus the specification of $\delta_i \geq 0.25$ mm may be too conservative.

If the alternative $K_I$ criterion were applied, the equivalent value of $\delta_i$ would be of the order of 0.05 mm which is much closer to the value observed in service.

The current experience with an in-service structural steel BS4360 50D would indicate that this steel used at -50°C would have a toughness of $K_c = 3000\text{N mm}^{-3/2}$ or $\delta_i \approx 0.05$ mm. It is probable that a Canadian produced grade 350 steel could meet similar specifications but cognizance must be taken both of the scatter in test data and the possible scatter in metallurgical structures on which these properties depend.

## Conclusion

### Proposal in regard to the development of a Canadian structural steel of yield stress 350 MPa for Arctic use

In developing a suitable grade 350 steel it would be of value to survey the values of $\delta_i$ for existing steels and the likely weld procedures to be used so that $\delta_i$ can be specified for the base plate, weld metal and heat-affected-zone. A test program could be developed in which the candidate steel is compared directly with the existing North Sea structural steel BS4360 50D to determine the following aspects of fracture behavior:

- the operative fracture initiation mechanism at the design temperature under conditions of full constraint
- the values of $\delta_i$ for samples from both actual weldments and Gleeble simulated samples over a range of temperatures
- a statistical analysis of the $\delta_i$ values and their scatter should be made.

# 1. INTRODUCTION

Fracture Mechanics is aimed at establishing the relationship between the level of the applied load, the size of existing defects, the material toughness and the degree of structural safety in service. In order to quantify these relationships it is necessary to consider, in detail, the following factors:

- methods for establishing safe operating stress levels
- specifications for allowable defect size, both for acceptance tests and service conditions
- determination of the required fracture toughness including,
  - selection of steels and welding procedures
  - requirement of PWHT
  - definition of the maximum thickness of the joint used
  - definition of the minimum temperature to be used
- prediction of safe life conditions for the structure including determining inspection periods and supplying a fracture control plan in the whole life of the structures

In the last two decades, fracture mechanics has successfully been used in areas where the applied stress level is lower than yield strength of materials used. Linear elastic fracture criteria have been shown to be valid in several areas including:

- the aircraft industry for high and ultra-high strength materials
- for nuclear pressure vessels constructed of low and medium strength steels in heavy section sizes

However, there is no extensive experience or specifications and standards for the application of fracture mechanics to offshore structures and ships, even though in the last two decades a mass of experimental and theoretical works have been performed aimed mainly at clarifying the following problems:

- the extent to which the CTOD design curve is valid and the definition of an alternative criterion
- the validity of the various CTOD fracture criteria
- assessment of the stress level in complex structures including stress concentration factors and residual stresses.

- studies of fracture toughness of welded joints in order to establish a rational fracture toughness testing procedure

- maximum defect size existing in both manufacture and service

- reliability criteria for offshore structures and ships

The existing literature provides a basis for evaluating the applicability of Arctic grade 350 structural plate using fracture mechanics methods. The successful development of Arctic grade structural steels must include:

- screening of both base plate and weldment properties

- classification of steels with respect to their resistance to brittle fracture

- quality control of steel production

- overall assessment of the applicability of new steels in Arctic service conditions, including corrosion and fatigue resistance

- development of data for use in fail-safe analysis

In defining the above objectives, it is assumed that three aspects of fail-safe analysis procedure schematically shown in Figure 1.1 have been previously established:

- definition of stress, temperature and loading rate, etc,
- maximum defect sizes and their likely location, and
- extent of service life and reliability required.

**Figure 1.1 - Scheme of fail-safe analysis**

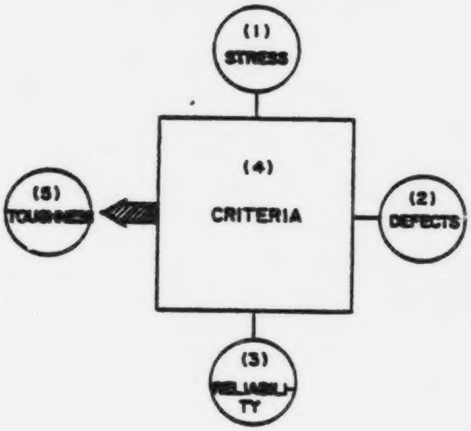

Thus, the essential problems are the establishment of a fracture criterion including its range of validity, reliability and accuracy and the design of a series of fracture toughness test methods and procedures of the material tested suitable for the various end-uses of the steel.

# 2. MECHANISMS OF FRACTURE AND FRACTURE TRANSITION

## 2.1 Definition

(1) For clarity, "Cleavage Fracture" and "Fibrous Fracture" are used to define two different microscopic fracture mechanisms which are easily differentiated by means of fractography.

"Elastic Fracture" and "Plastic Fracture" are used to define two alternative macroscopic fracture states, i.e., below and above the general yield condition. The identification of these two kinds of fracture states can be accomplished by reference to the load-displacement curves.

(2) Initiation, Extension and Unstable Growth of Cracks

The fracture process can be divided into three steps, i.e., crack initiation, crack extension (or stable crack growth) and unstable crack growth. The different stages may occur by different fracture mechanisms.

Determination of crack extension and the unstable growth mechanisms can be accomplished by a combination of fractographic studies and reference to the load-displacement curve for low and medium strength steels. However, the initiation mechanism is not easy to define in a unique manner.

(3) Fracture Initiation Mechanism (FIM)

The crack initiation mechanism can be defined with reference to the fractograph appearance in the region adjacent to the front of blunted crack as shown in Figure 2.1.

**Figure 2.1 - Crack Tip Blunting**

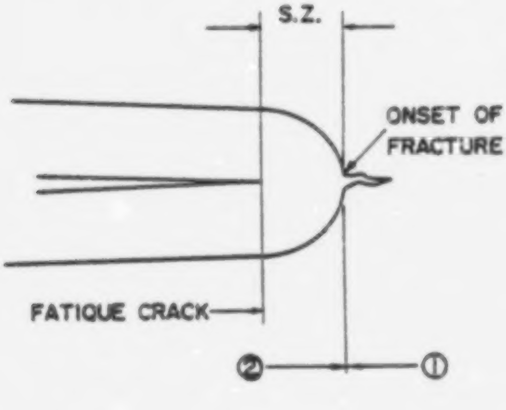

The nature and extent of the stretched zone is the deciding factor determining the initiation fracture toughness. Providing the extent and nature of the stretched zone is the same, then no matter what the mechanism of the successive crack extension, the initiation fracture toughness is the same, regardless of sample size.

For cleavage failure, there are two possibilities. The first is cleavage initiation within the stretched zone and the alternative is cleavage initiation after production of the stretched zone. Otsuka et al[1] (1975) have used similar definitions.

For simplicity, crack initiation can be defined as being either by the fibrous mode or by cleavage. With a sufficiently developed stretched zone, it is referred to as fibrous fracture initiation and in the case where fracture occurs by cleavage without a clearly developed stretched zone it is called cleavage fracture initiation. However, it should be noted that in hetergenous microstructures the mode of initiation may vary with position in the structure or occur by a mixed mode.

(4) Combination of Fracture Mechanisms and Processes

The various combinations of fracture initiation and propagation processes are summarized in Table 2.1.

Table 2.1 - The combination of fracture mechanisms and processes

| | Initiation | Fracture Processes | |
|---|---|---|---|
| | | Extension (stable growth) | Unstable |
| 1 | fibrous | fibrous | fibrous |
| 2 | fibrous | fibrous | cleavage |
| 3 | fibrous | - | cleavage |
| 4 | cleavage | - | cleavage |

## 2.2 Fracture Mechanism and Toughness

(1) Fracture Toughness

Fracture toughness tests of low-medium strength structural steels has shown that there are two regimes of temperature relating to two different toughness levels, as shown in Figure 2.2.

**Figure 2.2 - Fracture toughness as a function of temperature**

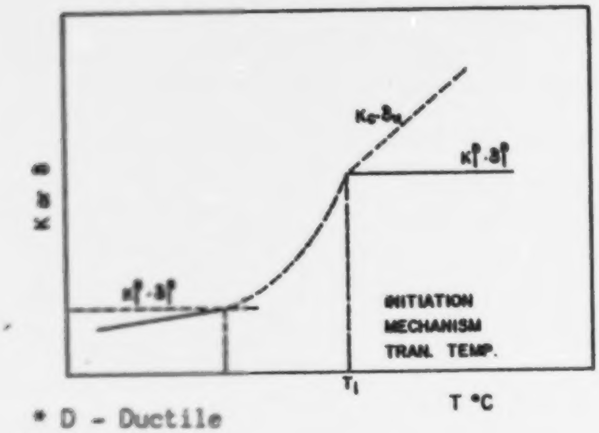

* D - Ductile
** B - Brittle

It is worth noting that when test temperature $T > T_i$ as shown in figure 2.2, the initiation fracture toughness referred to as $K_i^D$ or $\delta_i^D$ is almost independent of specimen size, test temperature and loading rate.

In the low temperature region, $T < T_i$ the initiation fracture toughness is only slightly dependent on temperature, but appears to be independent of specimen size and loading rate, and is referred to as $K_i^B$ or $\delta_i^B$.

In the initiation mechanism transition temperature region, i.e., when T is quite close to $T_i$, fracture toughness values exhibit very large scatter between fibrous initiation fracture toughness $K_i^D$ and cleavage fracture toughness $K_i^B$.

In general, $K_i^D$ varies from 4000 to 6000 $Nmm^{-3/2}$ and $K_i^B$ from 2000 to 3000 $Nmm^{-3/2}$ for medium strength structural steels. Their corresponding crack tip opening displacement (CTOD) values are from 0.12 to 0.24 mm and from 0.03 to 0.07 mm, respectively.

In contrast with initiation toughness $K_i^D$ and $K_i^B$, the unstable toughness corresponding to unstable growth, which is referred to as $K_c$ or $\delta_u$ in figure 2.2, is strongly dependent on specimen size or structural constraint.

(2) Cleavage Initiation Mechanism

The usual criterion used for cleavage is a critical stress criterion denoted as $\sigma_f^*$, i.e. cleavage will occur when:

$$(\sigma)_{max} = \sigma_f^*$$

The theory due to Ritchie, Knott and Rice[2] offers an explanation of the observed $K_{IC}(T)$ variation with temperature.

Curry[3] has given an analytical expression of $K_{IC}$ by taking the Hutchinson, Rice and Rosegren solution in a Ramberg-Osgood material with a strain hardening exponent n.

$$K_{IC} = k\ \sigma_{ys}^{2/(n-1)} \qquad (2.1)$$

where: $$\varepsilon/\varepsilon_{ys} = \sigma/\sigma_{ys} + \alpha(\sigma/\sigma_{ys})^n \qquad (2.2)$$

and k is a constant for a given material. For medium strength steel, n is about 5 and $\sigma_{ys}$ is a function of test temperature.

Otsuka et al[1] have measured the stretched zone width under conditions of cleavage crack initiation and found that as temperature decreases, the stretched zone width (SZW) decreases as shown in Figure 2.3.

**Figure 2.3 - Stretched zone width versus temperature**

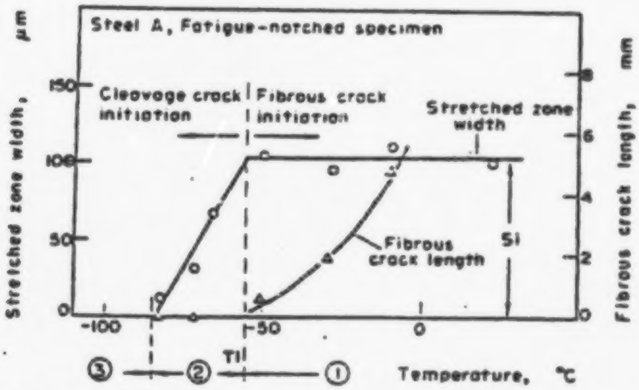

① : Fracture occurs by fibrous crack with streted zone
② : Fracture occurs by cleavage with stretched zone
③ : Fracture occurs by cleavage without stretched zone

This variation can be explained qualitatively by using the model given by Otsuka et al.[4] For a crack-bearing body, it is expected that as the applied load increases, the variation of maximum stress versus maximum effective strain ahead of a crack will go up as shown in figure 2.4 (b). Cleavage fracture will occur at $(\sigma_Z)_m = \sigma_f^*$, i.e. $P = P_c$. In Figure 2.4 (b), $T_2$ is lower than $T_i$, so at cleavage fracture, the $(\varepsilon_{eff})_m$ at $T_2$ is greater than at $T_1$.

**Figure 2.4 - Schematic diagram showing (a) stress, $\sigma_Z$ and strain $\varepsilon_{eff}$ as a function of distance from crack tip at P = P; (b) the trace of $(\sigma_Z)_m$ and $(\varepsilon_{eff})_m$**

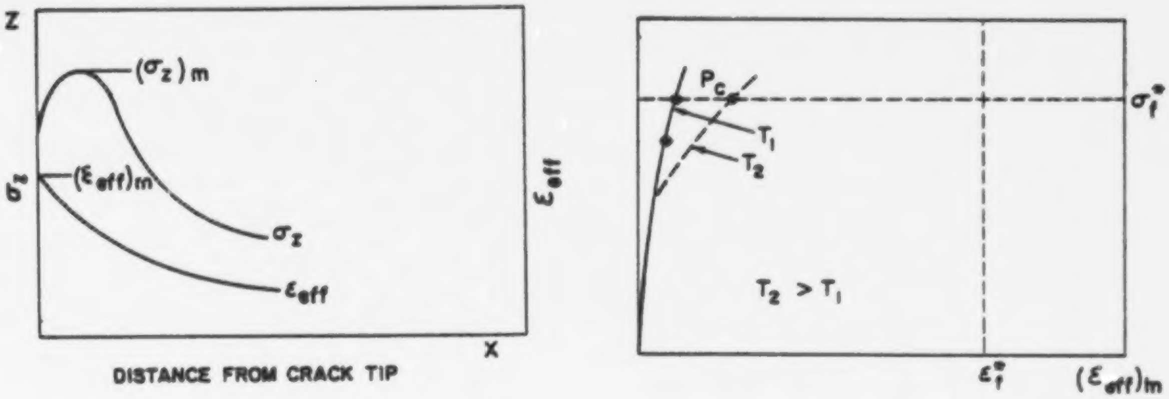

(3) Fibrous Initiation Mechanism

The criterion of fibrous fracture is usually assumed to be a critical strain criterion. The critical strain can be referred to as $\varepsilon_f^*$, and the criterion becomes:

$$(\varepsilon_{eff})_m = \varepsilon_f^*$$

Otsuka et al[4] have measured the dependence of effective strain at fibrous fracture initiation on the degree of triaxiality, $\sigma_m/\sigma$ at the notch root or crack tip (Figure 2.5).

Figure 2.5 - Dependence of effective strain at fibrous crack initiation on stress triaxiality

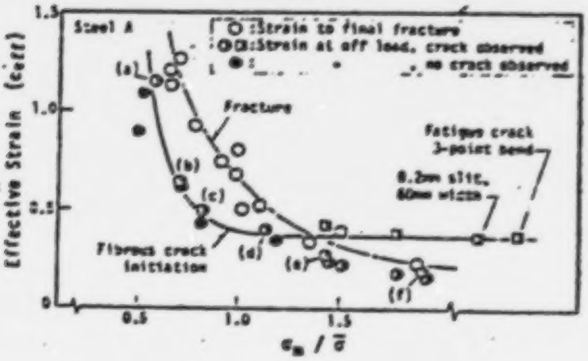

where: $$\sigma_m = \frac{\sigma_1 + \sigma_2 + \sigma_3}{3}$$

$\sigma_1$, $\sigma_2$ and $\sigma_3$ are principal stresses

and $$\sigma = \frac{1}{\sqrt{2}} \sqrt{(\sigma_1-\sigma_2)^2 + (\sigma_2-\sigma_3)^2 + (\sigma_3-\sigma_1)^2}$$

The effective strain at fibrous crack initiation varies sharply with increase of $\sigma_m/\sigma$ in the region $\sigma_m/\sigma$ <1.0 ~1.2, however it decreases to an almost constant value for large values of $\sigma_m/\sigma$. The constant effective strain at initiation is $\varepsilon_f* = 0.36$.

In the same paper[4] the authors calculated the trace of the maximum stress (z direction vertical to the crack plane), $(\sigma_z)_m$ and the maximum effective strain $(\varepsilon_{eff})_m$ for another steel, at -65°C by using FEM. The result is shown schematically in Figure 2.6 and in detail in Figure 2.8.

Figure 2.6 - Schematic diagram showing the variation of $(\sigma_z)_m$ and $(\varepsilon_{eff})_m$

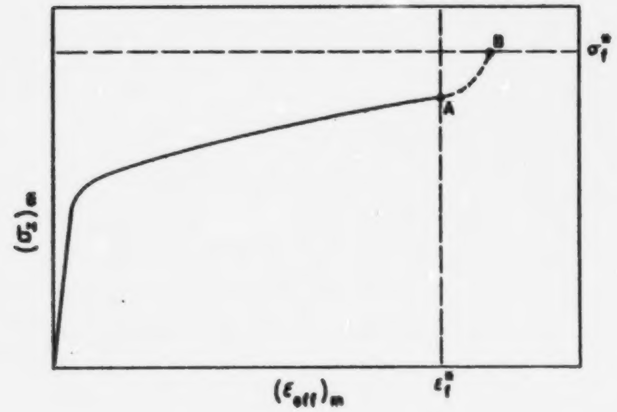

When $(\varepsilon_{eff})_m$ reaches $\varepsilon_f^*$ (for a given material) prior to the attainment of $(\sigma_z)_m$ equal to $\sigma_f^*$, then fibrous crack initiation occurs, followed by fibrous stable crack growth.

Because $\varepsilon_f^*$ is a constant for a given material and independent of temperature, specimen size and strain rate in the temperature range from -100°C to 20°C and crosshead speed range from 1.3 x $10^{-2}$ mm/sec to 4.8 x $10^3$ mm/sec[4], then the fibrous crack initiation fracture toughness $K_i^D$ or $\delta_i^D$ should be essentially independent of temperature, specimen size and strain rate. This is also supported by the observation of constant size of stretched zone width with increase of temperature as shown in figure 2.3.

It should be noted that the unstable fracture toughness $K_c$ or $\delta_u$ behaves in a different manner, increasing with increase of temperature and decrease of constraint in the specimen.

(4) Stable Crack Extension Mechanism

It can be seen in figure 2.6 that after the onset of fibrous crack initiation at point A, the process becomes one of fibrous stable crack growth accompanied by an increase of the applied load. As the crack grows, the applied load increases and the material work hardens, the values of $(\sigma_z)_m$ and $(\varepsilon_{eff})_m$ ahead of extended crack tip still increase, in the manner shown by the dashed line in figure 2.6. If $(\sigma_z)_m$ reaches the value of $\sigma_f^*$ before the onset of unstable plastic fracture, then fibrous stable crack growth will change into unstable crack growth by cleavage corresponding to an unstable fracture toughness denoted as $K_c$ or $\delta_u$.

If the value of $(\sigma_z)_m$ does not reach $\sigma_f$* then the sample fails by fibrqus unstable crack growth and its corresponding unstable fracture toughness can be denoted as $K_m$ or $\delta_m$.

It can be expected that the amount of stable crack growth depends on test temperature, specimen size or structural constraint and strain rate, as well as the crack extension resistance curve of the material.

It is worth noting that as specimen size increases, the amount of stable crack growth increases for high strength steels, while on the contrary, it decreases for medium strength steels.

## 2.3 Transition of Crack Initiation Mechanism

(1) Crack Initiation Mechanism Transition Temperature

As the temperature decreases, the crack initiation mechanism will change from fibrous to cleavage crack initiation at the crack initiation transition temperature $T_i$ (Otsuka[5]).

The temperature $T_i$ varies with specimen thickness B. Otsuka et al[5] have measured the dependence of $T_i$ on specimen thickness for five medium strength C-Mn steels, whose mechanical properties and chemical compositions are listed in Table 2.2.

**Table 2.2 - Mechanical properties and chemical compositions (%) of steels**

| Steel | Thickness (as-rolled) (mm) | Yield Strength (kg/mm$^2$) | UTS (kg/mm$^2$) | C | Si | Mn | P | S | Ni | Cr | Mo | V |
|---|---|---|---|---|---|---|---|---|---|---|---|---|
| Steel A JIS SM50C | 50 | 35 | 54 | 0.16 | 0.33 | 1.40 | 0.021 | 0.014 | 0.02 | 0.02 | - | - |
| Steel B ASTM A387B | 50 | 36.1 | 55.9 | 0.17 | 0.25 | 0.58 | 0.014 | 0.009 | - | 1.10 | 0.50 | - |
| Steel C JIS SM58Q | 50 | 50.0 | 60.7 | 0.13 | 0.42 | 1.02 | 0.013 | 0.005 | 0.170 | 0.010 | 0.250 | 0.014 |
| Steel D (HT80) | 25 | 77.7 | 82.9 | 0.15 | 0.22 | 1.00 | 0.015 | 0.006 | 0.017 | 0.29 | 0.27 | - |
| Steel E JIS SM50C | 25 | 34.7 | 52.2 | 0.16 | 0.30 | 1.40 | 0.013 | 0.013 | 0.013 | 0.05 | 0.02 | 0.02 |

The test results are shown in Figure 2.7.

**Figure 2.7 - Variation of $T_i$ with specimen thickness B for various steels[5]**

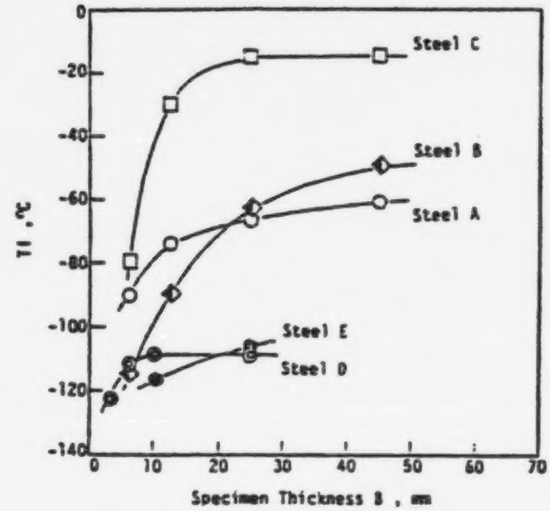

The transition temperature $T_i$ increases with increase of specimen thickness due to the variation in stress state. $T_i$ takes its upper limiting value when the plane strain state develops at the crack tip at the midthickness where crack initiation occurs. This upper value of $T_i$ denoted by $T_{ic}$ (plane strain $T_i$) may be regarded as a material parameter.

Otsuka[5] et al have expressed the specimen size requirement for plane strain $T_{ic}$ by the following formula:

$$a,\ B,\ w-a > 0.4\ \frac{\delta_i E}{\sigma_{ys} R} \qquad (2.3)$$

where E is Youngs modulus, $\sigma_{ys}$ is yield stress and R is the ratio of yield strength to ultimate tensile strength.

For medium strength C-Mn steels, it is usual to take the following expression:

$$J_i = 1.8\ \sigma_{ys}\delta_i \qquad (2.4)$$

based on the consideration of correlation of $J_p$ and $\delta$ being well satisfied with $J_p = k\sigma_{ys}\delta_p$, where k varies from 1.6 to 2.0, from the results given[6] for an API X70 pipeline steel.

Substituting equation (2.4) into equation (2.3) and taking $J_iE = K_i^2$ we obtain:

$$a,\ B,\ w-a > \frac{0.22}{R} \left( \frac{K_i}{\sigma_{ys}} \right)^2 \qquad (2.5)$$

Thus we can use $B_{ic}$ to denote the thickness required to meet the condition expressed in (2.5).

The important conclusion to be drawn from this, is that when the test temperature is higher than $T_{ic}$, the crack initiation mechanism no longer changes with increase of specimen thickness. It can be seen in Figure 2.7 that the $T_{ic}$ is lower than -50°C for steels with yield strength lower than 400 $Nmm^{-2}$.

The crack initiation mechanism transition caused by variation of temperature can also be expressed by making use of the relations given by Otsuka[4] shown in Figure 2.8.

**Figure 2.8 - (a) The relationship between $(\sigma_z)_m$ and $(\varepsilon_{eff})_m$; (b) the transition in initiation mechanism[4]**

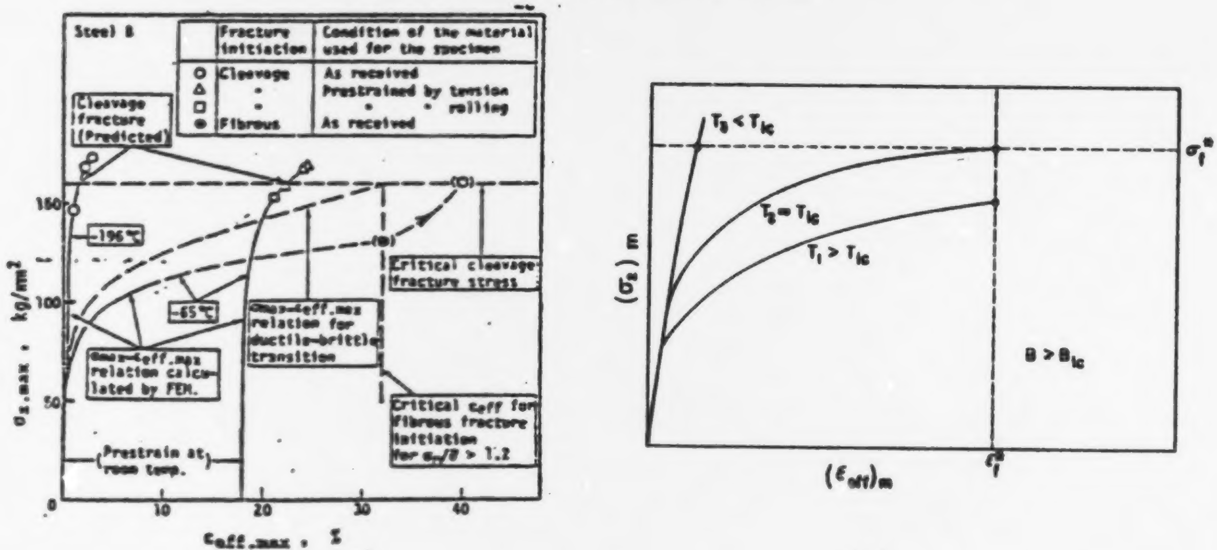

(a)

(b)

It can be seen that as the temperature decreases the $(\sigma_z)_m$ at fibrous crack initiation approaches $\sigma_f^*$. When $T = T_{ic}$, $(\sigma_z)_m = \sigma_f^*$ and $(\varepsilon_{eff})_m = \varepsilon_f^*$ at the same time.

### (2) Effect of Thickness

From the preceding section, it can be seen that if the test temperature $T < T_{ic}$, the increase of specimen thickness can always bring about the transition of crack initiation mechanism.

It is known that $T_i$ is a function of specimen thickness B, as shown in Figure 2.9.

**Figure 2.9 - $T_i$ as a function of thickness B**

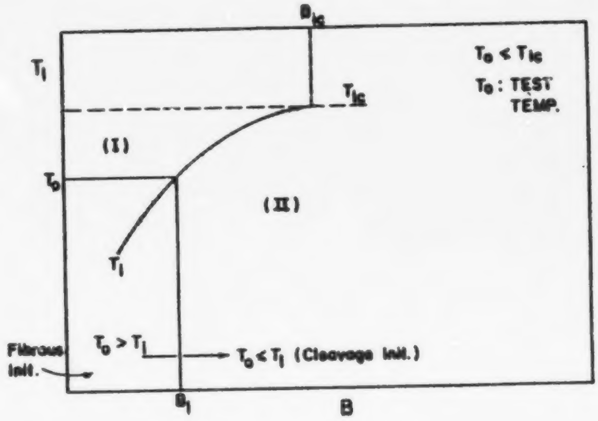

It can be seen that in region (I), $B < B_i$ and $T_o > T_i$, so fibrous initiation will occur, while in region II $B > B_i$ and $T_o < T_i$, then cleavage initiation will occur.

So far the only effect of thickness which has been considered is that on $T_i$. It is not known whether $T_i$ also varies with increase of a and w-a when thickness B is fixed.

For example, consider a plate of thickness B, and initiation mechanism transition temperature $T_i$. Suppose that the test temperature $T > T_i$, the initiation mechanism will be the fibrous mechanism for a proportional specimen, i.e. a and w-a approximately equal to B, but it is not known if the initiation mechanism varies if a or w-a increases whilst B is constant.

It can be expected that fracture toughness $K_i$ will vary with specimen thickness. When $T > T_{ic}$, it means that the initiation mechanism no longer changes with specimen size, so $K_i$ behaves as shown in Figure 2.10.

**Figure 2.10 - The effect of thickness on $K_i$ and $\delta_i$ (for $T > T_{ic}$)**

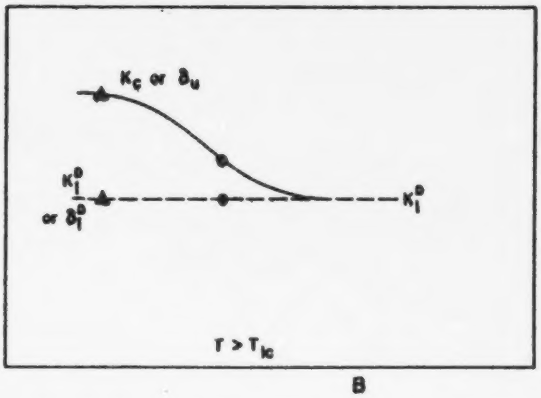

If the test temperature $T < T_{ic}$, then the fracture initiation toughness $K_i$ will change as the fracture mechanism changes, as shown in Figure 2.11.

**Figure 2.11 - The dependence of $K_i$ and $\delta_i$ on thickness B (for $T < T_{ic}$)**

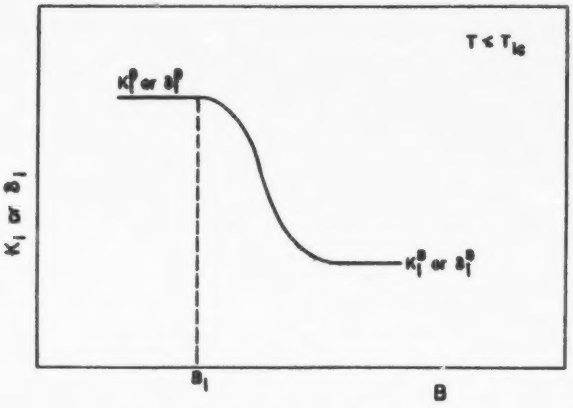

(3) Transition Temperature Range

The variation of fracture mechanisms and toughness within the transition temperature range $\Delta T_i (= T_i - T_{io})$ are shown schematically in Figure 2.12.

**Figure 2.12 - Schematic showing fracture mechanism and toughness within transition temperature range $\Delta T_i$**

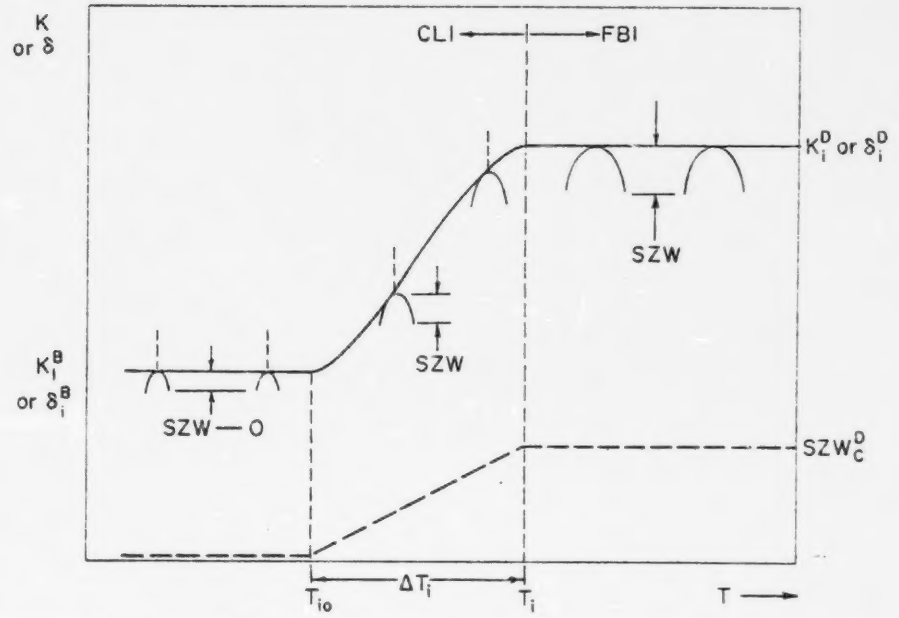

The initiation mechanism within $\Delta T_i$ is cleavage but with the stretched zone developed to various extents. The corresponding initiation fracture toughness $K_i$ or $\delta_i$ is between $K_i^D$ and $K_i^B$ or $\delta_i^D$ and $\delta_i^B$.

It can be expected that there is a transition thickness range where the fracture initiation mechanism and toughness have the same features as mentioned above when test temperature $T < T_{ic}$. This is shown in Figure 2.13.

**Figure 2.13 - Schematic showing initiation mechanism and toughness within the transition thickness range**

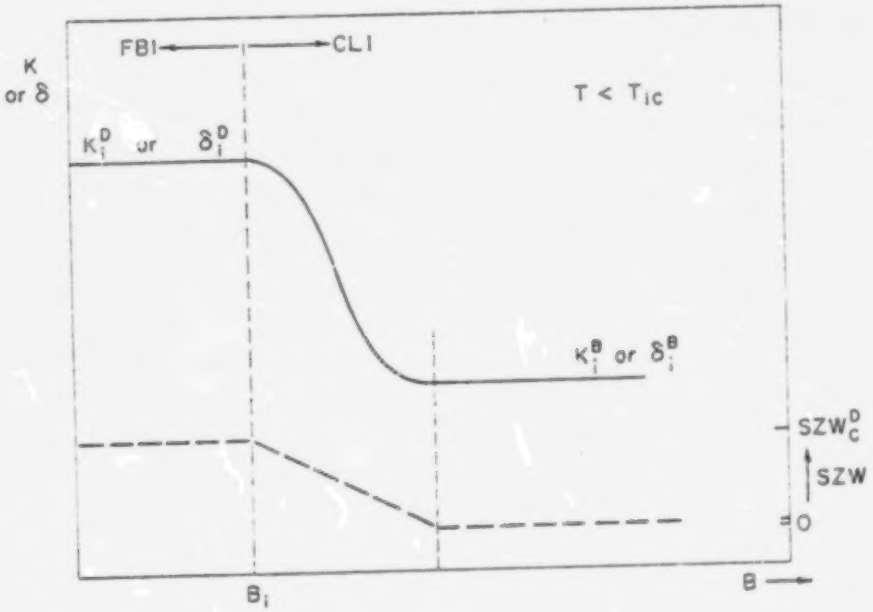

We can also use the model given by Otsuka to explain qualitatively the variation of stretched zone both with change of temperature and thickness. This has been shown in Figure 2.14.

The width of the transition range will depend predominantly on the sensitivity of the material strength and hardening to temperature and to the degree of stress triaxiality.

Figure 2.14 - Schematic showing the traces of $(\sigma_z)_m$ and $(\epsilon_{eff})_m$ ahead of crack tip vary with (a) temperature and (b) thickness when $T < T_{ic}$

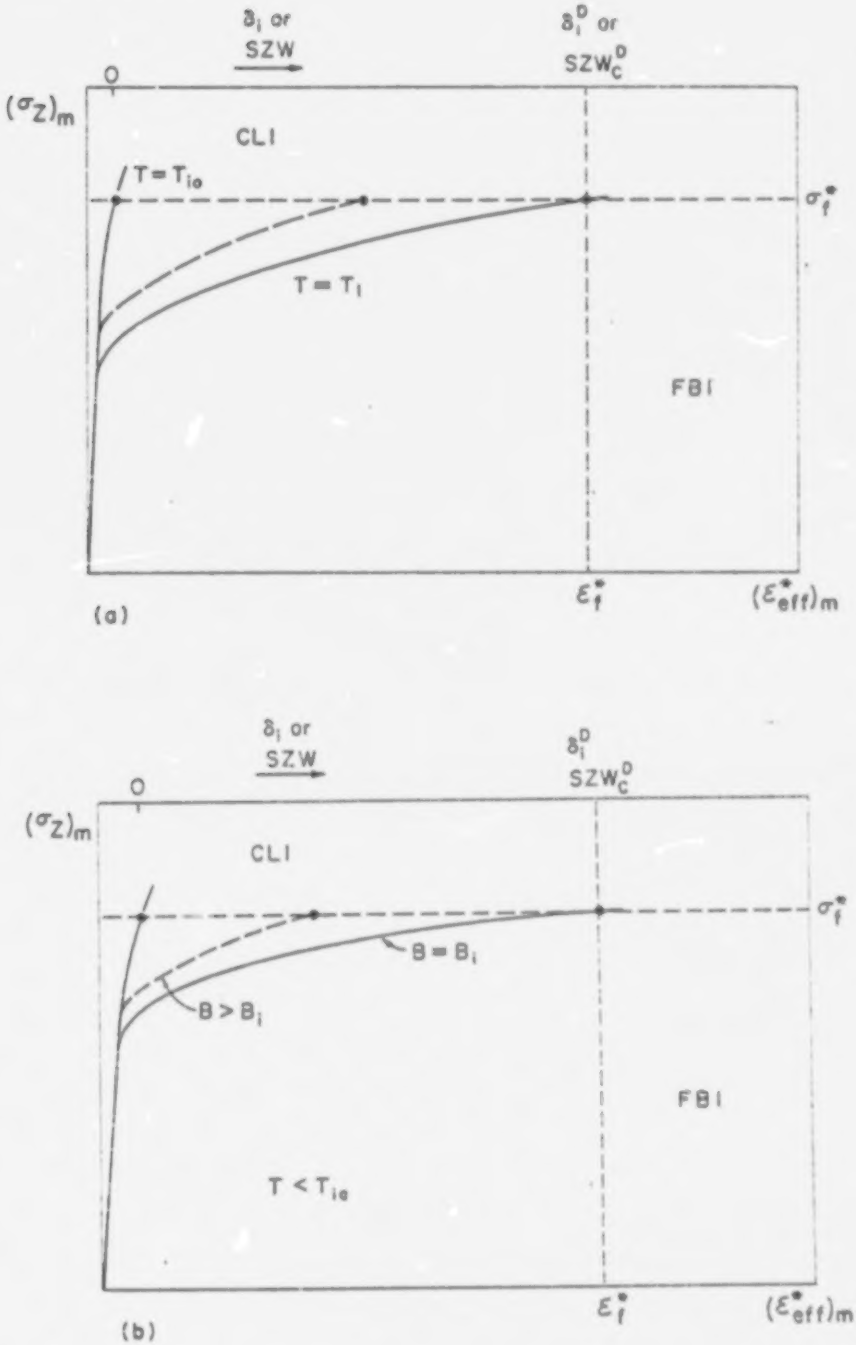
δ_i or SZW
δ_i^D or SZW_c^D
0
(σZ)m
CLI
T = T_io
σ_f*
T = T_i
FBI
ε_f*
(ε*_eff)m
(a)
δ_i or SZW
δ_i^D SZW_c^D
0
(σZ)m
CLI
σ_f*
B = B_i
B > B_i
FBI
T < T_io
ε_f*
(ε*_eff)m
(b)

## REFERENCES

1. A. Otsuka, T. Miyata, S. Nishimura and Y. Kashiragi: "Crack Initiation from a Sharp Notch and Stretched Zone", Engineering Fracture Mechanics, Vol 7, 1975, pp 419-128.

2. R. O. Ritchie, J. F. Knott and J. R. Rice: J of Mechanics and Physics in Solid, Vol 21, p 395, 1978.

3. D. A. Curry: "Micromechanisms of Crack Extension", Conf Preprints, Cambridge, 31/3-2/4, Paper No. 4, 1980.

4. A. Otsuka, T. Miyata, S. Nishimura and M. Orashi: "Effects of Stress Triaxiality on Ductile Fracture Initiation and Ductile-Brittle Transition in Prestrained Steel", Fracture Mechanics in Engineering Application by G. C. Sih and S. R. Valluri.

5. A. Otsuka, T. Miyata and S. Nishimura: "Fracture Toughness and the Transition in Fracture Initiation Mode in Low and Medium Strength Steel", Fracture Mechanics and Technology, Vol 1 by G. C. Sih and C. L. Chow, 1977 March 21-25, Hong Kong, pp 539-551.

6. P. Brozzo and G. Buzzichelli: "On the Metallurgical Design of Steels with High Fracture Toughness", Analytical and Experimental Fracture Mechanics by G. C. Sih and M. Mirabile, pp 45-79.

# 3. FRACTURE CRITERIA

## 3.1 General

In fracture mechanics, one can use either the stress intensity factor $K_1$ criterion used for linear elastic fracture mechanics or in the elastic plastic regime either the crack tip opening displacement CTOD criterion or the J-integral criterion.

Both the $K_1$ criterion and CTOD criterion are currently being used in pressure vessels, offshore structures and ship design. The $K_1$ criterion is simpler and more strictly defined than the CTOD criterion, but the application of $K_1$ criterion to welded structures of low and medium strength steels is still contentious.

In attempting to apply CTOD methods, the following aspects must be considered:

- How to delineate a factor of safety in the CTOD design curve; in the current literature, it ranges from 1 to 8.
- The reliability of the unstable fracture toughness $\delta_u$ (corresponding to maximum load).
- The currently preferred Bx2B CTOD specimen may not represent the maximum constraint operative in structures.

For Arctic grade 350 structural plates such as those of current interest, there may be some advantages in using a $K_1$ criterion, because:

- the design temperature is -50°C or lower
- sections of plate heavier than those used in shipbuilding may be utilized
- low nominal design stress are operative compared with those in shipbuilding applications

## 3.2 Validity of $K_1$ Criteria

### (1) General

Generally speaking, the low stress fracture regime is described by a $K_1$ criterion. However, the definition of the fracture stress is in dispute. There is so far no consistent opinions and the required value of $\sigma/\sigma_{ys}$ varies from 0.5 (CTOD design curve) to 0.9 (surface crack fracture toughness test) for uniform tensile stress, and from 1.0 (BS PD 6493[1] and ASME code[2]) to 1.4 (NK code[3]) for complex stress including tension and bending, stress concentration and residual or thermal stresses.

In order to determine an appropriate and simple fracture criterion, the validity of $K_I$ criterion will be further discussed in this section based on the limited available experimental work.

If the fracture or initiation occurs in the elastic part of the load-displacement curve, it is best described by a $K_I$ criterion, no matter what the specimen size (including crack length, thickness and ligament) and regardless how high some local stress will be, or how the load-displacement curve change after crack initiation as shown in Figure 3.1.

**Figure 3.1 - Schematic diagram showing the general stress state at crack initiation and unstable point; (a) elastic initiation and unstable; (b) elastic initiation and unstable; (c) plastic initiation and plastic unstable**

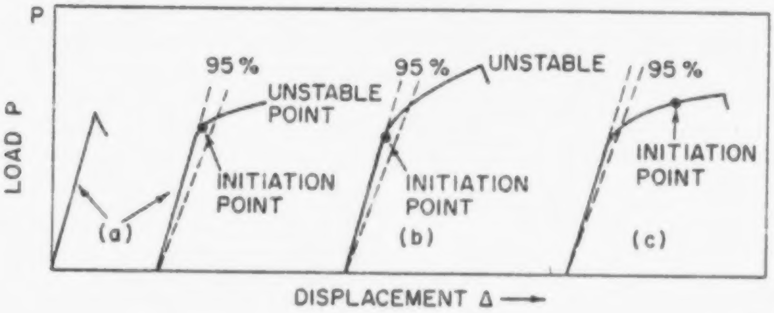

Note: For case (b) the deviation of the load-displacement curve from linear is caused by crack extension and supposes the applied stress is still lower than yield strength of the material.

So, in cases (a) and (b) in Figure 3.1, one can use $K_I$ criterion to predict the fracture load both at initiation and at unstable fracture, but for the latter, plane stress fracture toughness $K_c$ may be considered.

It is also worth noting that the 95 percent offset is adopted here to denote the limit of small scale yielding condition where the $K_I$ criterion is approximately valid according to experience of ASTM E399 testing method for $K_{Ic}$.

### (2) Tensile Stress

According to massive fracture toughness tests done with a surface crack under uniform tensile stress, the validity of the $K_1$ criterion can be expressed either by[4]

$$a, (t-a) \geq 0.5 \left( \frac{K_{IC}}{\sigma_{ys}} \right)^2$$

or by

$$\sigma_{net}/\sigma_{ys} = 0.9$$

This result is mainly based on tests for high strength steels. It is probable that the requirements for specimen size can be relaxed for medium strength steels relative to high strength steels.

Fedderson[5] has discussed the validity of the $K_1$ criterion for a surface-crack specimen made of high strength materials and pointed out that the limiting stress level is:

$$\sigma_c = 0.8\ \sigma_u$$

where $\sigma_c$ is the gross section fracture stress, $\sigma_u$ is ultimate tensile strength.

Mentl and Janda[6] have carried out fracture toughness tests of medium strength steel with surface crack under tensile loading. The material tested was CrMoV steel with $\sigma_{ys}$ = 565 $Nmm^{-2}$, $\sigma_u$ = 664 $Nmm^{-2}$ at 20°C and $\sigma_{ys}$ = 650 $Nmm^{-2}$, $\sigma_u$ = 761 $Nmm^{-2}$ at -100°C. The test results are shown in Figure 3.2.

Figure 3.2 - The dependence of fracture stress $\sigma_{max}$ on crack size a/t (Ref 6)

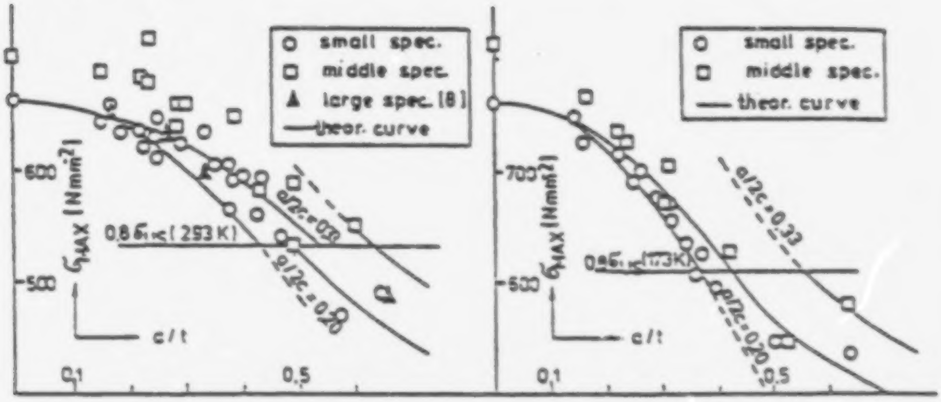

Mentl and Janda have found that the limiting stress level is of the order of 0.8 $\sigma_u$, which for a medium strength steel is equivalent to:

$$\sigma_c/\sigma_{ys} = 0.94$$

(3) Bending Stress

For offshore structures, the main stresses are compression and bending stresses.

It is well known that for three-point bending specimens the requirement of specimen sizes is:

$$B,\ a,\ w-a \geq 2.5\ (K_{IC}/\sigma_{ys})^2$$

It is useful to note that this requirement is based on earlier experience with high strength materials.

Ritter[7] (1977) has suggested that

$$B = 400\ \frac{K_{IC}^2}{E\sigma_{ys}} \qquad (3.1)$$

for structural steel. Thus taking $E=2\times10^5$ MPa, this becomes

$$B = \frac{\sigma_{ys}}{500}\ \left(\frac{K_{IC}}{\sigma_{ys}}\right)^2 \qquad (3.2)$$

For grade 350 steel at -50°C the yield strength is approximately 400 $\text{Nmm}^{-2}$, then

$$B = 0.8 \left( \frac{K_{IC}}{\sigma_{ys}} \right)^2$$

In fact, we will see later the requirement of specimen size can be relaxed still further.

Let us now consider the problem of deficiency when the load-displacement curve deviates from its straight line during the bending process.

It is known that the limit load can be obtained by using the following formula for a three-point bending specimen.

$$P_L = 1.5 \frac{B}{S} b^2 \sigma_{ys} \qquad (3.3)$$

where b is the width of uncracked ligament (i.e. w-a). In fact, the maximum load, Pm observed in the CTOD test is often greater than the value $P_L$ derived from an assumption of nonhardening material and the load at which the load-displacement deviates from its straight line is not smaller than 0.7 $P_L$. In other words, if the fracture load does not exceed 0.7 $P_L$, the fracture would be elastic and controlled by the $K_1$ criterion (see in Figure 3.3).

**Figure 3.3 - Schematic diagram showing common load-displacement curve**

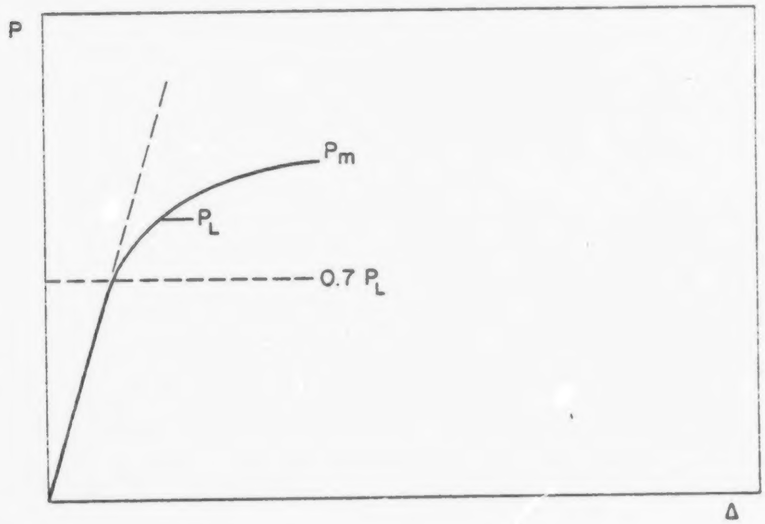

The maximum fibrous stress at crack tip, not considering the elastic stress concentration, can be written as

$$(\sigma_{net})_m = \frac{6PW}{Bb^2} \qquad (3.4)$$

substituting equation (3.3) into (3.4) and taking S=4W and P=0.7 $P_L$, then it becomes

$$(\sigma_{net})_m = 1.6\ \sigma_{ys} \qquad (3.5)$$

This means that under bending stresses even when the maximum fibre stress approaches 1.6 $\sigma_{ys}$, the general load-displacement remains in the elastic state. Thus, it can be expected that if the fracture occurs at this point, it would be controlled by the $K_1$ criterion.

Chell and Spink's work[8] supports the above analysis. The material used was CrMoV steel with a yield strength of 650 $Nmm^{-2}$ and ultimate strength of 757 $Nmm^{-2}$ and specimen size was 50 x 100 x 460 mm with crack length ranging from 6.1 mm to 52.3 mm. The test results are listed in Table 3.1.

**Table 3.1 - Test results**

| Spec No. | Crack Length a (mm) | $P_{max}$ (KN) | $K_{IC}$ $Nmm^{-3/2}$ | $\frac{P_{max}}{P_L}$ | $\frac{(\sigma_{net})_m}{\sigma_{ys}}$ |
|---|---|---|---|---|---|
| 3T | 6.1 | 858 | 4427 | 0.82 | 1.85 |
| 5T | 8.4 | 694 | 4142 | 0.70 | 1.58 |
| 4T | 13.5 | 583 | 4300 | 0.66 | 1.49 |
| 7T | 37.3 | 356 | 5059 | 0.73 | 1.64 |
| 2T | 52.3 | 195 | 4205 | 0.68 | 1.53 |

All the specimens showed linear elastic fracture behavior down to very small crack lengths. It can be seen that when the values of $P_{max}/P_L$ and $(\sigma_{net})_m/\sigma_{ys}$ increase up to 0.82 and 1.85, respectively, the $K_1$ criterion is still valid.

It is interesting to note that when the specimen thickness was decreased down to 25 mm, i.e., $B=0.66\ (K_{IC}/\sigma_{ys})^2$, the plane strain condition remained valid. Moreover, the shortest crack is just equal to plastic zone size, i.e. $a=0.16\ (K_{IC}/\sigma_{ys})^2 = 6$ mm.

The following analysis demonstrates that the ligament width is the deciding factor controlling whether fracture occurs in elastic condition.

It is well known that the $K_1$ expression can be written as:

$$K_1 = \frac{P}{B\sqrt{W}}\ Y(a/w) \qquad (3.6)$$

Where, for convenience, taking Y(a/w) for a short crack as

$$\begin{aligned} Y &= 3.5\ (1 - a/w)^{-3/2} \\ &= 3.5\ (w/b)^{3/2} \end{aligned} \qquad (3.7)$$

and substituting equation (3.7) and (3.4) into equation (3.6) it can be rewritten as

$$K_1 = \frac{1}{1.7}\ (\sigma_{net})_m \sqrt{b} \qquad (3.8)$$

Assuming that the elastic fracture condition is $P=0.7\ P_L$, i.e. $(\sigma_{net})_m = 1.6\ \sigma_{ys}$, equation (3.8) becomes

$$K_c = \frac{1.6}{1.7}\ \sigma_{ys} \sqrt{b} \qquad (3.9)$$

so that:

$$b = 1.1\ (K_c/\sigma_{ys})^2 \qquad (3.10)$$

Therefore, fracture or initiation can occur under elastic conditions if the size of the ligament width is sufficient.

Thus, it seems that for through thickness cracks in a large structure the fracture would be generally controlled by the $K_1$ criterion, because of the large ligament size.

(4) Stress Concentration

The most highly stressed region in structures is always related to stress concentrations associated with the discontinuity of the structure, such as weld toes, variation of thickness and nozzles, etc.

There is no direct experimental data to confirm the validity of the $K_1$ criterion under loading with stress concentration. However, it may be expected that the deciding factors determining whether the $K_1$ criterion is valid are the average net section stress and the peak value of stress concentration.

For example, the limiting stress level which meets the $K_1$ criterion is given below for a circumferential notched bar in tension.

$$\sigma_{net}/\sigma_{ys} = 1.1 \quad (3.11)$$

This criterion applies although the peak value of the stress at the notch root far exceeds the yield strength of the material. Also, due to the stress triaxiality at the notch, the required value of applied stress is raised.

The function of the side-groove in specimens for the $K_{Ic}$ test is similar. The local stress concentration can enlarge the valid range of the $K_1$ criterion.

For cracks located in welded joints and subjected to the stress concentration caused by variation of thickness or weld toes, and with ratios of crack length to a joint thickness t of the order of $a/t > 0.5$, it is only necessary to consider the average net section stress and to evaluate the validity of $K_1$ criterion.

Lereim[9] has reported that the local stress concentration caused by variation of thickness from 2t to t, influences the magnitude of stress intensity factor only for very shallow cracks relative to plate thickness ($a/t < 0.05$) for loading by bending stresses, as shown in Figure 3.4.

Figure 3.4 - The effect of stress concentration similar to T and cruciform plate joints

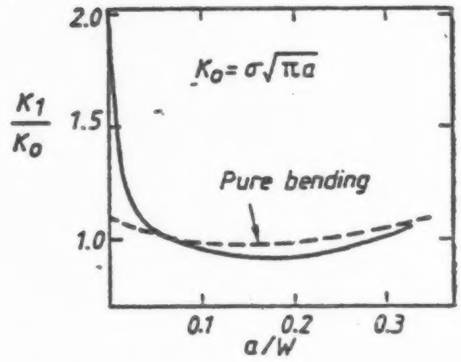

(5) Residual Stress

Residual stress is also a type of secondary stress. Both local stress concentrations and residual stresses are important when crack formation and subcritical crack growth are considered. The residual stress can be included as an equivalent K factor and this is outlined in section 5 of this report.

However, in the relevant NK code,[3] the residual strss is not taken into account when considering the validity of the $K_1$ criterion. After the determination of the $K_1$ criterion an equivalent tensile stress is taken as 0.3 $\sigma_{ys}$ for crack parallel to weld beam and 0.6 $\sigma_{ys}$ for cracks perpendicular to the weld beam.

Summary

The valid range of the $K_1$ criterion can be described in the following Figure 3.5 from the stress level point of view for uniform tension, bending and with stress concentrations.

**Figure 3.5 - Schematic diagram showing the range where the $K_1$ criterion is valid**

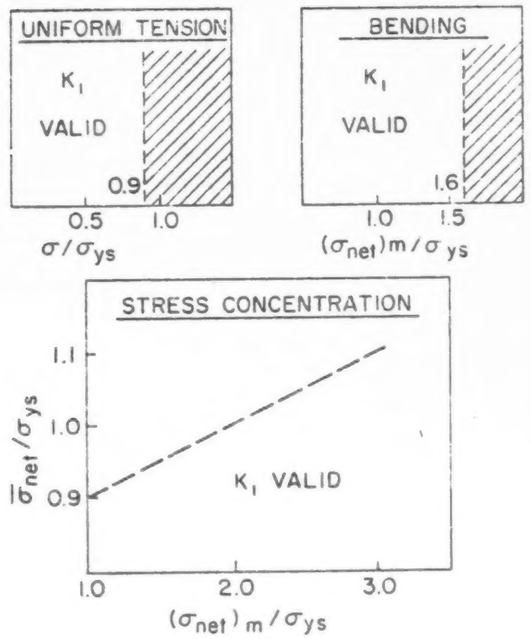

## 3.3 CTOD Criterion

If the stress level of interest exceeds the limitation of the $K_1$ criterion validity as shown in figure 3.5, other criteria are needed.

The one most widely used is the CTOD criterion. However, cognizance must be taken of the following points:

(1) CTOD Calibration Curve

Besides the existing CTOD design curve, a CTOD calibration curve is needed, based on both theoretical and experimental studies.

It is obvious that it is necessary to know how the CTOD in a real structure varies with applied load, crack length and geometry of components.

The CTOD design curve appears to be quite close to the calibration curve. Its establishment was based on experimental calibration by using a great number of wide plate tests, and the existing design curve also has a good agreement with computing results given by Goldman and Hutchinson[10] by using FEM.[11]

Many authors[9,12,13] have pointed out that the CTOD design curve involves a safety factor from 1 to 8 and even higher. This does not reflect the uncertainty of the relationship between the CTOD and applied load for wide plate specimens. However, it does demonstrate the uncertainties of fracture toughness of the materials, especially since unstable fractures are often preceded by different amounts of fibrous stable crack growth. The values of $\delta_u$ for a given material quite often differ by a factor of three to five, sometimes by a factor of more than ten.

The establishment of a CTOD calibration curve point, requires the direct measurement of CTOD. The replica technique using silicon rubber may be the best way for setting up of a CTOD calibration curve providing the rubber has dimensional stability.

However, the CTOD calibration curve is dependent on the materials properties particularly the hardening exponent. Thus, the CTOD calibration curves will be more complicated than K calibration curves.

(2) Superposition of Stresses or Strains

Due to the difficulties in establishing the CTOD calibration curve, it may be necessary to determine equivalent stress or strain for complex loading conditions.

(3) Effect of Constraint

The CTOD criterion requires that the fracture toughness be obtained under conditions of full constraint.

However, the condition for full constraint for the CTOD criterion in medium strength structural steels may be that where elastic fracture or initiation can occur, i.e., when the $K_1$ criterion is valid.

For example, for steel plate 30 mm thick and using the standard CTOD specimen of 30 x 60 mm section size, the crack initiation mechanism may be by the fibrous mode at -50°C. The influence of the ligament size and the amount of stable crack growth on the unstable fracture toughness $\delta_u$ is not well documented. Thus, it is difficult at this stage to adopt $\delta_u$ for medium strength steels, particularly for welded joints having a higher transition temperature compared with the minimum design temperature for the Arctic.

## 3.4 Other Criteria

Some fracture criteria are being developed for use where the stress level obviously exceeds the yield strength of the material.

One of them has been used in ASME code[2] by applying linear interpolation between the fracture load equivalent to the ultimate tensile strength $\sigma_u$ at crack length a=o and that given by the $K_1$ criterion at stress level $\sigma=\sigma_{ys}$. This is shown in Figure 3.6.

**Figure 3.6 - Schematic diagram showing the linear interpolation between $\sigma_{ys}$ and $\sigma_u$**

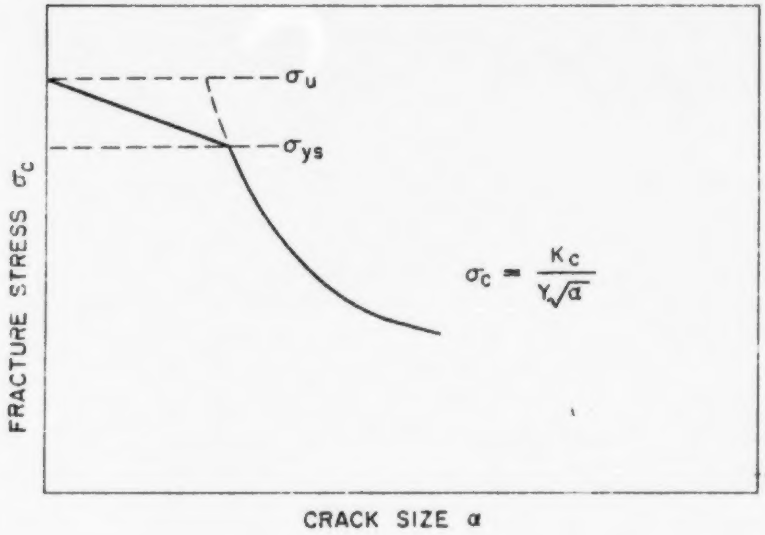

$\sigma_u$
$\sigma_{ys}$
$\sigma_c = \frac{K_c}{Y\sqrt{a}}$
FRACTURE STRESS $\sigma_c$
CRACK SIZE $a$

The conversion of the actual stresses can be approximated as follows:

$$\sigma = \sigma_{ys} + \frac{1}{30}(\sigma_p - \sigma_{ys}) \qquad (3.12)$$

where $\sigma_p = \sum\varepsilon\cdot E$ and $\sum\varepsilon$ is the sum of each strain component such as primary tension strain, strain caused by stress concentration and residual strain, etc.

For the assessment of defects, i.e., determination of critical and allowable crack size for stress levels below the lower limit of stress, the $K_1$ method is adequate.

If we wish to know the residual strength of structures having a given crack, e.g. an allowable crack size and which results in a strength level given by $K_1$ criterion which is higher than yield stress or even ultimate strength, then other fracture criterion are needed.

## REFERENCES

1. BS PD 6493:1980, "Guidance on Some Methods for the Derivation of Acceptance Levels for Defects in Fusion Welded Joints", British Standards Institution, March, 1980.

2. ASME Boiler and Pressure Vessel Code, Section III Nuclear Power Plant Components, App G; Protection against Non-ductile Failure, 1977.

3. H. Yajima, Lecture Notes, "Application of Fracture Mechanics in Shipbuilding" in Ship Research Centre of China, Wuxi 8-15, Apl 1982.

4. T. W. Orange, "Fracture Testing with Surface Crack Specimens", J of Testing and Evaluation, Vol 3, No. 5, September, 1975, pp 335-342.

5. C. E. Feddersen, "Fracture Behavior of Surface Cracked Tension Element", AIAA Journal, Vol 9, No. 12, 1971, pp 2309-2313.

6. V. Mentl and R. Janda, "Residual Strength of Surface Crack Specimens", Skoda Res Report, UV2U, Report T12 1158, P1ZEN, 1979, p 305.

7. J. C. Ritter, "A Modified Thickness Criterion for Fracture Toughness Testing", Engineering Fracture Mechanics, Vol 9, 1977, pp 521-540.

8. G. G. Chell and G. M. Spink, "A Post Yield Fracture Mechanics Analysis of Three-Point-Bend Specimens and Its Implications to Fracture Toughness Testing", Engineering Fracture Mechanics, Vol 9, 1977, pp 101-121.

9. J. Leriem, "Elastic-Plastic Fracture Analysis of Heavy Welded Structural Elements", 2nd Int Conf on Offshore Welded Structures, London 16-18 Nov, 1982, paper 13.

10. N. L. Goldman and J. W. Hutchinson, Int J of Solids Structures, No. 11, 1975, pp 575-591.

11. C. K. Tsai et al, "Crack Opening Displacement Analysis in Areas of High Nominal Strain", IIW Doc X-900-78, 1978.

# 4. FRACTURE TOUGHNESS AND ITS TESTING

## 4.1 Fracture Toughness of Medium Strength Steels

### 4.1.1 General Aspects

### (1) Literature Survey

The tensile properties of medium strength welded structural steels are dependent on temperature, strain rate and stress state; thus, it is necessary to know the probable range of these factors in service.

According to the literature[1,2] we can consider:

- minimum design temperature is of the order -50°C
- welded structures will involve plate thicknesses of up to 100 mm
- static loading rather than dynamic loading conditions are dominant

Let us consider the design philosophy with regard to protection against brittle fracture. Prevention of crack initiation is often used in design of offshore structures. This can also be considered as preventing cleavage initiation or unstable fracture if a certain amount of fibrous initiation is allowed.

For clarity we define the initiation fracture toughness as

$K_{i}^{D}$, $\delta_{i}^{D}$ and $J_{i}^{D}$ for fibrous initiation

$K_{i}^{B}$, $\delta_{i}^{B}$ and $J_{i}^{B}$ for cleavage initiation

These parameters are basically independent of specimen size as mentioned in section 2. There is no plane stress problem in crack initiation in the thickness range of interest.

We also have unstable fracture toughness denoted here as

$K_c$, $\delta_c$ and $J_c$ regardless of the fracture mechanism

These are plane stress parameters and are influenced by specimen size.

When the initiation mechanism is the same, then initiation fracture toughness can be converted from one to the other using the following formulas:

$$K_i = \sqrt{1.8\, E'\sigma_{ys}\, \delta_i} \qquad (4.1)$$

$$= 643 \sqrt{\sigma_{ys}\, \delta_i} \quad (\mathrm{Nmm}^{-3/2})$$

and

$$K_i = \sqrt{J_i E'} \qquad (4.2)$$

$$= 480 \sqrt{J_i} \quad (\mathrm{Nmm}^{-3/2})$$

and

$$J_i = 1.8\, \sigma_{ys}\, \delta_i \quad (\mathrm{Nmm}^{-1}) \qquad (2.4)(4.3)$$

where: $E' = E/(1-\nu^2) = 230\ 000\ \mathrm{N\ mm}^{-2}$ for low alloy steels

In relation to the design it would be very useful to know:

- the transition temperature $T_i$ under maximum constraint
- the critical thickness, $B_i$, causing transition of initiation mechanism at design temperature
- the variation of the amount of stable crack growth with constraint
- the design of specimen possessing maximum constraint compared with typical structures, and finally
- the two levels of initiation toughness values, i.e. $K_i^D$ and $K_i^B$.

### (2) Transition Temperature and Fracture Toughness

There are many correlations between transition temperature and fracture toughness. However only the following ones have been adopted in some standards and specifications related to pressure vessels, offshore structures and shipbuilding.

It is worth noting that all these correlations only give the lower bound of fracture toughness; it is sometimes very conservative, but may be acceptable in design. These correlations have been obtained based on extensive experimental results for the same kind of steels and welding procedures, so that it seems that fracture toughness data given by these empirical correlations are more reliable than those obtained directly using very limited specimens welded under laboratory conditions.

ASME Code[3]

The only specification required for toughness testing of A5338 or similar steels belonging to medium strength C-Mn steels is to measure nil-ductility transition (NDT) temperature by using the drop weight test. $K_{1c}$ can then be obtained from the diagram given in the ASME code.[3]

For convenience, an empirical formula is given for the variation of $K_{1c}$ with temperature,

$$K_{1c} = 1320 + 7.40 \times 10^{-7} (\Delta T + 80)^{4.65} \qquad (4.4)$$

where: $\Delta T = T - T_{NDT}$

T is the test temperature in °C and $K_{1c}$ in N $mm^{-3/2}$. Some typical data is tabulated below.

**Table 4.1 - The effect of test temperature on $K_{Ic}$**

| $\Delta T$ (°C) | $K_{1c}$ N $mm^{-3/2}$ |
|---|---|
| -30 | 1380 |
| 0 | 1840 |
| 30 | 3620 |
| 50 | 6320 |

## WES 2805 Standard[4]

This standard is based on the Charpy V-notch energy, $C_v$ at the specified temperature T* which depends on the design temperature, plate thickness and yield strength. Thus[4]

$$\delta_i = 0.01\ C_v\ (T^*) \qquad (4.5)$$

where: $T^* = T + 112 - \sigma_{ys} - 5 \sqrt{t}$

T = design temperature in °C, $\sigma_{ys}$ = yield strength in kg $mm^{-2}$ and t = plate thickness in mm.

For Arctic grade 350 steel with 25, 40 and 100 mm thickness the corresponding T* are 2°C, -5°C and -23°C, respectively, if the design temperature is taken as -50°C.

If at these temperatures the $C_v$ values are 200 J, 150 J and 100 J, respectively, then from (4.5) $\delta_i$ values are 0.2 mm, 0.15 mm and 0.10 mm, and the corresponding $K_i$ values are 5350 N $mm^{-3/2}$, 4660 $Nmm^{-3/2}$ and 3800 N $mm^{-3/2}$, respectively.

## NKK Code[5]

In the assessment of material toughness, including weld metal, of steels used in the Japanese shipbuilding industry, fracture toughness $K_c$ can be obtained based on the $C_v$ value at any temperature. The calculation procedures are as follows.

Through extensive tests it has been found that for the curve of Charpy V-notch energy versus temperature, only the relative position is different. If expressed as a function of the relative temperature T-FATT the lower bound of each steel of interest will overlap each other.

For convenience, the authors give a formula to describe the relation in the temperature range often used, that is for $C_v$ values from 6 to 14 kgf•m

$$FATT = \frac{10 - C_v(T)}{0.4} + T\ (^\circ C) \qquad (4.6a)$$

and for $C_v$ values from 1.2 to 6 kgf•m

$$FATT = T + 36\ (6.25\ C_v(T))^{1/1.12}\ (°C) \qquad (4.6b)$$

A fracture toughness transition temperature $T_K$ has been defined by using the wide plate test, with a central through thickness crack length 2C = 80 mm (w = 400 mm), i.e. at the temperature $T_K$, brittle fracture will occur at a stress of half the yield stress.

Summarizing the correlation between FATT and $T_K$ it is found that:

for base metal

$$T_K = (0.00321\ \sigma_{ys} + 0.391)\ FATT_B + 2.74 \sqrt{t} - 5.44\ (°K) \qquad (4.7a)$$

and for material at the fusion line

$$T_K = (0.00321\ \sigma_{ys} + 0.391)\ FATT_F + 2.74 \sqrt{t} + 4.96\ (°K) \qquad (4.7b)$$

where $FATT_F = FATT_B + \Delta T$

$\Delta T$ varies with heat input (HI); for typical values of HI of 2, 3 and 4 kJ/mm, the corresponding values of $\Delta T$ are 25, 35 and 45, respectively.

Finally, the fracture toughness $K_c$ can be obtained from the following formula

$$K_c = 3.81\ \sigma_{ys} \exp 562 \left( \frac{1}{T_k} - \frac{1}{T} \right) \qquad (4.8)$$

For example, if $C_v$ = 40 J at -50°C and for a plate thickness of 40 mm, we obtain

$K_c = 5350\ N\ mm^{-3/2}$ for base metal (at -50°C)

$K_c = 3850\ N\ mm^{-3/2}$ for weld metal (at -50°C)

and correspondingly, $\delta_c$ = 0.2 mm and 0.1 mm, respectively.

This method is used in classification of shipbuilding steels with respect to fracture toughness in Japan.

(3) Effect of Constraint

The effect of specimen sizes on fracture toughness seems much more complicated due to the influence of three dimensions, i.e. thickness B, ligament width b and crack length a.

It might be expected that when a and b are sufficient to meet the requirement of LEFM then the $K_1$ criterion is valid. In this case, $K_i$ and $K_c$ would vary with thickness as shown in Figure 4.1 where T is higher than $T_{ic}$.

**Figure 4.1 - Schematic diagram showing the variation of $K_i^D$ and $K_c$ with thickness B**

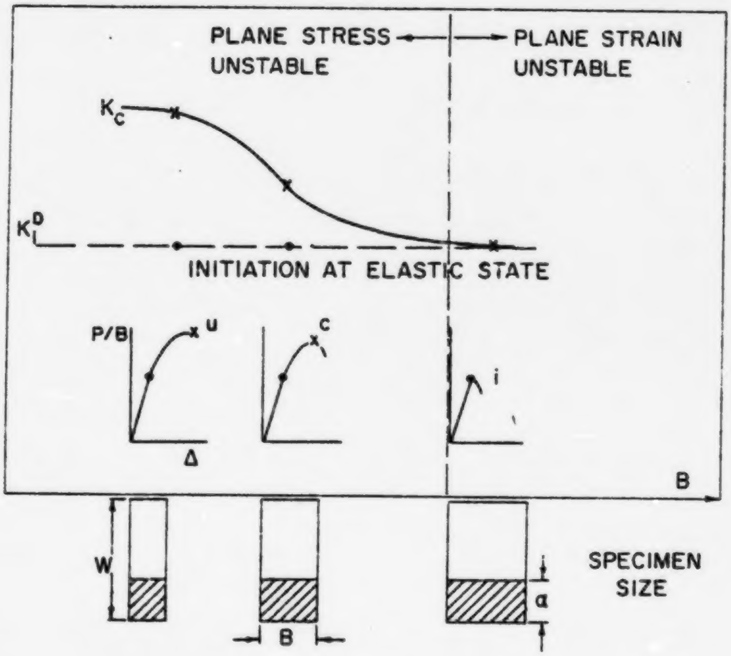
PLANE STRESS
UNSTABLE
PLANE STRAIN
UNSTABLE
$K_c$
$K_I^D$
INITIATION AT ELASTIC STATE
P/B
u
c
i
Δ
B
W
B
a
SPECIMEN SIZE

But it is not clear what the variation of $\delta_i$ and $\delta_c$ will be with an increase of ligament b keeping B constant and a or a/w constant. The plot may be as shown in Figure 4.2.

**Figure 4.2 - Schematic diagram indicating the possible variation of $\delta_i$ and $\delta_c$ with ligament width b**

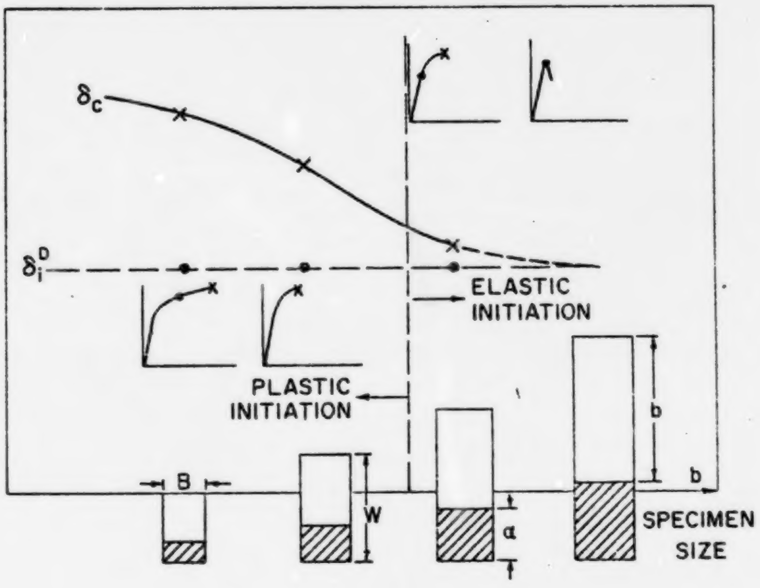

It can be seen from Figure 4.1 and 4.2 that the condition for the plane strain and triaxial constraint at crack initiation can be established, in general, if B and b > 5 mm, the $\delta_i$ is independent of specimen size, indicating that the constraint has reached saturation (for fibrous crack initiation).

Cleavage initiation needs two forms of constraint condition; one is the same as in fibrous initiation, i.e. plane strain and triaxial constraint, the other is the energy release rate condition. The latter one depends on the macroscopic stress state at crack initiation.

Generally speaking, the elastic constraint at crack initiation can be increased by increasing the crack length or the ligament size. For central through thickness cracks the variable is the crack length, and for a three-point bending specimen, it is the ligament size.

When the elastic constraint is not sufficient, crack initiation will occur in the elastic-plastic condition. Assuming the initiation fracture toughness is expressed by $J_i$ and

$$J_i = J_{ie} + J_{ip} \qquad (4.9)$$

the corresponding $K_i$ values are

$$K_i = \sqrt{J_i E'}$$

$$K_{ie} = \sqrt{J_{ie} E'} \qquad (4.10)$$

and $$K_{ip} = \sqrt{J_{ip} E'}$$

Thus $$K_i = \sqrt{K_{ie}^2 + K_{ip}^2} \qquad (4.11)$$

If we define an elastic constraint factor denoted as $\alpha$

$$\alpha = \frac{K_e}{K_p + K_e} \qquad (4.12)$$

at crack initiation it becomes

$$\alpha_i = K_{ie}/(K_{ip} + K_{ie})$$

When $\alpha = 1$, it means that the elastic constraint has reached saturation.

It is worth noting that the increase of thickness B can not vary the elastic constraint in either the tension or bending specimen for a through thickness crack. It can be expected that for different temperature T ($<T_{ic}$) the necessary value of $\alpha_i$ will vary with type of initiation mechanism. Similarly, it is important to realize that the amount of stable crack growth varies with constraint. This constraint consists of two factors.

- One is plane strain constraint of stable crack growth. Its increase can lead to cleavage or unstable crack growth at earlier stages, i.e. decreases the amount of stable crack growth.
- The other is the elastic constraint from the viewpoint of energy release rate.

The former constraint is supplied by thickness B. The latter one by elastic constraint factor $\alpha$.

Let us suppose that $\gamma$ denotes the constraint state during stable crack growth. $\gamma$ would be a function of $\alpha$ and $\beta$.

$$\gamma = f(\alpha,\beta) \tag{4.13}$$

where $\beta$ is the plane strain constraint factor and

$$\beta = B/\left(\frac{K_c}{\sigma_{ys}}\right)^2 \tag{4.14}$$

For medium strength steels it is reasonable to assume when $\beta = 1$, the plane strain constraint saturates.

If the contributions of both $\alpha$ and $\beta$ are the same form the expression (4.13) can be written

$$\gamma = 1/2(\alpha+\beta) \tag{4.15}$$

Also we can expect that the amount of stable crack extension $\Delta a$ can be expressed as follows

$$\Delta a = g(\gamma) \tag{4.16}$$

We need to establish the real forms of equation (4.13) and (4.16), i.e. the variation of $\Delta a$ with constraint $\alpha$ and $\beta$.

We can also define that when $\Delta a = 0$ the constraint saturates. On the other hand we can determine a limiting constraint factor $\gamma$ for a given structure.

The essential problem is how to design the specimen used in fracture toughness testing to have the same constraint condition as that operative in structures.

### 4.1.2 Fracture Toughness Data

#### (1) Scatter of Toughness Data

The scatter of fracture toughness value, $K_{1c}$ of ultra-high strength steels rarely exceeds ±20 percent, while it often exceeds ±100 percent for base metal of medium strength steels, and is even larger for weld metal.

There are various reasons for this scatter:

- inconsistency of constraint
- difference of testing and calculating methods
- discrepancy of defining the critical value of CTOD and the complicated behavior of weld metal

Recently the Welding Institute in the UK, has performed an extensive testing program on scatter in CTOD tests.[6] Some typical values are listed in Table 4.2.

**Table 4.2 - Scatter in CTOD results**

| **Material** | **Test Temp (°C)** | **CTOD (mm)** | | |
|---|---|---|---|---|
| | | **Mean (m)** | **SD (s)** | **s/m** |
| BS4360-50D: | | | | |
| plate A | -100 | 0.34 | 0.22 | 0.65 |
| plate B | -60 | 0.81 | 0.31 | 0.38 |
| SAW | 20 | 0.066 | 0.026 | 0.39[7] |
| MMA | -10 | 0.16 | 0.11 | 0.69 |

Johnson[7] has pointed out that the results of weld metal can be described as a normal distribution, shown in Figure 4.3.

Figure 4.3 - Histograms of data for welded 50D steel[7]

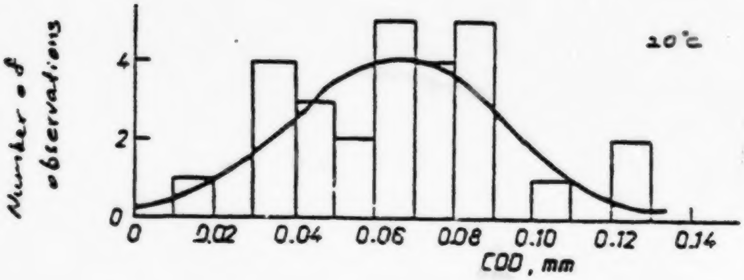

In the case of weld metal the position of the crack tip and the direction of crack growth can greatly influence the CTOD value, as shown in Figure 4.4 by Bukalrud and Karlsen.[8]

Figure 4.4 - Lower bound CTOD values for 100 mm thickness in as-welded condition[8]

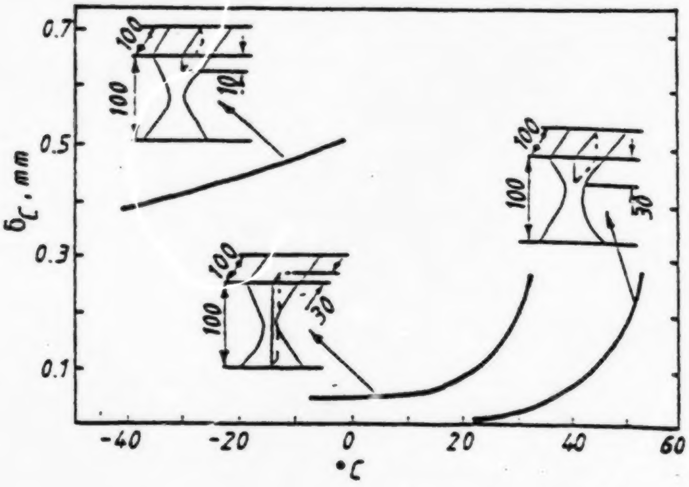

Currently there is an increasing tendency to apply statistical analysis to fracture toughness values for medium strength steel, particularly for welded structures.

(2) Fracture Toughness Data

Fracture toughness tests have been carried out on BS4360 50D in the Welding Institute of England. Some results are shown in Figures 4.5 and 4.6 for base metal, at different temperatures.[9]

Figure 4.5 - Fracture toughness $K_c$ versus test temperaure for BS4360 50D base metal[9]

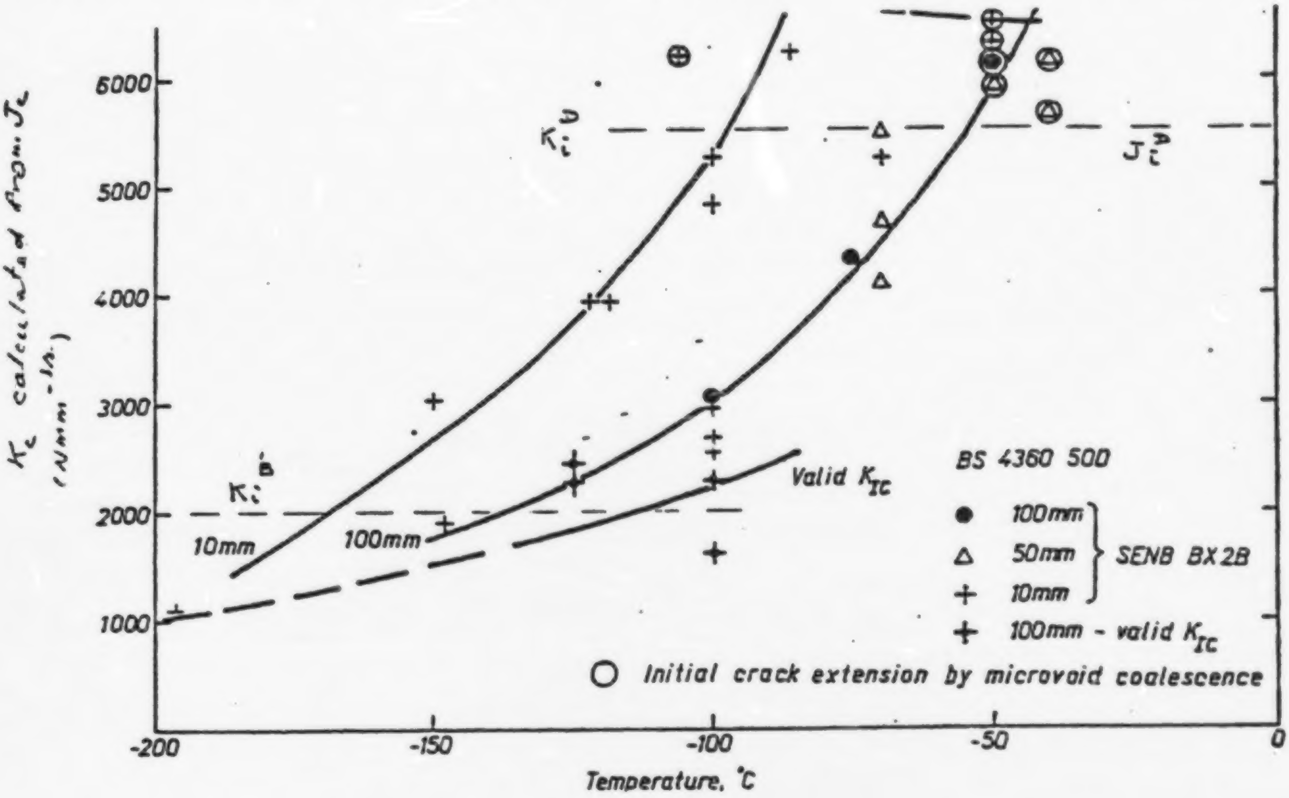

Figure 4.6 - Fracture toughness $\delta_c$ versus test temperature[9]

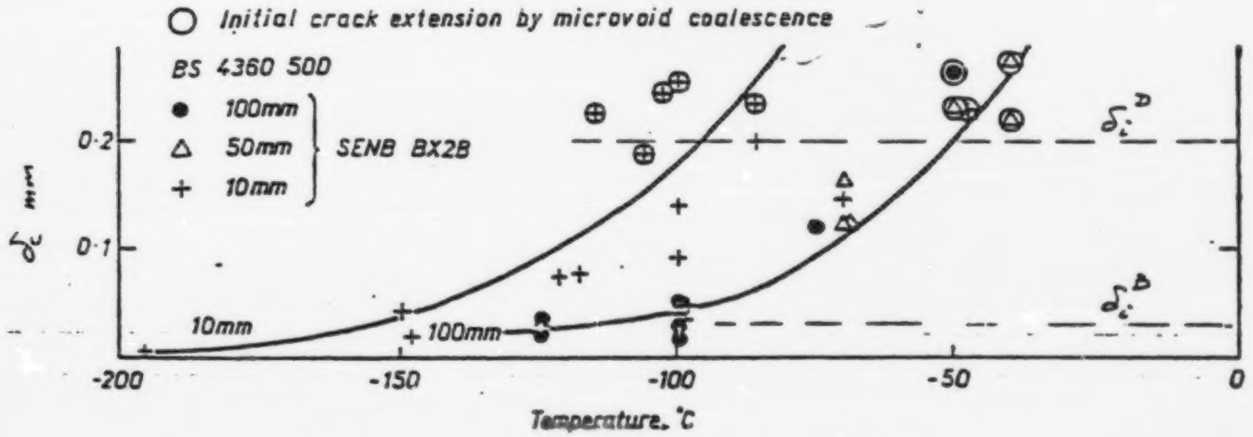

It should be explained that the dashed horizontal lines were added by the present authors; it seems more reasonable because the $K_i^D$ or $\delta_i^D$ must be lower than those points being signed by the circle at least. And it seems to be reasonable that the average value of fracture toughness at -100°C to -150°C is considered as the lower limit of cleavage initiation fracture toughness $K_i^B$ and $\delta_i^B$.

The following data can be obtained from these two figures:

$$k_i^D = 5500 \text{ N mm}^{-3/2}$$

$$k_i^B = 2000 \text{ N mm}^{-3/2}$$

$$\delta_i^D = 0.2 \text{ mm}$$

$$\delta_i^B = 0.03 \text{ mm}$$

The mechanical properties of the steel tested are listed in Table 4.3.

**Table 4.3 - Tensile properties of BS4360 50D**

| Stress (MPa) | Test Temperature (°C) | | |
|---|---|---|---|
| | 0 | -50 | -100 |
| $\sigma_{ys}$ | 330 | 355 | 410 |
| $\sigma_u$ | 530 | 560 | 620 |

It can be seen also that the fracture initiation mechanism transition temperature $T_{ic} < -50°C$, and the scatter of data for specimens with 50 mm and 100 mm thickness is much smaller than that for 10 mm thick specimens.

The fracture toughness values of $\delta_c$ have been obtained for grade NVA[10] the basic data of which are listed in Table 4.4.

**Table 4.4 - Mechanical Properties of grade NVA**

| Plate Thickness (mm) | Composition (%) | | | $\sigma_{ys}$ ($Nmm^{-2}$) | $\sigma_u$ ($Nmm^{-2}$) | $T_{NDT}$ (°C) |
|---|---|---|---|---|---|---|
| | C | Mn | S | | | |
| 25 | 0.17 | 1.15 | 0.032 | 285 | 457 | -20 |
| 50 | 0.12 | 1.15 | 0.018 | 286 | 449 | -20 |
| 100 | 0.11 | 1.33 | 0.021 | 276 | 443 | -10 |

The fracture toughness results are shown in Figures 4.7 and 4.8.

Figure 4.7 - Effect of plate thickness on $CTOD_c$[10]

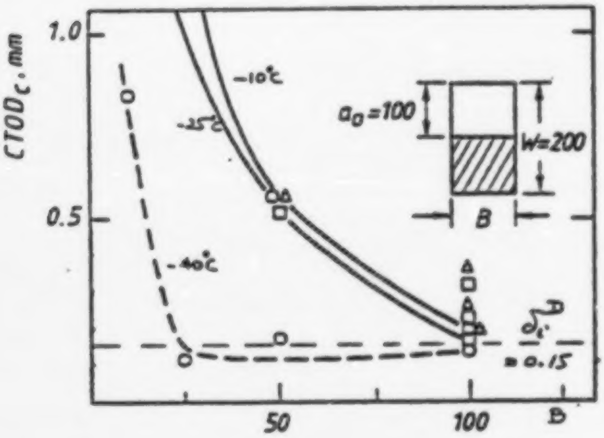

Figure 4.8 - $CTOD_c$ versus temperature obtained from wide plates with surface crack[10]

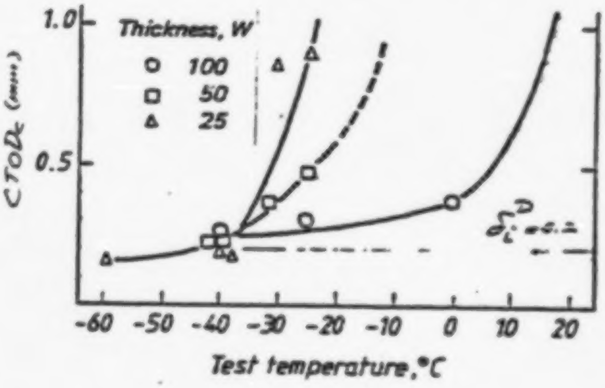

It can be seen that the values of fibrous initiation toughness $\delta_i^D$ at -40°C are 0.15 mm and 0.2 mm for through thickness and surface crack respectively. Although the unstable fracture toughness often shows much scatter, $\delta_i^D$ is relatively constant.

For the HAZ or weld metal a different situation ensues.

The fracture toughness of HAZ and weld metal has been reported in a recent paper.[11] The $\delta_c$ of HAZ's were measured for BS4360 steel for different conditions including plate thicknesses of from 50 to 100 mm, multipass and single-pass welding procedures with heat input of 1.5 and 4 kJ/mm for each welding cycle. The test temperature was approximately -10°C.

Of the 183 HAZ specimens tested, ninety-five gave values of $\delta_c$ greater than 0.87 mm. The rest of the specimens had $\delta_c$ greater than 0.3 mm with the exception of one which had a $\delta_c$ value of 0.14 mm.

Eighty specimens of weld metal were tested at -10°C with nine consumables, three plate thicknesses of 25, 38 and 60 mm, and two post weld conditions AW and PWHT (as welded and post weld heat treated).

The $\delta_c$ values ranged from 0.01 to 1.64 mm and most of them were within 0.05 to 0.1 mm.

The material used in Figure 4.4 was $O_x$ 522 D with yield strength $\sigma_{ys}$ = 330 N mm$^{-2}$. The $\delta_c$ varied from 0.01 to 0.4 mm at the temperature of -10°C and lower.[8]

It is worth noting that many authors[12-14] have pointed out that the $\delta_c$ value of the HAZ is much better than that of the weld metal. This should be born in mind when one assesses the applicability of a developing steel for a given service condition with respect to its fracture toughness.

## 4.2 Fracture Toughness Testing

### 4.2.1 Testing Methods

(1) Test for $K_i$ and $K_c$

It is preferable to carry out the $K_i$ test for the following reasons:

- the $K_i$ criterion is more definite and simpler than the CTOD criterion and can be used in the case of offshore structures, especially for Arctic use.
- the testing method is simple because the initiation point is very close to the instability point, i.e., the error of the test is small.
- the test results are relatively stable and less scattered because of fewer uncertainties in data processing; also as mentioned in figure 4.6 the larger specimens tend to give more consistent test results.

Prior to designing the $K_i$ specimens, it is worth stating that the elevated toughness values of some specimens are not very important; only the lower bound and its confidence limit is of engineering utility.

A few statistical analysis methods for fracture toughness data will be suggested in the latter part of this review. According to that, a required fracture toughness value should be given. For example, if it is assumed that the $K_i$ for the HAZ and the weld metal cannot be smaller than 3000 $Nmm^{-3/2}$ at the design temperature, the value of required toughness is hereafter denoted as $K_D$.

Design of Specimen for $K_i$ Test

According to Section 3, the factor controlling the elastic fracture initiation is the ligament width.

Let us suppose that $a/w = 0.2$ and the elastic fracture limit load equals $0.8\ P_L$, then the required ligament b can be obtained [from equation (3.6) to (3.10)].

$$b = (K_D/\sigma_{ys})^2 \qquad (4.17)$$

and

$$a = 0.25\ (K_D/\sigma_{ys})^2 \qquad (4.18)$$

so that

$$W = 1.25\ (K_D/\sigma_{ys})^2 \qquad (4.19)$$

By using a specimen of these dimensions, the $K_i$ values around $K_D$ and lower can be measured exactly. Values much higher than $K_D$ are themselves not very useful. However, the number of tests giving the elevated values of $K_i$ is important, in terms of estimating the confidence of the lower bound of the test results.

For example, if taking $K_D$ = 3000 $Nmm^{-3/2}$ and $\sigma_{ys}$ = 360 $Nmm^{-2}$ (at -50°C), the required specimen size can be obtained from the above formulas as:

$$w = 88 \text{ mm}$$
$$b = 70 \text{ mm}$$
$$a = 18 \text{ mm}$$

The loads required for both the fatigue precracking and the fracture test are listed in Table 4.5, for specimen thicknesses of 25, 40 and 100 mm.

**Table 4.5 - Loads required for Precracking and Fracture**

| Specimen Thickness (mm) | Load | | | |
|---|---|---|---|---|
| | Fatigue* | | Fracture | |
| | (ton) | (klb) | (ton) | (klb) |
| 25 | 7 | 15 | 21 | 46 |
| 50 | 11 | 24 | 34 | 75 |
| 100 | 28 | 62 | 84 | 185 |

* based on $K_f$ = 1000 $Nmm^{-3/2}$

## Testing Procedure

Because it is only of value to know the $K_i$ values which are greater than $K_D$, it is not necessary to completely break the sample.

The testing procedure can be designed as follows (see figure 4.9). First, the sample will be loaded up to $P_D$ corresponding to $K_D$; if the crack does not initiate, it can then be loaded until it reaches either 1.1 $P_D$ or to the intersection of the load-displacement curve and the 5 percent offset of the original straight line shown in Figure 4.9 (b).

**Figure 4.9 - Controlling the unload point**

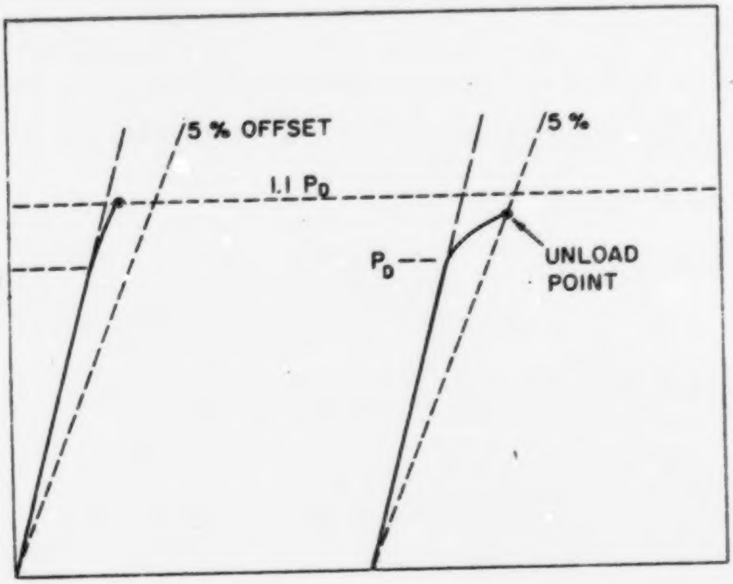

The 5 percent offset line can be plotted on the recording chart by means of preload procedure.

After unloading, the specimen can be fatigued to extend the crack tip past the elastic zone, and a further test can be performed.

Using this method, one sample can give one to five data points. If there are three specimens, it is possible to get more than ten data points and thus a reliable $K_i$ value can be obtained.

For base metal, $K_D$ can be taken as 5000 $Nmm^{-3/2}$. The $\sigma_{ys}$ is most likely $\approx 385$ $Nmm^{-2}$ and then the specimen sizes are W = 210 mm, a = 42 mm. The required loads for both the fatigue precracking and the fracture test are 170 KN and 520 KN respectively, for plate of 40 mm thick.

The measurement of crack length will be carried out on the fracture surface after the final test which breaks the specimen. The fracture sequence is shown schematically in Figure 4.10.

**Figure 4.10 - The fracture test sequence**

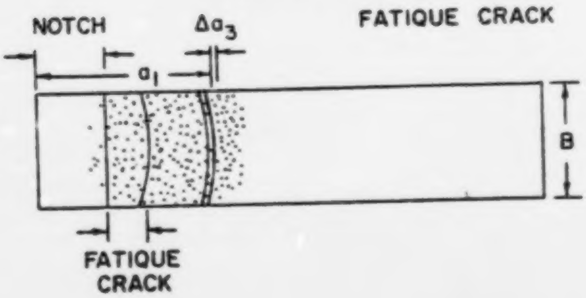

Substituting the actual values of load and crack length, the stress intensity factor can be obtained and referred to as $K_T$. And then the fracture toughness value can be obtained as follows:

$$\begin{array}{lll} K_i & > K_T & \text{for } \Delta a = 0 \\ K_i & = K_T & \text{for } 0 < \Delta a < 0.1 \text{ mm} \\ K_c(\Delta a) & = K_T & \text{for } \Delta a > 0.1 \text{ mm} \end{array}$$

The values of $K_c(\Delta a)$ may be used to construct a resistance curve according to which the $K_i$ can be obtained.

(2) Test for $CTOD_c$

The tests should be carried out according to the standard method, e.g. BS5762 (1978) using the preferred (Bx2B) and subsidiary (BxB) specimen.

The method of determination of $\delta_i$ and $\delta_u$ described in BS5762 is quite definitive using a single sample and identifying if there is fibrous stable crack growth.

It should be pointed out that $\delta_u$ is not a material constant, and is influenced by specimen size.

According to the initiation design philosophy, the value $\delta_i$ is needed.

The determination of $\delta_i$ is much more complicated, and there is no satisfactory method available at present. There are however five commonly used methods.

Prior to briefly describing these methods, it is necessary to state the definition of initiation point.

The crack initiation process is shown in Figure 4.11. The initiation process can be divided into six initiation states or stages, as follows:

| | |
|---|---|
| the first stage $i_0$: | individual grain cracking |
| the second stage $i_1$: | local micro-regions cracking |
| the third stage $i_2$: | local macro crack extension |
| the fourth stage $i_3$: | crack extension at most of crack front |
| the fifth stage $i_4$: | extension begins along the entire crack front |
| the sixth stage $i_5$: | a certain amount of macroscopic crack extension |

**Figure 4.11 - Schematic diagram showing different initiation states on (a) P-V curve and (b) fracture surface as well as corresponding test methods**

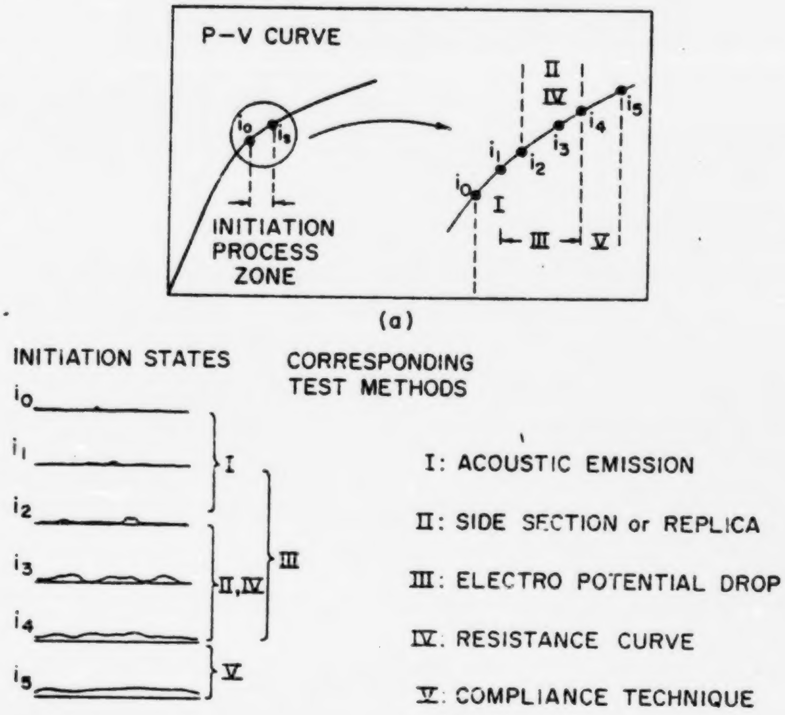
P–V CURVE
$i_0$
$i_s$
INITIATION PROCESS ZONE
II
IV
$i_0$
$i_1$
$i_2$
$i_3$
$i_4$
$i_5$
I
III
V
(a)
INITIATION STATES
CORRESPONDING TEST METHODS
$i_0$
$i_1$
$i_2$
$i_3$
$i_4$
$i_5$
I
II, IV
III
V
I: ACOUSTIC EMISSION
II: SIDE SECTION or REPLICA
III: ELECTRO POTENTIAL DROP
IV: RESISTANCE CURVE
V: COMPLIANCE TECHNIQUE

In the earlier stage of development of the CTOD standard testing method in DD19 the recommended method of determination of initiation point was the electro potential drop technique. Recently this has been changed into the resistance curve method by using multiple specimens as described in BS5762.

In fact, the methods are relevant to different initiation states as shown in Figure 4.11.

For engineering use, a stable and more definitive value of $\delta_i$ is needed. It is reasonable to define a $K_c$ corresponding a certain amount of stable crack growth, such as recommended in Chinese Standard method for $J_{Ic}$ test taking $\Delta a$ = 0.05 mm as initiation point or $\Delta a$ = 0.2 mm and associated with it $J_{0.05}$ or $J_{0.2}$ as the $J_i$[14].

It can be expected that the scatter of $\delta_i$ or $J_i$ will be much smaller than that of $\delta_u$, and thus make it easier to analyze statistically.

From this reason, perhaps, the resistance curve method has been recommended in BS5762[15] and GB2358-80[16] (Chinese standard for CTOD testing and in ASTM E813-81[17] and GB2038-80[14] (Chinese standard) for $J_{ic}$ testing.

One really wants to know the fracture initiation process in more detail, i.e., which of the stages described above is the more significant and useful for fail-safe analysis of welded structures and the relationship between them, as well as their variation with the degree of constraint.

It is preferable to use larger specimens, if possible, for measuring $\delta_i$ or $\delta_c$ at higher constraint thus making the constraint factor $\gamma$ as close as possible to 1.

If it is found that the fracture initiation mechanism is fibrous mode at the design temperature and the maximum constraint is operative, i.e., elastic initiation occurs at full thickness, it may be possible to use small specimens to measure the $\delta_i{}^D$ and $\delta_c$ using the same $\Delta a$ as that of the maximum constraint sample.

It would be convenient to use a specimen with fixed size, e.g. 20 x 24 x 100 mm as described in GB2358 and working out a much simpler testing and calculating procedure.

In this case, for the very high $\delta_i{}^D$ values, it is important to know both the number of tests performed and the values obtained in order to establish the lower bound of $\delta_i{}^D$ and its confidence limit.

This can be done by using a design value of $\delta_i{}^D$ denoted $\delta_D$ and the specimen will be loaded till $\delta = \delta_D$ by means of the following procedures with reference to the load (P) - displacement (V) diagram, Figure 4.11).

$$\delta = \delta_e + \delta_p \qquad (4.20)$$

where

$$\delta_e = \frac{K_1{}^2\ (1-\nu^2)}{2E\sigma_{ys}} = CP^2 \qquad (4.21)$$

where

$$c = \frac{Y^2}{2E\sigma_{ys}B^2W} \qquad (4.22)$$

and

$$\delta_p = DV_p \qquad (4.23)$$

where

$$D = \frac{0.4\ (W-a)}{0.4\ W + 0.6\ a + Z}$$

supposing $\delta = \delta_D$ and rewriting the above formula then the following is derived:

$$Vp = \frac{\delta_D - CP^2}{D} \qquad (4.24)$$

Using formula (4.24) it is possible to establish the required value of $V_p$ to maintain $\delta = \delta_D$ for different loads. If we use a specimen of fixed size, the coefficients C and D can be calculated and tabulated beforehand and a line with equal $\delta$ value plotted on the recording chart as shown in Figure 4.12.

**Figure 4.12 - Schematic diagram showing the equal $\delta$ line on the chart**

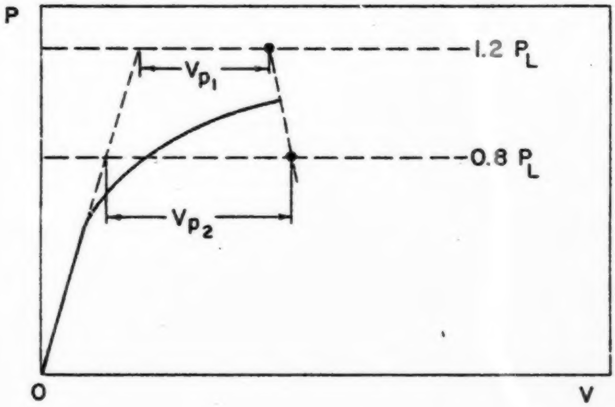

From preloading the data the original slope can be plotted as well as the lines of 1.2 $P_L$ and 0.8 $P_L$. Using formula (4.24) the values $V_{p1}$ and $V_{p2}$ can be obtained, the line through point $V_{p1}$ and $V_{p2}$ is the equal $\delta$ line. It can be shown that it is approximately a straight line within a small interval of the load.

If enough samples are tested, e.g. perhaps five for base metal and eight to ten for weld metal, the resistance curve can be obtained.

From this method, it is possible to establish the statistical distribution of the $\delta_i$ values by using more than 30 specimens and a lower bound of $\delta_i$, and its confidence can be provided for engineering use.

(3) Test for $J_{ic}$ (or $J_i$)

When only the $K_i^D$ or both the $K_i^D$ and $\delta_i^D$ are needed, it is suggested that it would be better to measure the $J_i^D$ in the same time, because the conversion formula from J to $K_1$ is more definite than that from $\delta$ to $K_1$.

There are three ways to get the $\delta_i$ and $J_i$ at the same time. By means of the following formula

$$\Delta p = \frac{W}{0.4\,W + 0.6\,a + Z}\,V_p \tag{4.25}$$

the first two ways are to record either load-crack tip opening displacement (p-v curve) as in CTOD test or load-load point displacement (p-$\Delta$ curve) as in $J_{ic}$ test.

It is obviously more accurate to record both the p-v and p-Δ curve in the same test.

The advantages of the $J_{ic}$ test are:

- $J_i$ can be calculated without knowing the yield strength. This is important because for weld metal, the value of the local yield strength is not well known.

- the strain gauge can be kept out of the medium in low temperature tests.

- there is no need to prepare knife edges for each specimen.

The disadvantages of $J_{ic}$ are:

- a more precise loading system is needed including fixtures of three-point bending test. Also the original slope of the p-Δ curve is not as well defined as that of the p-v curve.

- sometimes two strain gauges are needed to get the average value of displacements.

- the equal J line is not a straight line, as shown below. The expression to calculate the J value recommended in existing standards for the $J_{ic}$ test[14],[17] is:

$$J = J_e + J_p \qquad (4.26)$$

where

$$J_e = \frac{K_1{}^2}{E'} = c'p^2 \qquad (4.27)$$

where

$$c' = \frac{Y^2}{E'B^2W} \qquad (4.28)$$

and

$$J_p = \frac{2\ U_p}{B(W-a)} = D'P\Delta p \qquad (4.29)$$

where

$$D' = \frac{2}{(1 + n)B(W-a)} \qquad (4.30)$$

where n is equivalent to the work hardening exponent in a tension test. For medium strength steel without a yield point, n can be taken as 0.2.

Substituting and rewriting the above equations, the following formula can be obtained:

$$J = C'p^2 + D'p\Delta p \qquad (4.31)$$

for a given specimen C' and D' are known and taking $J = J_D$, where $J_D$ is design value similar to that for $K_i$ and $\delta_i$ tests.

By using equation (4.31) the line of equal J values can be plotted on the recording chart, as shown schematically in Figure 4.13.

**Figure 4.13 - Schematic diagram showing the equal J line on the load displacement chart**

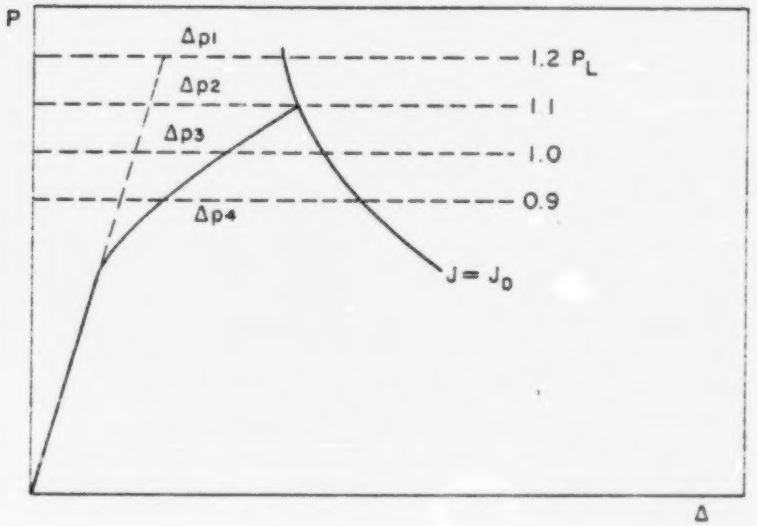

4.2.2 Some Subjects under Investigation

(1) Pop-ins

The significance of pop-in during CTOD testing has been the subject of much discussion.

Since the most characteristic feature of pop-in is that it does not appear to reduce the load bearing capacity of the specimen, this behavior has led some authors to dismiss pop-ins as insignificant events that do not reflect the true fracture resistance of the material. Also as many structures are essentially under load control, pop-ins seen in the CTOD may not be significant fracture events.

Nevertheless, pop-ins have been recorded and arrested brittle cracks seen on the fracture faces. Dawes et al[6] suggest a cautious approach to this problem until research work has established the true significance of pop-ins, and stated that such work is currently in hand at the Welding Institute in the UK.

According to previous experience, pop-ins can be divided essentially into two kinds. The front can arise due to local or microstructural heterogeneity of material and its characteristic features are:

- a small load drop
- very limited crack growth during pop-in on the fracture surface if loading is stopped as soon as pop-in occurs

If this is true and can be proved, then the pop-in CTOD value $\delta_{pop-in}$ can be dismissed. Only in this case, can it be said that it does not reflect the true fracture resistance of the material.

The other form of "pop-in" occurs due to crack initiation having a certain amount of crack extension, exceeding that defined for engineering purpose ($\Delta a = 0.1$ mm).

In this case, the pop-in CTOD value should be considered as an individual initiation event. However, it is different from unstable crack growth and thus it is suggested that the average value of $\delta_{pop-in}$ and the successive $\delta_c$ or $\delta_i$ of the same specimen also be measured.

If obvious crack growth occurs and the load drops, this is no longer called pop-in but is due to the arrest of brittle cracks.

For convenience, the following criteria can be used: for the first case where we neglect the $\delta_{pop-in}$ we can define:

- the ratio of load drop $\Delta p$ to the pop-in load

$$\Delta p / p_{pop-in} \leq 5 \%$$

- the amount of pop-in crack growth $\Delta a$. $\Delta a < 0.1$ mm for the second case taking the average value of $\delta_{pop-in}$ and $\delta_i$ when

  - $\Delta p / p_{pop-in} > 5$ percent or $\Delta a \geq 0.1$ mm and
  - final fracture load $P_c > p_{pop-in}$

The condition $P_c \leq P_{pop-in}$ might be seen as the limit between the pop-in initiation and arrested brittle cracks.

(2) Statistic Analysis of Data

The minimum value of three test results corresponds to an 88 percent lower bound value for the true population median. While that of six test results corresponds to 91 percent lower bound value. Thus, it is difficult to establish the reliability and the degree of confidence.

As Dawes et al[6] mentioned, the consumers risk of uncertainty inherent in using limited data subject to large scatter may be overcome by setting a high minimum CTOD requirement. However, this has a very damaging effect on the manufacturers risk. This problem can only be overcome by carrying out more extensive testing and using more elaborate acceptance/rejection criteria, agreed to by the consumer and manufacturer.

It can be seen from Table 4.2 that taking only a 0.5 percent confidence limit, the $\delta_c$ values become 0.023, 0.36, 0.029 and 0.002 mm, corresponding mean values of 0.34, 0.81, 0.066 and 0.16 mm.

It would be expected that the scatter of data would be decreased by using $\delta_c$ and $\delta_i$ instead of $\delta_u$. This approach is outlined in the example below.

Assumed 20 test pieces are used$^6$, and 10 $\delta_c$ and 10 $\delta_R$ have been obtained, where $\delta_R$ denotes the value of CTOD at an amount of crack extension of $\Delta a$.

## The Determination of Mean Value

Firstly, the average value of the 10 $\delta_c$ measurements can be calculated, as denoted $\delta_c$, and the R-curve can then be plotted obtaining $\delta_R$ and $\Delta a$ by extrapolating the $\delta_i{}^R$ to $\Delta a = 0$.

Then averaging the $\delta_c$ and $\delta_i{}^R$ obtained above, the final $\delta_i$ can be obtained for the 20 test pieces.

## Standard Deviaton, S

The calculation of S by using the following formula

$$S = \sqrt{\frac{\sum(\bar{\delta}_c - \delta_c)^2 + \sum\Delta\delta^2}{N-1}} \qquad (4.32)$$

where $\Delta\delta$ denotes the deviation of $\delta_R$ from the R-curve and N is the number of the test-pieces.

It is suggested here that extremely large values of $\delta_c$, say greater than $\delta_c + 2S$, or extremely large $\delta_R$ corresponding to extremely large $\Delta a$, say $\Delta a = 0.5$ mm or 6 percent of the ligament length (the former one is recommended in standard (14) and the latter one in standard (17)) will be rejected in calculating the values of $\delta_i$ and S.

The degree of confidence can be considered as follows.

Suppose that required degree of confidence is P (may be 90 percent or higher) and N is the number of tests associated with $\delta_i$ and S and n is the number with extremely high values of both $\delta_c$ or $\delta_R$, then the $\delta_i$ at confidence of P can be obtained.

$$\delta_i = \delta_i - sz(p') \qquad (4.33)$$

where

$$p' = p \frac{N + n}{N} \qquad (4.34)$$

The value of z corresponding to the probability P can be looked up in a table of probabilities.

It should be mentioned that for pop-in CTOD, it may be useful to treat this as described previously.

### (3) Fracture Toughness Tests for Weldments

#### Philosophy

From the design point of view, one wants to determine the fracture toughness of the so-called weakest region of the material.

This leads us to develop fracture toughness tests which are carried out on the specimen extracted from the center of weld metal, fusion line and HAZ, located different distances from the fusion line, so the fracture toughness distribution along the weldment can be obtained as shown in Figure 4.14.

**Figure 4.14 - Schematic diagram showing the distribution of $\delta_c$ along the weldment, WM: weld metal, BM: base metal**

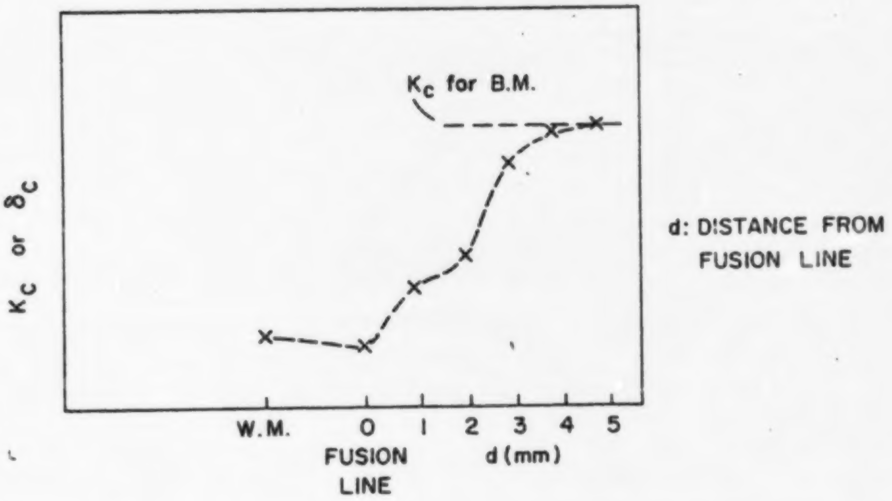

The lowest toughness region might be in any region of the weldment, depending on many factors.

It is worth noting that so far the data published seem to demonstrate that the weakest region of the steels used in offshore structures is located in the weld metal.

It is well known that the weld metal is not homogenous. However, we still need to know what location in the weld metal is the weakest part. From Figure 4.4 it can be seen that the weakest part seems to be located in the center of the double V multipass weld metal.

Even if the position where the crack front is located in this region, the fracture toughness may vary if the crack growth direction varies as shown in Figure 4.15.

**Figure 4.15 - Different fatigue crack growth methods**[18]

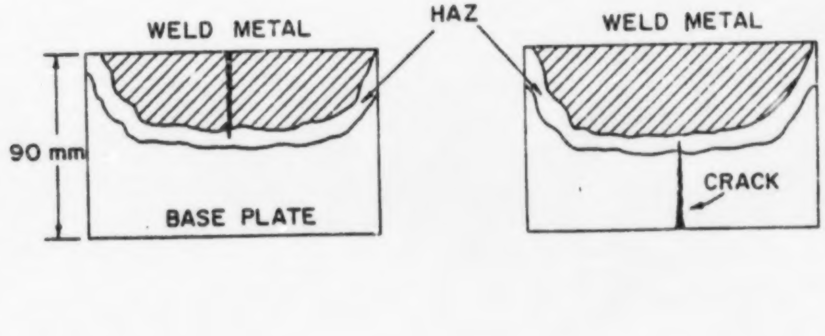

There are further reasons for considering the average properties of the weld and not the extreme value:

- the probability is very small that the entire crack front locates in the weakest region after sub-critical crack growth in service
- almost all the differences mentioned above might not be statistically significant because of the extreme scatter of data for the weldment
- extremely low fracture toughness can be obtained by increasing the number of tests, if this is taken into account it will lead to a very conservative criterion.

We need also to establish which combination of base plate welding procedures and consumables will give the lowest fracture toughness.

Thus, any reliable assessment of both material toughness and allowable crack size of structures must rely on extensive experimental results and their statistic analysis.

### Test Technique

There are no guidelines in existing standards for fracture toughness testing of weldments, which consider specimen preparation, the limitation of welding deformation, etc.

Some useful suggestions are given in reference 6. These include:

- applying a plastic compression of 1 percent of the specimen thickness, B, across the uncracked ligament prior to fatigue precracking.
- using a high R-ratio in fatigue cycle
- adding a high "reverse bending" load prior to fatigue precracking, being at the same load as subsequently used during precracking.

Dolby[18] has given many useful suggestions in design of fracture toughness specimens for HAZ studies.

# REFERENCES

1. G. H. Eide, K. O. Vilpponen et al. "Review of Steels used in the Construction of Offshore Structures", Report of Det Norske Veritas, April, 1982.

2. Fenco Consultants Ltd, Lloyd's Register of Shipping, "A Review of Steel Properties at Low Temperatures", Transport of Canada Research and Development Centre, TP 2717.

3. I. Milne and D. A. Curry, "The Effect of Triaxiality on Ductile-Cleavage Transition in a Pressure Vessel Steel".

4. WES/2805, "Method of Assessment for Defects in Fusion Welded Joints with Respect to Brittle Fracture", The Japan Welding Engineering Society, 1980.

5. H. Yajima: "Application of Fracture Mechanics in Shipbuilding", Lecture Notes in Ship Research Centre of China, 8-15 Apl 1982.

6. M. G. Dawes, H. G. Pisarski, O. L. Towers and S. Williams, "Fracture Mechanics Measurements of Toughness in Welded Joints", Int Conf on Fracture Toughness in Welded Joints", Int Conf on Fracture Toughness Testing Methods, Interpretation and Application, 9-10 June, 1982, London.

7. G. O. Johnston, Interim Process Report on Toughness Distributions in a Submerged Arc Weld", The Welding Institute Report 110/1980, June 1980.

8. T. Bokalrud and A. Karlson, "Fracture Toughness and Significance of Defects in heavy Offshore Structures", European Offshore Steels Research Seminar Cambridge, UK, 1978, Paper 37.

9. H. G. Pisarski, "Influence of Thickness on Critical Crack Opening Displacement (CTOD) and J Values", The Welding Institute Report 90/1979, May 1979.

10. J. Lereim, "Elastic-Plastic Fracture Analysis of Heavy Welded Structural Elements", 2nd Int Conf on Offshore Welded Structures, London, 16-18, Nov 1982, Paper 13.

11. H. G. Pisarski and J. D. Harrison, "Fracture Resistance of Materials used in Offshore Structures", European Offshore Steels Research Seminar, Cambridge, UK, 1978, Paper 2.

12. G. H. Eide, K. O. Vilpponen et al. "Review of Steels used in the Construction of Offshore Structures", Report of Det Norske Veritas, Apl 1982.

13. C. F. Berkhout, S. H. van den Brink and G. H. G. Vaessen, "Controlling Weld Metal Toughness of Manual Metal-Arc and Submerged-Arc Welds in Carbon-Manganese Steel", European Offshore Steels Research Seminar, Cambridge, UK, 1978, Paper 1.

14. GB2038 "Test Method for Ductile Fracture Toughness of Metallic Materials by usin $J_R$ Resistance Curve", Chinese State Standardization Bureau, 1982.

15. BS5762, "Methods for Crack Opening Displacement (CTOD) Testing", British Standards Institution, 1979.

16. ASTM E813-81, "Standard Test for $J_{Ic}$. A Measure of Fracture Toughness", Annual Book of ASTM Standard Part 10, 1981.

17. GB2358, "Test Method for Crack Opening Displacement", Chinese State Standardization Bureau, 1982.

18. R. E. Dolby, "Influence of Defect Orientation on HAZ Fracture-Toughness Measurements", Metal Construction and British Welding Journal, July 1974, pp 6-11.

## 5. ASSESSMENT OF FRACTURE TOUGHNESS

### 5.1 Principle

(1) Preparation of Data

It is necessary to supply three aspects of data as shown in figure 1.1 in order to assess the applicability of the material of interest. With respect to brittle fracture these are:

Stress Analysis

The compressive $\sigma_t$ and bending stresses $\sigma_b$ are the main applied stress components. The design stress used in most papers is taken as $2/3\ \sigma_{ys}$. But in paper (1) the nominal design stress of 75 $\mathrm{Nmm}^{-2}$ is taken to be approximately $1/4\ \sigma_{ys}$.

Let us assume that the design stress $\sigma_D$ can be expressed as:

$$\sigma_D = \frac{1}{2}\sigma_t + \frac{1}{2}\sigma_b \qquad (5.1)$$

$$= \frac{2}{3}\sigma_{ys}$$

Thus,

$$\sigma_t = \frac{1}{3}\sigma_{ys} \qquad (5.2)$$

and

$$\sigma_b = \frac{1}{3}\sigma_{ys}$$

With respect to the magnitude of the stress concentration factor, SCF = 3 is given in most papers (in paper 1 SCF = 8 is taken). The stress concentration at fillet weld toes, SCF = 3, and decreasing linearly to one at crack depths exceeding 15 percent of the section thickness.

From the brittle fracture point of view, the stress concentration is not important.

The structures include weld joints in both the as-welded and PWHT conditions. Thus the levels of residual stress $\sigma_R$ should be considered.

The minimum operating temperature in Arctic service will be -50°C, and the loading rate can be considered as static loading.

## Defect Analysis

Different defect sizes have been considered as listed in Table 5.1.

Due to the difficulty in inspecting defects in service, the period of inspection must be very long.

Now, the following defect sizes are assumed for surface cracks

$$a = B/4 \qquad \text{for } B \leq 50 \text{ mm}$$

and

$$a = 12.5 \text{ mm} \qquad \text{for } B > 50 \text{ mm} \tag{5.3}$$

**Table 5.1 - Assumed defect sizes**

| | **Surface Crack Depth (mm)** | **Reference** |
|---|---|---|
| Single Side Weld Joint<br>Double Side Weld Joint | 12<br>8 | [2] |
| $B \leq 50$ mm<br>$B \geq 50$ mm | 15% B<br>7.5 | [3] |
| $B \leq 50$ mm<br>$B \geq 50$ mm | B/4<br>12.5 | [4] |

for through-thickness cracks

$$2C = B \qquad \text{for } B \leq 50 \text{ mm} \tag{5.4}$$
$$2C = 50 \text{ mm} \qquad \text{for } B > 50 \text{ mm}$$

## Required Safety Factor

In the ASTM code[5] the safety factor required can be described below:

$$2K_{IM} + K_{IR} \leq K_C \tag{5.5}$$

where $K_{IM}$ corresponds to equivalent tensile stress and $K_{IR}$ corresponds to residual stress, i.e. a safety factor of 2 is required only for equivalent tensile stress intensity factor.

In BS PD 6493[6] a safety factor of 2 is required for the total stress intensity factor, i.e.,

$$2\ (K_{IM} + K_{IR}) \leq K_C \tag{5.6}$$

In this paper the expression (5.5) is adopted.

There are no guidelines in the available literature about the requirement of degree of confidence with respect to fracture toughness, and thus, the safety of the structures.

The requirement of 15 ft-lb (Charpy V-notch energy) for steels used in shipbuilding has been set up based on survival probabilitly of 75 percent.[7]

For our analysis it is assumed the degree of confidence is 80 percent.

(2) Determination of Fracture Criterion

Due to the low design stress, and possible low toughness at -50°C, the $K_I$ criterion is most likely valid, and used in this paper.

For surface cracks

$$K_I = \frac{M}{\Phi} \sigma_{eq} \sqrt{\pi a} \qquad (5.7)$$

where $\sigma_{eq}$ is the equivalent tensile stress and M is the geometry correction factor for tensile stress given in the ASTM code.

The equivalent tensile stresses for bending and residual stress are as follows:

For bending stress

$$\sigma_{eq} = \frac{1}{\sqrt{6}} \sigma_b \qquad (5.8)$$

where $\sigma_b$ is bending stress.[8]

For residual stress the equivalent tensile stresses are listed in Table 5.2.[9]

**Table 5.2 - Equivalent tensile stress of residual stress**

| Crack Type | Longitudinal Crack | Transverse Crack |
|---|---|---|
| Through Thickness | 0 | 0.6 $\sigma_{ys}$ |
| Buried | 0 | 0.5 $\sigma_{ys}$ |
| Surface | 0.2 $\sigma ys$ | 0.6 $\sigma_{ys}$ |

In reference (8) the equivalent stress of the residual stress for longitudinal crack is taken as 0.3 $\sigma_{ys}$, regardless of crack type, based on wide plate test.

(3) Assessment of Fracture Toughness

According to these assumptions mentioned above the required fracture toughness can be obtained.

For longitudinal surface crack and 40 mm thick plate in the as-welded condition, with a yield strength $\sigma_{ys}$ = 380 Nmm$^{-2}$ at -50°C.

$$\sigma_{eq} = \frac{1}{3}\sigma_{ys} + \frac{1}{3\sqrt{6}}\sigma_{ys} + 0.3\,\sigma_{ys} \qquad (5.9)$$

$$= 0.77\,\sigma_{ys} = 292 \text{ Nmm}^{-2}$$

taking a/c = 0.5, then

$$K_I = K_{IM} + K_{IR}$$

where

$$K_{IM} = \frac{M}{\Phi}\sigma_{im}\sqrt{\pi a} \qquad (5.10)$$

$$= \frac{1.18}{1.21}\,178\sqrt{10\,\pi}$$

$$= 973 \text{ Nmm}^{-3/2}$$

and

$$K_{IR} = 623 \text{ Nmm}^{-3/2}$$

so that the required fracture toughness $K_C$ is

$$K_C > 2K_{IM} + K_{IR} = 2570 \text{ Nmm}^{-3/2} \qquad (5.11)$$

For longitudinal through thickness crack the other parameters are the same as given above, supposing $K_{IR} = 0$.

$$K_I = \sigma_{eq} \sqrt{\pi c}$$

$$= 178 \sqrt{20 \pi} = 1410 \text{ Nmm}^{-3/2} \qquad (5.12)$$

Thus, the required fracture toughness $K_C$ is

$$K_C > 2K_I = 2800 \text{ Nmm}^{-3/2} \qquad (5.13)$$

The corresponding $\delta_c$ is 0.05 mm.

## 5.2 Empirical Assessment of Toughness

### (1) Based on Failure

Numerous brittle fractures occurred in the hull structures of ships in the 1940s. In order to develop a toughness criterion samples of steel were collected from approximately 100 fractured ships. The plates from fractured ships were divided into three groups:

- those plates in which fractures originated - source plates
- those plates through which the crack passed - through plates
- those plates in which a fracture stopped - end plates

They correspond to three grades of quality, and the average 15 ft-lb Charpy V-notch transition temperature of the three groups are listed in Table 5.3.

**Table 5.3 - Average 15 ft-lb transition temperature**

| | **Number of Plates** | **Transition Temperature** | |
|---|---|---|---|
| | | **°F** | **°C** |
| Source Plates | 38 | 95 | 35 |
| Through Plates | 52 | 65 | 18.3 |
| End Plates | 40 | 50 | 10 |

An absorbed energy at failure temperature greater than 10 ft-lb was found in only 10 percent of the source plates, 33 percent of the through plates and 73 percent of the end plates.

It was therefore concluded, based on these data and for steels of this quality of end plates, that in the large ship hull structures brittle fractures are not likely to initiate in a plate that absorbs more than 10 ft-lb in a Charpy V-notch test at the anticipated operating temperature.

Finally, a slightly higher level of performance, namely the 15 ft-lb transition temperature as measured with a CVN impact test specimen, was selected as a fracture criterion.

(2) Based on Safety

There have not been such a large number of failures in any other type of structure. Thus it is impossible to set up the fracture criterion based on the comparison between safe and unsafe structures.

However, based on the safety of the structure the necessary fracture toughness can be obtained by experience in the following ways:

Survey of Defects

Suppose that an offshore structure has been in service for eight years. A survey of cracks can be made in those regions where the components are subject to higher stress level, and the cracks are easy to form and propagate. By doing so, more reliable data pertaining to cracks, their size, type, position and growth direction, as well as the statistical nature of cracks, can be obtained, provided adequate NDT technology exists.

Survey of Toughness

A large number of fracture toughness tests should be performed on the specimens extracted from both high stress regions in actual structure used in service for long time and the fully simulated components which can represent the actual toughness level.

Such a statistical distribution of fracture toughness might be very useful for more reasonable and reliable establishment of a toughness criterion.

The recent requirement of fracture toughness, e.g., $\delta_c = 0.25$ mm at the design temperature, may be too conservative, as the requirement of lower bound of fracture toughness.

For example, some low fracture toughness values can be seen in Table 5.4 obtained from paper 10, for the PWHT condition.

**Table 5.4 - PWHT Fracture toughness data**

| Specimen Size (mm) | Crack Type | Test Temperature (°C) | $\delta_c$ (mm) |
|---|---|---|---|
| 12.5 x 25 | through thickness crack | -50 | 0.082 |
| 100 x 100 | | -50 | 0.057 |
| 100 x 100 | | -60 | 0.028 |
| 100 x 100 | | -40 | 0.188 |
| 100 x 650 wide plate | surface crack | -30 | 0.09 |
| | | -30 | 0.01 |
| | | -30 | 0.12 |
| | | -50 | 0.05 |

For the as-welded condition, the fracture toughness values are much lower than that for PWHT.

The relevant data given by Slatcher et al[10] are listed in Table 5.5, for the as-welded condition over the temperature range from -10°C to -30°C, but including those higher temperatures at which very low toughness values are obtained and also those lower temperatures at which very high toughness values are obtained.

**Table 5.5 - As-Welded Fracture toughness data[10]**

| | $\delta_c$ (mm) | Test Temp (°C) | IM* | $\delta_c$ (mm) | Test Temp (°C) | IM | $\delta_c$ (mm) | Test Temp (°C) | IM |
|---|---|---|---|---|---|---|---|---|---|
| 1 | 0.13 | -10 | C | 0.06 | -10 | C | 0.148 | -10 | F |
| 2 | 0.31 | -10 | F | 0.062 | 0 | C | 0.115 | -10 | C |
| 3 | 0.43 | -30 | F | 0.031 | -30 | C | 0.42 | -10 | F |
| 4 | 2.5 | -10 | F | 0.008 | -10 | C | 0.152 | -40 | C |
| 5 | 0.02 | -10 | C | 0.106 | -10 | C | 0.98 | -30 | F |
| 6 | 0.05 | +20 | C | 0.157 | -10 | C | 1.08 | -30 | F |
| 7 | 0.02 | -10 | C | 0.008 | +20 | C | 1.10 | -30 | F |
| 8 | 0.08 | -10 | C | 0.007 | +20 | C | 0.35 | -40 | F |
| 9 | 0.06 | -10 | C | 0.009 | -20 | C | 0.98 | -30 | F |
| 10 | 0.03 | -10 | C | 0.028 | +20 | C | >1.0 | -30 | F |
| 11 | | | | 0.103 | +20 | C | 0.346 | -40 | F |
| 12 | | | | 0.015 | -10 | C | 0.314 | -40 | F |
| 13 | | | | 0.011 | -10 | C | 0.99 | -40 | F |
| 14 | | | | | | | >1.0 | -30 | F |
| 15 | | | | | | | >1.0 | -40 | F |
| | Wide plate 100 x 650 mm | | | Three point bending 100 x 100 mm | | | Three-point bending 12.5 x 50 | | |

* IM: Initiation Mechanism
C: Cleavage
F: Fibrous

By using the statistical method mentioned in the previous section, firstly, the mean value and standard deviation will be calculated for the data associated with cleavage initiation. The results are:

$$\delta_c = 0.057 \text{ mm}$$

$$s = 0.049 \text{ mm}$$

By using a similar method to that used in establishment of the toughness criterion of 15 ft-lb for ship steels, a $\delta_c^*$ value can be obtained over which the probability of appearance of fracture toughness $\delta_c$ is 75 percent.

By using the equation (4.33) and (4.34)

$$\overset{*}{\delta_c} = \overline{\delta_c} - sz\,(p')$$

where $$p' = p \, \frac{N + n}{N}$$

$$= 0.25 \, \frac{22 + 16}{22}$$

$$= 0.43$$

so $$\overset{*}{\delta_c} = 0.057 - 0.047 \times 0.17$$

$$= 0.05 \text{ mm}$$

Thus, we would predict that if the fracture toughness of weld metal in the as-welded condition and at the design temperature possesses a value not less than 0.05 mm with degree of confidence of 80 or 85 percent, these structures can be operated safely.

$\delta_c$ = 0.05 corresponds to $K_i$ = 3000 $\text{Nmm}^{-3/2}$ for the material tested in paper 10 with yield strength $\sigma_{ys} = 425 \text{ Nmm}^{-2}$.

## 5.3 Assessment of Some Steels

(1) Assessment of BS4360 Grade 50D

Some data is available on the fracture toughness of BS 4360 50D node steels (Table 5.6).

**Table 5.6 - Test data of BS4360 50D Node**

| Steel | Thickness (mm) | $\sigma_{ys}$ | $\sigma_u$ | CVN (J) at -25°C | |
|---|---|---|---|---|---|
| | | ($Nmm^{-2}$) | | HAZ | WM |
| 50D node | 38 | 367 | 541 | | 35 (AW) |
| | 60 | 358 | 534 | 44 | 32* (PWHT) |

* at -20°C

The fracture toughness data shown in Table 5.7 was estimated from equations (4.6 - 4.8)

**Table 5.7 - Estimated fracture toughness of BS 4360 50D Node**

| Material | Thickness (mm) | Welded Condition | FATT (°C) | $T_K$ (°K) | $K_C$ $Nmm^{-3/2}$ | $\delta_c$ (mm) |
|---|---|---|---|---|---|---|
| HAZ | 60 | AW | -9 | 160 | 3679 | 0.09 |
| WM | 38 | AW | -5 | 159 | 3856 | 0.10 |
| WM | 60 | PWHT | 1 | 165 | 3308 | 0.07 |

If the analysis above is correct, i.e., fracture toughness $K_C$ = 3000 $Nmm^{-3/2}$, then it can be said that the BS4360 50D node steel can be used for Arctic use at temperature down to -50°C.

It is worth noting that it seems there is a great discrepancy between the above assessment of toughness based on $K_I$ criteria and the common toughness requirement based on CTOD design curve. The former suggests a requirement of $\delta_c = 0.05$, while the latter one, $\delta_c = 0.25$ for the as-welded condition and 60 mm thick.

It is of interest to read the paragraph quoted below:

> "Experience shows, however, that procedure test plates now often fail to meet these stringent specifications and that one or more retests are required. Furthermore, designers have, on occasion, had to relax specification requirements to accept results attained in the construction yard from production coupon plates. Such relaxation can have the effect of undermining the credibility of the original requirements in the eyes of the fabricator. This comment is particularly relevant to CTOD requirements where the specification for a minimum acceptable value has caused problems because of the inherent variability of toughness within fusion welds and where it is sometimes the practice to repeat the test program until satisfactory results are obtained."[12]

It has been stated[13] that "the reason why so few brittle fractures occur is perhaps that the probability of a defect of sufficient size being situated in a highly stressed region of low toughness is rather small" and "an appropriate design method should take the observed scatter into account".

Thus it can be seen that the problem remains unsolved even for offshore structures in non-Arctic regions, let alone for Arctic use.

### (2) Assessment of KST 24B and KST 33

These two kinds of steels have been developed for shipbuilding hull structures at low temperature service down to -50°C and have the best low temperature toughness values available so far in the literature.

The typical compositions and mechanical properties are listed in Tables 5.8 and 5.9.[14]

**Table 5.8 - Chemical compositions (%)**

| Designation | Heat Treatment* | Plate Thickness (mm) | C | Si | Mn | P | S | Ni | Al | $C_{eq}$ |
|---|---|---|---|---|---|---|---|---|---|---|
| KST 24B | N | 21 | 0.07 | 0.18 | 1.30 | 0.013 | 0.002 | - | 0.021 | 0.29 |
| KST 33 | QT | 21 | 0.08 | 0.20 | 1.30 | 0.014 | 0.002 | - | 0.030 | 0.30 |

* N: Normalizing;
QT: Quenching and Tempering

**Table 5.9 - Mechanical Properties**

| Designation | $\sigma_{ys}$ | $\sigma_u$ | Test Temperature (°C) | Average CVN (J) | FATT (°C) |
|---|---|---|---|---|---|
| | ($Nmm^{-2}$) | | | | |
| KST 24B | 290 | 429 | -60 | 209 | -85 |
| KST 33 | 403 | 500 | -60 | 357 | -106 |
| | 405 | 515 | -60 | 160 | -73 |

Double sided single pass SAW and single sided single run SAWs were applied to the steels in Tables 5.8 and 5.9. The Charpy V-notch energy values fully meet the IMCO code (Transverse direction: more than 25 J).

According to this value, i.e., 25 J at -50°C, the fracture toughness $K_C$ and $\delta_c$ can be estimated by using the formulas (4.6) and (4.8), that is:

$$K_C = 5450 \text{ Nmm}^{-3/2}$$

and

$$\delta_c = 0.2 \text{ mm}$$

This value would be adequate for use of offshore structures in Arctic service.

# REFERENCES

1. J. C. McKay, "Development of Grade 350 Structural Steel for Offshore Structures and Arctic Vessels", Stelco Inc, R&D 820108, September, 1982.

2. G. H. Eide, K. O. Vilpponen et al, "Review of Steels used in the Construction of Offshore Structures", Report of Det Noske Veritas, April, 1982.

3. H. G. Pisarski, "Design for Fracture Avoidance in Offshore Structures", Int Conf on Steel in Marine Structures, Paris, France, 5-8 October, 1981, Paper 3.

4. H. G. Pisarski and J. D. Harrison, "Background to the Material Selection Procedures for Steels and Weldment Contained in the Proposed Revisions to the Department of Energy Guidance Notes", Conference on Offshore Welded Structures, Paper 22.

5. ASTM Boiler and Pressure Vessel Code, Section III, Nuclear Power Plant Components, App G: Protection Against Non-ductile Failure.

6. BS PD6493: "Guidance on Some Methods for the Derivation of Acceptance Levels for Defects in Fusion Welded Joints", British Standards Institution, March, 1980.

7. S. T. Rolfe and J. M. Barsom, "Fracture and Fatigue Control in Structures: Applications of Fracture Mechanics", New Jersey, 1977.

8. H. Yajima, "Application of Fracture Mechanics in Shipbuilding", Lecture Notes in Ship Research Centre of China, Wuxi, 8-15 April, 1982.

9. WES/2805, "Method of Assessment for Defects in Fusion Welded Joints with Respect to Brittle Fracture", The Japan Welding Engineering Society, 1980.

10. S. Slatcher, S. Saether and J. Lereim, "Post Weld Heat Treatment of Welded Constructions. C-Mn Manual Metal Arc Weld-Metal Toughness", Report of Det norske Veritas, August, 1982.

11. H. G. Pisarski and J. D. Harrison, "Fracture Resistance of Materials Used in Offshore Structures", European Offshore Steels Research Seminar, Cambridge, UK 27-29 November, 1978, Paper 2.

12. V. G. Marshall, "The Procedural Requirements for Welded Joints in Offshore Structures: A Question of Validity", Int Conf on Fracture Toughness Testing Methods, Interpretation and Application, 9-10 June 1982, London.

13. T. Bokalrud and A. Karlson, "Fracture Toughness and Significance of Defects in Heavy Offshore Structures", European Offshore Steels Research Seminar, Cambridge, UK, 27-29 November, 1978, Paper 37.

14. M. Tomita, S. Takashima, T. Hosoya and Y. Kasamatsu, "Development of Steel Plate for High Heat Input Welding by Optimizing Small Amounts of Titanium and Nitrogen Contents", Seminar on the Use of Steel in Shipbuilding, Katowice, Poland, 15-19 September, 1980.